

XI: Modeling of Phosphorus Dynamics of Lake Okeechobee

Subtask Reports:

**Task 4.6 Determination of the Distribution of
Phosphorus in the Water Column**

and

Task 6.2 Simplified Mass Balance Approach

by

Robert E. Dickinson¹

and

Wayne C. Huber²

Department of Environmental Engineering Sciences

University of Florida

Gainesville, Florida 32611-2013

and

Curtis D. Pollman

KBN Engineering and Applied Science, Inc.

Gainesville, Florida 32607

July 1992



Sponsor:

South Florida Water Management District

P.O. Box 24680, 3301 Gun Club Road

West Palm Beach, Florida. 33416-4680

¹Now at WP Software, 8-10 Purdue St., Belconnen, A.C.T. 2617, Australia

²Now at Dept. of Civil Engineering, Oregon State University, Corvallis, OR 97331-2302

EXECUTIVE SUMMARY

1. Introduction

This is a report documenting the background, creation, and findings of an integrated suite of computer models used to simulate the phosphorus dynamics of Lake Okeechobee, the largest lake in Florida and second largest wholly within the (lower 48) United States. The models and the lake regions they are designed to simulate include:

- | | |
|----------|---|
| LOP0D | Model LOP0D is mass balance phosphorus model of Lake Okeechobee that simulates the phosphorus for time periods on the order of years. The model contains 5 large "boxes:" north lake, mud zone, sand zone, South Bay, and littoral area (macrophyte zone). |
| LOP3D | Model LOP3D is a three dimensional phosphorus model of Lake Okeechobee that meshes with model EHSMSED (developed by the University of Florida, Dept. of Coastal and Oceanographic Engineering = UF COE), a three dimensional model of the hydrodynamics and suspended sediment dynamics of Lake Okeechobee. LOP3D contains 486 boxes each with a surface area of 4 km ² and 5 vertical layers. Simulation times are on the order of weeks. |
| Pelagic | The phosphorus dynamics of the open water column are simulated. Seven phosphorus components are simulated: soluble reactive phosphorus (SRP), dissolved organic phosphorus (DOP), green algae (GRN), blue-green algae (BLU), zooplankton (ZOO), particulate inorganic phosphorus (PIP), and particulate organic phosphorus (ORG). An eighth component is total phosphorus (TP), the sum of the other seven components. |
| Sediment | The phosphorus dynamics of the bottom sediments of the lake are simulated. The genesis or the change of organic phosphorus to inorganic phosphorus in the sediment is simulated using 50 sediment layers. The sediment phosphorus interacts with the pelagic phosphorus through the processes of erosion, deposition, and diffusion. |

2. Report Format

The contents of this report are divided into 14 chapters and four appendices. The chapters discuss water quality characteristics of Lake Okeechobee, the basis of the finite difference formulation used in the two models, and summarize the models' results. The appendices define notation, discuss trends in Lake Okeechobee phosphorus data, and present some of the voluminous model output. Each chapter discusses a major component in the dynamic phosphorus model(s) of Lake Okeechobee:

- Chapter 1** Background information on the history of phosphorus concentrations in Lake Okeechobee.
- Chapter 2** The complexity of the phosphorus cycle in lake waters, measured phosphorus species, and modeled phosphorus components.
- Chapter 3** Loading and location of the tributaries to Lake Okeechobee.
- Chapter 4** An analysis of the trend in the major atmospheric, hydraulic, and phosphorus input components affecting Lake Okeechobee.
- Chapter 5** Background information on the history of phosphorus concentrations in Lake Okeechobee.
- Chapter 6** Solar radiation, temperature, and pelagic light attenuation.
- Chapter 7** Description of the suspended sediment model used in LOP0D.
- Chapter 8** Description of the diagenetic phosphorus model used in LOP0D and LOP3D.
- Chapter 9** Description of the littoral phosphorus model used in LOP0D and LOP3D.
- Chapter 10** Governing differential equations for advection and diffusion used in LOP3D.
- Chapter 11** Testing of the advection and diffusion finite difference scheme used to solve the equations discussed in Chapter 10.

- Chapter 12 Formulations of the phosphorus reactions used in models LOP0D and LOP3D.
- Chapter 13 Calibration and alternative analysis using the model LOP0D.
- Chapter 14 Calibration and analysis using the model LOP3D.

3. Major External or Environmental Factors

- Solar radiation is the source of energy for photosynthesis. The processes of algal uptake and release of SRP, algal light shading, suspended sediment light shading, and algal loss to the bottom sediments are all predicated on correctly calculating the vertical attenuation of light. The models contain mechanisms to predict the surface light intensity on a daily basis, and attenuate the light vertically based on the light absorption and light scattering properties of water, organic color, algae, and suspended sediments.
- Wind is the major source of mixing energy in the lake to drive horizontal and vertical advection. The wind generated waves generate bottom shear stresses that erode bottom sediment. The wind's cessation allows the suspended sediment to deposit on the sediment bed. Model LOP3D has an erosion/deposition model, developed by the University of Florida Department of Coastal and Oceanographic Engineering (UF COE), to predict the benthic contributions to the pelagic phosphorus pool. Model LOP0D has a simpler erosion/deposition model based on gross characteristics of wind-generated waves and bottom shear.
- The diurnal variation in temperature and light energy in Lake Okeechobee as well as the time scale of SRP uptake and phosphorus transformations predicate a model time step requirement of less than one day. Model LOP0D uses an approximate quarter-day time step (two daylight and two night). The time step duration is dependent on the day of the year. Model LOP3D uses time steps ranging from 15 minutes to 3 hours.
- Temperature affects the uptake and reaction rates of the algal species and remineralization of SRP. The models contain formulas for altering the reaction rates depending on the external temperature.

- The import of new SRP and TP loads through the tributaries strongly affects in-lake concentrations. Both models include these driving forces as well as loading due to rainfall on the lake.
- Due to the shallowness of Lake Okeechobee the mean flow is not as significant as the horizontal advection caused by direct wind action and associated wind-wave setup. The horizontal mixing due to littoral-pelagic gradients in temperature may also be significant in Lake Okeechobee. Temperature gradients affect the 3D hydrodynamic model of the UF COE and thus affect model LOP3D. However, they are not included in model LOP0D.
- The atmospheric contribution of phosphorus to the lake (302 mg/m^2 SRP plus 130 mg/m^2 DOP based on the nine-year simulation of Chapter 13) through the processes of wet and dry deposition is approximately equal to the phosphorus losses from the lake through the surface outflow canals (417 mg/m^2).

4. Summary of Impacts on Algal Components

Model simulations highlighted the following factors influencing algal growth in Lake Okeechobee:

- The light shading of algae by wind-mixed suspended sediment in the mud zone controls algal uptake and has the secondary effect of decreasing algal sedimentation loss, thus increasing the mean concentrations of SRP and TP concentration. This is demonstrated by the sensitivity of both models to light attenuation parameters.
- On the basis of runs of model LOP3D (Chapter 14), algal self shading may be one of the causes of blue-green algal dominance in Lake Okeechobee. Because of the lake's turbidity and algal self shading, most especially in the mud zone, phosphorus is likely not limiting algal populations in Lake Okeechobee. Similarly, other nutrients limiting algal growth are masked by the physical processes of light shading and temperature.

5. Summary of the Major Findings of This Study

Most of the major objectives and findings of this study are based on the LOP3D and LOP0D computer simulations presented elsewhere in this report. The reader should be cognizant of the fact that improvements, refinements and reduction

of errors always accompany computer model development. Thus, numerical values presented in the text below should be understood to be provisional and subject to moderate changes as models improve. Nonetheless, conclusions drawn from them are felt by the report authors to be qualitatively correct at the very least.

To place some of the concentrations listed below in context, the 1979-1988 measured whole-lake averages for TP and SRP are 90.2 and 29.5 ug/l, respectively (Table 13-12). Predicted values using model LOP0D are 93.3 and 28.4 ug/l, respectively, with similar variance (as indicated by coefficients of variation) for measured and predicted phosphorus time series.

1. Evaluate the phosphorus exchange between the bottom sediments and pelagic phosphorus on weekly and yearly time scales.

Based on the measured (from tributaries) and modeled phosphorus fluxes given for the nine-year simulation period in Chapter 13 and in Figures from Appendix D, the diagenetic diffusion of SRP across the pelagic-sediment interface (528 mg/m^2 , Figure D-63) was approximately 17 percent of the tributary loading of TP ($3,081 \text{ mg/m}^2$, Table D-1 at end of Appendix D) during the years 1979 to 1988. Short-term exchange (e.g., weekly) depends strongly on the loadings and wind conditions at the instant of time. The transfer of pelagic phosphorus to the bottom sediments was mainly accomplished by the twin loss processes of algal settling (Figure D-59) and PIP deposition to the sediment (Figure D-78). The losses were $1,853 \text{ mg/m}^2$ and $4,413 \text{ mg/m}^2$, respectively, for algal settling and PIP deposition. The total of $6,266 \text{ mg/m}^2$ is approximately balanced by the main sources of SRP and TP-SRP: diagenetic diffusion (D-63, 528 mg/m^2), erosion (D-77, $1,980 \text{ mg/m}^2$), tributary loading (Appendix D table, $3,081 \text{ mg/m}^2$), and atmospheric loading (D-60 and D-61, 432 mg/m^2), which totaled $6,021 \text{ mg/m}^2$.

2. Determine the role of phosphorus mineralization in the sediments as a source of supply to the pelagic region.

The anaerobic transformation from organic phosphorus to inorganic phosphorus is composed of a two stage transformation (Pollman, 1991). The first stage lasts ≈ 100 days and 30% of the organic phosphorus is transformed (Reddy et al., 1991). The second stage is the transformation and burial of refractory organic phosphorus.

3. Determine the effects of sediment mixing and resuspension on pelagic SRP release.

The adsorption of pelagic SRP on suspended sediment was a significant loss of SRP from Lake Okeechobee. Based on the ten-year simulation (Chapter 13 and Appendix D), this loss pathway ($2,832 \text{ mg/m}^2$ adsorption of PIP, Figure D-41) was 153 percent of the algal settling loss pathway ($1,853 \text{ mg/m}^2$). Desorption of PIP was 399 mg/m^2 (Figure D-40). Thus, the net

effect of sorption is still an SRP release of $2,832 - 399 = 2,433 \text{ mg/m}^2$ or a net release that is 131 percent of the algal settling loss pathway. The fate of most of the adsorbed phosphorus is settling: PIP deposition (Figure D-78) was $4,413 \text{ mg/m}^2$.

4. Determine the relative phosphorus retention capacity of the bottom sediments over a multi-year simulation.

Organic phosphorus erosion and deposition are in an approximate balance for each box and for the lake as a whole (compare Figures D-74 and D-75). However, the north lake and central mud zone are a net sink of inorganic sediment related phosphorus for the ten-year simulation period (compare Figures D-77 and D-78). The littoral area, sand zone and South Bay were net exporters of inorganic sediment-related phosphorus based on these phosphorus balances.

5. Develop an internal nutrient budget for the lake. The internal nutrient budget combines the sediment phosphorus transformation pathways with pelagic absorption-desorption, and algal settling.

The many diagrams of Chapter 13 and Appendix D quantify most of the phosphorus pathways in the lake. Because the fluxes vary among the eight phosphorus components and from area to area, the reader must refer to the diagrams, in units of mg/m^2 over the ten-year simulation, to determine the magnitude of the flux of interest. However, see item 1 above for an approximate balance for the lake as a whole.

6. Determine the relationship between lake stage and internal loading from the bottom sediments and littoral zone.

This was not accomplished as part of the modeling study. However, using time series analysis, Carey and Huber (1990) showed that SRP was more sensitive to lake stage (increasing with higher stage) than was TP, presumably because of flooding of the macrophyte (littoral) zone during high stages.

7. A management goal for Lake Okeechobee is likely to be the reduction of the tributary concentrations of SRP and TP. Because the net adsorption-desorption process is dependent on the equilibrium phosphorus concentration (EPC), a lake sediment type may change from a net sink of SRP to a net source of SRP if the new SRP < EPC.

The response of the bottom sediment to a reduction in SRP is negligible based on the ten-year simulation. The gradient at the sediment-water interface is so sharp that water column SRP concentrations under 200 ug/l almost always result in the net diffusion of SRP from the bottom sediment to the water column. Thus, the diagenetic modeling indicates that the sediment is not currently acting as a net sink. In addition, modeling results discussed below

indicate a reduction in SRP concentrations with a reduction in tributary loads. For the LOP0D modeling performed during this study, there is no sorption reversal effect as described above.

8. Determine the effect of tributary load reductions on TP and SRP concentrations in the lake.

Nine-year simulations of TP and SRP were made using model LOP0D under assumptions of 40 percent, 50 percent, and 70 percent reductions in tributary loads of TP and SRP (see Chapter 13 and Section 13.12). These simulations predicted corresponding reductions of 26, 33, and 46 percent in SRP and 19, 23, and 33 percent in TP (Table 13-12). The reduction is approximately a linear function of loading reduction, but the percent reduction in concentration is not 1:1 with percent reduction in loading because of other internal and rainfall loadings and because of internal recycling. For example, the magnitude of the SRP diffusive flux from bottom sediments is in the range of 500 to 700 mg/m², depending on the loading scenario, and erosion of PIP is in the range of 1,900 to 2,100 mg/m². Internal loading is insensitive to external loading and approximately constant.

A three-month simulation with model LOP3D was performed with the cooperation of the UF COE hydrodynamic and sediment modeling effort (Sheng et al., 1991b). Results are only summarized in Chapter 14 (due to the detailed presentation by Sheng et al., 1991b), but indicate that concentrations in the north lake zone were reduced with a reduction in loadings (eliminated for comparison purposes). Thus, localized effects of tributary reduction will be greater than the impact on the whole of Lake Okeechobee.

The principal point is that a reduction in loadings results in a reduction of in-lake concentrations, although the predicted percentage reductions given above are unlikely to be precise. Future model improvements and refinements should enhance the evaluation of management alternatives based on tributary load reduction.

9. What is the effect of limiting the TP concentration in Nubbin Slough/Taylor Creek to 180 ug/l?

When this alternative was run, it resulted in only an 8 percent reduction in SRP and 5 percent reduction in TP concentrations in the lake (Table 13-12). This option does not have a substantial effect on whole-lake concentrations.

10. Can TP concentrations in Lake Okeechobee be reduced to the 50 ug/l range of the early 1970s?

From the LOP0D modeling of Chapter 13, when tributary loads were reduced by 70%, the average TP concentration in the lake was predicted to be 62.9 ug/l, not down to 50 ug/l, but down. Again, this prediction is unlikely to

be precise but does indicate that significant in-lake TP reductions can be expected with large reductions in tributary loads.

11. What is the time scale for phosphorus changes in the lake?

This depends in part upon the residence time of phosphorus in the lake. As shown in Chapter 13, when based on the reciprocal of first-order kinetic coefficients, the residence time of phosphorus in the lake (on the order of a few months) is much shorter than the residence time of water (three to five years). Response time is a multiple of residence time (Chapra and Reckhow, 1983). This means that changes in lake phosphorus concentrations (in response to external changes) will occur faster -- on the order of one to ten years -- than one would assume based strictly on the hydraulic residence time .

12. What is the prognosis for phosphorus concentrations in Lake Okeechobee?

Mixing caused by Hurricane David in 1979 and the large influx of SRP and TP in the early 1980s is still causing elevated SRP and TP concentrations in the lake (Carey and Huber, 1990). However, in-lake concentrations and tributary loads concentrations show a decreasing trend from 1984 (see Appendix C and Carey and Huber, 1990). If tributary loads are reduced, in-lake TP concentrations should drop from their ten-year average level of near 90 ug/l. The exact drop cannot be precisely predicted, but the results discussed in items 8 and 10 above may serve as indicators.

ABSTRACT

As part of a comprehensive study of phosphorus dynamics and sediment interaction in Lake Okeechobee, Florida, two dynamic phosphorus simulation models were developed:

1. LOP3D - a three-dimensional, transient, five-layer model, running on a 15-min to 3-hr time step for simulation time periods on the order of weeks. This model is run in parallel with a hydrodynamic and sediment transport model developed by the University of Florida Department of Coastal and Oceanographic Engineering (UF COE).
2. LOP0D - a lumped, transient model simulating Lake Okeechobee as five "boxes" with distinct sediment characteristics, running on an approximate quarter-day time step for simulation time periods on the order of years.

Both models include the influence of tributary loadings, wind-driven resuspension and deposition, diagenetic exchange with the sediment, advection, diffusion, and in-lake phosphorus kinetics. Phosphorus species simulated are phosphorus contained in the lake as soluble reactive phosphorus (SRP), dissolved organic phosphorus (DOP), green algae (GRN), blue-green algae (BLU), diatom algae (DIA), zooplankton (ZOO), particulate inorganic phosphorus (PIP), and organic sediment phosphorus (ORG). The models also predict the sum of the phosphorus species as total phosphorus (TP). The LOP3D model uses sediment concentrations provided by the UF COE model for adsorption-desorption exchange.

This report summarizes the history of Lake Okeechobee insofar as its water quality characteristics are concerned. The development of model algorithms and procedures for all the processes mentioned above is described in separate chapters. Runs of the LOP0D model are described documenting calibration and use of the model for alternative analyses. The baseline TP value in the lake is predicted to average 93.3 ug/l for the time period 1979-88 (measured to be 90.2 ug/l). In particular, in-lake phosphorus reductions are predicted by the model for hypothetical tributary reductions in SRP and TP of 40, 50 and 70%. The lowest predicted TP at a 70% reduction is 62.9 ug/l. All predicted concentrations in this report are subject to improvements in model parameterization and calibration. Runs of the LOP3D model illustrate its calibration and application for spatial and temporal resolution of phosphorus distributions in the lake. A separate 3-month LOP3D simulation is described elsewhere.

ACKNOWLEDGEMENTS

This research has been supported by the South Florida Water Management District (SFWMD). Statements made in this report are the opinion of the authors and not necessarily those of the SFWMD.

The support and patience of Dr. Peter Sheng and his colleagues in the Department of Coastal and Oceanographic Engineering at the University of Florida is gratefully acknowledged. We also appreciate the support and patience of Dr. Ramesh Reddy of the Soil Science Department and other colleagues at the University of Florida for their input and support.

We wish to thank most of all Mr. Brad Jones and colleagues at the SFWMD for their untiring patience and good-willed support in the face of untoward delays in the production of this final report.

This report involved the work of several individuals, but there are two standouts: Ms. Doris Smithson of the University of Florida, Department of Environmental Engineering Sciences faithfully logged the progress of the project and report and provided a first pass through the report draft. As an interface and buffer alone, she deserves our thanks. Ms. Laurie Dockendorf of the Oregon State University, College of Engineering stepped in at the eleventh hour to provide expert word processing in a time of great need. The production of this report would have been even further delayed without the help of these persons.

TABLE OF CONTENTS

	<u>Page</u>
EXECUTIVE SUMMARY	1
1. Introduction	1
2. Report Format	2
3. Major External or Environmental Factors	3
4. Summary of Impacts on Algal Components	4
5. Summary of the Major Findings of This Study	4
1. INTRODUCTION TO THE PELAGIC PHOSPHORUS MODEL	1-1
1.1 Project Overview	1-1
1.2 Glossary	1-4
1.3 Project Approach	1-4
1.4 Model Overview	1-5
1.5 Physical Setting of Lake Okeechobee	1-7
1.5.1 Word Origins	1-7
1.5.2 Geological Beginnings of Lake Okeechobee	1-9
1.6 Ecological Setting of Lake Okeechobee	1-12
1.7 Trophic Status of Lake Okeechobee	1-15
2. PHOSPHORUS CYCLE AND COMPONENTS	2-1
2.1 Introduction	2-1
2.2 Phosphorus Cycle in Lake Okeechobee	2-3
2.3 Dissolved Organic Phosphorus (DOP)	2-4
2.4 Soluble Reactive Phosphorus (SRP)	2-5
2.5 Dissolved Organic Phosphorus (DOP)	2-5

2.6	Particulate Phosphorus	2-6
2.7	Particulate Algal and Detrital Phosphorus	2-7
2.8	Chlorophyll <i>a</i> and Phosphorus Relationship in Lake Okeechobee	2-7
2.9	Relationship Between SRP and TP-SRP in Lake Okeechobee	2-9
2.10	Nutrient and Yield Limitation on Lake Okeechobee Algae	2-11
2.11	Algae - Bacteria Pelagic Interaction	2-13
2.12	Zooplankton Particulate Phosphorus	2-14
2.13	Summary	2-15
3.	LAKE OKEECHOBEE BOUNDARY INFORMATION	3-1
3.1	Introduction	3-1
3.2	Tributary Flow and Loading Data for Lake Okeechobee	3-3
3.3	Seasonal Rainfall and Evaporation Patterns	3-7
3.4	Lake and Marsh Evaporation	3-9
3.5	Precipitation Loading Model	3-9
4.	LAKE OKEECHOBEE WATER QUALITY	4-1
4.1	Introduction	4-1
4.2	Chemical and Physical Data in Lake Okeechobee	4-2
4.2.1	Data Sources	4-2
4.2.2	Lake Okeechobee Turbidity and Suspended Solids	4-3
4.2.3	Lake Okeechobee Organic Color, pH, and Secchi Disc	4-5
4.3	Nutrient Data in Lake Okeechobee	4-8
4.4	Summary of Nutrients in Lake Okeechobee	4-10
5.	DOUBLE MASS TREND ANALYSIS	5-1
5.1	Introduction	5-1
5.2	Double Mass Trend Analysis of Mud and Non-Mud Stations	5-1

5.3	Double Mass Curve Analysis of Boundary Conditions	5-5
5.4	Rainfall, Evaporation and Wind Data	5-7
6.	SOLAR RADIATION AND TEMPERATURE MODEL	6-1
6.1	Daily and Seasonal Solar Radiation Model	6-1
6.1.1	Net Surface Heat Flux	6-1
6.1.2	Clear Sky Shortwave Radiation	6-2
6.1.3	Clear Sky Longwave Radiation	6-6
6.1.4	Longwave Back Radiation from the Lake Surface	6-8
6.1.5	Atmospheric Cloud Effect on Shortwave and Longwave	6-9
6.1.6	Nonradiative Heat Loss from Water Surface	6-11
6.2	Lake Temperature Model	6-12
6.3	Additional Temperature-Related Parameters	6-14
6.4	Vertical Light Attenuation in Water	6-15
6.4.1	Disposition of Radiation	6-15
6.4.2	Pelagic Light Absorbance and Scattering Coefficients	6-17
6.4.3	CaCO_3 Precipitation in Lake Okeechobee	6-20
6.4.4	Vertical Light Attenuation Coefficient	6-21
6.5	Light Limiting Growth Functions	6-22
6.6	Temperature Growth Limiting Functions	6-24
7.	PELAGIC SEDIMENT PHOSPHORUS	7-1
7.1	Introduction	7-1
7.2	Pelagic Adsorption-Desorption	7-2
7.3	Sediment Organic Phosphorus and PIP	7-5
7.4	Wind Fields Near Lake Okeechobee	7-6
7.5	Lake Okeechobee Wind Model	7-7
7.6	Magnitude of Internal Wind Loading	7-10
7.7	Interaction with Diagenetic Model	7-11
7.8	Interaction with Deposition-Resuspension Model	7-11

7.9	Summary	7-16
8.	DIAGENETIC ADVECTION-DIFFUSION MODEL	8-1
8.1	Introduction	8-1
8.2	Basic Equations and Boundary Conditions	8-1
8.3	Vertical Grid Resolution	8-3
8.4	Data Required for Diagenetic Model	8-3
8.5	Steady-State Numerical Solution	8-3
8.6	Time Scale Considerations	8-7
9.	LITTORAL ZONE PHOSPHORUS MODEL	9-1
9.1	Introduction	9-1
9.2	Littoral Source of Phosphorus to Pelagic Area	9-3
9.3	Lake Stage Influence on Pelagic Phosphorus Concentrations	9-3
10.	PELAGIC ADVECTION-DIFFUSION EQUATION	10-1
10.1	Introduction	10-1
10.2	Basic Equations and Boundary Conditions	10-2
10.3	3-D Equation in Sigma Coordinate System	10-2
10.4	Time Scales and Dimensionless Parameters	10-6
10.5	Transformation of Governing Equations to Dimensionless Form	10-9
11.	PELAGIC ADVECTION-DIFFUSION SCHEMES	11-1
11.1	Introduction	11-1
11.2	Upwind Solution	11-5
11.3	Central Difference	11-7
11.4	Combined Upwind and Central Difference	11-7
11.5	Vertical Advection and Diffusion	11-8

11.6	3-D Advection-Diffusion Solution	11-9
11.7	Advection and Diffusion Solution Testing	11-10
11.8	Summary	11-12
12.	REACTION MODEL FOR PELAGIC PHOSPHORUS	12-1
12.1	Introduction to the Pelagic Water Quality Model	12-1
12.2	Phosphorus Components in Lake Okeechobee	12-2
12.3	Simulated Pelagic Algae	12-3
	12.3.1 Algal Forms	12-3
	12.3.2 Allometric Differences Between Algal Classes	12-9
	12.3.3 Algal Blooms in Lake Okeechobee	12-10
12.4	Algal Growth Simulation	12-11
	12.4.1 Alternative Formulations	12-11
	12.4.2 Species Specific Growth Rates	12-15
	12.4.3 Algal Carbon/Chlorophyll a	12-16
	12.4.4 Algal Carbon/Phosphorus	12-18
	12.4.5 Model Formulation for Chlorophyll a Prediction	12-19
12.5	Effect of Light/Temperature on Algal Growth	12-19
12.6	Algal Respiration and Excretion	12-20
12.7	Algal Non-Predatory Mortality	12-21
12.8	Algal Settling	12-22
12.9	Zooplankton Uptake	12-24
12.10	Reaction Model for Littoral, Sediment and Pelagic Phosphorus	12-25
12.11	Phosphorus Boundary Conditions	12-29
12.12	Summary of Pelagic Phosphorus Model	12-29
13.	MASS BALANCE APPROACH TO PREDICTING PHOSPHORUS	13-1
13.1	Introduction	13-1
13.2	Previous Water Quality Models of Lake Okeechobee	13-2

13.3	Five-Box Model of Phosphorus in Lake Okeechobee	13-3
13.4	Algal Growth in Lake Okeechobee	13-5
13.5	Finite Difference Model of Lake Okeechobee	13-6
	13.5.1 Box Model Formulation	13-6
	13.5.2 Diffusion and Advection	13-7
	13.5.3 Reaction Pathway Finite Difference Equations	13-12
13.6	Sediment Erosion and Deposition	13-12
13.7	Stage-Area-Volume in Lake Okeechobee	13-16
13.8	Lake Okeechobee LOP0D Boundary Conditions	13-16
13.9	Normalized Nutrient and Hydraulic Loading	13-19
13.10	General Modeling Considerations	13-19
	13.10.1 Time Steps	13-19
	13.10.2 DOP Remineralization	13-20
	13.10.3 Lake Precipitation Loading	13-20
	13.10.4 Lake Diagenetic Flux	13-20
	13.10.5 Macrophyte, Corbicula, and Algal Mat fluxes	13-21
	13.10.6 Algal and Zooplankton Reaction Pathways	13-21
	13.10.7 Dynamic Adjustment of Algal Functions	13-22
	13.10.8 Algal Populations and Time Scales	13-24
	13.10.9 Phosphorus Import and Export	13-25
	13.10.10 Initial Phosphorus Conditions	13-26
	13.10.11 Lake Area and Lake Box Areas	13-27
	13.10.12 Conservation of Mass	13-28
13.11	Calibration and Verification of LOP0D Model	13-28
	13.11.1 Whole-Lake Results	13-28
	13.11.2 Individual Box Results	13-30
	13.11.3 Output of Miscellaneous Fluxes, Storages, etc.	13-36
13.12	Comparative Analysis: Baseline vs. Simulation with Load Reduction	13-39
13.13	General Discussion of Baseline Results	13-42
	13.13.1 Comparisons of Modeled Fluxes, Rates, Timing	13-42
	13.13.2 Comparison of Flux Magnitudes	13-49
	13.13.3 Sensitivity	13-49
	13.13.4 Further General Discussion	13-50

13.14 Summary	13-51
14. RESULTS OF 3-D PHOSPHORUS MODELING	14-1
14.1 Introduction	14-1
14.2 Synoptic Data Interpolation and Initial Conditions	14-1
14.3 Results	14-6
14.3.1 Interfacing and Time Steps	14-6
14.3.2 TP and SRP Comparisons	14-7
14.3.3 Other Phosphorus Parameters	14-16
14.3.4 Water Depths	14-28
14.4 Three-Month Simulation	14-28
14.5 Sensitivity	14-48
14.6 Summary	14-48
REFERENCES	Ref-1
Appendix A: Dictionary of FORTRAN Variables	A-1
Appendix B: List of Symbols	B-1
Appendix C: Lake Okeechobee SRP and TP-SRP Trends	C-1
Appendix D: Output from Baseline Run of LOP0D	D-1

LIST OF FIGURES

<u>Figure</u>		<u>Page</u>
1-1 Satellite photograph of Lake Okeechobee, showing the major regions of the lake		1-1
1-2 Lake Okeechobee is the largest lake in Florida, and the second largest in the lower 48 states		1-2
1-3 Location of Lake Okeechobee and its tributary drainage areas in Florida		1-2
1-4 TP and SRP concentrations in Lake Okeechobee for 1972 to 1989		1-4
1-5 Temporal variation in lake models		1-5
1-6 Spatial variation in lake models		1-5
1-7 Structure of the combined advection-diffusion-reaction three dimensional model of pelagic, littoral, and sediment phosphorus species in Lake Okeechobee		1-6
1-8 Florida coastline during the Pamilco period, showing the extension of the continental shelf and the coastline at the time of high water between glacial periods		1-9
1-9 Physiographical regions near Lake Okeechobee, showing the sculpturing effect the raising and lowering of the mean sea level by ice ages had on the features of Florida		1-10
1-10 An early map of Lake Okeechobee (1838), showing the greater extent of the lake especially in the western littoral zone and southern lake due to higher water surface elevations		1-11
1-11 Vegetation regions of Lake Okeechobee before 1900, showing custard apple groves in the southern lake, and less area of emergent macrophytes in the western lake compared to the present lake		1-12
1-12 Stage history of Lake Okeechobee since 1932, showing the periodicity of stages in the lake		1-13
1-13 Mean lake stage of each decade beginning in 1932		1-14
1-14 The total phosphorus (TP) and soluble reactive phosphorus (SRP) burdens in Lake Okeechobee have increased greatly since 1979		1-14

2-1	Definition of phosphorus forms in water	2-2
2-2	Conceptual model of Scavia (1980)	2-2
2-3	Size spectrum of particles in water	2-2
2-4	Particulate phosphorus grouping along axes of size and organic content	2-3
2-5	Biological movements of phosphorus from Lean (1975)	2-4
2-6	Phosphorus pathway between DOP and SRP is a combination of bacterial uptake of DOP and excretion of SRP in Subroutines REAC3D and REAC0D	2-4
2-7	SRP versus TP for the non-mud stations in Lake Okeechobee	2-10
2-8	SRP versus TP for mud stations in Lake Okeechobee	2-10
2-9	Lake Okeechobee mean station TN/TP	2-12
2-10	Lake Okeechobee mean station DIN/SRP	2-12
2-11	A zooplankter (<i>Daphnia spp.</i>)	2-15
3-1	Inflow tributaries and outflow control structures in Lake Okeechobee	3-1
3-2	Inflow drainage area and outflow canals in southern Lake Okeechobee	3-2
3-3	Major Lake Okeechobee inflow/outflows	3-4
3-4	Lake Okeechobee hydraulic loadings	3-4
3-5	Lake Okeechobee inflow time series for the period 1972-1989	3-5
3-6	Lake Okeechobee outflow time series for the period 1972-1989	3-5
3-7	Lake Okeechobee inflow time series for phosphorus	3-5
3-8	Lake Okeechobee phosphorus loading	3-5
3-9	SRP loading to Lake Okeechobee (1977-1988)	3-6
3-10	TP loading to Lake Okeechobee (1977-1988)	3-6
3-11	DOP loading to Lake Okeechobee (1977-1988)	3-7

3-12	Precipitation near Lake Okeechobee	3-8
3-13	Pan evaporation near Lake Okeechobee	3-9
3-14	Precipitation and evaporation difference	3-9
4-1	Long term sampling station locations in Lake Okeechobee	4-1
4-2	Correspondence between long term sampling station locations in Lake Okeechobee and the generalized areas in the box model of Lake Okeechobee	4-2
4-3	Mean station turbidity and TP during 1988-1989	4-3
4-4	Mean station suspended solids and TP during 1988-1989	4-3
4-5	Mean monthly suspended solids during 1988-1989	4-4
4-6	Mean monthly turbidity during 1988-1989	4-4
4-7	Mean lake TSS concentrations before and after 1979 from the SFWMD data set YPROJ.DAT	4-4
4-8	Mean station TP versus turbidity during 1988-89	4-5
4-9	Mean station TP versus TSS during 1988-1989	4-5
4-10	Mean monthly Lake Okeechobee organic color during 1988-1989	4-6
4-11	Mean monthly Lake Okeechobee pH 1988-1989	4-6
4-12	Mean Lake Okeechobee pH and conductivity station data during 1988-1989	4-6
4-13	Mean monthly Lake Okeechobee Secchi Disc (m)	4-7
4-14	Mean station SD, Color, TSS, and turbidity during 1988-1989	4-7
4-15	Mean Cond, pH by station	4-7
4-16	Mean Cond, pH by month	4-7
4-17	Turbidity (NTU) and suspended solids (TSS) by station	4-8
4-18	Turbidity (NTU) and suspended solids (TSS) by month	4-8
4-19	Mean SRP and TP by station	4-9

4-20	Mean SRP and TP by month	4-9
4-21	Mean station total nitrogen during 1988-1989	4-10
4-22	Mean station total phosphorus during 1988-1989	4-10
5-1	Lake Okeechobee volume weighted TP and SRP concentrations during 1972 to 1989	5-2
5-2	Lake Okeechobee TP and SRP concentrations for the five mud stations during 1972 to 1989	5-2
5-3	Lake Okeechobee TP and SRP concentrations for the three non-mud stations during 1972 to 1989	5-3
5-4	Mud zone TP double mass	5-3
5-5	Non-mud TP double mass	5-3
5-6	Mud zone SRP double mass	5-4
5-7	Non-mud SRP	5-4
5-8	Fractional increase in TP and SRP	5-5
5-9	Lake SRP change	5-5
5-10	Inflow double mass for years 1972-1989	5-6
5-11	Outflow double mass for years 1972-1989	5-6
5-12	Phosphorus loading double mass curve from 1979-1989	5-6
5-13	Lake Okeechobee mean rainfall double mass for 1965-1989	5-7
5-14	Evaporation double mass for 1965-1989	5-7
5-15	Monthly wind movement at Moore Haven, Florida	5-7
5-16	Double mass curve for squared monthly wind at Moore Haven	5-7
6-1	Major components of surface heat transfer	6-2
6-2	Definition of the solar altitude (α) and zenith angle (Z) of the incident solar ray	6-3

6-3	Normalized earth-sun radius. Solar declination as a function of M_{day} for the year	6-3
6-4	Shortwave radiation at the top of the atmosphere at noon and the horizontal clear sky shortwave radiation at the earth surface without clouds	6-4
6-5	Solar altitude and shortwave albedo for Lake Okeechobee	6-4
6-6	Length of daylight and the hour angle at noon	6-6
6-7	Atmospheric emissivity at various air temperatures	6-6
6-8	Net atmospheric longwave radiation from the water vapor, carbon dioxide and ozone in the atmosphere	6-7
6-9	Longwave back radiation from the lake surface	6-7
6-10	The transmittance, emissivity, and reflectivity of longwave radiation from the water surface of Lake Okeechobee	6-9
6-11	The optical air mass and shortwave radiation atmospheric transmission coefficient	6-10
6-12	The effect of cloud cover on shortwave and longwave radiation	6-10
6-13	Saturation vapor pressure [mbar] and the latent heat of evaporation	6-11
6-14	Mean monthly Lake Okeechobee water temperature measurements during the years 1988 and 1989	6-11
6-15	Mean monthly water temperature and dissolved oxygen concentration measurements for Lake Okeechobee during the period 1972 to 1987	6-12
6-16	Mean station water temperature and dissolved oxygen concentrations measurements for Lake Okeechobee during the period 1972 to 1987	6-12
6-17	Maximum and minimum air temperature for 1965 to 1989	6-13
6-18	Water density [$\text{gm} \cdot \text{cm}^{-3}$], viscosity [$\text{gm} \cdot \text{cm}^{-1} \cdot \text{sec}^{-1}$], and heat capacity [$\text{cal} \cdot \text{g}^{-1} \cdot \text{K}^{-1}$]	6-13
6-19	Differences in shortwave and longwave pelagic radiation characteristics	6-15
6-20	Definition of the measured and calculate pelagic light levels for SD depth, K_d , and photic depth	6-17
6-21	Permutations of mixing depth, photic depth, and the bottom of a lake	6-17

6-22	Mean turbidity and TSS station concentrations in Lake Okeechobee during 1972-1988	6-18
6-23	Mean monthly turbidity and TSS station concentrations in Lake Okeechobee during 1972-1988	6-18
6-24	Light scattering coefficients (b) and light extinction coefficients (b/TSS) attributable to TSS	6-20
6-25	Definition of the refracted angle in water of the incident solar ray	6-20
6-26	Monod light function	6-23
6-27	Smith light function	6-23
6-28	Bannister light function	6-23
6-29	Steele light function	6-23
6-30	Sensitivity of the temperature parameter, θ , used to modify reaction rates	6-25
7-1	Interaction between sediment and pelagic phosphorus	7-1
7-2	Bottom sediment map from Reedy et al. (1991)	7-3
7-3	Bottom sediment map from Messer et al. (1979)	7-3
7-4	Bottom sediment flag for the bottom of lake	7-3
7-5	Relationship between PIP and SRP in open water	7-4
7-6	Relationship between PIP and DOP is through SRP	7-4
7-7	Mean monthly wind at Moore Haven	7-6
7-8	Mean squared monthly wind at Moore Haven	7-6
7-9	Estimated internal loading from Lake Okeechobee for the years 1979-1988	7-10
7-10	Removal of pelagic phosphorus and regeneration of sediment phosphorus governs the removal capacity of the lake sediment	7-15
8-1	Layers in sediment diagenetic model	8-3
8-2	Tridiagonal solution for any k level C_{aq}	8-4

9-1	Submergent and emergent vegetation regions currently are primarily in western and southern Lake Okeechobee	9-1
9-2	Vegetation regions in Lake Okeechobee circa 1914 consisted primarily of custard apple trees in the South Bay region	9-2
9-3	Pelagic TP and SRP versus Lake Stage	9-5
9-4	Mean pelagic SRP has a polynomial relationship with stage in Lake Okeechobee	9-6
10-1	Advective movement of a concentration peak with the velocity field of the lake depends on the magnitude of the velocity	10-1
10-2	Diffusive movement of a concentration peak from a higher concentration to a lower concentration	10-1
10-3	Sigma-stretched coordinate system	10-3
10-4	Sigma (σ) levels in a five layer model	10-3
10-5	Longitudinal and transverse seiche periods	10-8
11-1	Cell nomenclature in x and y directions	11-1
11-2	Computational cell used in advection-diffusion reaction equation in $\sigma \equiv k$, $y \equiv j$, and $x \equiv i$ directions	11-2
11-3	X and Y directions in finite difference pelagic model	11-2
11-4	Computational cell nomenclature in x and σ directions for a five layer model	11-3
11-5	Center cell depth in meters for Lake Okeechobee	11-3
11-6	Cell nomenclature in y and σ directions for a five vertical layer model	11-4
11-7	The depth at the U face cell (meters)	11-4
11-8	The depth at the V face cells (meters)	11-5
11-9	Ending simulation concentrations at the end of 24 hours using a time step of 3 hours and a constant initial concentration of $100 \text{ ug} \cdot \text{l}^{-1}$ subject to a vertical σ -velocity of $+50 \text{ sec}^{-1}$	11-13

11-10	Ending simulation concentrations at the end of 24 hours using a time step of 3 hours and a constant initial concentration of $100 \text{ ug} \cdot \text{l}^{-1}$ for σ -layers 2, 3, 4, and 5 and $150 \text{ ug} \cdot \text{l}^{-1}$ for the bottom σ layer using a vertical σ -velocity of 50 sec^{-1}	11-14
11-11	Ending simulation concentrations at the end of 24 hours using a time step of 3 hours and a constant initial concentration of $100 \text{ ug} \cdot \text{l}^{-1}$ for σ -layers 1, 2, 3, and 4 and $150 \text{ ug} \cdot \text{l}^{-1}$ for the top σ layer subject to a vertical σ -velocity of 50 sec^{-1}	11-15
11-12	Ending simulation concentrations at the end of 24 hours using a time step of 3 hours and a constant initial concentration of $100 \text{ ug} \cdot \text{l}^{-1}$ for σ -layers 1, 2, 3, and 4 and $150 \text{ ug} \cdot \text{l}^{-1}$ for the top σ layer subject to a vertical σ -velocity of -50 sec^{-1}	11-16
11-13	Ending simulation concentrations at the end of 24 hours using a time step of 3 hours and a constant initial concentration of $100 \text{ ug} \cdot \text{l}^{-1}$ for σ -layers 2, 3, 4, and 5 and $150 \text{ ug} \cdot \text{l}^{-1}$ for the bottom σ layer subject to a vertical σ -velocity of -50 sec^{-1}	11-17
11-14	Ending simulation concentrations at the end of 1 hour using a time step of 15 minutes and a constant initial concentration of $100 \text{ ug} \cdot \text{l}^{-1}$ for σ -layers 2, 3, 4, and 5 and $150 \text{ ug} \cdot \text{l}^{-1}$ for the bottom σ layer using a vertical diffusion coefficient of $1.0 \text{ cm}^2 \cdot \text{sec}^{-1}$	11-18
11-15	Ending simulation concentrations at the end of 1 hour using a time step of 15 minutes and a constant initial concentration of $100 \text{ ug} \cdot \text{l}^{-1}$ for σ -layers 2, 3, 4, and 5 and $150 \text{ ug} \cdot \text{l}^{-1}$ for the bottom σ layer using a vertical diffusion coefficient of $5.0 \text{ cm}^2 \cdot \text{sec}^{-1}$	11-19
11-16	Beginning simulation concentrations (200 ug/l in macrophyte zone, 100 elsewhere) for comparison of advection schemes	11-20
11-17	Ending simulation concentrations at the end of 24 hours using a time step of 1 hour and a constant initial concentration of $100 \text{ ug} \cdot \text{l}^{-1}$ for mud, north lake, sand, and south bay and $200 \text{ ug} \cdot \text{l}^{-1}$ for the macrophyte zone subject to a constant u and v velocity of $0.1 \text{ cm} \cdot \text{sec}^{-1}$, using the LOP3D solution and ISOL value of 1	11-21
11-18	Ending simulation concentrations at the end of 24 hours using a time step of 1 hour and a constant initial concentration of $100 \text{ ug} \cdot \text{l}^{-1}$ for mud, north lake, sand, and south bay and $200 \text{ ug} \cdot \text{l}^{-1}$ for the macrophyte zone subject to a constant u and v velocity of $0.1 \text{ cm} \cdot \text{sec}^{-1}$, using the LOP3D solution and ISOL value of 2	11-22

11-19	Ending simulation concentrations at the end of 24 hours using a time step of 1 hour and a constant initial concentration of $100 \text{ ug} \cdot \text{l}^{-1}$ for mud, north lake, sand, and south bay and $200 \text{ ug} \cdot \text{l}^{-1}$ for the macrophyte zone subject to a constant u and v velocity of $0.1 \text{ cm} \cdot \text{sec}^{-1}$, using the LOP3D solution and ISOL value of 3	11-23
11-20	Ending simulation concentrations at the end of 24 hours using a time step of 1 hour and a constant initial concentration of $100 \text{ ug} \cdot \text{l}^{-1}$ for mud, north lake, sand, and south bay and $200 \text{ ug} \cdot \text{l}^{-1}$ for the macrophyte zone subject to a constant u and v velocity of $0.1 \text{ cm} \cdot \text{sec}^{-1}$, using the LOP3D solution and ISOL value of 4	11-24
11-21	Ending simulation concentrations at the end of 24 hours using a time step of 1 hour and a constant initial concentration of $100 \text{ ug} \cdot \text{l}^{-1}$ for mud, north lake, sand, and south bay and $200 \text{ ug} \cdot \text{l}^{-1}$ for the macrophyte zone subject to a constant u and v velocity of $0.1 \text{ cm} \cdot \text{sec}^{-1}$, using the LOP3D solution equivalent to the EHSMIT solution and ISOL value of 3	11-25
12-1	Advection, diffusive, and reactive components in the pelagic zone of the lake	12-2
12-2	Algal pathways in subroutines REAC3D and REAC0D	12-7
12-3	Doubling or reaction time for algal growth and respiration as a function of the reaction rate	12-12
12-4	Intracellular algal nutrient processes in the model	12-13
12-5	$\text{Carbon/Chla} = \Theta_c$	12-18
12-6	$\mu_{\max} = f(T)$	12-18
12-7	Zooplankton pathways in subroutines REAC3D and REAC0D	12-24
13-1	The 486 boxes of Lake Okeechobee 3-D model assigned to five sections in the coarse grid model	13-4
13-2	Lake Okeechobee boxes used in coarse grid model	13-5
13-3	Stage, area, and volume relationship	13-17
13-4	Normalized hydraulic inflow and outflow for 1979 to 1988	13-17
13-5	Normalized loading of SRP and TP for 1979 to 1988	13-17
13-6	Stage history for the period 1979 to 1988	13-17

13-7	Daily wind movement above the pan evaporation station at Belle Glade for 1979-1988	13-18
13-8	Average of pan evaporation measurements at Moore Haven, Clewiston, and Belle Glade for 1979-1988	13-18
13-9	Average of precipitation measurements at Moore Haven, Clewiston, and Belle Glade for 1979-1988	13-18
13-10	Major hydraulic input (rainfall and inflow) and output (evaporation and outflow) for 1979-1988	13-18
13-11	Predicted and measured stages for 1979-1988	13-29
13-12	Calibrated pan evaporation coefficient of 0.965 balances the total water inflows and outflows	13-29
13-13	Mean whole-lake TP in Lake Okeechobee	13-31
13-14	Mean whole-lake SRP in Lake Okeechobee	13-32
13-15	Mud zone total phosphorus in Lake Okeechobee	13-32
13-16	Mud zone SRP in Lake Okeechobee	13-33
13-17	North lake total phosphorus in Lake Okeechobee	13-33
13-18	North lake SRP in Lake Okeechobee	13-34
13-19	Sand zone total phosphorus in Lake Okeechobee	13-34
13-20	Sand zone SRP in Lake Okeechobee	13-35
13-21	South Bay total phosphorus in Lake Okeechobee	13-35
13-22	South Bay SRP in Lake Okeechobee	13-36
13-23	Whole-lake TP with 40% load reduction	13-40
13-24	Whole-lake SRP with 40% load reduction	13-40
13-25	Whole-lake TP with 70% load reduction	13-41
13-26	Whole-lake SRP with 70% load reduction	13-41
13-27	Algal concentrations in Lake Okeechobee	13-44

13-28	Deposition/erosion in Lake Okeechobee	13-44
13-29	Algal pathways in Lake Okeechobee	13-45
13-30	SRP pathways in Lake Okeechobee	13-45
13-31	Algal settling rates in Lake Okeechobee	13-46
13-32	Algal coefficients in Lake Okeechobee	13-46
13-33	PIP balance in Lake Okeechobee	13-47
13-34	Adsorption/desorption in Lake Okeechobee	13-47
13-35	Phosphorus components in Lake Okeechobee	13-48
13-36	Monthly phosphorus in Lake Okeechobee	13-48
13-37	Fractional increases in mean station SRP and TP concentrations for the years 1979-1982 and 1983-1988 over the baseline concentrations of 1972-1978	13-51
14-1	Location of Coastal Engineering data collectors	14-2
14-2	Synoptic station locations used in model LOP3D	14-3
14-3	Mean synoptic total phosphorus and suspended sediment concentrations in 1989	14-4
14-4	Straight line relationship obtained by linear regression between the mean synoptic TP and TSS for the five synoptic surveys during the spring of 1989	14-4
14-5	Box depths, areas, and volumes for the measured synoptic surveys during the spring of 1989	14-6
14-6	Starting TP synoptic concentrations in ug/l on 89147	14-8
14-7	SRP synoptic concentrations in ug/l on 89147	14-9
14-8	Center cell depth on Julian day 89147	14-10
14-9	Predicted SRP concentration in ug/l on day 89154	14-11
14-10	Predicted concentration for constituent DOP, in ug/l	14-12
14-11	Predicted concentration for constituent greens, ug/l	14-13
14-12	Predicted concentration for constituent blue-greens, ug/l	14-14

14-13 Predicted concentration for constituent ZOO, ug/l	14-15
14-14 Predicted concentration for constituent PIP, ug/l	14-17
14-15 Predicted concentration for constituent OrgP-Sed, ug/l	14-18
14-16 Predicted concentration for constituent sediment, mg/l	14-19
14-17 Predicted TP concentration in ug/l on day 89154	14-20
14-18 Upper layer uptake for all algae species in kilograms	14-21
14-19 Lower layer uptake for all algae species in kilograms	14-22
14-20 Upper layer losses for all algae species in kilograms	14-23
14-21 Lower layer losses for all algae species in kilograms	14-24
14-22 Total reaction change of zooplankton in kilograms	14-25
14-23 Total cell change of DOP in kilograms	14-26
14-24 Total cell change of SED in kilograms	14-27
14-25 Total mass flux of TP in an I,J center cell	14-29
14-26 Total adjusted thickness (cm) of cell at end of simulation	14-30
14-27 Total original thickness (cm) of center cell	14-31
14-28 Total advection-diffusion SRP change in kilograms	14-32
14-29 Total advection-diffusion DOP change in kilograms	14-33
14-30 Predicted chlorophyll <i>a</i> in ug/l	14-34
14-31 Total advection-diffusion algae change in kilograms	14-35
14-32 Total advection-diffusion ZOO change in kilograms	14-36
14-33 Predicted Secchi depth, meters	14-37
14-34 Total reaction SRP change in kilograms	14-38
14-35 Upper layer adsorption in kilograms	14-39
14-36 Lower layer adsorption in kilograms	14-40

14-37 Total sediment organic flux in kilograms	14-41
14-38 Total PIP flux from sediment to pelagic in kilograms	14-42
14-39 Total PIP flux from pelagic to sediment in kilograms	14-43
14-40 Measured TP synoptic concentrations in ug/l on day 89154	14-44
14-41 Measured SRP synoptic concentrations in ug/l on day 89154	14-45
14-42 Ending TP concentration differences in ug/l	14-46
14-43 Ending SRP concentration differences in ug/l	14-47

LIST OF TABLES

<u>Table</u>	<u>Page</u>
1-1 Physical characteristics of Lake Okeechobee during the years 1972-1988	1-8
1-2 Proposed boundary values for trophic categories based on the OECD Summary Report	1-15
2-1 Mean chlorophyll <i>a</i> concentrations in Lake Okeechobee by station ranked in order of decreasing concentration	2-8
3-1 Lake Okeechobee tributaries	3-2
3-2 Lake Okeechobee control structures at stations with significant flows	3-4
3-3 The inflow stations are ranked below in decreasing contribution to the phosphorus load over the period of record	3-6
3-4 South Florida rainfall for 1980s (Source: SFWMD, 1990)	3-8
4-1 Mean phosphorus concentrations and standard deviations of phosphorus measured in Lake Okeechobee ranked in order of decreasing mean concentration ($\mu\text{g} \cdot \text{l}^{-1}$)	4-9
4-2 Mean nutrient concentrations in Lake Okeechobee by station ($\mu\text{g} \cdot \text{l}^{-1}$), April 1973 to March 1980	4-10
6-1 Conversion factors used to convert other units of solar radiation to units of langleys $\cdot\text{day}^{-1}$ in the different models of Lake Okeechobee	6-1
6-2 Index of cloud cover index	6-10
6-3 Optical properties of the major phytoplankton classes	6-16
6-4 Linear light extinction coefficients for chlorophyll <i>a</i>	6-20
6-5 Background light extinction coefficients	6-20
6-6 Optimal light intensity or the half saturation constant for light limitation	6-24
6-7 Coefficients for the temperature dependence of biological rates	6-25
7-1 Extractable phosphorus in sediments	7-12
7-2 Nutrients in the sediments of Lake Okeechobee	7-12

7-3	Input data used for diagenetic and sediment model of Lake Okeechobee	7-14
8-1	Input data for diagenetic model	8-4
9-1	Estimates of macrophyte nutrient content and areal excretion rate from Brezonik et al. (1983)	9-4
9-2	Optimum range of growth for plants in Lake Okeechobee	9-4
9-3	The emergent vegetation of Lake Okeechobee	9-5
10-1	Physical parameters for Lake Okeechobee	10-7
10-2	Model dimensionless numbers and model values	10-13
11-1	Options for advection simulation in LOP3D model	11-12
12-1	Modeled phosphorus species and related components	12-3
12-2	Kinetic pathways of phosphorus components	12-4
12-3	Major functional differences between the phytoplankton classes	12-6
12-4	Lake Okeechobee algal species	12-7
12-5	Phytoplankton densities by algal class on July 15, 1981	12-8
12-6	Phytoplankton densities by algal class on August 24, 1981	12-8
12-7	Phytoplankton densities by algal class in Lake Okeechobee on October 8, 1981	12-9
12-8	Half saturation constant for algal growth	12-13
12-9	Maximum growth rate for algae at 20°C	12-14
12-10	Chlorophyll/Phosphorus	12-18
12-11	Algal respiration rate	12-20
12-12	Algal mortality rate	12-21
12-13	DOP to SRP regeneration rate at 20°C	12-21
12-14	Algal settling rates	12-22
12-15	Zooplankton ingestion rate	12-25

12-16 Zooplankton respiration rate	12-25
12-17 Michaelis constant for zooplankton uptake of algae	12-25
12-18 Residual phosphorus partitioning coefficients for partitioning TP-SRP synoptic data measurements	12-26
12-19 Water plus organic color light extinction coefficient ($1 \cdot m^{-1}$)	12-26
12-20 Phosphorus transformation coefficients ($1 \cdot day^{-1}$)	12-26
12-21 Maintenance respiration coefficients ($1 \cdot day^{-1}$)	12-27
12-22 Temperature adjustment coefficients	12-27
12-23 Minimum uptake rate ($1 \cdot day^{-1}$)	12-27
12-24 Half saturation constant for uptake ($ug \cdot day^{-1}$)	12-28
12-25 Maximum settling rate ($m \cdot day^{-1}$)	12-28
12-26 Half saturation constant for light ($ly \cdot day^{-1}$)	12-28
12-27 Light absorption coefficients ($m^2 \cdot ug^{-1}$)	12-28
12-28 Light scattering coefficients ($m^2 \cdot ug^{-1}$)	12-29
13-1 Symbols for the various modeled boxes used in the simulation of Lake Okeechobee	13-5
13-2 Advection and diffusion interbox connections	13-9
13-3 Interbox transfer coefficients	13-9
13-4 Phosphorus reaction pathways	13-13
13-5 Algal population limits (fraction of total population)	13-23
13-6 Specific nutrient loadings to Lake Okeechobee	13-25
13-7 Specific outflows from Lake Okeechobee	13-26
13-8 Residual C_{diff} phosphorus proportions (fractions of C_{diff})	13-27
13-9 Lake areas in km^2 for Model LOP0D	13-27
13-10 Weights used for volume weighting	13-31

13-11 List of figures in appendices	13-37
13-12 Comparison of means and standard deviations for various loadings	13-39

1. INTRODUCTION TO THE PELAGIC PHOSPHORUS MODEL

*The thought behind I strove to join
Unto the thought before.
But sequence ravelled out of reach
Like balls upon the floor.*

- Emily Dickinson

1.1 Project Overview

Lake Okeechobee (Figure 1-1), is the largest lake in Florida (Figure 1-2) and the center of the surface water system of South Florida (Figure 1-3), but the lake is stressed from the continued population growth in Central and South Florida. A partial listing of the benefits of Lake Okeechobee to South Florida include flood control, water storage, water supply, wildlife habitat, commercial and sport fishing, and climate modification.



Figure 1-1 Satellite photograph of Lake Okeechobee, showing the major regions of the lake. The north lake is dominated by the river flows of the Kissimmee River, Taylor Creek, Nubbins Slough, and Fisheating Creek. The western littoral zone is shallow with emergent and submersed vegetation. The shallow south lake has three large islands and surface outflow through canals to the south, east and west. The central region is deeper with organic mud sediments.

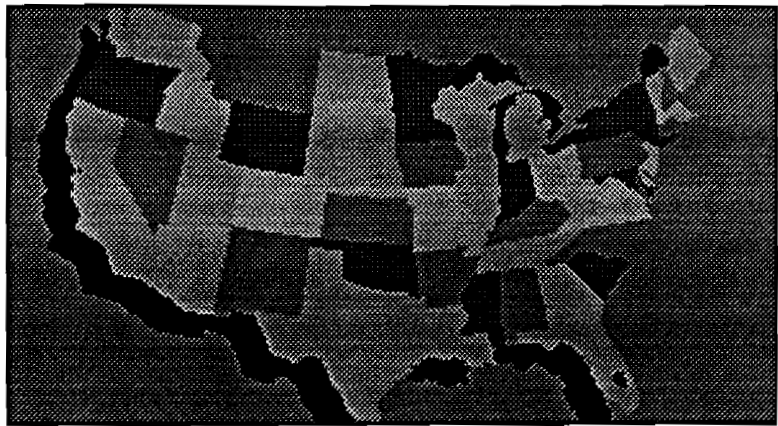


Figure 1-2 Lake Okeechobee is the largest lake in Florida, and the second largest in the lower 48 states.

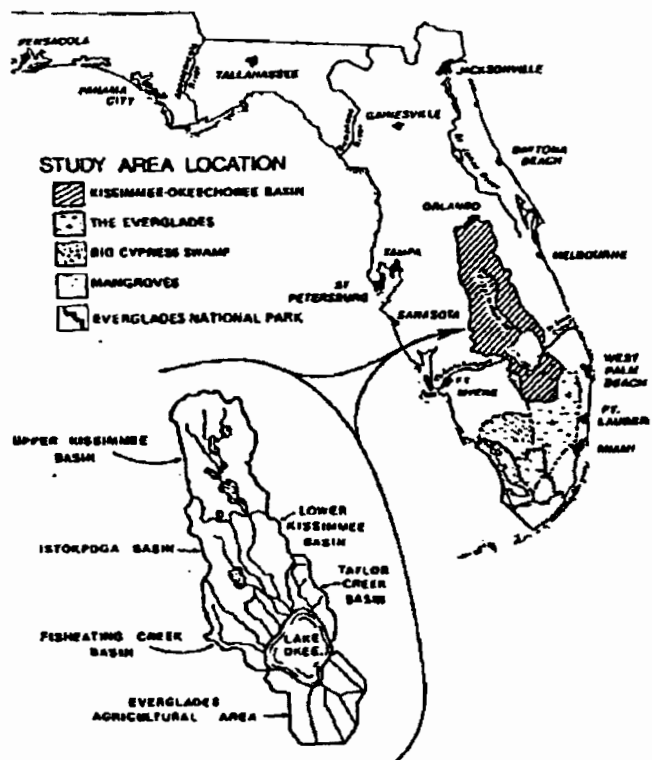


Figure 1-3 Location of Lake Okeechobee and its tributary drainage areas in Florida. The major inflow source is the Kissimmee river and rainfall. The major outflows are evaporation, Caloosahatchee River, and St. Lucie, Miami, New North River, and Hillsboro Canals.

This report describes a mass balance model and 3-D model of the phosphorus dynamics in Lake Okeechobee. Phosphorus, nitrogen and silica are the major limiting macronutrients in lakes (Schindler, 1978). However, because phosphorus is the most controllable nutrient in lakes, nitrogen and silica are not simulated in Lake Okeechobee. Phosphorus is more controllable by man since the source of phosphorus to lakes is either external (river loading and atmospheric deposition) or internal from the bottom sediments of a lake. Nitrogen is not as easily controlled as phosphorus, because nitrogen fixing bacteria and nitrogen fixing blue-green algae can directly utilize atmospheric nitrogen (Brezonik et al., 1979).

Phosphorus is probably the ultimate controller of algal productivity and biomass in Lake Okeechobee even though the lake more often limited by temperature, light and nitrogen limitation. The right conditions for algal growth may result in an algal bloom, which is a very dense concentration of algae. The algal bloom is limited by the concentration of available phosphorus. Blue-green and green algal blooms in Lake Okeechobee may cover up to 100 square miles of the lake, and create adverse biological conditions in the lake. The blooms are a primary concern of the South Florida Water Management District (SFWMD) and the people of South Florida.

The concentration of total phosphorus (TP) in the lake has increased 20 to 40 percent in the 1980s compared to a baseline concentration established in the 1970s (Figure 1-4). The greater total phosphorus lake concentrations degrade the overall water quality in the lake.

Thus, the overall goal of this comprehensive project for the South Florida Water Management District (SFWMD) was the quantification of the various external and internal sources of phosphorus to Lake Okeechobee, and the development of a predictive framework (e.g., a computer model) with which to assess the effects of changes in the various phosphorus loading mechanisms on pelagic phosphorus concentrations. This report focuses on two tasks delineated in the project proposal:

Task 4.6 Prediction of pelagic phosphorus, and

Task 6.2 Simplified mass balance approach

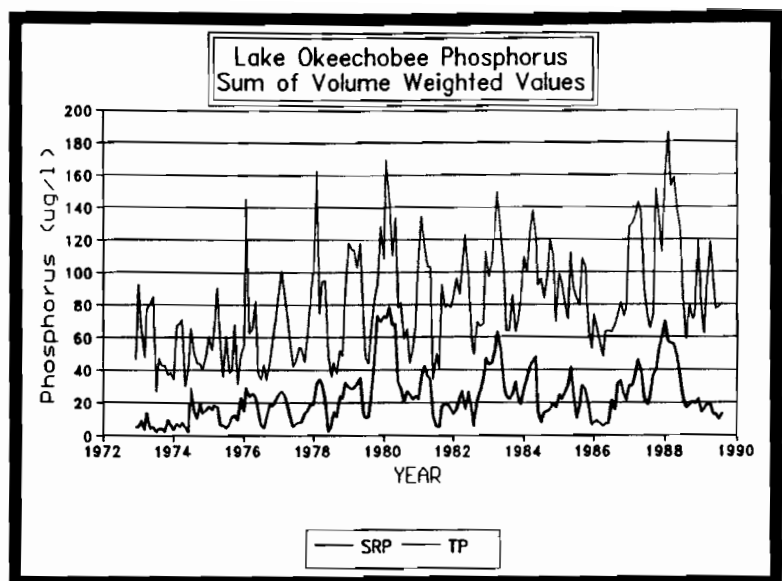


Figure 1-4 TP and SRP concentrations in Lake Okeechobee for 1972 to 1989. The TP and SRP values are the volume weighted average of 8 sampling stations.

1.2 Glossary

In this report on Lake Okeechobee we will use the following names for important areas and processes in the lake. The open water area of the lake will be called the **pelagic** area. This is the region of the lake without emergent macrophyte plants and is deeper than the **littoral** area, which is the shallow area in western Lake Okeechobee dominated by emergent and submersed macrophytes. An important chemical and physical process in Lake Okeechobee is **diagenesis**, or the changes occurring during and after the burial of phosphorus in the bottom sediments.

1.3 Project Approach

The transient, three-dimensional water quality model developed to simulate the major phosphorus species of Lake Okeechobee is called the Lake Okeechobee Phosphorus three-dimensional model (**LOP3D**). LOP3D is linked to the hydrodynamic (**EHSM3D**) and sediment models (**EHSMSD**) developed by the UF Coastal and Oceanographic Engineering (UF COE) Department (Sheng et al., 1991a) as well as to the Lake Okeechobee diagenetic sediment model (**LOPSED**) developed by KBN Applied Science and Engineering (Pollmann, 1991). The simplified mass balance model developed for use as a management tool is for the Lake Okeechobee Phosphorus zero-dimensional model (**LOP0D**). This final report describes the efforts devoted to these two tasks.

1.4 Model Overview

Many model classifications are possible. Temporally, models may produce only steady-state results or be completely transient (Figure 1-5). Spatially, models may range from completely lumped (e.g., a continuously stirred tank reactor or CSTR) to full variation in the x, y, and z directions (Figure 1-6).

Model LOP3D was created to incorporate the effects of light, temperature, and sediments on the phosphorus species in Lake Okeechobee. The combined abiotic, biotic and physical model moves phosphorus constituents through the physical processes of advection and diffusion and then solves the interacting phosphorus reactions using ordinary differential equations (Figure 1-7).

The LOP3D model output is aggregated in large boxes corresponding to the aggregated areas used in model LOP0D to aid in the comprehension of the multitude of reaction pathways and phosphorus components. Two dimensional picture representation of the average box and cell concentrations during the simulation aid in proving or disproving model input assumptions and the validity of the model output.

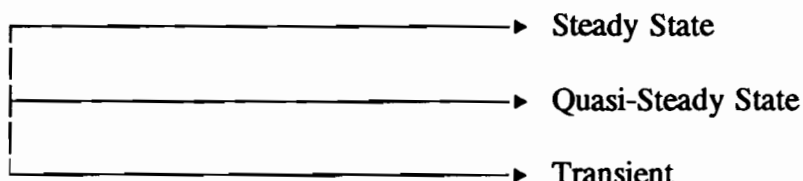


Figure 1-5 Temporal variation in lake models.

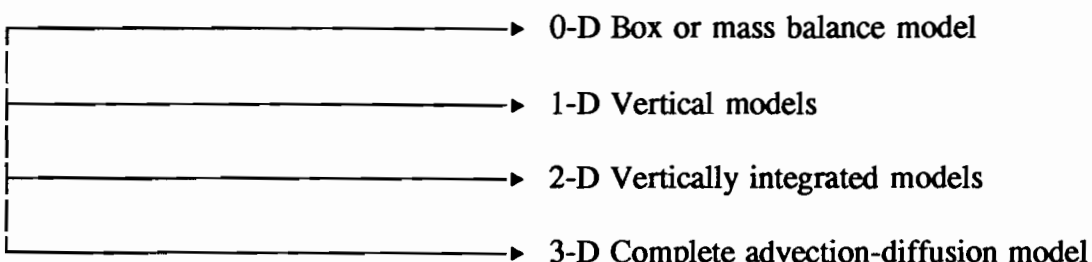


Figure 1-6 Spatial variation in lake models.

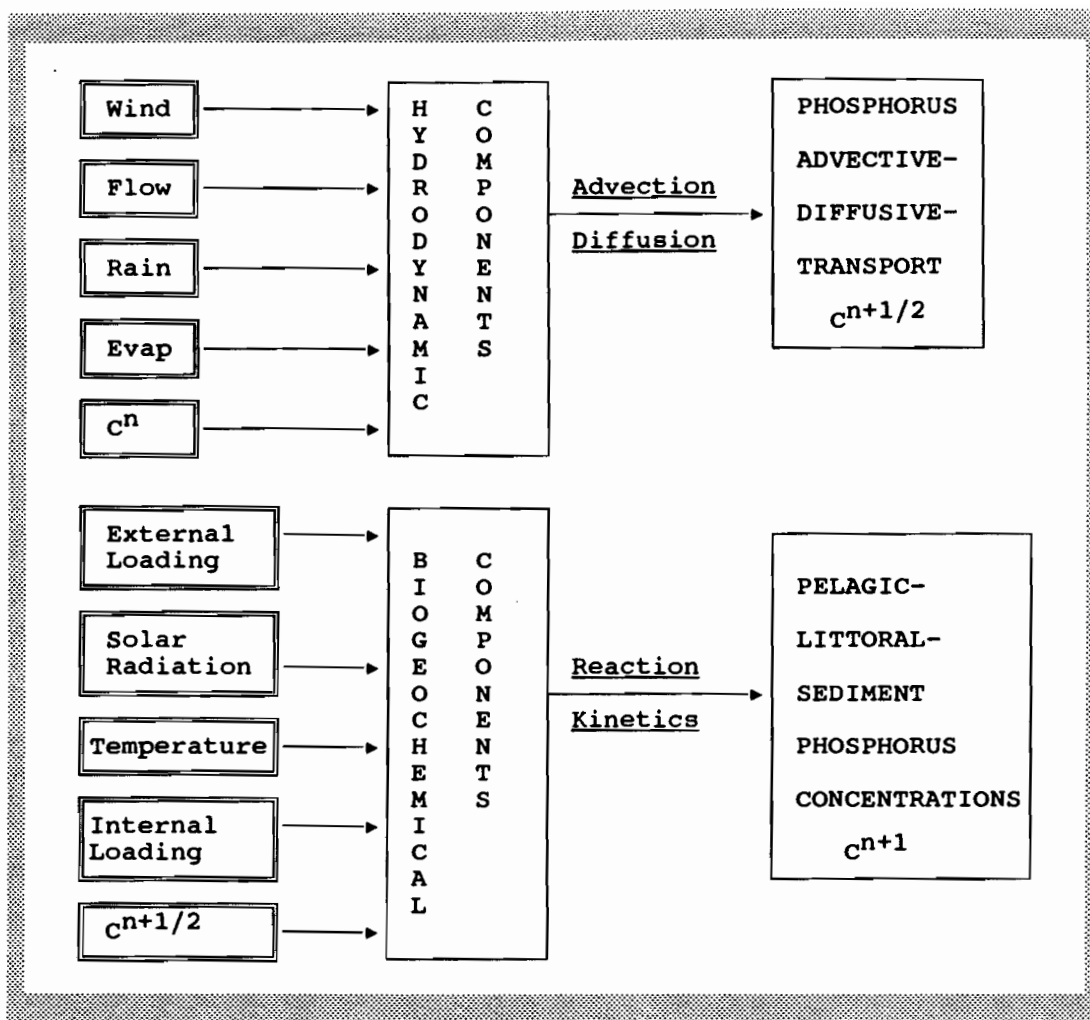


Figure 1-7 Structure of the combined advection-diffusion-reaction three dimensional model of pelagic, littoral, and sediment phosphorus species in Lake Okeechobee.

The models include basic assumptions about phosphorus dynamics that are almost universally accepted (Wetzel, 1983)

- (1) Temperature is important in governing reaction rates,
- (2) Light is a limiting factor in algal uptake. The abiotic factors of light and temperature are usually the most sensitive parameters simulations (Scavia et al., 1984; Bierman, 1980).
- (3) There are pronounced seasonal changes in the phytoplankton population. Spring algal populations are dominated by diatoms and summer algae are dominated by green and blue-green algae.

Lake Okeechobee shares the characteristics of temperate and sub-tropical lakes. The seasonal patterns of algal succession, e.g., diatoms in the spring followed by green algae and blue-green algae in the summer is typical of northern temperate lakes (Wetzel, 1983). However, modulated changes in algal biomass is more typical of sub-tropical lakes (Crisman and Beaver, 1988). Lake Okeechobee straddles the climate zone between temperate and sub-tropical in South Florida.

Complex environmental models are hard to visualize so the two models described herein include a sensitivity analyzer that determines the range of acceptable parameter values. Simply put, the model coefficients are varied + or - from selected starting points and the model simulation results are compared to the average synoptic values of phosphorus measured by the UF COE Department. Results deemed to be unacceptable invalidate that particular range of model coefficients. Tight bounds for most coefficients can be found based on this procedure.

Riverine input, atmospheric input, diagenetic flux from the lake sediments, solar radiation, temperature, wind and material transfer from the littoral zone are integral to the prediction of pelagic phosphorus concentrations. The pelagic phosphorus concentrations in turn are the boundary conditions for the diagenetic and littoral zone model transfer of phosphorus. The pelagic region is also the source of the autochthonous sediment phosphorus that supplies the mud zone of Lake Okeechobee.

1.5 Physical Setting of Lake Okeechobee

Lake Okeechobee, located between latitudes 27° 12'N and 26° 40'N and longitudes 80° 37'W and 81° 08'W in south Florida, is the third largest natural freshwater lake lying entirely within the United States. As the key element in the Kissimmee River - Lake Okeechobee - Everglades ecosystem, the three together form a shallow depression running from north to south in the Florida peninsula (Figure 1-3). General physical and morphometric features of Lake Okeechobee are listed in Table 1-1 and the lake and its watershed are shown in Figure 1-4.

1.5.1 Word Origins

The name Okeechobee comes from the words Oki = water and Chubi = big in the Hitchiti dialect of the Miccosukee Indian language. Lake Okeechobee was also known as Lake Mayaimi in the language of the original Florida Indians. Mayaimi means "Big Water" and the lake name was copied by the Miccosukee and Seminole Indians.

Table 1-1 Physical characteristics of Lake Okeechobee during the years 1972 to 1988.

Mean Surface Area	1598 km ²
Mean Depth	2.6 m
Mean Stage	4.4 m
Mean Volume	4.25x10 ⁹
Mean Hydraulic Inflow	1.52 m/yr
Mean Hydraulic Outflow	0.67 m/yr
Mean TP River Loading	429 mg/m ² /yr
Mean Precipitation Load	49
Mean TP Tributary Loss	52 mg/m ² /yr
Maximum Length	56.4 km
Maximum Width	48.0 km
Shoreline Length	172 km
Total Watershed Area	13,007 km ²
Watershed Land Area	11,116 km ²

1.5.2 Geological Beginnings of Lake Okeechobee

The foundation of Lake Okeechobee began a half a billion years ago as an ocean trench separating North America from an arc of steaming island volcanoes that now are the Caribbean Islands. The basement of the flat Florida landscape actually started as the result of this volcanic activity, and the original volcanic rocks can be as deep as 13,000 feet below the surface in Florida (Randazzo, 1986).

Florida slowly emerged from the ocean 20 to 30 million years ago as a shallow sea. Limestone deposits as deep as 18,000 feet in some areas formed on the volcanic beds. Sediment from the land soon filled in the northern trench and Florida touched the main continent. Worldwide glacier growth lowered the sea level up to 350 feet below their current level, and the Florida peninsula was twice its present size. The melting glaciers caused the ocean to wash over the extended coastline of Florida about six times during the ice ages (Figure 1-8). This strong tidal process chiseled a staircase of bluffs and terraces all across Florida. Geologists estimate the last high tide that crept into Florida occurred 120,000 years ago.



Figure 1-8 Florida coastline during the Pamilco period, showing the extension of the continental shelf and the coastline at the time of high water between glacial periods.

The lake is situated at the lower end of the Central Florida Highlands (Figure 1-9) and based on its history can be considered a self created system. The lake is a relic seabed (see Figure 1-9) that most recently formed \approx 6,300 years ago. The plant life in ancient Lake Okeechobee created a levee of peat at the southern end of the lake that slowly raised the water level of Lake Okeechobee.

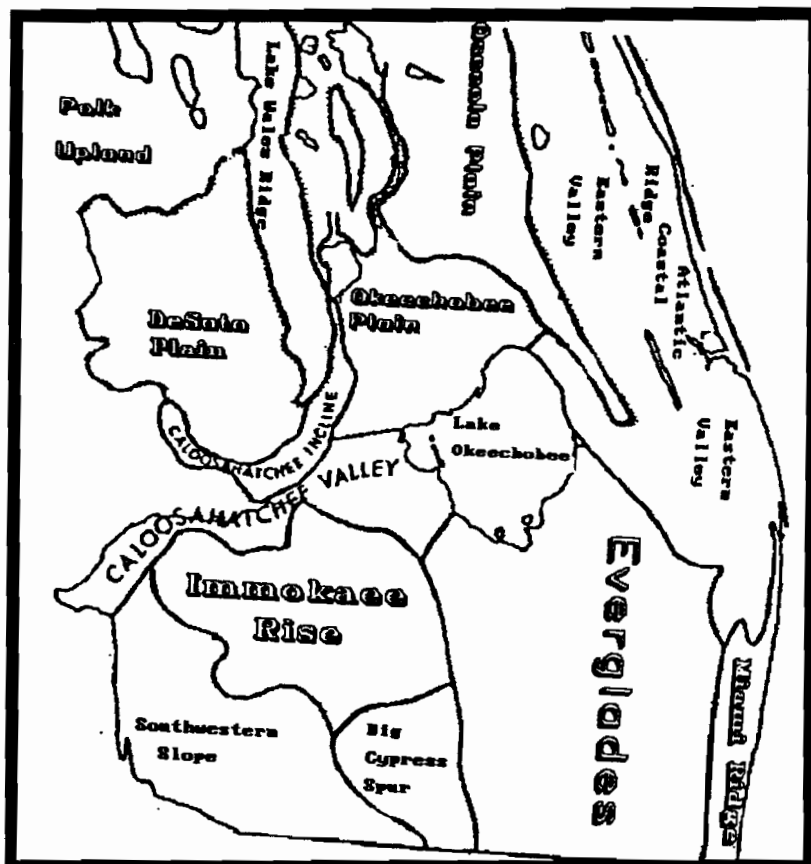


Figure 1-9 Physiographical regions near Lake Okeechobee, showing the sculpturing effect the raising and lowering of the mean sea level by ice ages had on the features of Florida.

This large area was a land of mystery until about a century ago (Figure 1-10). The area south and west of Lake Okeechobee had fewer than 50 Caloosa Indian villages before the year 1500. The Okeechobee drainage basin and the Everglades were almost entirely without human inhabitants after the year 1700 until the Seminole Indian wars of the 1820s and 1830s. The area south of Lake Okeechobee remained sparsely populated until this century.



Figure 1-10 An early map of Lake Okeechobee (1838), showing the greater extent of the lake especially in the western littoral zone and southern lake due to higher water surface elevations.

After the connection of the Caloosahatchee River to Lake Okeechobee in the 1870s, the Kissimmee-Okeechobee region began to be explored by hunters and naturalists who reported their discoveries as being the first of the lake, but thousands of early Caloosa and Seminole Indians were already familiar with Lake Okeechobee.

The lake and its watershed have been considerably altered by man for the goal of increased water storage and greater flood protection. Previously, before the year 1900, inflow to the lake came from Fisheating Creek, the Kissimmee River, and the Taylor Creek and Nubbin Slough drainage basins. Outflows from the lake consisted of surface evaporation, evapotranspiration, and sheet flow over the southern rim of the lake into the Everglades during some wet seasons. The drainage area of predevelopment Lake Okeechobee was approximately 10,360 km² (Federico et al., 1981).

Now, all natural tributaries except Fisheating Creek are regulated by the South Florida Water Management District (SFWMD) through control structures. Surface outflow is regulated through drainage canals, and the lake itself is completely surrounded by a 25 foot dike for flood protection purposes. The Caloosa Indians were probably the first to begin constructing canals in the area, as Buckingham Smith reported the presence of canals in his reconnaissance of South Florida in 1848 (Brooks, 1974). Hamilton Disston dredged these same canals in an attempt to open a

waterway from the Kissimmee River to the Gulf of Mexico in 1881 (Brooks, 1974, from earlier reference). Until the 1890s the water in the lake overtopped the natural levees at 20 to 22 feet with some water draining in the "blind" channels situated at 21 to 22 feet. The extensive system of canals since constructed has added approximately 1550 km² to the Lake Okeechobee watershed in the area south of the Lake (Federico et al., 1981).

1.6 Ecological Setting of Lake Okeechobee

The ecology of Lake Okeechobee has changed dramatically in the last 100 years. Large groves of custard apples and moonvine were present in the late 1890s and early 1900s (Figure 1-11). The groves would extend several miles into southern Lake Okeechobee and were periodically killed by frosts in the winter. Cattle grazing was practiced in the littoral zone of the lake. The dominant macrophyte community may be completely altered after extended periods of inundation (Milleson, 1987). Lake Okeechobee's natural hydroperiod was changed in the 1900s by the construction of the Hoover Dike, channelization of the Kissimmee River, back-pumping of the Everglades Agricultural Area (EAA), and regulation of the lake's water surface elevation and inflows/outflows (Milleson, 1987).

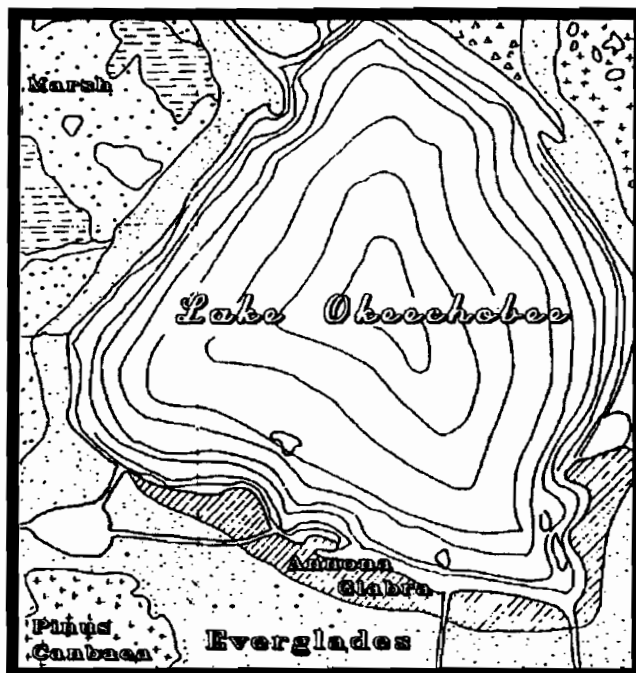


Figure 1-11 Vegetation regions of Lake Okeechobee before 1900, showing custard apple groves in the southern lake, and less area of emergent macrophytes in the western lake compared to the present lake.

The water residence time and lake stage (Figure 1-12) of Lake Okeechobee affect the feeding and nesting pattern of migratory birds. Successful bird feeding conditions require lake stages below 15 feet msl to concentrate the forage organisms for the birds. Nesting of wading birds only succeeds if the ground beneath the colony is flooded during the months of March to July or that the colony nest on an island (Zaffke, 1984).

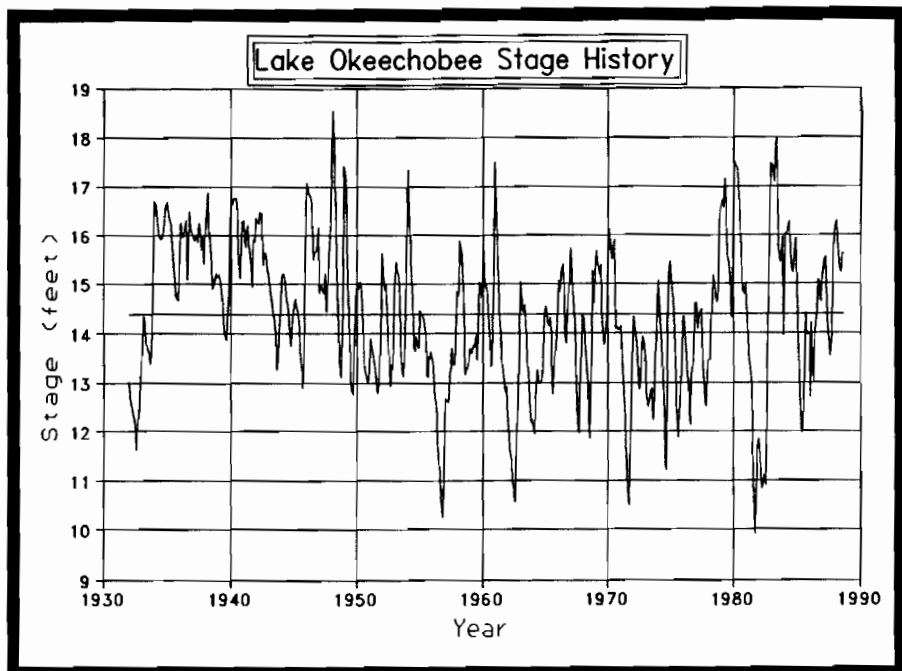


Figure 1-12 Stage history of Lake Okeechobee since 1932, showing the periodicity of stages in the lake.

The stage history of Lake Okeechobee has fluctuated between 10 and 19 feet for the last 60 years (Figure 1-12), with a mean stage of 14.4 feet. The mean depth actually increased during the 1980s (Figure 1-13). The change of lake regulatory schedule has succeeded in raising the mean lake stage (Milleson, 1986). The higher lake stage, however, has actually worsened the effect of the increase in TP and SRP concentrations. The total lake burden of Lake Okeechobee, which is the lake volume times the mean concentration of TP or SRP, has increased significantly in the 1980s (Figure 1-14). The mean lake burden of TP before 1979 was 210,000 kilograms, whereas after 1980 the burden increased to 398,000 kilograms. The mean lake burden of SRP increased from 51,000 to 125,000 kilograms over the same time frame.

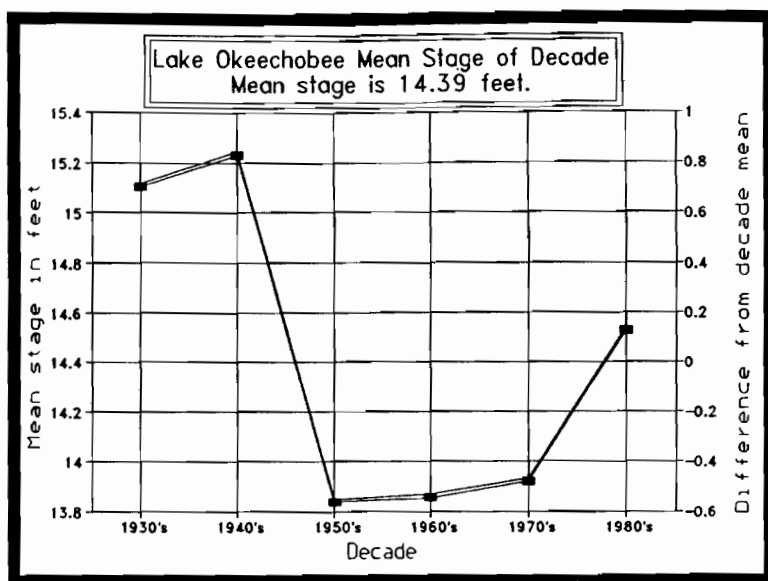


Figure 1-13 Mean lake stage for each decade beginning in 1932. The mean stage for the 1980s is higher than the 1950s, 1960s, and 1970s due to a change in the regulatory schedule.

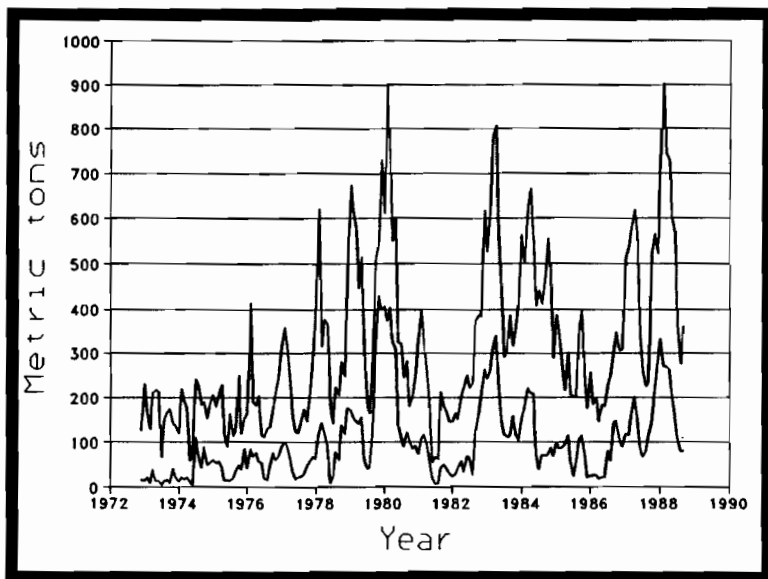


Figure 1-14 The total phosphorus (TP) and soluble reactive phosphorus (SRP) burdens in Lake Okeechobee have increased greatly since 1979. The phosphorus burden is defined as the volume weighted mean phosphorus concentration multiplied by the mean monthly lake volume.

1.7 Trophic Status of Lake Okeechobee

Lake Okeechobee is a naturally eutrophic lake based on typical lake trophic classification standards (Table 1-2), and the lake has made significant gains towards achieving hypereutrophic status in the 1980s. A classification of eutrophic or hypereutrophic for Florida lakes is common. Using a TP concentration of 20 ug/l to divide between oligotrophic, mesotrophic and eutrophic lakes, only 27 percent of the Florida lakes in a data set of 1039 lakes can be classified oligotrophic or mesotrophic (Huber et al., 1982).

Table 1-2 Proposed Boundary Values for Trophic Categories based on the OECD Summary Report (OECD, 1982).

Trophic Category	Mean TP (ug/l)	Mean CHLA (ug/l)	Max CHLA (ug/l)	Max Secchi (m)	Mean Secchi (m)
Ultra-Oligotrophic	≤ 4.0	≤ 1.0	≤ 2.5	≤ 12	≥ 6.0
Oligotrophic	≤ 10.0	≤ 2.5	≤ 8.0	≥ 6.0	≥ 3.0
Mesotrophic	10 - 35	2.5 - 8	8 - 25	6 - 3	3.0 - 1.5
Eutrophic	35 - 100	8 - 25	25 - 75	3 - 1.5	1.5 - 0.7
Hypereutrophic	≥ 100	≥ 25	≥ 75	≤ 1.5	≤ 0.7

The use of trophic state indicators (TSI) to classify lakes may be misleading or deceptive. The common TSI parameters total phosphorus (TP), chlorophyll *a*, and Secchi depth (SD) all have limitations in perception (Huber et al., 1982).

Florida lakes may generally be classified as warm monomictic (Beaver et al., 1981); ranging in trophic classification from oligotrophic to hypertrophic (Kratzer and Brezonik, 1981); and have a range in color from 0 to 416 Pt-Co units (Canfield et al., 1984). The primary productivity of the algae in Lake Okeechobee appears limited more by decreased light penetration and inorganic nitrogen limitation than by phosphorus, based on a lake mean TN/TP of 10.0, mean organic color measurements of 40-50 PCU, and high suspended sediment concentrations.

2. PHOSPHORUS CYCLE AND COMPONENTS

2.1 Introduction

The measured phosphorus species in Lake Okeechobee are typically soluble reactive phosphorus (SRP), dissolved phosphorus (DP), and total phosphorus (TP). In contrast, the phosphorus components simulated as part of this study include SRP, dissolved organic phosphorus (DOP), green algae (GRN), blue-green algae (BLU), diatom algae (DIA), zooplankton (ZOO), particulate inorganic phosphorus (PIP), and particulate organic phosphorus (ORG). This chapter has two purposes:

- (1) an introduction to the phosphorus cycle in lakes.
- (2) a discussion of the methods used to apportion the three measured phosphorus species to the eight simulated phosphorus components.

This apportionment is the fundamental problem in modeling phosphorus in lakes: the measured phosphorus species do not correspond exactly or even approximately to modeled phosphorus components. This problem arises because measured phosphorus species are operationally defined and their physical and biological significance or meaning is uncertain. Thus, Broberg and Persson (1988) state: "Classically operationally defined monitoring variables...are not congruent with known specific physical or chemical components in natural waters or their bio-availability."

The first criterion for classifying the different phosphorus species is their separation into soluble and particulate phosphorus, using a 0.45 μ membrane filter to separate the two fractions (Figure 2-1). Since 1974 when this operational scheme was first introduced, our understanding of the phosphorus cycle has grown and the complexity of lake phosphorus models has paralleled this understanding (Tarapchak and Nalewajko, 1986). Compare the three phosphorus forms in Figure 2-1 to the conceptual diagram of Scavia (1981) showing 22 phosphorus species (Figure 2-2).

Particulate matter in water can cover an enormous range (Figure 2-3). Particulate phosphorus includes both organic and inorganic particulates. Particulate organic matter in lakes typically comprises detritus, phytoplankton, bacteria, and zooplankton in relative order of biomass (Grobbelaar, 1985; Persson, 1984). Individual lakes can have a different ordering of particulate matter. For example, lakes with a high external loading of organic matter can have a bacterial biomass greater than the phytoplankton biomass (Grobbelaar, 1985).

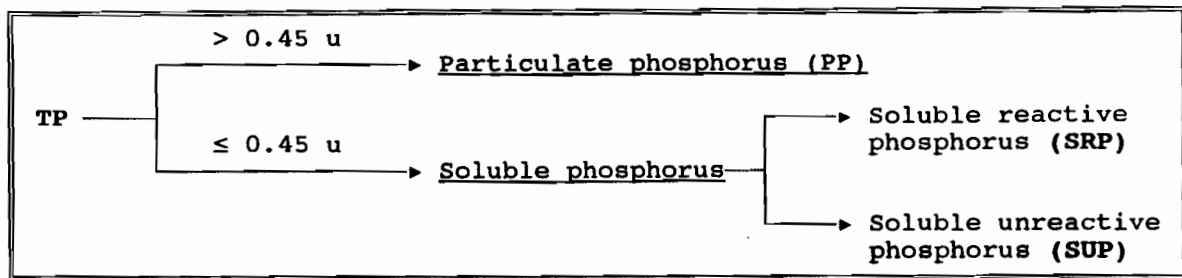


Figure 2-1 Definition of phosphorus forms in water, Rigler (1975). Micron = $u = 10^{-6}$ m.

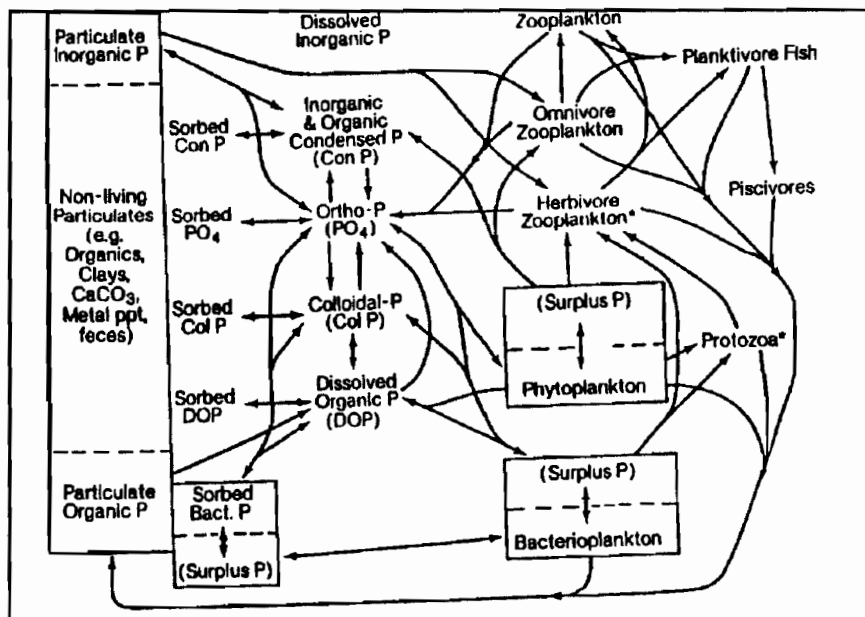


Figure 2-2 Conceptual model of Scavia (1981).

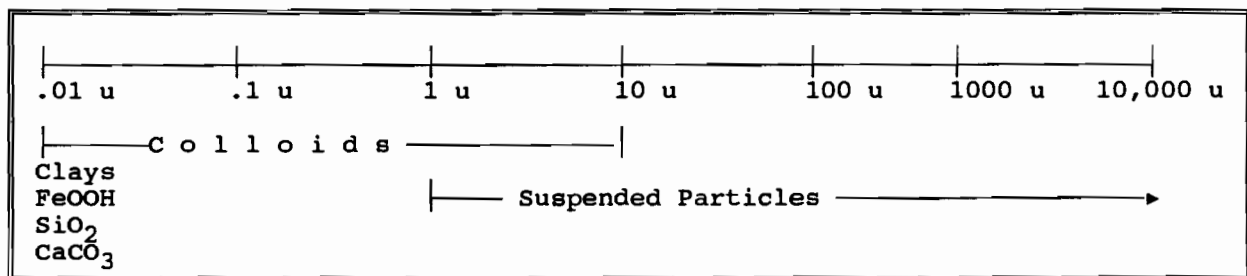


Figure 2-3 Size spectrum of particles in water (after Stumm, 1977). Micron = $u = 10^{-6}$ m.

2.2 Phosphorus Cycle in Lake Okeechobee

Phosphorus enters Lake Okeechobee in a variety of physical pathways via different phosphorus species. The magnitude of the pathway and its constituent makeup ultimately determine phosphorus availability and concentrations in the lake. Figures 2-1 and 2-4 show possible phosphorus species separations based on size and organic content. The sources of phosphorus to Lake Okeechobee include tributary dissolved and sediment associated phosphorus, resuspended bottom sediments containing inorganic and organic phosphorus, diffusion of dissolved phosphorus from lake sediments, internal pathways of recycled pelagic phosphorus, atmospheric deposition of dry particulates, and scavenged SRP in the rainfall (Brezonik et al., 1983).

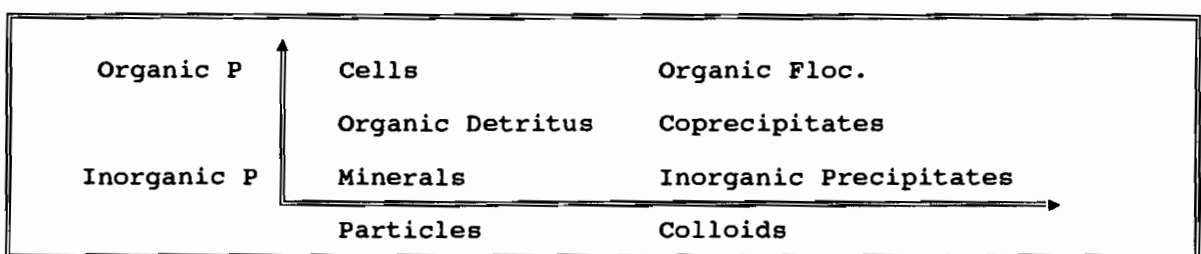


Figure 2-4 Particulate phosphorus grouping along axes of size and organic content, from Broberg and Persson (1988).

The cycle of phosphorus in lakes is in dynamic flux with constant movement between the four forms of phosphorus (Lean, 1973): (1) particulate phosphorus; (2) orthophosphorus (commonly measured as soluble reactive phosphorus); (3) colloidal phosphorus; and (4) low molecular weight phosphorus (Figure 2-5). The relative proportions of the four forms vary from lake to lake but generally particulate phosphorus > orthophosphorus > colloidal phosphorus > low molecular weight phosphorus (Lean, 1973; Rigler, 1973; Prepas and Vickery, 1984). Florida lakes have a mean orthophosphorus content of 39 percent ($n=267$). The OECD found the percentage of orthophosphorus to range from 20 percent to 45 percent (OECD, 1982). Schnoor and O'Connor (1980) found dissolved phosphorus to range from 35 to 75 percent in 81 northern lakes, and phytoplankton phosphorus to account for 10 to 40 percent of the total phosphorus. Prepas and Vickery (1984) found a range of 3 to 19 percent for colloidal phosphorus in 17 Alberta lakes.

The following sections describe in detail the various phosphorus species simulated in LOP0D and LOP3D models of Lake Okeechobee and their overall relationship to the cycling of phosphorus in lakes. Chapter 12 presents the formal algorithms used in the model to simulate the phosphorus cycle in Lake Okeechobee.

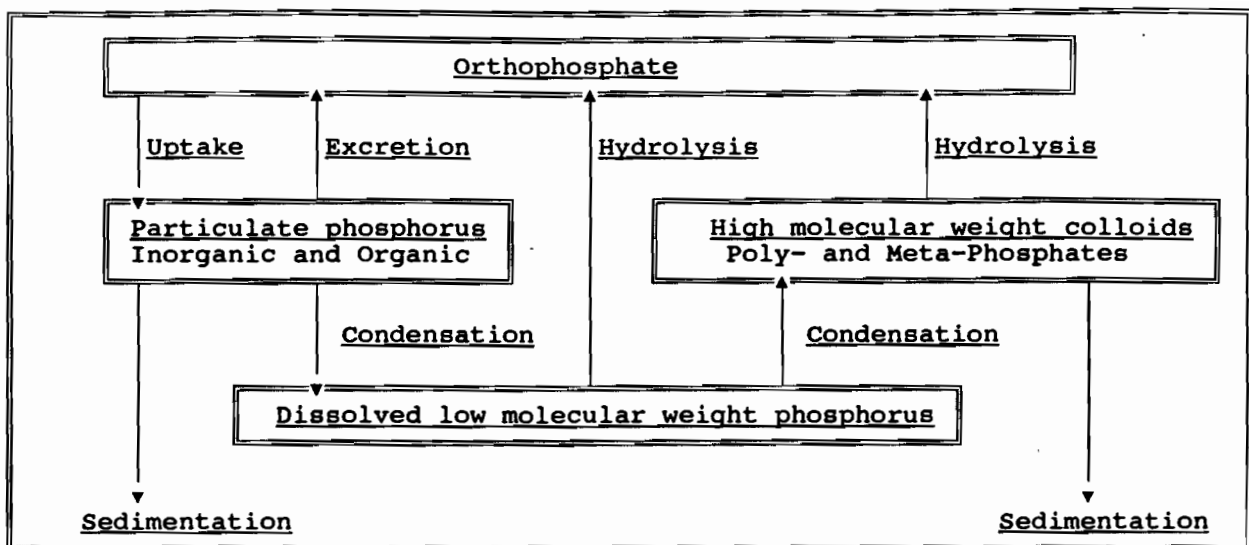


Figure 2-5 Biological movements of phosphorus from Lean (1973).

2.3 Dissolved Organic Phosphorus (DOP)

Dissolved organic phosphorus comprises a major portion of phosphorus in lake water (Wetzel, 1983). The transformation from DOP to SRP is mediated by bacteria through the process of uptake of DOP and excretion of SRP (Figure 2-6). This bacterial regeneration of SRP is modeled as a first-order decay of DOP to SRP (Chapter 12). Bacterial phosphorus biomass is not explicitly modeled.

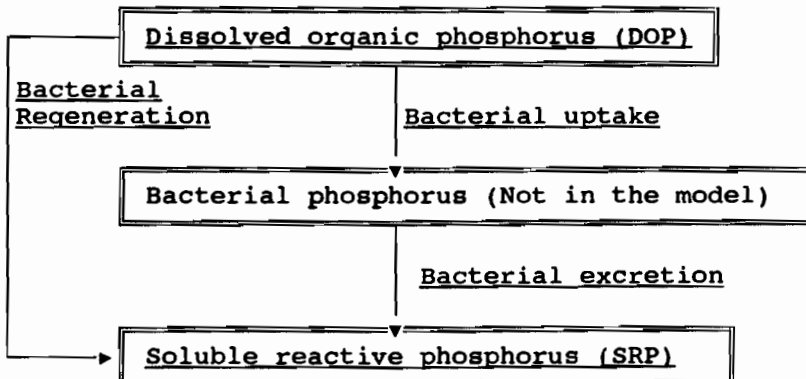


Figure 2-6 Phosphorus pathway between DOP and SRP is a combination of bacterial uptake of DOP and excretion of SRP in Subroutines REAC3D and REAC0D.

2.4 Soluble Reactive Phosphorus (SRP)

Dissolved inorganic phosphorus consists of orthophosphates, polyphosphates, and metaphosphates (Broberg and Persson, 1988). Orthophosphates are generated by chemical weathering or biological activity. Biological activity is the source of poly- and meta-phosphates. Much of the dissolved inorganic phosphorus is usually colloidal poly- and meta-phosphates. Ortho-phosphorus, PO_4 , is the phosphorus species involved in algal uptake.

Dissolved reactive phosphorus (DRP), also called soluble reactive phosphorus (SRP), is commonly used as the measure of the external nutrient source for algal growth in simulation models. However, SRP overestimates the concentration of ortho-phosphorus by at least one order of magnitude, since SRP is actually a combination of ortho-phosphorus and low molecular weight organic phosphorus (Barica and Allen, 1988). However, the low molecular weight organic phosphorus components are rapidly cycled and ultimately taken up by algae; thus SRP is still an acceptable measure of dissolved bioavailable phosphorus (Barica and Allen, 1988).

Bioavailable phosphorus is commonly defined as the sum of immediately available phosphorus and that which will become an available form by a naturally occurring process (Bostrom et al., 1988). NaOH-Extractable P, commonly assumed to correspond to aluminum- and iron-bound phosphorus, is the sediment form most readily available to algae (Bostrom et al., 1988). HCl-Extractable P, corresponding to calcium-bound phosphorus, and particulate organic P were found not to support algal growth.

The biological availability of phosphorus varies between and within lakes. Biologically unavailable phosphorus exists in both soluble and particulate form in lakes (Peters, 1981). Peters found 83 percent of the TP in Lake Memphremagog to be biologically available. The phenomenon of phosphorus luxury uptake also affects the relationship between algal biomass and phosphorus. Luxury uptake is the uptake and storage of phosphorus as inorganic polyphosphate with metachromatic or volutin granules (Keenan and Auer, 1974). A large fraction of the algal phosphorus exists in the form of polyphosphates (Kunikane and Kaneko, 1984).

The concentration of SRP in Lake Okeechobee averages 32 percent of the TP concentration. Station variability ranges from 22 percent at station L001 to 38 percent at station L007. (Please see Figure 3-1 for the location of sampling stations.)

2.5 Dissolved Organic Phosphorus (DOP)

The University of Florida Coastal and Oceanographic Engineering Department (UF COE) conducted four week-long synoptic surveys of phosphorus in Lake Okeechobee during the spring of 1989. Five days of phosphorus and sediment synoptic data were collected. The synoptic data included measurements of total dissolved phosphorus (TDP), which includes dissolved inorganic phosphorus (SRP),

dissolved organic phosphorus (DOP), as well as colloidal material (CM) and small organic and inorganic particles not retained on the 0.45 μ membrane filters (Broberg and Persson, 1988). The difference between TDP and SRP is dissolved unreactive phosphorus, or

$$\text{TDP} - \text{SRP} = \text{DOP} + \text{CM} + \text{ultra PP} \quad (2.5-1)$$

where ultra PP < 0.45 μ particulate organic and inorganic phosphorus.

2.6 Particulate Phosphorus

Sources and sinks of phosphorus in the pelagic zone of a lake are (Broberg and Persson, 1988):

- (1) Cells from plants (prokaryotic and eukaryotic algae, and multicellular plants) and animals (bacteria, protozoans, and zooplankton);
- (2) Primary or secondary minerals;
- (3) Sediment resuspension from the bottom of the lake (old detritus);
- (4) Organic detritus from plants and animals;
- (5) Direct precipitation of inorganic phosphorus;
- (6) Sorption to other organic/inorganic precipitates; and
- (7) Organic floc consisting of organic macromolecule.

The bulk of the particulate phosphorus (PP) in lakes is usually detritus (Wetzel, 1983). Lake Okeechobee PP is primarily detritus or attached to sediment (Reddy et al., 1991). Algal associated PP seldom dominates in lakes unless the lake system is very eutrophic or an algal bloom is occurring. Brezonik et al. (1983) found PP to constitute only 25 percent of the total pelagic phosphorus and 8 percent of the total littoral phosphorus, with DOP constituting most of the remaining littoral TP in Lake Okeechobee. Brezonik et al. (1983) hypothesized that DOP was produced in the littoral zone from macrophyte decomposition, was exported to the pelagic area, became mineralized by bacteria to SRP, and then utilized by the pelagic phytoplankton.

Suspended solids have multifarious effects on algal populations by altering the light regime and affecting zooplankton feeding and community structure. Suspended particles also may create microscale nutrient patches (Melack, 1985) which in turn govern microscale algal succession.

2.7 Particulate Algal and Detrital Phosphorus

Living algal cells are a major and dynamic component of the total phosphorus pool in the water. Based on the Redfield (1966) equation for algal biomass in the ocean, the ratio of chlorophyll *a* to phosphorus should be almost unity. Algal biomass is typically represented by chlorophyll *a*, which can be measured fluorometrically. For modeling purposes, chlorophyll *a* can be predicted from phosphorus concentrations by multiplying the ratio of carbon/chlorophyll *a* by the ratio of phosphorus/carbon in typical algal cells. In essence, this prediction is based on an average yield of chlorophyll *a* per unit mass of phosphorus. This formulation breaks down *sensu stricto* over short time intervals. For example, modelled carbon/chlorophyll *a* are derived from the average light intensity of the *previous* day. However, regression equations relating chlorophyll *a* to total phosphorus indicate that chlorophyll *a* is associated with only 25 to 30 percent of the mean annual total phosphorus (OECD, 1982; Huber et al., 1982).

Settling of algae to the bottom sediments is a major loss pathway of phosphorus from the water column in a shallow lake such as Lake Okeechobee. The three algal classes simulated in LOP0DX, green, diatom and blue-green algae, have widely varying settling rates (algal settling is further discussed in Chapter 12). Diatoms are not simulated in LOP3D because algal succession is not a dominant process over weekly periods.

Algal and non-algal particulate carbon fractions generally are about equal in the epilimnion of lakes (Wetzel, 1983). However, there may be a difference in algal and non-algal particulate phosphorus for any particular lake due to differing release rates of phosphorus, nitrogen and carbon from detritus and living cells.

LOP0D and LOP3D do not explicitly include detrital phosphorus. Rather, we make the assumption that upon death algae release all stored SRP and that the remaining cell phosphorus is rapidly changed to dissolved organic phosphorus (DOP) (this assumption is discussed fully in Chapter 12).

2.8 Chlorophyll *a* and Phosphorus Relationship in Lake Okeechobee

A tentative verification of the model "correctness" can be assessed by comparing the mean model chlorophyll *a* prediction for a long term simulation with the mean values of measured station chlorophyll *a* concentrations in Lake Okeechobee. Mean station chlorophyll *a* ranges from 18 to 28 $\mu\text{g} \cdot \text{l}^{-1}$ (Table 2-1). The mean simulated algal phosphorus multiplied by the CHLA/TP ratio should also range from 18 to 28 $\mu\text{g} \cdot \text{l}^{-1}$. A value for of CHLA/TP has to be input to the model to calculate a predicted chlorophyll *a* concentration. Vollenweider and others argue that this CHLA/TP ratio should be approximately 1.0 in algae (OECD, 1982).

Table 2-1 Mean chlorophyll *a* concentrations in Lake Okeechobee by station ranked in order of decreasing concentration.
 Mean monthly concentrations ($\mu\text{g} \cdot \text{l}^{-1}$) are also presented.
 Adapted from Jones and Federico (1984).

Mean Chlorophyll <i>a</i>		
Station	CHLA	CHLA/TP
L001	28.4	0.36
L002	25.6	0.34
L008	25.6	0.29
L005	25.2	0.44
L003	22.6	0.27
L004	21.5	0.24
L007	18.3	0.27
L006	17.9	0.20

Chlorophyll <i>a</i>			
Month	Mean	Month	Mean
January	19.7	July	25.3
February	17.4	August	23.7
March	20.7	September	25.8
April	21.0	October	25.7
May	22.1	November	32.7
June	22.1	December	17.8

The Organization for Economic Cooperation and Development (OECD, 1982) found a near linear exponent for TP in a log-transformed regression model relating chlorophyll *a* to TP (Eq. (2.8-1)). [The slope in a log transformed data set is the exponent in a power-law function.] The nonlinear exponents of previous empirical relationships derived by Sakamoto (1966), Dillon-Rigler (1974), and Jones-Bachmann (1976) were explained by the OECD as artifacts of using only spring concentrations of chlorophyll *a* and TP, not correcting for phaeophytin (Sakamoto, 1966), and using chlorophyll pigments other than *a* (Sakamoto, 1966).

TP exponents greater than 1.0 can be explained only by a hypothesis of increasing efficiency of phosphorus utilization at higher phosphorus concentrations (Kalff and Knoechel, 1978), or that the unit response in Chla to an unit increase in TP concentration is greater as TP increases (Reckhow and Chapra, 1983). For TP exponents less than 1.0 less the opposite situation applies.

CHLA/TP is greater in summer and fall than in the winter and spring for Florida lakes, but using log-transformed mean chlorophyll *a* ($\mu\text{g/l}$) and TP ($\mu\text{g/l}$) data from Huber et al. (1982), the following relationship is found for 354 Florida lakes:

$$\text{CHLA} = .282 \text{ TP}^{0.999} \quad R^2 = 0.74 \quad (2.8-1)$$

The relationship between chlorophyll *a* and TP may therefore be assumed to be approximately linear. The intercept in the log transformed model is the same as the CHLA/TP ratio in the linear model. A better estimate of the true intercept may be

the median CHLA/TP ratio of Florida lakes. The median Florida ratio of 0.25 is similar to the value of 0.24 found by the OECD (1982) using data from 78 lakes in the northern hemisphere.

The three multiplicative components that together comprise the CHLA/TP ratio in lakes are: (1) Carbon/AP ; (2) AP/TP; and (3) CHLA/Carbon, where AP = algal phosphorus. All three ratios vary temporally (within lakes) and spatially (between lakes). The combined effect of the three ratios results in an order of magnitude difference in mean lake CHLA/TP. The mean CHLA/TP appears to be statistically different between lakes (Dickinson et al., 1986). Watershed influences or inlake mechanisms keep the lake CHLA/TP ratio constant over a long time period.

The Carlson model predicts CHLA/TP ratios less than the median value for oligotrophic lakes and greater than the median value for mesotrophic and eutrophic lakes (Stauffer, 1991). The Carlson model is only adequate for TP concentrations less than 20 mg/m³ based on a comparison of the predicted CHLA/TP of the Carlson model to the predicted CHLA/TP of the curvilinear model. Only 29 percent of the 892 lakes have concentrations less than 20 mg/m³. The median linear model is adequate for lakes with TP concentrations less than 100 mg/m³ (76 percent) based on a comparison of predicted CHLA/TP's for the linear and curvilinear models (Stauffer, 1991).

The CHLA concentration and primary productivity in Lake Okeechobee is higher in the northern part of the lake than in the southern end of the lake. This may be due to tributary inflows and loading in the northern portion of the lake.

2.9 Relationship Between SRP and TP-SRP in Lake Okeechobee

The relationship between SRP and the TP-SRP difference was investigated using linear regression for the aggregated non-mud and mud Lake Okeechobee long term stations. The correlation between SRP and TP-SRP was less for the non-mud stations (Figure 2-7) than for the mud stations (Figure 2-8). This difference between the two types of stations may be due to: (1) the proximity of the non-mud stations to tributary sources (stations L001 and L005), closeness to surface outflows (L007), dissimilar sediments (L001, L005, and L007), different bottom sediment biota (L005 and L007), and proximity to the littoral zone of Lake Okeechobee (L005). (Sampling stations are shown in Figure 3-1.)

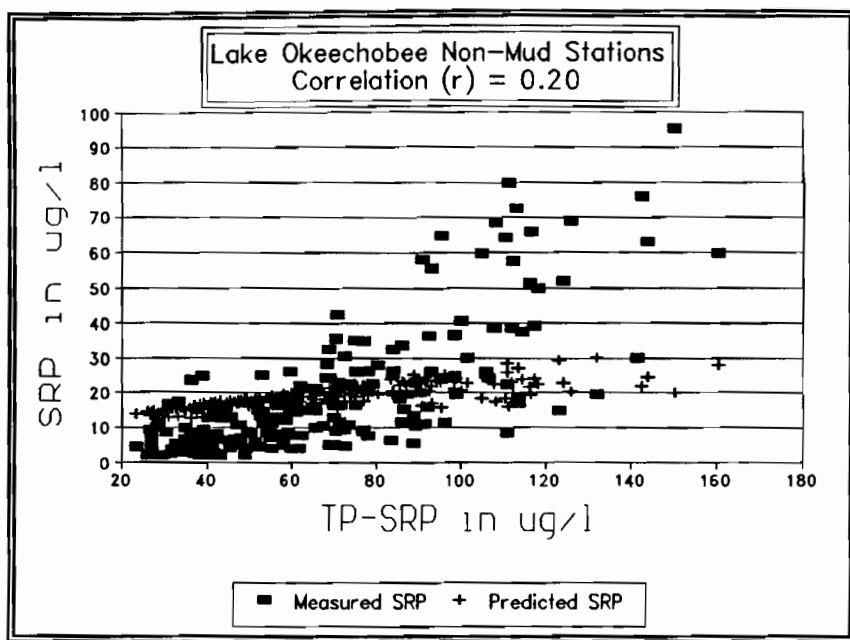


Figure 2-7 SRP versus TP for the non-mud stations in Lake Okeechobee.

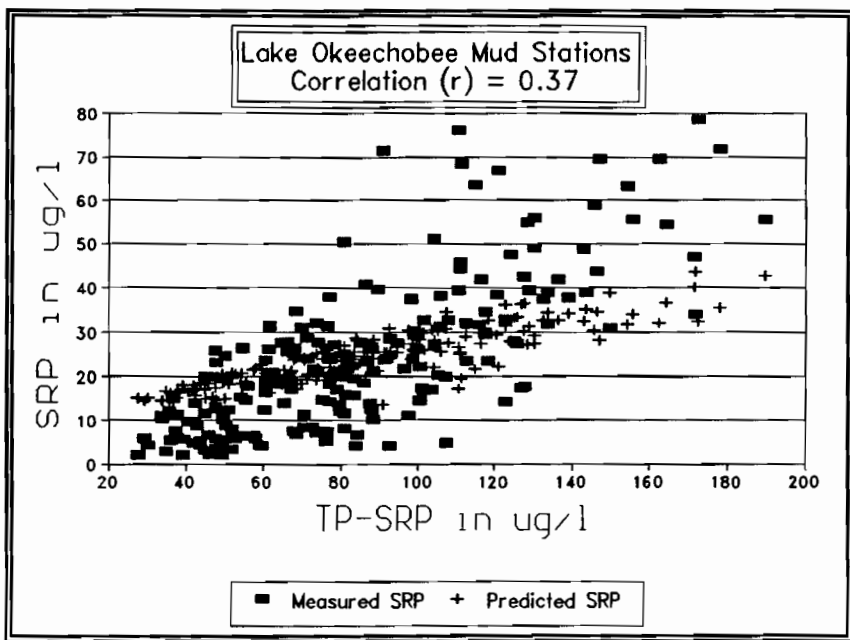


Figure 2-8 SRP versus TP for mud stations in Lake Okeechobee.

2.10 Nutrient and Yield Limitation on Lake Okeechobee Algae

The concept of a single nutrient, such as phosphorus, limiting algal growth in lakes is overly simplistic. The pelagic phytoplankton community is composed of many species which undergo different physiological responses to external nutrient limitation (Kunikane et al., 1981), light regime (intensity and length of sunshine) and temperature. Temperature influences the growth rate and the minimum cell quota (intracellular concentration) of Scenedesmus under phosphorus and nitrogen limitation (Rhee and Gotham, 1981a). This temperature effect was both nutrient and species specific. Light influences both the growth rate and minimum cell quota of Scenedesmus (Rhee and Gotham, 1981b).

Temperate lakes are primarily yield and light limited during most of the year and phosphorus limited during the summer months. Lakes generally may be seasonally phosphorus limited, nitrogen, limited, temperature limited or limited by a micronutrient. For example, nutrient limitation in Lake Titicaca in South America varies seasonally between summer nitrogen limitation, and winter nitrogen or phosphorus limitation (Vincent et al., 1984).

Lake Okeechobee is probably only seasonally or spatially phosphorus limited (Leslie, 1979). Ratios of total nitrogen to total phosphorus (TN/TP) are inconclusive regarding nutrient limitation (Figure 2-9). The ratio of dissolved inorganic nitrogen (DIN) to SRP is also commonly used as a coarse indicator of nitrogen or phosphorus limitation. Mean values of DIN/SRP show the lake to be nitrogen limited (Figure 2-10). [Values of DIN/SRP below 7.0 are indicative of nitrogen limitation, whereas values over 30.0 indicate phosphorus limitation.] Federico et al. (1981) concluded Lake Okeechobee is neither conclusively nitrogen or phosphorus limited. Brezonik et al. (1979) state nutrient limitation is a localized and transitory situation in Lake Okeechobee, but some values of the inorganic N:P ratio indicate phosphorus or nitrogen to be marginally limiting.

Using the algal assay procedure (AAP) Brezonik et al. (1979) showed that nutrient limitation in Lake Okeechobee varied spatially: a combination of phosphorus limitation in the South Bay, Fisheating Creek, and Miami Canal; nitrogen limitation in Fisheating Creek, and trace metal and EDTA limitation in the pelagic zone. Physiological tests of algal phosphorus limitation by Brezonik et al. (1979) also showed Lake Okeechobee to be only spatially and temporally phosphorus limited. Limnobag determinations of nutrient limitation by Leslie (1979) indicated phosphorus limitation was relatively minor except in the southern portion of the lake during the summer. Nitrogen limitation occurred at only a few stations in Lake Okeechobee (Leslie, 1979).

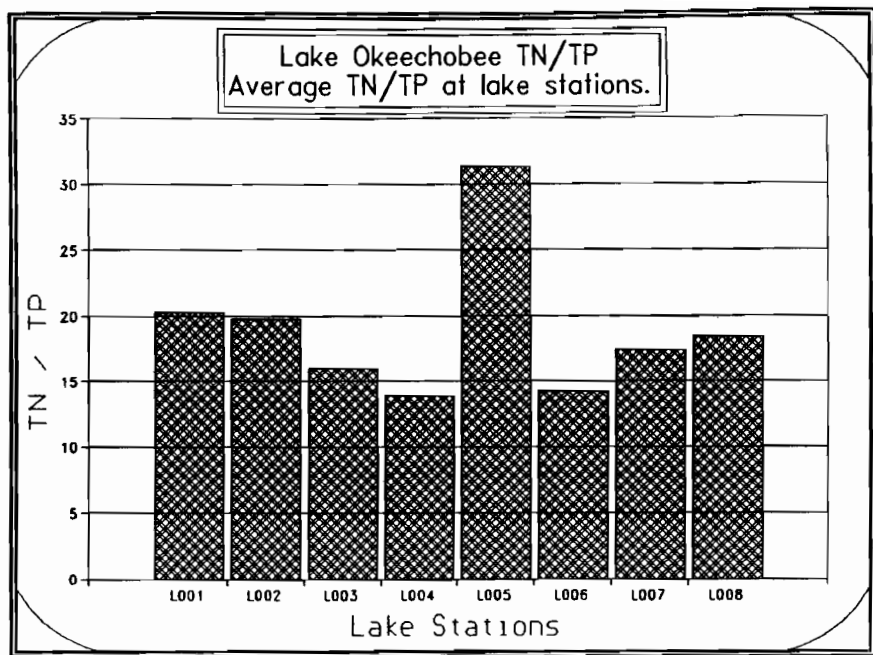


Figure 2-9 Lake Okeechobee mean station TN/TP.

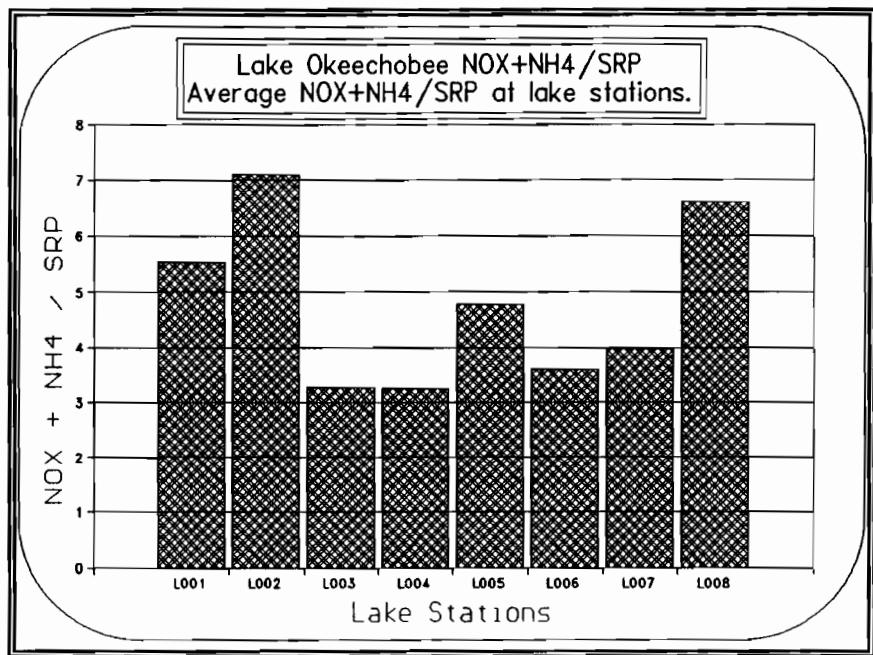


Figure 2-10 Lake Okeechobee mean station DIN/SRP.

Multivariate regression models to predict CHLA based on TN and TP have been investigated for groups of northern and Florida lakes by Smith (1982) and Canfield (1983). TP was more important than TN in predicting CHLA in northern lakes (Smith, 1982), and TN to be more important than TP in predicting CHLA in Florida lakes (Smith, 1982; Canfield, 1983; Baker et al., 1981). The regression results show a better correlation or tighter bound between total nitrogen concentrations and algal biomass as represented by chlorophyll *a* concentrations.

An important conclusion from these studies is the spatial and temporal transience of macronutrient limitation in Lake Okeechobee. The concentrations of SRP and inorganic nitrogen are usually large enough to preclude phosphorus and nitrogen limitation. The majority of the time the lake is light, temperature, micro-nutrient, or yield limited, i.e., the lake is controlled by abiotic factors and the balance of biotic factors.

2.11 Algae - Bacteria Pelagic Interaction

Bacteria and algae are dominant numerically in the plankton of lakes, (Cole, 1982). Together, they control the pelagic nutrient recycling and energy flow. The bacteria are less than 0.5 μ m in size and usually number 10^6 cells ml^{-1} (Cole, 1982). The phytoplankton of Florida lakes are greater than 2 μ m in size and range from $214 \cdot 10^3$ to $710 \cdot 10^6$ cells ml^{-1} with a mean of $320 \cdot 10^3$ cells ml^{-1} (Canfield et al., 1984).

The carbon limitation theory of Currie and Kalff (1984) explains the coexistence of bacteria and algae in the pelagic zone of a lake by showing bacteria controlling the P supply for algae and the algae controlling the energy supply for bacteria. This mutual regulation applies when phosphorus is the limiting nutrient and the external supply of carbon is low. Lake Okeechobee, with a high concentration of organic color, has an additional energy source for bacteria not supplied by algae. The ability of algae to store an internal supply of phosphorus gives algae a competitive advantage over bacteria despite their slow growth rate (Cole, 1982).

Bacteria have two mechanisms of phosphorus uptake (Jansson, 1988). At low SRP concentrations, a high affinity uptake system (called Pst) allows bacteria to out-compete algae. At high SRP concentrations, bacteria are still able to continuously take up phosphorus through a low affinity Pit system. The Pit system also increases the excretion rate of phosphorus; otherwise the cell would burst with accumulating internal phosphorus.

This continued dynamic exchange of phosphorus at high concentrations of phosphorus has been verified isotopically and reflects the phosphate exchange theory developed by Jansson (1988), which states that bacteria saturated with phosphorus excrete an internal phosphorus molecule for every phosphorus molecule actively taken up from the external pool. The practical significance of this dynamic exchange is that each molecule of phosphorus eventually will be consumed by algae, with the bacteria

functioning as a transitional pool. This exchange allows the available phosphorus to be used optimally for autotrophic algal production and heterotrophic bacterial production.

Jansson (1988) notes three possible reasons for this seemingly inefficient, continuous excretion of phosphorus from bacteria:

- (1) More energy might be expended by the bacteria activating and deactivating phosphate uptake mechanism,
- (2) The bacteria always have first access to an essential nutrient, and
- (3) Excess phosphorus is used by algae to produce new energy for the bacteria.

Bacteria and algae have both a symbiotic and a competitive interaction in lakes. The faster bacterial reaction rates compared to algal reaction rates means that bacteria need not be explicitly modeled. The bacteria effect may be simulated by adjusting the reaction rates of the algal pathways.

2.12 Zooplankton Particulate Phosphorus

Zooplankton (Figure 2-11) play an important role in recycling of phosphorus in lakes. Zooplankton phosphorus excretion after ingesting algae may be 90 percent SRP. Additionally, the selective zooplankton grazing of green algal cells shifts the algal population towards blue-green algal domination in the summer. Zooplankton grazing of algae enhances cycling of phosphorus and may be a major supply of SRP to algae during the summer. Zooplankton may supply $\approx 100\%$ of the SRP for algal growth during periods of low SRP concentrations (Devol, 1979).

Mean areal mass of zooplankton in Florida lakes $\approx 2 \text{ mg} \cdot \text{m}^{-2}$, with a time integrated mass of 100 to 1000 $\text{mg} \cdot \text{m}^{-2}$. At the mean depth of Lake Okeechobee this translates to an estimated zooplankton concentration of $0.67 \text{ ug} \cdot \text{l}^{-1}$.

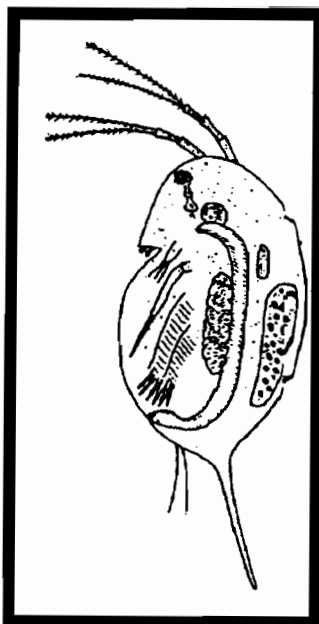


Figure 2-11 A zooplankter (*Daphnia spp.*).

2.13 Summary

The major components involved in phosphorus cycling in lakes and most of the major pathways for phosphorus cycling are implemented in the models LOP0D and LOP3D. The major assumption we have made is that bacterial transformations of phosphorus are not a rate limiting pathway. Bacteria are important in the conversion of DOP to SRP and the conversion of GRN, BLU, and DIA algal phosphorus to DOP.

Other assumptions incorporated directly or indirectly into the phosphorus models for Lake Okeechobee are:

- (1) Soluble reactive phosphorus (SRP) constitutes 32 percent of the total phosphorus (TP) in the lake. The mean concentration of SRP in the lake is 27.9 ug/l.
- (2) The mean chlorophyll α concentration in the lake is 25 ug/l, or 25 percent of the TP.

3. LAKE OKEECHOBEE BOUNDARY INFORMATION

3.1 Introduction

Lake Okeechobee has twelve tributaries that contribute a significant inflow to Lake Okeechobee, as shown in Figure 3-1 and listed in Table 3-1. The flow in most tributaries can be both into and out of Lake Okeechobee, as indicated in the table. In our model a negative flow indicates flow that is in the direction not typically taken by tributary [this applies primarily at the pumping stations at the southern end of Lake Okeechobee (Figure 3-2)].

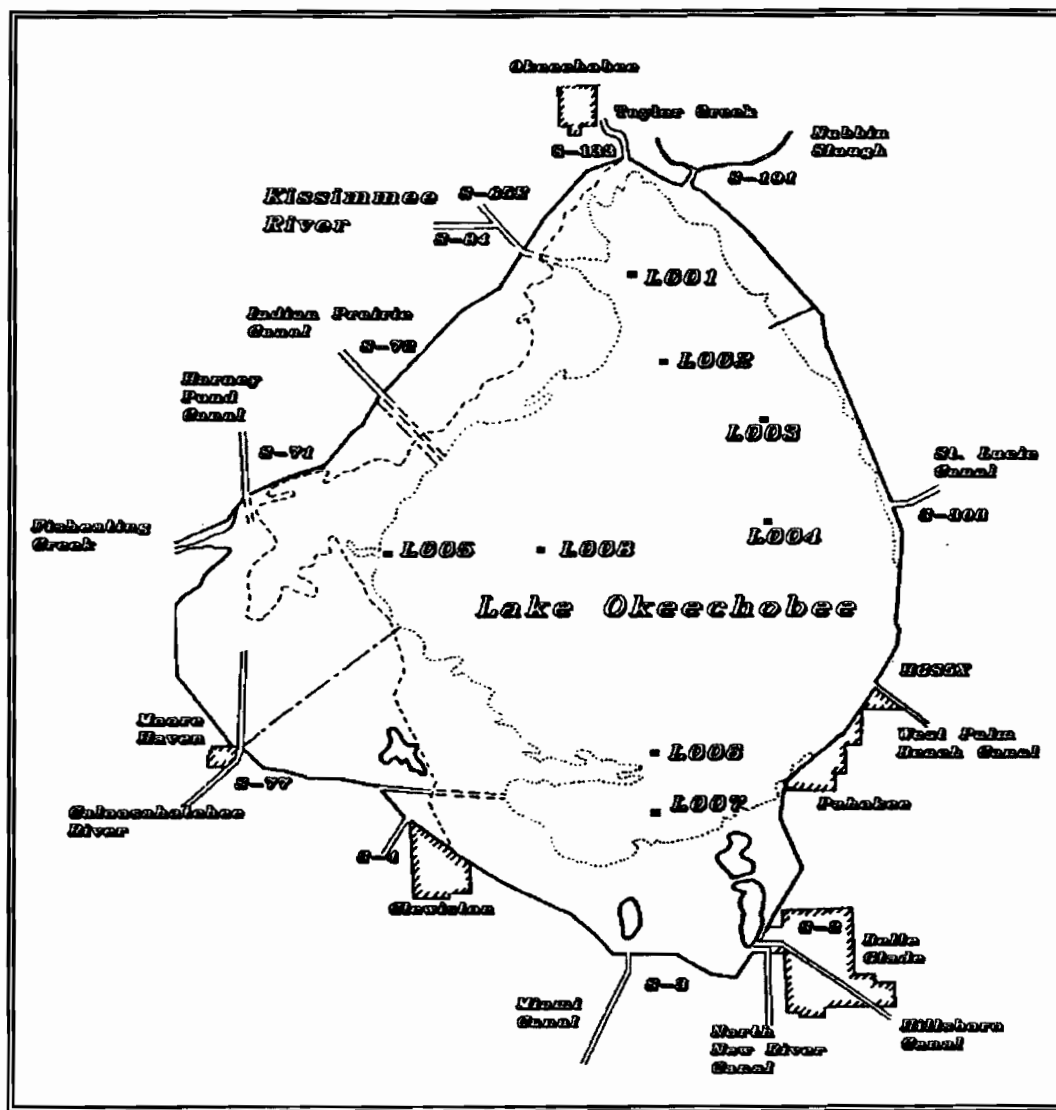


Figure 3-1 Inflow tributaries and outflow control structures in Lake Okeechobee. In-lake SFWMD sampling locations are also shown (L001 - L008).

Table 3-1 Lake Okeechobee tributaries.

Tributary	Type of flow
Fisheating Creek	Inflow
Harney Pond Canal	Inflow
Indian Prairie Canal	Inflow
Kissimmee River	Inflow
Taylor Creek/Nubbin Slough (S-191)	Inflow
West Palm Beach Canal	Inflow-Outflow
Hillsboro Canal	Inflow-Outflow
North New River Canal	Inflow-Outflow
Miami Canal	Inflow-Outflow
Caloosahatchee River	Inflow-Outflow
Istokpoga Canal (S-84)	Inflow
St. Lucie Canal	Inflow-Outflow

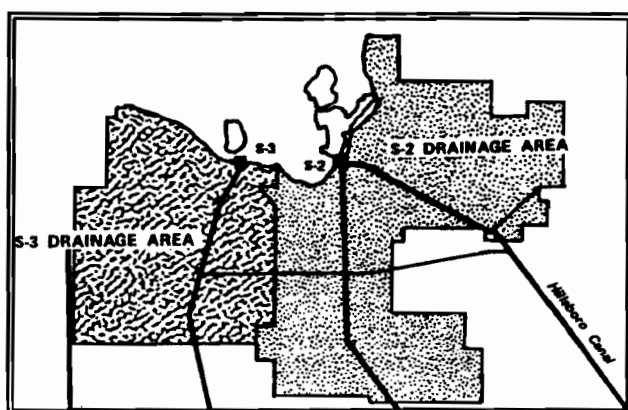


Figure 3-2 Inflow drainage area and outflow canals in southern Lake Okeechobee.

Data collected by the SFWMD as a result of its inflow/outflow monitoring program were used in the analysis of inputs to the lake. Figure 3-1 locates most of these sampling stations, where measurements were made of flow as well as SRP and TP. Inspection of the records for these stations reveals that many of these stations have very long periods of no inflow; only 18 of the 27 stations shown are considered to make significant inflow contributions to the lake (Table 3-2 and Figures 3-3 and 3-4).

3.2 Tributary Flow and Loading Data for Lake Okeechobee

The Kissimmee-Okeechobee-Everglades system historically experiences cycles of wet and dry years. These can be seen in the normalized total inflows to Lake Okeechobee shown in Figure 3-5. Highest total inflows for the period 1972-1990 occurred in 1979 (Hurricane David) and the wet year of 1983. Outflows (Figure 3-6) mimic inflows to a large degree but are about half the magnitude of the inflows. Inflows and outflows at the various stations shown in Figure 3-1 serve as boundary conditions to the phosphorus models.

Concentration and flow data for all tributaries (Figure 3-1) were used to prepare a time series of monthly flow-weighted average inflow concentrations for TP and SRP, shown in Figure 3-7. Interestingly, in spite of the rise in concentration values within the lake itself, tributary concentrations generally do not show very much of an upward trend. Highest inflow concentrations are found in Nubbin Slough and at the S-154 structure downstream from S-65E on the Kissimmee River. Concentrations at S-65E itself are not especially high. (In-lake TP and SRP concentrations are shown in Figure 5-1 and discussed in Chapters 4 and 5.)

In-lake concentrations should respond to mass loadings to the lake rather than to inflow concentrations as such. Normalized monthly TP and SRP loads (in units of mg/m^2) summed for all stations are shown in Figure 3-8. A very high phosphorus inflow pulse occurs in late 1979, followed by TP and SRP loadings that do not show a noticeable increasing trend that would correspond to the increase in lake concentrations (Figure 5-1). The high 1979 loadings correspond to a hydrograph peak, as shown in Figure 3-5. Huber and Carey (1990) show that the highest loadings occur from Nubbin Slough (S-191) and the Kissimmee River at S-65E.

This preliminary analysis has not formally addressed cause and effect. The most interesting point is that the in-lake TP and SRP concentrations have increased since 1979 in spite of an apparent lack of increase in tributary loadings.

The cumulative phosphorous load for each inflow station was determined May 1979 through June 1989 (Table 3-3). Comparing these results shows that approximately 80 percent of both SRP and TP is contributed by stations S-191, S-65E, S-71, S-154, and FECSR78 (Figures 3-9 and 3-10). DOP (TP-SRP) loadings show a similar ranking (Figure 3-11).

Table 3-2 Lake Okeechobee control structures at stations with significant flows.

Structure	Description of control structure
S-2	Pump station S-2 at south end of Lake.
S-3	Pump station S-3 at south end of Lake.
S-4	Pump station S-4 at south end of Lake.
S-71	Structure S-71 on Harney Pond Canal (C41).
S-72	Structure S-72 on Indian Prairie Canal (C40).
S-77	Caloosahatchee River and Lake Okeechobee.
S-84	Structure S-84 on C41A Canal.
S-65E	Structure S-65E on the Kissimmee River.
HGS-5	Hurricane gate near Card Point.
S-127	Pump station S-127 on northwest side of Lake.
S-129	Pump station S-129 on northwest wide of Lake.
S-131	Pump station S-131 on west side of Lake.
S-133	Pump station S-133 at Taylor Creek.
S-135	Pump station S-135 on northeast side of Lake.
S-154	Gate structure near S-310 at Kissimmee River.
S-191	Bridge at SR 441 and Nubbin Slough.
FECSR78	Fisheating Creek at SR 78.
S-308	St. Lucie Canal

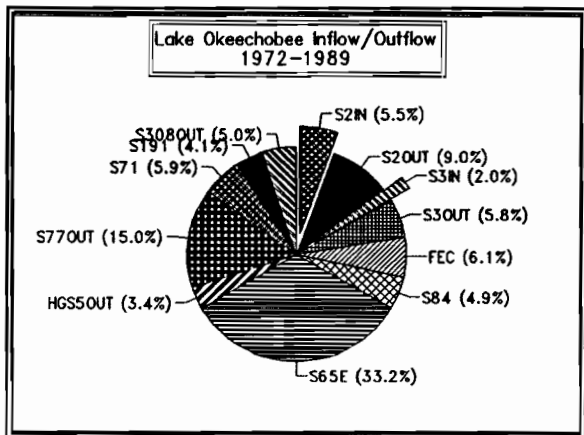


Figure 3-3 Major Lake Okeechobee Inflow/Outflows.

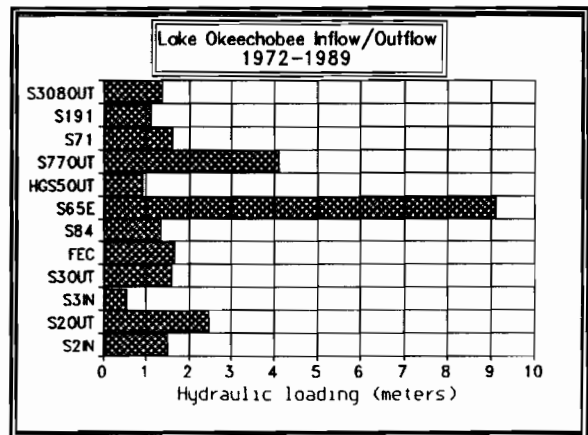


Figure 3-4 Lake Okeechobee hydraulic loadings.

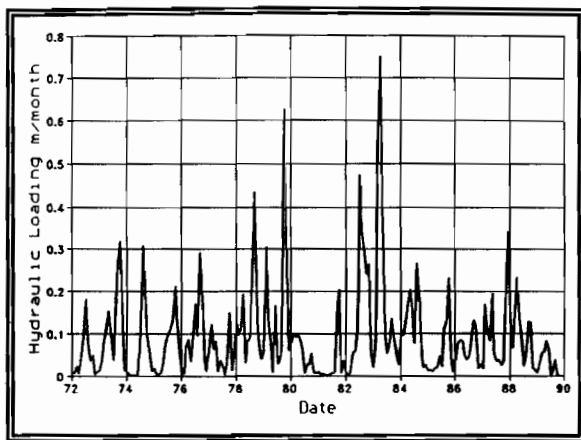


Figure 3-5 Lake Okeechobee inflow time series for the period 1972-1989.

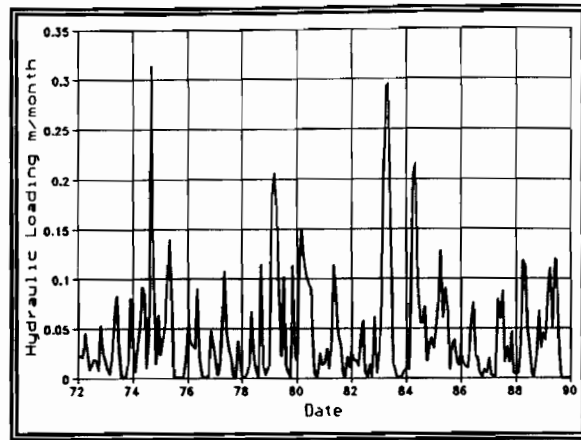


Figure 3-6 Lake Okeechobee outflow time series for the period 1972-1989.

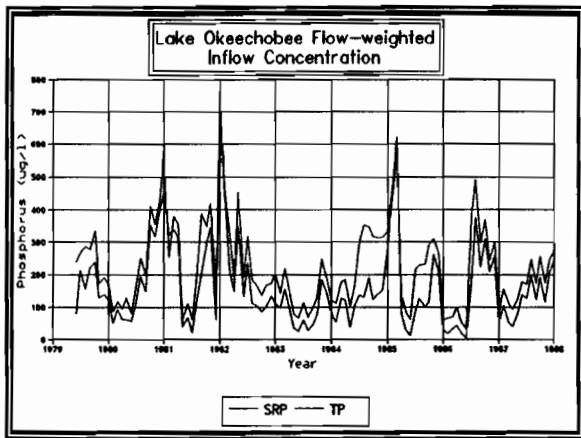


Figure 3-7 Lake Okeechobee inflow time series for phosphorus.

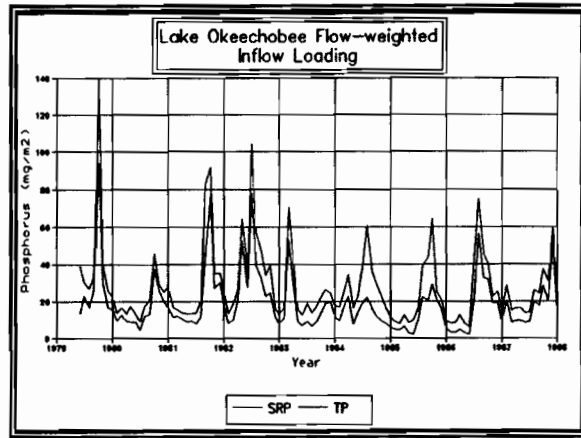


Figure 3-8 Lake Okeechobee phosphorus loading.

Table 3-3 The inflow stations are ranked below in decreasing contribution to the phosphorus load over the period of record (adapted from Carey and Huber, 1990).

Station	SRP Load (Kg)	Percent of Total Loading	Station	TP Load (Kg)	Percent of Total Loading
S191	823,691	30.25	S191	1,141,386	26.10
S65E	536,270	19.69	S65E	1,073,685	24.55
S71	312,800	11.49	S71	453,206	10.36
S154	276,047	10.14	FEC/CSR78	382,995	8.76
FECSR78	257,646	9.46	S154	352,237	8.05
S2	112,926	4.15	S2	225,674	5.16
S4	80,051	2.94	S4	124,106	2.84
S127	65,166	2.39	S3	113,807	2.60
S133	59,611	2.19	S84	108,032	2.47
S3	46,315	1.70	S133	95,115	2.17
S84	46,266	1.70	S127	92,545	2.12
S72	41,488	1.52	S72	72,169	1.65
S129	18,789	0.69	S77	40,506	0.93
S77	17,230	0.63	HGS5	32,327	0.74
S135	15,817	0.58	S135	32,014	0.73
HGS5	8,687	0.32	S129	27,039	0.62
S131	4,213	0.15	S131	6,755	0.15
Total	2,723,018		Total	4,373,606	

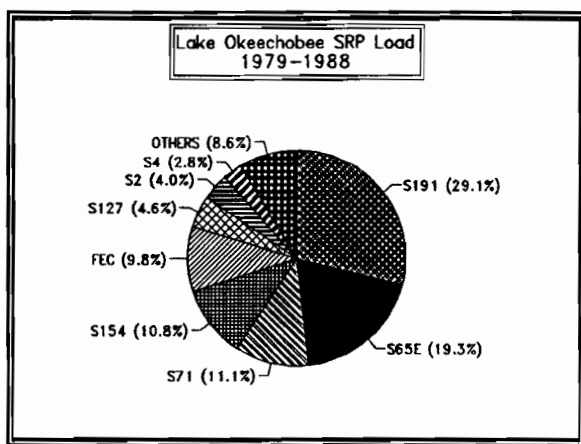


Figure 3-9 SRP loading to Lake Okeechobee (1977-1988).

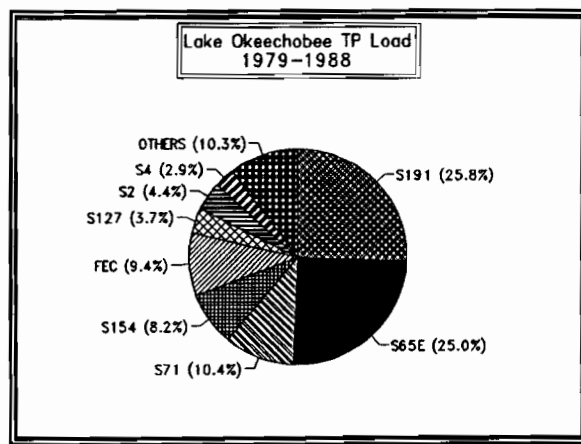


Figure 3-10 TP loading to Lake Okeechobee (1977-1988).

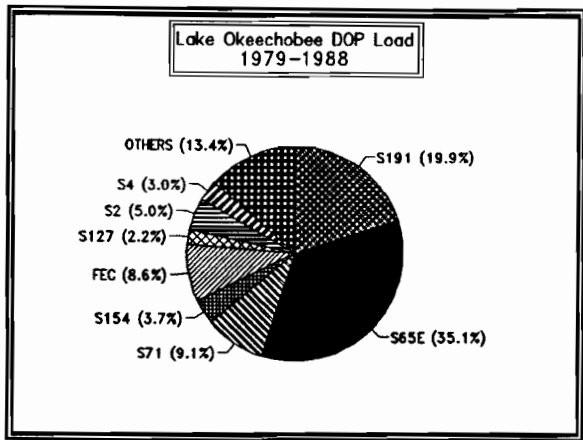


Figure 3-11 DOP loading to Lake Okeechobee (1977-1988).

There is considerable disagreement between published phosphorus budgets for Lake Okeechobee concerning the degree of net phosphorus retention, R_p , which is calculated as:

$$R_p = \frac{\text{Outflow load}}{\text{Inflow load}} \quad (3-2.1)$$

Joyner (1974) reports that 36 percent of the phosphorous entering the lake is retained in the bottom sediments and biota, whereas Federico et al. (1981) estimate that 84 percent of the phosphorous load is retained. The disparity largely reflects differing estimates of phosphorus input; the export rates for all the predicted budgets are relatively similar.

3.3 Seasonal Rainfall and Evaporation Patterns

The forty-year average rainfall near Lake Okeechobee is 55 inches per year. This is a decrease of about 8 to 9 inches per year since the 1960s primarily due to the absence of hurricanes in the area since that period (SFWMD, 1990). Table 3-4 shows the South Florida Rainfall for 1980s.

The pattern of the winter rainfall is dominated by cold front passage through the State. The convective patterns of summer rainfall are influenced by the sea-breeze circulation along the Atlantic Ocean and Gulf of Mexico. Lake Okeechobee is located between the two fronts and has sufficient areal extent and water mass to contribute its own lake-land breeze circulation pattern to the complex regional wind pattern (Pielke, 1974). This complex pattern of frontal movement results in the minimum rainfall in South Florida typically being located over Lake Okeechobee (MacVicar, 1983).

Table 3-4 South Florida Rainfall for 1980s (Source: SFWMD, 1990).

Year	Rainfall (inch)	Year	Rainfall (inch)
1981	43	1986	52
1982	64	1987	50
1983	67	1988	43
1984	47	1989	43
1985	48	1990	43

Blosser (1986) used a rainfall volume adjustment factor of 0.8 to estimate the lower lake precipitation compared to the precipitation measured at land precipitation stations. This adjustment factor should be lower in the summer convective storm season and higher during winter cyclonic storms. The precipitation from 1965 to 1989 was 52.1 inches at Belle Glade, 47 inches at Moore Haven, and 46.1 inches at Clewiston, Florida (Figure 3-12). The average rainfall over Lake Okeechobee can estimated to be 38.3 inches for the period 1965 to 1989 by using the mean precipitation from Belle Glade, Moore Haven, and Clewiston and a constant rainfall adjustment factor of 0.8.

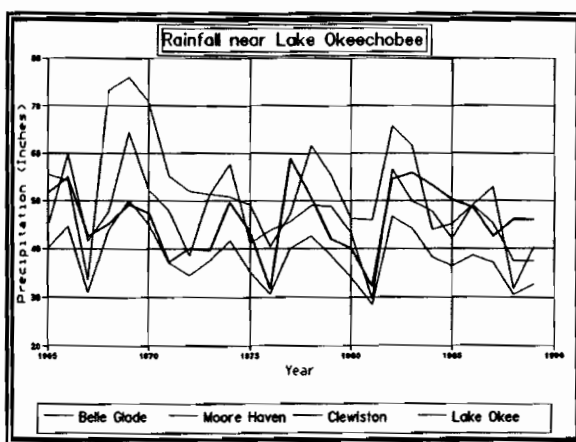


Figure 3-12 Precipitation near Lake Okeechobee.

3.4 Lake and Marsh Evaporation

Pan evaporation data are available at Moore Haven, Belle Glade, and Clewiston (Figure 3-13). Pan coefficients of 0.865 for the open lake areas (Shih, 1980) and 1.2 for the western marsh or littoral zone (Shih, 1980) were used in the modeling to convert pan evaporation measurements to estimates of open water evaporation and marsh evapotranspiration. Rainfall minus pan evaporation (annual totals) at the three stations is shown in Figure 3-14. Peaks correspond to periods during which higher than average runoff and lake stages would be expected.

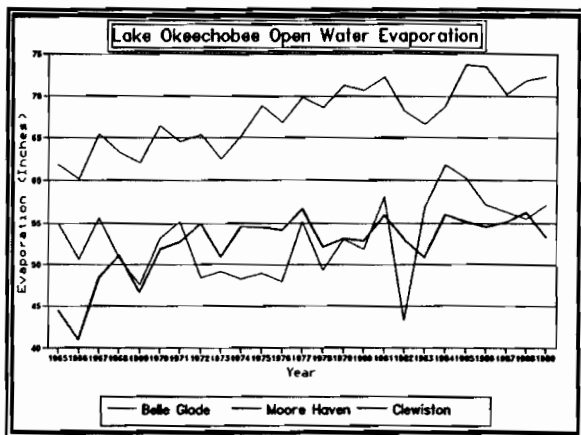


Figure 3-13 Pan evaporation near Lake Okeechobee.

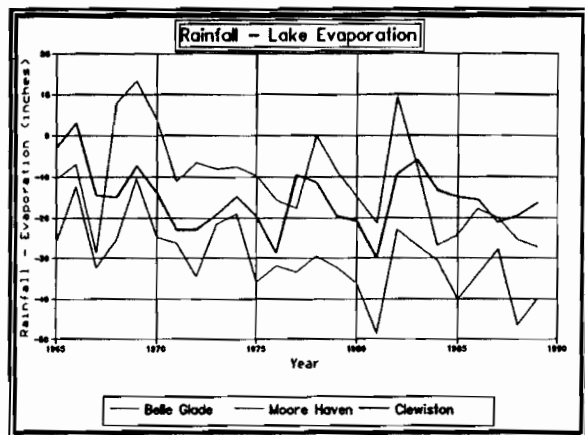


Figure 3-14 Precipitation and evaporation difference.

3.5 Precipitation Loading Model

Atmospheric input of nutrients occurs via both wet (direct precipitation) and dry (gaseous and particulate) deposition. The summation of wet and dry precipitation is termed bulk precipitation (Brezonik et al., 1983). The largest contribution to atmospheric nutrient input is via dry deposition for phosphates and wet deposition for nitrates (Ecternacht, 1975). The total amount of wet and dry precipitation input varies year by year and depends on the nutrient concentrations and measured precipitation used in the model LOP0D.

Bulk precipitation concentrations were 600 to 700 percent higher than wet-only concentrations near Lake Michigan (Eisenreich et al., 1977). Eisenreich et al. measured higher concentrations of TP in collection stations over Lake Michigan than over nearby land precipitation collectors. The average bulk concentrations of TP over Lake Michigan was $50 \text{ ug} \cdot \text{l}^{-1}$ in the northern basin and $64 \text{ ug} \cdot \text{l}^{-1}$ in the southern basin (Eisenreich et al., 1977).

Precipitation contributes about 19 percent of the nitrogen load and "dry fallout" accounts for 11 percent of the phosphorus load to Lake Okeechobee (Ecternacht, 1975). Brezonik et al. (1983) found that Florida bulk precipitation concentrations are 500 percent higher than wet-only precipitation in Florida, and summer precipitation concentrations in Florida were 1.5 greater than winter precipitation concentrations. Lake Okeechobee precipitation nutrient concentrations were higher in the summer and fall than winter and spring precipitation concentrations (Joyner, 1974).

Holtan et al.(1988) estimate a mean worldwide TP loading of $43 \text{ mg P} \cdot \text{m}^{-2} \cdot \text{yr}^{-1}$. Distributed over the surface area of Lake Okeechobee this would be an average TP load of 81,270 kilo-rams/year. Brezonik et al. (1983) measured a TP loading of $82 \text{ mg P} \cdot \text{m}^{-2} \cdot \text{yr}^{-1}$ at Clewiston and $67 \text{ mg P} \cdot \text{m}^{-2} \cdot \text{yr}^{-1}$ at Lake Alfred to the northwest of the Lake. The Clewiston TP loading would contribute 155,060 kilograms per year to Lake Okeechobee. The mean bulk precipitation concentrations in Florida were 21 ug/l for SRP and 36 ug/l for TP (Brezonik et al., 1983).

The average total phosphorus concentration in rainfall was $61 \text{ ug} \cdot \text{l}^{-1}$ and the SRP concentration was $41 \text{ ug} \cdot \text{l}^{-1}$ based on averages between 1973 and 1979 (Federico et al., 1981). The concentration of total nitrogen in precipitation is $1090 \text{ ug} \cdot \text{l}^{-1}$ and the inorganic nitrogen concentration ($\text{NO}_2 + \text{NO}_3 + \text{NH}_4$) is $565 \text{ ug} \cdot \text{l}^{-1}$ (Federico et al., 1981). Blosser (1986) used an SRP concentration of $40 \text{ ug} \cdot \text{l}^{-1}$ and a total phosphorus concentration of $100 \text{ ug} \cdot \text{l}^{-1}$. Brezonik et al., 1981 measured bulk TP concentrations of $64 \text{ ug} \cdot \text{l}^{-1}$ at Clewiston, wet-only TP concentrations of $9 \text{ ug} \cdot \text{l}^{-1}$ at Belle Glade, and bulk concentrations of $50 \text{ ug} \cdot \text{l}^{-1}$ at Lake Alfred for stations near Lake Okeechobee.

For LOP0D modeling, rainfall concentrations were varied somewhat during model runs, but final runs used concentrations of 35 ug/l for SRP and 15 ug/l for DOP (TP-SRP). These were then multiplied by rainfall to provide loads to the lake.

4. LAKE OKEECHOBEE WATER QUALITY

4.1 Introduction

In-lake data used in this study were originally collected by the South Florida Water Management District (SFWMD) from the Lake Okeechobee limnetic and littoral zone water quality monitoring program. Measurements of soluble reactive phosphorous (SRP) and total phosphorous (TP) were made at 43 stations within Lake Okeechobee (Figure 4-1).

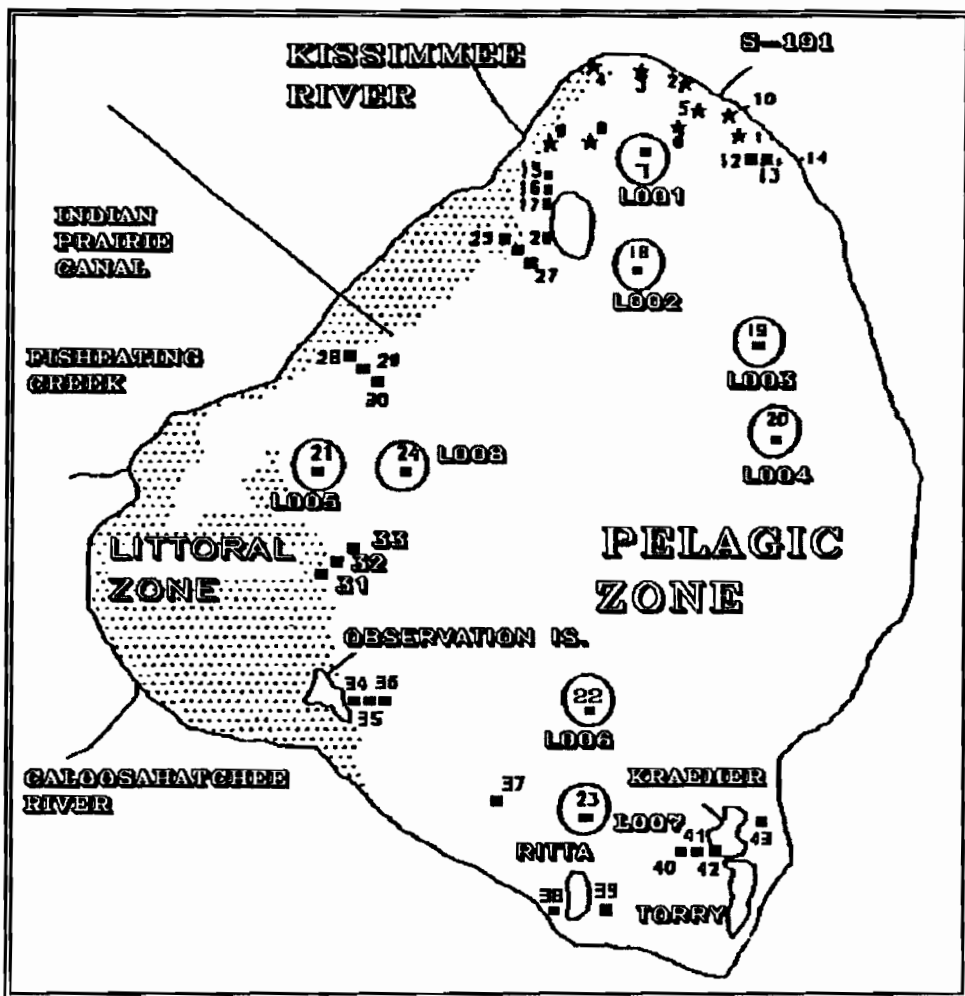


Figure 4-1 Long term sampling station locations in Lake Okeechobee.

However, most of these stations have a short or intermittent record length and only eight of these stations are used in this report. The eight remaining stations are stations seven, eighteen, nineteen, twenty, twenty-one, twenty-two, twenty-three, and twenty-four. Further reference to these stations will be as stations L001, L002, L003, L004, L005, L006, L007, and L008 respectively. Data were available for these stations for the period from December 1972 through August 1989. The

sampling frequency was predominantly twice per month; however, in some months four measurements were made, one in others, and there are months when no sample was taken at a station.

The eight long term stations are used in model LOPOD to approximate the measured phosphorus concentrations (Figure 4-2). Station L001 is used to estimate the phosphorus in northern Lake Okeechobee. The central mud zone of the lake is covered by station L002, L003, L004, L006, and L008. Stations L005 and L007 are the most dissimilar statistically (Blosser, 1986; Federico et al., 1981) since they straddle two dissimilar sediment areas. Station L005 borders the sand zone and macrophyte area on the western side of the lake. Station L007 is on the border between the South Bay of Lake Okeechobee and the central mud zone and has peat bottom sediment. Physical mechanisms are probably dominant at every long-term station except L007, which is dominated by biological activities [D. Soballe, SFWMD, personal communication, 1990].

L001	- Northern Lake
L002	- Mud zone
L003	- Mud zone
L004	- Mud zone
L005	- Sandy area between mud and macrophyte area
L006	- Mud zone
L007	- South bay
L008	- Mud zone

Figure 4-2 Correspondence between long term sampling station locations in Lake Okeechobee and the generalized areas in the box model of Lake Okeechobee.

4.2 Chemical and Physical Data in Lake Okeechobee

4.2.1 Data Sources

The chemical and physical data discussed in this chapter and subsequent chapters consist of two different data sets collected by the SFWMD. The first data set covers the period between 1972 and 1988, and is used in this report to quantify the long term reaction rates and constants specific to Lake Okeechobee. The second data set was collected during the years 1988 and 1989. This period of time corresponds to the data collection period for this study of the phosphorus dynamics of Lake Okeechobee (Reddy et al., 1991; Sheng et al., 1991c).

4.2.2 Lake Okeechobee Turbidity and Suspended Solids

The measured turbidity and suspended solids concentrations of Lake Okeechobee are used to estimate the light absorption and light scattering coefficients in the different areas of Lake Okeechobee [see Chapter 6]. Additionally, partitioning coefficients for the organic and inorganic phosphorus associated with the total suspended solids (TSS) are estimated from these data.

The mean station turbidity and suspended solids of the long term stations of Lake Okeechobee indicate lower concentrations at stations L005 and L007, which are located in the western sand area and South Bay of Lake Okeechobee respectively, compared to the stations in the central mud zone [L002, L003, L004, L006 and L008], and station L001 located near the northern end of the lake (Figures 4-3 and 4-4).

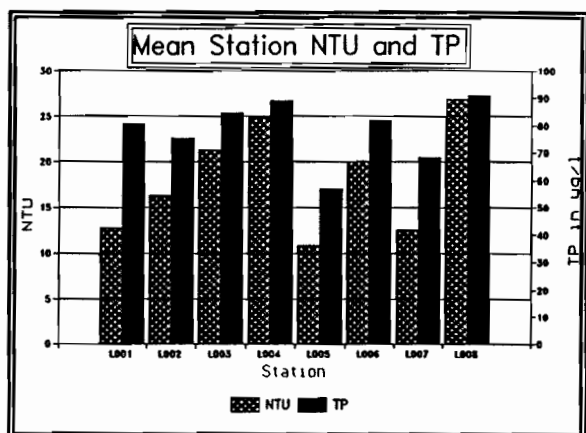


Figure 4-3 Mean station turbidity and TP during 1988-1989.

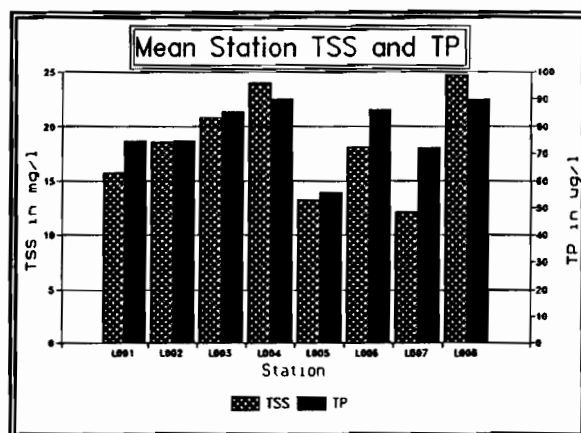


Figure 4-4 Mean station suspended solids and TP during 1988-1989.

The central mud zone has flocculent sediment that is more susceptible to resuspension due to the action of wind (Hwang and Mehta, 1989). This resuspended flocculent sediment is the cause of the higher pelagic suspended sediment. The suspended sediment scatters light and causes higher turbidity measurements in the central mud zone than in the border sandy areas of Lake Okeechobee. The mud area of Lake Okeechobee exhibits a localized effect on TSS concentrations (i.e., there is vertical movement but little lateral movement of TSS in Lake Okeechobee). This is also a finding of the 3-D TSS model of Lake Okeechobee (Sheng et al., 1991a).

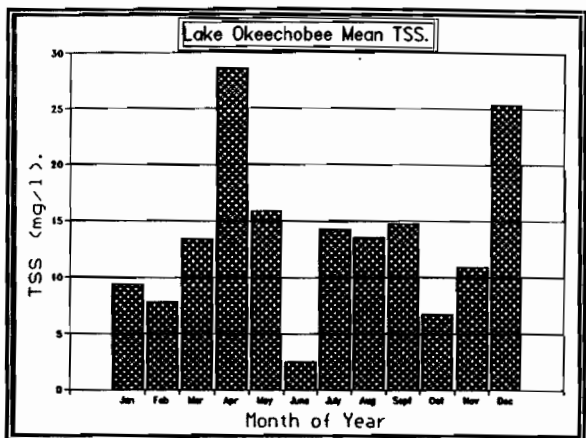


Figure 4-5 Mean monthly suspended solids during 1988-1989.

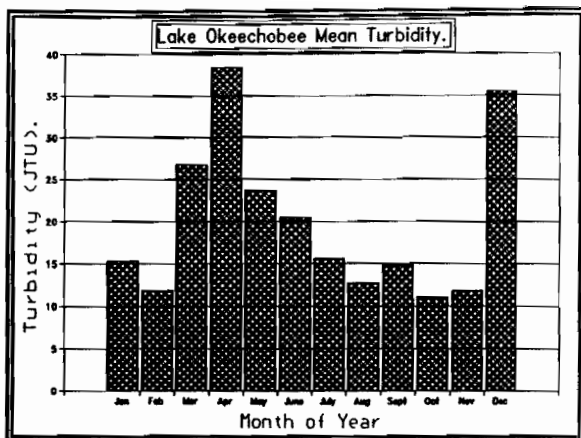


Figure 4-6 Mean monthly turbidity during 1988-1989.

The mean Lake Okeechobee monthly TSS concentrations and turbidity measurements are higher during the months of frontal or cyclonic storm movement (Figures 4-5 and 4-6). The smallest monthly concentration of TSS is during the summer months when the wind movement over Lake Okeechobee is lessened because the lake affects the movement of convective storm systems over South Florida (Pielke, 1974). Wind movement and lake TSS concentrations are significantly higher in the months of March, April, May and December, because Florida experiences a complex interaction of convective and cyclonic storm systems during the year that maximizes wind movement in the spring and winter (Balling and Cerveny, 1983).

We found a decreasing trend in mean lake TSS using the data set YPROJ.DAT, which was supplied by the SFWMD (Figure 4-7).

Mean lake total suspended solids (TSS) concentration before 1979.	26.5 mg/l
Mean lake total suspended solids (TSS) concentration after 1979.	17.2 mg/l

Figure 4-7. Mean lake TSS concentrations before and after 1979 from the SFWMD data set YPROJ.DAT.

Turbidity generally follows the pattern of suspended solids except in the summer months when high concentrations of algae scatter light and compensate for the decrease in light scattering due to lower TSS concentrations (Figure 4-6).

The mud area of Lake Okeechobee occupies one third of the total lake area (Kirby et al., 1989), and contains approximately 193×10^6 m³ of material with a maximum depth of 70 to 80 cm in the deepest portion of the lake. The other major surface sediments types are sand, peat, and marl (Reddy et al., 1991). The bottom sediment type influences greatly the phosphorus dynamics and concentrations in Lake Okeechobee.

We investigated this influence by using linear regression on measured TP, turbidity, and TSS data. TP is strongly correlated with turbidity (Figure 4-8) and TSS (Figure 4-9), except for stations L001 and L005. The stronger relationship for the mud stations may be attributable to the attached organic phosphorus on the suspended sediments. The unreactive sediment phosphorus may be 30 to 50 percent of the measured TP at a mud station based on bottom sediment data collected by Reddy et al. (1991).

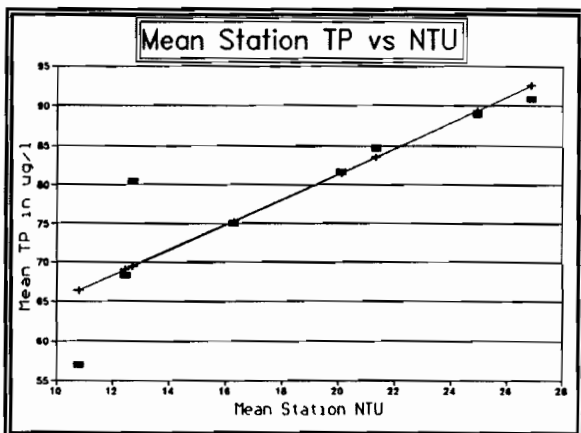


Figure 4-8 Mean station TP versus turbidity during 1988-89.

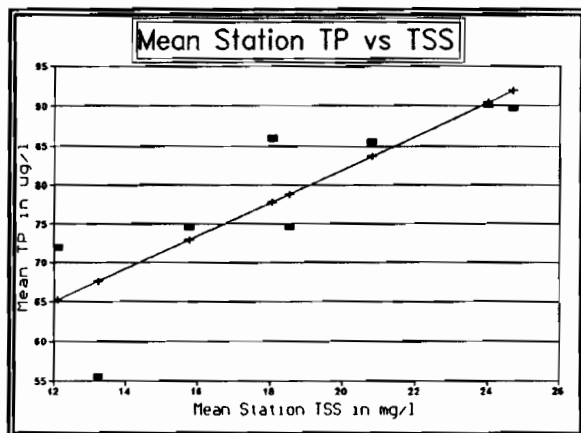


Figure 4-9 Mean station TP versus TSS during 1988-1989.

4.2.3 Lake Okeechobee Organic Color, pH, and Secchi Depth

Organic color in lake water is described by the platinum-cobalt scale which measures the "yellowness" of filtered water samples (Davies-Colley et al., 1988). Organic color in Lake Okeechobee is strongly seasonal due to the influence of river loading (Figure 4.10). The primary sources of organic color in Lake Okeechobee are the wetlands of the Kissimmee River, Taylor Creek/Nubbin Slough, and Fisheating Creek (Joyner, 1974). Mean lake dissolved organic color is 42 Pt-Co units (Canfield and Hoyer, 1989).

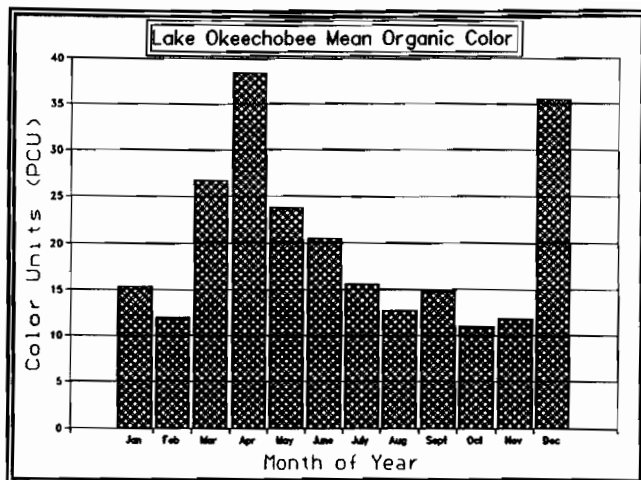


Figure 4-10 Mean monthly Lake Okeechobee organic color during 1988-1989.

The pH of Lake Okeechobee is nearly uniform seasonally (Figure 4-11) and uniform spatially (Figure 4-12). The mean pH of the lake ranges from 7.0 in January to 8.5 in October, which reflects the influence of river loading, lake biota, and calcite dissolution from the *rangia* beds in Lake Okeechobee (Joyner, 1974). Conductivity was also spatially uniform in the lake (Figure 4-11).

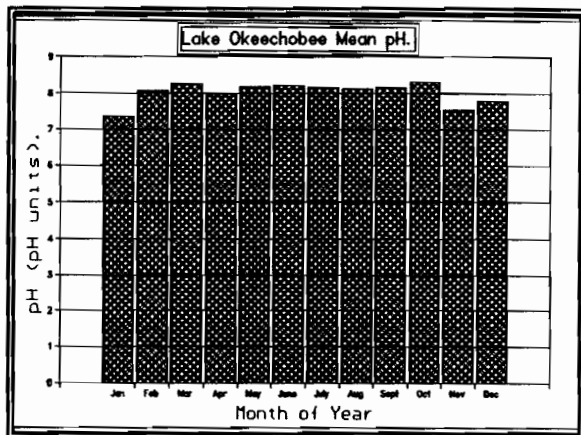


Figure 4-11 Mean monthly Lake Okeechobee pH 1988-1989.

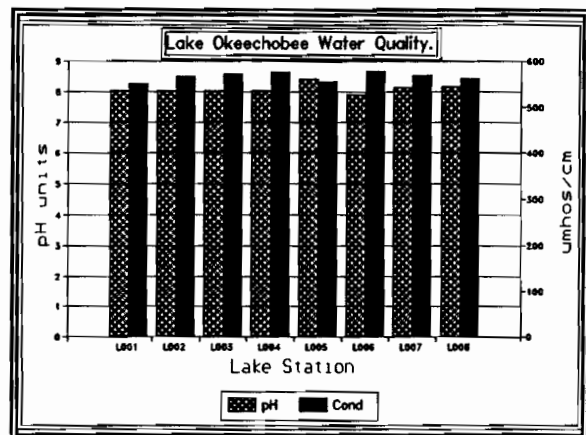


Figure 4-12 Mean Lake Okeechobee pH and conductivity station data during 1988-1989.

The uniformity of the pH and conductivity measurements is due to the calcareous white deposit that forms the basement of the lake. This calcareous material is exposed to the open water at over 50 percent of the lake area and is a major source of dissolved solids to Lake Okeechobee (Joyner, 1974). The CaCO_3 dissolution of the beds increases the conductivity of Lake Okeechobee above the concentration expected from river input alone.

The secchi disc depth (see later discussion in Chapter 6) is the complex realization of the influence of absorbing agents (water, organic color, and algal cells) and scattering agents (suspended solids and algal cells). Secchi depth in Lake Okeechobee is temporally (Figure 4-13) and spatially variable (Figure 4-14). The actual measurement of secchi disc depth may vary as much as 15 percent depending on whether the observer of the black and white disc places the disc on the shady or sunny side of the boat (Davies-Colley and Vant, 1988).

Additional data showing the variation of conductivity, pH, turbidity and suspended solids are shown in Figures 4-15 — 4-18. The reduction of turbidity and suspended solids during the summer months is particularly noticeable (Figure 4-18).

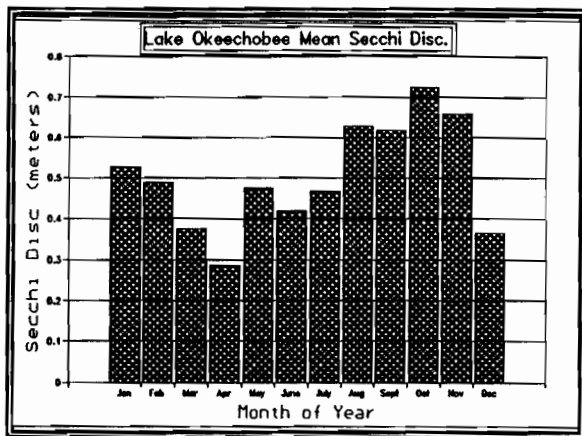


Figure 4-13 Mean monthly Lake Okeechobee Secchi depth (m).

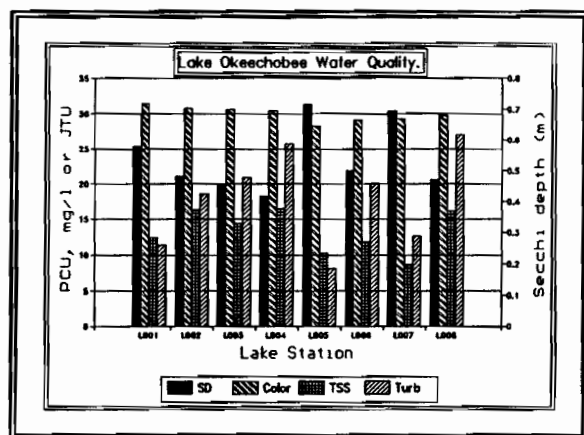


Figure 4-14 Mean station SD, Color, TSS, and turbidity during 1988-1989.

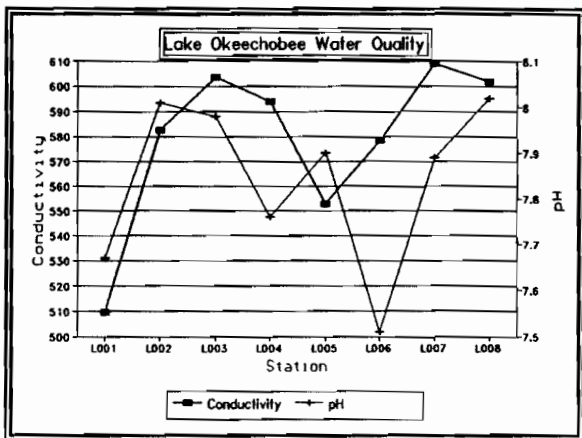


Figure 4-15 Mean Cond, pH by station.

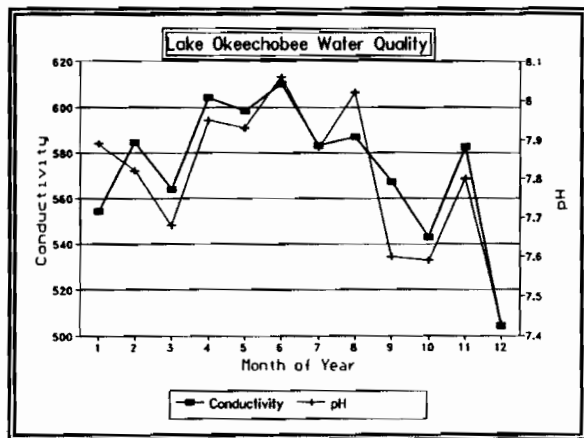


Figure 4-16 Mean Cond, pH by month.

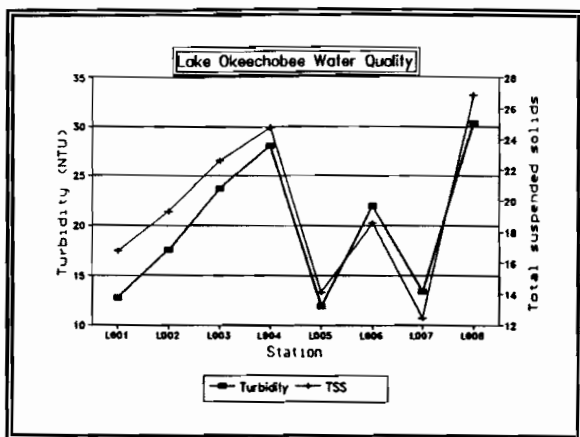


Figure 4-17 Turbidity (NTU) and suspended solids (TSS) by station

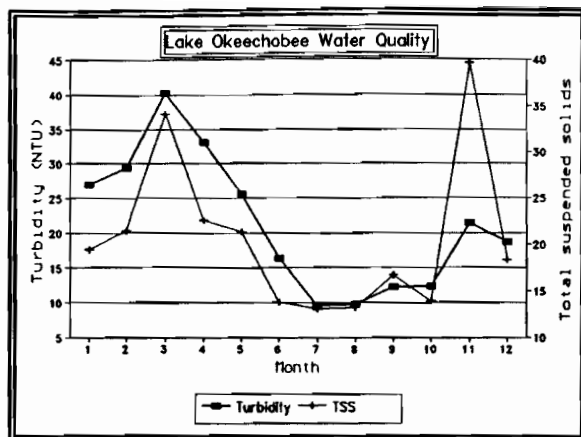


Figure 4-18 Turbidity (NTU) and suspended solids (TSS) by month.

4.3 Nutrient Data in Lake Okeechobee

Mean concentrations and standard deviations were calculated by lake station for nutrient data collected between December, 1972 and August, 1989 (Table 4-1 and Figure 4-19 and 4-20). Mean station SRP concentrations were $16 \text{ ug} \cdot \text{l}^{-1}$ to $30 \text{ ug} \cdot \text{l}^{-1}$, and mean station TP concentrations ranged $57 \text{ ug} \cdot \text{l}^{-1}$ through $91 \text{ ug} \cdot \text{l}^{-1}$. The lower mean SRP concentrations were near inflow tributaries (i.e., stations L005, L002, and L001), with two of these stations (L005 and L001), having the largest standard deviations of SRP. An additional difference between station L005 and the other lake stations is its proximity to the macrophyte or littoral zone. The highest SRP concentrations were in the deepest area of Lake Okeechobee, an area also referred to as the mud zone (i.e., stations L006, L004, and L003) as were the highest mean and standard deviations of TP concentrations. The mud zone of Lake Okeechobee also had the highest concentrations of TP-SRP which is indicative of the importance wind resuspended bottom sediments play in the prediction of TP in the mud zone.

The nitrogen species concentrations at each of the 8 long term stations are approximately the same for concentration and percentage composition (Table 4-2 and Figure 4-21), except for station L005 which has a smaller percentage of inorganic nitrogen.

Table 4-1 Mean phosphorus concentrations and standard deviations of phosphorus measured in Lake Okeechobee ranked in order of decreasing mean concentration ($\mu\text{g} \cdot \text{l}^{-1}$). Adapted from Carey and Huber (1990).

SRP Concentrations			TP Concentrations			TP-SRP Concentrations	
Station	Mean	Std.	Station	Mean	Std.	Station	Mean
L006	30	20	L004	91	40	L008	67
L004	27	21	L008	87	43	L004	64
L003	24	19	L003	84	38	L003	60
L007	24	21	L006	84	39	L001	58
L008	21	21	L001	78	34	L002	56
L001	20	22	L002	74	37	L006	54
L002	18	19	L007	67	35	L005	44
L005	13	23	L005	57	37	L007	43

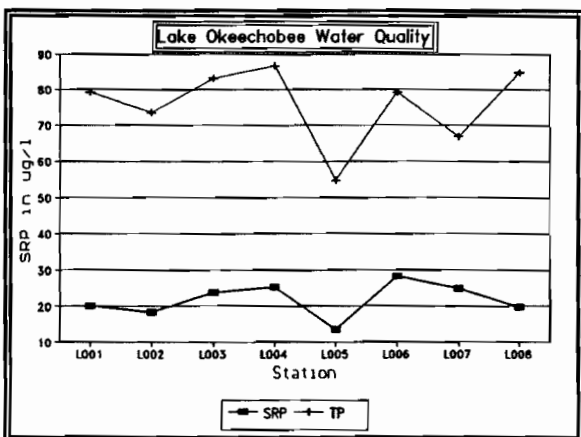


Figure 4-19 Mean SRP and TP by station.

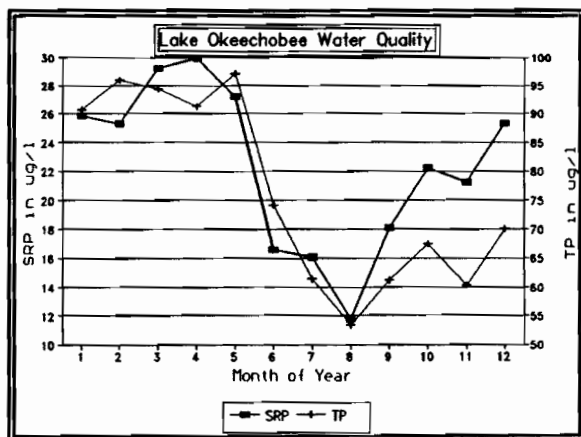


Figure 4-20 Mean SRP and TP by month.

Table 4-2 Mean nutrient concentrations in Lake Okeechobee by station ($\mu\text{g}\cdot\text{l}^{-1}$), April 1973 to March 1980. Adapted from Frederico et al. (1981).

Station	TP	SRP	TN	DIN	ORGN
L005	46.	12.	1630.	80.	1550.
L007	55.	21.	1830.	230.	1600.
L002	63.	16.	1720.	150.	1570.
L003	64.	18.	1740.	160.	1580.
L001	67.	15.	1700.	130.	1590.
L006	67.	25.	1680.	210.	1470.
L008	68.	16.	1760.	170.	1590.
L004	73.	20.	1780.	180.	1610.

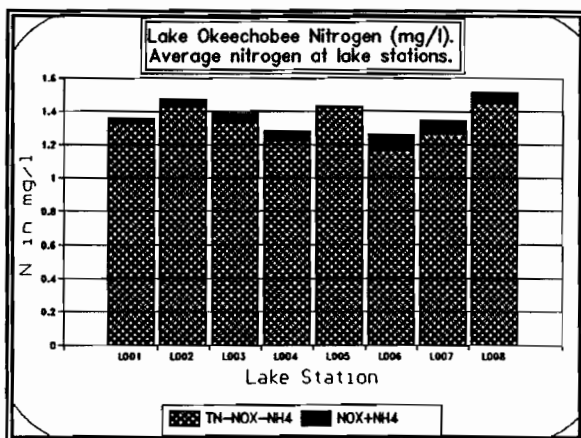


Figure 4-21 Mean station total nitrogen during 1988-1989.

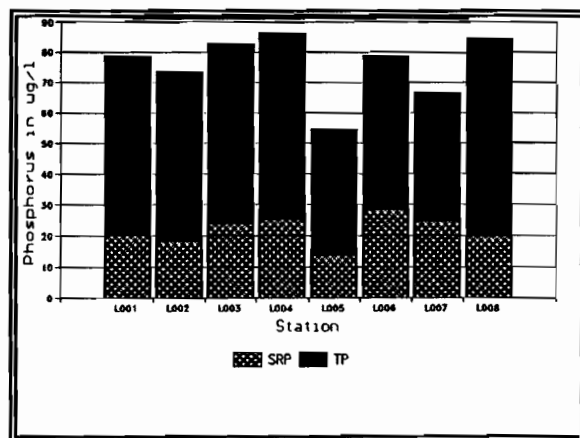


Figure 4-22 Mean station total phosphorus during 1988-1989.

4.4 Summary of Nutrients in Lake Okeechobee

The mean concentrations of SRP and TP during the study period of 1988 and 1989 (Figure 4-22) are similar to the concentrations measured during the period 1972 to 1988 (Figure 4-19). The dissimilarities in the long term lake station's measured TP and SRP concentrations are related to bottom sediment type, and station proximity to littoral or inflow tributaries.

5. DOUBLE MASS TREND ANALYSIS

5.1 Introduction

We have utilized the concept of the double mass curve to examine trends in the input loading, input concentration, in-lake concentration, rainfall, evaporation, stage history, tributary inflow, and surface outflow of Lake Okeechobee. The double mass curve is a plot of the cumulative parameter of interest versus time. Any change over time in the parameter characteristics will be apparent by a change of slope. If there is no change in the characteristics of the parameter over time the result will be a curve approximating a straight line. More typically the double mass curve will exhibit both positive and negative deviations from a straight line but tend to return to a straight line.

The basis for detecting the change in slope was a straight line constructed from the mean slope of the first half of each time series. This line was then extended the entire length of the time series and visually compared to the double mass curve.

5.2 Double Mass Trend Analysis of Mud and Non-Mud Stations

That TP and SRP concentrations in Lake Okeechobee have increased in the 1980s is readily apparent based on the volume weighted mean average SRP and TP data (Figure 5-1). This increase is approximately the same for both the mud and non-mud stations in Lake Okeechobee (Figures 5-2 and Figure 5-3) for both measured SRP and TP. Based on the double mass analysis (Figures 5-4 and 5-5 for TP and Figures 5-6 and 5-7 for SRP), the increase appears to have taken place in the years 1979 to 1981. Carey and Huber (1990) also concluded in-lake concentrations have been increasing since 1973, with perhaps a step increase in 1979 or 1980. Three major events took place between 1979 and 1981 that affected the water quality of Lake Okeechobee:

- Hurricane David in the year 1979.
- High lake stages in 1979 and 1980 that overtopped the islands in the South Bay of Lake Okeechobee.
- A severe drought in 1981 that caused near record low lake stages.

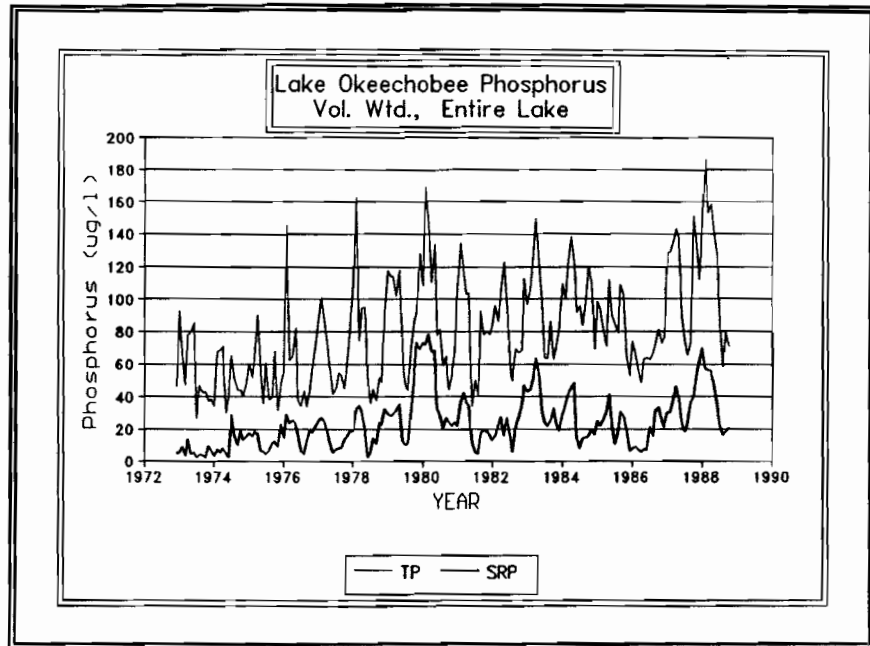


Figure 5-1 Lake Okeechobee volume weighted TP and SRP concentrations during 1972 to 1989.

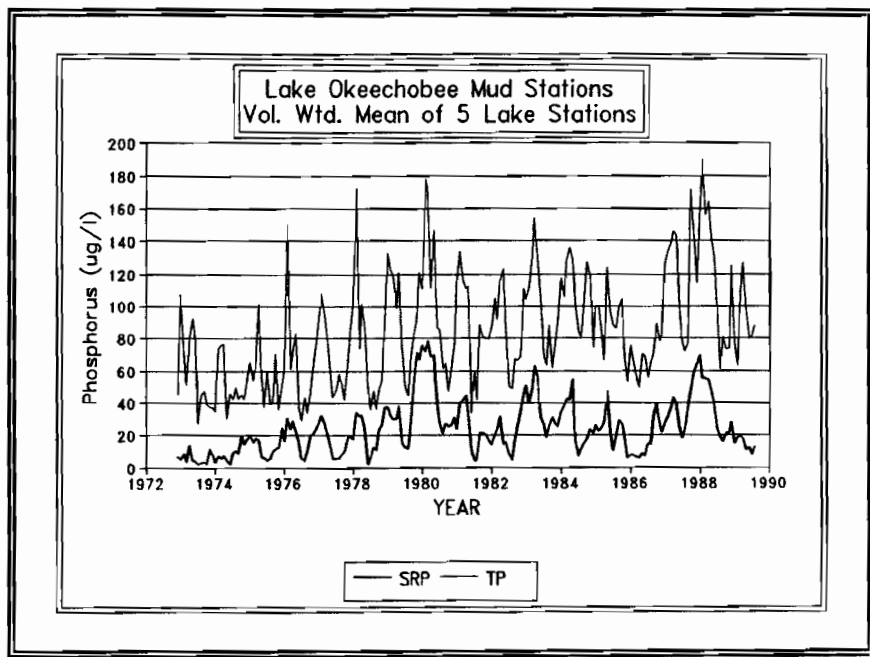


Figure 5-2 Lake Okeechobee TP and SRP concentrations for the five mud stations during 1972 to 1989.

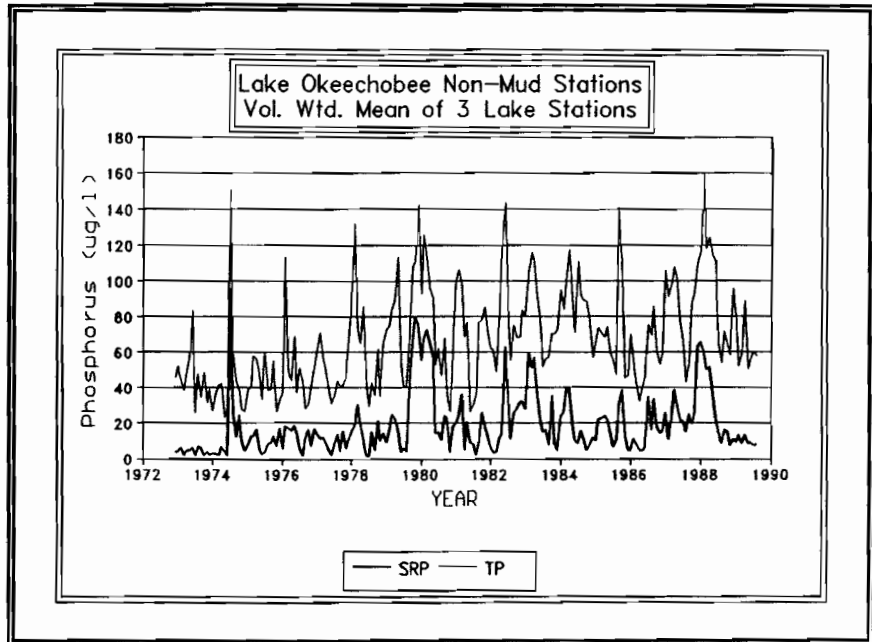


Figure 5-3 Lake Okeechobee TP and SRP concentrations for the three non-mud stations during 1972 to 1989.

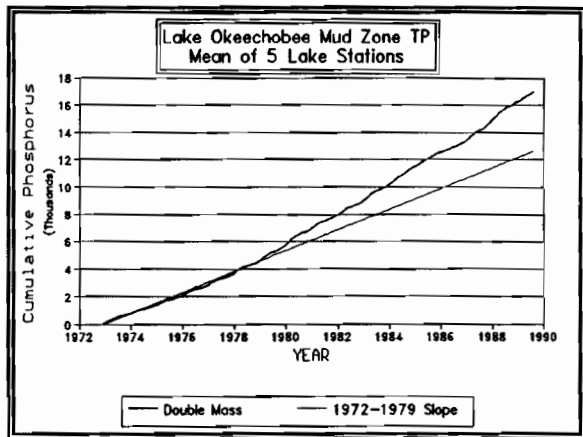


Figure 5-4 Mud zone TP double mass.

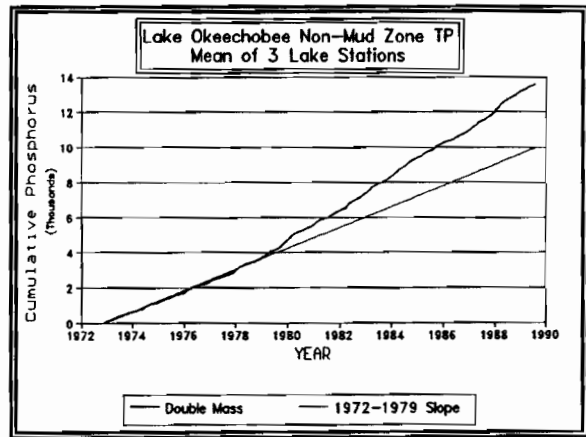


Figure 5-5 Non-mud TP double mass.

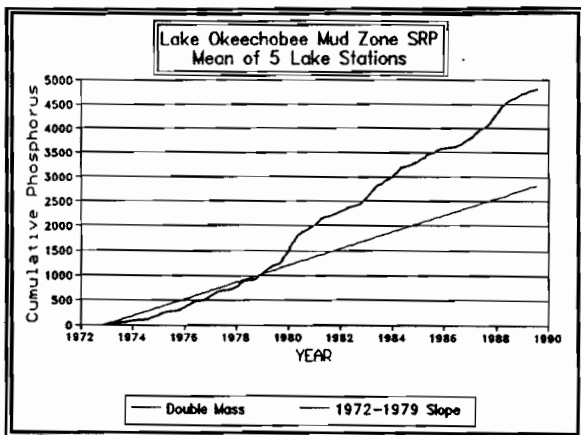


Figure 5-6 Mud zone SRP double mass.

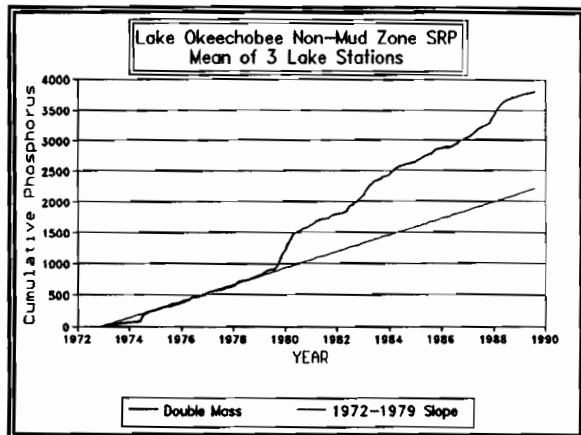


Figure 5-7 Non-mud SRP.

Fractional TP and SRP increases are shown in Figure 5-8, and the magnitude of SRP concentration changes is shown for two different time periods in Figure 5-9. Lake Okeechobee mean annual SRP concentrations increased from $5 \text{ ug} \cdot \text{l}^{-1}$ in 1973 to $45 \text{ ug} \cdot \text{l}^{-1}$ in 1979, and mean annual total phosphorus concentrations increased from $48 \text{ ug} \cdot \text{l}^{-1}$ in 1973 to $97 \text{ ug} \cdot \text{l}^{-1}$ in 1979 (Federico et al., 1981). This increase in TP concentration began between 1977 and 1979, which coincided with a 1978 change in the regulation schedule to raise the mean stage from 15.5 feet to 17.5 feet (Canfield and Hoyer, 1989). This higher stage caused further inundation of the macrophyte or littoral zone, and inundated several islands in the South Bay region of Lake Okeechobee (Federico et al., 1981). These islands had been used for agricultural purposes, and their inundation may have caused a pulsed release of mineralized phosphorus from soil that had been exposed to the air and oxidizing before 1979.

A statistical survey of SFWMD lake data by Blosser (1986), encompassing the period 1973 to 1980, showed SRP and TP concentrations were increasing over time, that the lowest TP concentrations were located at station L005, near submerged and emergent vegetation (Figure 4-1). Contours constructed by Schelske (1989) of mean SRP and mean TP using data from forty SFWMD stations collected between May 20, 1978 and September 15, 1979, also showed lower concentrations near the littoral zone of Lake Okeechobee.

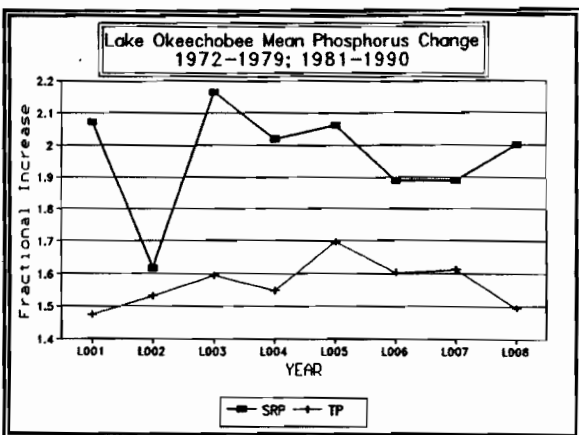


Figure 5-8 Fractional increase in TP and SRP.

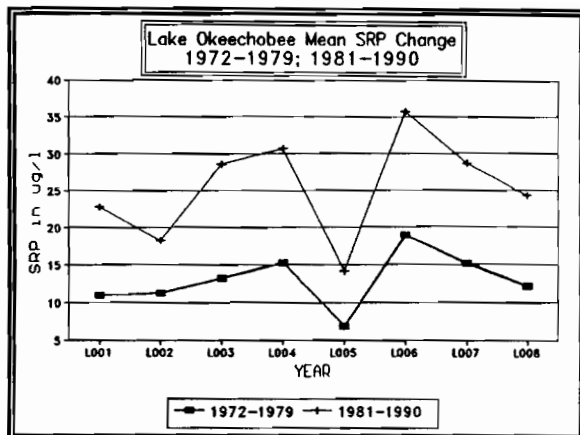


Figure 5-9 Lake SRP change.

5.3 Double Mass Curve Analysis of Boundary Conditions

A key question is the reason for the increase in-lake phosphorus concentrations in the 1980s compared to concentrations in the 1970s. Perhaps an examination of the trends in the major inputs to Lake Okeechobee will shed some light on the important external processes that singly or in combination are causing the increase in phosphorus concentrations.

The surface inflow to Lake Okeechobee has remained the same for the last 18 years (Figure 5-10), whereas the measured outflow has increased during the same period (Figure 5-11). The mean hydraulic loading was $0.093 \text{ m} \cdot \text{month}^{-1}$ during the years 1972 to 1979 and $0.091 \text{ m} \cdot \text{month}^{-1}$ for the following years. The measured outflow from Lake Okeechobee was $0.039 \text{ m} \cdot \text{month}^{-1}$ during the years 1972 to 1979 and $0.047 \text{ m} \cdot \text{month}^{-1}$ for the following years.

An increasing trend was not found for external nutrient loads (Federico et al., 1981; Carey and Huber, 1990), indicating increased lake concentrations may be linked to internal cycling of phosphorus. An analysis of SFWMD data collected between 1973 and 1984 by Canfield and Hoyer (1989) also showed no significant correlation ($r = 0.16$) between annual in-lake concentrations and phosphorus loading rates.

The surface phosphorus loading to Lake Okeechobee has decreased over the last 18 years (Figure 5-12). The inflow SRP loading has been decreasing since 1979, and inflow TP seems to holding steady or decreasing (Figure 3-8). Large peaks are seen in both the inflow loading series (Figure 3-8) and the in-lake concentration series (Figure 5-1) in late 1979, which are a result of Hurricane David, which struck the Lake in September 1979. Time series analysis of inflow loadings (Carey and Huber, 1990) did not identify any useful natural cycles beyond the annual cycle evident from annual peaks in both series.

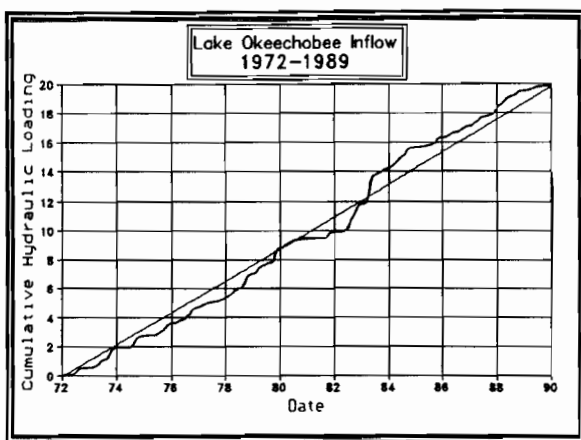


Figure 5-10 Inflow double mass for years 1972-1989. Loading is in units of m/yr.

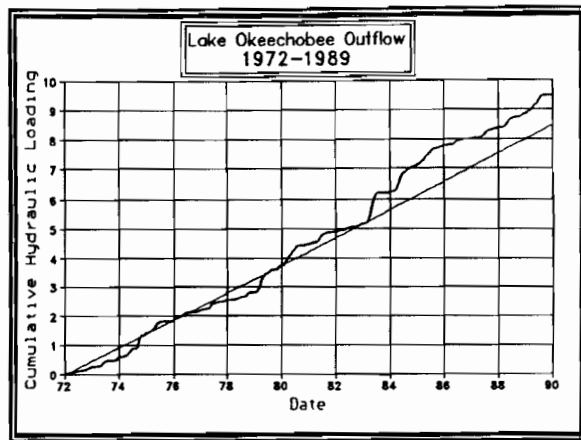


Figure 5-11 Outflow double mass for years 1972-1989. Loading is in units of m/yr.

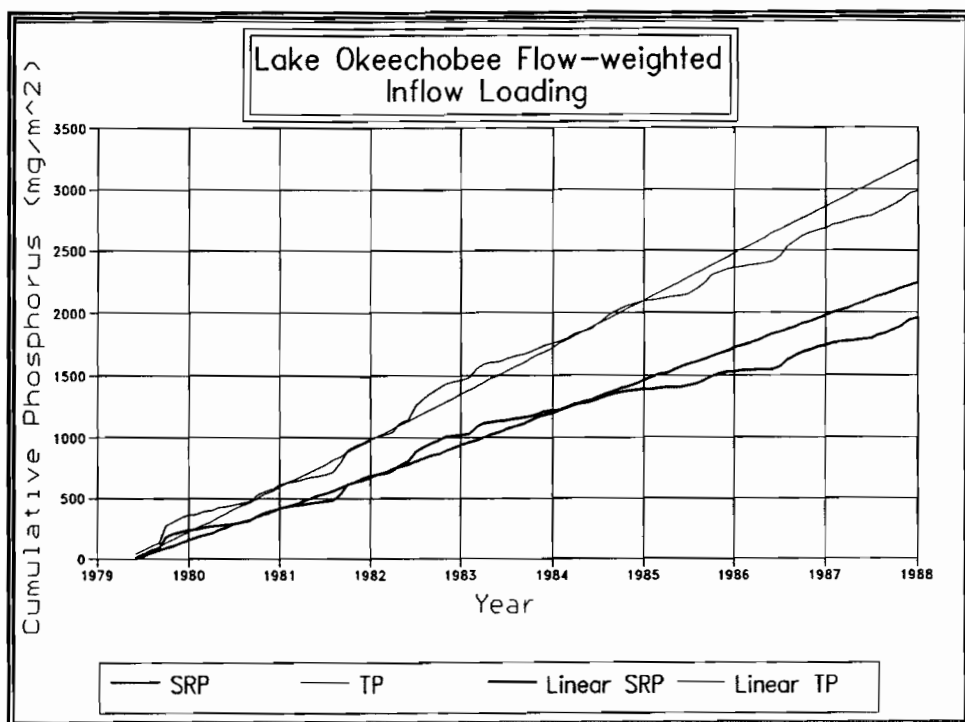


Figure 5-12 Phosphorus loading double mass curve from 1979-1989.

5.4 Rainfall, Evaporation and Wind Data

Rainfall is a major source of water to Lake Okeechobee (20 percent), and evaporation from the water surface is the largest outflow from Lake Okeechobee (65 percent). The mean rainfall over Lake Okeechobee has remained approximately the same for the last 25 years (Figure 5-13), whereas the estimated evaporation has increased during the same 25 year period (Figure 5-14) according to the mean pan evaporation measurements for stations located near Lake Okeechobee. The mean rainfall was 0.083 m/month during the years 1965 to 1979 and 0.078 m·month for the subsequent years. The estimated surface water evaporation from Lake Okeechobee was 0.12 m/month during the years 1965 to 1979 and 0.13 m/month for the following years. The difference between rainfall and evaporation increased from -0.037 m/month before 1979 and -0.058 m/month after 1979.

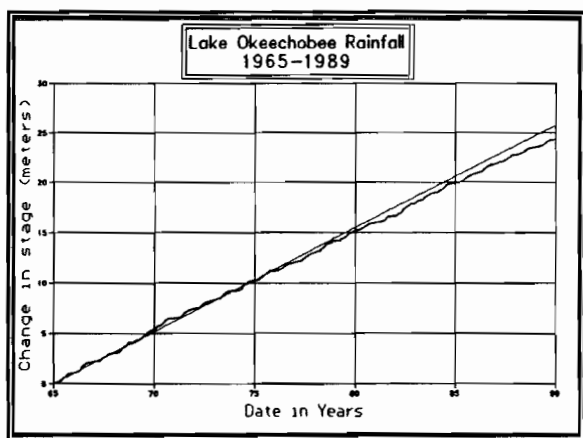


Figure 5-13 Lake Okeechobee mean rainfall double mass for 1965-1989.

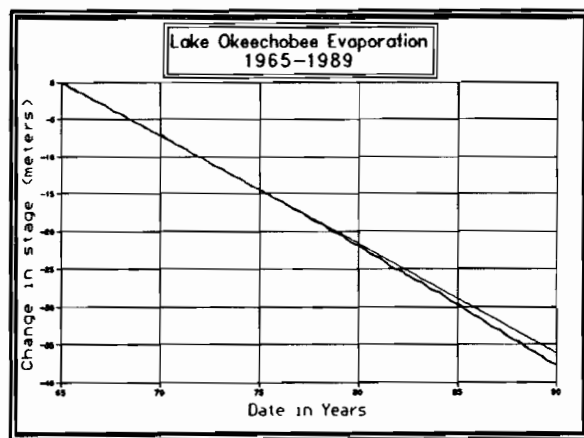


Figure 5-14 Evaporation double mass for 1965-1989.

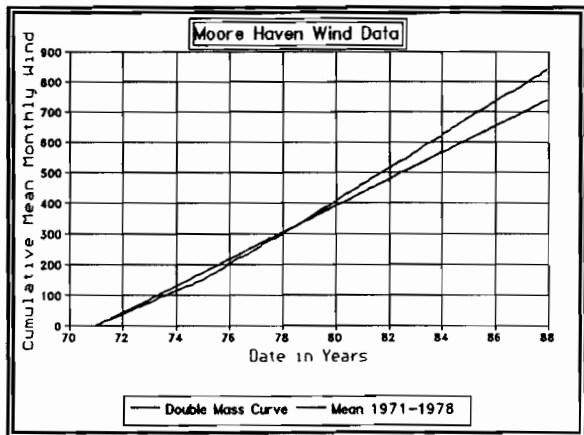


Figure 5-15 Monthly wind movement at Moore Haven, Florida.

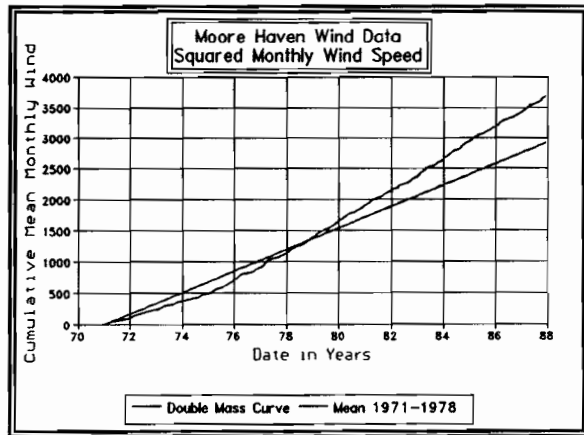


Figure 5-16 Double mass curve for squared monthly wind at Moore Haven.

Wind speeds have apparently increased since 1978 (Figure 5-15). Because surface wind shear is proportional to the squared wind velocity, the effect on lake turbulence is even more noticeable (Figure 5-16). That is, an increase in wind speeds during the 1980s could account for some increase in sediment scour and phosphorus cycling.

6. SOLAR RADIATION AND TEMPERATURE MODEL

6.1 Daily and Seasonal Solar Radiation Model

6.1.1 Net Surface Heat Flux

The sun supplies the light energy to drive algal and macrophyte photosynthesis and is a source of heat to Lake Okeechobee. The seasonal cycle of solar intensity and duration drives (both explicitly and implicitly via water temperature) the seasonal dynamics of Lake Okeechobee's aquatic biota. The approximation of Lake Okeechobee's diurnal and seasonal solar radiation flux involves either the average daily clear sky radiation at Lakeland, Florida, or the calculated cloudless sky solar radiation as defined in Section 6.1.2 is used by models LOP0D and LOP3D. The equations used in the models, variable sensitivity, and background information are discussed and presented in this chapter.

Heat and solar radiation flux units are commonly $\text{cal} \cdot \text{cm}^{-2} \cdot \text{day}^{-1}$ [$\text{langleys} \cdot \text{day}^{-1}$], $\text{kcal}/\text{m}^2/\text{hr}$, $\text{BTU} \cdot \text{ft}^{-2} \cdot \text{day}^{-1}$, or $\text{watt} \cdot \text{m}^{-2}$ in the literature. The units in the Lake Okeechobee models are always $\text{langleys} \cdot \text{day}^{-1}$ [$\text{ly} \cdot \text{day}^{-1}$]. The conversion factors used to convert from other common units of measurements to units of $\text{ly} \cdot \text{day}^{-1}$ are listed in Table 6-1.

Table 6-1 Conversion (multipliers) factors used to convert other units of solar radiation to units of $\text{langleys} \cdot \text{day}^{-1}$ in the different models of Lake Okeechobee.

Other Units	Conversion Factor
1 BTU/ ft^2/day	0.271
1 kcal/ m^2/hr	2.40
1 watt/ m^2	2.07
1 Einsteins $\text{m}^{-2} \text{ s}^{-1}$	4.6
$^{\circ}\text{C}$	$(^{\circ}\text{F} - 32) / 1.8$
$^{\circ}\text{F}$	$^{\circ}\text{C} - 1.8 + 32$

The net surface heat flux for a lake consists of terms for solar and atmospheric shortwave and longwave radiation, longwave back radiation, lake evaporation, and conduction of heat from/to the water surface (Figure 6-1). The net surface heat flux equation can be written:

$$\phi_n = \phi_s - \phi_{sr} + \phi_a - \phi_{ar} - \phi_{br} - \phi_e \pm \phi_c \quad (6.1-1)$$

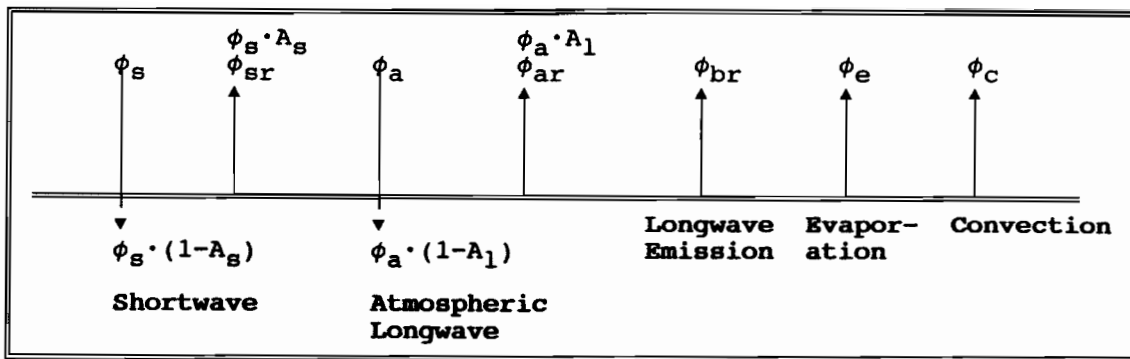


Figure 6-1 Major components of surface heat transfer (adapted from Henderson-Sellers (1986) and others).

The seven terms of the above surface heat flux equation can be simplified to five terms by combining the four terms for the shortwave and longwave radiation from the atmosphere into net shortwave and longwave:

$$\phi_n = \phi_{sn} + \phi_{an} - \phi_{br} - \phi_e \pm \phi_c \quad (6.1-2)$$

6.1.2 Clear Sky Shortwave Radiation

The net shortwave radiation (incident minus reflected shortwave) is calculated as follows in the model (Henderson-Sellers, 1986):

$$\phi_{sn} = \phi_s - \phi_{sr} \approx a_t \cdot (1 - A_s) \cdot \phi_{sc} \cdot [1 - 0.65 \cdot C_1^2] \quad (6.1-3)$$

where a_t = transmission coefficient, A_s = shortwave albedo, ϕ_{sc} = incident solar radiation at edge of atmosphere, and C_1 = fraction of sky covered by clouds.

The net shortwave radiation is the energy used to drive the process of photosynthesis in the model. The assumption we make is that ϕ_{sn} is equivalent to the photosynthetically active radiation (PHAR) used by algae in Lake Okeechobee.

The solar radiation at the outer edge of the atmosphere (ϕ_{sc}) has the value of $2.0 \text{ ly} \cdot \text{min}^{-1}$ at the mean earth-sun distance. The actual solar radiation for any day of the year is calculated from the solar altitude α , which is the angle between the sun's rays and a plane tangent to the earth's surface (or from the zenith angle Z of the incident ray defined in Figure 6-2) and the normalized earth-sun radius. Variation of the normalized radius and of the earth's declination is shown in Figure 6-3.

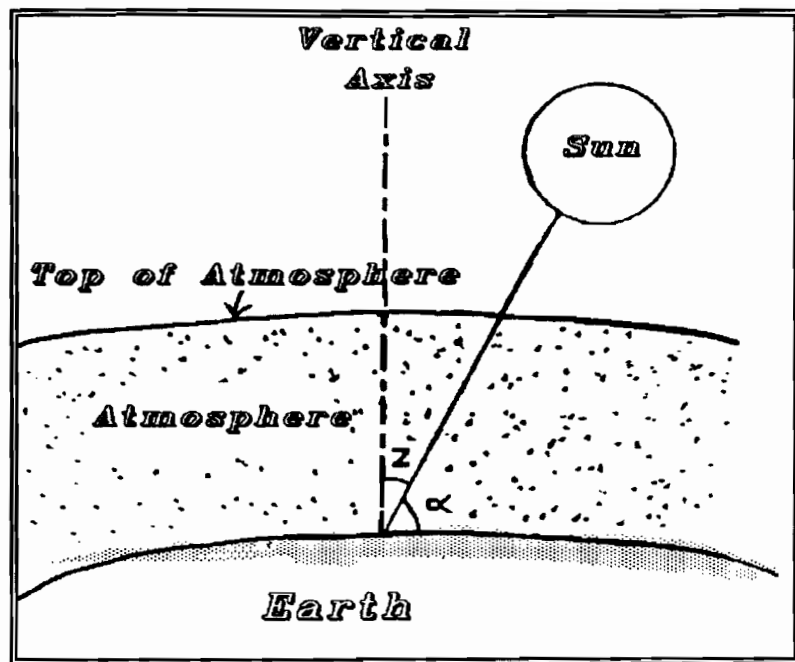


Figure 6-2 Definition of the solar altitude (α) and zenith angle (Z) of the incident solar ray.

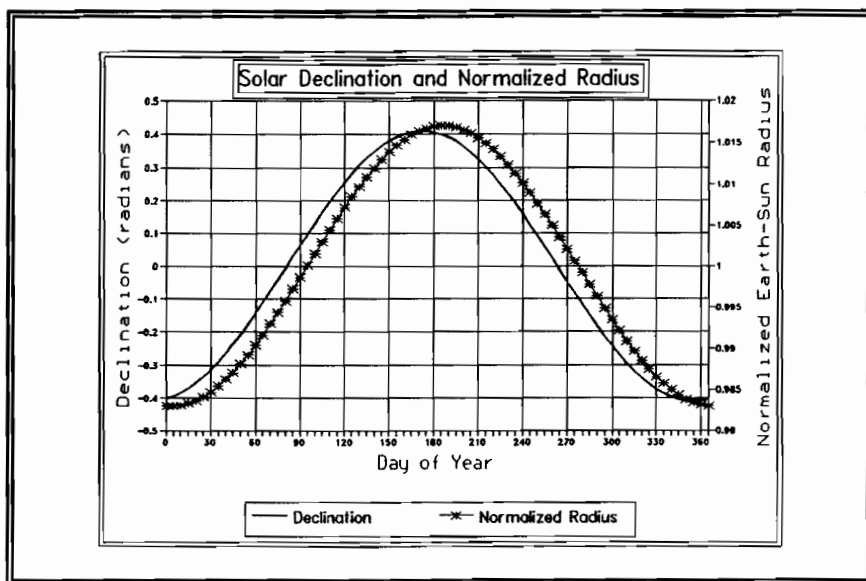


Figure 6-3 Normalized earth-sun radius. Solar declination as a function of M_{day} for the year.

The normalized earth-sun radius (r_{rad}) is the actual radius of the earth orbit divided by the mean radius of the earth orbit (Huber and Perez, 1970):

$$r_{\text{rad}} = 1 + 0.017 \cdot \cos \left[\frac{2 \cdot \pi}{365} \cdot (186 - M_{\text{day}}) \right] \quad (6.1-4)$$

where M_{day} is the number of the day of the year.

The value of ϕ_{sc} at the edge of the atmosphere on any day is $2.0 \cdot \sin(\alpha) \cdot r_{\text{rad}}^{-2}$ $\text{ly} \cdot \text{min}^{-1}$, or $2.0 \cdot \cos(Z) \cdot r_{\text{rad}}^{-2}$ $\text{ly} \cdot \text{min}^{-1}$. The shortwave wavelength ranges from 0.1 μm to 4 μm (Brutsaert, 1980). The net shortwave radiation over Lake Okeechobee without clouds is shown in Figure 6-4 for a typical year. The upper curve is the solar radiation at the edge of the atmosphere and the lower curve the solar radiation at the earth's surface. The shortwave radiation is almost constant for the months May, June, July, and August which is the period of the spring 1989 synoptic data collection.

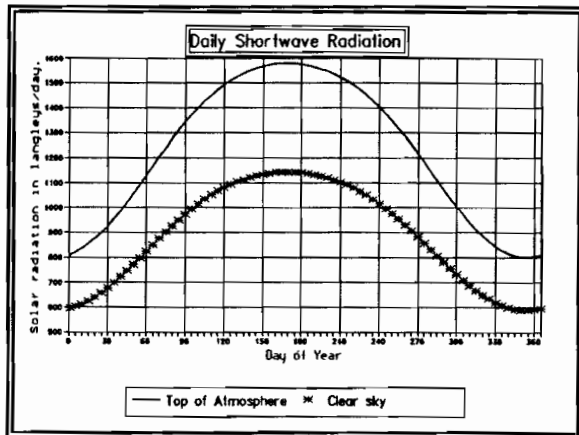


Figure 6-4 Shortwave radiation at the top of the atmosphere at noon and the horizontal clear sky shortwave radiation at the earth surface without clouds.

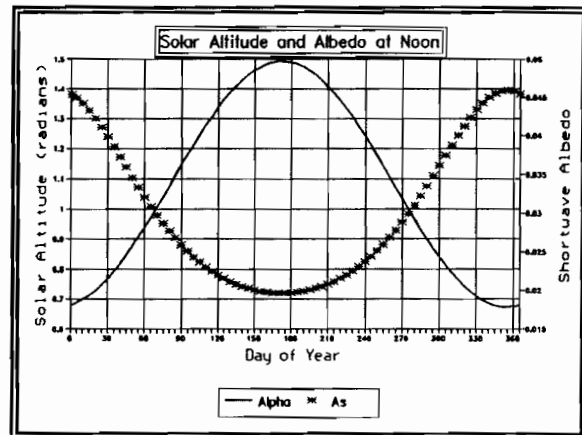


Figure 6-5 Solar altitude and shortwave albedo for Lake Okeechobee.

The solar altitude (α) is calculated from (List, 1966):

$$\sin(\alpha) = \sin(\delta_{\text{decl}}) \cdot \sin(E_\phi) + \cos(\delta_{\text{decl}}) \cdot \cos(E_\phi) \cdot \cos(HR_\alpha) \quad (6.1-5)$$

where δ_{decl} = declination, E_ϕ = latitude, and HR_α = hour angle of the sun.

The above calculation of α is accurate to within 0.05 radians (Holtslag and Ulden, 1983). The solar declination (δ_{decl}) is calculated as a function of the day of the year:

$$\delta_{\text{decl}} = \frac{23.45 \cdot \pi}{180.0} \cdot \cos \left[\frac{2 \cdot \pi}{365} \cdot (172 - M_{\text{day}}) \right] \quad (6.1-6)$$

or, as an arsine function of the solar longitude (Holtslag and Ulden, 1983):

$$\delta_{\text{decl}} = \arcsin[0.398 \cdot \sin(S_L)] \quad (6.1-7)$$

where the solar longitude (S_L) has the units of radians and is function of the day of the year (Holtslag and Ulden, 1983):

$$S_L = 4.871 + 0.0175 \cdot M_{\text{day}} + 0.033 \cdot \sin(0.0175 \cdot M_{\text{day}}) \quad (6.1-8)$$

The shortwave albedo or reflectivity is assumed a function (Figure 6-5) of the solar altitude α (Henderson-Sellers, 1986):

$$A_s = \frac{a_0}{a_0 + \sin \alpha} \quad (6.1-9)$$

where $a_0 = 0.02 + 0.01 \cdot [0.5 - C_l] \cdot \{1 - \sin[\pi \cdot (M_{\text{day}} - 81)/183]\}$

The hour angle (HR_α) through which the earth must turn to bring a location directly under the sun is a function of the declination and latitude (E_ϕ) of a location on earth (List, 1966).

$$HR_\alpha = \frac{12}{\pi} \cdot \arccos[-\tan(\delta_{\text{decl}}) \cdot E_\phi] \quad (6.1-10)$$

or alternatively the hour angle is calculated (Holtslag and Ulden, 1983):

$$\begin{aligned} HR_\alpha &= -L_\phi + 0.043 \cdot \sin(2 \cdot S_L) - 0.033 \cdot \sin(0.0175 \cdot M_{\text{day}}) \\ &\quad + 0.262 \cdot t - \pi \end{aligned} \quad (6.1-11)$$

The hour angle of the sun represents the time difference from noon and thus negative in the morning (Topper et al., 1981). The hour of sunrise (HR_{sr}) and sunset (HR_{ss}) are calculated simply as noon \pm the hour angle (HR_α), and the length of daylight (D_L) is HR_{ss} minus HR_{sr} . The length of daylight over Lake Okeechobee increases from 11 hours in December to 14 hours in June (Figure 6-6).

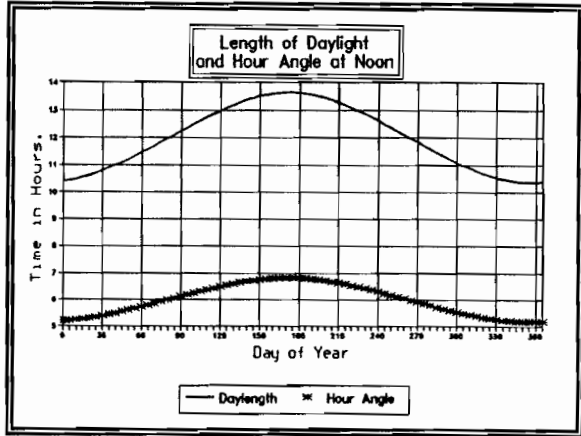


Figure 6-6 Length of daylight and the hour angle at noon.

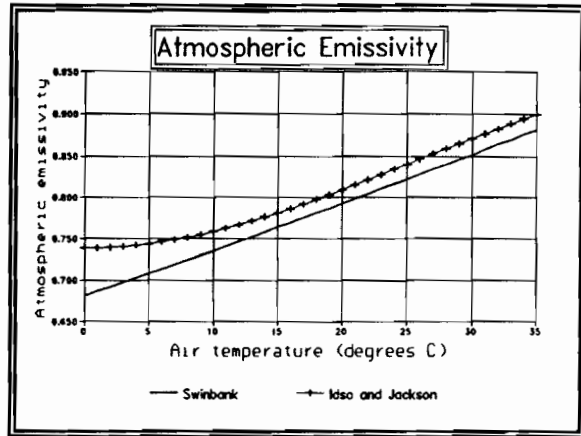


Figure 6-7 Atmospheric emissivity at various air temperatures.

6.1.3 Clear Sky Longwave Radiation

The longwave back radiation wavelength from the lake and atmosphere ranges from 4 to 100 μm (Brutsaert, 1980). The net atmospheric longwave radiation is the radiation emitted by water vapor, carbon dioxide, ozone and aerosols in the atmosphere (Idso, 1981). Longwave radiation is commonly calculated as blackbody emission (Huber and Perez, 1970):

$$\phi_{an} = \phi_a - \phi_{ar} \approx \epsilon_a \cdot \sigma_{sb} \cdot (T_a + 272.16)^4 \quad (6.1-12)$$

where ϵ_a = atmospheric emissivity, T_a = air temperature ($^{\circ}\text{C}$), and σ_{sb} = Stefan-Boltzmann constant.

The atmospheric emissivity in the model is related empirically to air temperature (Figure 6-8), and is a function of the density of H_2O , CO_2 , the $\text{H}_2\text{O}-\text{CO}_2$ overlap, O_3 , trace gases and aerosols (Idso, 1981). The greatest uncertainty in the estimation of atmospheric emissivity is the contribution by aerosols (Staley and Jurica, 1972). Emissivity may be estimated using either the base air temperature above the ground or the surface vapor pressure (Idso, 1981). The LOP0D model uses the base air temperature above the ground. The average of the Swinbank (1963) relationship from Brutsaert (1980):

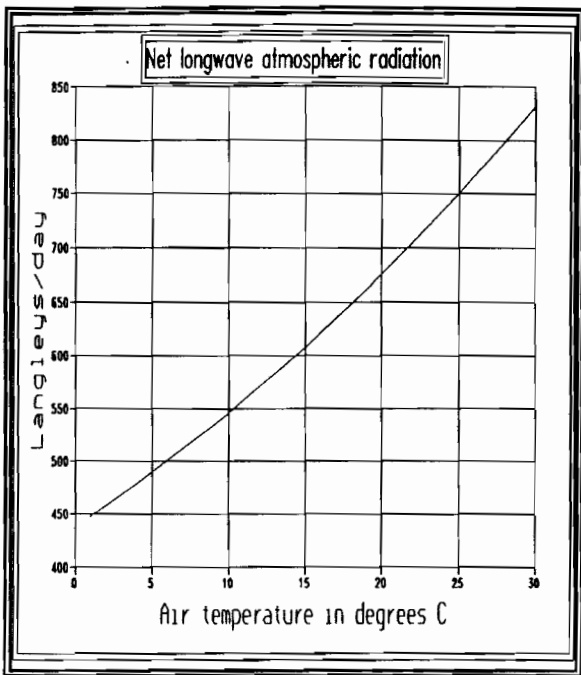


Figure 6-8 Net atmospheric longwave radiation from the water vapor, carbon dioxide and ozone in the atmosphere.

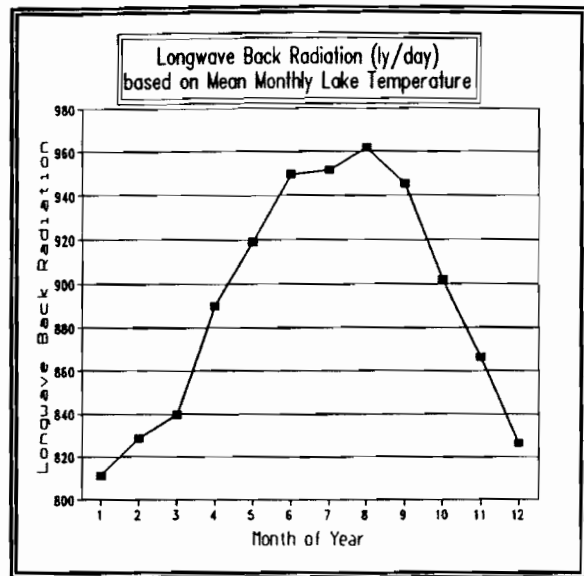


Figure 6-9 Longwave back radiation from the lake surface.

$$\epsilon_a = 3.98 \times 10^{-6} \cdot (T_a + 273.16)^{2.148} \quad (6.1-13)$$

and the Idso and Jackson (1969) relationship is:

$$\epsilon_a = [1 - 0.261 \cdot \exp(-0.000777 \cdot (273.16 - T_a)^2)]^2 \quad (6.1-14)$$

is used to calculate the total emissivity.

The ratio of the diffuse irradiance to direct normal was found to be practically constant on any given day by Peterson and Dirmhirn (1981). Direct measurements of shortwave radiation can then be related to the indirect longwave radiation.

The atmospheric emission is increased by cloud cover and the associated increase in water vapor (Jirka et al., 1977). This cloud effect is modeled as follows (Salhotra et al., 1986):

$$\epsilon_a = \epsilon_{a_0} \cdot (1 + 0.17 C_1^2) \quad (6.1-15)$$

Combining the effects of longwave emission and cloud cover on longwave radiation from the atmosphere results in the following model equation:

$$\phi_{an} = \phi_a - \phi_{ar} \approx 9.36 \times 10^{-6} \cdot \sigma_{sb} \cdot (1 + 0.17 C_1^2) \cdot (1 - A_l) \cdot (T_a + 272.16)^6 \quad (6.1-16)$$

The biota of the lake (especially algae) alter the light and heat regime of a lake by altering the shortwave and longwave reflection from the lake. Large algal reflection of heat wavelengths greater than $0.7 \mu\text{m}$ reduce the heating of the water. Smaller algal reflection of wavelengths less than $0.1 \mu\text{m}$ increase the energy to drive photosynthesis.

6.1.4 Longwave Back Radiation from the Lake Surface

The long-wave back radiation from a water surface (ϕ_{br}) is the largest flux in the energy budget and the most accurate because the emissivity of water is so well known (Adelaja and Adams, 1990). The reflectivity, absorbance and transmittance through a water body must sum to one (Salhotra et al., 1986).

Since water is opaque to longwave radiation the reflectivity and transmittance of water is low and the absorbance is high (Figure 6-10). The long-wave back radiation from the surface of Lake Okeechobee is (Figure 6-9):

$$\phi_{br} = 0.97 \cdot \sigma_{sb} \cdot (T_s + 273.16)^4 \quad (6.1-17)$$

where σ_{sb} = Stefan-Boltzmann constant = 8.26×10^{-11} , cal/cm²/min/°K⁴.

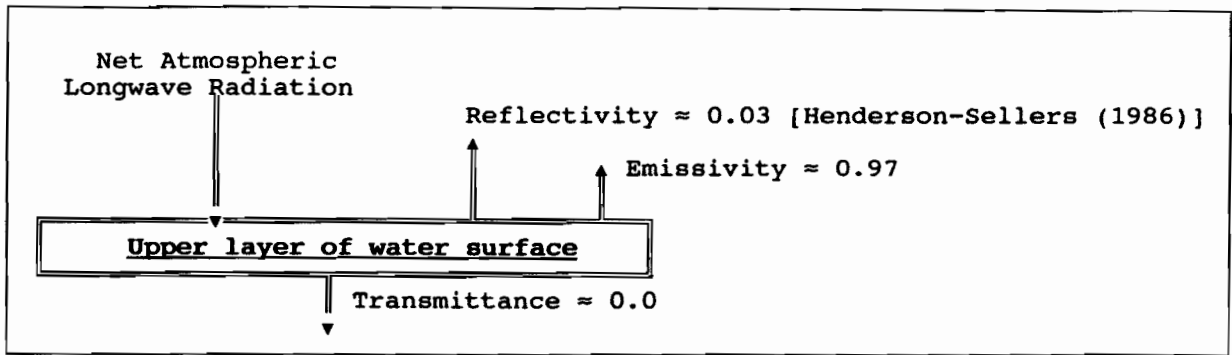


Figure 6-10 The transmittance, emissivity, and reflectivity of longwave radiation from the water surface of Lake Okeechobee.

6.1.5 Atmospheric Cloud Effect on Shortwave and Longwave Radiation

The fraction of the horizontal solar radiation transmitted through the atmosphere to the surface is the parameter a_t (Balling and Cerveny, 1983). The mean annual a_t for the area near Lake Okeechobee is 0.5 (Balling and Cerveny, 1983).

A harmonic analysis of U.S. measured values of a_t found three harmonics that explained most of the variance (Balling and Cerveny, 1983). The maximum values of a_t in Florida are associated with a lack of cyclonic movement and convective storms in late winter and early spring. This is atypical compared to most of the U.S. which has a maximum value of a_t in July. The lowest a_t levels in Florida were due to storms in October and convective systems in April.

The first harmonic explains the annual variance in a_t . It explained 50 percent of the variance in a_t in Florida versus 80 percent for most of the continental U.S. The second harmonic explained the semi-annual variance of a_t and was unusually high in Florida [greater than 60 percent versus an average of 11 percent in the whole U.S.]. The first two harmonics together explained 94.8 percent of the U.S. variance compared to only 75 to 80 percent near Lake Okeechobee. The third harmonic explained peaks of a_t in early April, August, and December. These peaks were four months apart and were due to the combination of low convective and cyclonic activity during these months.

The optical air mass, M , is the ratio of the path length of the solar rays for a given α to the path length through the zenith angle (Huber and Perez, 1970). M is related to the solar altitude (α) after Kasten (1964) from Huber and Perez (1970) in Eq. (6.1-18). The atmospheric transmission, a_t , is calculated from the optical air mass using Eq. (6.1-19) (Huber and Perez, 1970). The solar noon atmospheric transmission has a short range over Lake Okeechobee (Figure 6-11).

$$M = \frac{1}{\sin\alpha + 0.15 \cdot (\alpha + 3.885)^{-1.253}} \quad (6.1-18)$$

$$a_t = 0.74 \cdot M^{0.0882} \quad (6.1-19)$$

The cloudiness functions included in Eqs. (6.1-3) and (6.1-15) are plotted in Figure 6-12. The relation of fraction cloudiness, C_l , to sky cover is shown in Table 6-2. LOP0D uses an average value of cloudiness to vary the solar radiation and lake temperature on a daily basis in Lake Okeechobee. LOP3D uses an average value of cloudiness to vary the solar radiation at the time step used in the simulation, typically 15 minutes to 3 hours.

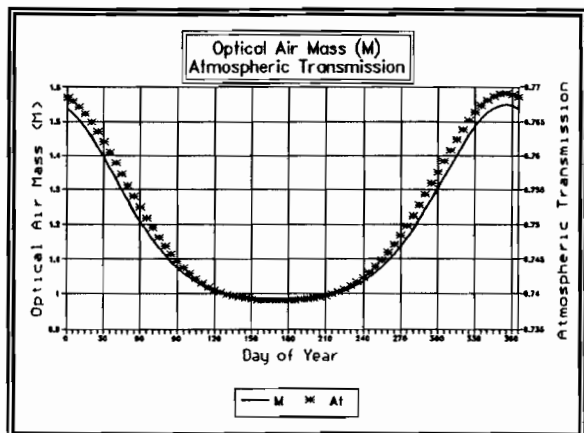


Figure 6-11 The optical air mass and shortwave radiation atmospheric transmission coefficient.

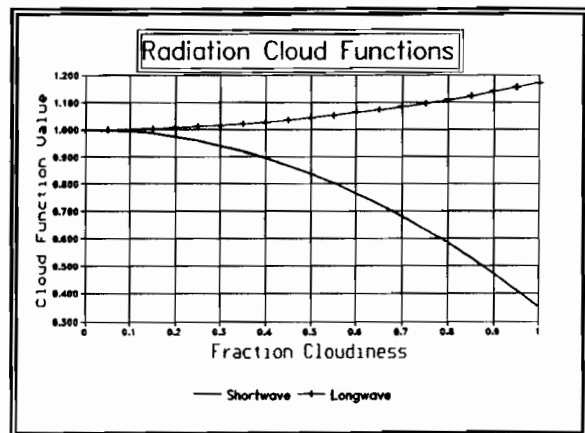


Figure 6-12 The effect of cloud cover on shortwave and longwave radiation. Clouds block shortwave and increase the emission of atmospheric longwave radiation.

Table 6-2 Index of cloud cover index (after Anderson, 1954).

Type of Cloud Cover	Cloudiness Index
Clear sky	0.0
Scattered clouds	0.1 - 0.5
Broken clouds	0.6 - 0.9
Overcast	1.0

6.1.6 Non-radiative Heat Loss from Water Surface

The net nonradiative heat loss is usually written as the sum of evaporation and sensible heat convection while ignoring the gain by precipitation since it does not involve a change of state (Henderson-Sellers, 1986). The evaporative heat flux (ϕ_e , ly/day) is the product of the latent heat of evaporation and the rate of evaporative mass transfer ($\rho_w \cdot E$) across the air-water interface:

$$\phi_e = 2.40 \cdot 3600 \cdot / 1000 \cdot \rho_w \cdot L_w \cdot E \quad (6.1-20)$$

where

$$L_w = 597 - 0.57 \cdot T_s, \text{ latent heat of vaporization [kcal/kg]},$$

or alternatively,

$$L_w = 1.91846 \times 10^6 \cdot [T_s / (T_s - 33.91)]^2$$

where ρ_w = water density (kg/m^3), E = evaporation rate (m/sec), and T_s = water surface temperature ($^\circ\text{C}$). The linear relationship for L_w is plotted in Figure 6-13.

The conductive heat flux, ϕ_c , from the water surface to the atmosphere is related to the evaporative flux, ϕ_e , through the Bowen ratio (B_r):

$$B_r = \frac{\phi_c}{\phi_e} = \frac{T_s - T_a}{0.46 \cdot (e_s - e_a)} \quad (6.1-21)$$

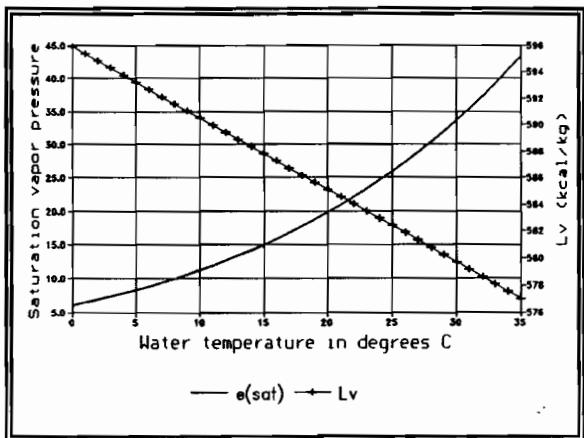


Figure 6-13 Saturation vapor pressure [mbar] and the latent heat of evaporation.

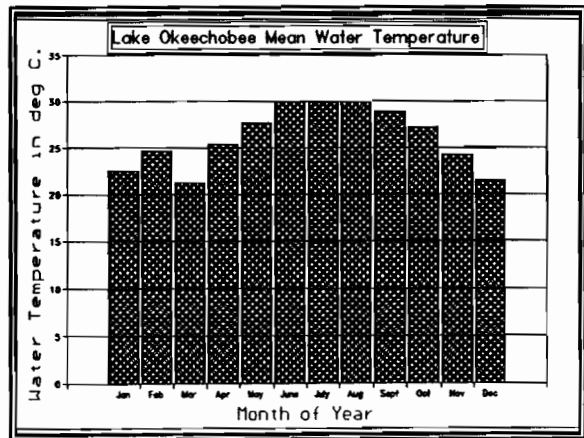


Figure 6-14 Mean monthly Lake Okeechobee water temperature measurements during the years 1988 and 1989.

The Thackston (1974) formula is used to estimate the saturation vapor pressure (for e_s in mbar using the conversion factor of 33.0 to convert in Hg to mbar) (Figure 6-13):

$$e_s = 33.0 \cdot e^{[17.62 - 9500 / (T_a + 460)]} \quad (6.1-22)$$

and the vapor pressure of air (e_a in mbar) is:

$$e_a = R_h \cdot 33.0 \cdot e^{[17.62 - 9500 / (T_a + 460)]} \quad (6.1-23)$$

where R_h = relative humidity (fraction).

6.2 Lake Temperature Model

LOP3D uses average monthly Lake Okeechobee water temperatures based on SFWMD monitoring in the 1970s and 1980s. The mean lake temperature ranges from 15°C to 34°C for the period 1972 to 1989; however, the water temperature for the years 1988 and 1989 was always over 20°C (Figure 6-14).

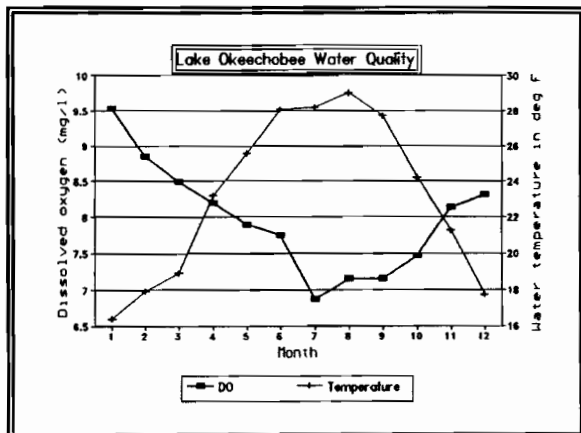


Figure 6-15 Mean monthly water temperature and dissolved oxygen concentration measurements for Lake Okeechobee during the period 1972 to 1987.

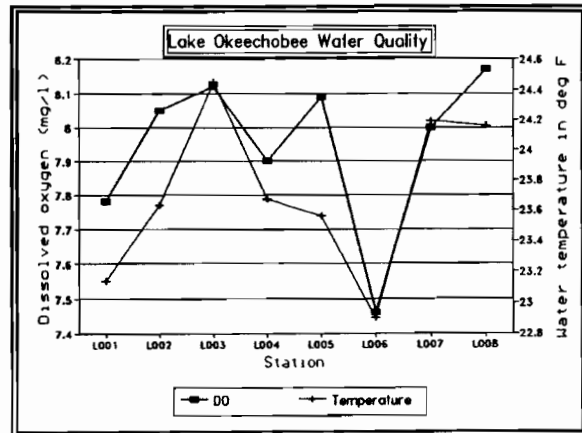


Figure 6-16 Mean station water temperature and dissolved oxygen concentrations measurements for Lake Okeechobee during the period 1972 to 1987.

Synoptic monitoring showed that differential heating between the surface and bottom of Lake Okeechobee resulted in a 3°C variation in daily temperature at the surface and only 1°C at the bottom of the lake (Sheng et al., 1991c). This differential heating promotes density stratification and may inhibit the short term exchange of nutrients, plankton, heat and momentum between layers (Sheng et al., 1989). Cooler air masses above the surface destroy the stratification before sunset every day. Currents were found to increase at 6 p.m. without a corresponding increase in wind, apparently due to the cooling and heating of the lake water. The difference between daily maximum and minimum air temperatures is typically about 20°F (Figure 6-17).

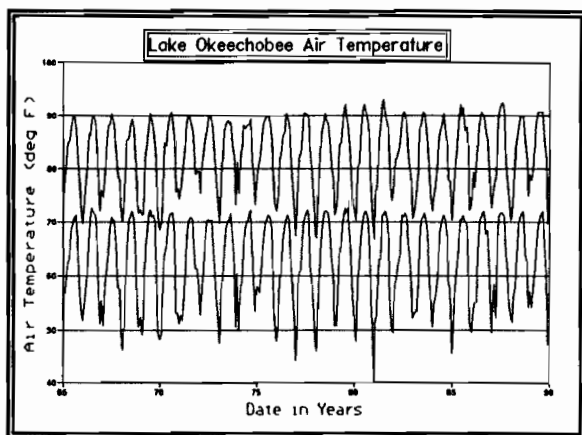


Figure 6-17 Maximum and minimum air temperature for 1965 to 1989.

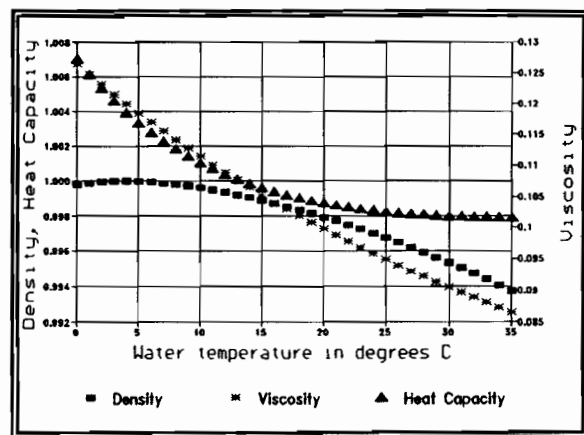


Figure 6-18 Water density [$\text{gm} \cdot \text{cm}^{-3}$], viscosity [$\text{gm} \cdot \text{cm}^{-1} \cdot \text{sec}^{-1}$], and heat capacity [$\text{cal} \cdot \text{g}^{-1} \cdot \text{K}^{-1}$].

A one-dimensional vertical model of heat transport (Adelaja and Adams, 1990) was used in the LOP0D model of Lake Okeechobee. The 1-D equation for temperature (T) may be written:

$$\frac{\partial T}{\partial t} = \frac{1}{A} \cdot \frac{\partial}{\partial z} \left[A_v \cdot A \cdot \frac{\partial T}{\partial z} \right] \quad 0 \leq z \leq H \quad (6.2-1)$$

where A = horizontal area, and A_v = turbulent diffusivity.

The surface boundary condition is:

$$A_v \cdot \frac{\partial T_s}{\partial z} = \phi_n \quad \text{at } z = H \quad (6.2-2)$$

The bottom boundary condition assumes zero heat flux through the lake bottom:

$$\frac{\partial T_s}{\partial z} = 0 \quad \text{at } z = 0 \quad (6.2-3)$$

The LOP0D model has one temperature for each box. Since the area of the box does not change with depth Eq. (6.2-1) can be simplified by canceling the area term:

$$\frac{\partial T}{\partial t} = \frac{\partial}{\partial z} \left[A_v \cdot \frac{\partial T}{\partial z} \right] \quad (6.2-4)$$

A further simplification is possible by linearizing the heat-flux equation:

$$\phi_n = -K_{sht} \cdot (T_s - T_e) \quad (6.2-5)$$

where K_{sht} = transfer coefficient and T_e = equilibrium temperature.

6.3 Additional Temperature-related Parameters

Other temperature-related properties of water used in the various Lake Okeechobee models are the density of water, viscosity of water, and heat capacity of water (Figure 6-18).

The water density (ρ_w), with units of $\text{gm} \cdot \text{cm}^{-3}$, is calculated (Heggen, 1983):

$$\rho_w = (1.0 - 1.9549 \times 10^{-5} \cdot |T_s - 277|^{1.68}) \cdot 1000 \quad (6.3-1)$$

where T is in $^{\circ}\text{C}$. The heat content of water (c_p), with units of $\text{cal} \cdot \text{g}^{-1} \cdot \text{K}^{-1}$, also from Heggen (1983) is:

$$c_p(T) = 0.99716 + 3.979 \times 10^{-4} \cdot f(T) \quad (6.3-2)$$

where

$$f(T) = e^{r1/10.6} + e^{(-r1/10.6)} \quad (6.3-3)$$

in which

$$r1 = 34.5 - T \quad T \leq 34.5^{\circ}\text{C}$$

$$r1 = 2.08 \cdot (T - 34.5)^{2/3} \quad T > 34.5^{\circ}\text{C}$$

The viscosity, η , of water in $\text{gm} \cdot \text{cm}^{-1} \cdot \text{sec}^{-1}$, is calculated for water temperature T_s in $^{\circ}\text{C}$ as:

$$\eta = 0.1 \cdot \exp^{[-1.65 + 262/(T_s + 139)]} \quad (6.3-4)$$

6.4 Vertical Light Attenuation in Water

6.4.1 Disposition of Radiation

The incoming solar radiation at any depth z (ϕ_z) can be described by the equation (Dake and Harleman, 1969)

$$\phi_z = (1 - \beta) \cdot \phi_{sn} \cdot e^{(-\epsilon \cdot z)} \quad (6.4-1)$$

The surface absorption coefficient, β , is approximately 1.0 for longwave radiation (Babajiimopoulos and Papadopoulos, 1986) and 0.0 for shortwave radiation (Figure 6-19).

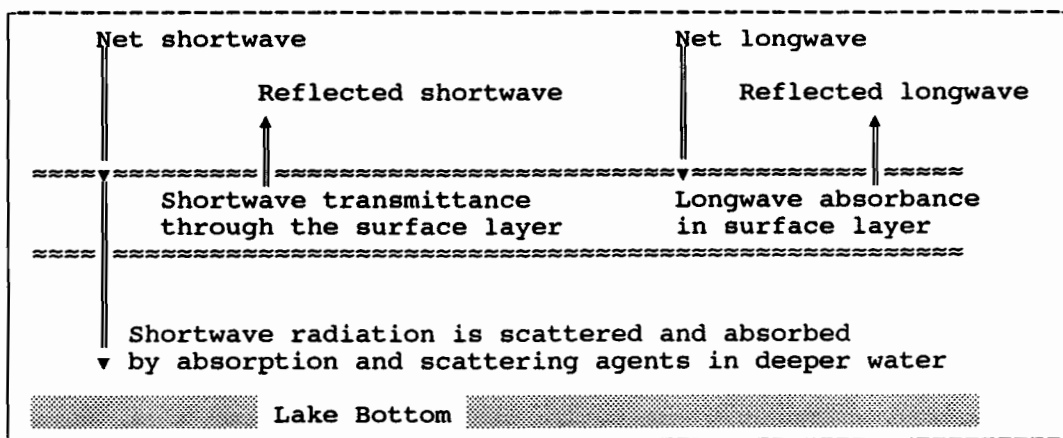


Figure 6-19 Differences in shortwave and longwave pelagic radiation characteristics.

The light extinction coefficient, ϵ , can be related to K_d , the diffuse light attenuation coefficient (units of m^{-1} for both coefficients). K_d is a function of pelagic absorption and scattering agents (Effler et al., 1987b). Pelagic absorption agents include water, dissolved yellow substances (Gelbstoff), which are measured as organic color, and algal cells. Pelagic scattering agents include suspended solids, algae, and suspended calcium carbonate particles (Effler et al., 1987b).

Algal absorption and scattering coefficients are species specific. However, the algal classes in general show distinct characteristics. For example, diatoms scatter more light than green and blue-green algae (Table 6-3) since diatom cells are larger. The use of chlorophyll a concentrations alone to estimate the algal contribution to K_d is not sufficiently valid since measured chlorophyll a includes all algal classes (Effler et al., 1987b).

Table 6-3 Specific absorption (a^*) and scattering (b^*) coefficients of the major phytoplankton classes, adapted from Bricaud et al., 1988. Coefficients have units of m^{-1} per concentration.

Algal Class	a^* ($m^2 mg^{-1}$)	b^* ($m^2 mg^{-1}$)
Diatoms	0.0025	0.241
Green algae	0.0105	0.047
Blue-green algae	0.0199	0.146

Lake specific values of K_d can be found based on a regression analysis using Secchi depth (SD) and assuming a value of $K_d \cdot SD$ equal to 1.9 (Effler et al., 1987b). However, K_d and SD respond differently to changes in absorption and scattering agents and the product of $K_d \cdot SD$ is lake specific (Effler, 1988). Secchi depth is most sensitive to changes in scattering agents and K_d is most sensitive to changes in absorption agents (Effler et al., 1987b). The values of $K_d \cdot SD$ and b/a (to be discussed) are both spatially and temporally variable Effler et al., 1987b).

SD depth, K_d , and photic depth are related since they are all measurements of pelagic light penetration (Figures 6-20 and 6-21). The depth at which 15 percent of the surface light intensity is transmitted is the SD depth (Wofsy, 1983), the 10 percent light level is K_d (Effler et al., 1987b; Davies-Colley and Vant, 1988), and the photic depth is the 1 percent level. The photic depth is approximately $2.3 \cdot SD$ (OECD, 1982) and $4.6/K_d$ (Davies-Colley and Vant, 1988).

Algal cells have sufficient light to photo-synthesize only within the photic depth, but are viable within the mixing depth of a lake as long as they spend sufficient time in the photic zone and their net growth is positive.

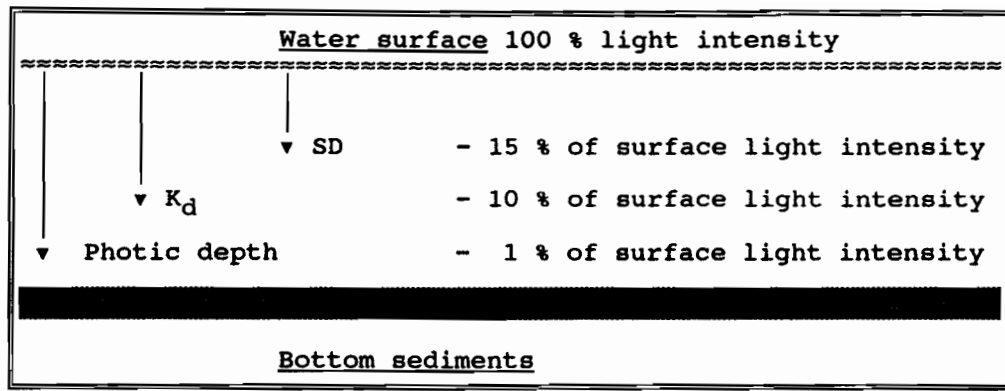


Figure 6-20 Definition of the measured and calculated pelagic light levels for SD depth, K_d , and photic depth.

<u>Permutation a</u>	<u>Permutation b</u>	<u>Permutation c</u>
Water surface =====	Water surface =====	Water surface =====
Photic depth _____	Mixing depth -----	Photic depth _____
Mixing depth -----	Photic depth _____	Lake bottom [diagonal lines]
Lake bottom [diagonal lines]	Lake bottom [diagonal lines]	Mixing depth -----
<u>Permutation d</u>	<u>Permutation e</u>	<u>Permutation f</u>
Water surface =====	Water surface =====	Water surface =====
Lake bottom [diagonal lines]	Lake bottom [diagonal lines]	Mixing depth -----
Photic depth _____	Mixing depth -----	Lake bottom [diagonal lines]
Mixing depth -----	Photic depth _____	Photic depth _____

Figure 6-21 Permutations of mixing depth, photic depth, and the bottom of a lake.

6.4.2 Pelagic Light Absorbance and Scattering Coefficients

A relation for K_d was developed by Effler (1988) from Kirk (1981), who performed a Monte Carlo simulation of light attenuation in water. Their relation for K_d is:

$$K_d = (a^2 + 0.256a \cdot b)^{1/2} \quad (6.4-2)$$

with the absorption (a in Eq. 6-4.2, units of m^{-1}) and scattering coefficients (b in Eq. 6-4.3, units of m^{-1}) being the sum of the individual pelagic adsorption and scattering agents (Effler et al., 1987a).

The most common estimate for the scattering coefficient (b) is found from the measurement of lake turbidity (T_n) using:

$$T_n = \alpha_n \cdot b \quad (6.4-3)$$

where the parameter α_n is a constant that ranges from 0.8 to 1.27 $\text{NTU} \cdot \text{m}$ (Effler, 1988). Lake Okeechobee turbidity, TSS, color and SD depths from 1988 and 1989 (with the exclusion of the month of June due to a low average TSS concentration of $2.50 \text{ mg} \cdot \text{l}^{-1}$) were used to estimate the scattering coefficient (b) for suspended solids (Figures 6-22 and 6-23). During this period the mean turbidity was 19.77 NTU, and the mean TSS $14.6 \text{ mg} \cdot \text{l}^{-1}$. Assuming an average value of $1.0 \text{ NTU} \cdot \text{m}$ for α_n the estimate of the mean total scattering coefficient (b) in Lake Okeechobee is 19.77 m^{-1} .

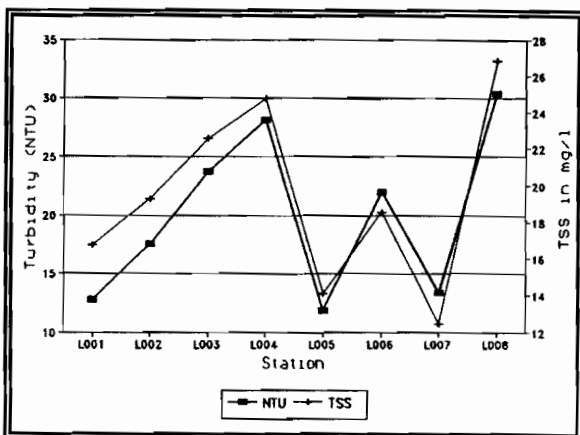


Figure 6-22 Mean turbidity and TSS station concentrations in Lake Okeechobee during 1972-1988.

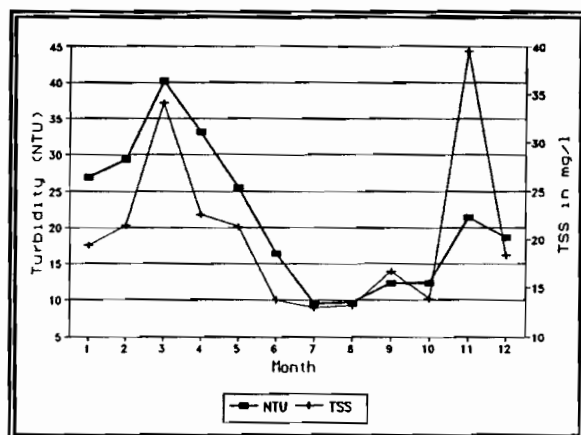


Figure 6-23 Mean monthly turbidity and TSS concentrations in Lake Okeechobee during 1972-1988.

We used an empirical relationship between turbidity and TSS to estimate the contribution of TSS to light scattering. The following equation was obtained from 1988 and 1989 turbidity and TSS data using linear regression:

$$\text{Turbidity} = 6.18 + 1.0 \cdot \text{TSS} \quad (6.4-4)$$

This regression explained 62 percent of the variance in measured turbidity. The scattering attributable due to TSS is [Mean turbidity - 6.18] or 13.6 m^{-1} , which is 69 percent of the total scattering. The estimated light extinction coefficient for TSS is thus $(13.6/\text{m}) \cdot (\text{l}/14.6 \text{ mg}) \cdot (\text{m}^3/1000 \text{ l})$, or a lakewide mean of $0.00095 \text{ m}^2 \cdot \text{mg}^{-1}$ for the years 1988 and 1989.

The universality of the these estimated scattering coefficients was investigated using Lake Okeechobee data from 1972 to 1987. The following equation was obtained from 1972 to 1987 mean station turbidity and TSS data:

$$\text{Turbidity} = 1.34 + \text{TSS} - 6.12 \quad (6.4-5)$$

This linear regression explained 89 percent of the variance in measured turbidity. The scattering attributable due to TSS for each station is [Mean station turbidity + 6.12]/1.34.

The mean station scattering (b) and light extinction coefficients (b/TSS) are shown in Figure 6-24. There appears to be two groupings in the station scattering coefficients for TSS: periphery stations [L001, L005, and L007] which have a mean estimated b of 14 m^{-1} , and central mud zone stations [L002, L003, L004, L006, and L008] which have a mean estimated b of 22.7 m^{-1} . However, the mud stations also have higher mean concentrations of TSS (Figure 6-22), thus the mean b/TSS values in Lake Okeechobee are $0.000986 \text{ m}^2 \cdot \text{mg}^{-1}$ for the 3 periphery stations and $0.01015 \text{ m}^2 \cdot \text{mg}^{-1}$ for the 5 mud stations. The mean lakewide b/TSS of $0.010 \text{ m}^2 \cdot \text{mg}^{-1}$ obtained for the period 1972-1987 is the value used in the models of Lake Okeechobee.

Light extinction coefficients for suspended sediments are usually in the range 0.02 to $0.045 \text{ l} \cdot \text{mg}^{-1}$. Stefan et al. (1982) estimated a light extinction coefficient of $0.045 \text{ m}^{-1} \cdot \text{l} \cdot \text{mg}^{-1}$ for suspended sediments.

A literature review of the linear light extinction coefficients used in other lake and estuary models is presented in Tables 6-4 and 6-5, respectively. Linear extinction coefficients per unit of chlorophyll a ranged from 0.01 to $0.02 \text{ m}^2 \cdot \text{mg}^{-1}$, with a mean of $0.016 \text{ m}^2 \cdot \text{mg}^{-1}$. The background light extinction coefficients for water were more diverse in the literature because this parameter must account for light extinction due to water and organic color.

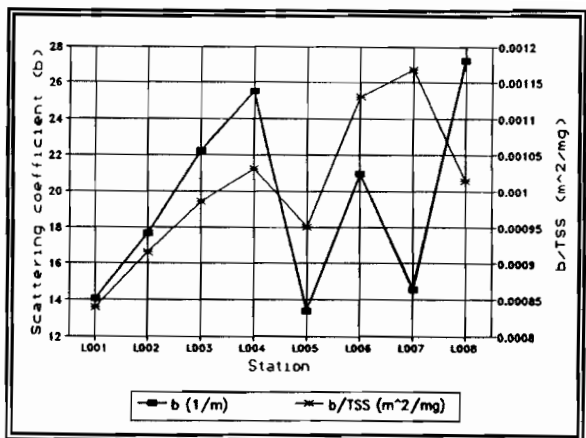


Figure 6-24 Light scattering coefficients (b) and light extinction coefficients (b/TSS) attributable to TSS.

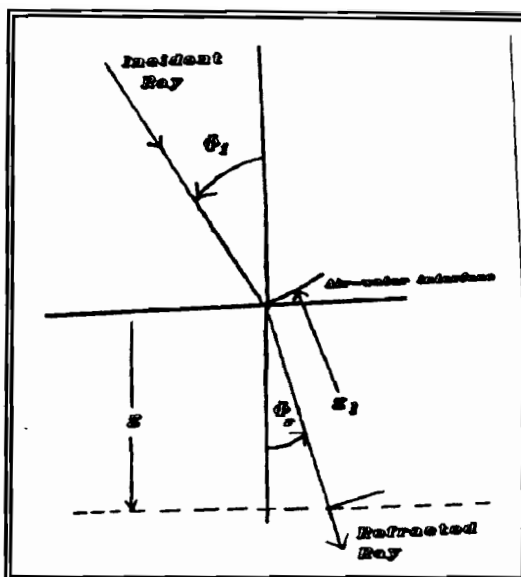


Figure 6-25 Definition of the refracted angle in water of the incident solar ray.

Table 6-4 Linear light extinction coefficients for chlorophyll a .

Field and Effler (1982)	0.0109 $\text{m}^2 \cdot \text{mg}^{-1}$
Shanahan and Harleman (1981)	0.0150 $\text{m}^2 \cdot \text{mg}^{-1}$
Griffin and Ferrara (1984)	0.0088 $\text{m}^2 \cdot \text{mg}^{-1}$
Van Beneschoten and Walker (1984)	0.0430 $\text{m}^2 \cdot \text{mg}^{-1}$
Blosser (1986)	0.0140 $\text{m}^2 \cdot \text{mg}^{-1}$

Table 6-5 Background light extinction coefficients.

Griffin and Ferrara (1984)	0.054 m^{-1}
Van Beneschoten and Walker (1984)	0.33 m^{-1}
Blosser (1986)	0.01 m^{-1}

6.4.3 CaCO_3 Precipitation in Lake Okeechobee

CaCO_3 precipitation, or "whiting" is a common phenomenon in hard water lakes during summer months when the temperature is high (Effler et al., 1987). For example, 32 to 70 percent of the turbidity in Lake Ostico in New York was attributable to whiting during the summer (Effler and Johnson, 1987). Lake

Okeechobee is a hard water lake with high summer water temperatures (Joyner, 1974).

6.4.4 Vertical Light Attenuation Coefficient

The relationship between the Secchi depth (SD) and K_d (Effler, 1988 from Tyler, 1968) is:

$$SD = \frac{8.69}{a + b + K_d} \quad (6.4-6)$$

or relating SD to the coefficients a and b

$$SD = \frac{8.69}{a + b + (a^2 + 0.256 a \cdot b)^{1/2}} \quad (6.4-7)$$

The simultaneous solution of Eqs. (6.4-2), (6.4-3), and (6.4-4) for absorption (a) and scattering (b) coefficients (Effler, 1985) yield lake specific estimates.

Butaka et al. (1989) improved Kirk's (1981) empirical relationship for K_d as a function of time of day, the absorption coefficient (a), and scattering coefficient (b):

$$K_{vsun}(\theta_r) = \frac{1}{\cos\theta_r} \cdot (a^2 + 0.425 \cdot \cos\theta_r - 0.190) \cdot a \cdot b^{1/2} \quad (6.4-8)$$

$$K_{vsky} = 1.168 \cdot (a^2 + 0.162 \cdot a \cdot b)^{1/2} \quad (6.4-9)$$

The combined direct and diffuse radiation can be written as (Butaka et al., 1989):

$$K_d(\theta_r) = F_2 \cdot K_{dsky} + (1 - F_w) \cdot K_{dsun}(\theta_r) \quad (6.4-10)$$

The angle of refraction in water, θ_r , (Figure 6-25) may be found from the solar zenith angle (Z) and the water index of refraction (m) using Snell's Law:

$$m \cdot \sin(\theta_r) = \sin(Z) \quad (6.4-11)$$

The function $f_1(I_z)$ is an exponential attenuation with increasing depth of water by using Beer's Law for irradiance at depth z

$$I_z = I_0 e^{(-\epsilon \cdot z)} \quad (6.4-12)$$

The light extinction coefficient, ϵ , is defined as the summation of the effect of the various absorbing and scattering agents in the water:

$$\epsilon = \epsilon_w + \epsilon_{col} + C_G \cdot \epsilon_g + C_B \cdot \epsilon_b + C_C \cdot \epsilon_c + C_{sed} \cdot \epsilon_s \quad (6.4-13)$$

An integrated Eq. 6.4-12 is used to calculate the mean pelagic solar insolation (I_z) in model LOP0D over the lake box depth y_k :

$$I_z = \frac{I_0 \cdot [1 - \exp^{-\epsilon \cdot y_k}]}{\epsilon} \quad (6.4-14)$$

6.5 Light Limiting Growth Functions

The model contains four formulations for calculating the algal growth limiting factor based on the light intensity or irradiance at a depth z in the water column, I_z (Orlob, 1983; Bowie et al., 1985). All four methods are used to calculate the light limiting function, $f_1(I_z)$, but differ in their approach to photo-inhibition, which is the suppression of algal growth at high light intensities (Field and Effler, 1982). Field and Effler (1982) recommend either Smith's or Bannister's function. The first option is the half saturation or Monod light limitation which is an S-shaped transfer function (Figure 6-26) (this does not model photo-inhibition):

$$f_1(I_z) = \frac{I_z}{K_L + I_z} \quad (6.5-1)$$

The second option is Smith's function (Figure 6-27), (which does not include photo-inhibition):

$$f_1(I_z) = \frac{I_z}{(K_L^2 + I_z^2)^{1/2}} \quad (6.5-2)$$

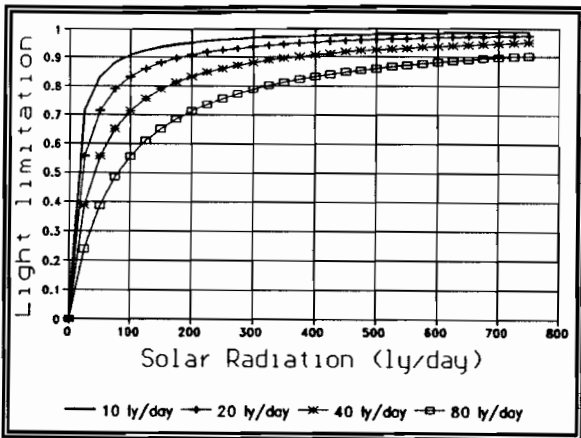


Figure 6-26 Monod light function.

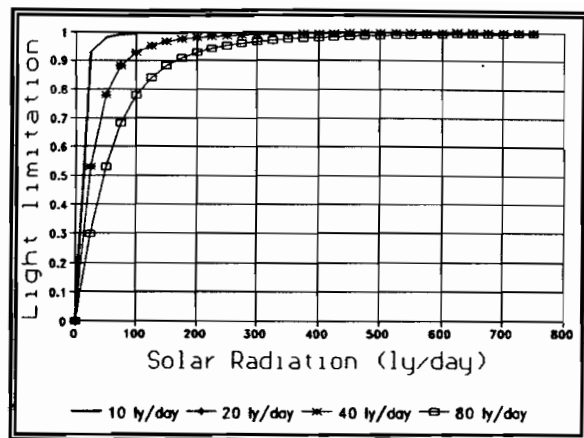


Figure 6-27 Smith light function.

The third option is Bannister's function (Figure 6-28), which also does not include photo-inhibition:

$$f_1(I_z) = \frac{I_z}{(K_L^{2.5} + I_z^{2.5})^{1/2.5}} \quad (6.5-3)$$

The fourth option is Steele's equation (Figure 6-29), which does include photo-inhibition:

$$f_1(I_z) = \frac{I_z}{K_{opt}} \exp \left[1 - \frac{I_z}{K_{opt}} \right] \quad (6.5-4)$$

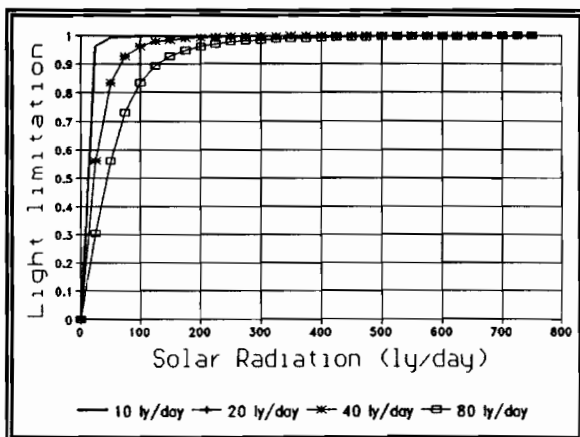


Figure 6-28 Bannister light function.

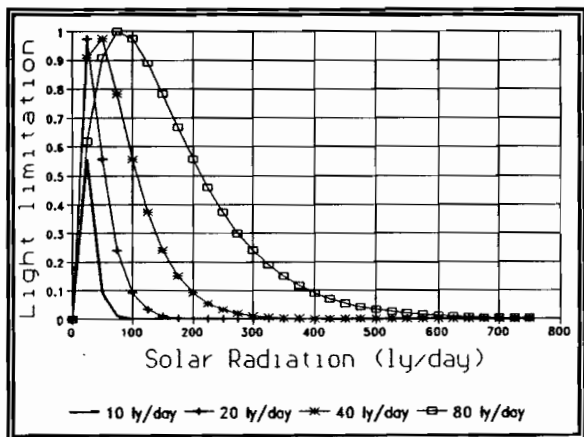


Figure 6-29 Steele light function.

The default model option for light (radiation) attenuation is equation 6.5-1. The half saturation constant, K_L , in that equation is also sometimes called the optimal light intensity, I_{opt} . Literature values for K_L and I_{opt} are shown in Table 6-6.

Table 6-6 Optimal light intensity or the half saturation constant for light limitation.

Source	Optimal light intensity		
Griffin and Ferrara (1984)	GRN	300	ly/day
Salas and Thomann (1978)		200	ly/day
Goldman (1979)		0.025	ly/min
Jorgensen (1983)		0.667	ly/min
Van Benschoten and Walker (1984)		0.024	ly/min
Jaffe (1988)		329	ft/candle
Keesman and Van Stratten (1990)		72-104	ly/day
Boers et al. (1991)	BLU	48	ly/day
	GRN	83	ly/day

The calculation of the mean pelagic solar intensity must include the following factors:

- (1) Vertical variation in solar intensity due to algal self shading, suspended sediment, and background light extinction.
- (2) Diurnal variation in incident solar radiation at the surface.

Simply using the calculated means of pelagic solar radiation and surface solar radiation is inadequate to represent the light conditions algae experience in the water column (Field and Effler, 1982). Thus, the integrated daily mean pelagic light intensity is used in the model. For example, a mean intensity of 100 ly/day can be achieved by many combinations of surface light and light extinction coefficients.

6.6 Temperature Growth Limiting Functions

Temperature effects are simulated using the function $f_2(T)$ that modifies the maximum rate for the various growth, excretion, and decay pathways. Two options for function $f_2(T)$ have been formulated. First is the algorithm from Chen and Orlob (1975) based on measured rate coefficients at 20°C and adjusted by a coefficient of temperature dependence (Table 6-7):

$$f_2(T) = K_{20} \cdot \theta^{(T-20)} \quad (6.6-1)$$

Table 6-7 Coefficients for the temperature dependence of biological rates.

Source	θ
Salas and Thomann (1978)	1.045
Lastein and Gargas (1978)	1.07
Jorgensen (1981)	1.02
Bowie et al. (1985)	1.08
Virtanen et al. (1986)	1.274
Keesman and Van Stratten (1990)	1.05-1.20

The temperature dependence of the coefficient θ is shown in Figure 6-30. The second option is the two stage algorithm of Lehman et al. (1975) that calculates $f_2(T)$ as a function of an optimal temperature for growth:

$$f_2(T) = \exp\{-2.3 \cdot [(T - T_{opt})/(T_{max} - T_{opt})]^2\}^2 \quad T > T_{opt} \quad (6.6-2)$$

$$f_2(T) = \exp\{-2.3 \cdot [(T - T_{opt})^2/(T_{min} - T_{opt})]^2\}^2 \quad T \leq T_{opt} \quad (6.6-3)$$

Equation 6.6-1 is generally used in the models of this study due to the wide literature on coefficient θ (e.g., Table 6-6).

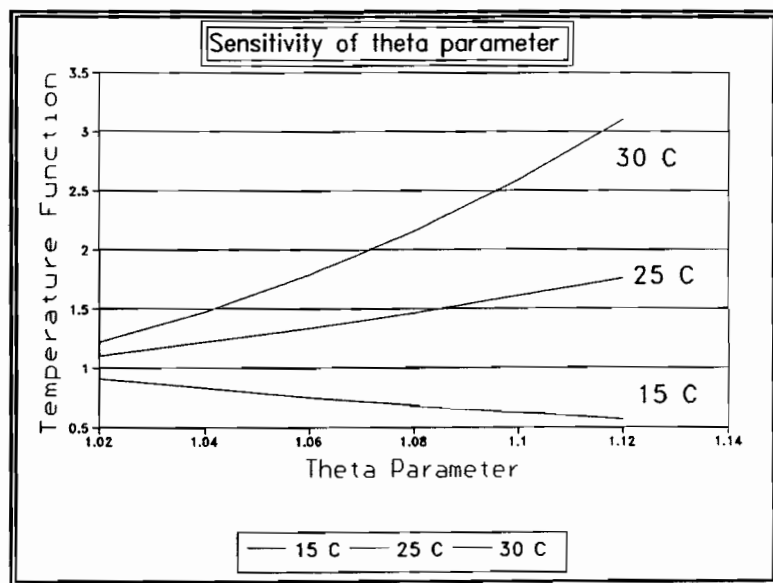


Figure 6-30 Sensitivity of the temperature parameter, θ , used to modify reaction rates.

7. PELAGIC SEDIMENT PHOSPHORUS

7.1 Introduction

Model LOP3D is based on the advection-diffusion equation with cartesian surface coordinates and σ stretched vertical coordinates (see the later discussion in chapters 10 and 11). This conceptualization matches the 3-D suspended sediment model (EHSMSED) of the UF COE group, which in turn is linked to a curvilinear 3-D hydrodynamic model (Sheng et al., 1991a). An important component of LOP3D is the interaction with the 2-D sediment resuspension model, the 3-D pelagic suspended sediment model, and the 1-D diagenetic model of sediment phosphorus [Figure 7-1]. The models have a flux boundary condition at the sediment-water interface to connect the diagenetic model to the 3-D pelagic sediment and multi-component pelagic phosphorus models.

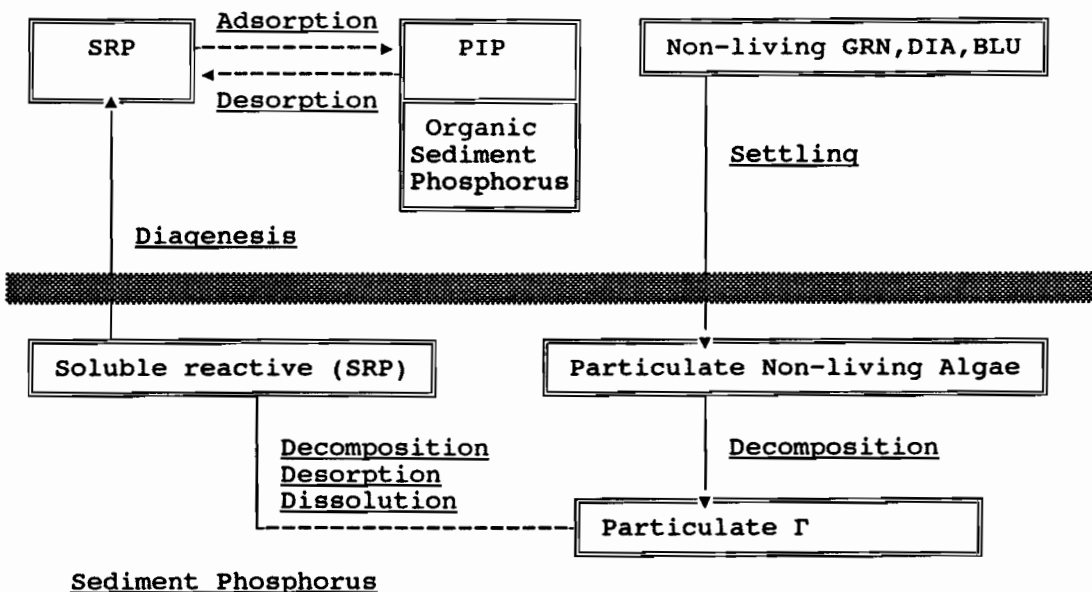


Figure 7-1 Interaction between sediment and pelagic phosphorus.

The wind affects all the major lake components. Wind acts to influence biological activity primarily through direct and indirect effects on the photic zone. For example, increasing wind leads to sediment suspension and compression of the photic zone because the optical properties of the lake are changed by suspended sediments. Wind induced vertical currents can reduce the net settling rates of diatoms and green and blue-green algae. Essentially, the "mixing zone" increases by keeping algae continually suspended and well-mixed in the water column. In addition, wind mixing alters nutrient conditions by increasing or decreasing the local supply of nutrients depending on the antecedent pelagic nutrient conditions (Pollman, 1983).

The effective erosion depth of a shallow lake is approximated by the following function of the effective fetch (L_f):

$$D_{\text{erosion}} = 30.4 \cdot L_f / [L_f + 34.2] \quad (7.1-1)$$

The erosion depth for Lake Okeechobee's fetch length of 48 km is greater than 17 meters, which compared to the lake mean depth (2.6 m) shows that 100 percent of the lake bottom is subject to wind erosive forces. Linear wave theory predicts that Lake Okeechobee's average wind velocity (9 mph) creates an average wave height of 1.4 feet (0.43 m) (Joyner, 1974). In Lake Okeechobee [average depth of 10 feet, (3.05 m)], a wave height in excess of 2 feet (0.61 m) would cause effective mixing to all depths regardless of stage (Blosser, 1986).

Considerable variation exists in the nature of Lake Okeechobee's bottom sediment (Figures 7-2 and 7-3). The model characterization is shown in Figure 7-4.

7.2 Pelagic Adsorption-Desorption

The particulate inorganic phosphorus (PIP) pathway in the pelagic zone is an algebraic relation involving exchangeable inorganic phosphorus on the suspended sediment (C_p) and the pelagic dissolved SRP (C_{aq}) as shown in Figures 7-5 and 7-6. The equations described in this chapter are used in models LOP0D and LOP3D.

There are two equations and two unknowns (the ending PIP and SRP concentrations at the $n+1^{\text{st}}$ time step) involved in the solution of the PIP and SRP pelagic dynamics. The two equations are the linear relationship between C_p and C_{aq} at the n^{th} , or beginning time step

$$\frac{C_p^n}{C_{\text{sed}}^n} = K_{\text{sp}} \cdot C_{\text{aq}}^n \quad (7.2-1)$$

where C_p , C_{aq} and C_{sed} are the concentrations of PIP, SRP and sediment, respectively. At the $n+1^{\text{st}}$, or ending time step

$$\frac{C_p^{n+1}}{C_{\text{sed}}^{n+1}} = K_{\text{sp}} \cdot C_{\text{aq}}^{n+1} \quad (7.2-2)$$

The linear relationship is the same as the Freundlich adsorption isotherm with the exponent n in $C_{\text{aq}}^{1/n}$ (not to be confused with the old time step n) equal to 1.

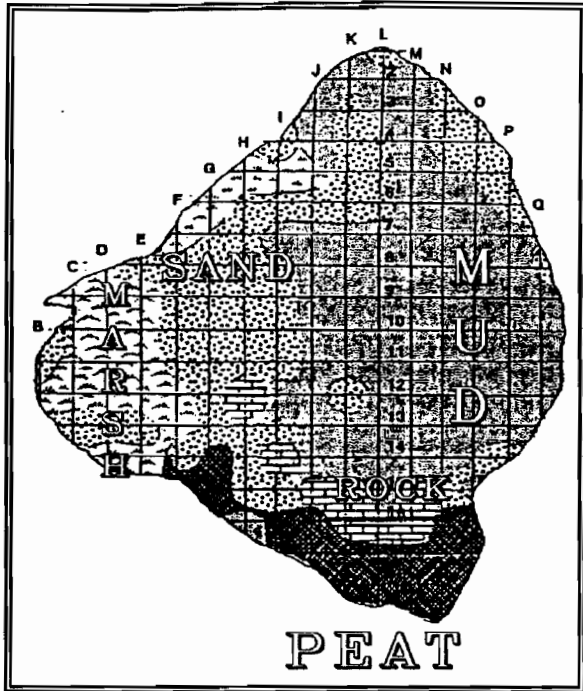


Figure 7-2 Bottom sediment map from Reedy et al. (1991).

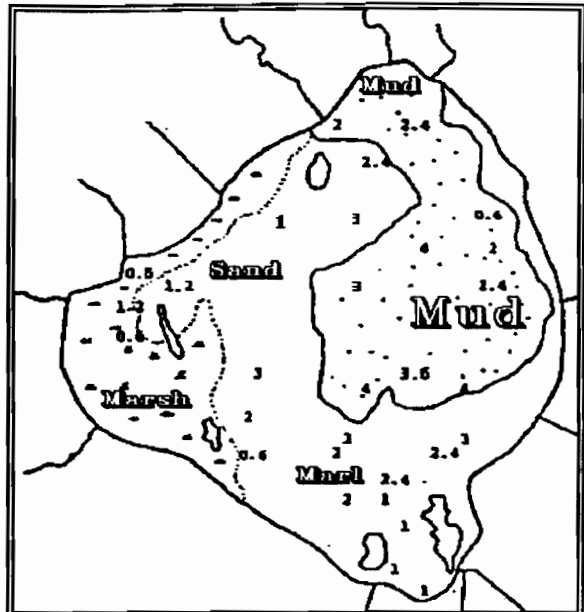


Figure 7-3 Bottom sediment map from Messer et al. (1979).

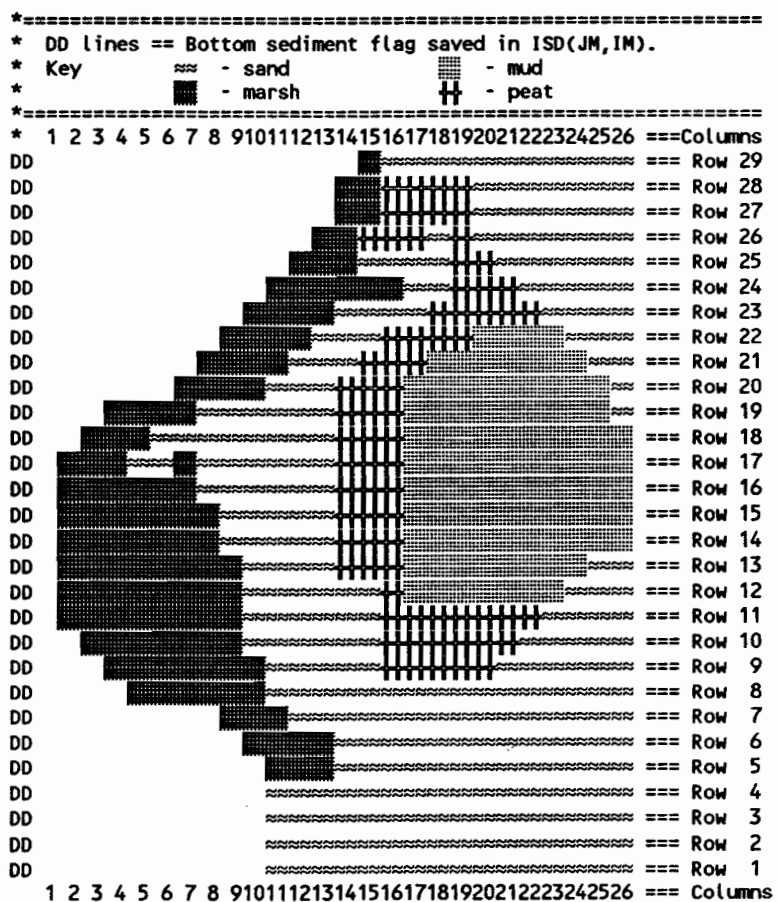


Figure 7-4 Bottom sediment flag for the bottom of lake.

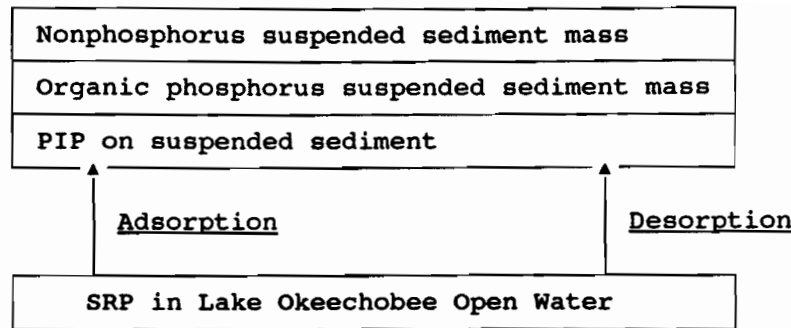


Figure 7-5 Relationship between PIP and SRP in open water. Organic phosphorus is unreactive with SRP.

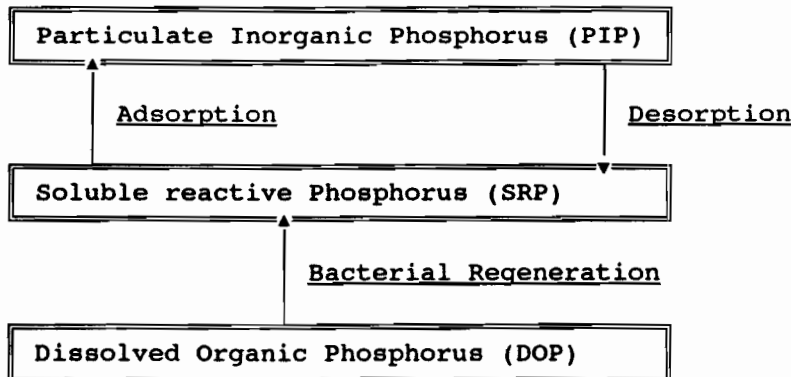


Figure 7-6 Relationship between PIP and DOP is through SRP.

However, we still need an equation relating the $n+1^{\text{st}}$ time step to the n^{th} time step. Two other equations are possible using the created variable δ_m , which is defined as the change in SRP or PIP concentration during the time step. Using $\delta_m \leq 0$ for desorption from the sediment to the water and $\delta_m > 0$ for adsorption from the water to the sediment, the following two algebraic relations are defined:

$$C_{\text{aq}}^{n+1} = C_{\text{aq}}^n - \delta_m \quad (7.2-3)$$

$$\frac{C_p^{n+1}}{C_{\text{sed}}^n} = \frac{C_p^n}{C_{\text{sed}}^n} + \frac{\delta_m}{C_{\text{sed}}^n} \quad (7.2-4)$$

Solving for the change in concentration (δ_m) algebraically:

$$K_{sp}C_{aq}^{n+1} = \frac{C_p^n}{C_{sed}^n} + \frac{\delta_m}{C_{sed}^n} \quad (7.2-5)$$

$$K_{sp}C_{aq}^n - K_{sp}\delta_m = \frac{C_p^n}{C_{sed}^n} + \frac{\delta_m}{C_{sed}^n} \quad (7.2-6)$$

$$\delta_m = \frac{K_{sp}C_{aq}^n C_{sed}^n - C_p^n}{1.0 + K_{sp}C_{sed}^n} \quad (7.2-7)$$

The model solves for δ_m at the end of every time step by using the known partition coefficient, n^{th} sediment concentration, n^{th} SRP concentration, and n^{th} PIP concentration.

The linear partition coefficient based on calibration and literature search is 500 l/kg (liters per kilogram) for the mud and peat sediment and 100 l/kg the sand and littoral zone sediments. The model uses a partition coefficient with units of 1/mg to correspond to the suspended sediment unit of mg/l.

Example desorption or adsorption calculations for a mud zone partition coefficient of 0.0005 l/mg and suspended sediment concentration under 250 mg/l show that desorption will occur for SRP concentrations less than 20 ug/l and adsorption for SRP concentrations greater than 20 ug/l. A typical desorption is 0.268 ug for the combination of SED = 50 mg/l and SRP = 10 ug/l, and a typical adsorption is 0.638 ug for the combination of SED = 50 mg/l and SRP = 50 ug/l.

7.3 Sediment Organic Phosphorus and PIP

The primary forms of sediment organic phosphorus (SOP) are labile organic P associated with microbial biomass; moderately labile organic P - extracted with HCL; moderately resistant organic P or fulvic acid P_o ; and highly resistant organic P or humic acid P_O and resistant organic P not extractable with HCL and NaOH (Reddy et al., 1991).

Within the original project proposal, three components of phosphorus were to be modeled in the water column: particulate organic phosphorus (POP), particulate inorganic phosphorus (PIP), and soluble reactive phosphorus (SRP) or dissolved inorganic phosphorus (DIP). There were major problems with this approach: PIP was not measured during the synoptic surveys, a major form of phosphorus (dissolved organic phosphorus, DOP) was not measured, and the importance of organic phosphorus on the suspended sediment was not understood. The historical data

surveys and the current synoptic surveys measured (and continue to measure) mainly SRP and total phosphorus (TP), except for the synoptic surveys associated with this study that measured total dissolved phosphorus (TDP).

Isotherm data assembled by the Soil Science group (Reddy et al., 1991) from their sediment work as part of the project included anaerobic and aerobic sediments. The aerobic decomposition of the organic phosphorus was substantially faster (20 days versus 120 days).

7.4 Wind Fields Near Lake Okeechobee

Intensive meteorological data for Lake Okeechobee are limited. Three-hour wind data are available at Port Mayaca, Okeechobee and Clewiston prior to 1980 but were not collected after that date. The nearest three hour wind station is in West Palm Beach. Daily wind movement over the pan evaporation stations is available for Port Mayaca, Okeechobee and Clewiston (locations are shown in Figure 5-1). Moreover, cumulative monthly wind movement data are available from Moorehaven, Florida by the National Oceanographic and Atmospheric Administration with units of miles per month. The Moore Haven meteorological period of record is from 1950 through 1989.

Average wind speeds at Moore Haven are shown in Figure 7-7, in which lower velocities in the summer are obvious. Because shear stress is proportional to the square of wind speed, an even greater seasonal distinction can be seen in Figure 7-8, and a corresponding seasonal difference in erosive capability.

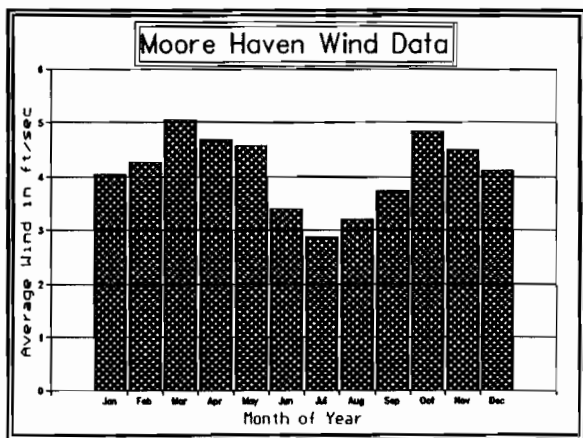


Figure 7-7 Mean monthly wind at Moore Haven.

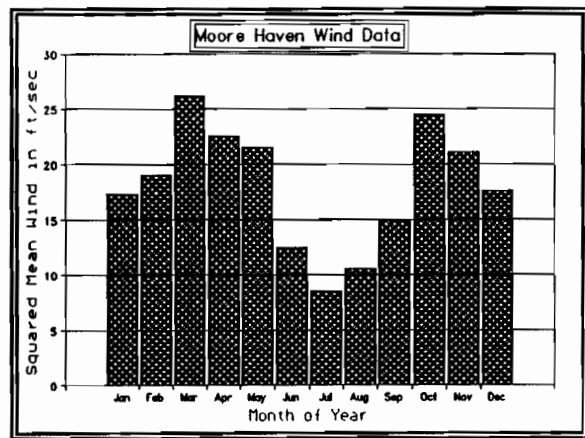


Figure 7-8 Mean squared monthly wind at Moore Haven.

The most common wind direction during the summer is from the southeast in South Florida (Pielke, 1974). The typical pattern of summer afternoon thunderstorms in Florida is radically changed because of the presence of Lake Okeechobee. The cooling effect of the lake suppresses convergence (Pielke, 1974) and minimizes cloud formation over the lake in the summer. This is readily apparent from weather photographs of South Florida, which typically show a hole in the cloud cover over Lake Okeechobee. Pielke's (1974) three dimensional atmospheric model predicts that the lake breeze generated by Lake Okeechobee reinforces the convergence pattern east of the lake generated by the regional sea breeze.

The summer pattern of little cloud cover means more solar radiation reaches the lake, increasing the water temperature and maximizing algal uptake. The rainfall and wind over the lake is minimal in the summer due to this effect.

7.5 Lake Okeechobee Wind Model

The wind model used in the mass balance model of Lake Okeechobee (Task 6.2) is derived from the models of Blosser (1986) and Pollman (1983) which in turn are based on the Sverdrup-Munk-Bretschneider (SMB) wave model (U.S. Army CERC, 1977). The SMB model is a semi-empirical representation of wave generation in shallow water. The method is based on successive approximations in which wave energy due to wind stress is subtracted from wave energy due to bottom friction and percolation. The model requires wind speed over the lake, fetch length and water depth. The model output includes significant wave height (H_s in m) and significant wave period (T_s in seconds).

The wind energy shear stress is calculated from the air wind speed and air density:

$$\tau_a = C_d \cdot \rho_a \cdot W_a^2 \quad (7.5-1)$$

where τ_a = surface shear stress, N/m²; ρ_a = air density, kg/m³; W_a = wind speed at a point 10 meters above the ground, m/sec; and C_d = 0.001 for wind speeds less than 5 m/sec.

The wind energy is transferred from the atmosphere, making surface waves in the lake. The energy of the surface waves makes the water move in an orbital motion. U_m is the maximum orbital velocity outside the bottom wave boundary layer, and is calculated from H_s and T_s .

Blosser (1986) used the following predictive equations for the wave height and wave period in Lake Okeechobee:

$$H_s = 5.22 \cdot W_{\text{mph}}^{0.7454} \quad (7.5-2)$$

and

$$T_s = 0.7541 \cdot W_{\text{mph}}^{0.4389} \quad (7.5-3)$$

where H_s has units of cm, T_s seconds, and wind velocity mph. The model assumptions are a constant depth of 10 feet (3.05 m) in Lake Okeechobee and a fetch length of 15 miles (24 km).

The over-lake wind speed based on nearby land wind stations needs to be corrected for measurement height and the difference in air-water interface temperature (Schwab and Morton, 1984). The correction factor is usually 1.2 (SethuRaman and Raynor, 1981). The wind movement above the evaporation gage at Moore Haven was measured at a height of 2 meters. A power law profile for wind speed uses an exponent of (1/7) for changing the wind speed from that measured at 2 m to an estimated wind speed at 10 m (Schwab and Morton, 1984). The wind speed is increased by a factor $(10/2)^{1/7} = 1.26$ to be usable in the wind shear formulas. The relationship between over-lake wind speed and land wind speed is also a function of the wind speed class and the air-lake temperature difference. Neglecting the wind speed class and air-lake temperature difference the best predictor of over-lake wind speed (W_w) is a constant $1.18 \cdot W_1$ in the Great Lakes (Schwab and Morton, 1984). We use a value of $1.26 \cdot 1.18 = 1.44$ to estimate the mean over-lake wind speed in Lake Okeechobee at a height of 10 meters. The calculation of the average daily wind is better approximated by doubly weighting the evening winds (Barnstan et al., 1983). Using the same procedure the mean daily wind speed coefficient over Lake Okeechobee is 1.44^*3 . This is used in the model LOP0D to estimate over-lake wind speed.

The Sheng and Lick (1980) sediment model uses the results of the SMB wave model in an approximation of the maximum horizontal velocity at the bottom boundary caused by the periodic wave. The maximum horizontal velocity, U_m , and the wavelength, L_d [m], associated with the oscillatory motion are computed from the following equations:

$$U_m = \frac{\pi \cdot H_s}{[T_s \cdot \sinh(2 \cdot \pi \cdot Y_k/L_d)]} \quad [\text{cm/s}] \quad (7.5-4)$$

$$L_d = L \cdot \tanh(2 \cdot \pi \cdot d/L) \quad (7.5-5)$$

$$L = \frac{g \cdot T_s^2}{2 \cdot \pi} \quad [\text{m/s}^2 \cdot \text{s}^2] \quad (7.5-6)$$

Next, assuming that the shear stress due to wave action is much more significant than shear stress due to large scale currents, the bottom shear stress generated by the periodic motion of the waves, τ_b , is:

$$\tau_b = 0.5 \cdot \rho_w \cdot f_w \cdot U_m^2 \quad [\text{gm/cm}^2 \cdot \text{cm}^2/\text{sec}^2] \quad (7.5-7)$$

The erosion flux (F_e) is determined by excess shear stress above the critical shear stress for bed movement, τ_{crm} , using the following set of equations:

$$\tau_{br} = \tau_b / \tau_{crm} \quad (7.5-8)$$

$$\tau_{br} = 0.5 \cdot [\tau_{br} - 1] + |\tau_{br} - 1| \quad (7.5-9)$$

$$F_e = C_{susp} \cdot \tau_{br} \quad [\text{sec/cm} \cdot \text{gm/cm/sec}^2] \quad (7.5-10)$$

where C_{susp} = resuspension rate (sec/cm). τ_{crm} was estimated to be 0.1 N/m^2 [0.01 dynes/cm²] by Hwang and Mehta (1989). However, we use a value of 0.30 dynes/cm² in model LOP0D.

The wave friction factor (f_w) is a function of the wave boundary layer and bottom roughness characteristics. Typically a value of 0.004 is used for f_w (Blosser, 1986; Sheng et al., 1991a). The respective conditions for deposition from the pelagic to the sediment and erosion from the sediment to the pelagic are:

$$\tau_b < \tau_{crm} \quad (7.5-11)$$

$$\tau_{cr} < \tau_b < \tau_{crm} \quad (7.5-12)$$

The maximum value of τ_b is restricted to be less than 1.5 dynes in model EHSMSD (Sheng et al., 1991a) and models LOP0D and LOP3D. A C_{susp} value of $1.2 \times 10^{-7} \text{ s/cm}$ [0.01037 day/cm] was used by Sheng et al. (1991a) in their 3-D model of the suspended sediment of Lake Okeechobee. The erosion rate, E_r , (cm/sec) is calculated from the erosion flux and sediment density:

$$E_r = F_e / \rho_s \quad [\text{gm/cm}^2/\text{sec} \cdot \text{cm}^3/\text{gm}] \quad (7.5-13)$$

The pelagic TSS concentration is correlated with the cubic wind speed (Hellstrom, 1991). Sand has little effect on algal growth dynamics since it quickly settles from the water column. Fine silt or mud resuspended in the water column

may reduce the algal uptake by 10 to 20 percent since it remains suspended for many days. The residence time of resuspended inorganic sediment (\approx 7 days) is longer than the residence time for resuspended organic sediment (\approx 3 days) Hellstrom (1991). This is simulated in the models by using different settling velocities for PIP and ORG sediment phosphorus.

7.6 Magnitude of Internal Wind Loading

An estimate of the magnitude of the internal loading of TP to the pelagic Lake Okeechobee can be obtained by using the time history of stage, TP, and loading in Lake Okeechobee. The monthly internal loading is:

$$\text{Internal Load} = ([V \cdot TP]^{n+1} - [V \cdot TP]^n - [Q \cdot TP]_{in} - [Q \cdot TP]_{out}) / A^{n+1} \quad (7.6-1)$$

where $n+1$ is the new month's volume, outflow and volume weighted mean lake TP concentration and n is the old month's volume, outflow, and lake TP concentration. The monthly loading of TP includes tributary loading plus precipitation loading minus the estimated surface outflow loading from the lake (De Groot, 1983).

The estimated net internal loading for Lake Okeechobee is 3356 mg/m² to the bottom sediments (Figure 7-9). The minimum monthly, -194 mg/m², maximum monthly, 152 mg/m², and average monthly, -32.3 mg/m² shows the wide variability in monthly internal loading. The average monthly loss to the sediments almost matches the mean monthly tributary loading, 35.8 mg/m². Thus, the sediments, through the process of algal settling and inorganic phosphorus deposition, remove 91 percent of the phosphorus loading to Lake Okeechobee.

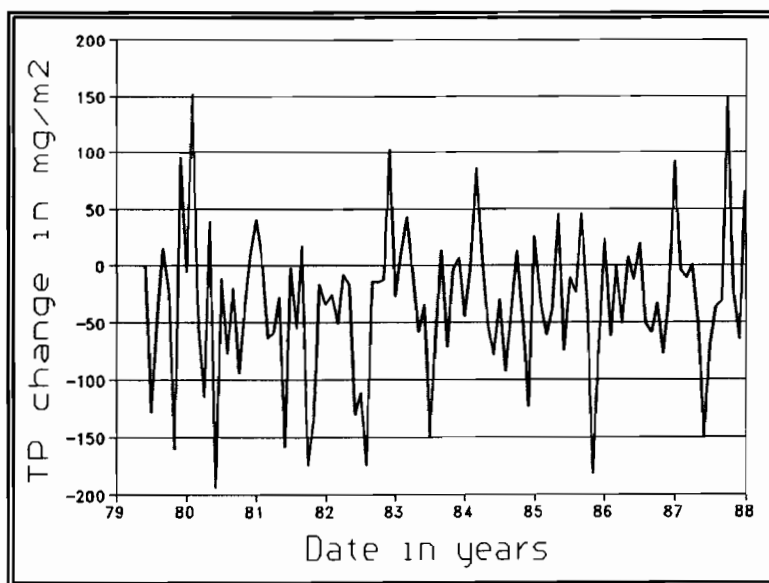


Figure 7-9 Estimated internal loading from Lake Okeechobee for the years 1979-1988.

7.7 Interaction with Diagenetic Model

The calculation of the bottom diffusive flux of inorganic phosphorus (SRP) from the sediment to the pelagic involves the daily update of the diffusive flux by Subroutine SDIAG. The model calculates the flux based on the previous day's mean pelagic SRP concentration. The added pelagic SRP concentration (ΔM in units of mg/m^3) from the diffusive flux (F_{srp}) is calculated as:

$$\Delta M = \Delta t \cdot F_{\text{srp}} / Y_k \quad [\text{day} \cdot \text{mg/m}^2/\text{day}/\text{m}] \quad (7.7-1)$$

The interstitial water in the sediment also contains dissolved inorganic phosphorus, or SRP, which becomes entrained into the pelagic zone during resuspension events. The added pelagic concentration of this erosion-entrained SRP is computed from the pelagic depth, Y_k , and sediment porosity, ϕ , as:

$$\Delta M = \Delta t \cdot F^e \cdot C_{\text{srp}} \cdot \phi / Y_k \quad [\text{day} \cdot \text{cm/day} \cdot \text{mg/m}^3/\text{m}/Z_{\text{ref}}] \quad (7.7-2)$$

7.8 Interaction with Deposition-Resuspension Model

The sediment organic phosphorus (ORG) is related algebraically to the suspended sediment in the water column using the partitioning coefficient (K_{org}) and the equation:

$$C_{\text{org}}^{n+1} = K_{\text{org}} \cdot C_{\text{sed}}^{n+1} \quad (7.8-1)$$

at the new time step $n+1$.

Kirby et al. (1989) and Hwang (1989) hypothesized a fluidized mud layer called the lutocline that may range up to 10 cm in depth. The lutocline has a lower density ($\leq 1.065 \text{ g} \cdot \text{cm}^{-3}$) and a near zero shear strength, implying the mud of the lutocline essentially behaves as a fluid. Conversely, the shear strength of the mud and sand just below the lutocline is generally three times the critical shear stress for erosion according to Kirby et al. (1989).

Phosphorus can be extracted from lake sediments by various methods (Table 7-1). Istvanovics (1988) measured a total phosphorus content of $721 \text{ mg P} \cdot \text{kg}^{-1}$ dry weight in hypereutrophic Lake Balaton (Hungary) sediments. Brezonik et al. (1989) measured values for total phosphorus of 1188, 1306, 866, 1517, 305, 1604, 1395, 1246 mg P/kg dry wt. in the upper 1 cm of eight Lake Okeechobee sediment cores. This is an average of 1178 mg P/kg dry wt. in Lake Okeechobee. Similar results were found by Reddy and Ivanoff (1990) and are presented in Table 7-2. An earlier study by Messer et al. (1979) found an average total phosphorus concentration of

Table 7-1 Extractable phosphorus in sediments (adapted from Reddy et al., 1991).

Extraction Method	Type of Phosphorus Extracted from Sediment
Sodium Hydroxide NaOH-SRP Extraction	Iron (Fe) and Aluminum (Al) bound phosphorus, and labile organic phosphorus.
Sodium Hydroxide NaOH-ORP Extraction	Hydrolyzable organic phosphorus calculated as NaOH-TP - N.
Hydrogen Chloride HCl-P Extraction	Calcium (Ca) bound phosphorus or apatite inorganic phosphorus (AIP).
Potassium Chloride (KCl-P) Extraction	Exchangeable inorganic phosphorus, or PIP.
Sulfuric Acid H ₂ SO ₄ -P Digestion	Total phosphorus in the sediment (TP).
Porewater Total Phosphorus (PW-TP)	Measurement of dissolved total phosphorus in interstitial water.
Residual Phosphorus (RP)	RP = TP - (PW-TP KCl-P + NaOH-TP + HCl-P). Assumed to be a measure of organic phosphorus and inorganic phosphorus not extracted by NaOH and HCl reagents.

Table 7-2 Nutrients in the sediments of Lake Okeechobee (adapted from Reddy and Ivanoff, 1990).

Sediment Type	Total P (mg/kg)	Total N (mg/kg)	Total N/ Total P
Mud (Station K8)	1064	6800	6.39
Peat (Station M17)	641	23700	36.97
Sand (Station J7)	150	500	3.33
Littoral (Station J5)	18	200	11.11

800 mg P/kg dry wt. in the upper 5 cm of six Lake Okeechobee sediment cores. Joyner (1974) found a range of 80 mg P/kg dry wt. to 690 mg P/kg dry wt. in fifteen sediment samples from Lake Okeechobee.

Reddy and Ivanoff (1990) suggest that external loads of SO_4 and NO_3 associated with wind-induced mixing can stimulate organic matter decomposition in the sediments and contribute to highly variable spatial and temporal release of labile P. The variability in sediment labile P release is also due to the dynamic microbial biomass P on the sediment. The release of phosphorus from the bottom sediment and suspended sediment is a function of the available redox conditions in the overlying water column. The redox depends on the amount of dissolved oxygen present, which changes diurnally due to sediment oxygen demand, algal growth and algal respiration. Fortunately, isotherm data assembled by the Soil Science group (Reddy et al., 1991) from their sediment work as part of the project are all for anaerobic sediments and do not apply to the aerobic conditions of the water column.

The data used in the diagenetic and suspended sediment model of Lake Okeechobee are presented in Table 7-3. The data required include: K_{sp} , the adsorption partition coefficient for PIP (l/kg); ρ_s , the bottom sediment density (gm/cm^3); K_{pip} , inorganic phosphorus partition coefficient for suspended sediment (mg/kg); and, K_{org} , the organic phosphorus partition coefficient for suspended sediment (mg/kg).

The model calculates the settling of organic phosphorus sediment (C_{org}) and inorganic phosphorus (C_{pip}), respectively, as:

$$\Delta M_{org} = \Delta t \cdot C_{pip} \cdot K_{sorg}/y_k \quad [\text{day} \cdot \text{mg}/\text{m}^3 \cdot \text{m}/\text{day}/\text{m}] \quad (7.8-2)$$

$$\Delta M_{pip} = \Delta t \cdot C_{pip} \cdot K_{spip}/y_k \quad [\text{day} \cdot \text{mg}/\text{m}^3 \cdot \text{m}/\text{day}/\text{m}] \quad (7.8-3)$$

The erosion of C_{org} and C_{pip} from the bottom of the lake are calculated as:

$$\Delta M_{org} = \Delta t \cdot F_e/Y_k \cdot K_{org} \quad [\text{day} \cdot \text{gm}/\text{cm}^2/\text{day}/\text{m} \cdot \text{mg}/\text{gm}] \quad (7.8-4)$$

$$\Delta M_{pip} = \Delta t \cdot F_e/Y_k \cdot K_{pip} \quad [\text{day} \cdot \text{gm}/\text{cm}^2/\text{day}/\text{m} \cdot \text{mg}/\text{gm}] \quad (7.8-5)$$

where Δt = time step, F_e = erosive flux, Y_k = lake depth, and K_{org} and K_{pip} are partition coefficients.

Table 7-3 Input data used for diagenetic and sediment model of Lake Okeechobee.

Variable	Sediment Type	FORTRAN Variable	Simulation Value
K_{sp}	Sand	OPFRAC(1)	100
K_{pip}	Sand	PFRAC(1)	4.1
ρ_s	Sand	DRHO(1)	2.6
K_{org}	Sand	OPFRAC(1)	204
K_{sp}	Mud	OPFRAC(2)	400
K_{pip}	Mud	PFRAC(2)	14.23
ρ_s	Mud	DRHO(2)	1.1
K_{org}	Mud	OPFRAC(2)	2286
K_{sp}	Littoral	OPFRAC(3)	100
K_{pip}	Littoral	PFRAC(3)	1.04
ρ_s	Littoral	DRHO(3)	2.6
K_{org}	Littoral	OPFRAC(3)	1150
K_{sp}	Peat	OPFRAC(4)	200
K_{pip}	Peat	PFRAC(4)	16.5
ρ_s	Peat	DRHO(4)	1.1
K_{org}	Peat	OPFRAC(4)	193

Erosion is constrained in model LOP0D to only occur during the night (one time step). The units of shear stress are usually Newtons [$1 \text{ kg} \cdot \text{m/sec}^2$] per m^2 , or dynes [$1 \text{ gm} \cdot \text{cm/sec}^2$]. The range of shear stresses used in the model range from 0.1 dynes to 10 dynes/ cm^2 for the critical shear stress. We start the simulation using a starting ORG partition coefficient in the sediment similar to one measured by (Brezonik et al. 1979).

Many of the units in the model are equivalent. For example, the following solid/solid and solid/liquid concentrations are equivalent:

$$\frac{\text{ug}}{\text{mg}} = \frac{\text{mg}}{\text{gm}} = \frac{\text{gm}}{\text{kg}} , \text{ and}$$

$$\frac{\text{ug}}{1} = \frac{\text{mg}}{\text{m}^3}$$

The deposition flux [mg/m_2] is determined from the settling velocity and pelagic concentration of PIP and ORG:

$$F_d = C_{pip} \cdot K_{spip} \Delta t \text{ [mg/m}^3 \cdot \text{m/day} \cdot \text{day}] + \\ C_{org} \cdot K_{sorg} \Delta t \text{ [mg/m}^3 \cdot \text{m/day} \cdot \text{day}] \quad (7.8-6)$$

The magnitude of the deposition and erosion flux is on the order of 1 cm per week based on 3-D simulations using the model EHSMSED. These simulations were done for one week, one month and three month time periods during the months of maximum wind movement.

The conversion from the flux form of erosion and deposition to an estimate of the depth (cm) eroded (E_e) or deposited (E_d) from the sediment bed in one day is:

$$E_e = F_e / \rho_s / \phi \text{ [gm/sec/cm}^2 \cdot \text{cm}^3/\text{gm} \cdot 86,400 \text{ sec/day]} \quad (7.8-7)$$

$$E_d = F_d / \rho_s / \phi \text{ [mg/m}^2/\text{day} \cdot \text{cm}^3/\text{gm} \cdot \text{m}^2/10,000 \text{ cm}^2] \quad (7.8-8)$$

or the ratio between the shear rate and sediment density and porosity. In general, deposition and erosion are cyclic processes (Figure 7-10).

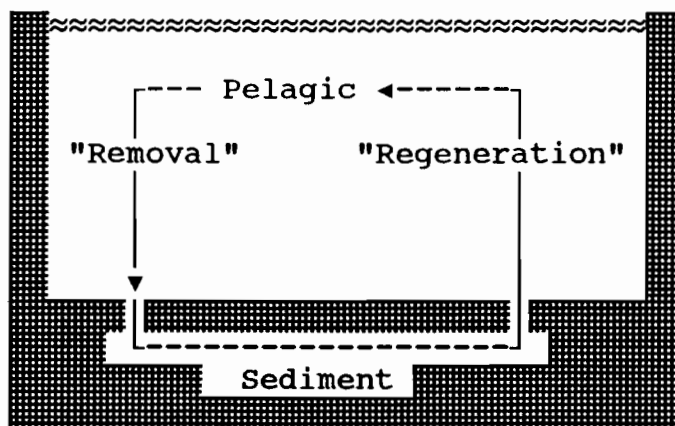


Figure 7-10 Removal of pelagic phosphorus and regeneration of sediment phosphorus governs the removal capacity of the lake sediment. The fraction lost in permanent burial will never contribute phosphorus to the pelagic region again - Or will it?

7.9 Summary

The movement of wind over the water surface and its action on the bottom sediment is an extremely important factor in predicting the pelagic total phosphorus (TP) concentration of Lake Okeechobee.

The components of phosphorus affected the most by the action of wind include the following:

C_{org} Organic phosphorus on the suspended sediment particle.

C_{pip} Inorganic phosphorus on the suspended sediment particle. C_{pip} and pelagic C_{srp} interact through the process of adsorption-desorption. The adsorption of C_{srp} to C_{pip} and its subsequent deposition to the bottom sediment is an important loss of pelagic SRP.

The simulation model(s) of Lake Okeechobee used the average monthly wind movement over the pan evaporation station at Moore Haven. The assumptions used to transform the Moore Haven data were:

- (1) The wind data were transformed using a power law to convert from the measured wind at 2 meters height to model input wind at 10 meters height.
- (2) A further transformation was necessary to convert a land based wind measurement to an over-lake wind measurement.
- (3) The mean wind estimate was subsequently altered by the ratio of the total day length (24 hours) to the length of night, since the model has wind movement only during the night time step of model LOP0D.

The key calibration parameters in the resuspension model were f_w , C_{susp} , τ_{cr} , and the maximum value of τ_b . The values of f_w tested ranged from 0.002 to 0.0010. The most common literature value was 0.004 and this has been used in Lake Okeechobee by Blosser (1986) and Sheng et al. (1991a). The highest values of f_w were suggested by Hwang and Mehta (1989). The final calibrated value of f_w was 0.008 in model LOP0D. The resuspension rate (C_{susp}) was estimated or calculated to be $1.2 \cdot 10^{-7}$ sec/cm by Sheng et al. (1991a) and this value is used in the model. Higher or lower values of C_{susp} yield mean predicted concentrations of TSS inconsistent with measured Lake Okeechobee TSS concentrations.

The critical shear stress, τ_{crm} , is loosely based on the work of Sheng et al. (1991a). We used τ_{crm} values of 1.0 dynes/cm² for peat sediment, 10.0 dynes/cm² for sand and marsh sediment, and 0.2 dynes/cm² for mud sediment. The maximum value of τ_b was 2 dynes/cm² in model LOP0D, which is consistent with the

simulations of Sheng et al. (1991a). The maximum value of τ_b suppresses the generation of large erosion rates leading to subsequent unrealistic TSS, ORG, and PIP concentrations.

The predicted sediment concentration has the required diurnal, monthly, and mean concentrations of suspended sediment (TSS), particulate organic phosphorus (ORG), and particulate inorganic phosphorus (PIP) as measured in Lake Okeechobee. The predicted measurements of ORG ranged from 40 ug/l during the winter months to < 5 ug/l during the summer months.

8. DIAGENETIC ADVECTION-DIFFUSION MODEL

8.1 Introduction

An important source of pelagic phosphorus occurs due to the diffusion of interstitial SRP from the bottom sediments. Conversely, the diffusion of pelagic SRP to the bottom sediments is a sink of pelagic phosphorus. The overall process of bottom sediment phosphorus change is called diagenesis. This section describes the linkage of the diagenetic model separately developed by Pollman (1991) to the pelagic phosphorus model.

8.2 Basic Equations and Boundary Conditions

The diagenetic model is based on the one dimensional model of Berner (1980). The aqueous phase of phosphorus in the sediment (C_{aq}) is the porewater or interstitial water concentration of SRP,

$$\frac{\partial C_{aq}}{\partial t} = \frac{1}{\phi} \cdot \frac{\partial}{\partial z} \left[\phi \cdot D_{eff} \frac{\partial C_{aq}}{\partial z} \right] - \nu_{aq} \cdot \frac{\partial C_{aq}}{\partial z} + \frac{\partial C_{aq}}{\partial t_{ads}} + \Sigma R_{aq} \quad (8.2-1)$$

and the solid phosphorus phase (Γ) in the bottom sediment consists of the organic phosphorus and exchangeable phosphorus on the sediment particles,

$$\frac{\partial \Gamma}{\partial t} = \frac{1}{\phi \cdot F} \frac{\partial}{\partial z} \left[\phi \cdot F \cdot D_r \frac{\partial \Gamma}{\partial z} \right] - \nu_s \cdot \frac{\partial \Gamma}{\partial z} + \frac{\partial \Gamma}{\partial t_{ads}} + \Sigma R_r \quad (8.2-2)$$

The aqueous and solid phase equations can be combined by expressing Γ as a function of C_{aq} and the formation factor, F :

$$F = \rho_s \cdot \frac{(1 - \phi)}{\phi} \equiv \text{"Formation factor"} \quad (8.2-3)$$

$$F \frac{\partial \Gamma}{\partial t} = \phi \frac{\partial C_{aq}}{\partial t_{ads}} \quad (8.2-4)$$

or, assuming a linear adsorption relationship between Γ and C_{aq} and a fast adsorption - desorption reaction, the following relationship is found:

The combined equation for phosphorus diagenesis in the lake sediment is:

$$\frac{\partial}{\partial t} \cdot (\phi \cdot C_{aq}) = \frac{1}{(1+K^*)} \frac{\partial}{\partial z} \left[(1+K^*) \cdot \phi \cdot D_r \cdot \frac{\partial \Gamma}{\partial z} + \phi \cdot D_{eff} \cdot \frac{\partial C_{aq}}{\partial z} \right] - \frac{\phi}{(1+K^*)} \cdot \left[(\nu_{aq} + \nu_s \cdot K^*) \cdot \frac{\partial C_{aq}}{\partial z} \right] + \frac{\Sigma R_r}{(1+K^*)} + \frac{\Sigma R_{aq}}{(1+K^*)} \quad (8.2-7)$$

where K^* , the modified linear adsorption coefficient, is $[F \cdot K]$.

The reaction terms include a first order decomposition of organic phosphorus

$$\Sigma R_{eff} \equiv R_{decomp} = F \cdot K_{org} \cdot P_{org} \quad (8.2-8)$$

and kinetically controlled chemical precipitation or dissolution of a mineral phase (e.g., hydroxyapatite in deeper sediments) that include ortho-phosphorus in its stoichiometry:

$$\Sigma R_r \equiv R_{ppt} = K_{ppt} \cdot (C_{aq} - C_{eq}) \quad (8.2-9)$$

Using the steady state assumption of $\frac{\partial \phi \cdot C_{aq}}{\partial t} = 0$ simplifies the model to the following combined equation:

$$\frac{\partial}{\partial z} \left[(1+K^*) \cdot \phi \cdot D_r \cdot \frac{\partial \Gamma}{\partial z} + \phi \cdot D_{eff} \cdot \frac{\partial C_{aq}}{\partial z} \right] = \phi \cdot \left[(\nu_{aq} + \nu_s \cdot K^*) \cdot \frac{\partial C_{aq}}{\partial z} \right] \Sigma R_r - \Sigma R_{aq} \quad (8.2-10)$$

An implicit finite difference scheme with a tridiagonal solution was used to solve for the steady state concentration of C_{aq} at each layer based on the average SRP concentration in the bottom σ layer of the pelagic model for the *previous* day. The flux of SRP across the sediment-water interface (assuming steady state conditions and negligible advection) is:

$$Flux = D_{eff} \cdot \left[\frac{\partial C_{aq}}{\partial z} \right]_{z=0} \quad (8.2-11)$$

in units of $\mu g \cdot cm^{-2}$ per time step.

8.3 Vertical Grid Resolution

The surface bottom sediment in the diagenetic model is divided into an upper aerobic layer and a lower anaerobic layer (Figure 8-1). The aerobic zone of 5 cm depth is influenced by benthic organisms which cause bioturbation. The concentration of C_{aq} in the upper zone is maintained by high rates of organic decomposition. The lower anaerobic layer extends to a depth of 50 cm without benthic organisms and their associated bioturbation. This lower zone is a region in which the C_{aq} concentration is in thermodynamic equilibrium with solid phase hydroxyapatite phosphorus.

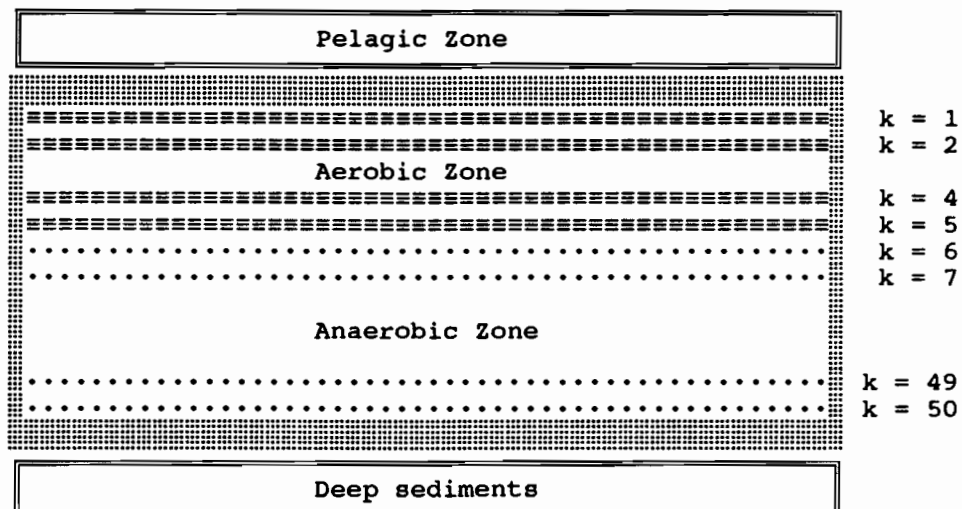


Figure 8-1 Layers in sediment diagenetic model.

8.4 Data Required for the Diagenetic Model

The data listed in Table 8-1 are required to run the diagenetic model. They are part of the input data stream of the models.

8.5 Steady-State Numerical Solution

This section documents the tridiagonal matrix elements for the numerical solution of the steady-state 1-D advection-diffusion-reaction equation for sediment diagenesis (Eq. 8.2-10)). Coefficients have different values for the aerobic layer (henceforth designated by the subscript up) and the anaerobic layer (henceforth designated by the subscript low).

Table 8.1 Input data for diagenetic model.

Diagenetic Data	Sand Sediment	Mud Sediment	Macrophyte Sediment	Peat Sediment
ρ_s (gm/cm ³)	2.474	1.381	2.474	1.255
(ug · l ⁻¹)	120.0	220.0	120.0	300.0
ν_{aq} (cm/yr)	0.0336	0.168	0.056	0.1025
K_{up} (l/kg)	100.0	400.0	100.0	200.0
K_{low} (l/kg)	100.0	400.0	100.0	200.0
ϕ (fraction)	0.45	0.892	0.45	0.892
K_{ppt} (1 · yr ⁻¹)	1.0	2.0	1.0	2.0
K_{org} (1 · yr ⁻¹)	0.002	0.005	0.002	0.005
C_{eq} (ug · l ⁻¹)	300.0	600.0	500.0	150.0
D_{eff} (cm ⁻² · yr ⁻¹)	5010.0	1980.0	1670.0	1990.0
DD_{eff} (cm ⁻² · yr ⁻¹)	501.0	198.0	167.0	199.0
D_{Γ} (cm ⁻² · yr ⁻¹)	0.0	0.0	0.0	0.0
DD_{Γ} (cm ⁻² · yr ⁻¹)	0.0	0.0	0.0	0.0

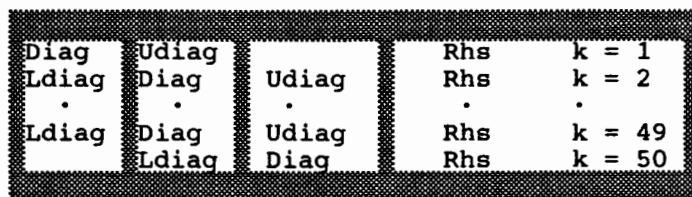


Figure 8-2 Tridiagonal solution for any k level C_{aq} .

With reference to Figure 8-2 for the definition of the matrix elements, the matrix elements for the first aerobic layer ($k=1$) are:

$$\text{Diag} = -2 \cdot \frac{\frac{D_{\text{eff}}}{(1+K^*)} - D_r}{\Delta z^2} \cdot C_1^{n+1} - \frac{\nu_{\text{aq}}}{\Delta z} \cdot C_1^{n+1} - \frac{K_{\text{ppt}}}{(1+K^*)} \cdot C_1^{n+1} \quad (8.4-1)$$

$$\text{Udiag} = \frac{\frac{D_{\text{eff}}}{(1+K^*)} - D_r}{\Delta z^2} \cdot C_1^{n+1} \quad (8.4-2)$$

$$\text{Rhs} = -\frac{\frac{D_{\text{eff}}}{(1+K^*)} - D_r}{\Delta z^2} \cdot C_\sigma - \frac{\nu_{\text{aq}}}{\Delta z} \cdot C_\sigma - \frac{K_{\text{ppt}}}{(1+K^*)} \cdot C_{\text{eq}} - \frac{F \cdot K_{\text{org}} \cdot P_{\text{org}}}{(1+K^*)} \quad (8.4-3)$$

The matrix elements for aerobic layers 2 through k_{low} :

$$\text{Ldiag} = \frac{\frac{D_{\text{eff}}}{(1+K^*)} - D_r}{\Delta z^2} \cdot C_{k-1}^{n+1} - \frac{\nu_{\text{aq}}}{(1+K^*)} \cdot C_{k-1}^{n+1} \quad (8.4-4)$$

$$\text{Diag} = -2 \cdot \frac{\frac{D_{\text{eff}}}{(1+K^*)} - D_r}{\Delta z^2} \cdot C_k^{n+1} - \frac{\nu_{\text{aq}}}{\Delta z} \cdot C_k^{n+1} - \frac{K_{\text{ppt}}}{(1+K^*)} \cdot C_k^{n+1} \quad (8.4-5)$$

$$\text{Udiag} = \frac{\frac{D_{\text{eff}}}{(1+K^*)} - D_r}{\Delta z^2} \cdot C_{k+1}^{n+1} \quad (8.4-6)$$

$$\text{Rhs} = -\frac{K_{\text{ppt}}}{(1+K^*)} \cdot C_{\text{eq}} - \frac{F \cdot K_{\text{org}} \cdot P_{\text{org}}}{(1+K^*)} \quad (8.4-7)$$

The matrix elements for the last aerobic layer k_{low} is:

$$\text{Ldiag} = \frac{\frac{DD_{\text{eff}}}{(1+K^*)} - DD_r}{\Delta z^2} \cdot C_{k-1}^{n+1} - \frac{\nu_{\text{aq}}}{(1+K^*)} \cdot C_{k-1}^{n+1} \quad (8.4-8)$$

$$\begin{aligned}
\text{Diag} &= - \frac{\frac{DD_{eff}}{(1+K^*)} - D_r}{\Delta z^2} \cdot C_k^{n+1} - \frac{\frac{DD_{eff}}{(1+K^*)} - DD_r}{\Delta z^2} \cdot C_k^{n+1} \\
&\quad - \frac{\nu_{aq}}{\Delta z} \cdot C_k^{n+1} - \frac{k_{ppt}}{(1+K^*)} \cdot C_k^{n+1}
\end{aligned} \tag{8.4-9}$$

$$Udiag = \frac{\frac{D_{eff}}{(1+K^*)} - D_r}{\Delta z^2} \cdot C_{k+1}^{n+1} \tag{8.4-10}$$

$$Rhs = - \frac{K_{ppt}}{(1+K^*)} \cdot C_{eq} - \frac{F \cdot K_{org} \cdot P_{org}}{(1+K^*)} \tag{8.4-11}$$

The matrix elements for each anaerobic layer k_{low+1} through layer $k_{layers-1}$ is:

$$Ldiag = \frac{\frac{DD_{eff}}{(1+K^*)} - DD_r}{\Delta z^2} \cdot C_{k-1}^{n+1} - \frac{\nu_{aq}}{(1+K^*)} \cdot C_{k-1}^{n+1} \tag{8.4-12}$$

$$\begin{aligned}
\text{Diag} &= - \frac{\frac{DD_{eff}}{(1+K^*)} - DD_r}{\Delta z^2} \cdot C_k^{n+1} - \frac{\frac{DD_{eff}}{(1+K^*)} - DD_r}{\Delta z^2} \cdot C_k^{n+1} \\
&\quad - \frac{\nu_{aq}}{\Delta z} \cdot C_k^{n+1} - \frac{K_{ppt}}{(1+K^*)} \cdot C_k^{n+1}
\end{aligned} \tag{8.4-13}$$

$$Udiag = \frac{\frac{D_{eff}}{(1+K^*)} - DD_r}{\Delta z^2} \cdot C_{k+1}^{n+1} \tag{8.4-14}$$

$$Rhs = - \frac{k_{ppt}}{(1+K^*)} \cdot C_{eq} - \frac{F \cdot K_{org} \cdot P_{org}}{(1+K^*)} \tag{8.4-15}$$

The matrix elements for the last anaerobic layer k_{layers} is:

$$L_{\text{diag}} = \frac{\frac{DD_{\text{eff}}}{(1+K^*)} - DD_r}{\Delta z^2} \cdot C_{k-1}^{n+1} + \frac{\nu_{\text{aq}}}{(1+K^*)} \cdot C_k^{n+1} \quad (8.4-16)$$

$$\begin{aligned} \text{Diag} &= -\frac{\frac{DD_{\text{eff}}}{(1+K^*)} - DD_r}{\Delta z^2} \cdot C_k^{n+1} - \frac{\frac{DD_{\text{eff}}}{(1+K^*)} - DD_r}{\Delta z^2} \cdot C_k^{n+1} \\ &\quad - \frac{\nu_{\text{aq}}}{\Delta z} \cdot C_k^{n+1} - \frac{K_{\text{ppt}}}{(1+K^*)} \cdot C_k^{n+1} \end{aligned} \quad (8.4-17)$$

$$Rhs = -\frac{K_{\text{ppt}}}{(1+K^*)} \cdot C_{\text{eq}} - \frac{F \cdot K_{\text{org}} \cdot P_{\text{org}}}{(1+K^*)} - \frac{(1+K^*)}{\Delta z^2} \cdot C_{\text{eq}} \quad (8.4-18)$$

Following computation of the matrix elements, the set of tridiagonal linear equations is easily solved for C_k^{n+1} ($k = 1-50$) by Gauss reduction.

8.6 Time Scale Considerations

The difference between the steady state and dynamic models is only significant over a time period of 1 - 2 months. We use the steady state solution of the organic and inorganic phosphorus concentrations in the bottom sediment for the estimated diffusion flux of SRP. The mean previous day's concentration of SRP in a lake box or the bottom σ -layer is the top boundary of the diagenetic model.

9. LITTORAL ZONE PHOSPHORUS MODEL

9.1 Introduction

The shallow area (littoral zone) in western and southern Lake Okeechobee is currently dominated by submergent and emergent vegetation (Figure 9-1). This is significantly different from the vegetation existing in Lake Okeechobee during the lake 1800s and early 1900s when the mean lake stage was higher (Figure 9-2). The fraction of the lake area covered by open water has decreased and the littoral vegetation area has increased since the 1920s.

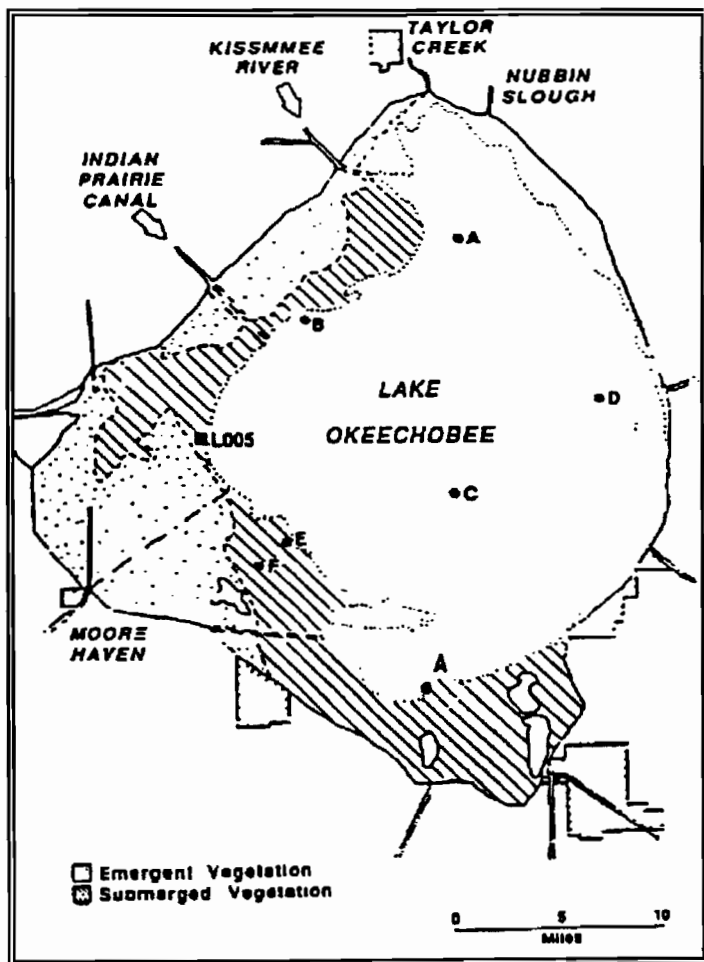


Figure 9-1 Submergent and emergent vegetation regions currently are primarily in western and southern Lake Okeechobee.

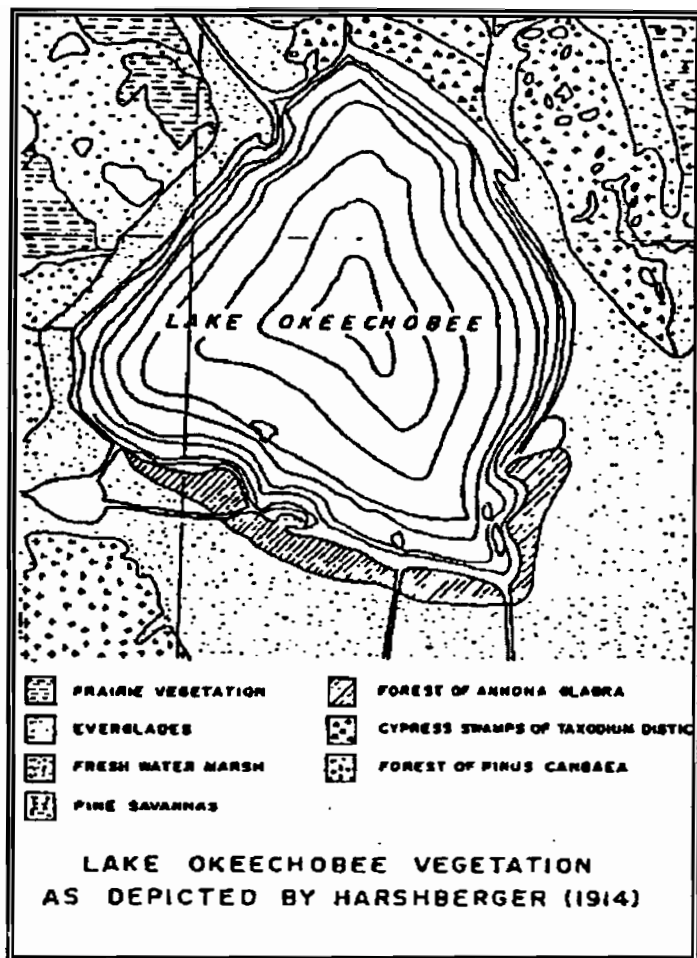


Figure 9-2 Vegetation regions in Lake Okeechobee circa 1914 consisted primarily of custard apple trees in the South Bay region.

The composition of the littoral zone and its effect on the phosphorus cycling in Lake Okeechobee was one of the primary concerns of this project. This chapter seeks to quantify the influence of the littoral zone on pelagic phosphorus concentrations. Primarily we seek to answer the question — Are the macrophytes a source, a sink, or a seasonal source and sink of phosphorus to the pelagic region of Lake Okeechobee?

Wetlands generally are assumed to retain phosphorus (Kilham and Kilham, 1991). Retention processes include chemical precipitation, adsorption/desorption, mineralization of organic phosphorus, plant tissue incorporation and ultimately sediment burial of detritus. The excretion of soluble phosphorus by macrophytic plants and macrophyte particulate detritus oppose these retention processes in the littoral zone.

The littoral zone increases the size of the phosphorus exported to the pelagic region of Lake Okeechobee by creating large detrital particles that become more likely to be retained in the lake's bottom sediments (Kilham and Kilham, 1991). The littoral zone of a lake is a

significant contributor of organic carbon and dissolved organic nitrogen (Wetzel, 1983). The dissolved organics are a primary source of food to the open water population of heterotrophic organisms such as bacteria, protozoa and zooplankton.

The littoral zone provides habitat for nesting and feeding migratory birds. Wading birds primarily utilize beakrush (*Rhynchospora tracyi*) wet prairie, spikerush (*Eleocharis cellulosa*) sloughs, and the mixed grasses (*Panicum repens*, *Spartina bakeri*, and *Panicum hemitomon*) as feeding habitat. These species grow optimally at elevations of 13 to 15 feet in Lake Okeechobee (Table 9-2). The willow community provides the major nesting areas in the macrophyte area of Lake Okeechobee (Zaffke, 1984). Willows require a periodic reduction in lake levels below 13 feet for long term maintenance. The major submergent macrophyte is Vallisneria which is estimated to comprise 76.4 percent by weight of the submerged vegetation.

The regulation of Lake Okeechobee's water surface elevation was changed in 1979 to increase the mean depth of the lake (Trimble and Marban, 1989). The mean depth of water in the lake did increase in the 1980s despite severe droughts and the greater depth of water had a drastic effect on the littoral zone vegetation (Table 9-3). The dominant spikerush community of the 1970s was nearly eliminated and cattail and torpedo grass increased their coverage of the littoral zone (Milleson, 1987). This had the effect of decreasing the feeding habitat available to birds in Lake Okeechobee, and perhaps decreasing the littoral zone contribution of phosphorus to the pelagic area due to lower phosphorus release by the newer dominant emergent macrophytes (Table 9-1).

9.2 Littoral Source of Phosphorus to Pelagic Area

Possible sources for littoral phosphorus export are the excretion of phosphorous from the macrophyte zone during periods of high stage and during plant senescence at the end of the growing season. Supporting evidence of this littoral source for phosphorus includes the observations of lower summer phosphorous concentrations during the period of the highest inflow loadings, and higher phosphorus concentrations during the winter, when aquatic plants in the littoral area undergo senescence releasing SRP and DOP, and frontal systems generate greater wind mixing. The amount of phosphorus estimated to be released from macrophytes in Lake Okeechobee range from $0.0 \text{ ug} \cdot \text{m}^{-2} \cdot \text{day}^{-1}$ net (Gayle, 1975) to a total macrophyte release of $400 \text{ ug} \cdot \text{m}^{-2} \cdot \text{day}^{-1}$ (Brezonik et al., 1979).

9.3 Lake Stage Influence on Pelagic Phosphorus Concentrations

A significant correlation ($r = 0.7$, $P < 0.05$) exists between annual average total phosphorous concentration and lake mean depth (Canfield and Hoyer, 1989). However, this annual relationship between TP and lake stage disappears using monthly or semi-monthly data (Figure 9-3). A second order polynomial best describes the shape of a regression of SRP versus lake stage for the period 1972 to 1988 (Figure 9-4). This excellent relationship fits the assumption of littoral zone senescence being a source of SRP to the pelagic region of Lake Okeechobee. In other words, macrophytes are a seasonal source of phosphorus to the

Table 9-1 Estimates of macrophyte nutrient content and areal excretion rate from Brezonik et al. (1983).

Macrophyte	Total Area (ha)	TP Content (kg)	Littoral Zone Excretion (ug/m ² -day)
Potamogeton	4760	21400	37.0
Vallisneria	1008	9240	28.0
Hydrilla	1800	17900	0.0
Typha	5650	73000	0.0

Table 9-2 Optimum range of growth for plants in Lake Okeechobee (Pesnell and Brown, 1977).

	Optimum Range (feet msl)
Indian Prairie	
<i>Spartina bakeri</i>	13.0 — 14.5
<i>Typha angustifolia</i>	12.0 — 13.0
<i>Eleocharis cellulosa</i>	10.7 — 12.0
<i>Scirpus californicus</i>	10.1 — 10.7
Moore Haven Transect	
<i>Spartina bakeri</i>	13.1 — 14.6
<i>Rhynchospora tracyi</i>	13.1 — 14.6
<i>Salix carolina</i>	13.2 — 14.3
<i>Typha angustifolia</i>	12.4 — 13.1
<i>Eleocharis cellulosa</i>	10.6 — 12.4
<i>Scirpus californicus</i>	11.1 — 12.3
Composite Transect	
<i>Spartina bakeri</i>	13.1 — 15.0
<i>Rhynchospora tracyi</i>	13.1 — 14.6
<i>Salix carolina</i>	13.2 — 14.3
<i>Typha angustifolia</i>	12.4 — 13.1
<i>Eleocharis cellulosa</i>	10.6 — 12.4
<i>Scirpus californicus</i>	10.1 — 10.6

Table 9-3 The emergent vegetation of Lake Okeechobee (from the supplement to Pesnell and Brown, 1977).

Vegetation	Hectares
Guava	84
Water Hyacinth	499
Water-Lily (<i>Nuphar advena</i>)	991
Bog	1,438
Melaleuca	2,402
Buttonbush	3,524
Mixed Forest	4,057
Bulrush (<i>S. validis</i>)	5,997
Sawgrass	9,985
Wire Cordgrass	17,067
Mixed Grasses	23,603
Willow (<i>Salix spp.</i>)	25,745
Beak-rush (<i>Rhynchospora tracyi</i>)	37,362
Spike-rush (<i>Eleocharis cellulosa</i>)	43,512
Cattail (<i>Typha spp.</i>)	59,620
Total	235,886

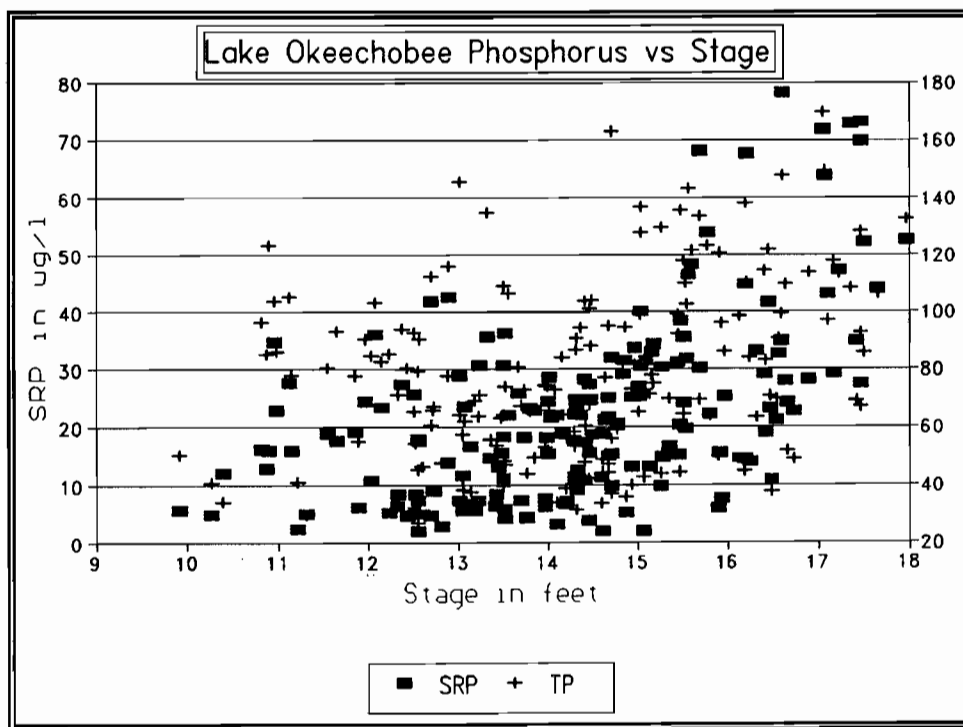


Figure 9-3 Pelagic TP and SRP versus Lake Stage.

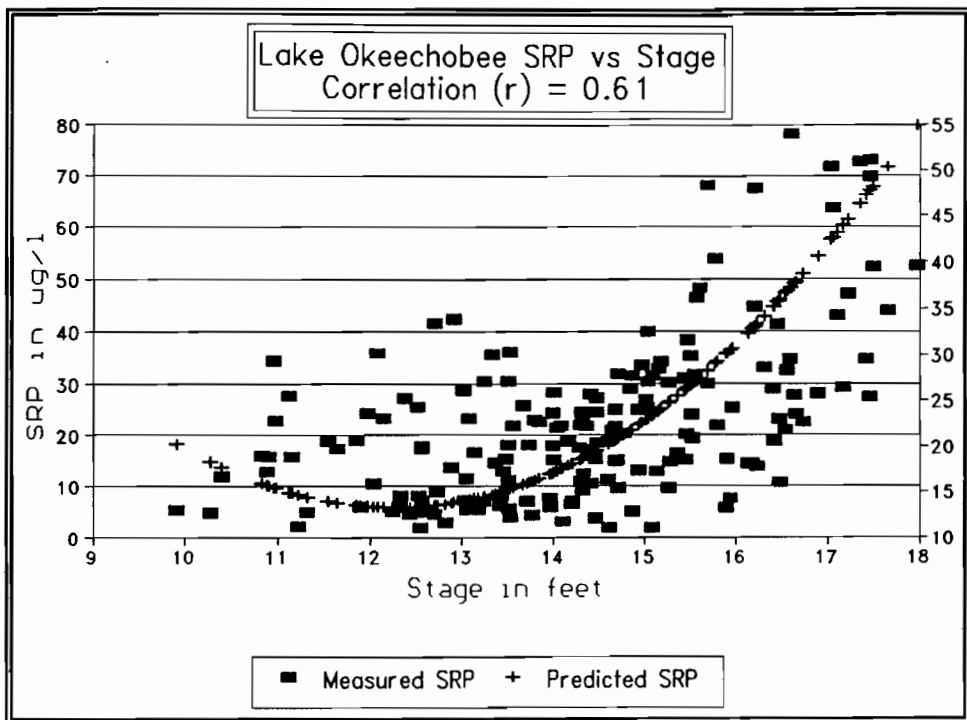


Figure 9-4 Mean pelagic SRP has a polynomial relationship with stage in Lake Okeechobee.

main lake area. At other times, surrounding macrophyte vegetation reduces P-loading to lakes by direct uptake and storage of TP and packaging the phosphorus in large particulates that are more easily buried.

10. PELAGIC ADVECTION-DIFFUSION EQUATION

10.1 Introduction

This section describes the governing transport equations used in the three dimensional phosphorus advection-diffusion model for Lake Okeechobee (LOP3D). The processes of advection and diffusion are coupled with the phosphorus reactions and kinetics described in Chapter 12.

Advection is the physical translation of concentration in the direction of the prevailing velocity field (Figure 10-1). Advection in Lake Okeechobee causes the various phosphorus species to move in response to wind generated water velocities. Diffusion is the movement of phosphorus from a location of higher concentration to a location of lower concentration (Figure 10-2). Important contributions to net diffusion in Lake Okeechobee are river loadings with higher or lower concentrations of phosphorus, biological transformations of phosphorus species, and advection, which all create spatial heterogeneity in the phosphorus concentration field of Lake Okeechobee.

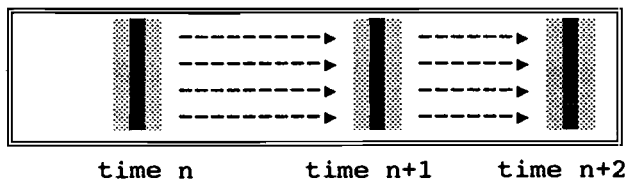


Figure 10-1 Advective movement of a concentration peak with the velocity field of the lake depends on the magnitude of the velocity (the darker hatching represents higher concentrations).

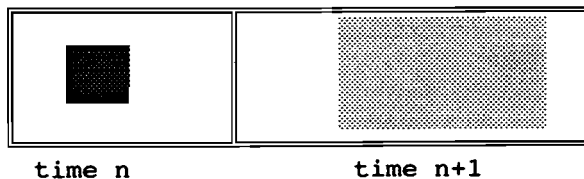


Figure 10-2 Diffusive movement of a concentration peak from a higher concentration (darker shading) to a lower concentration (lighter shading).

10.2 Basic Equations and Boundary Conditions

The governing equation for a three dimensional advective diffusion equation (Harleman, 1988):

$$\frac{\partial C_i}{\partial t} + \frac{\partial u \cdot C_i}{\partial x} + \frac{\partial v \cdot C_i}{\partial y} + \frac{\partial w \cdot C_i}{\partial z} = \frac{\partial}{\partial x} E_x \frac{\partial C_i}{\partial x} + \frac{\partial}{\partial y} E_y \frac{\partial C_i}{\partial y} + \frac{\partial}{\partial z} E_z \frac{\partial C_i}{\partial z} \pm R_i \quad (10.2-1)$$

where C_i = phosphorus species concentration,
 E_x = horizontal diffusivity in x direction,
 E_y = horizontal diffusivity in y direction,
 E_z = vertical diffusivity in z direction,
 R_i = reaction terms in cell,
 u = velocity in x direction,
 v = velocity in y direction, and
 w = velocity in z direction.

The equation represents the rate of change of the concentration of a constituent due to the combined effects of advection, diffusion, and reactions. Although analytical solutions are available for constant flow fields and simple geometries, for most realistic cases the equation has to be solved numerically.

10.3 3-D Equation in Sigma Coordinate System

All components are subject to advection and diffusion according to Eq. (10.2-1). The equation is now written for the sigma coordinate system employed by UF COE for its hydrodynamic and sediment transport models. The vertical coordinate, σ is

$$\sigma = \frac{z - \eta}{h + \eta} = \frac{z - \eta}{H} \quad (10.3-1)$$

where z = elevation above datum (zero at water surface at the average depth (h), and negative downward),
 h = average local water depth in cell,
 η = the local change in water surface elevation at the cell center (e.g., due to waves or wind set-up),
 H = total depth of lake.

The sigma coordinate system divides the total depth (H), at each location into equal non-dimensional increments to avoid "squeezing" the vertical layers as the water becomes shallower near the shoreline (Figure 10-3). For example, the five layer model used in Lake Okeechobee would have the following 5 σ levels as shown in Figure 10-4.

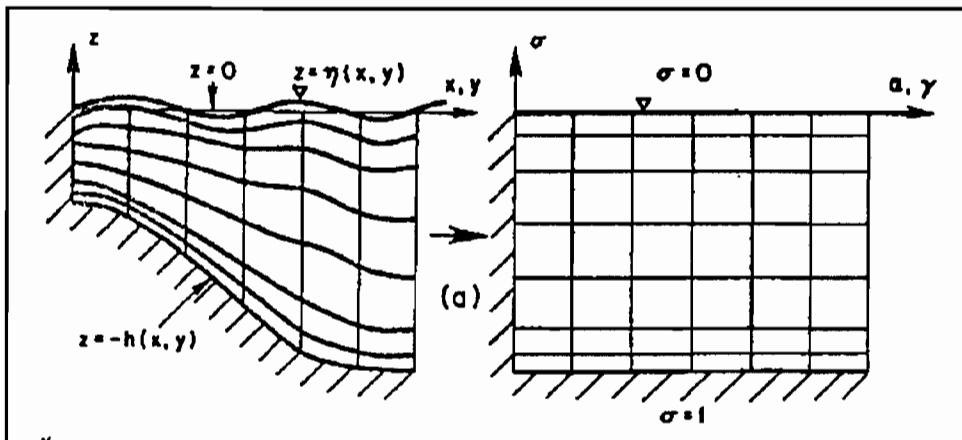


Figure 10-3 Sigma-stretched coordinate system.

$\sigma = 0$	
σ layer 5	$\sigma = -1/5$
σ layer 4	$\sigma = -2/5$
σ layer 3	$\sigma = -3/5$
σ layer 2	$\sigma = -4/5$
σ layer 1	$\sigma = -1$

Figure 10-4 Sigma (σ) levels in a five layer model.

In this model σ layer 5 is nearest the water surface and σ layer 1 is nearer the bottom of the lake.

The coordinate system is changed from (x, y, z) to (x, y, σ) by using the chain rule of calculus and Eq. (10.3-1) (Sheng and Lick, 1980).

$$\frac{\partial}{\partial x} = \frac{\partial}{\partial x} - \frac{\sigma}{H} \cdot \frac{\partial H}{\partial x} \cdot \frac{\partial}{\partial \sigma} \quad (10.3-2)$$

$$\frac{\partial}{\partial y} = \frac{\partial}{\partial y} - \frac{\sigma}{H} \cdot \frac{\partial H}{\partial y} \cdot \frac{\partial}{\partial \sigma} \quad (10.3-3)$$

$$\frac{\partial}{\partial z} = \frac{1}{H} \cdot \frac{\partial}{\partial \sigma} \quad (10.3-4)$$

$$\frac{\partial^2}{\partial x^2} = \frac{\partial^2}{\partial x^2} + 2 \cdot \frac{\partial \sigma}{\partial x} \cdot \frac{\partial^2}{\partial x \partial \sigma} + \frac{\partial^2 \sigma}{\partial x^2} \cdot \frac{\partial}{\partial \sigma} + \frac{\partial \sigma}{\partial x} \cdot \frac{\partial \sigma}{\partial x} \cdot \frac{\partial^2}{\partial \sigma^2} \quad (10.3-5)$$

$$\frac{\partial^2}{\partial y^2} = \frac{\partial^2}{\partial y^2} + 2 \cdot \frac{\partial \sigma}{\partial y} \cdot \frac{\partial^2}{\partial y \partial \sigma} + \frac{\partial^2 \sigma}{\partial y^2} \cdot \frac{\partial}{\partial \sigma} + \frac{\partial \sigma}{\partial y} \cdot \frac{\partial \sigma}{\partial y} \cdot \frac{\partial^2}{\partial \sigma^2} \quad (10.3-6)$$

$$\frac{\partial^2}{\partial z^2} = \frac{1}{H^2} \cdot \frac{\partial^2}{\partial \sigma^2} \quad (10.3-7)$$

The first four terms

$$\frac{\partial C_i}{\partial t} + \frac{\partial(u \cdot C_i)}{\partial x} + \frac{\partial(v \cdot C_i)}{\partial y} + \frac{\partial(w \cdot C_i)}{\partial z}$$

in the 3-D advective diffusion equation are transformed into the following form in σ -stretched coordinates:

$$\frac{\partial C_i}{\partial t} + \frac{\partial(u \cdot C_i)}{\partial x} - \frac{\sigma}{H} \cdot \frac{\partial H}{\partial x} \cdot \frac{\partial(u \cdot C_i)}{\partial \sigma} + \frac{\partial(v \cdot C_i)}{\partial y} - \frac{\sigma}{H} \cdot \frac{\partial H}{\partial y} \cdot \frac{\partial(v \cdot C_i)}{\partial \sigma} + \frac{1}{H} \cdot \frac{\partial(w \cdot C_i)}{\partial \sigma}$$

If we define $\omega = d\sigma/dt$ as the vertical velocity in the σ direction then w is related to ω , the velocity in the z direction, by:

$$\omega = w \cdot H + \sigma \cdot \left| u \cdot \frac{\partial H}{\partial x} + v \cdot \frac{\partial H}{\partial y} \right| \quad (10.3-8)$$

Substituting ω in the transformed terms of the 3-D equation we find for the first four terms:

$$\begin{aligned}
 \frac{\partial C_i}{\partial t} + \frac{\partial(u \cdot C_i)}{\partial x} - \frac{\sigma}{H} \cdot \frac{\partial H}{\partial x} \cdot \frac{\partial(u \cdot C_i)}{\partial \sigma} + \frac{\partial(v \cdot C_i)}{\partial y} - \frac{\sigma}{H} \cdot \frac{\partial H}{\partial y} \cdot \frac{\partial(v \cdot C_i)}{\partial \sigma} \\
 + \frac{\partial(\omega \cdot C_i)}{\partial \sigma} + \frac{\omega}{H} \cdot \frac{\partial(H \cdot C_i)}{\partial \sigma} + \frac{\sigma}{H} \cdot \frac{\partial H}{\partial x} \cdot \frac{\partial(u \cdot C_i)}{\partial \sigma} \\
 + \frac{\sigma}{H} \cdot \frac{\partial H}{\partial y} \cdot \frac{\partial(v \cdot C_i)}{\partial \sigma} + \frac{u}{H} \cdot \frac{\partial H}{\partial x} \cdot \frac{\partial(\sigma \cdot C_i)}{\partial \sigma} \\
 + \frac{v}{H} \cdot \frac{\partial H}{\partial y} \cdot \frac{\partial(\sigma \cdot C_i)}{\partial \sigma}
 \end{aligned}$$

Cancelling terms results in

$$\begin{aligned}
 \frac{\partial C_i}{\partial t} + \frac{\partial(u \cdot C_i)}{\partial x} + \frac{\partial(v \cdot C_i)}{\partial y} + \frac{\partial(\omega \cdot C_i)}{\partial \sigma} + \frac{\omega}{H} \cdot \frac{\partial(H \cdot C_i)}{\partial \sigma} \\
 + \left| \frac{u}{H} \cdot \frac{\partial H}{\partial x} + \frac{v}{H} \cdot \frac{\partial H}{\partial y} \right| \frac{\partial(\sigma \cdot C_i)}{\partial \sigma}
 \end{aligned}$$

which can be further simplified to:

$$\frac{1}{H} \cdot \frac{\partial(C_i)}{\partial t} + \frac{1}{H} \cdot \frac{\partial(H \cdot u \cdot C_i)}{\partial x} + \frac{1}{H} \cdot \frac{\partial(H \cdot v \cdot C_i)}{\partial y} + \frac{1}{H} \frac{\partial(H \cdot \sigma \cdot C_i)}{\partial \sigma}$$

Finally, the complete transformed equation is given below for an arbitrary constituent with concentration C ,

$$\begin{aligned}
 \frac{1}{H} \frac{\partial Hc}{\partial t} + \frac{1}{H} \left[\frac{\partial u Hc}{\partial x} + \frac{\partial v Hc}{\partial y} + H \frac{\partial \omega c}{\partial \sigma} \right] = \\
 \frac{1}{H} \left[\frac{\partial}{\partial x} E_x H \frac{\partial C}{\partial x} + \frac{\partial}{\partial y} E_y H \frac{\partial C}{\partial y} + \frac{\partial}{\partial \sigma} E_z H \frac{\partial C}{\partial \sigma} \right] \pm \text{Sources}
 \end{aligned}$$

where	$C(x,y,\sigma,t)$	= concentration of constituent,
	$H(x,y,t)$	= total depth = $h(x,y) + \eta(x,y,t)$,
	$h(x,y)$	= average depth,
	$\eta(x,y,t)$	= temporal variation (e.g., due to wind set-up),
	u,v	= x and y velocities,
	ω	= $d\sigma/dt$ = the "sigma" velocity, and
	E_x, E_y, E_z	= turbulent diffusivities in x , y and z (σ) directions.

The sources and sinks of Eq. (10.3-9) will be discussed extensively below. In addition to the kinetic formulations, the flux to and from the bottom due to erosion and deposition is also included as are horizontal fluxes at tributaries, both through the interface file generated by the hydrodynamic and sediment model of the UF COE group.

As described in Chapter 11, Eq. (10.3-9) is solved by a finite difference scheme that is explicit in the x and y directions and implicit in the σ direction (z or vertical direction). This is followed at each time step by an explicit evaluation of the source-sink terms. Advective velocities (u,v,x) and diffusivities (E_x, E_y, E_z) are input from the hydrodynamic model at 3-hr intervals. The time step for the finite difference solution has been varied from 15 minutes to 3 hours and works satisfactorily at the longer value, hence, the 3-hr value is routinely used. The code is written in Fortran 77 and was developed on a 486/25 microcomputer using an OS386 Leahy Fortran compiler.

10.4 Time Scales and Dimensionless Parameters

Lake Okeechobee is a highly complex set of interacting microscopic and macroscopic components that work together on short and long time scales that alter the water quality and trophic status of the lake.

The longitudinal and transverse frictionless seiche periods for Lake Okeechobee, respectively T_l and T_t , [defined in Table 10-1 after Hutchinson (1957)], show the effect of the long fetch length and shallow depth (Figure 10-5).

The Proudman number was defined by Platzman (1963) as the squared ratio of the viscous damping frequency, A_V/H^2 , to the gravitational frequency, $k\sqrt{gH}$, (proportional to the inverse of the seiche period), where A_V = vertical eddy viscosity, H = depth, g = gravitational acceleration, and k = wave number = $n\pi/L$, where L = characteristic length, and n = frequency number. For $n = 1$ (unimodal seiche), the Proudman number becomes

$$P_r = \frac{A_V^2}{(\pi/L)^2 g H^5} = 0.0143 \quad (10.4-1)$$

Table 10-1 Physical parameters for Lake Okeechobee.

$H = 4.7 \text{ m}$	Maximum depth
$L = 56.4 \text{ km}$	Maximum length
$W = 48.0 \text{ km}$	Maximum width
$(A_H)_r = 100,000 \text{ cm}^2/\text{s}$	Reference lateral eddy viscosity
$(A_V)_r = 5 - 10 \text{ cm}^2/\text{s}$	Reference vertical eddy viscosity
$f = 0.0000662 \cdot \text{s}^{-1}$	Coriolis parameter
$X_{\text{ref}} = 5.6 \times 10^6 \text{ cm}$	Reference horizontal distance
$Z_{\text{ref}} = 100.0 \text{ cm}$	Reference vertical distance
$U_{\text{ref}} = 10 \text{ cm/s}$	Reference horizontal velocity
$w_{\text{ref}} = 0.1 \text{ cm/s}$	Reference vertical velocity
$D_e = \pi \cdot (2 \cdot A_V / f)^{1/2} = 15 \text{ m}$	Ekman friction depth
$T_i = \frac{2 \cdot \pi}{f} = 26.4 \text{ hr}$	Inertial period
$T_1 = \frac{2 \cdot L}{(g \cdot H)^{1/2}} = 4.6 \text{ hr}$	Longitudinal seiche period
$T_t = \frac{2 \cdot W}{(g \cdot H)^{1/2}} = 3.9 \text{ hr}$	Transverse seiche period

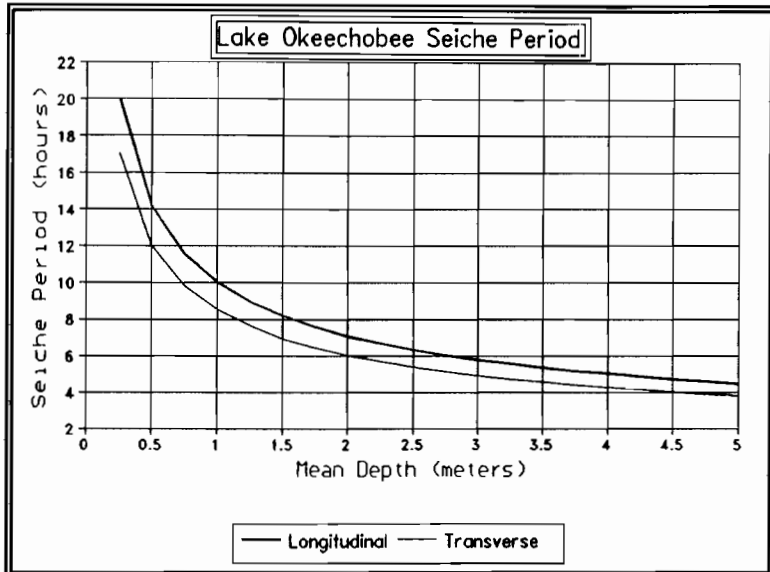


Figure 10-5 Longitudinal and transverse seiche periods.

for Lake Okeechobee, using the characteristic physical parameters given in Table 10-1 and an eddy viscosity, $A_V = 10 \text{ cm}^2/\text{s}$.

Platzman (1963) showed that gravitational modes (i.e., seiches) are under-damped (oscillatory) for $P_r < 0.53$ and over-damped (non-oscillatory) for $P_r > 0.53$. Even if the mean depth were used in Eq. (10.4-1) (instead of the maximum depth of 4.7 m), the Proudman number would still be less than 0.53, indicating that frictional damping in Lake Okeechobee will dampen seiches slowly.

The governing 3-D equation (10.3-9) may be converted to a non-dimensional form by using the following relationships. Note that in the following presentation, the variables in **bold** are the dimensionless variables.

$$\mathbf{u} = \frac{\mathbf{u}}{U_{\text{ref}}} \quad (10.4-2)$$

$$\mathbf{v} = \frac{\mathbf{v}}{U_{\text{ref}}} \quad (10.4-3)$$

$$\omega = \frac{\omega \cdot X_{\text{ref}}}{Z_{\text{ref}} \cdot U_{\text{ref}}} \quad (10.4-4)$$

$$x = \frac{x}{X_{ref}} \quad (10.4-5)$$

$$y = \frac{y}{X_{ref}} \quad (10.4-6)$$

$$z = \frac{z \cdot X_{ref}}{Z_{ref} \cdot X_{ref}} \quad (10.4-7)$$

$$t = t \cdot f \quad (10.4-8)$$

$$\eta = \frac{\eta \cdot g}{f \cdot X_{ref} \cdot U_{ref}} \quad (10.4-9)$$

$$H = \frac{H}{Z_{ref}} \quad (10.4-10)$$

$$A_H = \frac{A_H}{(A_H)_r} \quad (10.4-11)$$

$$A_v = \frac{A_v}{(A_v)_r} \quad (10.4-12)$$

10.5 Transformation of Governing Equations to Dimensionless Form

In anticipation of the forthcoming finite difference scheme, Equation 10.3-9 is first written in dimensional form, but distinguishing between values of depth predicted at the center (H_s), left-hand side or U-face (H_u), and bottom or V-face (H_v) of computational cells.

$$\begin{aligned} \frac{1}{H_s} \frac{\partial H_s C_i}{\partial t} + \frac{1}{H_s} \left[\frac{\partial u \cdot H_u \cdot C_i}{\partial x} + \frac{\partial v \cdot H_v \cdot C_i}{\partial y} + \frac{\partial \omega \cdot H_s \cdot C_i}{\partial \sigma} \right] = \\ \frac{1}{H_s} \left[\frac{\partial}{\partial x} E_x H_s \frac{\partial C_i}{\partial x} + \frac{\partial}{\partial y} E_y H_s \frac{\partial C_i}{\partial y} + \frac{\partial}{\partial \sigma} E_\sigma \frac{\partial C_i}{\partial \sigma} \right] \pm R_i \end{aligned} \quad (10.5-1)$$

where C_i = phosphorus species concentration in center of cell,
 E_x = horizontal diffusivity in x direction,
 E_y = horizontal diffusivity in y direction,
 E_σ = vertical diffusion in σ direction,
 H_s = center dimensionless cell depth,
 H_u = U face dimensionless cell depth,
 H_v = V face dimensionless cell depth,
 R_i = reaction terms in cell,
 u = dimensionless velocity in x direction,
 v = dimensionless velocity in y direction,
 ω = $d\sigma/dt$ or σ velocity
 σ = sigma coordinate,
 ∂x = length of a computational cell in dimensionless x direction
 ∂y = length of a computational cell in dimensionless y direction, and
 $\partial \sigma$ = length of a computational cell in the σ direction.

Substituting the relationships between the dimensional and non-dimensional coordinates and variables into the 3-D equation results in the following non-dimensional equation:

$$\frac{1}{Z_{ref} \cdot H_s} \frac{f \cdot Z_{ref} \cdot \partial H_s \cdot C_i}{\partial t} + \frac{1}{Z_{ref} \cdot H_s} \left[\frac{\partial u \cdot U_{ref} \cdot H_u \cdot Z_{ref} \cdot C_i}{X_{ref} \cdot \partial x} + \right. \\ \left. \frac{\partial v \cdot U_{ref} \cdot H_v \cdot Z_{ref} \cdot C_i}{X_{ref} \cdot \partial y} + \frac{Z_{ref} \cdot U_{ref} \cdot Z_{ref} \cdot \partial x \cdot H_s \cdot C_i}{Z_{ref} \cdot X_{ref} \cdot \partial \sigma} \right] = \\ \frac{1}{Z_{ref} \cdot H_s} \left[\frac{\partial}{X_{ref} \cdot \partial x} A_{Href} \cdot A_H \cdot Z_{ref} \cdot H_s \frac{\partial C_i}{X_{ref} \cdot \partial x} + \right. \\ \left. \frac{\partial}{X_{ref} \cdot \partial y} A_{Href} \cdot A_H \cdot Z_{ref} \cdot H_s \frac{\partial C_i}{X_{ref} \cdot \partial y} + \frac{\partial}{Z_{ref} \cdot H_s \cdot \partial \sigma} A_{vref} \cdot A_v \frac{\partial C_i}{\partial \sigma} \right] \pm R_i \quad (10.5.2)$$

Dividing each term of Eq. (10.5-2) by f and canceling Z_{ref} in the numerator and denominator leads to the following equation for the bold non-dimensional variables:

$$\begin{aligned}
& \frac{1}{H_s} \frac{\partial H_s \cdot C_i}{\partial t} + \frac{1}{H_s} \left[\frac{\partial u \cdot U_{ref} \cdot H_u \cdot C_i}{f \cdot X_{ref} \cdot \partial x} + \frac{\partial v \cdot U_{ref} \cdot H_v \cdot C_i}{f \cdot X_{ref} \cdot \partial y} + \right. \\
& \left. \frac{U_{ref} \cdot \partial x \cdot H_s \cdot C_i}{f \cdot X_{ref} \cdot \partial \sigma} \right] = \frac{1}{f \cdot H_s} \left[\frac{\partial}{X_{ref} \cdot \partial x} A_{H_{ref}} \cdot A_H \cdot Z_{ref} \cdot H_s \frac{\partial C_i}{X_{ref} \cdot \partial x} + \right. \\
& \left. \frac{\partial}{X_{ref} \cdot \partial y} A_{H_{ref}} \cdot A_H \cdot H_s \frac{\partial C_i}{X_{ref} \cdot \partial y} + \frac{\partial}{Z_{ref}^2 \cdot H_s \partial \sigma} A_{v_{ref}} \cdot A_v \frac{\partial C_i}{\partial \sigma} \right] \pm R_i/f
\end{aligned} \tag{10.5.3}$$

In terms of the dimensionless Rossby number (R_o), horizontal Ekman number (E_h) and vertical Ekman number (E_v) (all defined in Table 10-1), Eq. (10.5-3) becomes

$$\begin{aligned}
& \frac{1}{H_s} \frac{\partial H_s \cdot C_i}{\partial t} + \frac{R_o}{H_s} \left[\frac{\partial u \cdot H_u \cdot C_i}{\partial x} + \frac{\partial v \cdot H_v \cdot C_i}{\partial y} + \frac{\partial x \cdot H_s \cdot C_i}{f \cdot X_{ref} \cdot \partial \sigma} \right] = \\
& \frac{E_h}{H_s} \left[\frac{\partial}{\partial x} A_H \cdot H_s \frac{\partial C_i}{\partial x} + \frac{\partial}{\partial y} A_H \cdot H_s \frac{\partial C_i}{\partial y} \right] + \frac{E_v}{H_s \cdot H_s} \frac{\partial}{\partial \sigma} A_v \frac{\partial C_i}{\partial \sigma} \pm R_i/f
\end{aligned} \tag{10.5-4}$$

Equation (10.5-4) is the basic equation solved using the numerical finite difference solutions in LOP3D.

The dimensionless numbers in Table 10-2 are based on the characteristic parameter values for Lake Okeechobee given in Table 10-1. A small Peclet number (P_e) means diffusion is dominant, whereas a large P_e means advection is dominant. Thus, diffusion dominates vertically, while advection dominates horizontally.

The dimensional vertically averaged continuity equation can be written as follows:

$$\frac{\partial \eta}{\partial t} + \Sigma \left[\frac{\partial u \cdot H_u}{\partial x} + \frac{\partial v \cdot H_v}{\partial y} \right] = 0 \tag{10.5-5}$$

Substituting the relationships between the dimensional and non-dimensional coordinates and variables in the continuity equation results in the following non-dimensional equation:

$$\frac{Z_{ref} \cdot f \cdot f \cdot U_{ref} \cdot X_{ref} \cdot \partial\eta}{\eta \cdot \partial t} + \Sigma \left[\frac{U_{ref} \cdot Z_{ref} \cdot \partial u \cdot H_u}{X_{ref} \cdot \partial x} + \frac{U_{ref} \cdot Z_{ref} \cdot \partial v \cdot H_v}{X_{ref} \cdot \partial y} \right] = 0 \quad (10.5-6)$$

where the bold variables are dimensionless. Dividing by U_{ref} and Z_{ref} and using the non-dimensional variable β (Table 10-2) results in the following dimensionless continuity equation:

$$\frac{\partial\eta}{\partial t} + \frac{\beta}{Z_{ref}} \cdot \Sigma \left[\frac{\partial u \cdot H_u}{\partial x} + \frac{\partial v \cdot H_v}{\partial y} \right] = 0 \quad (10.5-7)$$

Equation (10.5-7) is used to balance the mass flux through a cell during a simulation that uses longer time steps than the hydrodynamic model. Typically 3 hour time steps are used on a microcomputer because the output from the UF COE hydrodynamic model is extracted only every three hours from a simulation that uses 15 minute time steps.

Table 10-2 Model dimensionless numbers and model values.

A_r	$= \frac{Z_{ref}}{X_{ref}}$	Aspect Ratio	0.0000177
β	$= \frac{g \cdot Z_{ref}}{f^2 \cdot X_{ref}^2}$	Eq. (10.5-7)	0.0704
E_v	$= \frac{A_v}{f \cdot Z_{ref}^2}$	Vertical Ekman Number	15.1
E_H	$= \frac{A_H}{f \cdot X_{ref}^2}$	Horizontal Ekman Number	0.000048
F_r	$= \frac{U_{ref}}{(g \cdot Z_{ref})^{1/2}}$	Froude Number	0.0319
P_{eh}	$= \frac{U_{ref} \cdot X_{ref}}{(A_H)_r}$	Horizontal Peclet Number	564.0
P_{ev}	$= \frac{w_{ref} \cdot Z_{ref}}{(A_v)_r}$	Vertical Peclet Number	10.0
P_r	$= \frac{A_v^2}{(\pi/L)^2 \cdot g \cdot H^5}$	Proudman Number	0.0143
R_o	$= \frac{U_{ref}}{f \cdot X_{ref}}$	Rossby Number	0.027
s_b	$= \frac{F_r^2}{R_o}$	Surface boundary parameter	0.0377
s_c	$= \frac{Z_{ref} \cdot \sqrt{E_v}}{X_{ref} \cdot \sqrt{E_H}}$	Slope parameter	0.994

11. PELAGIC ADVECTION-DIFFUSION SCHEMES

11.1 Introduction

This section describes the numerical techniques used to solve the dimensionless 3-D advection-diffusion (Eq. (10.5-4)). The equation is solved using a finite difference method, and is consistent with the finite difference method used by the UF COE group.

The finite difference scheme utilizes 2-km grid intervals as were used in the development of the sediment-hydrodynamic model. Each grid cell of the model is a square box with an area of 4 km^2 (Figures 11-1 and 11-2). There are a maximum of 26 horizontal (east-west) cells and 29 vertical (north-south) cells for a total of 754 cells in the finite difference model. However, only 486 of these cells are actually computational cells which means a total simulated area of 1944 km^2 for Lake Okeechobee (Figure 11-3). The maximum depth of Lake Okeechobee occurs near the center of the lake (Figure 11-5). Five vertical σ -layers (Figures 11-4 and 11-6) are used in the simulation to minimize the vertical distortion in the abrupt transition between the deep pelagic to the shallow littoral zone of the model (Figure 11-5). The phosphorus or sediment concentration for 2438 model data points must be calculated for each time step simulated.

The model uses a staggered grid for the computation of phosphorus. The calculated concentration is the center point of the cell in the x , y , and σ directions (Figures 11-2, 11-3, 11-4 and 11-6). A staggered grid has the computational points for velocity a half grid cell from the concentration computational data point. The concentrations are thus at the cell center and the u , v , and ω velocities are located on the cell faces. The model has a greater density of depths since it uses the depth at the u and v cell faces in the calculation of the advective flux (Figures 11-7 and 11-8).

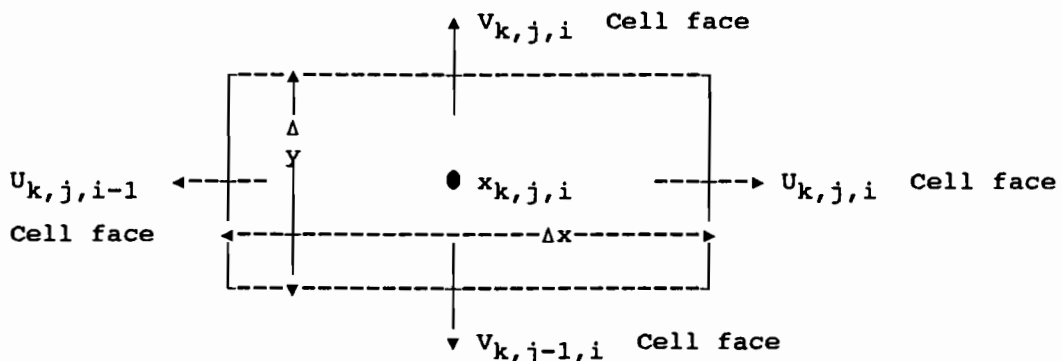


Figure 11-1 Cell nomenclature in x and y directions.

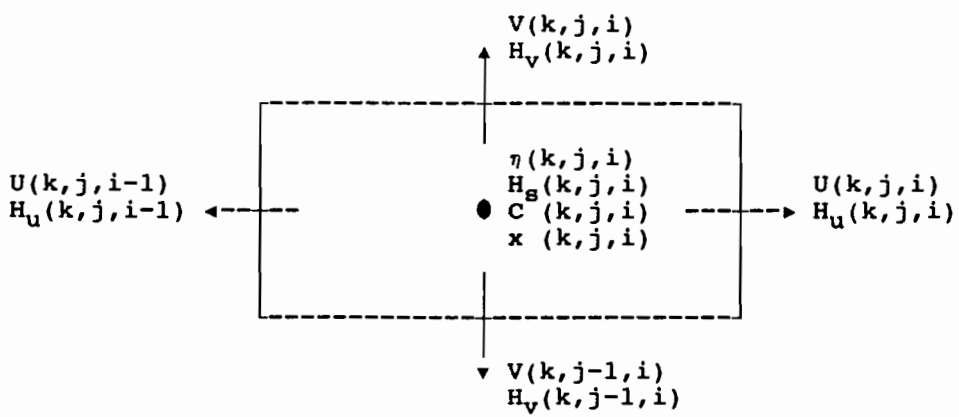


Figure 11-2 Computational cell used in advection-diffusion reaction equation in $\sigma \equiv k$, $y \equiv j$, and $x \equiv i$ directions.
Note: η is contained in array S in the computer program.

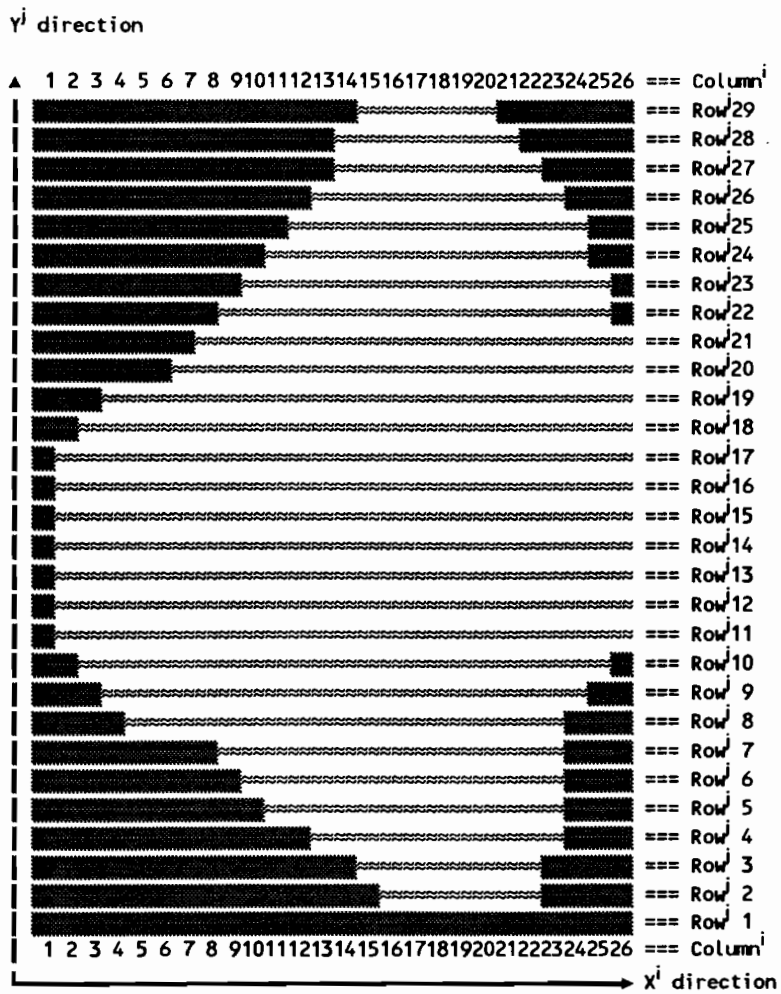


Figure 11-3 X and Y directions in finite difference pelagic model.

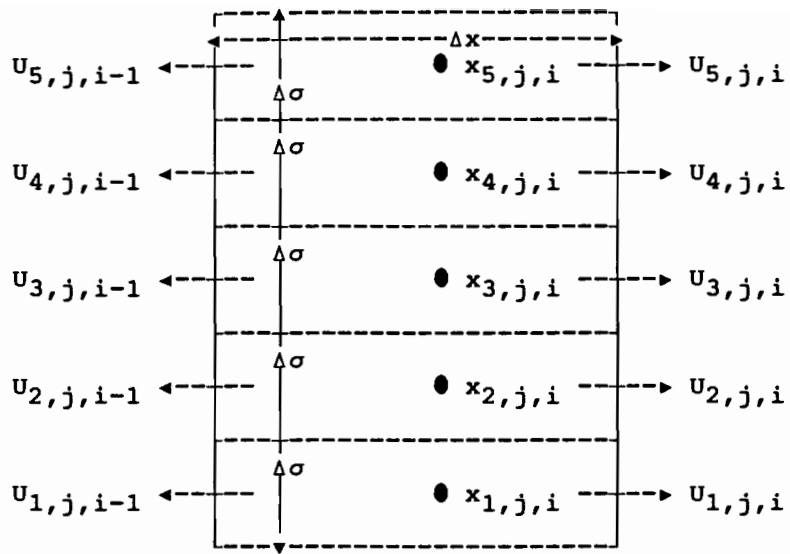


Figure 11-4 Computational cell nomenclature in x and σ directions for a five layer model.

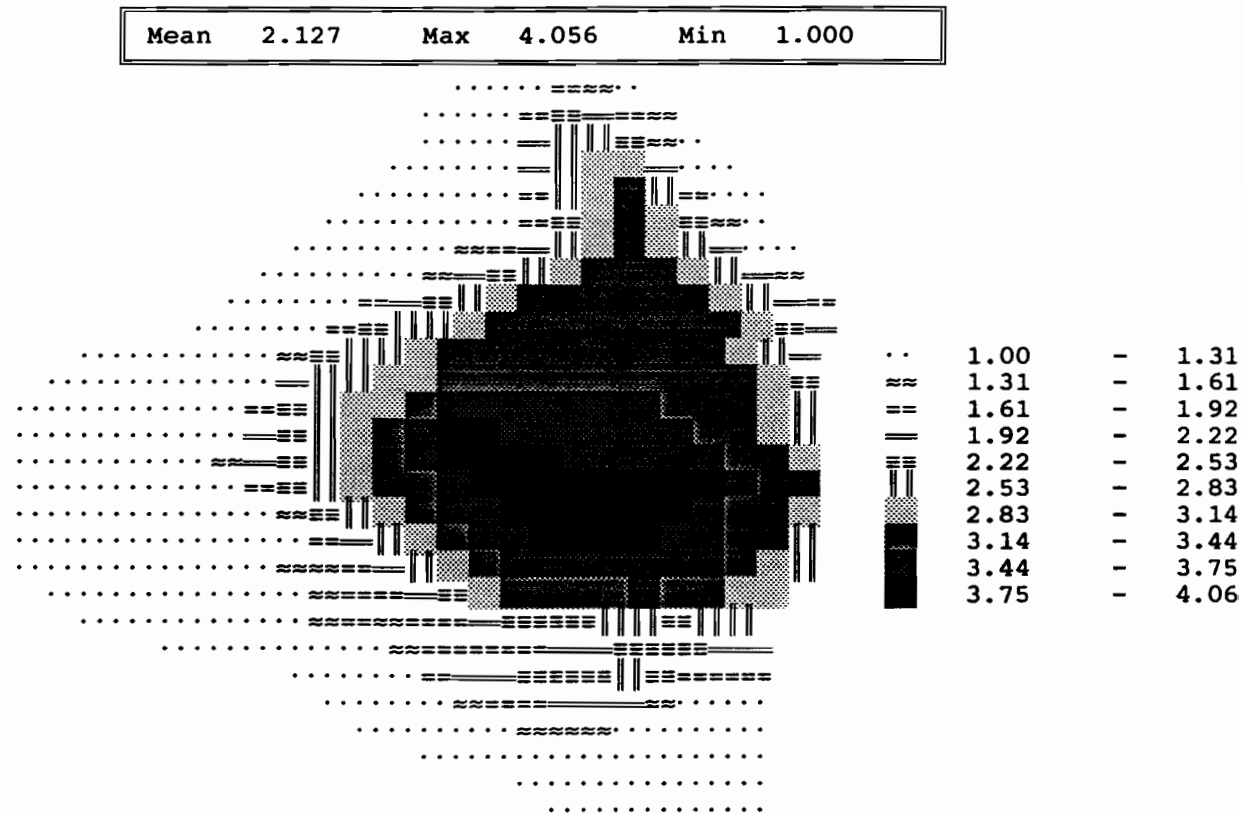


Figure 11-5 Center cell depth in meters for Lake Okeechobee.

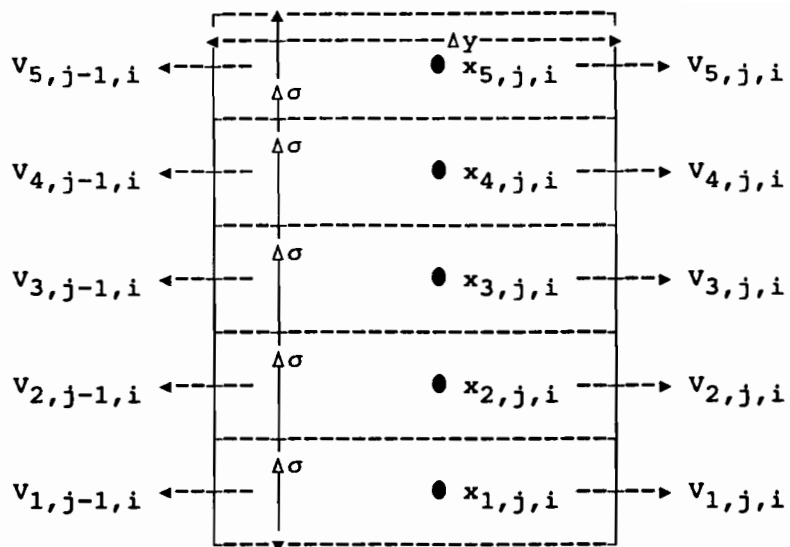


Figure 11-6 Cell nomenclature in y and σ directions for a five vertical layer model.

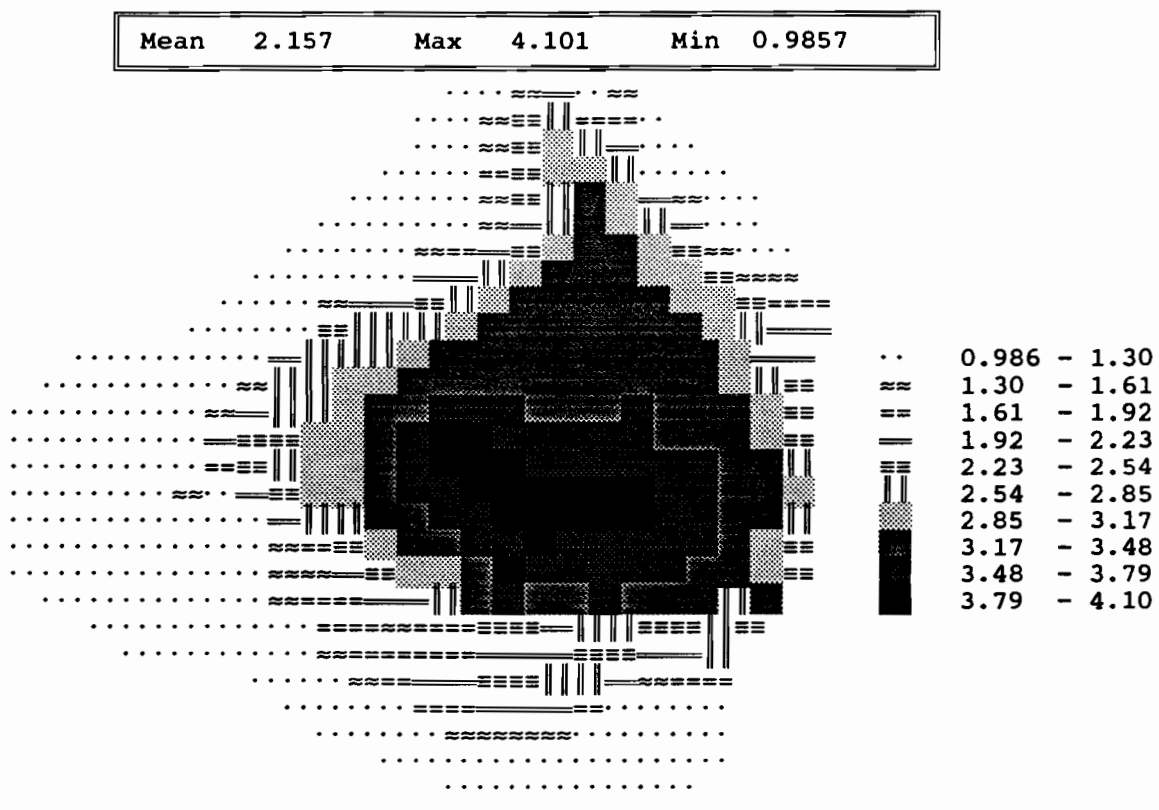


Figure 11-7 The depth at the U face cell (meters).

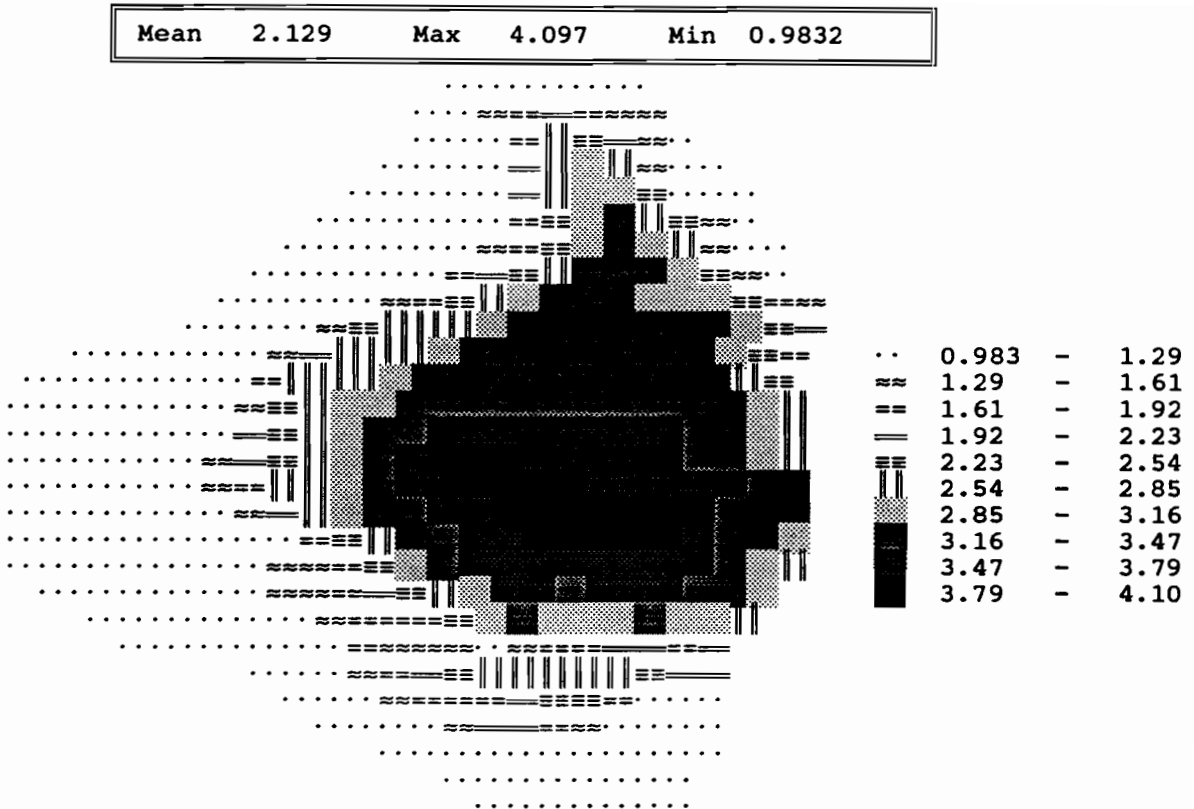


Figure 11-8 The depth at the V face cells (meters).

11.2 Upwind Solution

The upwind method for is a finite difference numerical scheme for solving the advective terms in the advection equation. Fluxes are defined according to the direction of flow along a boundary. For example, the flux component to the right (east), f_R , is:

$$f_R = u_{k,j,i} \cdot H_{uj,i} \cdot C_{k,j,i+1} \quad \text{if } u_{k,j,i} \leq 0 \quad (11.2-1)$$

$$= u_{k,j,i} \cdot H_{uj,i} \cdot C_{k,j,i} \quad \text{if } u_{k,j,i} > 0$$

The concentration used in the upwind method is the concentration in the cell **downstream** from the current cell. The u component to the left (west), f_L , is:

$$f_L = u_{k,j,i-1} \cdot H_{uj,i-1} \cdot C_{k,j,i} \quad \text{if } u_{k,j,i-1} \leq 0 \quad (11.2-2)$$

$$= u_{k,j,i-1} \cdot H_{uj,i-1} \cdot C_{k,j,i-1} \quad \text{if } u_{k,j,i-1} > 0$$

and the v component up (north), f_{up} , is:

$$\begin{aligned} f_{up} &= v_{k,j,i} \cdot H_{vj,i} \cdot C_{k,j+1,i} && \text{if } v_{k,j,i} \leq 0 \\ &= v_{k,j,i} \cdot H_{vj,i} \cdot C_{k,j,i} && \text{if } v_{k,j,i} > 0 \end{aligned} \quad (11.2-3)$$

and the v component down (south), f_{dn} , is:

$$\begin{aligned} f_{dn} &= v_{k,j-1,i} \cdot H_{vj-1,i} \cdot C_{k,j,i} && \text{if } v_{k,j-1,i} \leq 0 \\ &= v_{k,j-1,i} \cdot H_{vj-1,i} \cdot C_{k,j-1,i} && \text{if } v_{k,j-1,i} > 0 \end{aligned} \quad (11.2-4)$$

where the f-terms are the upwind fluxes through the walls of the computational cell (Sheng, 1983; Peyret and Taylor, 1983).

The upwind scheme has the following stability requirements:

$$\frac{u \cdot \Delta t}{\Delta x} \leq 1 \quad (11.2-5)$$

$$\frac{v \cdot \Delta t}{\Delta x} \leq 1 \quad (11.2-6)$$

$$\frac{E_x \cdot \Delta t}{(\Delta x)^2} + \frac{E_y \cdot \Delta t}{(\Delta x)^2} \leq 1/2 \quad (11.2-7)$$

The upwind method is satisfactory only when the Courant numbers (defined by Eqs. (11.2-5) and (11.2-6)) are < 1.0 ; otherwise there is excessive numerical diffusion.

The horizontal diffusive flux components in the x and y directions, d_R , d_L , d_{up} , and d_{dn} to the right, left, up and down directions respectively, are calculated based on the concentration differences in the computational cell centers. For example, the diffusive flux to the right is:

$$d_R = \frac{H_s \cdot (C_{k,j,i+1} - C_{k,j,i})}{\Delta x} \quad (11.2-8)$$

and the diffusive flux to the left is written as:

$$d_L = \frac{H_s \cdot (C_{k,j,i} - C_{k,j,i-1})}{\Delta x} \quad (11.2-9)$$

11.3 Central Difference

The central difference numerical scheme for solving the advective terms in Eq. (10.5-4) uses the average of the concentration across a boundary. For example, the flux component to the right (east), f_R , is:

$$f_R = u_{k,j,i} \cdot H_{uj,i} \cdot (C_{k,j,i+1} + C_{k,j,i})/2.0 \quad (11.3-1)$$

the u component to the left (west), f_L , is:

$$f_L = u_{k,j,i-1} \cdot H_{uj,i-1} \cdot (C_{k,j,i-1} + C_{k,j,i})/2.0 \quad (11.3-2)$$

the v component up (to the north), f_{up} , is:

$$f_{up} = v_{k,j,i} \cdot H_{vj,i} \cdot (C_{k,j+1,i} + C_{k,j,i})/2.0 \quad (11.3-3)$$

and the v component down (south), f_{dn} , is:

$$f_{dn} = v_{k,j-1,i} \cdot H_{vj-1,i} \cdot (C_{k,j-1,i} + C_{k,j,i})/2.0 \quad (11.3-4)$$

The main drawback of the central difference solution is the oscillatory concentration solutions if the cell P_e number is greater than 2.

11.4 Combined Upwind and Central Difference

The combined upwind and central difference method for the solution of the advective terms in Eq. (10.5-4) combines the simplicity of the upwind method with the higher order accuracy of the central difference method (Sheng, 1983). Fluxes are defined according to the direction of flow along a boundary and concentration differences between adjacent computational cells. For example, the flux component to the left (west), f_L , is:

$$f_L = u_{k,j,i-1} \cdot H_{uj,i-1} \cdot C_{k,j,i} \quad \text{if } u_{k,j,i-1} \leq 0 \text{ and } C_{k,j,i-1} > C_{k,j,i} \quad (11.4-1)$$

$$f_L = u_{k,j,i-1} \cdot H_{uj,i-1} \cdot (C_{k,j,i} + C_{k,j,i-1})/2 \quad \text{if } u_{k,j,i-1} \leq 0 \text{ and } C_{k,j,i-1} \leq C_{k,j,i} \quad (11.4-2)$$

$$f_L = u_{k,j,i-1} \cdot H_{uj,i-1} \cdot C_{k,j,i} \quad \text{if } u_{k,j,i-1} > 0 \text{ and } C_{k,j,i-1} \leq C_{k,j,i} \quad (11.4-3)$$

$$f_L = u_{k,j,i-1} \cdot H_{uj,i-1} \cdot (C_{k,j,i} + C_{k,j,i-1})/2 \quad \text{if } u_{k,j,i-1} > 0 \text{ and } C_{k,j,i-1} > C_{k,j,i} \quad (11.4-4)$$

Similar forms to Eqs. (11.4-1) through (11.4-4) are used to calculate f_R , f_{dn} , and f_{up} .

11.5 Vertical Advection and Diffusion

The advective and diffusive flux for the first σ layer ($k=1$) is:

$$d_k = \frac{H^n \cdot GB_{k+1}^{n+1}}{\Delta\sigma^2 \cdot H^{n+1} \cdot H^{n+1}} \cdot C_{k+1}^{n+1} - \frac{H^n \cdot GB_{k+1}^{n+1}}{\Delta\sigma^2 \cdot H^{n+1} \cdot H^{n+1}} \cdot C_k^{n+1} \quad (11.5-1)$$

$$f_k = \frac{\omega_k^{n+1}}{\Delta\sigma} \cdot C_k^{n+1} \quad \text{if } \omega_k^{n+1} > 0 \quad (11.5-2)$$

$$f_k = \frac{\omega_k^{n+1}}{\Delta\sigma} \cdot C_{k+1}^{n+1} \quad \text{if } \omega_k^{n+1} \leq 0 \quad (11.5-3)$$

The advective and diffusive fluxes through the intermediate σ layers are:

$$\begin{aligned} d_k &= \frac{H^n \cdot GB_k^{n+1}}{\Delta\sigma^2 \cdot H^{n+1} \cdot H^{n+1}} \cdot C_{k+1}^{n+1} - \frac{H^n \cdot GB_k^{n+1}}{\Delta\sigma^2 \cdot H^{n+1} \cdot H^{n+1}} \cdot C_k^{n+1} \\ &\quad - \frac{H^n \cdot GB_{k-1}^{n+1}}{\Delta\sigma^2 \cdot H^{n+1} \cdot H^{n+1}} \cdot C_k^{n+1} - \frac{H^n \cdot GB_{k-1}^{n+1}}{\Delta\sigma^2 \cdot H^{n+1} \cdot H^{n+1}} \cdot C_{k-1}^{n+1} \end{aligned} \quad (11.5-4)$$

$$f_k = \frac{\omega_k^{n+1}}{\Delta\sigma} \cdot C_{k+1}^{n+1} + \frac{(\omega_k - \omega_{k-1})}{2 \cdot \Delta\sigma} \cdot C_k^{n+1} - \frac{\omega_{k-1}}{\Delta\sigma} \cdot C_{k-1}^{n+1} \quad (11.5-5)$$

The advective and diffusive flux for the last σ layer is:

$$d_k = \frac{H^n \cdot GB_{k-1}^{n+1}}{\Delta\sigma^2 \cdot H^{n+1} \cdot H^{n+1}} \cdot C_{k-1}^{n+1} - \frac{H^n \cdot GB_{k-1}^{n+1}}{\Delta\sigma^2 \cdot H^{n+1} \cdot H^{n+1}} \cdot C_k^{n+1} \quad (11.5-6)$$

$$f_k = \frac{-\omega_{k-1}^{n+1}}{\Delta\sigma} \cdot C_{k-1}^{n+1} \quad \text{if } \omega_{k-1}^{n+1} > 0 \quad (11.5-7)$$

$$f_k = \frac{-\omega_{k-1}^{n+1}}{\Delta\sigma} \cdot C_k^{n+1} \quad \text{if } \omega_{k-1}^{n+1} \leq 0 \quad (11.5-8)$$

11.6 3-D Advection-Diffusion Solution

If the grid scheme of Figure 11-1 is used (Sheng, 1983), an explicit advective scheme for the advection terms in the x and y directions, an explicit central difference scheme for the diffusion in the x and y directions is combined with an implicit solution for the vertical advection and diffusion. The solution for any phosphorus species C at the new time step n+1 (denoted by C^{n+1} in Eq. (11.6-4) below) can be written for any cell k,j,i as:

$$F_{xy} = \frac{\Delta t \cdot R_b \cdot (f_r - f_l)}{\Delta x} + \frac{\Delta t \cdot R_b \cdot (f_{up} - f_{dn})}{\Delta y} \quad (11.6-1)$$

$$D_{xy} = \frac{\Delta t \cdot E_h \cdot (d_r - d_l)}{\Delta x} + \frac{\Delta t \cdot E_h \cdot (d_{up} - d_{dn})}{\Delta y} \quad (11.6-3)$$

$$C^{n+1} = \frac{H^n \cdot C^n}{H^{n+1}} + \frac{D_{xy} + F_\sigma + F_{xy}}{H^{n+1}} + \frac{\Delta t \cdot E_v \cdot d_k}{H^{n+1}} + \frac{\Delta t \cdot R_b \cdot f_k H^{n+1}}{H^{n+1}} \quad (11.6-4)$$

The principal numerical difficulty arising from a finite-difference solution is that of numerical diffusion, i.e., an apparent spreading or diffusive effect resulting from the treatment of the advective terms.

The total water depth at the center cell is the sum of the starting depth stored in the H_s array and the dynamic depth η which changes at every time step. The total water depth H for the center cell denoted by the subscripts j,i is:

$$H = H_{sj,i} + \frac{\eta_{j,i} + \eta_{j,i+1}}{2.0} \quad (11.6-5)$$

The total water depth H_u at the u face for a non-boundary cell is:

$$H_u = H_{uj,i} + \frac{\eta_{j,i} + \eta_{j,i+1}}{2.0} \quad (11.6-6)$$

and for a boundary cell H_u is:

$$H_u = H_{uj,i} + \eta_{j,i} \quad (11.6-7)$$

The total water depth H_v at the v cell face for a non-boundary cell is:

$$H_v = H_{vj,i} + \frac{\eta_{j,i} + \eta_{j,i+1}}{2.0} \quad (11.6-8)$$

and for a boundary cell H_v is:

$$H_v = H_{vj,i} + \eta_{j,i} \quad (11.6-9)$$

11.7 Advection and Diffusion Solution Testing

The basic model was first tested using a constant starting concentration of $100 \text{ ug} \cdot \text{l}^{-1}$ for each of the 486 cells and 5 σ -layers. The first series of tests was solely a test of the finite difference solution for vertical advection. The model lake had the same number of grid cells and the same shape as Lake Okeechobee. The model lake used a constant cell depth of 2 meters, had no change in water surface elevation over time, and constant horizontal and vertical velocities and diffusivities. The time step was 3 hours and the total simulation time was 24 hours in the first series of tests.

The result of this first test is shown in Figure 11-9. The average concentration is 100 ug/l , indicating mass is conserved by the finite difference scheme. The top

layer gains a small amount and the bottom layer loses a small amount because the hypothetical vertical velocity advects from zero concentration at the bed and does not advect through the water surface. This is not a problem during actual LOP3D simulations, because the velocity field entered into the model from the UF COE simulations maintains continuity by providing for horizontal convergence (divergence) if the net vertical velocity is out of (into) a cell.

When the bottom layer begins with an initial concentration of 150 ug/l, the result shown in Figure 11-10 again indicates mass is conserved since the average concentration should remain at $(100+100+100+100+150)/5 = 110$. Mass is removed from the bottom layer, and the top layer accumulates some mass because the hypothetical vertical velocity "ends" at the top layer, as explained above. A very similar result is shown in Figure 11-11 for the situation in which all layers but the top start at 100 ug/l. The result shown in Figure 11-12 is essentially the reverse of the case for Figure 11-10; that is, the velocity is negative (downward), and the top layer starts at 150 while the four lower layers start at 100 ug/l. Likewise, the result shown in Figure 11-13 is the reverse of the case for Figure 11-11. Thus, the advective scheme conserves mass in the model, as shown by the results of Figures 11-9 - 11-13.

Diffusion calculations are tested simply in Figures 11-14 and 11-15. In these figures, the results of vertical diffusion are shown from a bottom layer starting at 150 ug/l into upper layers starting at 100 ug/l. With a vertical diffusivity of 1 cm²/sec, mass is diffused upward, but a limited gradient remains (from 118 to 104). With a diffusivity of 5 cm²/sec, the gradient is completely eliminated, and the final concentration ends at a mass-conserving value of 110 ug/l.

Many advective schemes have been developed to minimize numerical diffusion, most of which utilize a higher order difference scheme for the advective derivatives. Other methods include the combined upwind and central difference scheme of Sheng (1983) and the flux-corrected transport (FCT) scheme of Zalesak (1979) and Steinle and Morrow (1989). The FCT scheme substantially decreases the incidence of numerical diffusion and was used by Sheng (1983) for the simulation of sediment transport in estuaries. However, the UF COE model for sediment transport in Lake Okeechobee (EHSMIT) uses Sheng's (1983) combined upwind-central difference scheme. Thus, although the FCT scheme was evaluated, the combined upwind-central was eventually used for consistency with the UF COD modeling. This latter scheme was marginally superior when tested against various analytical solutions for line and plane source releases (Harleman, 1988).

Figures 11-17 - 11-21 illustrate the results of alternative finite difference schemes for advection. These alternatives are listed in Table 11-1, in which parameter ISOL corresponds to an input parameter in the 3-D model LOP3D. The simulations shown in Figures 11-16 - 11-20 illustrate trials using the geometry of Lake Okeechobee. Each simulation begins with a concentration of 200 ug/l in the macrophyte zone and 100 ug/l elsewhere (Figure 11-16) and with a velocity distribution that should move mass toward the north and east.

Table 11-1 Options for advection simulation in LOP3D model.

Model Parameter ISOL	Option	Comment
1	Upwind Method	Section 11.2
2	Donor Cell Method	Not discussed in text
3	Combined Upwind-Central	Section 11.4
4	Central Difference	Section 11.3

The upwind solution shown in Figure 11-17 (ISOL=1) provides a reasonable distribution after 24 hours on the basis of the vertically-averaged cell concentrations indicated by the shading in the figure. Figures 11-18, 11-19 and 11-20 illustrate an implementation of the donor cell method (11-18), an early implementation of the combined upwind-central method (11-19), and the central difference method (11-20). All three suffer in a minor way from maximum concentrations greater than 200 ug/l, due to high concentrations that result from numerical approximations along the concentration boundary. The final scheme used in the LOP3D model corresponds to the combined upwind-central scheme used in the EHSMIT model, and results are shown in Figure 11-21. In this example, concentrations are correctly advected "away from" the values of 200 ug/l, resulting in no values greater than 200 and a reasonable movement into the remainder of the lake.

11.8 Summary

Many numerical schemes are possible for solution of the governing advective-diffusion Eq. (10.5-4) presented in Chapter 10. In this chapter, the five-layer schematization and notation have been presented, along with descriptions of the finite difference schemes and numerical tests for three options. Because of good test results and in order to maintain consistency with the UF COE sediment model, the combined upwind-central difference scheme is recommended for users of the 3-D, transient, LOP3D phosphorus transport model.

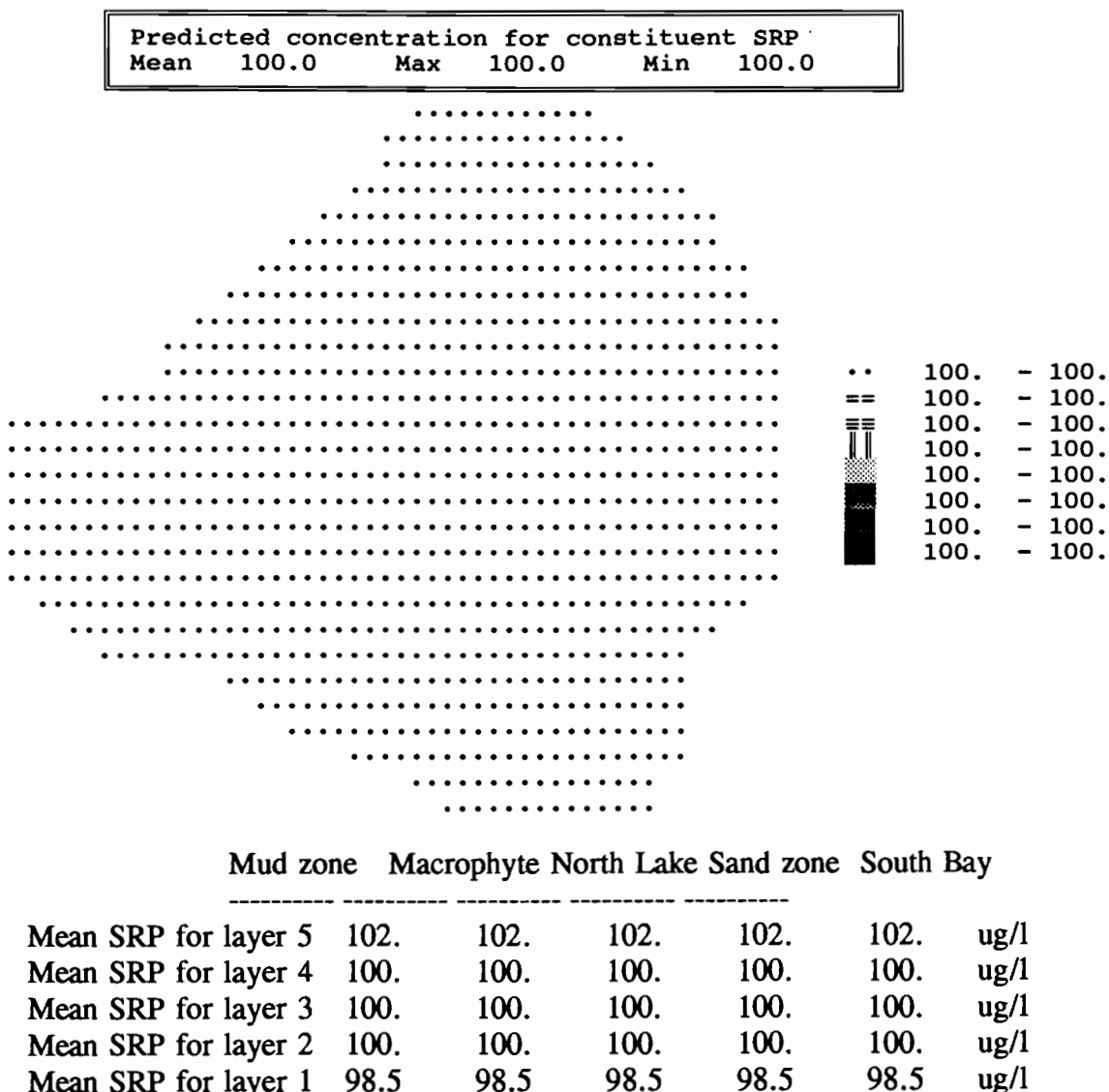


Figure 11-9 Ending simulation concentrations at the end of 24 hours using a time step of 3 hours and a constant initial concentration of $100 \text{ ug} \cdot \text{l}^{-1}$ subject to a vertical σ -velocity of $+50 \text{ sec}^{-1}$. Scale to right of graph represents average concentration of the five layers.

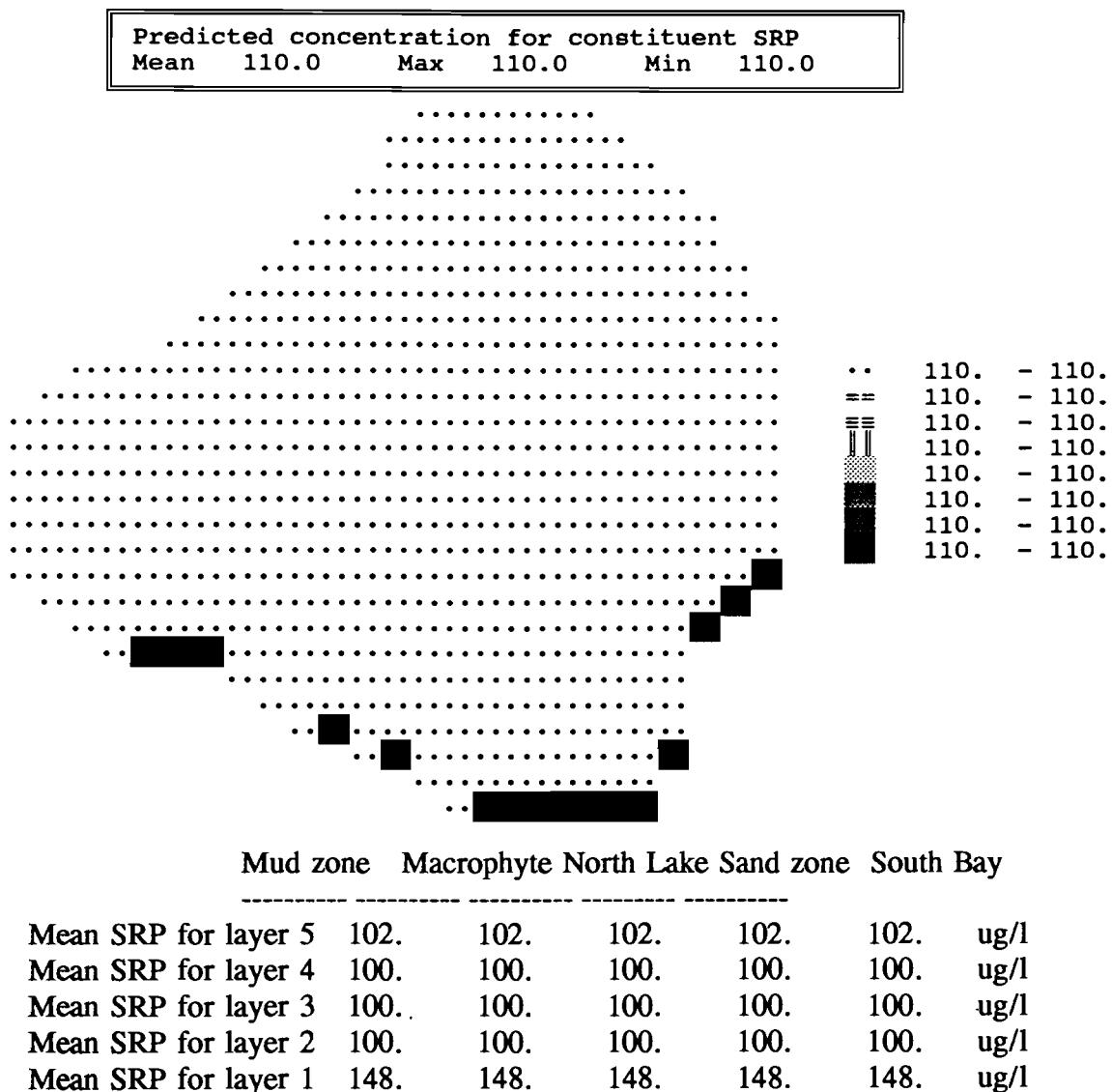


Figure 11-10 Ending simulation concentrations at the end of 24 hours using a time step of 3 hours and a constant initial concentration of $100 \text{ ug} \cdot \text{l}^{-1}$ for σ -layers 2, 3, 4, and 5 and $150 \text{ ug} \cdot \text{l}^{-1}$ for the bottom σ layer using a vertical σ -velocity of 50 sec^{-1} .

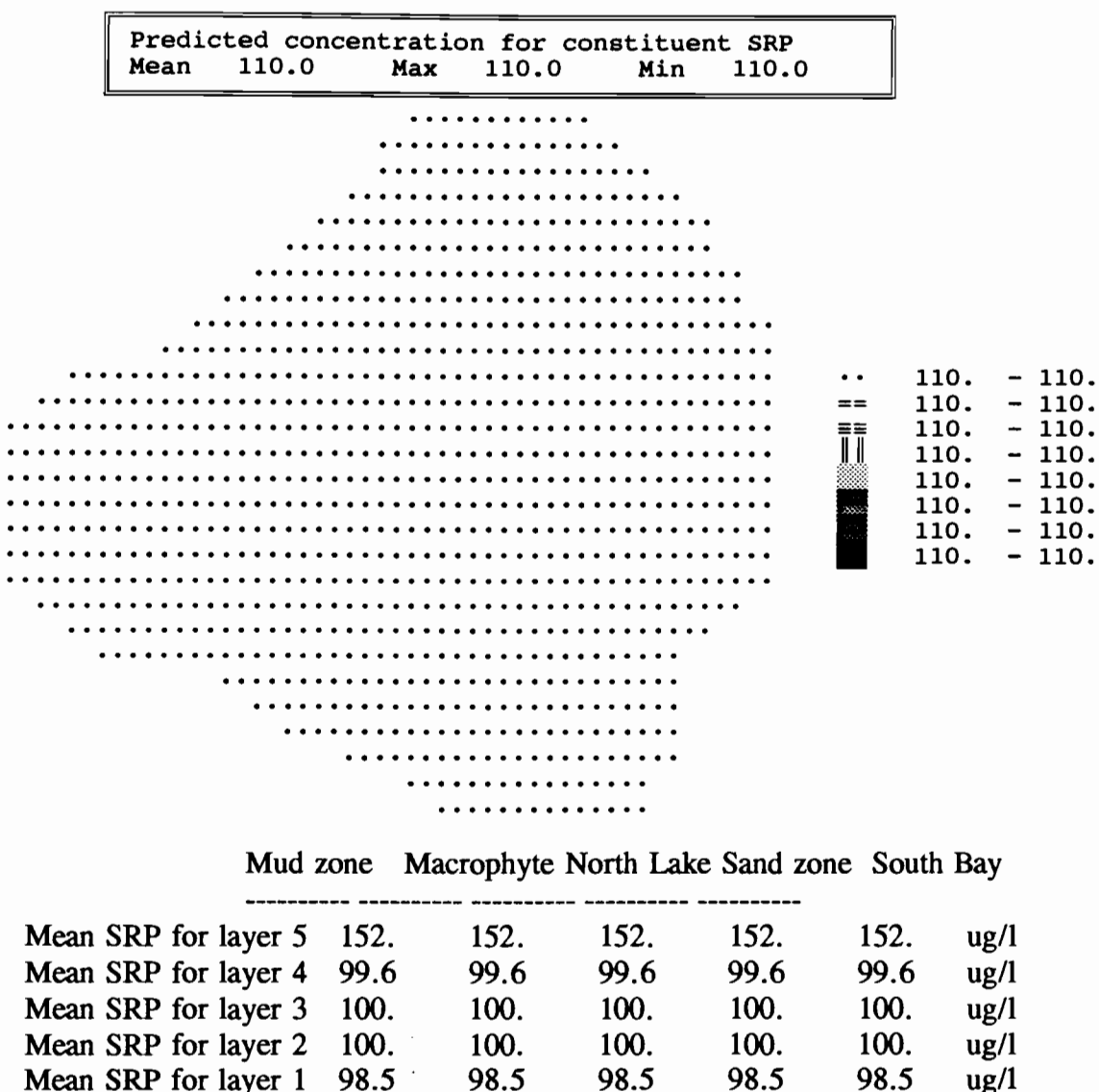


Figure 11-11 Ending simulation concentrations at the end of 24 hours using a time step of 3 hours and a constant initial concentration of $100 \text{ ug} \cdot \text{l}^{-1}$ for σ -layers 1, 2, 3, and 4 and $150 \text{ ug} \cdot \text{l}^{-1}$ for the top σ layer subject to a vertical σ -velocity of 50 sec^{-1} .

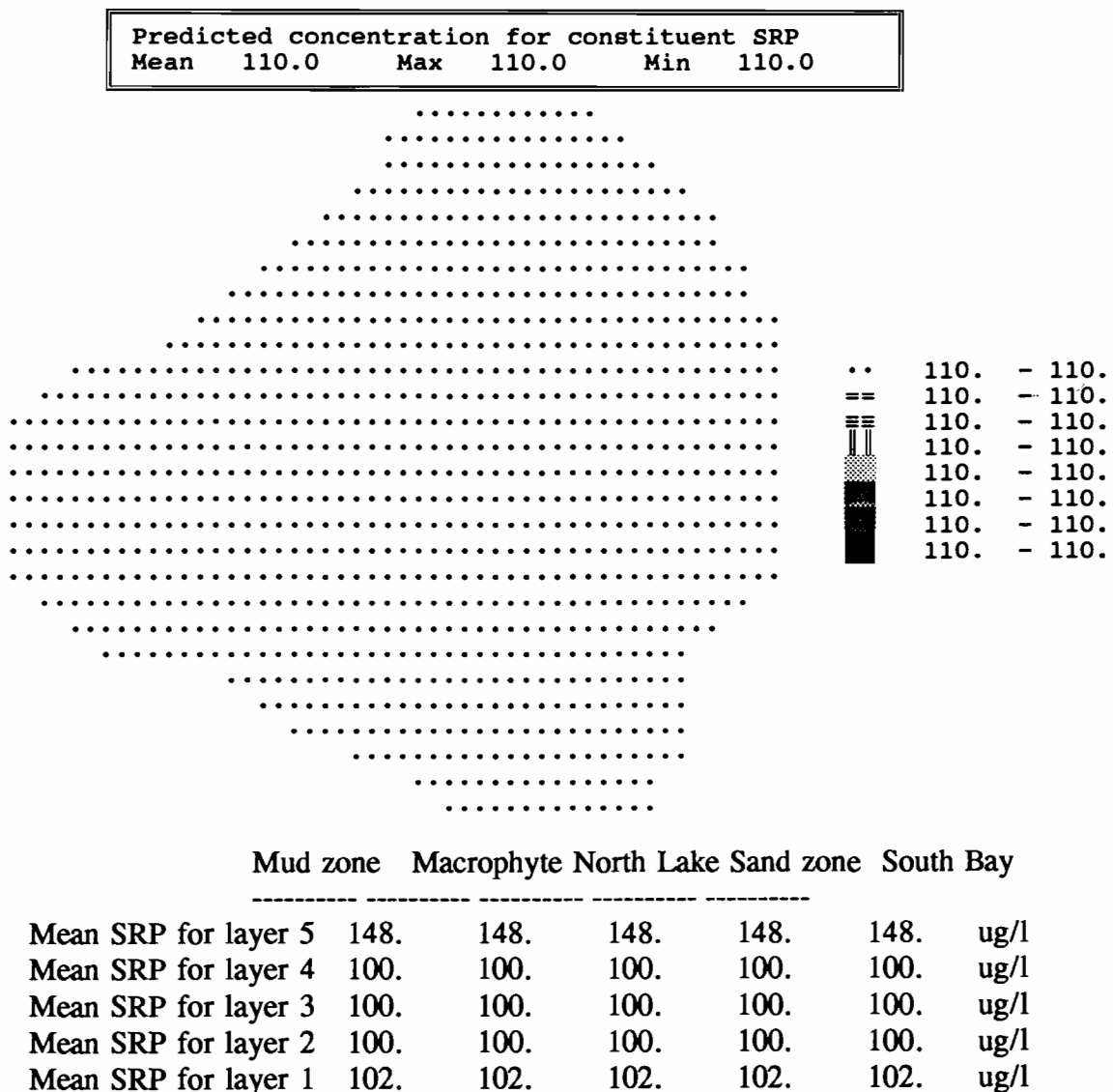


Figure 11-12 Ending simulation concentrations at the end of 24 hours using a time step of 3 hours and a constant initial concentration of $100 \text{ ug} \cdot \text{l}^{-1}$ for σ layers 1, 2, 3, and 4 and $150 \text{ ug} \cdot \text{l}^{-1}$ for the top σ -layer subject to a vertical σ -velocity of -50 sec^{-1} .

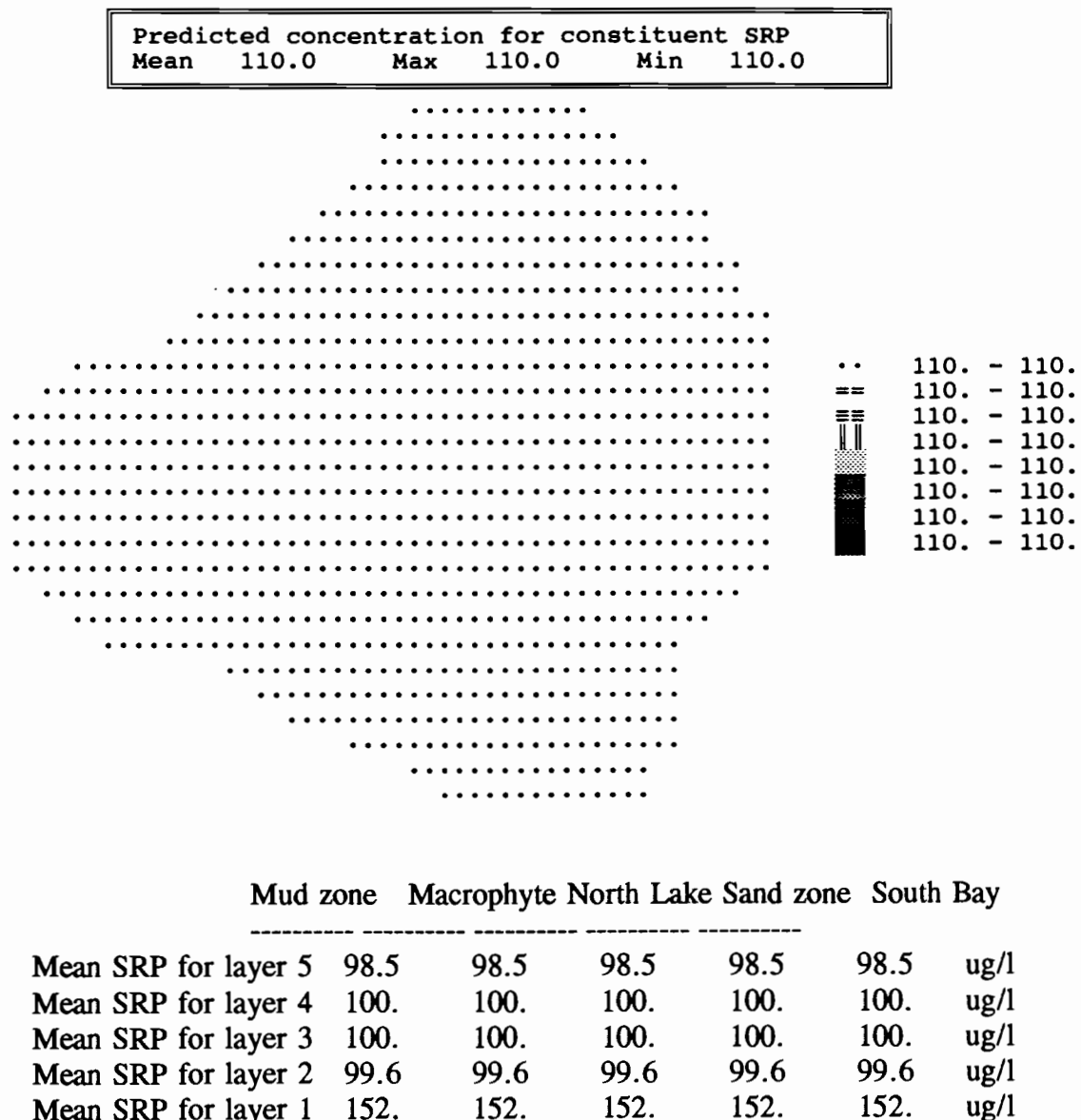


Figure 11-13 Ending simulation concentrations at the end of 24 hours using a time step of 3 hours and a constant initial concentration of $100 \text{ ug} \cdot \text{l}^{-1}$ for σ layers 2, 3, 4, and 5 and $150 \text{ ug} \cdot \text{l}^{-1}$ for the bottom σ layer subject to a vertical σ -velocity of -50 sec^{-1} .

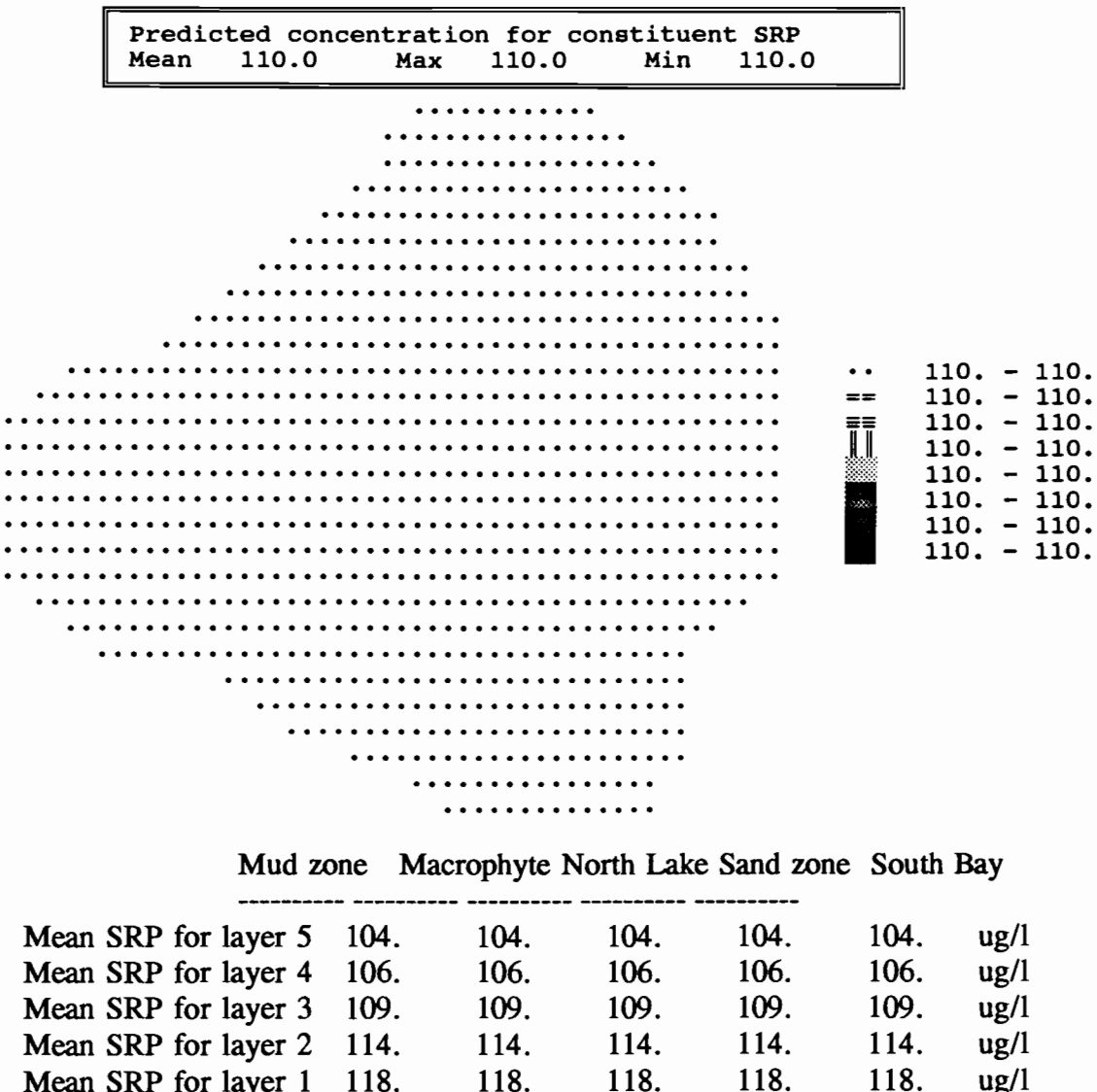


Figure 11-14 Ending simulation concentrations at the end of 1 hour using a time step of 15 minutes and a constant initial concentration of $100 \text{ ug} \cdot \text{l}^{-1}$ for σ layers 2, 3, 4, and 5 and $150 \text{ ug} \cdot \text{l}^{-1}$ for the bottom σ -layer using a vertical diffusion coefficient of $1.0 \text{ cm}^2 \cdot \text{sec}^{-1}$.

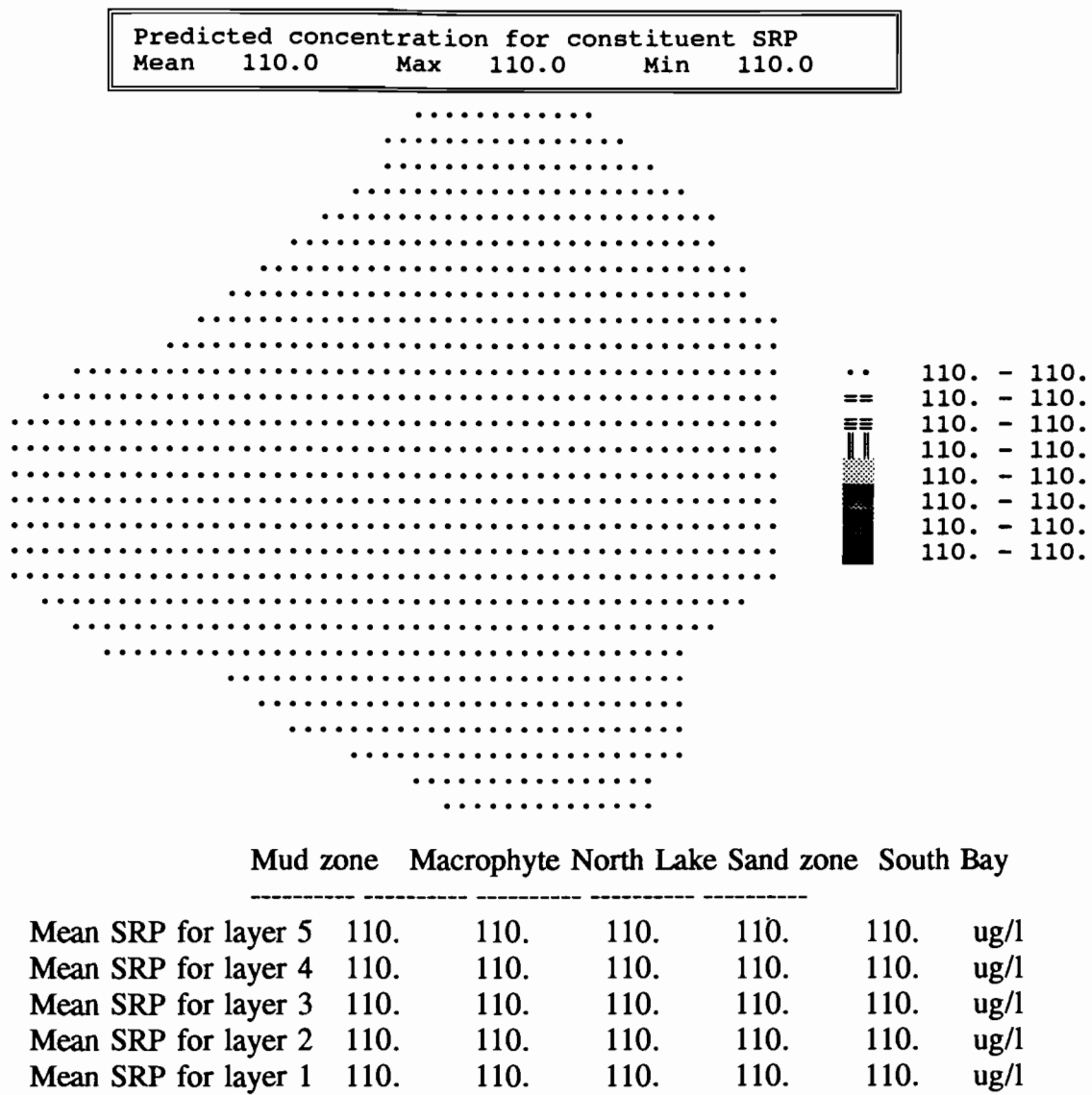


Figure 11-15 Ending simulation concentrations at the end of 1 hour using a time step of 15 minutes and a constant initial concentration of $100 \text{ ug} \cdot \text{l}^{-1}$ for σ layers 2, 3, 4, and 5 and $150 \text{ ug} \cdot \text{l}^{-1}$ for the bottom σ layer subject to a vertical diffusion coefficient of $5.0 \text{ cm}^2 \cdot \text{sec}^{-1}$.

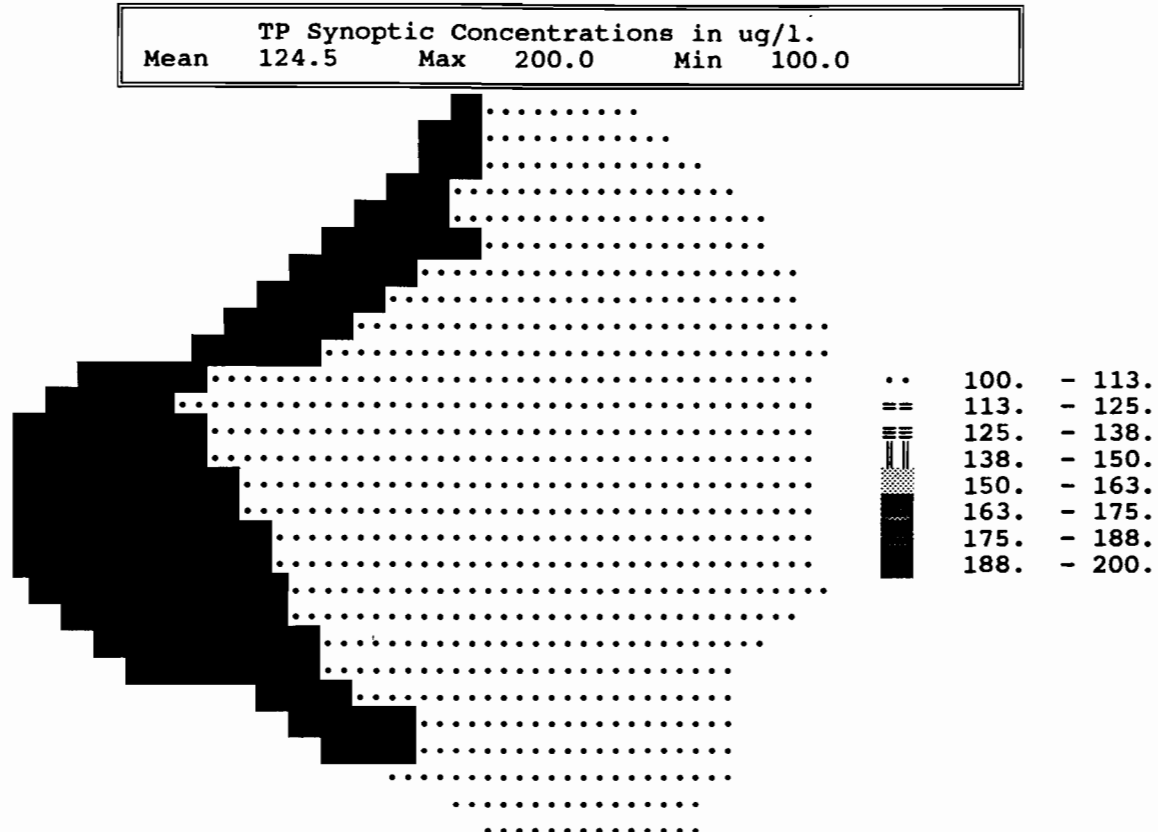


Figure 11-16 Beginning simulation concentrations (200 ug/l in macrophyte zone, 100 elsewhere) for comparison of advection schemes.

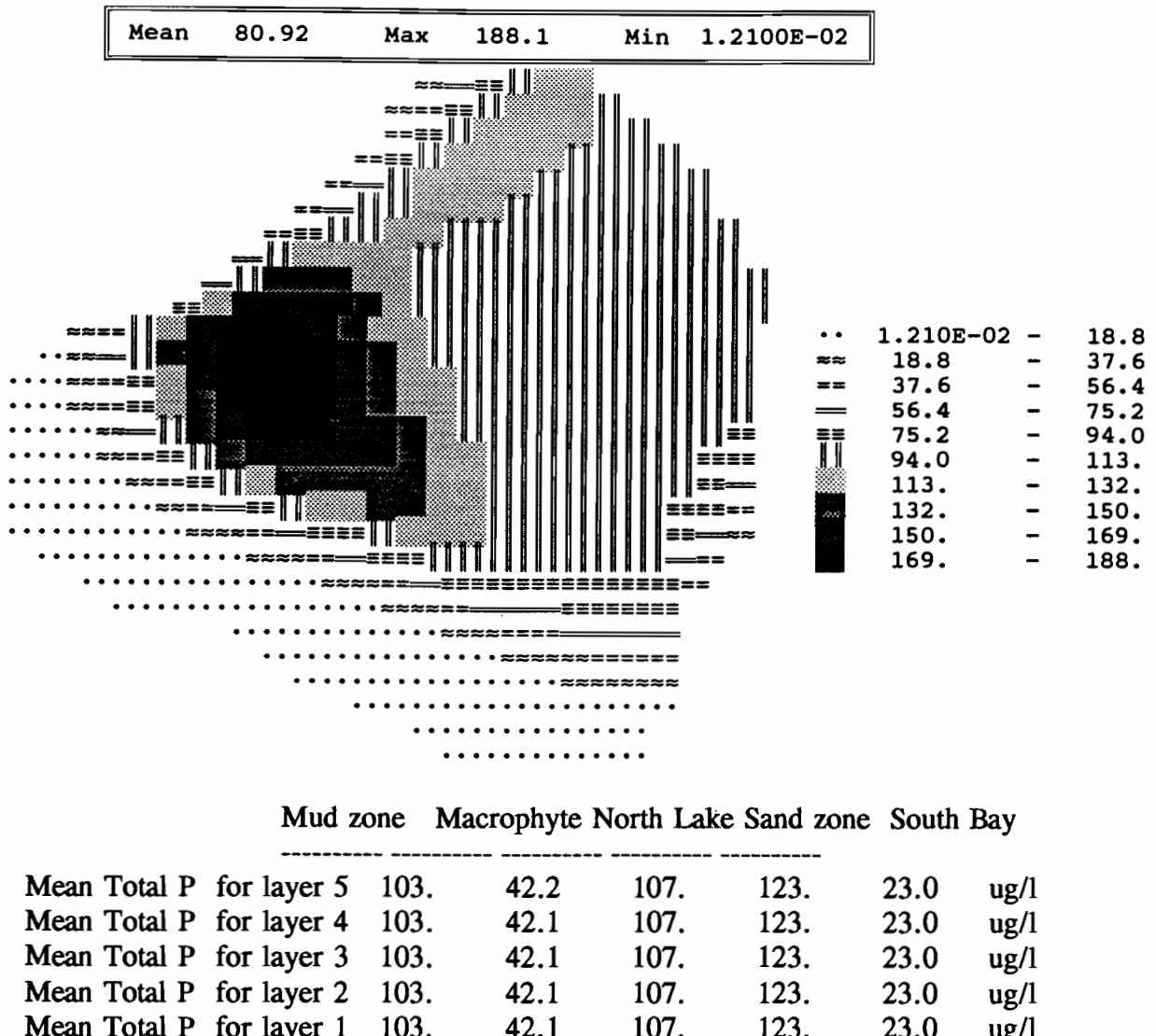


Figure 11-17 Ending simulation concentrations at the end of 24 hours using a time step of 1 hour and a constant initial concentration of $100 \text{ ug} \cdot \text{l}^{-1}$ for mud, north lake, sand, and south bay and $200 \text{ ug} \cdot \text{l}^{-1}$ for the macrophyte zone subject to a constant u and v velocity of $0.1 \text{ cm} \cdot \text{sec}^{-1}$, using the LOP3D solution and ISOL value of 1.

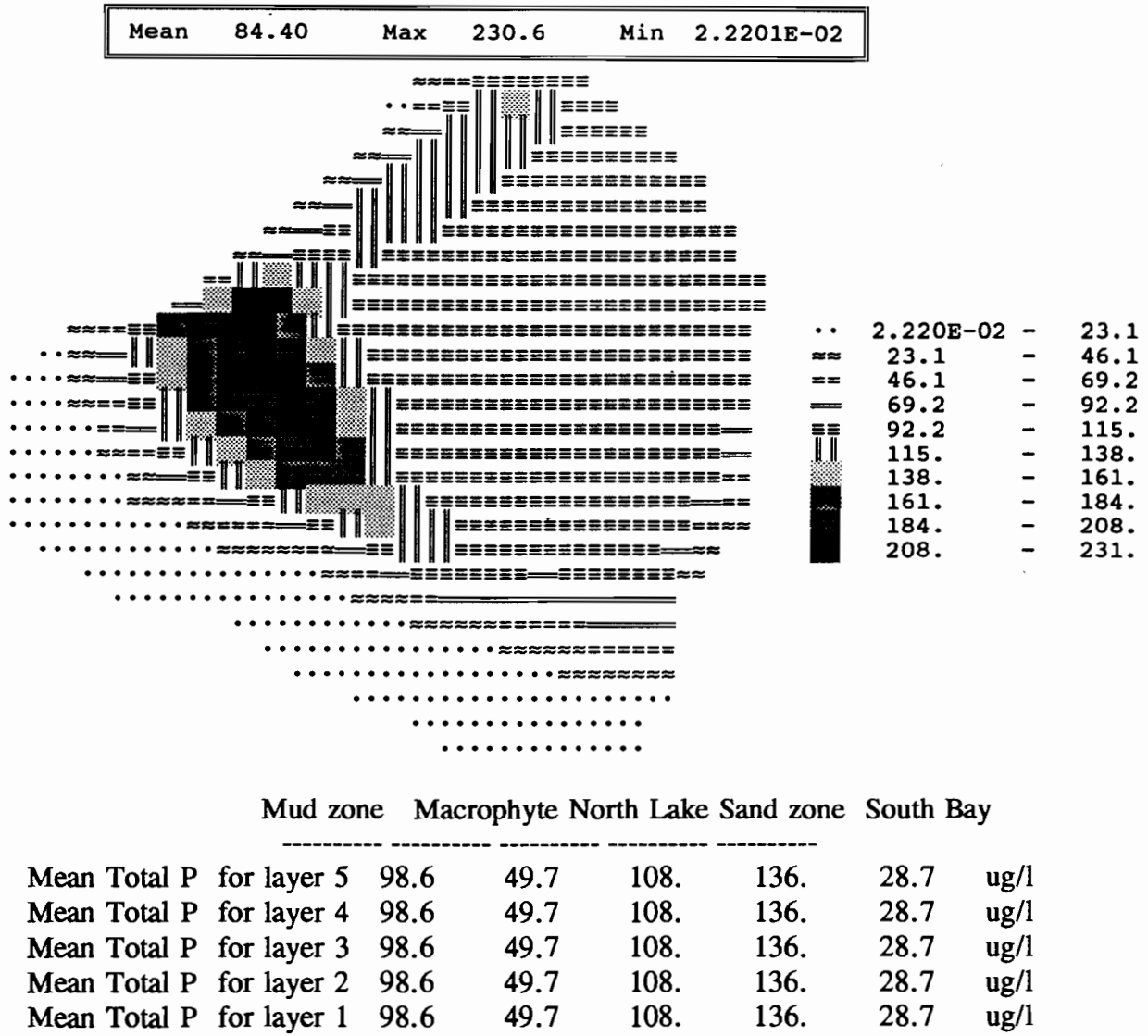


Figure 11-18 Ending simulation concentrations at the end of 24 hours using a time step of 1 hour and a constant initial concentration of $100 \text{ ug} \cdot \text{l}^{-1}$ for mud, north lake, sand, and south bay and $200 \text{ ug} \cdot \text{l}^{-1}$ for the macrophyte zone subject to a constant u and v velocity of $0.1 \text{ cm} \cdot \text{sec}^{-1}$, using the LOP3D solution and ISOL value of 2.

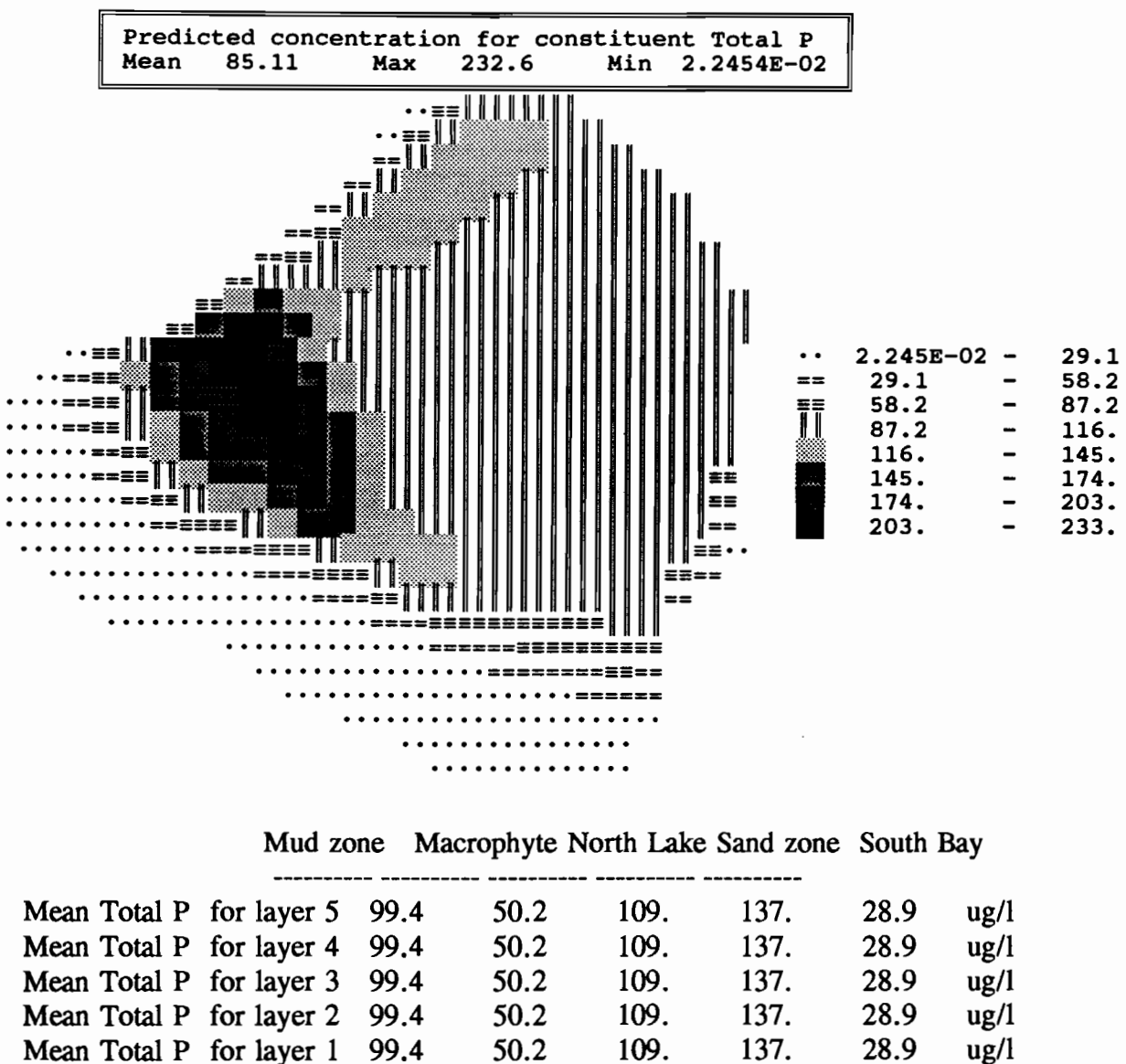


Figure 11-19 Ending simulation concentrations at the end of 24 hours using a time step of 1 hour and a constant initial concentration of $100 \text{ ug} \cdot \text{l}^{-1}$ for mud, north lake, sand, and south bay and $200 \text{ ug} \cdot \text{l}^{-1}$ for the macrophyte zone subject to a constant u and v velocity of $0.1 \text{ cm} \cdot \text{sec}^{-1}$, using an early LOP3D solution and ISOL value of 3.

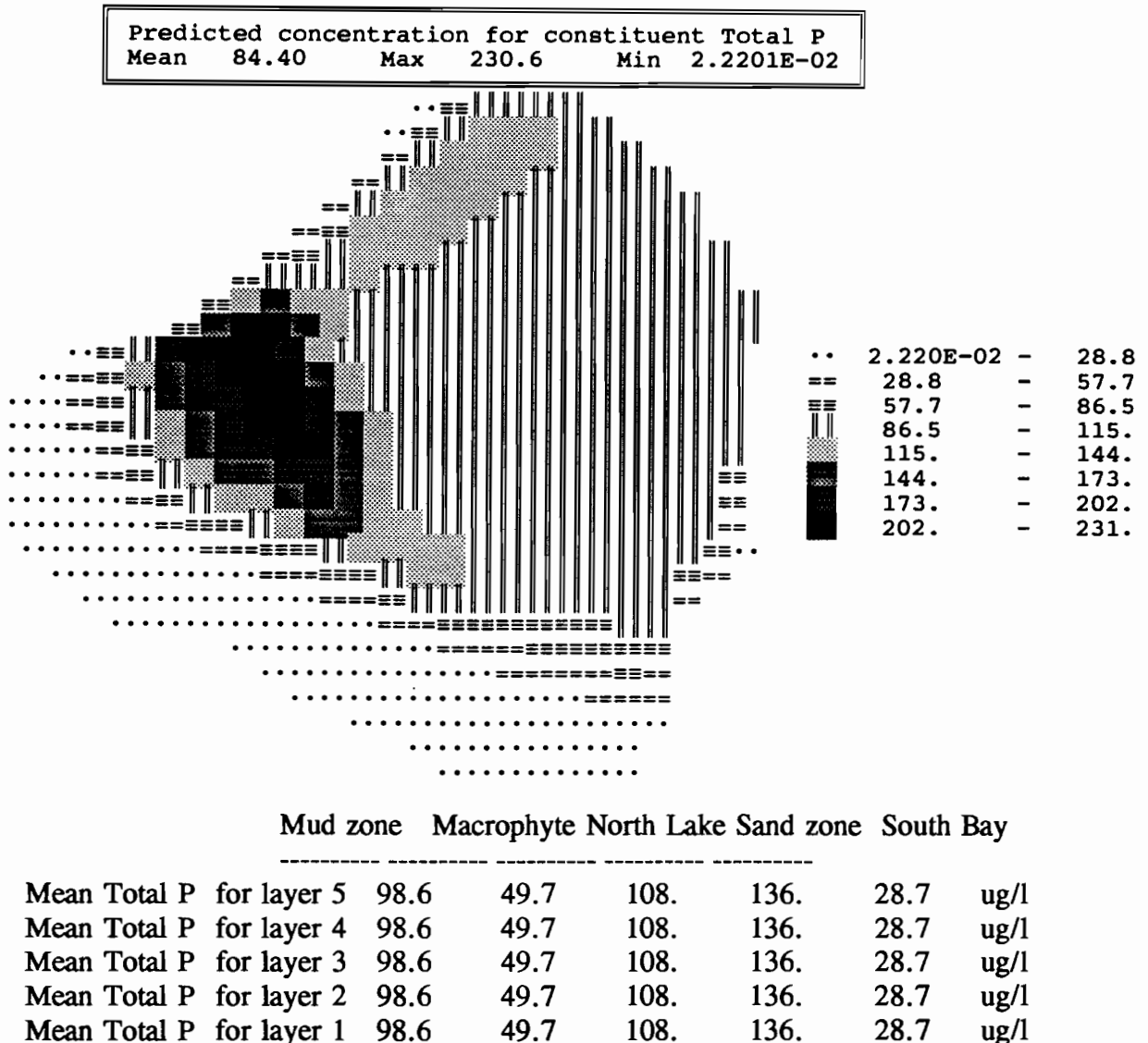


Figure 11-20 Ending simulation concentrations at the end of 24 hours using a time step of 1 hour and a constant initial concentration of $100 \text{ ug} \cdot \text{l}^{-1}$ for mud, north lake, sand, and south bay and $200 \text{ ug} \cdot \text{l}^{-1}$ for the macrophyte zone subject to a constant u and v velocity of $0.1 \text{ cm} \cdot \text{sec}^{-1}$, using the LOP3D solution and ISOL value of 4.

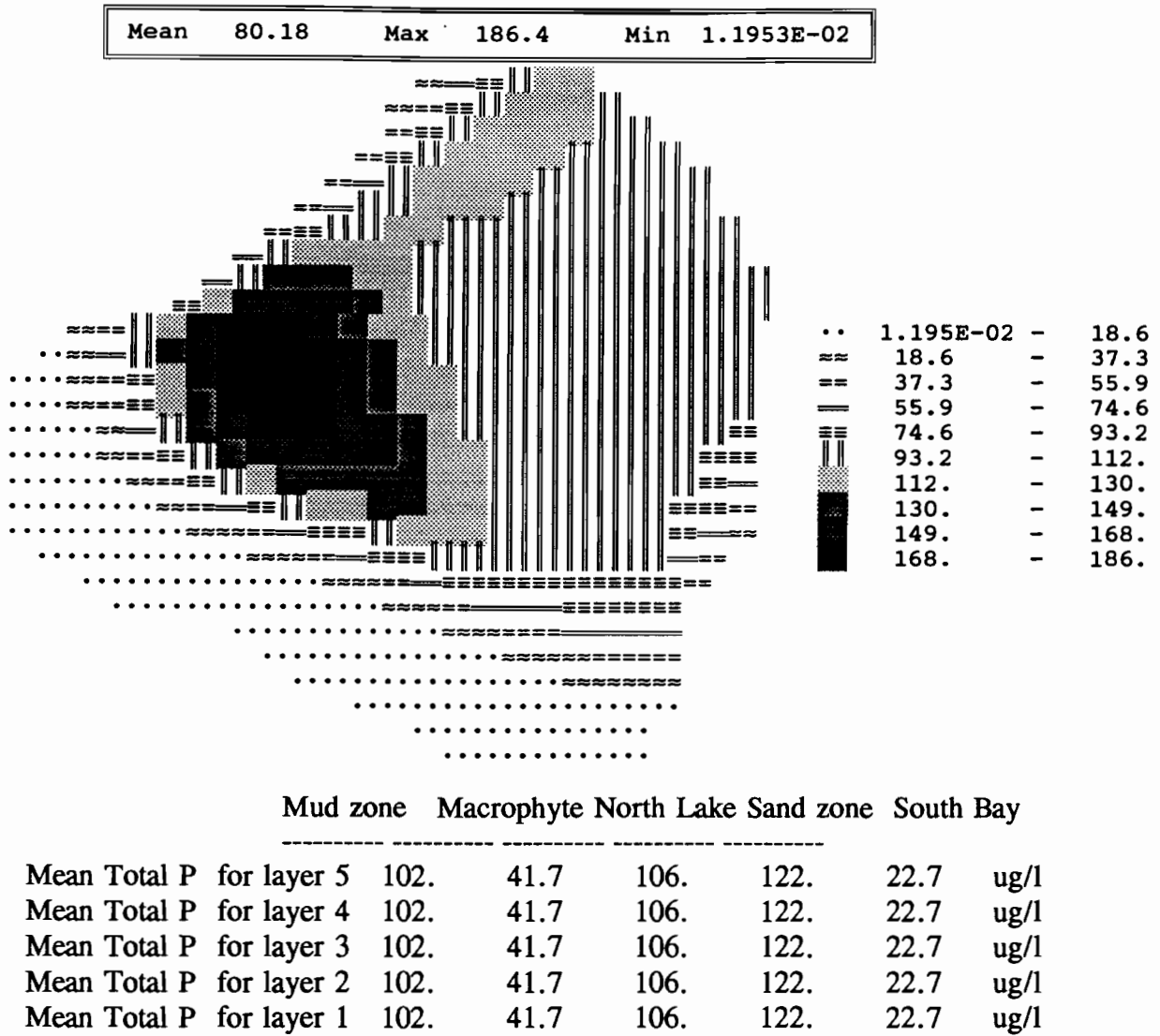


Figure 11-21 Ending simulation concentrations at the end of 24 hours using a time step of 1 hour and a constant initial concentration of $100 \text{ ug} \cdot \text{l}^{-1}$ for mud, north lake, sand, and south bay and $200 \text{ ug} \cdot \text{l}^{-1}$ for the macrophyte zone subject to a constant u and v velocity of $0.1 \text{ cm} \cdot \text{sec}^{-1}$, using the LOP3D solution equivalent to the EHSMIT solution and ISOL value of 3.

12. REACTION MODEL FOR PELAGIC PHOSPHORUS

Facilius per partes in cognitonem totius adducimer.

We are more easily led part by part to an understanding of the whole.

- Seneca

12.1 Introduction to the Pelagic Water Quality Model

The development of the comprehensive model for prediction of pelagic phosphorus species in Lake Okeechobee was broken into several tasks, including development of models for hydrodynamics (EHSM3D), sediment deposition and resuspension (EHSMSD), phosphorus transport within the sediment bed (LOPSED), and pelagic phosphorus reactions (LOP0D and LOP3D). This chapter describes how the pelagic phosphorus reactions are calculated in the models LOP0D and LOP3D.

The model reaction kinetics described in this chapter are the summation of four important processes:

1. A comprehensive literature review of reaction mechanisms, values for the kinetic constants, the range of acceptable kinetic values, and finite difference schemes for calculating the reaction terms. A range of kinetic values was used to initialize the calibration process.
2. Mathematical formulation of important biological, chemical and physical processes in Lake Okeechobee.
3. Finite difference formulation of mathematical relations.
4. Quantification of the sensitivity of the model used in the various finite difference schemes.

Phosphorus is subject to the physical transport mechanisms of advection and diffusion (Chapter 10). The advective velocities and turbulent diffusivities are obtained from the hydrodynamic model EHSM3D developed by the UF COE Department (Sheng et al., 1991a). Equally important are the "source and sink" terms (i.e., the kinetic formulations) that govern the interaction of the pelagic phosphorus species with their respective boundary conditions, including the settling and erosion of particulate algae and sediment. These terms are described first below in the context of a "box model," that is, considering only the effects of kinetics and neglecting lake circulation. [Note: this is Task 6.2 of the project proposal, which we call the Lake Okeechobee Phosphorus 0-Dimension model (LOP0D)]. These reaction terms when coupled to the 3D advection-diffusion model described in Chapter 10 constitute the LOP3D model.

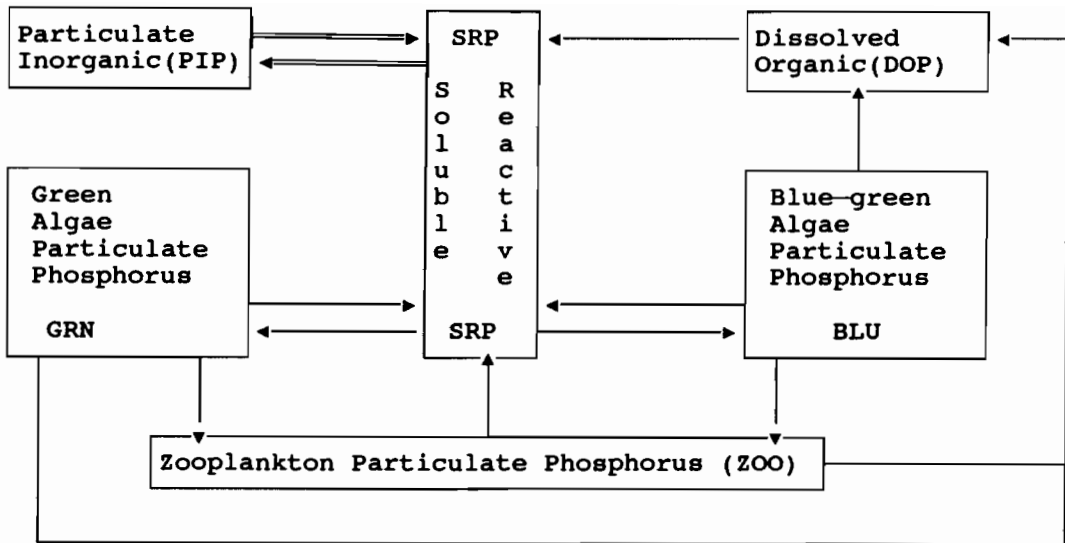


Figure 12-1 Advection, diffusive, and reactive components in the pelagic zone of the lake. The symbol " | " or "-·" indicates a combination advective, diffusive and reactive pathway. The symbol "==" indicates the pathway is solely an algebraic reaction pathway.

12.2 Phosphorus Components in Lake Okeechobee

Phosphorus occurs in water in both particulate and dissolved forms (Figure 12-1). The total phosphorus measurement is by definition all encompassing, including bound and readily available dissolved and particulate forms of organic and inorganic phosphorus that can be converted to orthophosphorus by acid digestion. Unlike macronutrients carbon and nitrogen, which are mainly associated with inorganic and dissolved organic matter (Wetzel, 1983), total phosphorus is almost entirely associated with living and nonliving particulate matter (Rigler, 1975). Phosphorus is the appropriate macronutrient to simulate in Lake Okeechobee because it is usually the most limiting nutrient in lakes (Reckhow and Chapra, 1983), cannot be obtained by biological mechanisms from the atmosphere, and the macronutrient most easily controlled.

We use the concentration of chlorophyll *a* to represent the phytoplankton biomass (carbon) because it is a convenient surrogate that is easier to measure and less subjective than calculating the actual algal biomass (Canfield et al., 1985). Additionally, phytoplankton carbon is hard to distinguish from non-phytoplankton carbon (Yentsch and Campbell, 1991).

The phosphorus components included in the model are listed in Table 12-1 and shown in Figure 12-1, along with their linkages. Note that the sum of the first seven modeled phosphorus components is total phosphorus (TP).

Table 12-1 Modeled phosphorus species and related components.

Phosphorus Component	Concentration Symbol
SRP (soluble reactive phosphorus)	C_{aq}
DOP (dissolved organic phosphorus)	C_D
GRN (green algae particulate phosphorus)	C_G
BLU (blue-green algae particulate phosphorus)	C_B
DIA (diatom algae particulate phosphorus)	C_d
ZOO (zooplankton particulate phosphorus)	C_Z
PIP (particulate inorganic phosphorus)	C_P
ORG (sediment organic particulate phosphorus)	C_{ORG}
CORB (corbicula particulate phosphorus)	C_{CB}
EMM (emergent macrophyte particulate phosphorus)	C_{EM}
SUB (submerged macrophyte particulate phosphorus)	C_{SM}
SED (suspended sediment)	C_{sed}

Kinetic formulations for the first seven reactive components are listed in Table 12-2. The maximum growth of the reactive components is modified by variations in temperature through the function $f_1(T)$, and with light intensity at a depth z through the function $f_2(I)$. The rate equations of Table 12-2 are written as ordinary differential equations. These are applied at each time step after completing the advective-diffusive computations described in Chapters 10 and 11.

All kinetic and other model coefficients are summarized in the equations of Table 12-2, with values used in models LOP3D and LOP0D listed in Tables 12-19 to 12-28. A review of literature values and the background for the coefficients are discussed in the remainder of Chapter 12.

12.3 Simulated Pelagic Algae

12.3.1 Algal Forms

The majority of lake models combine all algal species into one generic algal compartment without internal heterogeneity. An immense literature would suggest the

Table 12-2 Kinetic pathways of phosphorus components

Soluble reactive phosphorus (SRP) pathways		
$\frac{dC_{aq}}{dt} = - C_G \cdot \mu_G \cdot f_1(T) \cdot f_2(I) \cdot \frac{C_{aq}}{K_G + C_{aq}}$		Uptake by GRN
$- C_B \cdot \mu_B \cdot f_1(T) \cdot f_2(I) \cdot \frac{C_{aq}}{K_B + C_{aq}}$		Uptake by BLU
$- C_d \cdot \mu_d \cdot f_1(T) \cdot f_2(I) \cdot \frac{C_{aq}}{K_d + C_{aq}}$		Uptake by DIA
$+ K_D \cdot f_1(T) \cdot C_D$		Release by DOP
$+ K_{Gx} \cdot f_1(T) \cdot C_G$		Excretion by GRN
$+ K_{Bx} \cdot f_1(T) \cdot C_B$		Excretion by BLU
$+ K_{Zx} \cdot f_1(T) \cdot C_Z$		Excretion by ZOO
		(12.2-1)
Dissolved organic phosphorus (DOP) pathways		
$\frac{dC_D}{dt} = - K_D \cdot f_1(T) \cdot C_D$		Release to SRP
$+ K_{Gd} \cdot f_1(T) \cdot C_G$		Mortality of GRN
$+ K_{Bd} \cdot f_1(T) \cdot C_B$		Mortality of BLU
$+ K_{Cd} \cdot f_1(T) \cdot C_C$		Mortality of DIA
$+ K_{Zd} \cdot f_1(T) \cdot C_Z$		Mortality of ZOO
		(12.2-2)
Green algae particulate phosphorus (GRN) pathways		
$\frac{dC_G}{dt} = + C_G \cdot \mu_G \cdot f_1(T) \cdot f_2(I) \cdot \frac{C_{aq}}{K_G + C_{aq}}$		Uptake of SRP
$- C_Z \cdot \mu_{ZG} \cdot f_1(T) \cdot \frac{C_G}{K_{ZG} + C_G}$		Uptake by ZOO
$- K_{Gx} \cdot f_1(T) \cdot C_G$		Excretion to SRP
$- K_{Gd} \cdot f_1(T) \cdot C_G$		Mortality to DOP
		(12.2-3)

Table 12-2 Kinetic pathways of phosphorus components (continued)

Blue-green algae particulate phosphorus (BLU) pathways			
$\frac{dC_B}{dt}$	$= + C_B \cdot \mu_B \cdot f_1(T) \cdot f_2(I) \cdot \frac{C_{aq}}{K_B + C_{aq}}$	Uptake of SRP	
	$- C_Z \cdot \mu_{ZB} \cdot f_1(T) \cdot \frac{C_{aq}}{K_{ZB} + C_B}$	Uptake by ZOO	
	$- K_{Bx} \cdot f_1(T) \cdot C_B$	Excretion to SRP	
	$+ K_{Bd} \cdot f_1(T) \cdot C_B$	Mortality to DOP	(12.2-4)
Diatom algae particulate phosphorus (DIA) pathways			
$\frac{dC_d}{dt}$	$= + C_d \cdot \mu_C \cdot f_1(T) \cdot f_2(I) \cdot \frac{C_{aq}}{K_d + C_{aq}}$	Uptake of SRP	
	$- C_Z \cdot \mu_{Zd} \cdot f_1(T) \cdot \frac{C_d}{K_{Zd} + C_d}$	Uptake by ZOO	
	$- K_{dx} \cdot f_1(T) \cdot C_d$	Excretion to SRP	
	$- K_{dd} \cdot f_1(T) \cdot C_d$	Mortality to DOP	(12.2-5)
Zooplankton particulate phosphorus (ZOO) pathways			
$\frac{dC_Z}{dt}$	$= + C_Z \cdot \mu_{ZB} \cdot f_1(T) \cdot \frac{C_B}{K_{ZB} + C_B}$	Uptake of BLU	
	$+ C_Z \cdot \mu_{ZG} \cdot f_1(T) \cdot \frac{C_G}{K_{ZG} + C_G}$	Uptake of GRN	
	$+ C_Z \cdot \mu_{Zd} \cdot f_1(T) \cdot \frac{C_d}{K_{Zd} + C_d}$	Uptake of DIA	
	$- K_{Zx} \cdot f_1(T) \cdot C_Z$	Excretion to SRP	
	$+ K_{Zd} \cdot f_1(T) \cdot C_Z$	Mortality to DOP	(12.2-6)

need for multi-segmented algal simulations. If there is one thing we know it is the heterogeneity of algal populations (Hutchinson, 1961). Nonetheless, numerical models are written as if Hutchinson's "The Paradox of the Plankton" were "Plankton and Principle of Competitive Exclusion." This section discusses the reasons three algal classes are simulated in the models LOP0D and LOP3D. The three simulated algal classes in Lake Okeechobee are green algae, blue-green algae and diatoms.

The three algal classes are differentiated by a plethora of characteristics (Table 12-3). Diatoms require silica as well as nitrogen and phosphorus as a macronutrient. They maintain silicon cell walls in pinnate shape and usually have one flagella for mobility in the water column. Diatoms have a brown-yellow appearance because carotenoid pigments are more abundant than chlorophyll pigments. Green algae have a high concentration of chlorophyll *b*.

Table 12-3 Major functional differences between the phytoplankton classes.

Algal Class	Major Nutrient Requirements	Optimum Growth Rate	Saturation Light Intensity	Sinking Rate	Grazing Pressure
Diatoms	Phosphorus Nitrogen Silica	High	High	High	High
Green algae	Phosphorus Nitrogen	High	High	High	High
Blue-Green	Phosphorus	Low	Low	Low	None

The single biggest reason for blue green algal dominance in lakes is nitrogen limitation and light limitation (Klemer and Borko, 19??). As already discussed in Chapter 3, the evidence for any nutrient limitation in Lake Okeechobee is limiting, but the effects of light limitation are severe and drastically affect the algal population of the lake.

The phytoplankton of Lake Okeechobee have characteristics suggestive of both temperate and tropical lakes (Wetzel, 1983):

1. A spring maximum of diatoms less than 3 months in duration.
2. A spring maximum followed by a summer minimum of low algal density followed by a summer maximum dominated by blue green algae.

3. A winter decline in phytoplankton population. However, the magnitude of the winter decline is similar to tropical lakes and does not approach drastic decline in temperate lake phytoplankton induced by low water temperatures and low solar insolation.

The relationship among the several forms of modeled phosphorus species and the modeled phytoplankton classes are illustrated in Figure 12-2. Quantities of various algal forms found in Lake Okeechobee on three different dates are given in Tables 12-4, 12-5, 12-6 and 12-7. General characteristics of the algal forms are listed in Table 12-3.

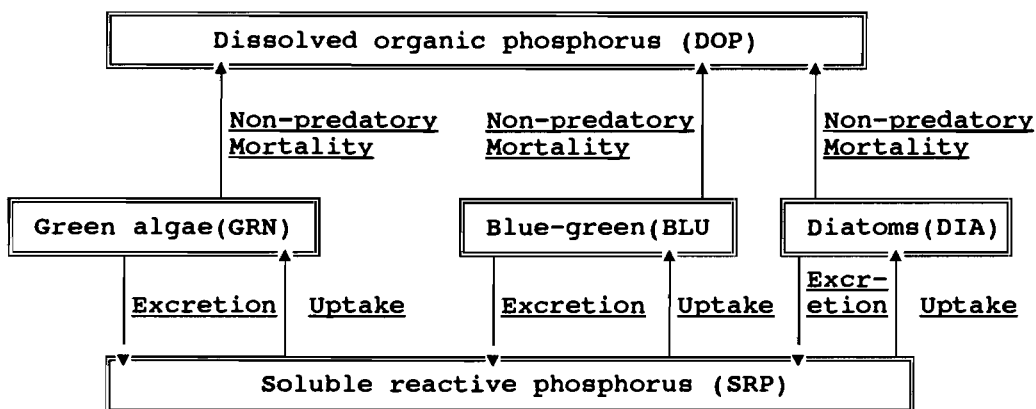


Figure 12-2 Algal pathways in subroutines REAC3D and REAC0D.

Table 12-4 Lake Okeechobee algal species (Marshall, 1977).

Algal Group	Number of Species	Percent Biovolume	Percent Density
Diatoms Chrysophyta Class Bacillariophyceae	67	41	20
Greens Chlorophyta	79	12	14
Blue-Greens Cyanophyta	38	34	59
Euglenoids Euglenophyta	29	2	<1
Cryptomonads Pyrrhophyta Class Cryptophyceae	8	10	7
Dinoflagellates Pyrrhophyta Class Dinophyceae	12	2	<1

Table 12-5 Phytoplankton Densities by Algal Class on July 15, 1981 (Jones and Federico, 1984).

Algal Group	Station 2 North lake Density (units/ml)	Station 6 South lake Density (units/ml)
Diatoms Chrysophyta Class Baccillariophyceae	13,022	563
Greens Chlorophyta	334	179
Blue-Greens Cyanophyta	105,512	870
Others	0	101

Table 12-6 Phytoplankton Densities by Algal Class on August 24, 1981 (Jones and Federico, 1984).

Algal Group	Station 2 North lake Density (units/ml)	Station 6 South lake Density (units/ml)
Diatoms Chrysophyta Class Baccillariophyceae	7,504	1,102
Greens Chlorophyta	750	67
Blue-Greens Cyanophyta	15,651	2,271
Others	107	0

Table 12-7 Phytoplankton Densities by Algal Class in Lake Okeechobee on October 8, 1981 (Jones and Federico, 1984).

Algal Group	Station 2 North lake Density (units/ml)	Station 5 Sand zone Density (units/ml)	Station 6 South lake Density (units/ml)
Diatoms Chrysophyta Class Baccillariophyceae	3,340	1,366	2,004
Greens Chlorophyta	267	1,069	264
Blue-Greens Cyanophyta	2,806	22,378	5,344
Others	0	0	534

12.3.2 Allometric Differences Between Algal Classes

Neibauer and Smith (1989) divided their model phytoplankton into nanoplankton ($< 20 \mu\text{m}$) and netplankton ($> 20 \mu\text{m}$) and differentiated the two classes in their algal simulation model on the basis of maximum growth rate and settling rate. Larger phytoplankton fare better in nutrient-rich environments, conversely, smaller phytoplankton dominate in nutrient-poor environments because smaller phytoplankton have faster nutrient uptake velocities and out-compete the larger phytoplankton.

Generally, the smaller the unicellular organism the faster the specific growth rate in the Monod functions of Eqs. (12.2-1) to (12.2-6) (Joint, 1991). The size-dependent, or allometric relationship, has the form

$$\mu_x = a \cdot C^b \quad (12.3-1)$$

where μ_x = (generic) rate constant (specific growth rate) in the Monod functions of Eqs. (12.2-1) - (12.2-6) (1/day),
 b = -0.15 for natural phytoplankton populations (Joint, 1991),
 a = a species specific constant (0.14 for dinoflagellates) (Banse, 1982), and
 C = cell carbon in picograms.

The allometric model only predicts the potential growth rate of algae and bacteria. Thus, the allometric estimate is an upper limit on the maximum growth rate

of algal cells. The ultraplankton were the predominant size class of phytoplankton in Lake Okeechobee (Marshall, 1977). The ultraplankton consisted of filamentous blue green algae and pennate diatoms ranging from 0.3μ to 3μ (Table 12-4). Ninety-five percent of the algae were less than 50μ in length along the major axis and could be classified as either nannoplankton or ultraplankton. Plankton are often separated according to the classification scheme developed by (Strickland, 1960) in which:

Macroplankton	$> 500 \mu$
Microplankton	50 to 500μ
Nannoplankton	10 to 50μ
Ultraplankton	$< 10 \mu$

The competitive advantage blue-green algae have over green algae and diatoms may be due to a minimization of grazing and settling loss during periods of high biomass (Kalff and Knoechel, 1978). Low loss rates are more important than high growth rates in determining the dominant algal species in lakes (Kalff and Knoechel, 1978 and Vincent et al., 1984)). Zooplankton are selective grazers of green algae and diatoms in preference to blue-green algae.

The most dominant algae class is blue green algae. The species *Lyngbya limnetica* is the most common blue green. However, most blue-green species are ultraplankton which have a small bio-volume. Diatoms, such as *Fragilaria sp.* and *Melosira*, are larger and dominate the other algae in terms of bio-volume. Green algae are common but rarely are as abundant as the blue-green algae or have large cell sizes like the diatoms.

Halterman and Toetz (1984) in a study of the uptake of NO_3 show the half saturation constants for diatoms and blue-greens are about three times greater than green algae, and the maximum up-take rate for diatoms was twice the uptake rate of green algae and three times the uptake rate of blue-greens. The larger phytoplankton have a greater μ_{\max} than smaller phytoplankton (Langdon, 1988).

12.3.3 Algal Blooms in Lake Okeechobee

Historically, the major species involved in algal blooms in Lake Okeechobee were the blue green algae, *Raphidiopsis curvata*, the diatom, *Fragilaria pinnata*, and the green algae, *Chlorella* (Joyner, 1974; Marshall, 1977). Algal productivity in northern Lake Okeechobee is much higher than in the South Bay or mud zone (Davis and Federico, 1984). The highest pelagic productivity does not occur near the water surface but the intermediate depth of 2.2 meters (Marshall, 1977).

Algal blooms commonly wash up on the western shore of Lake Okeechobee. Lake areas not light limited such as the south bay and western sandy area are more susceptible to experiencing algal blooms. Inflows to the lake are possible starting points for the algal blooms, which end up being wind blown to the western shore.

Other blue-green bloom species contributing to observed blooms are *Anacystis* sp., *Lyngbya contorta*, and *Agmenellum quadruplicatum*.

Blue-green and green algal blooms, are important biologically because of their effect on fish and benthic macroinvertebrates by increasing the diurnal amplitude of dissolved oxygen. Resultant lower dissolved oxygen concentrations at night stress the sediment macroinvertebrates and fish and may induce fish kills. The public then perceives the algal blooms as a symptom of a dying lake.

The onset of a bloom may be triggered by low NO_3 concentrations leading to dominance by nitrogen-fixing filamentous blue-green algae (e.g. *Anabaena flos-aquae* and *Aphanizomenon flos-aquae*). Lake Okeechobee, however, had algal blooms dominated by non-nitrogen fixing blue-greens *Lyngbya contorta*, *Agmenellum quadruplicatum*, and *Rhaphidiopsis curvata*. Smith et al. (1987) found the best predictors of the summer biomass of non-nitrogen fixing blue greens was total nitrogen, total phosphorus and mean depth, whereas the best predictors of nitrogen-fixing blue-greens included total phosphorus, temperature, CO_2 and mean depth.

The dominance of a single algal species during a bloom, as suggested by solitary sampling efforts is often illusory. For example, a succession of small phytoplankton pulses created the spring bloom of a hypereutrophic lake in Japan (Seki and Takahashi, 1983). Each phytoplankton pulse was dominated by a single organism or group of organisms. Depending on the time of sampling, a different algal species would appear to dominate the algal population in a lake. The onset of algae and the process of algal succession in general is affected by wind: storm events in a small reservoir hastened population shifts in phytoplankton once succession started, and had minor effects during periods of community stability (Edson and Jones, 1988).

12.4 Algal Growth Simulation

12.4.1 Alternative Formulations

There are two competing approaches to modeling algal growth: (1) Monod kinetics based on the external concentration of nutrients, and (2) growth rate based on internal cellular nutrient concentrations (Droop, 1968).

The dynamics of nutrient uptake by algae typically are simulated as a first order wherein the rate or velocity of nutrient uptake (v_{up}) is a function of the living biomass (B) and the specific growth rate of the species (μ):

$$v_{up} = \frac{dB}{dt} = \frac{1}{B} \cdot \mu \quad (12.4-1)$$

The turnover time (τ) for phosphorus is defined as the time necessary to replace the amount of phosphorus biomass in the water. Figure 12-3 illustrates the relationship between the response time for algal growth and the growth rate, μ .

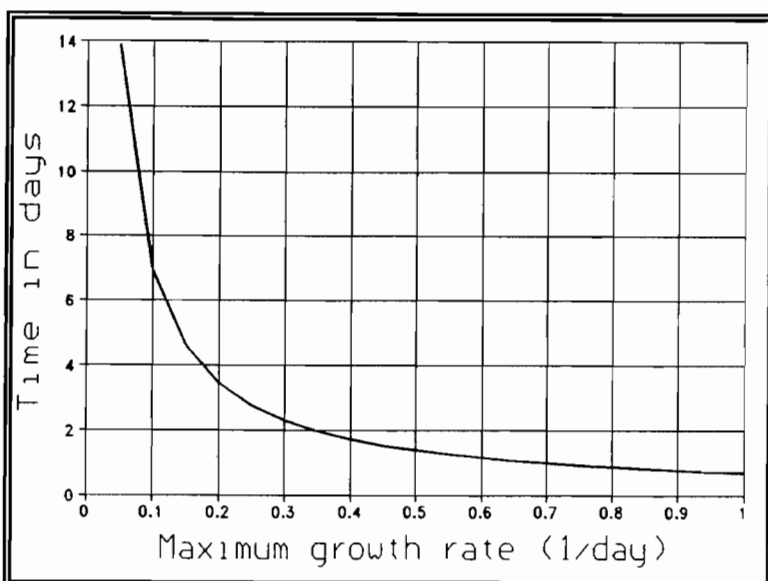


Figure 12-3 Doubling or reaction time for algal growth and respiration as a function of the reaction rate.

The specific growth rate varies depending upon antecedent nutrient, light, and temperature conditions. The conceptualization of μ is the basic difference between the two approaches to simulating algal growth uptake dynamics. Monod growth kinetics assume μ approaches asymptotically the maximum uptake rate μ_{\max} . Two constants are required to simulate algal growth: (1) K_s [the half saturation constant] is the concentration at which the specific growth rate, μ , equals one-half μ_{\max} (Table 12-8), and (2) the maximum growth rate, μ_{\max} (Table 12-9). The specific growth rate, μ , is related to the external nutrient concentration, C_{aq} (i.e., the concentration of SRP), by the hyperbolic or Monod function (Ahlgren, 1988):

$$\mu = \mu_{\max} \frac{C_{aq}}{K_s + C_{aq}} \quad (12.4-2)$$

Alternatively, μ is assumed to be a function of the internal phosphorus content of the cell as defined by the cell quota concept. According to the cell quota model, external SRP is taken up by the cell and stored; subsequent cell growth is dependent on the internal phosphorus concentration in the cell (Figure 12-4). The advantage over Monod kinetics is that uptake of nutrients and cell growth are decoupled. Q_{cell} is the cell quota and q_o is the minimum cell quota, or the subsistence cell quota at zero growth rate, of the algal class simulated.

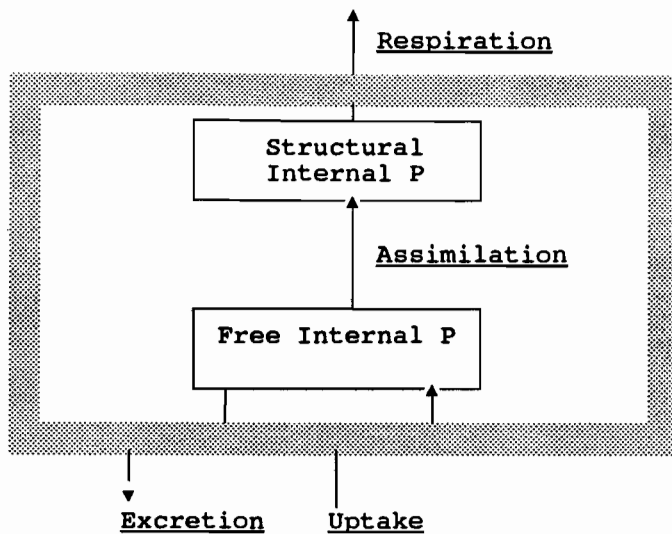


Figure 12-4 Intracellular algal nutrient processes in the model.

Table 12-8 Half saturation constant for algal growth.

Source	K_s (ug/l)
Griffin and Ferrara (1984)	20.
Salas and Thomann (1978)	5.
Bierman et al. (1980)	5.
Scavia et al. (1981b)	5.
Jorgensen (1976)	30.
Van Benschoten and Walker (1984)	5.
Virtanen et al. (1986)	10.
Jaffe (1988)	30.
Blosser (1986)	1.5
Keesman and Van Stratten (1990)	5.0 - 10.0
Grover (1988)	
<i>Chlamydomonas sp.</i>	0.68
<i>Chlorella sp.</i>	2.12
<i>Cryptomonas sp.</i>	1.35
<i>Oocystis pusilla</i>	1.16
<i>Scenedesmus quadricauda</i>	3.38
<i>Sphaerocystis schroeteri</i>	2.42
<i>Nitzschia acicularis</i>	0.22
<i>Nitzschia linearis</i>	1.83
<i>Nitzschia palea</i>	4.54
<i>Synedra radians</i>	0.01
<i>Synedra rumpens</i>	0.67

Table 12-9 Maximum growth rate for algae at 20°C.

Source		μ_{\max} (1/day)
Griffin and Ferrara (1984)		0.584
Salas and Thomann (1978)		2.0
Lastein and Gargas (1978)		1.50
Bierman et al. (1980)		0.627
Scavia et al. (1981b)		0.58
Jorgensen (1976)		0.0035
Canale and Vogel (1974)	GRN	0.43
	BLU	0.48
	DIA	0.48
Van Benschoten and Walker (1984)		2.3
Jaffe (1988)		3.23
Virtanen et al. (1986)		0.65
Blosser (1986)		1.5
Keesman and Van Stratten (1990)		0.5-2.0
Wroblewski et al. (1988)		2.0
Boers et al. (1991)	BLU	1.7
	GRN	2.25
Grover (1988)		
<i>Chlamydomonas</i> sp.		1.55
<i>Chlorella</i> sp.		1.59
<i>Cryptomonas</i> sp.		0.96
<i>Oocystis pusilla</i>		1.02
<i>Scenedesmus quadricauda</i>		1.24
<i>Sphaerocystis schroeteri</i>		0.94
<i>Nitzschia acicularis</i>		0.69
<i>Nitzschia linearis</i>		1.10
<i>Nitzschia palea</i>		1.73
<i>Synedra radians</i>		1.18
<i>Synedra rumpens</i>		1.43

$$\mu = \mu_{\max} \frac{Q_{cell} - q_o}{Q_{cell}} \quad (12.4-3)$$

The external nutrient and cell quota formulations are equivalent if the internal cell concentration is assumed to be in dynamic equilibrium with the external concentration (Di Toro, 1980). Di Toro (1980) estimated that the uptake of internal cell storage occurs in 1/8th to 1/2th of the time required for the uptake of external nutrients. The internal cell concentrations are thus in dynamic equilibrium with the external concentration. Equation (12.4-3) is difficult to use directly since the cell quotas and minimum cell quotas are species specific and we use generalized green,

blue-green, and diatom algal classes in LOP0D and LOP3D. The difficulties of working directly with cell quotas is obviated by expressing μ as a function of internal phosphorus and chlorophyll a concentrations (Riley and Stefan, 1988):

$$\mu = \mu_{\max} \frac{P_{\text{cell}} - \text{Chla} \cdot P_{\min}}{P_{\text{cell}}} \quad (12.4-4)$$

where P_{cell} = internal nutrient concentration ($\mu\text{g} \cdot \text{l}^{-1}$),
 P_{\min} = minimum ratio of phosphorus to chlorophyll a , and
 Chla = concentration of chlorophyll a .

The internal nutrient limitation and the external nutrient limitation as been combined as follows (Jorgensen, 1983):

$$\mu = \mu_{\max} \frac{\text{Chla} \cdot P_{\max} - \text{Chla} \cdot P_{\text{cell}}}{\text{Chla} \cdot (P_{\max} - P_{\min})} \cdot \frac{C_{\text{aq}}}{K_s + C_{\text{aq}}} \quad (12.4-5)$$

The yield (Y) is defined a the biomass produced divided by the amount of consumed SRP. Y as a function of μ and temperature (Ahlgren, 1988) is:

$$Y = A(T) + B(T) \cdot \mu + C(T) \cdot \mu^2 \quad (12.4-6)$$

12.4.2 Species Specific Growth Rates

Green and blue-green algae are distinguished by differing capacities for growth (uptake of SRP), maintenance of growth (non-predatory excretion of SRP), mortality (release of DOP) and settling rate (maintenance of position in the water column). These differing capacities for uptake of nutrients can be categorized as r-selective or K-selective species (Padisak et al., 1988). Algae that are r-selective have smaller cell sizes and are the better competitors in nutrient-rich environments than K-selective algae. The K-selective algae are larger and the better competitors in nutrient limited environments. Padisak et al. (1988) estimate 5-7 calm days are required before a K-selective species begins to dominate an algal population.

Some of the key factors influencing algal uptake were listed in Chapter 6 (Jansson, 1988):

1. Algae generally have a single uptake mechanism.
2. Uptake capacity is enhanced by phosphorus starvation.

3. The polyphosphate content of a cell (or the internal phosphorus pool in the cell) is negatively correlated with the cell's uptake capacity.
4. Light energy is the force driving phosphorus uptake.

12.4.3 Algal Carbon/Chlorophyll a

Commonly a single carbon to chlorophyll ratio is used in lake models to predict phytoplankton biomass. For example, Scavia et al. (1981b) used a value of 30.0 ug · Carbon/ug · Chla. The most commonly used Carbon/Chla ratio is 50:1 (Jorgensen, 1983), and was averaged across species and season for northern temperate lakes. Chmyr and Berseneva (1984) found a range of Carbon/Chla from 17:1 to 83:1 in ten algal species. Carbon/Chla can range over an order of magnitude under various combinations of light limitation, nutrient limitation, and temperature (Hunters and Laws, 1981). Granberg and Harjula (1982) in a study of Finnish lakes found that no constant ratio existed between Chla and carbon because of confounding differences in antecedent light intensity, nutrition, transparency, temperature, cell age and species composition. The Carbon/Chla in nanoplankton varied seasonally, whereas the Carbon/Chla in net plankton vary daily (Malone, 1982).

Smith (1980) found Carbon/Chla to be related to temperature and light intensity by the following expression:

$$\text{Carbon/Chla} = 136 \cdot I_o / \mu_{\max} \quad (12.4-7)$$

where I_o = incident light intensity (langleys/min) at the surface.

For example, using the Eppley function for μ_{\max} as a function of temperature (Eq. (12.4-8)) at a temperature of 25°C and 0.78 langleys/min (700 langleys/day) in June the θ_c is 37:1. At a temperature of 5°C and 0.52 langleys/min (250 langleys/day) in February the Carbon/Chla ratio (θ_c) is 87:1. The larger the Carbon/Chla ratio the smaller the Chla/TP ratio (Eq. (12.4-12)). The Chla/TP ratio should be smaller in fall and winter than in the spring and summer because of the influence of the Carbon/Chla ratio. The value of θ_c is constrained to be greater than a minimum value of 20.0 in the model.

The Carbon/Chla ratio (θ_c) increases with increasing light and decreases with increasing temperature (Smith, 1980). θ_c is higher during nitrogen and phosphorus deficiency, lower during exponential growth, and higher for colonial algae (Riemann et al., 1989). Measured values of θ_c range from 27 (1.5 percent chlorophyll a) to 67 (3.7 percent chlorophyll a) for green and diatom algae (Riemann et al., 1989). The value of θ_c is species specific, and only when one or two species dominate will chlorophyll data give reasonable estimates of phytoplankton biomass.

Most often algae respond to nutrient limitation through lowered chlorophyll a content and higher carbohydrate content (Ahlgren, 1988), or a higher θ_c . This categorization of the carbon/chlorophyll a is generally true depending on antecedent light conditions, since θ_c is also a function of the light regime. Diatoms are the best adapted to low-light and usually have the lowest values of θ_c (Langdon, 1988). Light adapted algae have low chlorophyll content and shade adapted algae have high chlorophyll content (Falkowski, 1981). In laboratory experiments using low light adapted and high light adapted Chlorella pyrenoidosa, a higher phosphorus content per cell (3.55 times greater) and lower uptake rates (0.35 times less) under low light conditions were found that were similar to conditions in Lake Superior when the mixing depth is 20-25 meters (Nalewajko et al., 1981). Lake Superior is often light limited rather than nutrient limited (Nalewajko et al., 1981). Generally, non-optimal growth conditions cause the internal content of the limiting nutrient to increase in the cell.

A θ_c predictive equation can be formulated based on lake temperature and optimum light saturation (Eq. (12.4-10) and Figure 12-5). Eppley's (1972) function for μ_{max} as a function of T ($^{\circ}$ C), Figure 12-6 is:

$$\mu_{max} = 10^{(0.0275 \cdot T - 0.230)} \quad (12.4-8)$$

Smith's (1980) function for the growth rate as a function of previous light conditions is:

$$\mu_g = \frac{\mu_{max} \cdot (\epsilon_g/\theta_c) \cdot I_z}{\mu_{max}/\Phi_{max} + (\epsilon_g/\theta_c) \cdot I_z} \quad (12.4-9)$$

where additional parameters have been defined in Chapter 6.

We use a value for θ_c based on the previous day's average layer light intensity:

$$\theta_{opt} = \frac{\Phi_{max} \cdot \epsilon_g \cdot I_0}{e \cdot \mu_{max}} \quad (12.4-10)$$

where Φ_{max} = P_{max} / K_{LG} = maximum quantum yield,
 e = the value of the transcendental function $e=2.318$, and
 I_0 = average daily irradiance for the previous day.

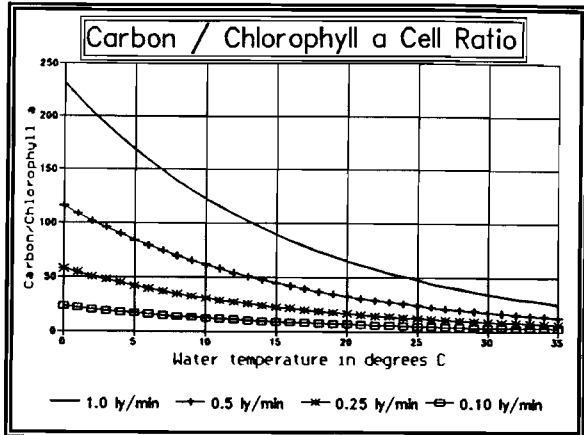


Figure 12-5 $\text{Carbon/Chla} = \theta_c$.

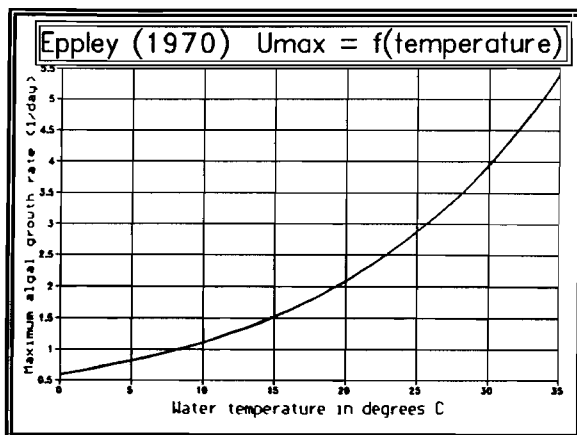


Figure 12-6 $\mu_{\max} = f(T)$.

12.4.4 Algal Carbon/Phosphorus

The stoichiometric relationship between algal biomass and phosphorus is given by Redfield et al. (1966) as:

$$\text{Algal Biomass} = C_{106} H_{263} O_{110} N_{16} P_1 \quad (12.4-11)$$

This expression, derived originally for marine phytoplankton, indicates the carbon/phosphorus ratio of the algal particulate matter should be 41.1:1 on a per weight basis. This ratio divided by a mean carbon/Chla ratio of 50 translates to an expected Chla/phosphorus ratio of 0.822. This estimate is valid only if the carbon/phosphorus ratio and the carbon/Chla ratio is constant. Unfortunately, neither assumption is true, as the two ratios are spatially and temporally variable in a lake (Table 12-10).

Table 12-10 Chlorophyll/Phosphorus.

Source	mg Chlorophyll / mg P
Scavia et al. (1981a)	0.70
Scavia et al. (1984)	0.60
Van Benschoten and Walker (1984)	0.91
Jaffe (1988)	0.58
Boers et al. (1991) BLU	0.89
GRN	0.78

The actual CHLA/phosphorus for algae is:

$$\text{Chla/AP} = \text{Carbon/AP} \cdot \text{Chla/Carbon} \quad (12.4-12)$$

where AP is algal phosphorus.

The ratio of carbon/algal phosphorus changes by species and lake system. Goldman et al. (1972) found the carbon/phosphorus in 15 algae to vary from 40.7:1 to 510:1 with a mean of 144:1. Vollenweider (1985) found the carbon/phosphorus ratio to range from half to two or three times the Redfield et al. (1966) ratio in freshwater systems.

12.4.5 Model Formulation for Chlorophyll *a* Prediction

The method for predicting chlorophyll *a* model applies Monod growth kinetics and uses Eq. (12.4-12) to estimate the Chla/Carbon ratio for a fixed ratio of Carbon/phosphorus in the lake. This approximates the known variability in the ratio of Carbon/phosphorus, seasonally and temporally.

12.5 Effect of Light/Temperature on Algal Growth

The combined effect of the two physical factors and interacting nutrients on algal growth may be summarized (Ahlgren, 1988):

1. With increasing light/growth rate the algae require additional phosphorus.
2. "Below an optimum temperature the minimum phosphorus content (subsistence quota) is inversely correlated with temperature". The phosphorus content of a cell increases at low temperature.
3. "The transition between light- and phosphorus-limitation...varies with growth rate".
4. At present, some chemostat results show better agreement with the non-interactive model.

The combined effect on the rate of algal uptake of SRP by the light and temperature regime is multiplicative in this model

$$\mu = \mu_{\max} \cdot f_1(I_z) \cdot f_2(T) \quad (12.5-1)$$

where $f_1(I_z)$ = light limiting function at depth z , and
 $f_2(T)$ = temperature limiting function at a temperature T in °C.

The light limiting function, $f_1(I_z)$, and temperature limiting function $f_2(T)$ are discussed in full detail in Chapter 6.

12.6 Algal Respiration and Excretion

Algal respiration can be separated into two components: a maintenance respiration rate (r_{oB} , r_{od} or r_{oG} for the three algal classes) when the growth rate is zero, and $k_{rG} \cdot \mu$, the amount respired during new growth (Langdon, 1988). For example, the total algal respiration rate for green algae, r_G , is:

$$r_G = r_{oG} + k_{rG} \cdot \mu \quad (12.6-1)$$

Langdon (1988) measured an average r_G of 0.15 day⁻¹ and k_{rG} of 0.20 for a variety of algal species. Scavia (1980) used 0.20 for k_{rG} and 0.05 day⁻¹ for r_{oG} . Typical respiration rates ($K_{Gd} \equiv r_G$) are shown in Table 12-11.

Table 12-11 Algal respiration rate.

Source	K_{Gd} (1/day)
Scavia et al. (1981b)	0.12
Bierman et al. (1980)	0.60
Jorgensen (1981)	0.01-0.06
Benschoten and Walker (1984)	0.11
Jaffe (1988)	0.15
Blosser (1986)	0.27
Keesman and Van Stratten (1990)	0.05-0.30
Wroblewski et al. (1988)	0.10
Boers et al. (1991) BLU	0.05
GRN	0.20

Takamura and Yasuno (1988) estimated 48 percent of the algal production in a shallow lake is algal respiration. The maintenance rate includes the extracellular release of dissolved organic carbon (DOC). Most investigators estimate that this is less than 5 percent of the cells' organic content (Cole, 1982).

12.7 Algal Non-Predatory Mortality

Algal mortality involves the conversion of algal phosphorus to biologically available phosphorus. This can be conceived as a two step process (De Pinto et al., 1986). First, algal death and lysis of the cell membrane releases any stored excess inorganic phosphorus. Typical values for the rate constant K_{Gx} governing this process for green algae (Eqs. (12.2-1) and (12.2-3)) are shown in Table 12-12. De Pinto et al. (1986) found that cellular phosphorus exceeding the minimum cell quota was released in an available form rapidly after cell death and lysis. Lysed material is usually 20-50 percent of the cell's organic content (Cole, 1982), and this excess inorganic phosphorus is immediately available for algal uptake. Secondly, bacteria mineralize the remainder of the cell organic phosphorus to available phosphorus.

Table 12-12 Algal mortality rate.

Source	K_{Gx} (day ⁻¹)
Jorgensen (1981)	0.015

Typical values for the rate coefficient K_D governing the mineralization of DOP to SRP (Eqs. (12.2-1) and (12.2-2)) are presented in Table 12-13.

Table 12-13 DOP to SRP regeneration rate at 20°C.

Source	K_D (1/day)
Salas and Thomann (1978)	0.10 - 0.20
Jorgensen (1981)	0.10
Bierman et al. (1980)	0.005
Van Benschoten and Walker (1984)	0.10
De Pinto et al. (1986)	0.056 <i>Chlorella</i> 0.03 <i>Microcystis</i> 0.023 <i>Scenedesmus</i>
Jaffe (1988)	0.0176
Keesman and Van Stratten (1990)	0.1 - 1.0
Boers et al. (1991)	0.5

12.8 Algal Settling

Phosphorus loss to the sediments is a significant fraction of the total incoming phosphorus loading. The loss to the sediments is via two main mechanisms: (1) algal sedimentation; and (2) non-algal phosphorus sedimentation. Some of the phosphorus is regenerated and later mixed with the water column due to biologic movement and wind action. The sediment usually undergoes "sediment focusing" towards deep holes in the lake. All lakes have a long term buildup of refractory nutrients in their sediments.

Deposition estimates obtained by sediment traps suspended in the water column are lower than the actual deposition since particulate phosphorus is transformed by bacterial action to DOP or SRP (Peng and Broecker, 1987). The settling velocity in a lake varies throughout the year; for example, in Lake Superior the settling rate ranges from 0.034 m/day to 0.088 m/day. Typical rates are shown in Table 12-14.

Table 12-14 Algal settling rates.

Source	K_{SG} , K_{Sd} , K_{SB} ($m \cdot day^{-1}$)
Salas and Thomann (1978)	0.0-0.10
Jorgensen (1981)	0.04
Van Benschoten and Walker (1984)	0.76
Jaffe (1988)	0.14
Virtanen et al. (1986)	0.03
Keesman and Van Stratten (1990)	0.01-0.50
Blosser (1986)	0.23
Takamura and Yasuno (1988)	<i>Melosira</i> 0.2-1.7 <i>Synedra</i> 0.2-2.0 <i>Microcystis</i> 0.0045-0.24 <i>Anabaena</i> 0.06

The classic ratio of algal carbon/phosphorus is 106 (Redfield et al., 1966), however, measured carbon/phosphorus ranges from 95 to 143 in marine detritus, and the mean carbon/phosphorus is nearer 112 using a carbon/nitrogen value of 7 (Peng, 1987). The amount of oxygen required to oxidize carbon and hydrogen in algal detritus is $1.2 O_2/C$ and the actual carbon/phosphorus ratio is 127 ± 7 in corrected marine detrital data (Peng, 1987). The meaning of the carbon/phosphorus ratio is keyed to the amount of carbon per unit of chlorophyll in algal biomass. The same amount of nutrient produced more or less chlorophyll *a* depending on antecedent light conditions and nutrient regimes.

Sedimentation is incorporated as part of the phosphorus models LOP0D and LOP3D. The three algal classes simulated have distinctive differences in settling rates and mechanisms. Takamura and Yasuno (1988) measured algal sinking rates in a

shallow hypereutrophic lake and found blue-greens to settle much slower than green and blue-green algae. The sinking rate of senescent algae was much higher than algae in exponential growth. Diatoms sank as living cells and blue-greens sank as detritus. The cell structure of the blue-green algae *Microcystis* collapsed rapidly after losing its function of carbon fixation (Takamura and Yasuno, 1988).

Blue-green algae use three mechanisms to control buoyancy: (1) cell turgor pressure increases at high light intensities causing the collapse of cell gas vacuoles and decreased buoyancy; (2) algae alter the rate of gas vacuole synthesis in response to the cell C/N internal ratio (a low C/N ratio increases gas vacuole synthesis); and (3) the cell may accumulate high-density storage products that act as ballast and affect cell buoyancy (Spencer and King, 1989). Some blue-green algae that use one or more of these mechanisms are *Anabaena* sp., *Aphanizomenon flos-aque*, *Microcystis*, *Oscillatoria*, and *Nostoc muscorum*.

Light intensity and CO₂ concentration interact to affect the buoyancy of the blue-green algae (Spencer and King, 1989), as indicated by its density, ρ_B . Carbon dioxide is held constant in the model. The effect of light on algal density is calculated as a function of the light intensity during the previous day. For blue green algae the new density is:

$$\rho_B^{n+1} = \rho_B^n + \Delta t \cdot \left[\frac{c_1 \cdot I_{mz}}{K_{BI} + I_{mz}} - c_2 I_a - c_3 \right] \quad (12.8-1)$$

where $n+1$ = new time step,
 n = old time step,
 c_1 = rate constant of density increase ($gm \cdot cm^{-3} \cdot sec^{-1}$),
 c_2 = rate constant of density decrease ($gm \cdot cm^{-3} \cdot sec^{-1}$),
 c_3 = minimal rate of density decrease ($gm \cdot cm^{-3} \cdot sec^{-1}$),
 K_{BI} = half saturation irradiance for maximum rate of density increase,
 I_a = average irradiance experienced when $I_z > I_c$,
 I_c = compensation irradiance,
 I_{mz} = Integrated value of I_z since dawn, and
 ρ_B = density of blue-green algae.

The new algal density is then used to calculate the new settling velocity using Stoke's equation:

$$v_{SB} = 2 \cdot g \cdot r^2 \cdot (\rho_B - \rho_w) \cdot \frac{A}{9 \cdot \phi \cdot \eta} \quad (12.8-2)$$

where v_{SB} = settling velocity (cm/sec),
 g = gravitational acceleration (cm^2/sec),
 ρ_w = density of water (gm/cm^3),

ϕ = coefficient of form resistance,
 A = ratio of cell volume to colony volume,
 r = effective radius of colony or filament, and
 η = dynamic viscosity.

12.9 Zooplankton Uptake

Zooplankton uptakes contributes another pathway between green, blue-green, and diatom algae and SRP, as indicated in Figure 12-7.

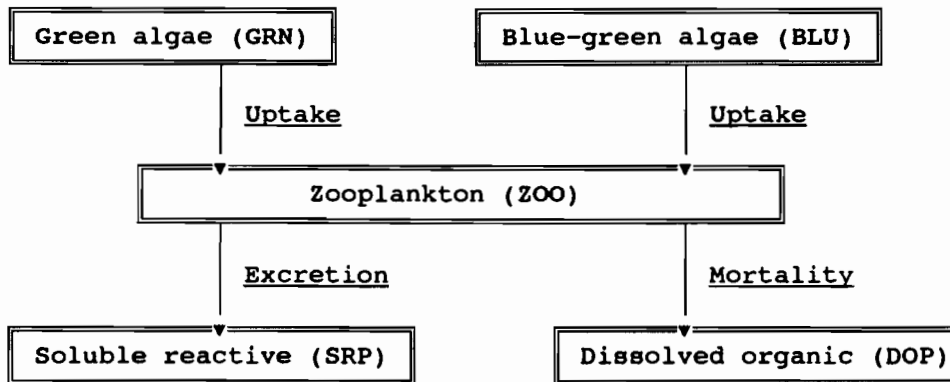


Figure 12-7 Zooplankton pathways in subroutines REAC3D and REAC0D.

Gayle (1975) found the zooplankton population of Lake Okeechobee to comprise 48 percent *Copepods*, 29 percent protozoans, 22 percent rotifers, and 1 percent cladocerans and others. Canfield et al. (1984) found an average of 100 copepods/l, 32 cladocerans/l, and 95 rotifers/l.

There are three possible representations of the zooplankton grazing of algae:

1. Mass action procedure based solely on the multiplicative concentrations of algae and zooplankton.
2. Michaelis-Menten model similar to other Michaelis-Menten (Monod) models discussed in this chapter.
3. A consumer density model based on an optimal concentration of algae.

Typical values for the Michaelis-Menten coefficients used in our model (Eq. (12.2-6)) are shown in Tables 12-15 to 12-17.

Table 12-15 Zooplankton ingestion rate.

Source	μ_{ZG} (day ⁻¹)
Jorgensen (1981)	0.175
Boers et al. (1991)	1.1

Table 12-16 Zooplankton respiration rate.

Source	μ_{Zd} (day ⁻¹)
Jorgensen (1981)	0.02-0.125
Wroblewski et al. (1988)	0.20
Boers et al. (1991)	0.13

Table 12-17 Michaelis constant for zooplankton uptake of algae.

Source	K_{ZG} (ug · l ⁻¹)
Jorgensen (1981)	5.0

12.10 Reaction Model for Littoral, Sediment and Pelagic Phosphorus

Values of coefficients used in Eqs. (12.2-1) to (12.2-6) and in related equations discussed in this and Chapter 6 are shown in Tables 12-18 to 12-28. These values were established for model use after initial model runs using literature values followed by subsequent calibration exercises.

Table 12-18 Residual phosphorus partitioning coefficients for partitioning TP-SRP synoptic data measurements.

Variable	Phosphorus Species	FORTRAN Variable	Simulation Value
K_{res}	DOP	AFRAC(1)	0.50
K_{res}	Zooplankton	AFRAC(2)	0.01
K_{res}	Blue greens	AFRAC(3)	0.30
K_{res}	Green algae	AFRAC(4)	0.19

Table 12-19 Water plus organic color light extinction coefficient ($1 \cdot m^{-1}$).

Variable	Lake Section	FORTRAN Variable	Simulation Value
$\epsilon_w + \epsilon_c$	Mud zone	EATA(1)	0.5
$\epsilon_w + \epsilon_c$	Macrophyte	EATA(2)	1.0
$\epsilon_w + \epsilon_c$	North Lake	EATA(3)	0.5
$\epsilon_w + \epsilon_c$	Sandy zone	EATA(4)	0.5
$\epsilon_w + \epsilon_c$	South Bay	EATA(5)	2.5

Table 12-20 Phosphorus transformation coefficients ($1 \cdot day^{-1}$).

Variable	Phosphorus Pathway	FORTRAN Variable	Simulation Value
K_D	DOP to SRP	RESPIR(1)	0.075
K_{Gx}	GRN to SRP	RESPIR(2)	0.20
K_{Gd}	GRN to DOP	RESPIR(3)	0.05
K_{Bx}	BLU to SRP	RESPIR(4)	0.10
K_{Bd}	BLU to DOP	RESPIR(5)	0.05
K_{Zx}	DIA to SRP	RESPIR(6)	0.20
K_{Zd}	DIA to DOP	RESPIR(7)	0.05
K_{dx}	ZOO to SRP	RESPIR(8)	0.50
K_{dd}	ZOO to DOP	RESPIR(9)	0.02

Table 12-21 Maintenance respiration coefficients ($1 \cdot \text{day}^{-1}$).

Variable	Phosphorus Pathway	FORTRAN Variable	Simulation Value
r_{oG}	GRN to SRP	RESBAK(1)	0.1
r_{oB}	BLU to SRP	RESBAK(2)	0.1
r_{od}	DIA to SRP	RESBAK(3)	0.0
r_{oZ}	ZOO to SRP	RESBAK(4)	0.0

Table 12-22 Temperature adjustment coefficients.

Variable	Phosphorus Pathway	FORTRAN Variable	Simulation Value
θ	DOP to SRP	THETA(1)	1.08
θ	GRN to SRP	THETA(2)	1.08
θ	GRN to DOP	THETA(3)	1.08
θ	BLU to SRP	THETA(4)	1.08
θ	BLU to DOP	THETA(5)	1.08
θ	ZOO to SRP	THETA(6)	1.08
θ	ZOO to DOP	THETA(7)	1.08
θ	DIA to SRP	THETA(8)	1.08
θ	DIA to DOP	THETA(9)	1.08

Table 12-23 Minimum uptake rate ($1 \cdot \text{day}^{-1}$).

Variable	Phosphorus Pathway	FORTRAN Variable	Simulation Value
μ_G	SRP to GRN	UPMAX(1)	2.0
μ_B	SRP to BLU	UPMAX(2)	1.25
μ_d	SRP to DIA	UPMAX(3)	0.1
μ_{ZG}	GRN to ZOO	UPMAX(4)	1.75
μ_{ZB}	BLU to ZOO	UPMAX(5)	0.75
μ_{Zd}	DIA to ZOO	UPMAX(6)	0.05

Table 12-24 Half saturation constant for uptake ($\mu\text{g} \cdot \text{day}^{-1}$).

Variable	Phosphorus Pathway	FORTRAN Variable	Simulation Value
K_G	SRP to GRN	KMIM(1)	1.0
K_B	SRP to BLU	KMIM(2)	15.0
K_d	SRP to DIA	KMIM(3)	10.0
K_{ZG}	GRN to ZOO	KMIM(4)	10.0
K_{ZB}	BLU to ZOO	KMIM(5)	5.0
K_{Zd}	DIA to ZOO	KMIM(6)	10.0

Table 12-25 Maximum settling rate ($\text{m} \cdot \text{day}^{-1}$).

Variable	Phosphorus Pathway	FORTRAN Variable	Simulation Value
v_{sG}	Green algae	WDOWN(1)	0.50
v_{sB}	Blue green	WDOWN(2)	0.20
v_{sd}	Diatoms	WDOWN(3)	1.20
v_{sZ}	Zooplankton	WDOWN(4)	0.08

Table 12-26 Half saturation constant for light ($\text{ly} \cdot \text{day}^{-1}$).

Variable	Phosphorus Pathway	FORTRAN Variable	Simulation Value
I_{oG}	GRN	AMAX(1)	300
I_{oB}	BLU	AMAX(2)	20
I_{od}	DIA	AMAX(3)	50

Table 12-27 Light absorption coefficients ($\text{m}^2 \cdot \mu\text{g}^{-1}$).

Variable	Phosphorus Pathway	FORTRAN Variable	Simulation Value
ϵ_{aG}	Green algae	SSA(1)	0.0105
ϵ_{aB}	Blue green	SSA(2)	0.20
ϵ_{ad}	Diatoms	SSA(3)	0.0025
ϵ_{as}	Sediment	SSA(4)	0.00

Table 12-28 Light scattering coefficients ($\text{m}^2 \cdot \text{ug}^{-1}$).

Variable	Phosphorus Pathway	FORTRAN Variable	Simulation Value
ϵ_{bG}	Green algae	SSC(1)	0.047
ϵ_{bB}	Blue green	SSC(2)	0.146
ϵ_{bd}	Diatoms	SSC(3)	0.241
ϵ_{bs}	Sediment	SSC(4)	0.87

12.11 Phosphorus Boundary Conditions

SRP and DOP are subject to loads from tributaries to the lake. The SRP and DOP loads are calculated from the daily flow in the tributary and either a semi-monthly or monthly average tributary concentration of SRP. The semi-monthly or monthly concentration is treated as a step-function, that is, the inflow concentration is held constant for approximately two or four weeks. However, the load (product of inflow and concentration) varies daily with inflow rates. DOP is the difference between TP and SRP in the tributary. All other phosphorus components are assumed to have zero concentration in the tributaries.

12.12 Summary of Pelagic Phosphorus Model

The simulation of pelagic phosphorus involves many kinetic coefficients. These are listed in the output of each run; representative literature values have been applied to Lake Okeechobee and are summarized in the tables of this chapter.

13. MASS BALANCE APPROACH TO PREDICTING PHOSPHORUS

13.1 Introduction

This chapter describes the mass balance approach to modeling phosphorus in Lake Okeechobee. This was Task 6.2 in the overall Lake Okeechobee phosphorus dynamics study. The mass balance approach ignores the complexities of lateral, transverse and vertical heterogeneities of phosphorus. A model that neglects these spatial complexities can be described as a 0-dimensional (0-D) model. The 0-D model uses the acronym LOP0D (Lake Okeechobee phosphorus 0-D model). LOP0D enables us to examine seasonal trends in phosphorus transformation rates, algal uptake and dissolved organic phosphorus mineralization rates, and littoral and diagenetic seasonal and annual phosphorus dynamics. Naturally, the same abiotic and biotic forcing functions and phosphorus components already described in Chapters 6 through 12 are used in LOP0D.

The approach we have taken is first to define the important internal and external physical, chemical, and biological factors for Lake Okeechobee that influence and affect the phosphorus dynamics of the lake. A few of these factors are:

1. Lake Okeechobee is a large body of water with a shallow depth. The action of wind on water is important because it causes bottom sediment erosion and is the primary cause of the pelagic and the littoral circulation patterns in the saucer shaped lake.
2. Solar radiation is a source of energy for macrophyte and phytoplankton growth in the littoral and pelagic regions of the lake. The solar radiation also causes heating or cooling of the lake water which in turn affects biological rates and vertical and horizontal lake circulation.
3. Tributary loadings of SRP and TP to Lake Okeechobee provide macronutrients nitrogen, phosphorus, and silica to fuel macrophyte, phytoplankton, and bacterial growth.
4. The bottom sediments of Lake Okeechobee are a source of recycled nutrients to the pelagic phytoplankton. The phytoplankton modify the sediment boundary condition affecting the diagenetic nutrient flux to and from the sediments.
5. The phytoplankton of Lake Okeechobee can be separated into three classes -- blue-green, green and diatom algae -- that have different growth, decay, settling, and other physical characteristics.

6. The phytoplankton have distinct seasonal cycles that interact with the other main phosphorus components.
7. Zooplankton and fish are a small fraction of the total phosphorus, but their selective feeding of algae influences the dominant algal class. Zooplankton and fish are important to the pelagic recycling of phosphorus through the processes of algal ingestion and SRP excretion.
8. Littoral macrophyte plants and associated epiphytic algae cover a large area (25,000 acres) of Lake Okeechobee. The quantitative effect of benthic organisms (e.g., corbicula and larvae) is best approximated in the model by using a range of possible uptake and release rates of phosphorus from the benthic animals.
9. The lake is not modeled as one reactive entity. Distinct lake areas are modeled based on bottom sediment type, average depth, submerged or emergent vegetation, river input, regulated releases of water, and the presence or absence of islands. The five lake sections are the central mud zone, macrophyte zone, north lake, South Bay, and the sandy fringe between the littoral zone and central mud zone of Lake Okeechobee.

Secondly, we review a previous modeling effort similar to LOP0D, followed by development, explanation, testing and application of LOP0D. The remainder of this chapter is a full description of the mass balance model of Lake Okeechobee. The period of record we have simulated is 1979 to 1988. The model has seven pelagic phosphorus components, two sediment phosphorus components and one littoral phosphorus component. Measured TP and SRP concentrations from eight long term lake stations are used to calibrate a five box-model of Lake Okeechobee phosphorus (see discussion in Chapter 4).

13.2 Previous Water Quality Models of Lake Okeechobee

In general, models can be classified into three categories: (1) simple input-output models; (2) linked hydrodynamic-nutrient models; and (3) ecosystem models. Hydrodynamic models have been discussed generally in Chapter 10, and ecosystem modeling as a component of the overall phosphorus modeling has been discussed in Chapter 12. The following section summarizes one of the previous simple input-output modeling studies done on Lake Okeechobee.

Blosser (1986) developed a variety of spatially varied models (i.e., one-box, two box, and three box models) to predict TP and SRP concentrations in Lake Okeechobee (Brezonik et al., 1983; Blosser, 1986). His goal was to develop and describe models without excessive data requirements that would be useful in managing

the lake. We will briefly describe the results of Blosser's modeling results, strengths, and limitations, plus improvements we make to the model to enhance its credibility both scientifically and from a lake management viewpoint.

Blosser's (1986) division of TP into only SRP and particulate phosphorus (PP) components is an inadequate representation of the total phosphorus pool. PP comprises only 25 percent of the TP in the middle of the lake and 8 percent in the macrophyte zone of the lake (Brezonik et al., 1983). The primary component of the TP pool was dissolved organic phosphorus (DOP) in the macrophyte zone and SRP in the lake center. Brezonik et al. (1983) hypothesized that DOP was produced in the littoral zone, became mineralized to SRP by pelagic bacteria, and then utilized by pelagic algae.

Blosser (1986) did not include the effect of temperature on primary production. All chemical and biological process rates are strongly dependent on temperature and the temperature response of phytoplankton and zooplankton must be modeled realistically, else large discrepancies can arise between model and observations (Jorgensen, 1983). This may be the most important drawback of the Blosser model.

The primary production submodel of Blosser (1986) included light as a function of depth and a light extinction coefficient. The light extinction coefficient (ϵ) was assumed by Blosser (1986) to be proportional to algal biomass. But, a non-linear relationship between the light extinction coefficient and algal biomass exists, due to increasing chlorophyll per cell as the total algal biomass increases (Carlson, 1977). A constant proportionality between biomass and extinction coefficient overestimates the extinction coefficient for large algal biomass. Another problem with Blosser's approach was the use of PP to represent algal biomass in the light extinction equation.

13.3 Five-Box Model of Phosphorus in Lake Okeechobee

Five separate and distinct areas of Lake Okeechobee were delineated based on the bottom sediment type, average depth, presence of submerged or emergent vegetation, river tributary input, regulated releases of water, and the presence/absence of islands. The five selected lake zones to model (shown in Figure 13-1) are:

1. The central mud zone. This is the deepest area of the lake with phosphorus dynamics dominated by suspended sediment.
2. Littoral or macrophyte zone in western Lake Okeechobee. This area has a shallow depth and dense emergent and submergent macrophyte vegetation. The vegetation and shallow depth dampen horizontal water movement and nutrient exchange mechanisms.

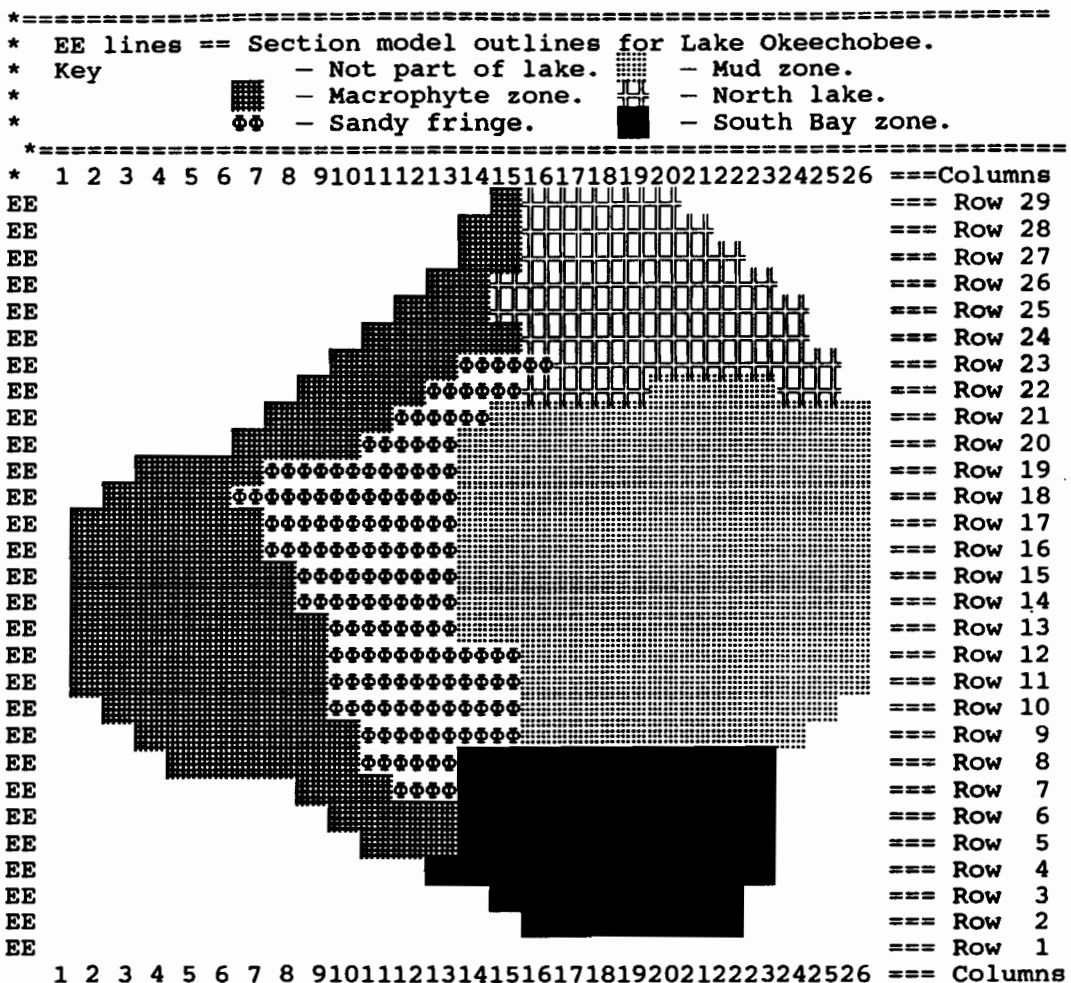


Figure 13-1 The 486 boxes of Lake Okeechobee 3-D model assigned to five sections in the coarse grid model.

3. Northern Lake Okeechobee. This area receives large tributary flows and SRP loading from central Florida.
4. The sand zone or sandy fringe between the littoral zone and central mud area.
5. South Bay. This area has a shallow depth, large islands, and is the area of the lake affected by the surface outflow canals to the Everglades.

The longitudinal Peclet number (Table 10-3), or the Bodenstein number, is an indicator of the spatial independence of the lake (Goda and Matsuoka, 1986). The P_e for the lake is low (564) meaning there is large scale spatial independence in Lake Okeechobee. The lake can be separated into large aggregated boxes with little loss of accuracy compared to a finer grid model.

The pictorial "stick" figure of Lake Okeechobee used in the rest of this chapter is shown in Figure 13-2. The delineation of the Lake Okeechobee finite difference boxes into coarse grid sections is defined based on the depth of the box, presence/absence of vegetation, and the bottom sediment type. Some of the frequently-used symbols for this schematization are listed in Table 13-1.

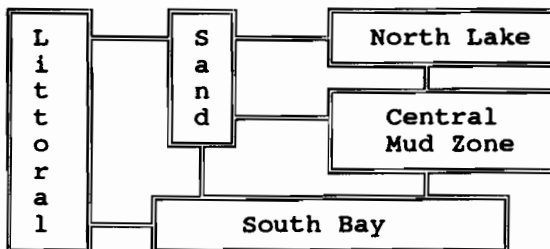


Figure 13-2 Lake Okeechobee boxes used in coarse grid model.

Table 13-1 Symbols for the various modeled boxes used in the simulation of Lake Okeechobee.

NL	North Lake	LT	Littoral area
MD	Mud zone	SN	Sand area
SB	South Bay		

13.4 Algal Growth in Lake Okeechobee

Model calibration and verification was accomplished by trying to match the long-term averages of water quality variables in Lake Okeechobee. The long term mean chlorophyll a was used to estimate the proportion of the total phosphorus associated with living algae. The long term measurements (Chapter 4) of suspended solids (TSS), turbidity (NTU), color (PCU), and secchi disc were used to estimate region specific absorption and scattering coefficients for light attenuation. Large algae are able to accumulate greater biomass than smaller algae before self-shading results in light limitation (Agusti, 1991). This accounts for the dominance of large algae in shaded, dense algal communities.

Phytoplankton growth represents a composite pattern of many species and algal classes. The literature values on algal growth, respiration and excretion usually apply to single species (see Chapter 12). Primary productivity applies to whole populations and growth rate applies to single cells. The Talling column compensation is the point where photosynthesis equals algal respiration over a diel cycle. Chlorophyll a serves as an integrative measure of phytoplankton biomass and photosynthetic potential.

The net growth of an algal species is a complex realization of internal and external biological and physical conditions. The net growth rate of algae in the model is based on the work of Langdon (1988), as discussed in Chapter 12. Using Eq. 12.6-1, a net algal growth rate (for green algae in this example) is:

$$r_{\text{lake}} = \mu_{\text{max}} \cdot f_1(I_z) \cdot f_2(T) \cdot k_{rG} + r_{oG} \quad (13.4-1)$$

where r_{lake} = net rate of algal growth (day^{-1}),
 μ_{max} = maximum growth rate (day^{-1}),
 f_1 = light intensity function (Chapter 6),
 f_2 = temperature function (Chapter 6),
 k_{rG} = respiration constant for new growth, and
 r_{oG} = respiration rate for zero growth (day^{-1}).

Values from this equation are consistent with net algal growth rates from data collected on Lake Okeechobee (Jones and Frederico, 1984). The net growth rate averaged 0.5/day to 0.6/day.

A yield controlled system (Chapra and Reckhow, 1983) is controlled primarily by the balance between gross primary production and the physical processes of sinking and vertical mixing.

13.5 Finite Difference Model of Lake Okeechobee

13.5.1 Box Model Formulation

The box model is a supplemental approach to the deterministic 3-D model. The main goal of this modeling is to predict the extent and rate of recovery of Lake Okeechobee in response to reductions in external loading rates. The objective is to predict annual changes in P concentrations in the lake. We attempt to incorporate the effects of pulsed events, e.g., major storms that cause accompanying pulsed releases from the sediment or littoral zone. These pulsed releases may in turn generate phytoplankton blooms in the lake. The main concern is to evaluate the averaged effects of reductions of P loading rates to Lake Okeechobee.

The Blosser box model of Lake Okeechobee was found to simulate the long term mean and variance of SRP and TP (Blosser, 1986). The weakness of Blosser's model was in matching peak values of TP. This was attributed by Blosser to problems with the sediment erosion model.

The total phosphorus concentration equation used in predicting the whole lake concentration on a yearly basis is (Canale and Effler, 1988):

$$\frac{d(V \cdot C)}{dt} = W - Q \cdot C - v \cdot A \cdot C \quad (13.5-1)$$

where V = volume of lake (m^3),
 C = average lake-wide concentration ($mg \cdot m^{-3}$),
 v = annual average net settling velocity of total phosphorus from the pelagic zone to sediments ($m \cdot yr^{-1}$),
 Q = annual outflow from lake ($m^3 \cdot yr^{-1}$),
 A = lake surface area (m^2),
 W = annual loading to the lake in $mg \cdot yr^{-1}$, and
 t = time (yr).

The water continuity equation for a lake box is:

$$A_m \cdot \frac{dy_m}{dt} + y_m \cdot \frac{dA_m}{dt} = Q_{mi} - Q_{mo} + (Q_{mr} - Q_{me}) \cdot A_m \quad (13.5-2)$$

where y_m = box m stage (m),
 A_m = box m area (m^2),
 Q_{mi} = box m inflow (m^3/mo),
 Q_{mo} = box m outflow (m/mo),
 Q_{mr} = box m average monthly rainfall (m/mo), and
 Q_{me} = box m average monthly evaporation (m/mo).

Conservation of mass for a phosphorus species i in box m is:

$$V_m \cdot \frac{dC_{im}}{dt} + C_{im} \cdot \frac{dV_m}{dt} = Q_{im} \cdot C_{im} + A_m \cdot Q_{mr} \cdot C_{imr} - C_{im} \pm R_{im} \quad (13.5-3)$$

where V_m = box m volume (m^3),
 R_{im} = reactions of phosphorus species i in box m ,
 Q_{im} = inflow rate containing species i to box m (m^3/mo),
 Q_{mi} = outflow rate containing species i from box m (m^3/mo),
 C_{im} = concentration of phosphorus species i in box m , and
 C_{mr} = rainfall concentration of species i into box m .

13.5.2 Diffusion and Advection

The terms that are products of flow \times concentration, $Q \cdot C$, are fluxes of phosphorus between boxes. Because actual flows between the various combinations of the five boxes are unknown, the fluxes have been considered in a heuristic fashion, in which the flux is broken into a pseudo-diffusive (PD) and pseudo-advective (PA) term. If the depths of adjacent zones are approximately equal, then multiplication by

area approximates differences in volume. Thus, the change in concentration due to the PD flux for transport, for example, from the north lake (higher concentration) to the mud zone (lower concentration) in the model is:

$$\Delta M_{mz} = X_i \cdot A_{nl} \cdot \Delta C \cdot \Delta t / (A_{mz} \cdot y_{mz}) \quad (13.5-4)$$

where ΔM_{mz} = change in concentration in mud zone due to diffusion from north lake,
 A_{nl} = surface area of north lake,
 ΔC = $C_{nl} - C_{mz}$, assumed positive for this example,
 A_{mz} = surface area of mud zone,
 y_{mz} = depth of mud zone, and

X_i is a parameter incorporating a coefficient, DIFCON_i, characteristic width between the north lake and mud zone, Y_i , and characteristic distance between the two zones, x_i ,

$$X_i = \text{DIFCON}_i \cdot Y_i / x_i \quad (13.5-5)$$

Parameters DIFCON_i, Y_i , and x_i (and thus, parameter X_i) differ for the eight different pathways between lake boxes shown in Table 13-2. This table also indicates the numerical interpretation of subscript i. Values used in the modeling for the three input parameters are shown in Table 13-3. Parameter DIFCON is not a diffusivity because it has units of length/time, but rather an empirical transport coefficient.

Note: in model LOPOD, parameter $Y \equiv YTRANS$ and $x \equiv XTRANS$. After input, the meaning of XTRANS is converted to parameter X (Eq. 13.5-5) for internal computations in the model. Additionally in the model, parameter ΔM is called DM.

Diffusion occurs from the area of higher concentration to the area of lower concentration. Thus, if $C_{nl} > C_{mz}$, the diffusive flux occurs only from the north lake to the mud zone. The north lake surface area (instead of the north lake depth) is included in Eq. 13.5-4 as a conceptual way to indicate the magnitude of the volume of water containing phosphorus that can be diffused from box to box. This accounts for the units of DIFCON (units of length/time instead of the units of a diffusivity of length²/time).

Organic phosphorus and particulate inorganic phosphorus are not advected or diffused across box boundaries because of the widely varying bottom sediment types. In addition the time scale of erosion and deposition is much shorted than the time scale of advection and diffusion.

Diffusion always takes place from the box of higher concentration to the box of lower concentration. Thus, for example if the north lake concentration of SRP is higher than the mud zone concentration of SRP then $C_{nl} - C_{mz} \equiv \Delta C_1 > 0$ and the flux from the north lake box to the mud zone box would be positive, and the diffusive

Table 13-2 Advection and diffusion inter-box connections.

1 - NL to Mud	2 - Mud to SB	3 - NL to Sand
4 - Sand to SB	5 - NL to Litt	6 - Litt to SB
7 - Sand to Mud	8 - Litt to Sand	

Table 13-3 Interbox transfer coefficients.

Lake Box Interface	Transfer Distance x_i , km	Interface Width Y_i , km	DIFCON
1 North Lake — Mud Zone	20	20	0.5
2 Mud Zone — South Bay	20	16	0.25
3 North Lake — Sand Zone	26.8	6	0.05
4 Sand Zone — South Bay	26.8	8	0.05
5 North Lake — Littoral Zone	12	12	0.05
6 Littoral Zone — South Bay	36	6	0.05
7 Sand Zone — Mud Zone	18	28	0.05
8 Littoral Zone — Sand Zone	12	26	0.05

flux from the mud zone box to the north lake box would be zero. In Eqs. (13.5-6) to (13.5-10) that follow, without resorting to complicated mathematical notation, if $\Delta C_i > 0$, then the positive (left-hand) term in the numerator applies (and the right-hand term is zero), and if $\Delta C_i < 0$, then the negative (right-hand) term in the numerator applies (and the left-hand term is zero). This is the way in which these terms are programmed in Subroutine CMOV of the LOPOD model. With the notation of Tables 13-2 and 13-3, the diffusive flux into (and out of) the five boxes are given below.

The diffusive flux for the mud zone (mz) is calculated as follows:

$$\Delta M_{mz} = \frac{+ X_1 \cdot A_{nl} \cdot \Delta C_1 - X_1 \cdot A_{mz} \cdot \Delta C_1}{A_{mz} \cdot y_{mz}} \cdot \Delta t + \frac{X_2 \cdot A_{sb} \cdot \Delta C_2 - X_2 \cdot A_{mz} \cdot \Delta C_2}{A_{mz} \cdot y_{mz}} \cdot \Delta t + \frac{X_7 \cdot A_{sz} \cdot \Delta C_7 - X_7 \cdot A_{mz} \cdot \Delta C_7}{A_{mz} \cdot y_{mz}} \cdot \Delta t \quad (13.5-6)$$

The diffusive flux for the north lake (nl) is calculated as follows:

$$\Delta M_{nl} = \frac{+ X_1 \cdot A_{mz} \cdot \Delta C_1 - X_1 \cdot A_{nl} \cdot \Delta C_1}{A_{nl} \cdot y_{nl}} \cdot \Delta t + \frac{X_3 \cdot A_{sz} \cdot \Delta C_3 - X_3 \cdot A_{nl} \cdot \Delta C_3}{A_{nl} \cdot y_{nl}} \cdot \Delta t + \frac{X_5 \cdot A_{mc} \cdot \Delta C_5 - X_5 \cdot A_{nl} \cdot \Delta C_5}{A_{nl} \cdot y_{nl}} \cdot \Delta t \quad (13.5-7)$$

The diffusive flux for the macrophyte (or littoral) area (mc or lt) is calculated as follows:

$$\Delta M_{mc} = \frac{X_5 \cdot A_{nl} \cdot \Delta C_5 - X_5 \cdot A_{mc} \cdot \Delta C_5}{A_{mc} \cdot y_{mc}} \cdot \Delta t + \frac{X_6 \cdot A_{sb} \cdot \Delta C_6 - X_6 \cdot A_{mc} \cdot \Delta C_6}{A_{mc} \cdot y_{mc}} \cdot \Delta t + \frac{X_8 \cdot A_{sz} \cdot \Delta C_8 - X_8 \cdot A_{mc} \cdot \Delta C_8}{A_{mc} \cdot y_{mc}} \cdot \Delta t \quad (13.5-8)$$

The diffusive flux for the sand zone (sz) is calculated as follows:

$$\begin{aligned}
\Delta M_{sz} = & \frac{+ X_3 \cdot A_{n1} \cdot \Delta C_3 - X_3 \cdot A_{sz} \cdot \Delta C_3}{A_{sz} \cdot y_{sz}} \cdot \Delta t + \\
& \frac{X_4 \cdot A_{sb} \cdot \Delta C_4 - X_4 \cdot A_{sz} \cdot \Delta C_4}{A_{sz} \cdot y_{sz}} \cdot \Delta t + \\
& \frac{X_7 \cdot A_{mz} \cdot \Delta C_7 - X_7 \cdot A_{sz} \cdot \Delta C_7}{A_{sz} \cdot y_{sz}} \cdot \Delta t + \\
& \frac{X_8 \cdot A_{mc} \cdot \Delta C_8 - X_8 \cdot A_{sz} \cdot \Delta C_8}{A_{sz} \cdot y_{sz}} \cdot \Delta t
\end{aligned} \tag{13.5-9}$$

The diffusive flux for the South Bay (sb) is calculated as follows:

$$\begin{aligned}
\Delta M_{sb} = & \frac{+ X_2 \cdot A_{mz} \cdot \Delta C_2 - X_2 \cdot A_{sb} \cdot \Delta C_2}{A_{sb} \cdot y_{sb}} \cdot \Delta t + \\
& \frac{X_4 \cdot A_{sz} \cdot \Delta C_4 - X_4 \cdot A_{sb} \cdot \Delta C_4}{A_{sb} \cdot y_{sb}} \cdot \Delta t + \\
& \frac{X_6 \cdot A_{mc} \cdot \Delta C_6 - X_6 \cdot A_{sb} \cdot \Delta C_6}{A_{sb} \cdot y_{sb}} \cdot \Delta t
\end{aligned} \tag{13.5-10}$$

Advective fluxes are assumed to occur on the basis of various current patterns in the lake. As for diffusion, the magnitude of these currents is unknown, and an inter-box flow, Q_{mi} , in Eq. 13.5-3 is assumed proportional to the surface area of the box and a constant, S. Thus, the change in concentration for a box i due to inflow Q_{mi} is assumed to be

$$\Delta MM_i = C_m \cdot A_m \cdot S \cdot \Delta t / (A_i \cdot y_i) \tag{13.5-11}$$

In the model, $\Delta MM \equiv$ parameter DMM. Input parameter S (SPEED in the model) has units of velocity and represents a conceptual rate of change of the water surface, per time step. In almost all model runs advection plays a very minor role due the small value of S (approximately 0.005 m/day). Thus, the model is not sensitive to advection assumptions.

As only one example of the code, the advective flux into and out of the mud zone (mz) is calculated as:

$$\begin{aligned}
 \Delta MM_{mz} &= \frac{A_{nl} \cdot C_{nl} - A_{mz} \cdot C_{mz}}{A_{mz} \cdot y_{mz}} \cdot S \cdot \Delta t + \\
 &\quad \frac{A_{sb} \cdot C_{sb} - A_{mz} \cdot C_{mz}}{A_{mz} \cdot y_{mz}} \cdot S \cdot \Delta t + \quad (13.5-12) \\
 &\quad \frac{A_{sz} \cdot C_{sz} - A_{mz} \cdot \Delta C_{mz}}{A_{mz} \cdot y_{mz}} \cdot S \cdot \Delta t
 \end{aligned}$$

13.5.3 Reaction Pathway Finite Difference Equations

The phosphorus concentration at the end of a time step, C^{n+1} , is solved using two iterations. The first estimate (iteration) of the average phosphorus concentration is $C^{n+1/2}$, the concentration after advection and diffusion have been calculated from Eqs. (13.5-6) to (13.5-12). The second and final estimate (Iteration) of the average phosphorus concentration is the volume-weighted mean of $C^{n+1/2}$ and ΣR , the concentration changes due to reactions. The new concentration of a phosphorus species at the end of a time step, C^{n+1} , is thus calculated as follows:

$$C^{n+1} = \frac{C^{n+1/2} \cdot V^n + \Sigma R \cdot V}{V^{n+1}} \quad (13.5-13)$$

where V^n = lake box volume at the last time step,
 V^{n+1} = lake box volume at the next time step,
 V = average lake volume over the time step, and
 ΣR = summation of phosphorus species reaction pathways for the timestep.

The many phosphorus species reaction pathways are enumerated in Table 13-4, where the subscripts correspond to the subscripts used in Subroutine REAC0D.

13.6 Sediment Erosion and Deposition

The bottom sediment type in Lake Okeechobee is considered homogeneous in each of the five areas (boxes) of the models LOP0D and LOP3D. This assumption is backed by the mapping of bottom sediments of Lake Okeechobee by Reddy et al. (1991). The lake contains mud sediments in the north and central lake areas, a broad sandy area between the littoral area and mud area, peat sediments and a rocky reef in the southern lake, and littoral sediments in the western area of Lake Okeechobee. The bottom coverage of sediments were 44.3 percent mud, 24.5 percent sand, 12.6 percent peat and rocky reef, and 18.6 percent littoral (Reddy et al., 1991).

Table 13-4 Phosphorus reaction pathways.

Pathway	Description
ΔM_1	DOP to SRP Remineralization
ΔM_2	GRN uptake of SRP
ΔM_3	GRN release of SRP
ΔM_4	GRN release of DOP
ΔM_5	BLU uptake of SRP
ΔM_6	BLU release of SRP
ΔM_7	BLU release of DOP
ΔM_8	ZOO uptake of GRN
ΔM_9	ZOO uptake of BLU
ΔM_{10}	ZOO release of SRP
ΔM_{11}	ZOO release of DOP
ΔM_{12}	Adsorption/Desorption of SRP
ΔM_{13}	DIA uptake of SRP
ΔM_{14}	DIA release of SRP
ΔM_{15}	DIA release of DOP
ΔM_{19}	SRP Tributary Load
ΔM_{20}	DOP Tributary Load
ΔM_{21}	SRP export through surface water
ΔM_{22}	DOP export through surface water
ΔM_{23}	GRN export through surface water
ΔM_{24}	BLU export through surface water
ΔM_{25}	DIA export through surface water
ΔM_{26}	ZOO export through surface water
ΔM_{28}	GRN settling loss
ΔM_{29}	BLU settling loss
ΔM_{30}	DIA settling loss
ΔM_{31}	SRP Precipitation Load
ΔM_{32}	DOP Precipitation Load
ΔM_{33}	Diagenetic flux of SRP
ΔM_{35}	ZOO uptake of DiA
ΔM_{36}	Erosion flux of ORG
ΔM_{37}	Deposition flux of ORG
ΔM_{38}	Erosion flux or PIP
ΔM_{39}	Deposition flux or PIP
ΔM_{40}	Advection flux of bottom SRP
ΔM_{47}	Bottom biota source of DOP
ΔM_{48}	Bottom biota sink of SRP

The surficial storage (upper 10 centimeters) of phosphorus in the bottom sediments is 28.7 million kilograms (Reddy et al., 1991). This storage of phosphorus is almost evenly divided between mud storage (42 percent) and sand storage (41 percent). The mud storage of phosphorus is more susceptible to wind mixing than the sand storage (Sheng et al., 1991c), but the diffusive flux of SRP from the sand area is greater than from the mud area (Pollman, 1991).

The possible pathways for phosphorus transfer across the sediment water interface include those listed below. In this list, the numbers in parentheses refer to monitored pathways in model LOP0D that are numbered in Table 13-11 (discussed later).

1. Erosion of organic sediment phosphorus (#74).
2. Erosion of inorganic sediment phosphorus (#77).
3. Deposition of organic sediment phosphorus (#75).
4. Deposition of inorganic sediment phosphorus (#78).
5. Diffusion of inorganic phosphorus (SRP) across the sediment-water interface (#63).
6. Entrainment of interstitial SRP during erosion and transfer to the pelagic (#76).
7. Pelagic adsorption of SRP to PIP and pelagic desorption of PIP to SRP (#40 and 41). This two-way process coupled to the process of erosion-deposition of PIP means that a particular sediment may function as a source or sink of pelagic SRP.
8. Settling algae to the bottom sediments (#59). This means that new organic phosphorus is being accumulated to replace the organic phosphorus transformed to inorganic phosphorus and the organic phosphorus loss to the deeper bottom sediments.

Additional material examined in the box model of Lake Okeechobee is the time a lake box $EPC > SRP$, where EPC = equilibrium phosphorus concentration. This indicates the time suspended sediment is a source and/or sink of pelagic SRP.

$SRP < EPC$ (Pathway #67, Table 3-11). Sediments are a source of pelagic SRP. This occurs primarily in the sand zone.

$SRP > EPC$ (Pathway #66, Table 3-11). Sediments are a sink of pelagic SRP. This occurs primarily in mud, littoral, and peat sediments.

The sink of absorbed SRP to PIP is a significant loss term in the phosphorus model. The absorbed phosphorus settles to the bottom of the lake, where it subsequently either is eroded or transformed in the diagenetic model.

The current average sediment accumulation rate is $282.5 \text{ g} \cdot \text{m}^2/\text{yr}$ in Lake Okeechobee (Brezonik et al., 1989). Sediment accumulation has accelerated in the 1900s, with the largest increase in the phosphorus sedimentation rate occurring in the last 40 to 50 years (Brezonik et al., 1989). The post 1900 sediment accumulation rate is 500 percent greater than the pre 1900 rate. The phosphorus accumulation rate can be estimated from the sediment accumulation rate and the ratio of total phosphorus to sediment ($1178 \text{ mg P/kg dry weight sediment}$). Thus, the phosphorus accumulation rate is $282.5 \times 1178/1000 = 333 \text{ mg P} \cdot \text{m}^2/\text{yr}$. A similar value of $257 \text{ mg P} \cdot \text{m}^2/\text{yr}$ was found by Messer et al. (1979). Lennox (1984) estimated an internal loading of $132 \text{ mg P} \cdot \text{m}^2/\text{yr}$ from the littoral area of Lough Ennell.

Sediment erosion only occurs during the two night-time steps (see Section 13.10.1). Sediment deposition occurs during every time step. This gives a diurnal pattern to the pelagic sediment concentration. A similar pattern was measured in Lake Okeechobee by Sheng et al. (1991c).

Using the mean daily wind in m/sec (W), the fetch length (FL) in meters and the depth (y) in meters the mean daily bottom shear stress (τ) is calculated as:

$$GG = 9.806/W^2 \quad (13.6-1)$$

$$ARG1 = TANH(0.530 \cdot (GG \cdot Y^{0.75})) \quad (13.6-2)$$

$$ARG2 = 0.00565 \cdot (FL \cdot GG)^{1/2} \quad (13.6-3)$$

$$ARG3 = TANH(0.833 \cdot (GG \cdot Y^{0.375})) \quad (13.6-4)$$

$$ARG4 = 0.0379 \cdot (FL \cdot GG)^{0.333333} \quad (13.6-5)$$

$$ARG5 = W/9.806 \quad (13.6-6)$$

$$TS = 7.54 \cdot ARG3 \cdot TANH(ARG4/ARG3) \cdot ARG5 \quad (13.6-7)$$

$$HS = 100 \cdot 0.283 \cdot ARG1 \cdot TANH(ARG2/ARG1)/GG \quad (13.6-8)$$

$$LFET = 9.81 \cdot TS^2/(2 \cdot \Pi) \quad (13.6-9)$$

$$LD = LFET \cdot TANH(2.0 \cdot \Pi \cdot Y/LFET) \quad (13.6-10)$$

$$UF = 2 \cdot \Pi \cdot HS / (TS \cdot SINH(2.0 \cdot \Pi \cdot Y/LD)) \quad (13.6-11)$$

$$\tau = UF^2 \cdot F_W/2 \quad (13.6-12)$$

The daily erosion value rate is:

$$\tau = [(\tau/\tau_{cr} - 1.0) + |\tau/\tau_{cr} - 1.0|]/2 \quad (13.6-13)$$

$$\tau \leq \tau_{max} \quad (13.6-14)$$

$$Fe = C_{susp} \cdot \tau \quad (13.6-15)$$

13.7 Stage-Area-Volume in Lake Okeechobee

The depth-area-volume relations used for Lake Okeechobee is shown in Figure 13-3. This relationship is important since a primary cause of increased TP concentrations is a lower lake depth and volume, and a primary cause of increased SRP concentrations is a higher lake stage. The modeled surface area in the 3-D model of Lake Okeechobee is 1944 km². This is a maximum surface area and is inappropriate for the 0-D model of Lake Okeechobee based on stage data from 1932 to 1988. The LOP0D model uses a maximum surface area of 1805 km² (Shih, 1980), which is a better approximation of the real surface area of Lake Okeechobee. The translation from the aggregate boxes in the 3-D model and the lake area in model LOP0D was accomplished by subtracting 35 km² from the north lake, sand zone, littoral, and South Bay boxes of Lake Okeechobee. The discrepancy between the lake surface area at high lake stages is significant only at high lake stages (Shih, 1980).

Each lake box has the same stage and depth, but differing lake areas. The lake depth for the remaining days of the month are based on separate pan coefficients for the macrophyte (P_{mc}) and other lake boxes (P_{lk}), and the average monthly precipitation (RAIN). The lake depth is calculated as follows:

$$\begin{aligned} y^{n+1} = & y^n + \Delta t \cdot [RAIN - A_{mc} \cdot P_{mc} - A_{nl} \cdot P_{lk} - A_{mz} \cdot P_{lk} \\ & - A_{sz} \cdot P_{lk} - A_{sb} \cdot P_{lk} + \\ & + KR + FEC + S23 + S191 + Inflow - \\ & - CALOO - HGSX - Outflow] / A_{lake} \end{aligned} \quad (13.7-1)$$

Acronyms for lake inflows and outflows correspond to locations shown on Figure 5-1. (See also Section 13.10.11 and Tables 13-6 and 13-7 later in this chapter.)

13.8 Lake Okeechobee LOP0D Boundary Conditions

The simulation period used in the 0-D Lake Okeechobee modeling covered the period 1979 to 1988. The time series history of the loading and boundary conditions to Lake Okeechobee are presented in Figures 13-4 through 13-10. The changes in

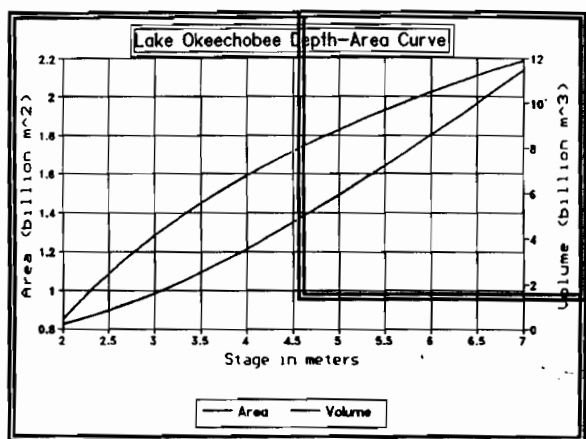


Figure 13-3 Stage, area, and volume relationship.

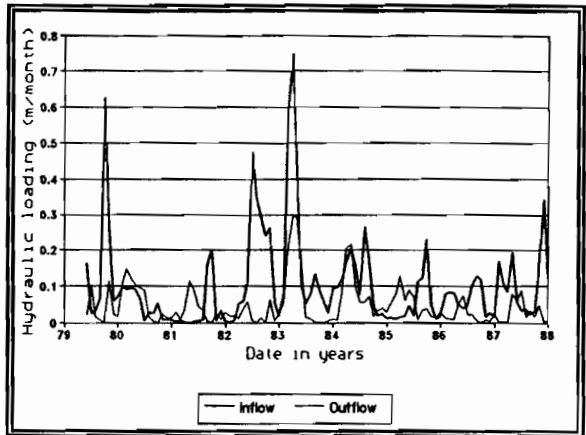


Figure 13-4 Normalized hydraulic inflow and outflow for 1979 to 1988.

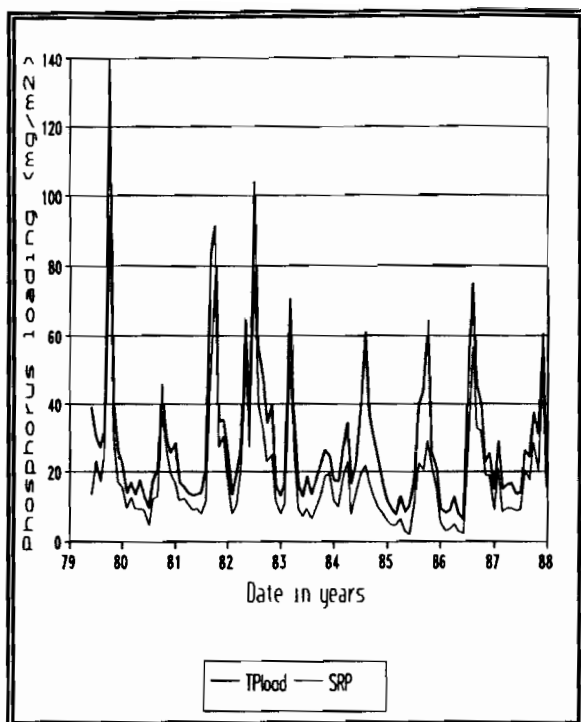


Figure 13-5 Normalized loading of SRP and TP for 1979 to 1988.

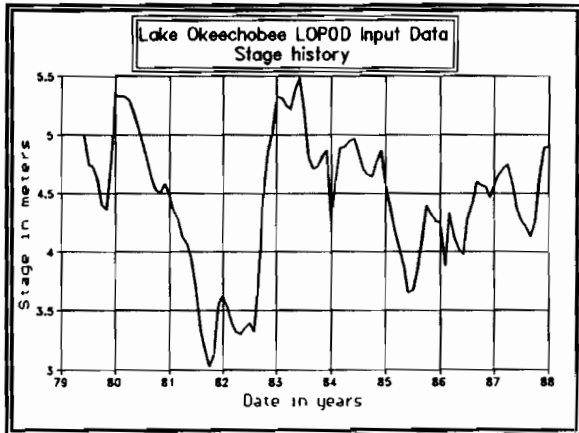


Figure 13-6 Stage history for the period 1979 to 1988.

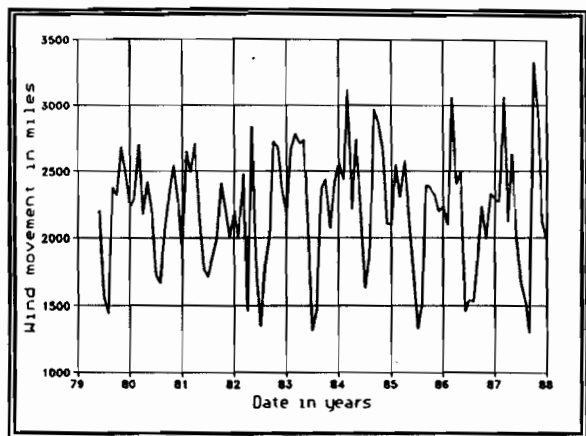


Figure 13-7 Daily wind movement above the pan evaporation station at Belle Glade for 1979-1988.

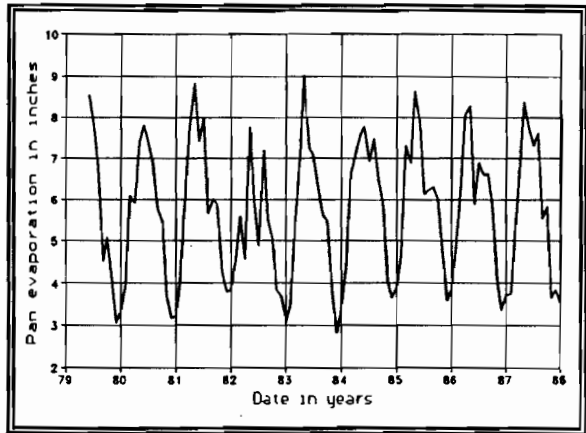


Figure 13-8 Average of pan evaporation measurements at Moore Haven, Clewiston, and Belle Glade for 1979-1988.

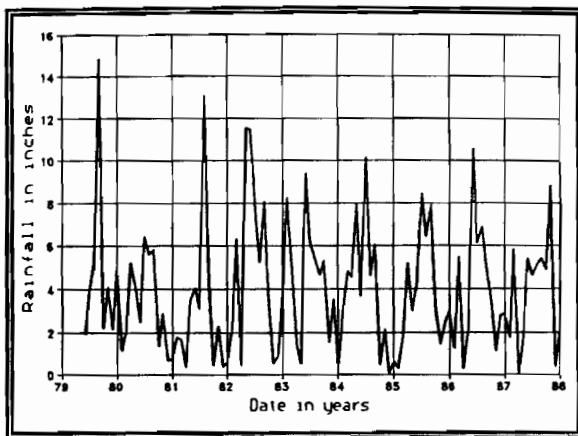


Figure 13-9 Average of precipitation measurements at Moore Haven, Clewiston, and Belle Glade for 1979-1988.



Figure 13-10 Major hydraulic input (rainfall and inflow) and output (evaporation and outflow) for 1979-1988.

loading, wind, inflow, outflow, precipitation, evaporation and stage between the 1970s and the 1980s were discussed in Chapter 4.

The wind movement above the evaporation pan is measured at a height of 2 meters. A power law profile for wind speed uses an exponent of (1/7) for changing the wind speed from that measured at 2 m to an estimated wind speed at 10 m (Schwab and Morton, 1984). The wind speed should be increased by a factor $(10/2)^{1/7} = 1.26$ to be usable in wind shear formulas. The relationship between over-lake wind speed and land wind speed is also a function of the wind speed class and the air-lake temperature difference. Neglecting the wind speed class and air-lake

temperature difference, the best predictor of over-lake wind speed (W_w) is a constant $1.18 \cdot W_l$ in the Great Lakes (Schwab and Morton, 1984). We will use a value of $1.26 \cdot 1.18$ to estimate the mean overlake wind speed in Lake Okeechobee at a height of 10 meters.

13.9 Normalized Nutrient and Hydraulic Loading

The total phosphorus load (kg) and total hydraulic load (m^3) are often divided by the lake surface area to normalize the loading for inter- and intra-lake comparisons. The smaller numbers are also easier to understand and comprehend. The external nutrient loading is usually presented in units of mg/m^2 (Figure 13-5), and the hydraulic loading in units of meters (Figure 13-4). The normalized external loading can be compared to internal loading, algal uptake, algal respiration, areal nutrient transformation rates, sediment erosion and deposition, and nutrient concentrations. Time integrated concentration can be compared to the total areal transformation rates, external and internal loading, and net flux from the sediments.

Using volume weighted concentrations to compare measured synoptic data is preferable to arithmetic weighting comparisons with synoptic data. We tried to minimize this problem by segregating the statistics by lake box (each box has approximately the same depth). (Note: A confounding factor in using data from 1979 is the overflowing of Kreamer Island and Ritta Island in South Bay resulting in large and unquantifiable loading of phosphorus to Lake Okeechobee (Federico et al., 1981).

13.10 General Modeling Considerations

13.10.1 Time Steps

Four time steps per day are used in the model: two daylight and two night time steps. The first daylight time step is from sunrise to solar noon, and the second is from solar noon to sunset. The first night time step is from sunset to midnight, and the second from midnight to sunrise. Four daily time steps are necessary because of the importance of diurnal variation of suspended sediment, solar radiation, temperature, the high rate of algal uptake of SRP, and the high rate of zooplankton uptake of algal species.

Even with four time steps per day some reaction pathways result in negative concentrations of a phosphorus component. Any reaction pathway that results in a negative concentration is disallowed, and only 25 percent of the reaction pathway is used by the model. For example, if the green algal uptake of SRP is $10\ mg/m^3$, the concentration of SRP $5\ mg/m^3$, then the modified green algal uptake will be $2.5\ mg/m^3$. The lowest limit for any phosphorus species in the model is $0.001\ mg/m^3$ ($1\ \mu g/l$).

13.10.2 DOP Remineralization

The reaction pathway rate between DOP and SRP is linear, and the typical calibrated remineralization rate is based on turnover times of DOP from 10 days to 20 days. Slower turnover rates of DOP result in unrealistic concentrations of DOP in Lake Okeechobee. Higher turnover rates of DOP result in low concentrations of DOP and high concentrations of SRP in Lake Okeechobee. A mean value of 0.075/day with a range from 0.05/day to 0.100 day results in reasonable values of DOP and SRP in the simulated Lake Okeechobee.

13.10.3 Lake Precipitation Loading

The dry and wet deposition loading of SRP and DOP to Lake Okeechobee is simulated using a constant concentration of SRP and DOP, a shading coefficient of 0.8 for rainfall over the lake, and measured monthly rainfall from stations located around the periphery of the lake. The mean Florida bulk precipitation concentrations were 21 ug/l for SRP and 36 ug/l for TP (Brezonik et al., 1983). The parameters used for precipitation loading are discussed in more detail in Chapter 6 of this report.

13.10.4 Lake Diagenetic Flux

The diagenetic flux of SRP from the bottom sediments occurs in all five lake boxes. The parameters used for estimating the bottom flux is discussed in more detail in Chapter 8. All bottom fluxes are predicted or simulated in units of mg/m²-day. The added concentration per time step is simply the flux · Δt divided by the mean box depth in meters.

The top boundary condition for the diagenetic model is the average box SRP concentration for the previous day. The magnitude of the diagenetic flux is only updated daily.

Transfer of SRP across the sediment-water interface is a two way process.

$C_{srp} > C_{aq}$ The diffusive transfer is from the pelagic to the sediment.

$C_{srp} < C_{aq}$ The diffusive transfer is from the sediment to the pelagic.

An important interaction between sediment and pelagic SRP is occurs through the process of pelagic adsorption/desorption. The details are discussed in Chapter 8.

It was necessary to develop an internal sediment phosphorus model to balance the many-fold pathways of pelagic-sediment interaction. The source of new organic phosphorus is algal settling. The organic phosphorus is modeling differently than in Pollman's diagenetic model. We consider only the top ten centimeters of the

sediment to viable and interacting. We thus use a small vertical segmentation through the aerobic and anaerobic sediment.

13.10.5 Macrophyte, Corbicula, and Algal Mat Fluxes

An additional flux of SRP and DOP is simulated in the macrophyte, sand, and South Bay areas of Lake Okeechobee. The purpose of this flux is to acknowledge in the model the effect of macrophytes, benthic organisms such as Corbicula, and algal mats on the pelagic concentrations of phosphorus in Lake Okeechobee. The parameters used for estimating the bottom flux are discussed in more detail in Chapter 9 of this report. Since we have incomplete information on the magnitude and timing of these pathways we must make the following realistic assumptions:

1. The net yearly flux is assumed negligible. We assume that half of the year the three boxes are a sink of SRP and the rest of the year the boxes are a source of DOP. The boxes are assumed to be a sink of SRP in the spring and summer, and a source of DOP in the fall and winter.
2. The magnitude of the daily source or sink is assumed to be comparable to the diagenetic flux of SRP.

13.10.6 Algal and Zooplankton Reaction Pathways

The uptake of SRP by the simulated algal species utilize Subroutine ATEMP to calculate the reaction rates based on the current lake water temperature. Algal uptake only occurs during the two daily time steps. The maximum algal uptake rate is moderated by the effects of light, temperature, and SRP concentration as discussed in Chapter 12. The uptake of SRP is calculated in units of concentration per time step.

The release of SRP and DOP by the simulated algal species utilizes Subroutine ATEMP to calculate the reaction rates based on the current lake water temperature. Algal release occurs during both the two nightly and two daily time steps. A lower limit of 1 or 2 mg/m³ is used for all algal loss pathways. This lower limit allows the simulated algal species a continued presence in each lake box. Otherwise, the concentration of algae may become unviable and affect the prediction of phosphorus in the lake. The reaction mechanisms of algal excretion and death are discussed in Chapter 12. The excretion and release of DOP and SRP, respectively, are calculated in units of concentration per time step.

The settling rate for green, and blue-green is based on a variant of Stoke's Law and varies daily throughout the year. The settling rate of sediment organic phosphorus is constant throughout the year. The settling rate units are m/day. The settling rate loss is calculated as $\Delta t \cdot \text{rate}/\text{depth}$. Settling occurs during both the

daylight and night time steps. The antithesis of settling, erosion occurs only during the two night time steps.

The settling velocity of algae (K_{sG} or K_{sB}) is a function of the water density (ρ), viscosity (η), daily wind (W), algal shape factor (A_{shape}), algal radius (A_{rad}), and wind factor (ψ). For example, for blue-green algae:

$$K_{sB} = 0.001884 \cdot A_{rad}^2 \cdot [A_{shape} \cdot \rho] / \eta \cdot \psi / W \quad (13.10-1)$$

Zooplankton uptake of algal species is based on Michaelis-Menten kinetics. A lower limit of 1 or 2 mg/m³ is used in modeling the algal uptake by zooplankton. The predation by zooplankton is assumed to be impossible for smaller algal concentrations. Zooplankton uptake occurs during all daily and night time steps.

Zooplankton excretion of SRP is 50 percent of the total algal uptake. This conversion of algal biomass to SRP by zooplankton is an important source of SRP during the summer months. The death of zooplankton is simulated as a quadratic function. The quadratic loss term represents the consumers of zooplankton, i.e., fish. This quadratic loss pathway places an upper limit on the zooplankton concentration. Typically, the upper range of zooplankton concentration is 5 to 10 mg/m³ in the lake simulation. Zooplankton phosphorus pathways are discussed in more detail in Chapter 12.

13.10.7 Dynamic Adjustment of Algal Fractions

The species of algae included in the model have quite different characteristics:

Blue-green	Slow growth and death, these algae remain in the water column by maintaining buoyancy and minimizing predation.
Green	Fast growth and recycle, these small algae are responsible for most of the pelagic community metabolism.
Diatom	A small component of the algal population, except during very turbulent months when they are able to maintain their position in the water column.

The blue-green algae include both N₂-fixing and non-N₂-fixing algae. Nitrogen is not simulated in this model and is only infrequently and locally limiting in Lake Okeechobee.

The numerical difficulties in modeling multiple algal species is center around ensuring that one species does not totally dominate the entire algal population. This undesirable result can occur because the large space scale of the models LOP0D and

LOP3D do not reflect the heterogeneity and small scale patchiness of the real algal population that ensures the survival of multiple algal species. Harkening back to the discussion in Section 12.3.1 of Hutchinson's "Paradox of the Plankton", the paradox in algal modeling is akin to Hutchinson's paradox.

How then, do we ensure that algal classes survive the hustle and bustle of pelagic existence? The only conceivable way is to use the vast knowledge of algal behavior in literature. For example, the diatom algal dominance of the spring bloom is due to wind mixed turbulence in both northern temperate and Florida lakes. The model replicates this condition by making diatom algal settling a function of turbulence (i.e., wind action). This is further elaborated in Chapters 7 and 12. The periodic green algal blooms are modeled as windows of opportunity in the general blue-green algal dominance of the lake phytoplankton (Chapter 12).

The algal loss pathway of GRN and BLU death and excretion to DOP are adjusted every two days to prevent the dominance of any one algal class in the simulated lake algal population. Each algal class has a lower and upper fraction of the total algal population, which is defined by the user of the program. The values used in the calibration are shown in Table 13-5. The adjustment procedure is as follows:

When an algal class falls below its allowable percentage the value of K_{Gd} or K_{Bd} is decreased by 0.005/day.

When an algal class exceeds its allowable percentage the value of K_{Gd} or K_{Bd} is increased by 0.005/day.

The allowable lower and upper limits of K_{Gd} and K_{Bd} are 0.01/day and 0.20/day, respectively.

Table 13-5 Algal population limits (fraction of total population).

Algal Class	Lower Limit	Upper Limit
Green	0.10	0.50
Blue-green	0.10	0.90

The reason for this procedure was the extreme sensitivity of the algal phosphorus concentrations to the choice of the algal uptake, release, settling, and death parameters. Basically, given a suite of GRN (green) algal parameters and a suite of BLU (blue-green) algal parameters, one algal class would always dominant (> 99 percent) in the simulation. This would have a drastic effect on the other simulated phosphorus species since the behavior of the two algal species varied dramatically. By dynamically adjusting one loss coefficient during the course of the 9

year simulation the apparent distribution of Lake Okeechobee algal species was mimicked by the model, and the overall simulation became less sensitive to the choice of the initial algal parameters.

13.10.8 Algal Populations and Time Scales

The most serious issue we wrestled with in the calibration of the model was finding the best and most accurate representation of the reaction rate formulations and constants used in this dynamic phosphorus model of Lake Okeechobee. We selected the coefficients for green algal growth to have the following characteristics:

1. High settling rate to remove green algal cells to the bottom sediment. Green algal settling was 66 percent of the total algal settling.
2. Green algae are subject to a high grazing pressure from zooplankton and fish.
3. Fast uptake of SRP.

Blue-green algae have the following selected characteristics in the lake:

1. Lower settling rates -- arbitrarily set to 25% of rate for green in LOP0D.
2. Blue-green algae are subject to lower grazing pressure from zooplankton and fish.
3. Slower uptake of SRP.

The reaction rates (μ and K with units of 1/time) have important implications on algal time scales. The inverse of a reaction rate (K_τ) indicates the time scale of the pelagic response (τ).

$$\tau \approx 1 / K_\tau \quad (13.10-2)$$

For example, $\tau = 20$ days for $K_\tau = 0.05/\text{day}$, $\tau = 2$ days for $K_\tau = 0.5/\text{day}$, and $\tau = 1$ day for $K_\tau = 1.0/\text{day}$.

The background release of SRP and DOP from the modeled algae must be reasonable for the entire year. Consider that a release rate of $0.10/\text{day}$ ($\tau = 10$ days) means the algal concentrations in the colder (less reactive) winter months will drop to near zero. Conversely, a release rate of $0.05/\text{day}$ ($\tau \approx 20$ days) ensures the algal concentration remain at a viable level for summer growth.

Algal growth and growth stimuli are uncoupled in time. A lag time exists between the application of a nutrient and subsequent algal growth. One explanation is that of an "intrinsic" lag time due to a period of biochemical adjustment, plus and "extrinsic" lag time due to variability in growth and loss rates. The lagged growth phenomenon occurs in laboratory, microcosms, and lakes (Duarte, 1990). The response time of lake phytoplankton to increased external algal growth is 11 days from vertical mixing to 23 days to whole lake enhancement.

Algae with high net growth rates can be expected to show a short lag time. Small species, with high growth rates, should dominate fluctuating environments. The models LOP0D and LOP3D have a lower limit of algal concentration ($\approx 1 \text{ ug/l}$). The lag time phenomenon also accounts for the spatial separation that occurs between the source of nutrients (i.e., the tributaries) and the manifestation of the nutrient load (i.e., higher algal growth and larger standing crops of algae). This may lead to wrong conclusions about the source of algal blooms. The source may be the northern lake tributaries, but the right conditions for algal growth may only take place in the south bay of Lake Okeechobee.

The residence time of the lake was 2.1 years based on the hydraulic loading and 4.3 years based on the surface outflow rate. However, the phosphorus residence time is appreciably shorter based on summing the phosphorus transformation rates. The response time of the lake is predicated on the reactive residence time of the lake. A lake with a residence time of 2 to 5 years will take at least 10 years to completely respond to external and structural changing conditions.

13.10.9 Phosphorus Import and Export

Tributary loadings to Lake Okeechobee in the model occur in the north lake, South Bay, mud zone and macrophyte zone. The loadings are mean daily loads in mg/m^2 and are based on the mean monthly concentrations of SRP and TP in the tributaries of Lake Okeechobee (Carey and Huber, 1990). The loads are entered based on a whole lake area and converted to a box-specific areal loading on the current value of the lake box area (see Table 13-6).

Table 3-6 Specific nutrient loadings to Lake Okeechobee.

Tributary Name	Lake Box
S191	North Lake
KR	North Lake
FEC	Macrophyte
S23	South Bay
Residual SRP	North Lake
Residual DOP	North Lake

Phosphorus export from Lake Okeechobee via the surface outflow canals in the model occurs in the South Bay, mud zone and macrophyte zone. The export loads are in mg/m² and are based on the current box concentration of the various phosphorus species and mean monthly surface outflow rates (see Table 13-7).

Table 3-7 Specific outflows from Lake Okeechobee.

Tributary Name	Lake Box
CALOO	Macrophyte
HGSX	Mud Zone
Residual	South Bay

Three special facilities are used in the input of the tributary loads to Lake Okeechobee. The concentration of phosphorus in the inflow from Nubbins/Slough can be limited. For example, the inflow concentration can be limited to 200 mg/m³. The total tributary loading can be reduced or increased by using the parameter REDLOW in the input data file. For example, load reduction alternatives tested for the SFWMD used 50 percent and 70 percent reduction in total load (REDLOW = 0.5, 0.3, respectively).

13.10.10 Initial Phosphorus Conditions

The beginning phosphorus species concentrations of both model LOP0D and model LOP3D are initialized using the following procedure based on measured SRP, TP and TSS concentrations:

First the concentration of particulate inorganic phosphorus or PIP (C_p) is estimated based on the measured TSS concentration (C_{sed}) and a partition coefficient, or $C_p = C_{sed} \cdot K_{pip}$.

Secondly, the sediment organic particulate phosphorus or ORG concentration (C_{org}) is estimated based on the measured TSS concentration and a partition coefficient, or, $C_{org} = C_{sed} \cdot K_{org}$.

Thirdly, the concentration of residual phosphorus, C_{diff} , is estimated as:

$$C_{diff} = C_{TP} - C_{aq} - C_p - C_{org} \quad (13.10-3)$$

where C_{TP} = TP concentration, and
 C_{aq} = SRP concentration.

The residual phosphorus concentration is then partitioned into starting concentrations of dissolved organic phosphorus or DOP (C_D), green algae (C_G), blue-green algae (C_B), and zooplankton (C_z) using the proportions shown in Table 13-8. The models are not overly sensitive to the starting values of phosphorus since the rates of phosphorus transformations are sufficiently high to alter the proportion of phosphorus components in two to three days.

Table 13-8 Residual C_{diff} phosphorus proportions (fractions of C_{diff}).

DOP 0.60	GRN 0.19	BLU 0.20	ZOO 0.01
----------	----------	----------	----------

13.10.11 Lake Area and Lake Box Areas

The area of each box is adjusted every time step based on the current lake stage and depth. The base of every box is 1.76 meters and the stage is simply depth (meters) plus 1.76 meters. The starting lake areas are shown in Table 13-9.

Table 13-9 Lake Areas in km^2 for Model LOP0D.

North Lake	216.0	Macrophyte	448.0
Mud Zone	616.0	Sand Zone	288.0
South Bay	236.0	Whole Lake	1804.0

The starting lake stage for day 1 of the month is the measured lake stage. The lake depth in meters is calculated as follows during the course of a month: First, the whole lake area in km^2 for a time step is calculated from the lake stage in meters as (Shih, 1980):

$$\text{Area} = 1067 \cdot \log_e [\text{stage} + 0.105] \quad (13.10-4)$$

The difference in lake area between the full lake area (1804 km^2) and the area given by the above equation is assigned to the five lake boxes as follows:

The entire areal difference when less than 224 km^2 is assigned to the macrophyte area of Lake Okeechobee. In other words the north lake, mud zone, sand zone, and South Bay lake areas are constant when the total lake area $\geq 1580 \text{ km}^2$ ($1804 - 224$).

Lake area differences greater than 224 km² are assigned equally to all five lake boxes based on the ratio of the lake area difference / 1580 km². This ratio is never allowed to go below 0.20.

13.10.12 Conservation of Mass

The global continuity of each phosphorus component in the lake model must be considered. The model computes the global continuity of SRP, DOP, GRN, BLU, DIA, PIP, ORG, and ZOO phosphorus components.

13.11 Calibration and Verification of LOP0D Model

13.11.1 Whole-Lake Results

The eight measured Lake Okeechobee stations that were discussed in Chapter 5 were used to calibrate and verify the LOP0D model for the period 1979-1988. Model LOP0D predicts the eight phosphorus components that together equal total phosphorus (TP) as discussed in Chapter 2 of this report.

Large sources of uncertainty in calibrating the box model of Lake Okeechobee include the spatial variation in TP at any time and imprecisions in TP measurements. The large-scale box model LOP0D uses a single phosphorus species concentration to represent the spatially variable phosphorus concentrations. The measured TP concentrations used in calibrating the model are subject to uncertainty in measurement and errors in matching measured species and modeled components of phosphorus.

The first step in the model calibration was the simulation of the lake stage using measured precipitation, estimated evaporation, and measured lake tributary inflows and outflows. Additional information on the characteristics of these boundary conditions are discussed in earlier chapters of this report. The measured and predicted lake stages using monthly time steps are shown in Figure 13-11. The match is very good, signifying that the basic hydrologic boundary conditions of Lake Okeechobee are correctly defined for the model. A key calibration parameter, the pan evaporation coefficient, required a value of 0.965 to match the predicted and measured lake stages (Figure 13-12). A value of 0.865 was used by Shih (1980) in a simulation of the lake stage of Lake Okeechobee during the 1960s and 1970s. The larger pan coefficient may be due to a larger evapotranspiration loss in the 1980s from the increased littoral zone surface area.

The second step in the process of model calibration is comparison of measured and predicted volume-weighted-average TP and SRP concentrations for the whole lake. These were prepared using the QuattroPro spreadsheet file OUTPUT.WQ1, supplied to the South Florida Water Management District in conjunction with this final report, which prepares volume-weighted average concentrations based on the LOP3D predictions and on the SFWMD eight-station measurements. Weights are

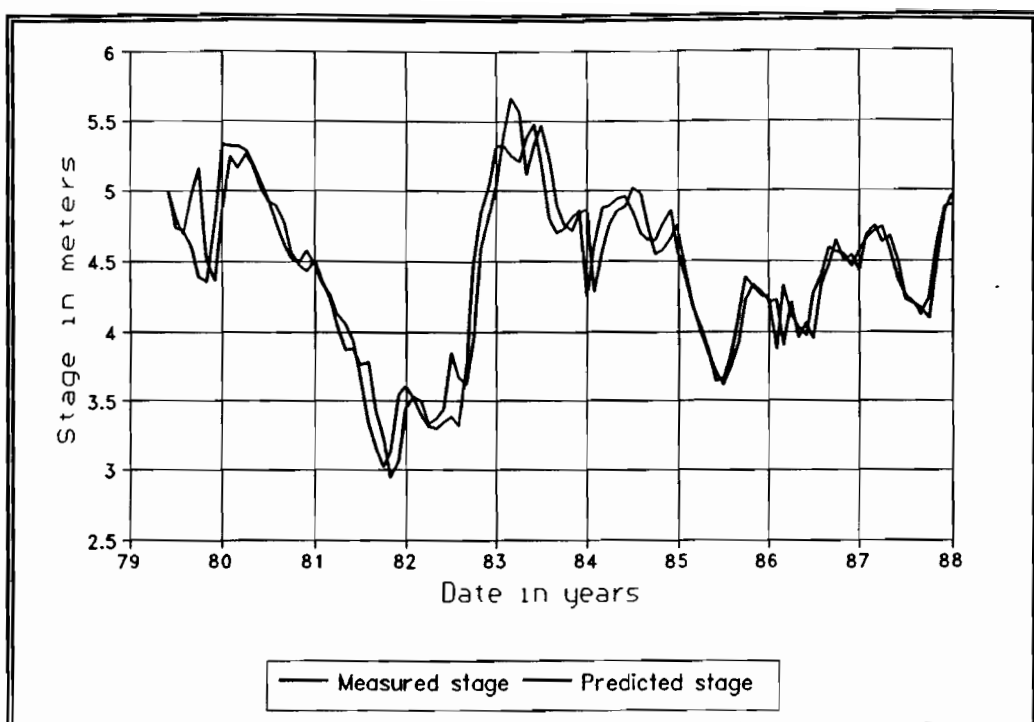


Figure 13-11 Predicted and measured stages for 1979-1988.

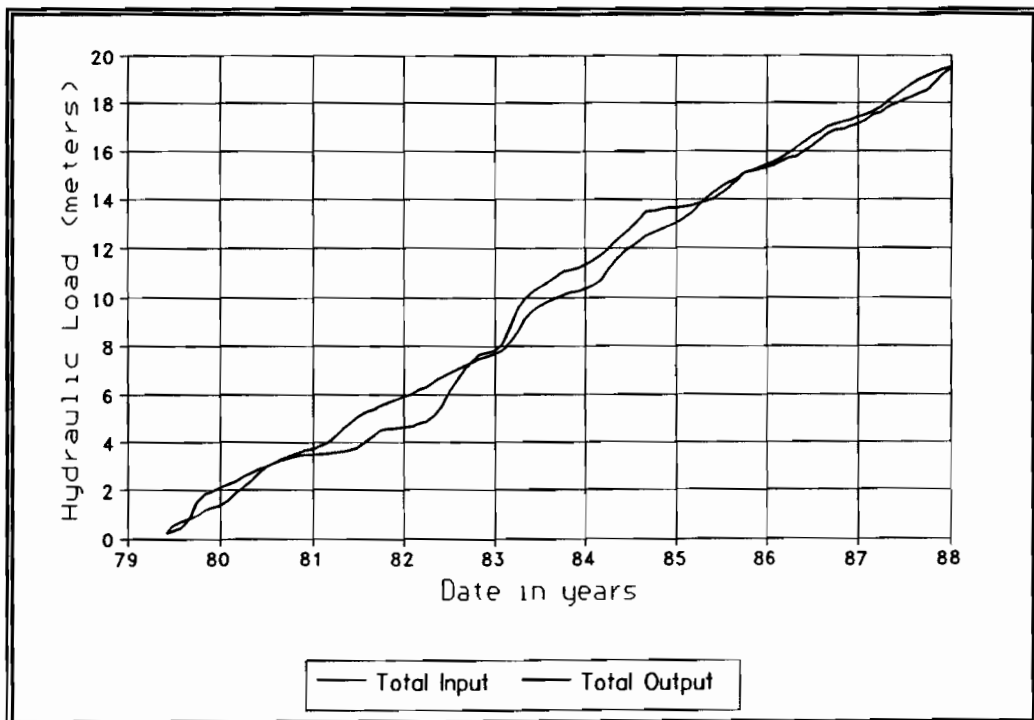


Figure 13-12 Calibrated pan evaporation coefficient of 0.965 balances the total water inflows and outflows.

given in Table 13-10 and are based on the areas and average depths of the lake regions (Carey and Huber, 1990). The comparison for the simulation period of 1979 - 1988 is shown for TP in Figure 13-13 and for SRP in Figure 13-14. (The time series of measured values for each measurement station are also shown in Appendix D of this report.) The simulation is driven by the phosphorus loadings shown in Figure 13-5 along with wind and other forcing functions described earlier.

Total phosphorus concentrations predicted by LOP0D (Figure 13-13) follow the highs and lows of the measured values marginally well. (However, the statistical comparison is good: see Section 13.12). The over-prediction in 1982 is vexing, and the writers have been unable to avoid it after having made many reasonable adjustments to parameters. This period of 1982 corresponds to a very low lake stage, when the model is especially sensitive to wind shear. The model typically predicts high algal and DOP concentrations. Some natural processes that are not included in the model are evidently able to reduce both TP and SRP in the lake during the unusual time period. Without arbitrary, time-specific parameter adjustments, the model cannot reproduce this condition well; fortunately, the remainder of the measured time series of both TP and SRP are reasonably well mimicked.

Predicted TP values for 1979-1982 are slightly higher than predicted values for 1983-1988, consistent with the measurements at stations L003-L008, as shown in Figure 13-13. That is, the ratio of TP values in time period 1979-82 to values from 1972-1979 is higher than the similar ratio for 1983-1988:1972-79 for all stations but L001 and L002 which are influenced by lower loadings from the Kissimmee River and other north lake inflows during the 1983-88 time period. (Additional statistical comparisons may be found in Section 13.12.)

Predicted SRP concentrations agree better with measured values for the lake, as shown in Figure 13-14. Annual cycles are followed reasonably well, with the exception of 1982, for which the model over-predicts, in response to the similar over-prediction of TP for those time periods. The SRP prediction is better because it responds more directly to inflows to the lake, as indicated by Carey and Huber (1990). These authors also indicated a response of TP to wind, on the basis of time series analysis, that relates to the problems of TP prediction discussed in the previous paragraph. (Additional statistical comparisons may be found in Section 13.12.)

13.11.2 Individual Box Results

In addition to the whole-lake TP and SRP comparisons, Figures 13-15 - 13-22 show measured and predicted TP and SRP time series for the four boxes of the lake for which individual stations can be used for comparison (all except the littoral or macrophyte zone). Note: in these figures, the solid squares indicate predicted phosphorus, and the plus signs indicate measured phosphorus, as in Figures 13-13 and 13-14. The comments made above for the whole lake apply reasonably well to the comparison in the four zones as well, e.g., over-prediction in 1982, under-prediction in 1986, and for the same reasons. Measured sand zone SRP values (Figure 13-20) are often at a threshold level that the model seldom achieves, although there are distinct peaks in measured as well as predicted sand zone SRP.

Table 13-10 Weights used for volume weighting

Lake Segment	Volume Weight	Lake Segment	Volume Weight
North Lake	0.315	L001	0.178
Mud Zone	0.258	L002	0.102
Sandy Zone	0.125	L003	0.076
Macrophyte Zone	0.166	L004	0.216
South Bay	0.136	L005	0.084
	-----	L006	0.203
	$\Sigma 1.000$	L007	0.072
		L008	0.069

			$\Sigma 1.000$

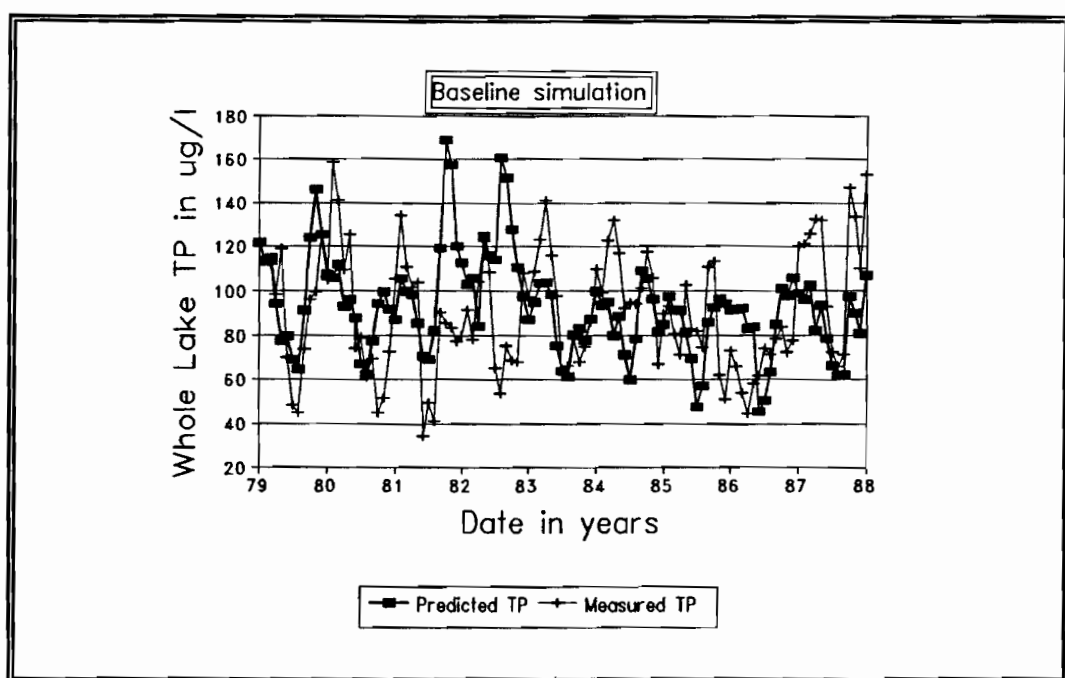


Figure 13-13 Mean whole-lake TP in Lake Okeechobee.

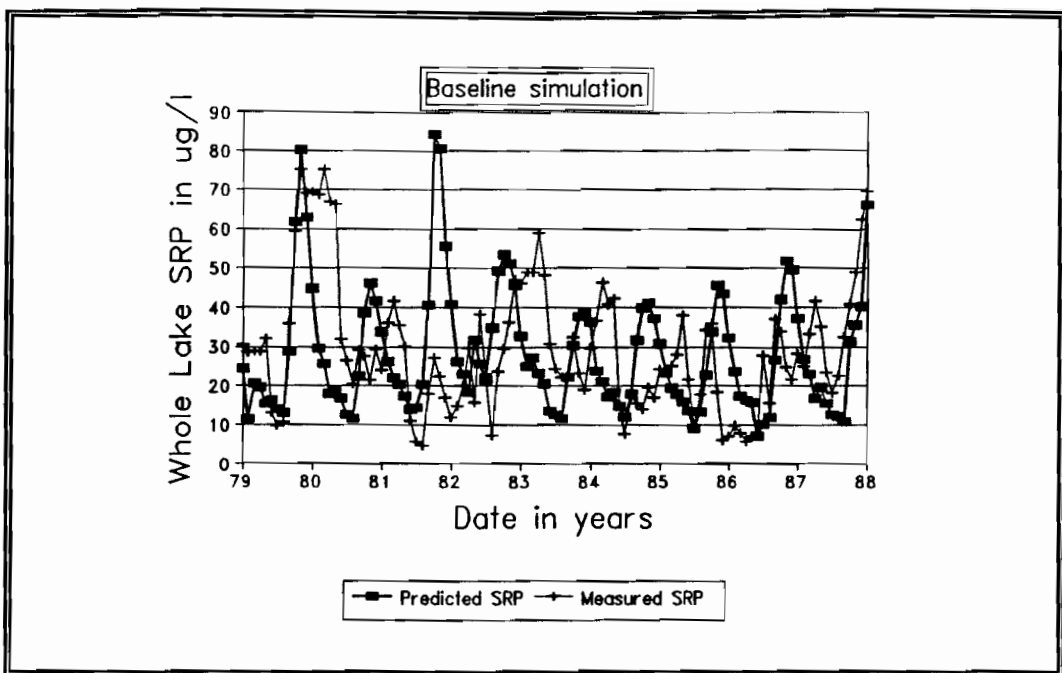


Figure 13-14 Mean whole-lake SRP in Lake Okeechobee.

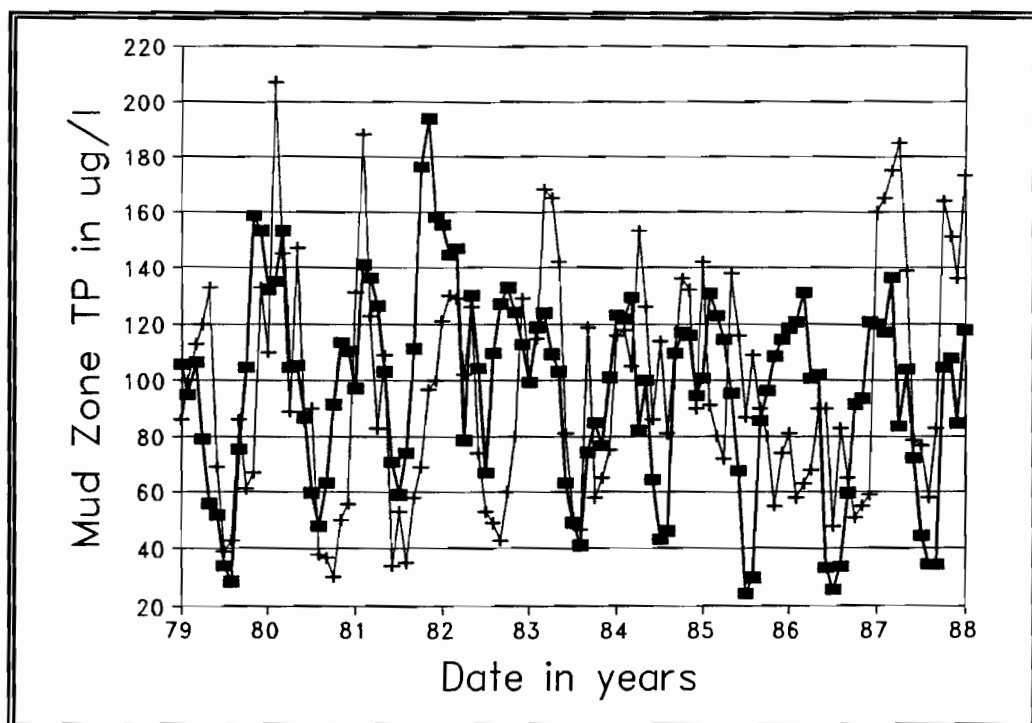


Figure 13-15 Mud zone total phosphorus in Lake Okeechobee.

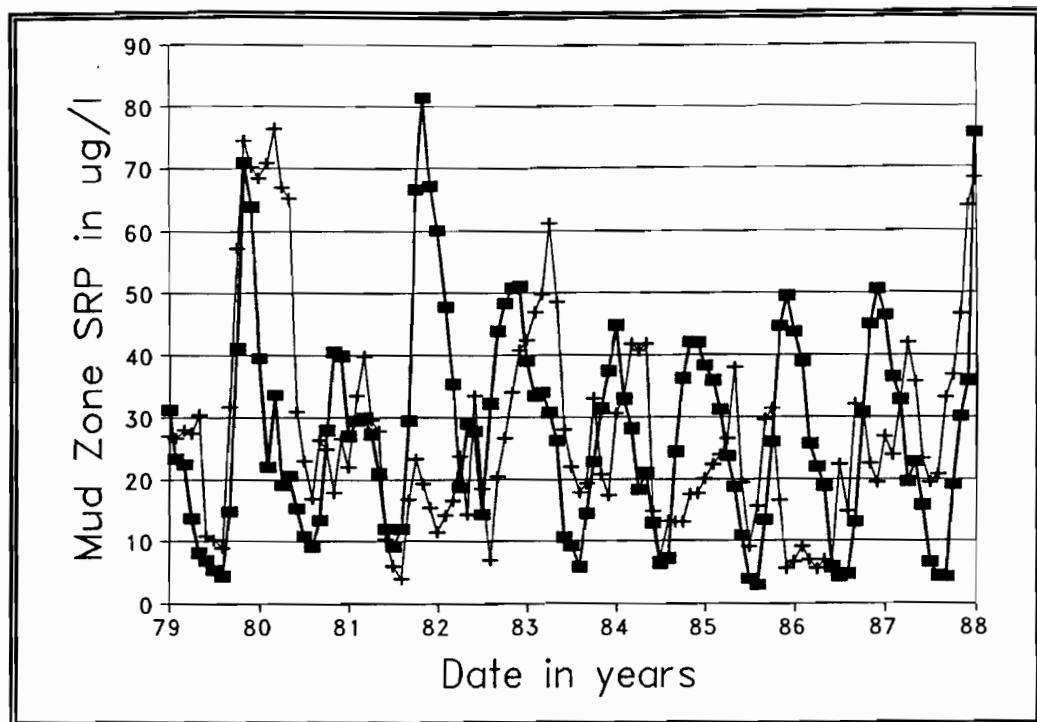


Figure 13-16 Mud zone SRP in Lake Okeechobee.

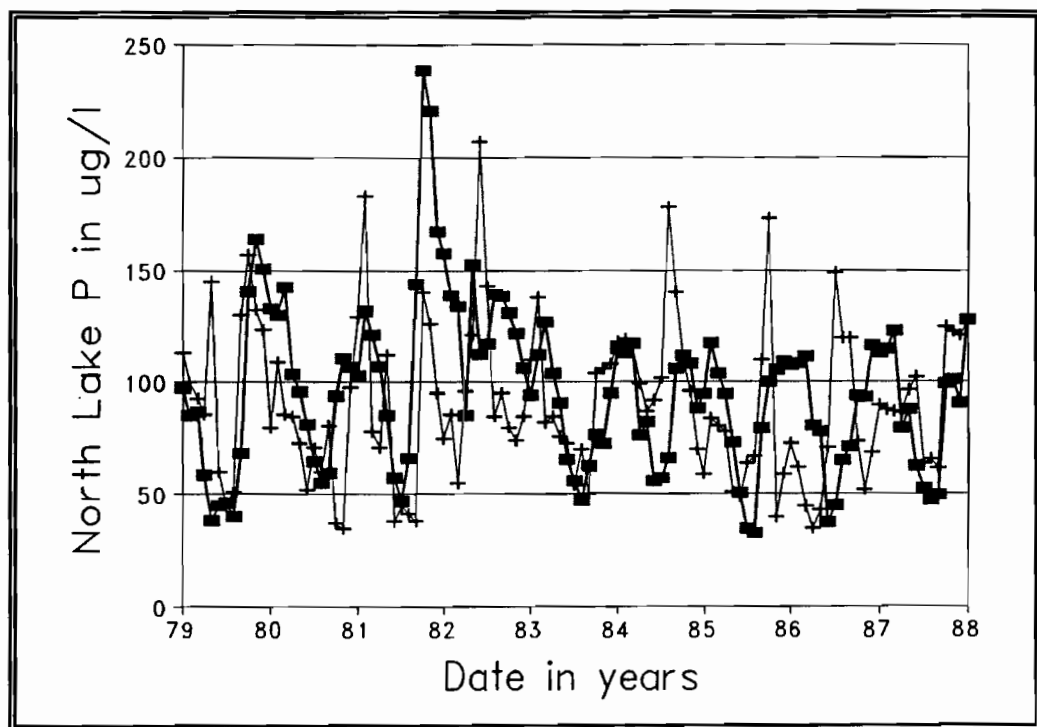


Figure 13-17 North lake total phosphorus in Lake Okeechobee.

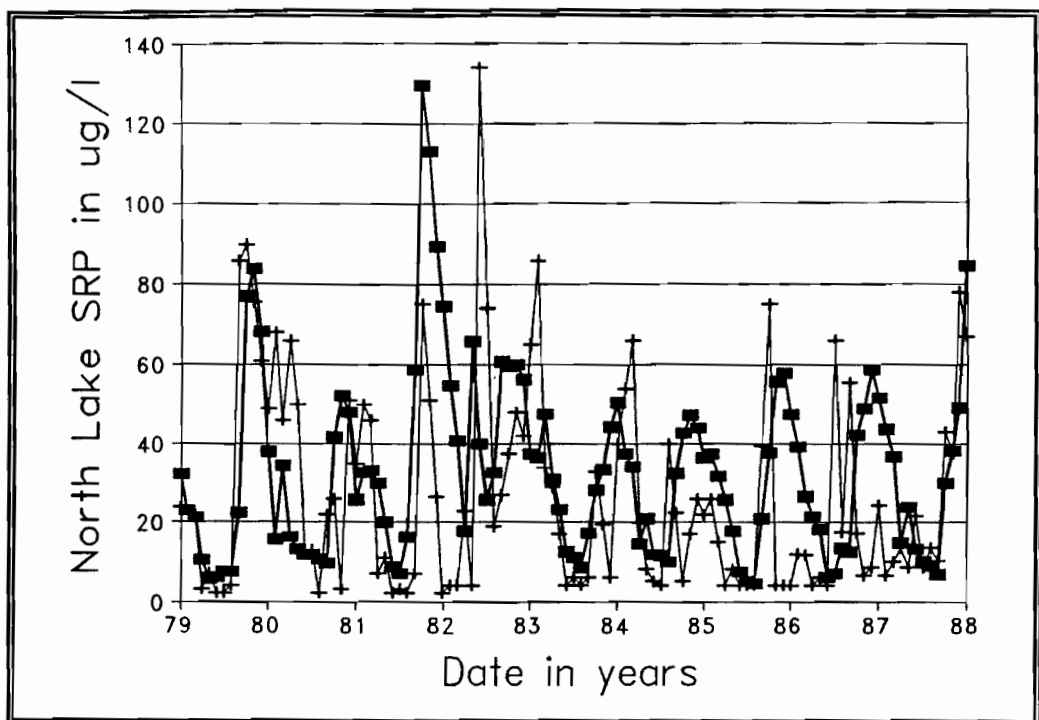


Figure 13-18 North lake SRP in Lake Okeechobee.

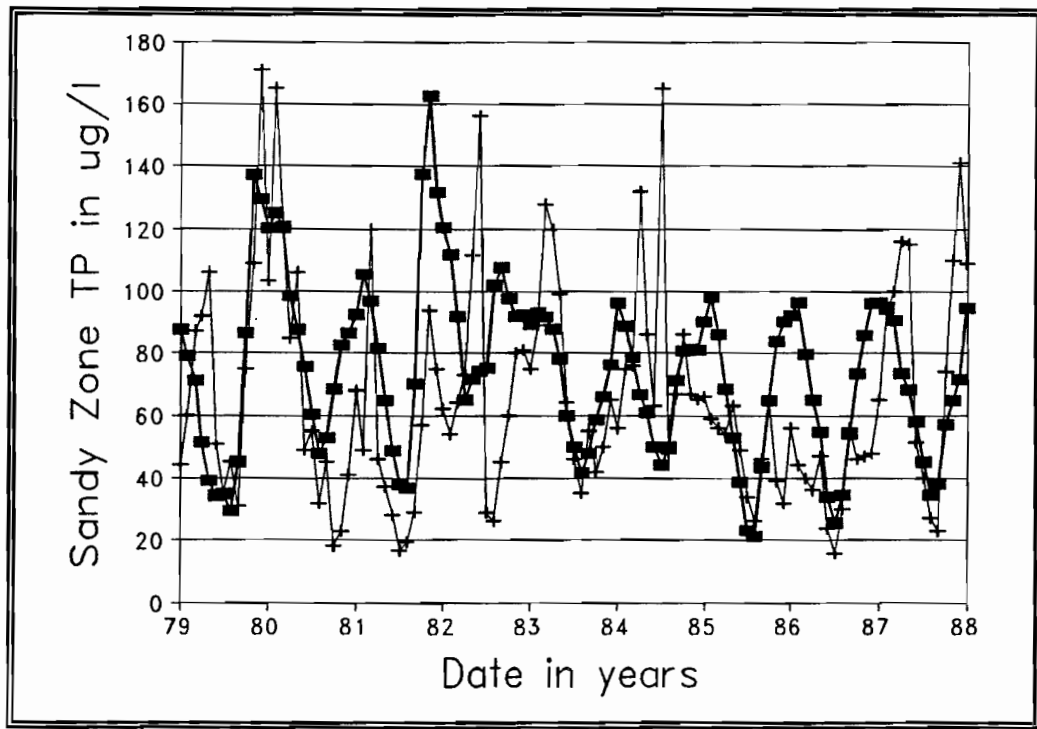


Figure 13-19 Sand zone total phosphorus in Lake Okeechobee.

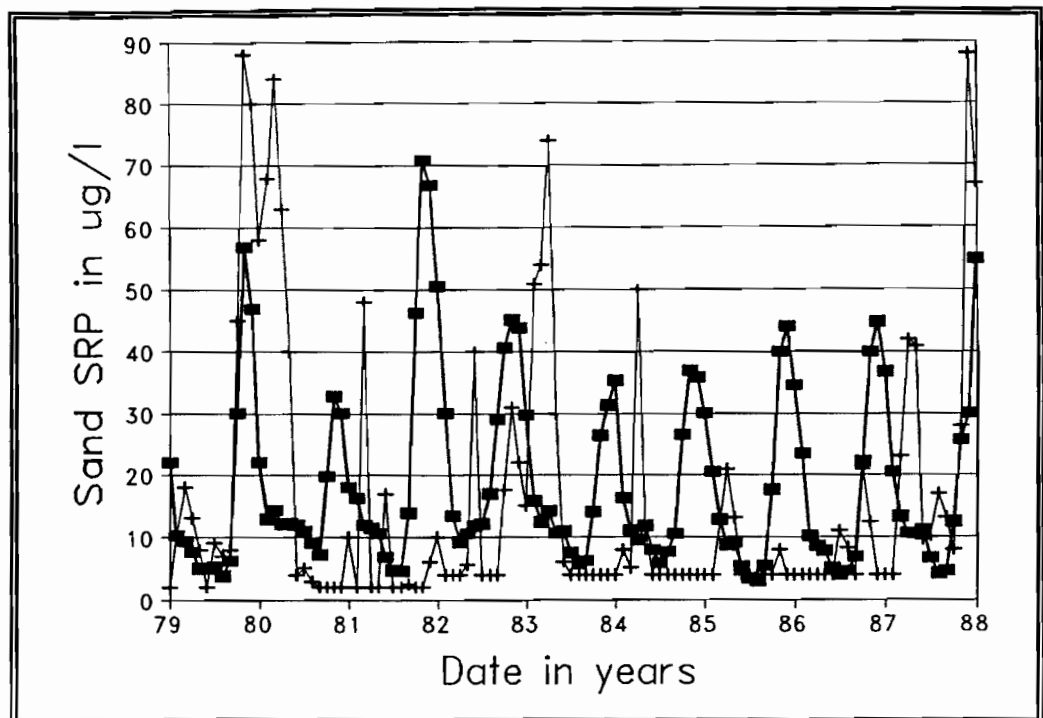


Figure 13-20 Sand zone SRP in Lake Okeechobee.

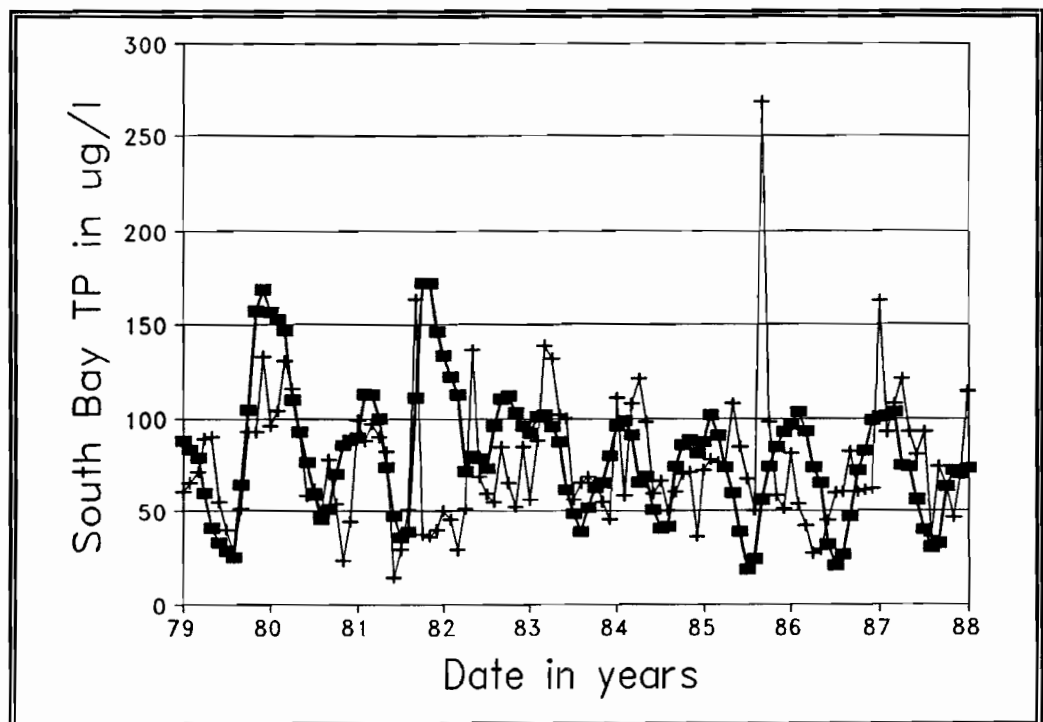


Figure 13-21 South Bay total phosphorus in Lake Okeechobee.

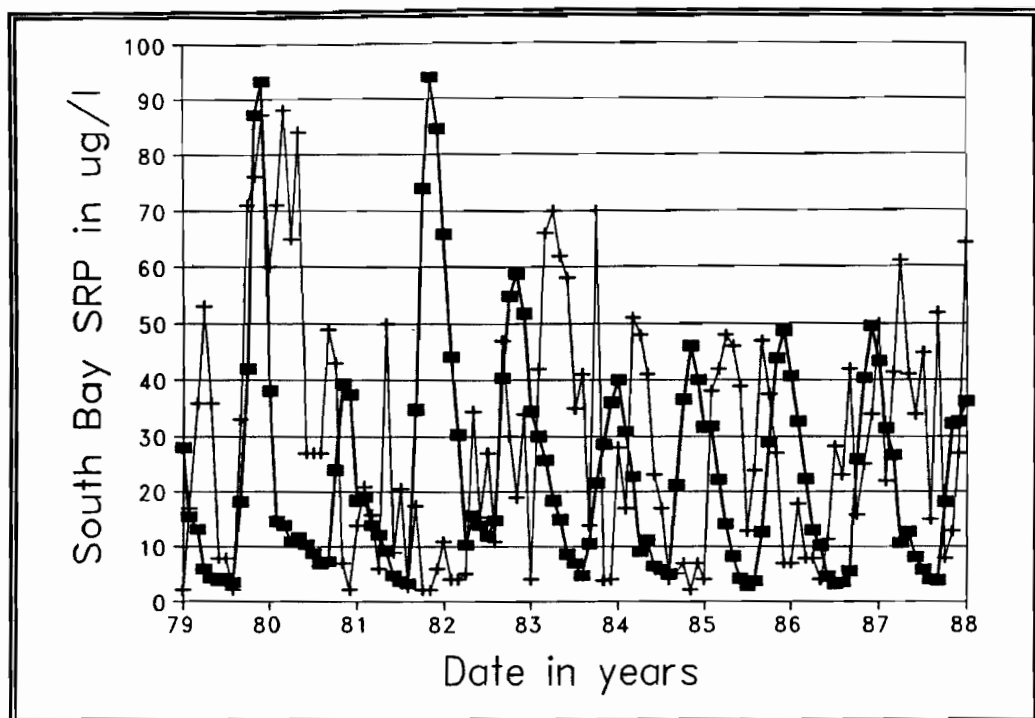


Figure 13-22 South Bay SRP in Lake Okeechobee.

Subsequent sections include further discussion on model calibration, phosphorus fluxes along various pathways, and figures containing concentrations and fluxes for each of the five lake "boxes," averaged over the simulation period. In Section 13.12, comparisons are made for various loading scenarios. Finally, complete output of average concentrations and fluxes is provided in Appendix D (for the 100% load scenario).

13.11.3 Output of Miscellaneous Fluxes, Storages, etc.

The LOP0D model provides a multitude of output in the form of sums, averages, etc. of fluxes, stages, storages, etc. The output is in the graphical form of Figure 13-2. That is, each box contains a summary of a flux, etc. for each lake sub-area, with the lower right-hand box containing the summary for the whole lake. There are 102 different summary graphics, as listed in Table 13-11. Because of this large number, this output is provided in Appendix D, but occasional reference will be made to numerical values obtained from that summary.

Table 13-11 List of figures in appendices.

Figure No.	Figure Name
01	Inflow
02	Outflow
03	Evaporation
04	Precipitation
05	Mean box stage
06	Mean box depth
07	SRP mean box concentration
08	DOP mean box concentration
09	GRN mean box concentration
10	BLU mean box concentration
11	DIA mean box concentration
12	ZOO mean box concentration
13	PIP mean box concentration
14	ORG mean box concentration
15	SED mean box concentration
16	TP mean box concentration
17	SRP time integrated burden
18	DOP time integrated burden
19	GRN time integrated burden
20	BLU time integrated burden
21	DIA time integrated burden
22	ZOO time integrated burden
23	PIP time integrated burden
24	ORG time integrated burden
25	SED time integrated burden
26	SRP remineralization from DOP
27	GRN uptake of SRP
28	GRN respiration to SRP
29	GRN death to DOP
30	BLU uptake of SRP
31	BLU respiration to SRP
32	BLU death to DOP
33	DIA uptake of SRP
34	DIA respiration to SRP
35	DIA death to DOP
36	ZOO uptake of GRN
37	ZOO uptake of BLU
38	ZOO respiration to SRP
39	ZOO death to DOP
40	Desorption. PIP to SRP.
41	Adsorption. SRP to PIP.
42	Mean GRN uptake rate
43	Mean GRN respiration rate
44	Mean GRN death rate
45	Mean BLU uptake rate
46	Mean BLU respiration rate
47	Mean BLU death rate
48	Mean DIA uptake rate
49	Mean DIA respiration rate
50	Mean DIA death rate

Table 13-11 List of figures in appendices (continued).

Figure No.	Figure Name
51	Mean ZOO uptake of GRN
53	Mean ZOO uptake of BLU
54	Mean ZOO respiration rate
55	Mean ZOO death rate
56	Green algal settling loss
57	Blue-green settling loss
58	Diatom algal settling loss
59	Total algal settling loss
60	Added SRP loading from rainfall
61	Added DOP loading from rainfall
62	Net diagenetic SRP diffusion
63	Up diagenetic SRP diffusion
64	Down diagenetic SRP diffusion
65	Equilibrium PC (EPC)
66	Days SRP > EPC
67	Days SRP < EPC
68	Diagenetic boundary flux
69	Top SRP concentration
70	Top diagenetic layer
71	Top diagenetic organic P (mg/kg)
72	Mean GRN settling rate (m/day)
73	Mean BLU settling rate (m/day)
74	Organic phosphorus erosion
75	Organic phosphorus deposition
76	Diagenetic SRP sediment advection
77	Inorganic phosphorus erosion
78	Inorganic phosphorus deposition
79	Total SRP interbox mass transfer
80	Total DOP interbox mass transfer
81	Total GRN interbox mass transfer
82	Total BLU interbox mass transfer
83	Total DIA interbox mass transfer
84	Total ZOO interbox mass transfer
85	Total PIP interbox mass transfer
86	Total ORG interbox mass transfer
87	Seiche (advection) SRP mass transfer
88	Seiche (advection) DOP mass transfer
89	Seiche (advection) GRN mass transfer
90	Seiche (advection) BLU mass transfer
91	Seiche (advection) DIA mass transfer
92	Seiche (advection) ZOO mass transfer
93	Seiche (advection) PIP mass transfer
94	Seiche (advection) ORG mass transfer
95	Secchi disc depth
96	KDD - light attenuation coef
97	CAA - sum of absorbing agents
98	KBB - sum of scattering agents
99	Erosion of sediment
100	Deposition to sediment
101	Macrophyte sink of SRP
102	Macrophyte loading of DOP
103*	*Ending lake TP burden

*Found in tabular information at end of output.

13.12 Comparative Analysis: Baseline vs. Simulation with Load Reduction

The LOP0D model was run with a 40 percent, 50 percent and 70 percent load reductions (both SRP and TP), in accordance with desired SFWMD alternative scenarios. A comparison of means and standard deviations is shown in Table 13-12, and predicted TP and SRP time series for the 40 percent and 70 percent reductions are shown in Figures 13-23 to 13-26, respectively, along with the measured (volume-weighted) values for the 1979-88 time period. (A time series plot for the 50 percent reduction is not shown. It essentially falls between the 40 and 70 percent reductions.) In the LOP0D model, for a 40 percent reduction, parameter REDLOW = 0.6, etc. A final option considered is to set a maximum limit on Nubbin Slough total phosphorus of 200 ug/l. Statistics for this option are also included in Table 13-12. [Note, slight differences in means between Table 13-12 and Figures D-7 and D-16 result from the use of a spreadsheet for computation of the Table 13-12 statistics, vs. slightly different computations in the Fortran LOP0D code.]

Table 13-12 Comparison of means and standard deviations for various loadings.
Based on volume-weighted, whole-lake concentrations.
(Values in parentheses are percent of 100% predicted-load means.)

	SRP, ug/l			TP, ug/l		
	Mean	Std.Dev.	CV	Mean	Std.Dev.	CV
Measured, 1979-88	29.5	17.2	0.58	90.2	27.3	0.30
Predicted, 0% reduction	28.4	15.9	0.56	93.3	22.4	0.24
Predicted, 40% reduction	20.9 (74)	11.3	0.54	75.8 (81)	18.6	0.25
Predicted, 50% reduction	19.0 (67)	10.3	0.54	71.4 (77)	18.2	0.25
Predicted, 70% reduction	15.4 (54)	8.7	0.56	62.9 (67)	17.8	0.28
Predicted, 200 ug/l, Nubbin Sl.	26.0 (92)	14.0	0.54	88.4 (95)	21.5	0.24

CV = coefficient of variation = std. dev./mean

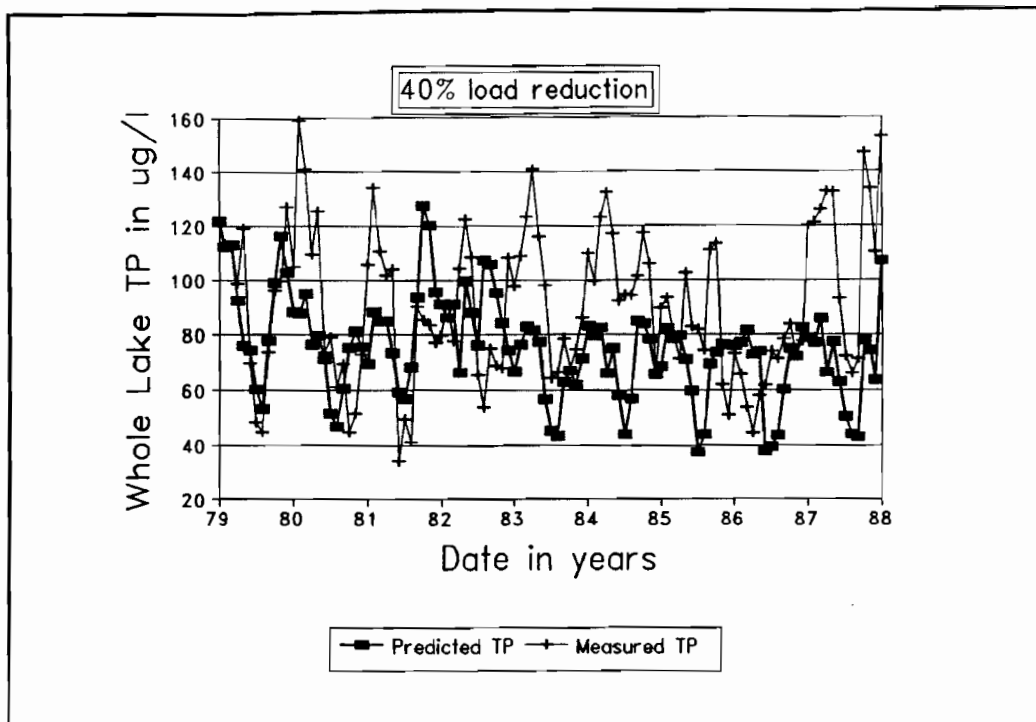


Figure 13-23 Whole-lake TP with 40% load reduction.

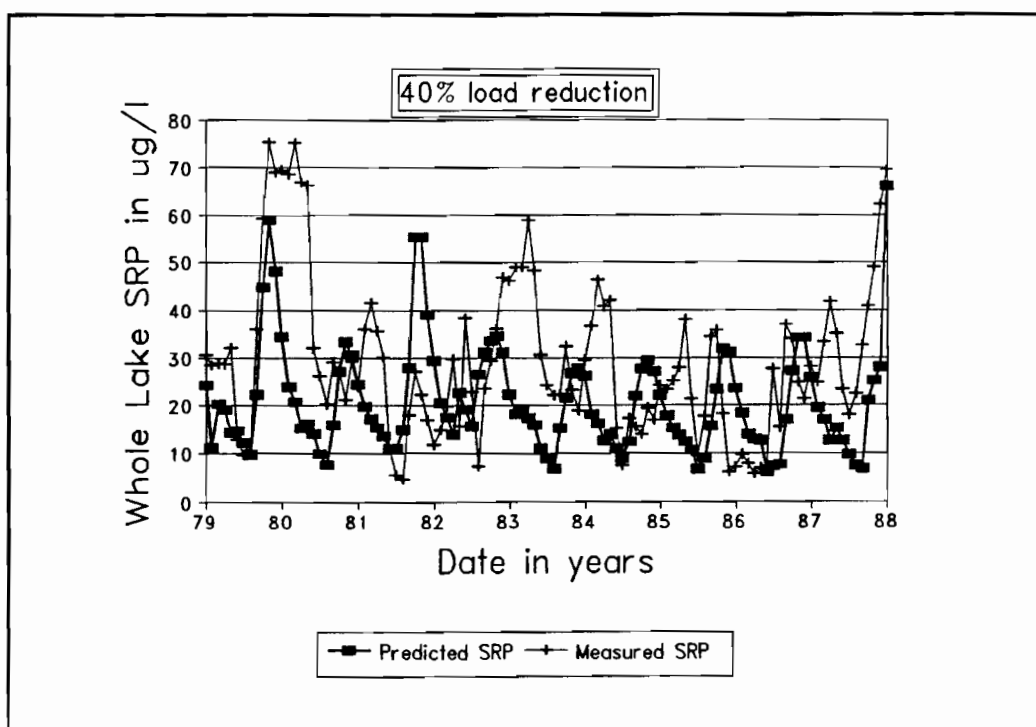


Figure 13-24 Whole-lake SRP with 40% load reduction.

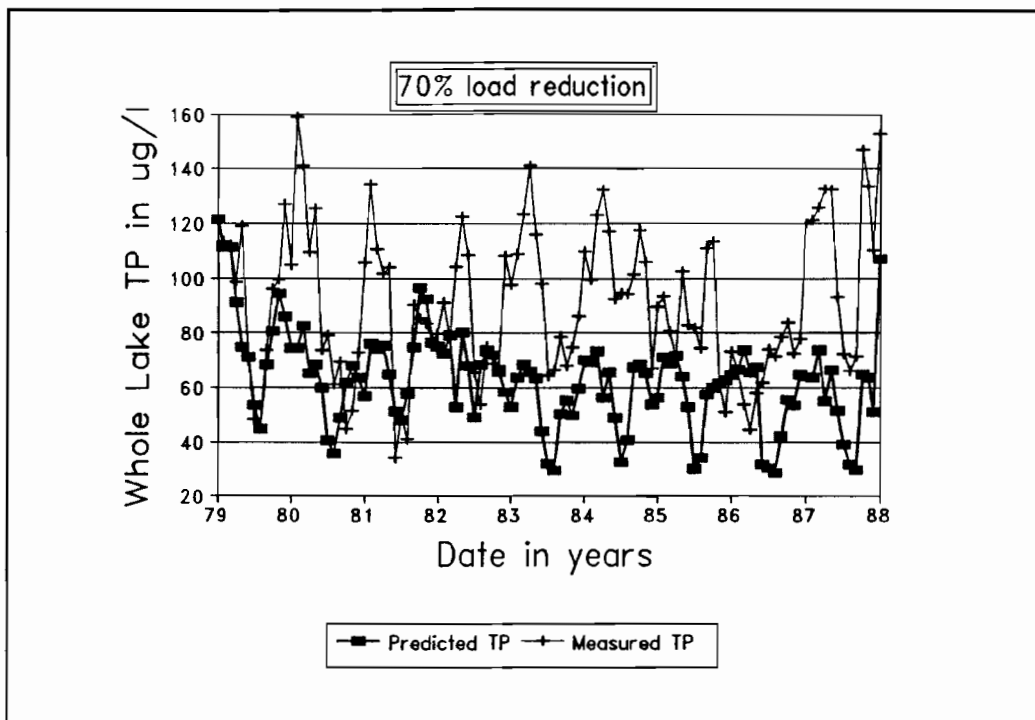


Figure 13-25 Whole-lake TP with 70% load reduction.

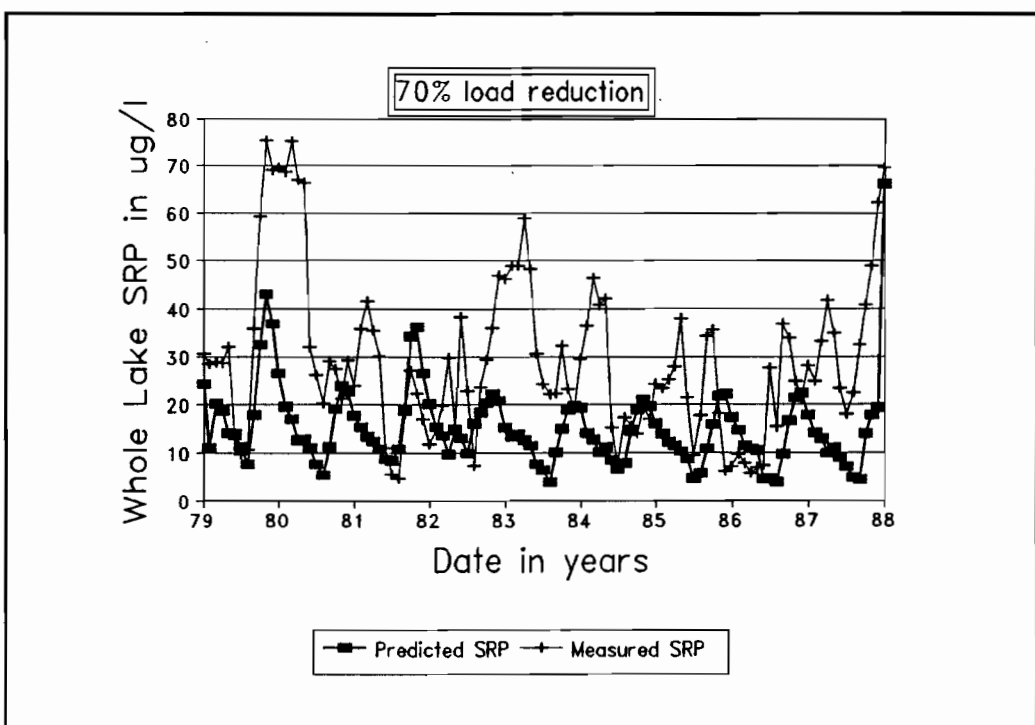


Figure 13-26 Whole-lake SRP with 70% load reduction.

Table 13-12 illustrates that the LOP0D model predicts about as much variation as is evident in measured in-lake concentrations. This reflects favorably on the simulation model because it is often difficult to duplicate the natural variability of a natural time series. Both measured and predicted lake concentrations respond to brief transients in the weather, e.g., convective storms, for which it is often difficult to provide data for model input. However, in the variety of temporal input provided to LOP0D, there is apparently enough variation to reflect the variation of monitored phosphorus data.

Time series of the predicted SRP and TP values (Figures 13-23 - 13-26) illustrate that peaks tend to be reduced more than minimum P values in response to the load reductions. This effect is more noticeable for SRP which is stabilized somewhat by the sorption exchange with sediment. This also accounts for the somewhat greater reduction in variance for SRP than for TP.

The effect of load reduction on in-lake concentrations is approximately linear but not on a one to one basis with the load reductions (Table 13-12). For TP, loads of 60 percent, 50 percent and 30 percent of baseline values result in TP values 81 percent, 77 percent and 67 percent of baseline. With a 70 percent load reduction, mean TP values are 62.9 ug/l, still above a value of 50 ug/l (a concentration of interest to the SFWMD because it typifies TP values in the early 1970s), but decreasing. This cannot be called a definitive prediction due to anticipated modeling improvements, but it does illustrate that reductions in loads will produce reductions in in-lake TP concentrations. For SRP, loads of 60 percent, 50 percent and 30 percent of baseline values result in SRP values 74 percent, 67 percent and 54 percent of baseline. The SRP is stabilized somewhat by sediment sorption-desorption. Reduction of influent concentration from Nubbin Slough to a maximum TP concentration of 200 ug/l results in a minor load reduction to the north lake and has much less of an effect than does a 40 percent total load reduction. The time series plots are similar to the 100 percent-load plots, and are not shown.

Regarding timing of changes, the discussion of residence time in Section 13.10.8 indicates a time period on the order of ten years for a complete response to changing loading conditions, based on a factor of two to five times the residence time. For example, for an exponential process, a 90 percent change requires 2.3 times the residence time (Chapra and Reckhow, 1983). The LOP0D model responds more rapidly to changes, on the order of a year or less, because of the greater importance of reaction rates in the lake as opposed to a pure "flushing" mechanism based on water exchange. As discussed previously, the inverse of first-order reaction rate coefficients is a time scale for changes. Thus, for time scales on the order of weeks, kinetic changes may result in less than a year. Thus, the time required for the response of Lake Okeechobee to changes in external loads is probably between one and ten years -- a broad range. This can be narrowed with improvements to LOP0D that will permit the model to be run with loading rates that are reduced as a function of time.

13.13 General Discussion of Baseline Results

13.13.1 Comparisons of Modeled Fluxes, Rates, Timing

Each LOP0D simulation produces voluminous information in addition to the time series plots discussed in the previous two sections. The many fluxes, storages, etc. are summarized for the total simulation in figures of the type of Figure 13-2 for the quantities listed in Table 13-11. These are shown in Appendix D, and some results are discussed below.

The seasonal distribution of algae (in its three modeled forms) is shown in Figure 13-27. Blue-green algae dominate during the period December-March during periods of highest erosion/deposition (cycling of bottom material), as shown in Figure 13-28. Green algae lag and dominate for most of the period April-October, with zooplankton highest in March and decreasing until January. Thus, the green algae appear to prevail during periods of lower winds (and erosion/deposition), while the blue-green with their lower settling rate prevail during periods of greater turbulence. On an annual basis, Figure 13-27 indicates that blue-green have a somewhat higher concentration than green, and both are 4-5 times higher than zooplankton.

The various production-loss mechanisms for algae are illustrated in Figure 13-29. Clearly, the dominant flux for green and blue-green algae is growth due to the presence (and uptake) of SRP. The higher the SRP concentration, the greater the growth of algae. Especially for green, the SRP uptake pathway is more than a factor of two greater than any other. Note that continuity is maintained for the various production-loss mechanisms. That is, the production of green is approximately 33 mg/m² for the 9-year simulation. This equals the sum of approximately 12 (release of SRP), 8 (release of DOP), 10 (ZOO uptake), and 3 (settling).

The parallel pathways for SRP are illustrated in Figure 13-30. Again, uptake by green has the largest magnitude, followed by remineralization of DOP. The relative magnitudes of the pathways of blue-green algae and associated SRP are similar to those for green (Figures 13-29 and 13-30).

Not surprisingly, the highest rate of algal settling occurs during the summer months of least wind shear and erosion-deposition (Figure 13-31). The lower settling velocity of blue-green can clearly be inferred from this figure. Rate coefficients used for algae in the simulation are compared in Figure 13-32. The largest magnitude is the zooplankton uptake rate (sum of values for green, blue-green and diatoms).

Particulate inorganic phosphorus (PIP) has the fluxes shown in Figure 13-33. Deposition of PIP (and a small amount of desorption to SRP) is balanced first by adsorption from SRP and, of a lesser magnitude, erosion from the sediment layer. The greatest amount of adsorption of PIP occurs during the December-April time period of greatest erosion-deposition, as shown in Figure 13-34.

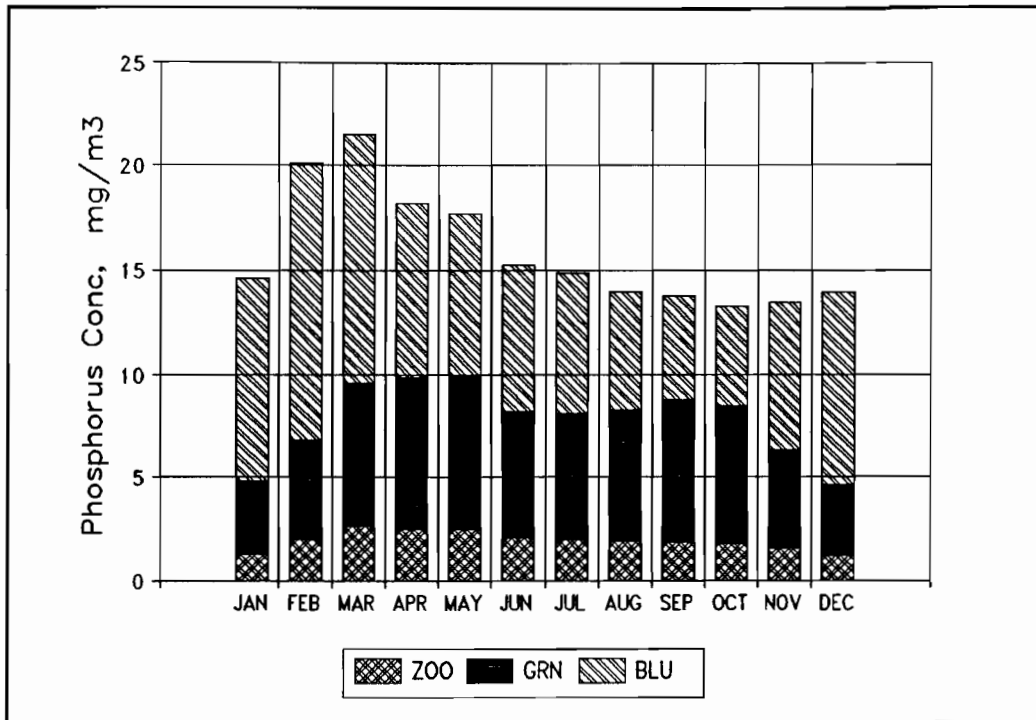


Figure 13-27 Algal concentrations in Lake Okeechobee.

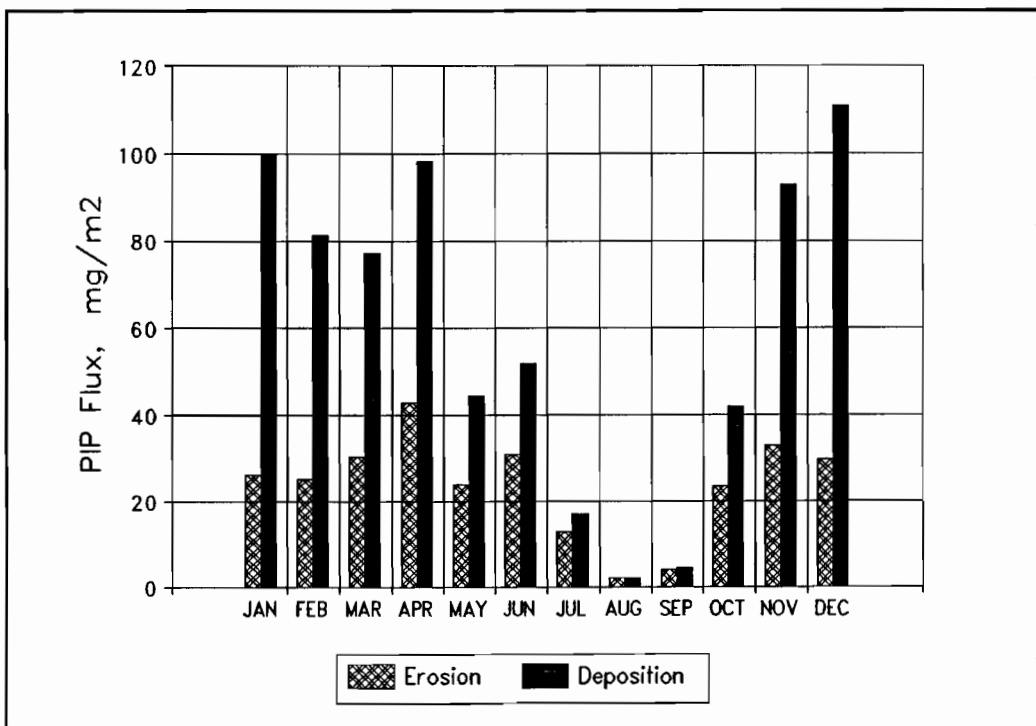


Figure 13-28 Deposition/erosion in Lake Okeechobee.

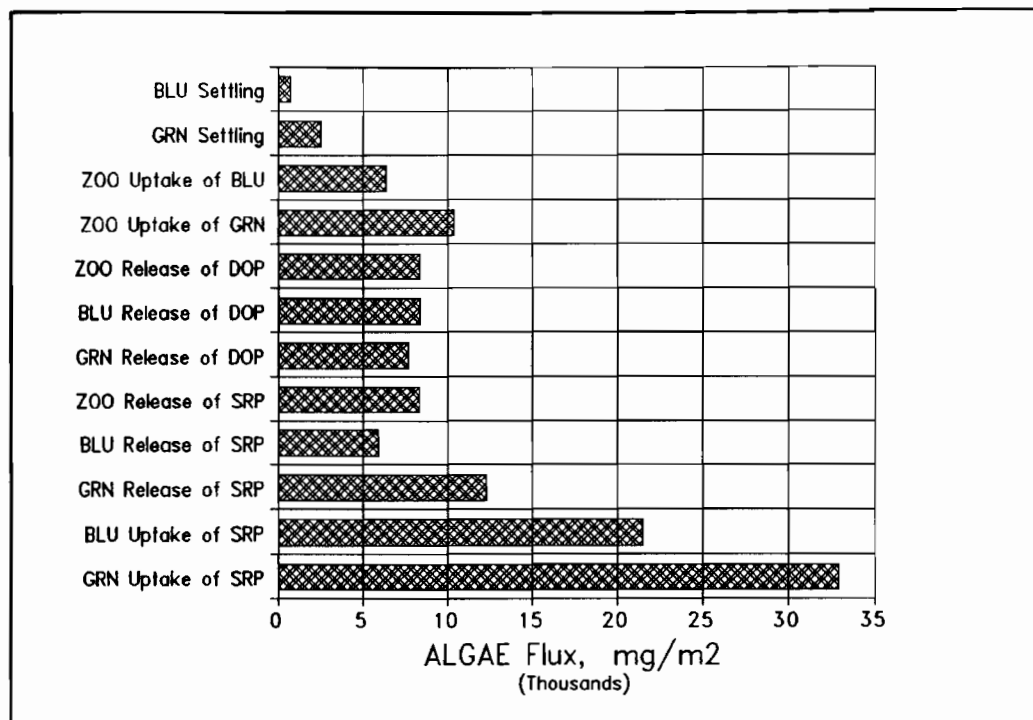


Figure 13-29 Algal pathways in Lake Okeechobee.

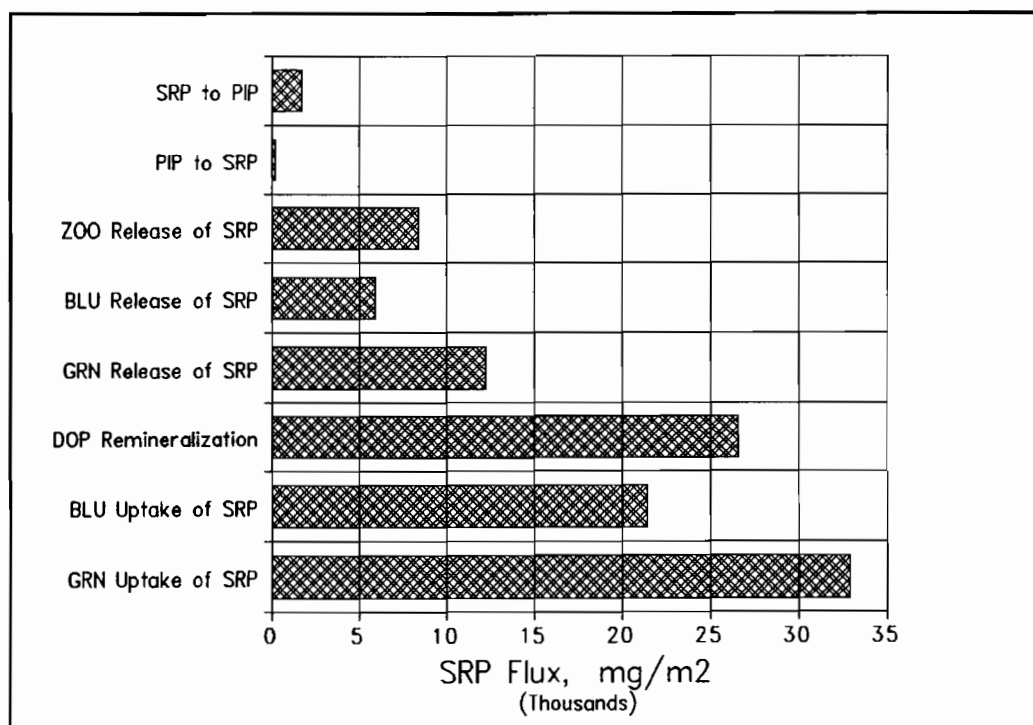


Figure 13-30 SRP pathways in Lake Okeechobee.

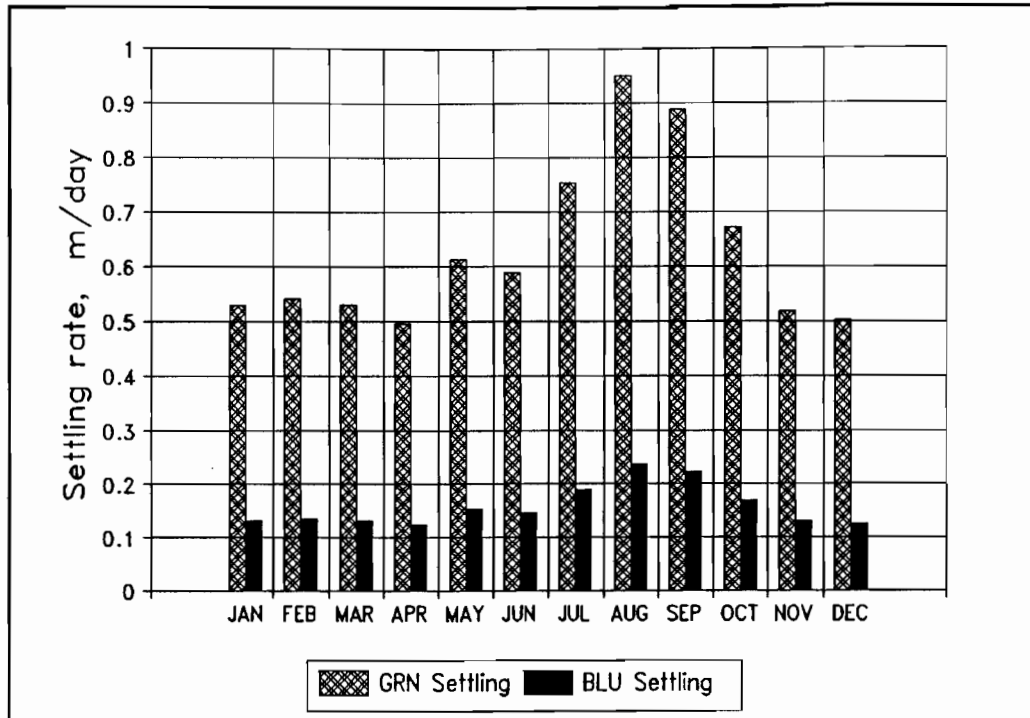


Figure 13-31 Algal settling rates in Lake Okeechobee.

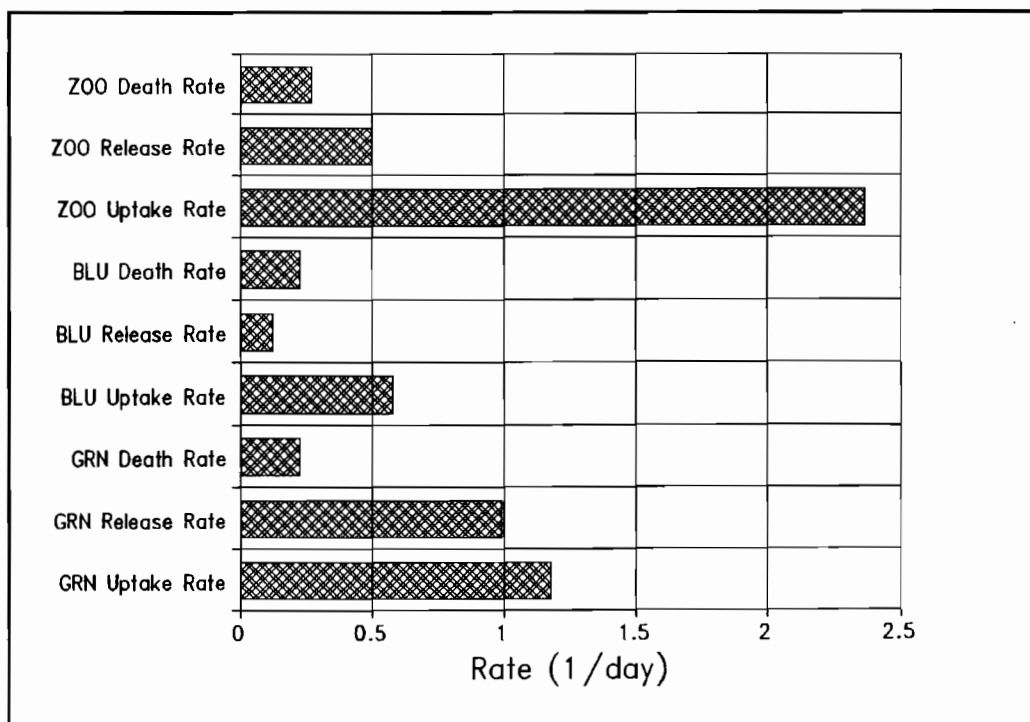


Figure 13-32 Algal coefficients in Lake Okeechobee.

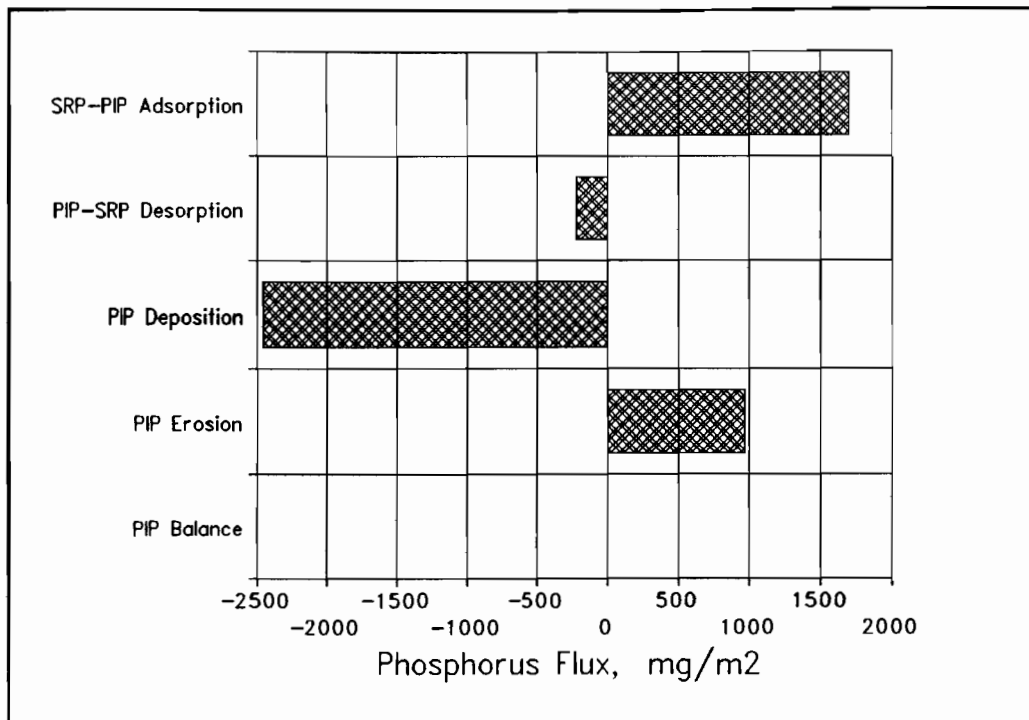


Figure 13-33 PIP balance in Lake Okeechobee.

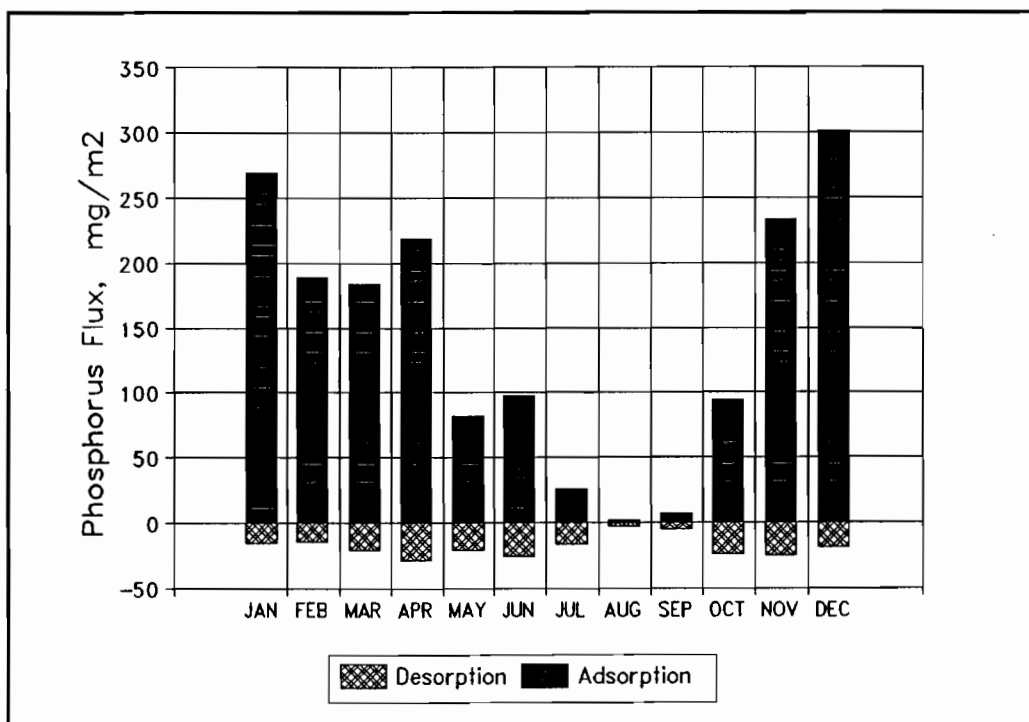


Figure 13-34 Adsorption/desorption in Lake Okeechobee.

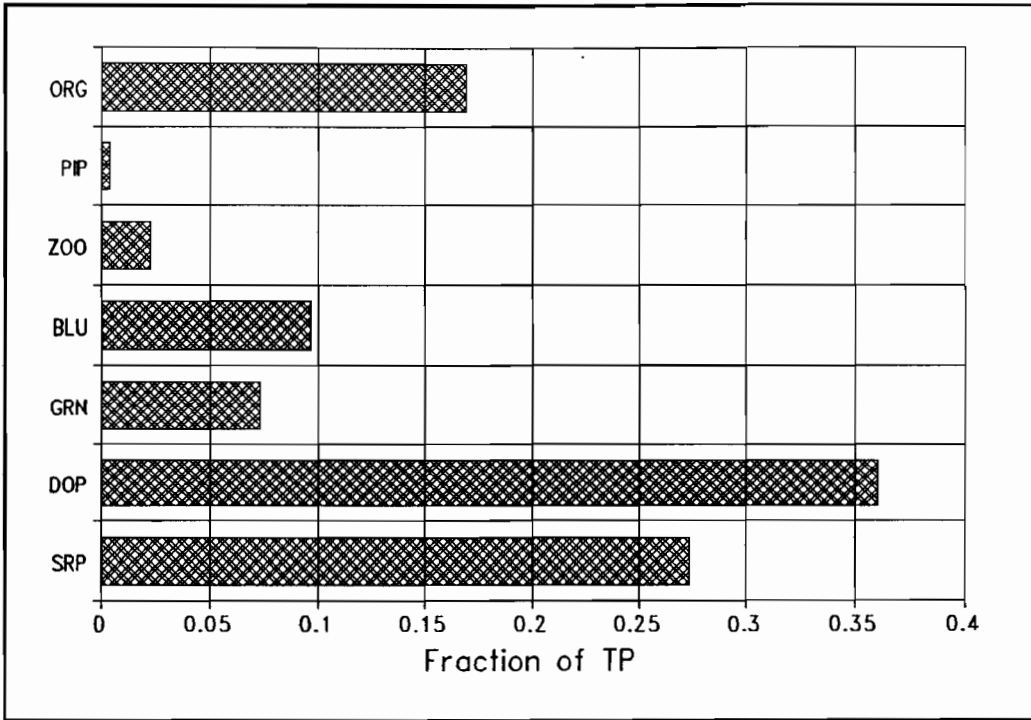


Figure 13-35 Phosphorus components in Lake Okeechobee.

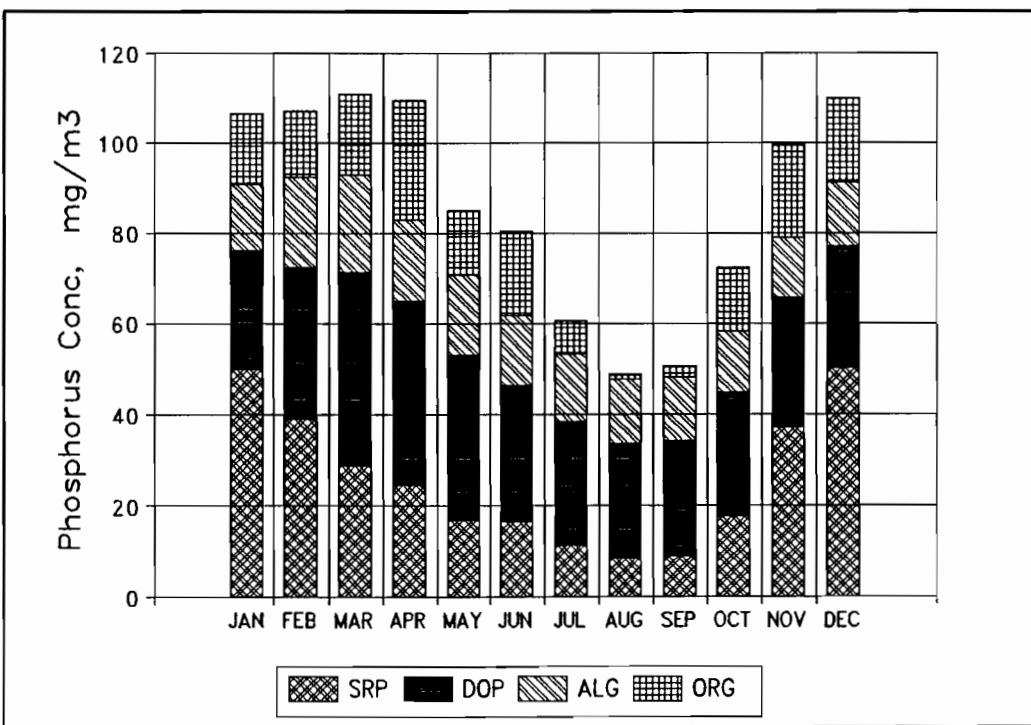


Figure 13-36 Monthly phosphorus in Lake Okeechobee.

In what form and at what time are the greatest phosphorus concentrations in Lake Okeechobee? These questions are addressed in Figures 13-35 and 13-36, respectively. The greatest quantity (as a fraction of TP) of phosphorus is in the form of dissolved organic phosphorus (DOP), followed by SRP. (These fractions are an average for the total simulation period.) The smallest fraction is that associated with PIP. SRP concentrations are greatest during the December-March time period of highest erosion-deposition (and hence, desorption and diagenetic flux). DOP concentrations remain relatively constant throughout the year, while organic concentrations mimic SRP timing. Algal concentrations tend to approach a maximum in early spring, corresponding to the timing shown in Figure 13-27. Interestingly, phosphorus concentrations are lowest in the summer months when rainfall increases in the region, indicating that higher seasonal inflows to the lake apparently do not necessarily raise total phosphorus (the sum of individual "bars" in Figure 13-36) levels. Rather, TP (and SRP) are highest following winter winds.

13.13.2 Comparison of Flux Magnitudes

The following comments are based on magnitudes for various phosphorus pathways, as indicated in the model output summarized in the "boxes" of Appendix D. (See Table 13-11 for key to figure numbers.) The normalized fluxes are totals for the 9-year simulation.

The diffusion of SRP from the bottom sediments to the pelagic region of the lake was 528 mg/m^2 for the baseline simulation (Figure D-63). This was overwhelmed by the total tributary TP loading of $3,081 \text{ mg/m}^2$ and precipitation TP load of 432 mg/m^2 (Table near end of Appendix D and values from Figures D-60 and D-61, respectively). The total surface outflow TP loss of 417 mg/m^2 was smaller than the estimated precipitation load.

The transfer of pelagic phosphorus to the bottom sediments was mainly accomplished by the twin loss processes of algal settling (Figure D-59) and PIP deposition to the sediment (Figure D-78). The losses were $1,853 \text{ mg/m}^2$ and $4,413 \text{ mg/m}^2$, respectively, for algal settling and PIP deposition. The total of $6,266 \text{ mg/m}^2$ balanced the main sources of SRP and TP-SRP: diagenetic diffusion (D-63, 528), erosion (D-77, 1,980), tributary loading (Appendix D table, 3,081), and atmospheric loading (D-60 and D-61, 432), which totaled $6,021 \text{ mg/m}^2$.

The loss of PIP to the bottom sediment resulted from the net adsorption of pelagic SRP on suspended sediment particles. Suspended sediment is a slight scavenger of SRP from the water column.

The transfer for phosphorus components between lake boxes was generally from the north lake (NL) box to the South Bay (SB) box (Figures D-79 to D-94). This is consistent with the predominance of major inflows into the north lake zone.

Recalling the conclusions of Canfield and Hoyer (1989) and Carey and Huber (1990) that the concentrations of SRP and TP in Lake Okeechobee are not correlated with external loading, we can see that the low correlation was because of suspended sediment loading, diffusion loading, and algal settling. However, we cannot conclude that the cause of high phosphorus concentrations in Lake Okeechobee are not high external loads. The external loading is driving the lake system. Decreasing the loads will only decrease the lake concentrations of SRP and TP as shown in Section 13.12, but at a slower rate than would occur without the considerable internal loadings.

13.13.3 Sensitivity

The LOP0D model (and its 3-dimensional cousin, LOP3D) are most sensitive to the parameters related to mortality (K_{Gx} and K_{Bx} in this report, RESPIR in the model) and SRP excretion (K_{Gd} and K_{Bd} in this report, RESBAK in the model) of green and blue-green algae. These parameters strongly affect the algal life span and increase of SRP in the water column. The relative quantities of algae can fluctuate depending on these parameter values. Organic settling also significantly influences the balance of phosphorus in the lake.

13.13.4 Further General Discussion

What is the reason for the humped trend in SRP and TP measured data (Figure 5-1)? The trend is also evident in Figure 13-37, in which the ratio of 1983-89 measured SRP and TP to 1972-78 baseline values is greater at most stations than the ratio of 1983-89 values to 1972-78 values. The following factors are relevant.

1. TP and SRP data increased in the early 1980s over the concentration in the 1970s. The trend in concentration since 1984 appears level or decreasing at non-mud stations of Lake Okeechobee.
2. The increase in TP, SRP and TP-SRP concentration is almost the same at all 8 long term monitoring stations. This means that the same mechanism must account for both the increase in SRP and non-SRP phosphorus concentrations.
3. The phosphorus concentration of the organic bottom sediment may have increased in 1980s.
4. Hurricane David occurred in 1979.
5. Regeneration rates are greater than removal rates for phosphorus in tropical lakes (subject to biological control) than for temperate lakes (subject to physical control) (Kilham and Kilham, 1991).

SRP is positively correlated with lake stage in Lake Okeechobee (Chapter 9) as are tropical African lakes (Kilham and Kilham, 1991). The source of the additional SRP at high lake stages may be:

1. The greater fetch length may increase the mixing of bottom sediments.
2. Particulate phosphorus from the macrophyte area may be transported to the pelagic region of the lake.
3. Sediments
4. Littoral zone plants or sediments.

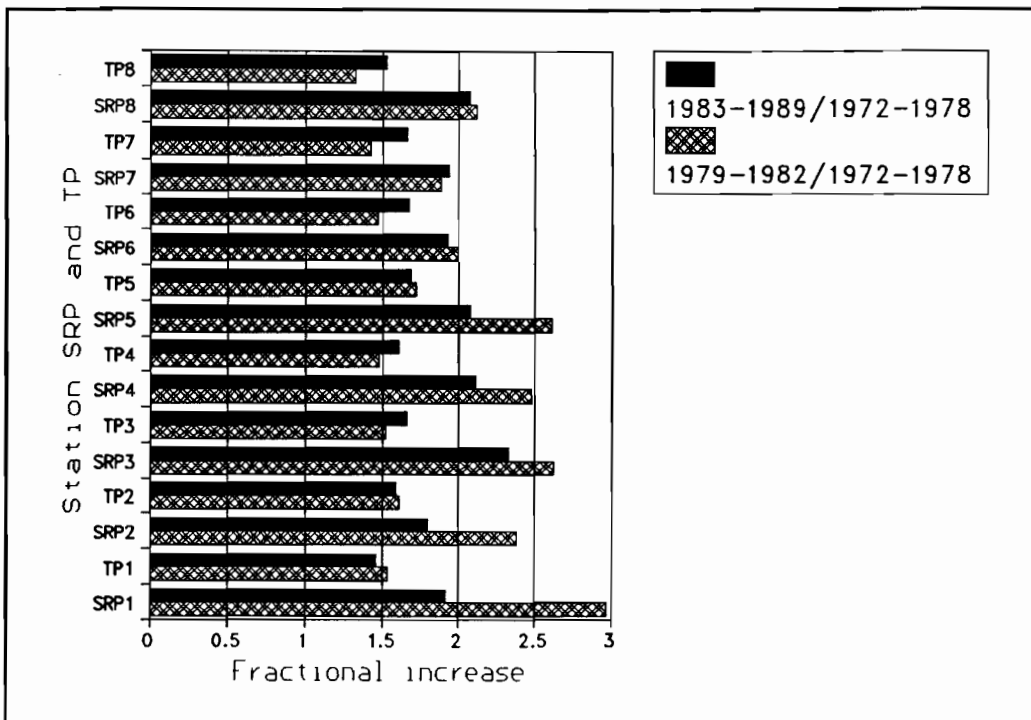


Figure 13-37 Fractional increases in mean station SRP and TP concentrations for the years 1979-1982 and 1983-1988 over the baseline concentrations of 1972-1978.

13.14 Summary

The Lake Okeechobee phosphorus 0-dimensional model (LOP0D) includes transport by diffusive and advective mechanisms, loadings (and export) by inflowing tributaries (and lake outflows) and by rainfall, water-column reactions for seven phosphorus species plus two sediment-related species, diagenetic flux from the sediment, and sediment resuspension-deposition. For application to Lake Okeechobee, five "boxes" were used: north lake, mud zone, sand zone, littoral (macrophyte) zone, and South Bay. The model runs on an approximate quarter-day time step (two daylight steps and two night-time steps) and was used to simulate the period 1979-1988 for which loading data (monitored phosphorus at tributaries) and in-lake concentration data exist.

Volume-weighted predicted TP and SRP concentrations for the whole lake were compared to monitored counterparts from eight SFWMD sampling stations. The 1979-88 predicted and measured time series compared reasonably well except for 1982, a time at which the lake experienced very low stages. The statistical comparison of means, standard deviations, and coefficients of variation is very good (e.g., predicted TP mean and CV = 93.3 ug/l and 0.24, respectively; measured TP mean and CV = 90.2 ug/l and 0.30). A full comparison is given in Table 13-12, along with a discussion of the impact of hypothetical control options.

Simulated management options include reductions in tributary loads by 40, 50 and 70 percent (for both TP and SRP). These reduced the TP mean by 19, 23 and 33 percent respectively, and the SRP mean by 26, 33, and 46 percent, respectively. A 70 percent load reduction resulted in an average in-lake TP concentration of 63 ug/l. A reduction of TP concentrations in Taylor Creek/Nubbin Slough to a maximum of 180 ug/l resulted in a predicted in-lake TP reduction of only 5 percent, to 88 ug/l. These predictions are by no means precise, but indicate first that reductions in loads translate to reductions in in-lake phosphorus concentrations, and second that a very large load reduction (> 70 percent) is probably necessary to reduce average in-lake TP concentrations to, say, 50 ug/l.

Output from the LOP0D model contains extensive tables of phosphorus quantities, fluxes, etc. These are included in Appendix D and summarized in this chapter.

14. RESULTS OF 3-D PHOSPHORUS MODELING

14.1 Introduction

The three-dimensional, transient phosphorus model for Lake Okeechobee developed as part of this project is designated LOP3D. Details are given in preceding chapters regarding model governing transport equations (Chapter 10), finite difference formulations (Chapter 11), and reactions (Chapter 12). Reactions are treated identically in models LOP0D and LOP3D. Thus, some of the details presented in Chapter 13 regarding phosphorus and sediment pathways also apply to LOP3D. This chapter describes the comparisons of LOP3D modeling with synoptic data from Lake Okeechobee and is basically the culmination of Task 4.6 of the SFWMD project. Because of the extended detail already presented in earlier chapters, this chapter will focus only on the comparisons with measured data. A 3-month simulation already described elsewhere (Sheng et al., 1991b) will be very briefly discussed as well.

14.2 Synoptic Data Interpolation and Initial Conditions

Five week-long synoptic surveys were performed during the spring of 1989 by the UF COE department (Sheng et al., 1991c). The collection Julian dates were 89141, 89147, 89154, 89161. Long-term UF COE monitoring locations are shown in Figure 14-1, while synoptic survey locations are shown in Figure 14-2. Data for the synoptic surveys are summarized in Figure 14-3. As can be seen, the fifth synoptic survey had the largest concentrations of total phosphorus and suspended sediments. Data from survey number 2 were used for comparisons presented in this chapter because of the need to correspond to hydrodynamic and sediment simulations performed by the UF COE group.

The total lake-wide total phosphorus and suspended solids appear to be a related (Figure 14-4). Sheng et al., (1991c) show similar correlation using The higher the suspended solids synoptic concentration the greater the total phosphorus synoptic concentration. This relationship was investigated using linear regression with the synoptic suspended solid as the dependent variable and synoptic total phosphorus as the independent variable (Figure 14-4). The empirical relation has an r^2 of 0.78 and the following intercept and slope coefficients for TP in ug/l and TSS in mg/l is :

$$TP = 2.48 \cdot TSS + 37.92 \quad (14.2-1)$$

The value of $2.48 \text{ ug} \cdot \text{mg}^{-1}$ (equivalent to $2,480 \text{ ug} \cdot \text{mg}^{-1}$) obtained from this empirical relationship is similar to the mean organic phosphorus value of $2,480 \text{ ug} \cdot \text{mg}^{-1}$ measured by Reddy et al. (1991) in the mud zone sediments of Lake Okeechobee. In addition, Sheng et al. (1991c) show significant log-log (power function) correlation between TP and TSS using all the data points from the 1989 and similar 1988 synoptic surveys. These results based on

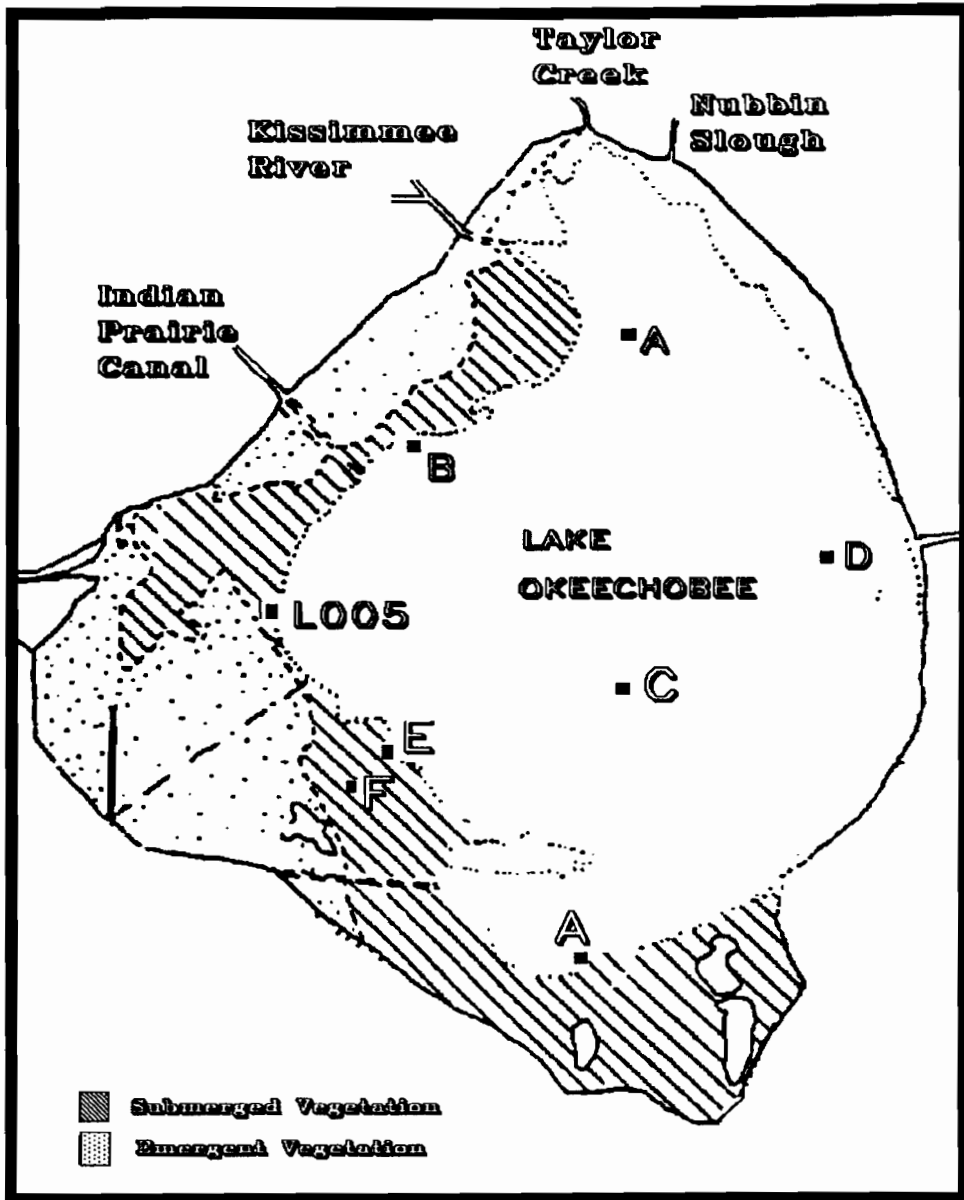


Figure 14-1 Location of Coastal Engineering data collectors.

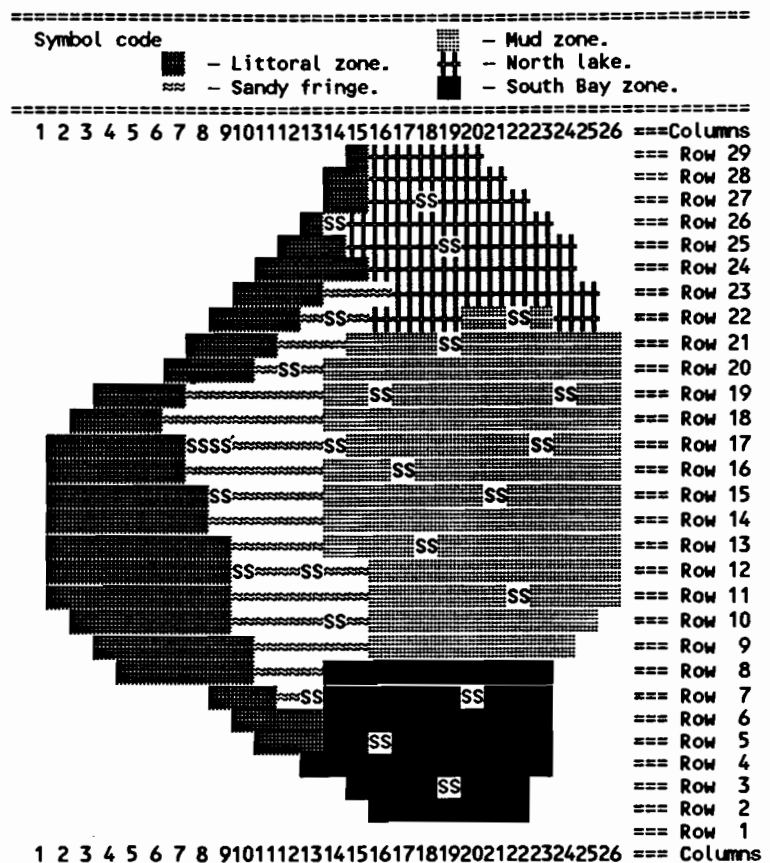


Figure 14-2 Synoptic station locations used in model LOP3D. The symbol for the location of a synoptic station is SS.

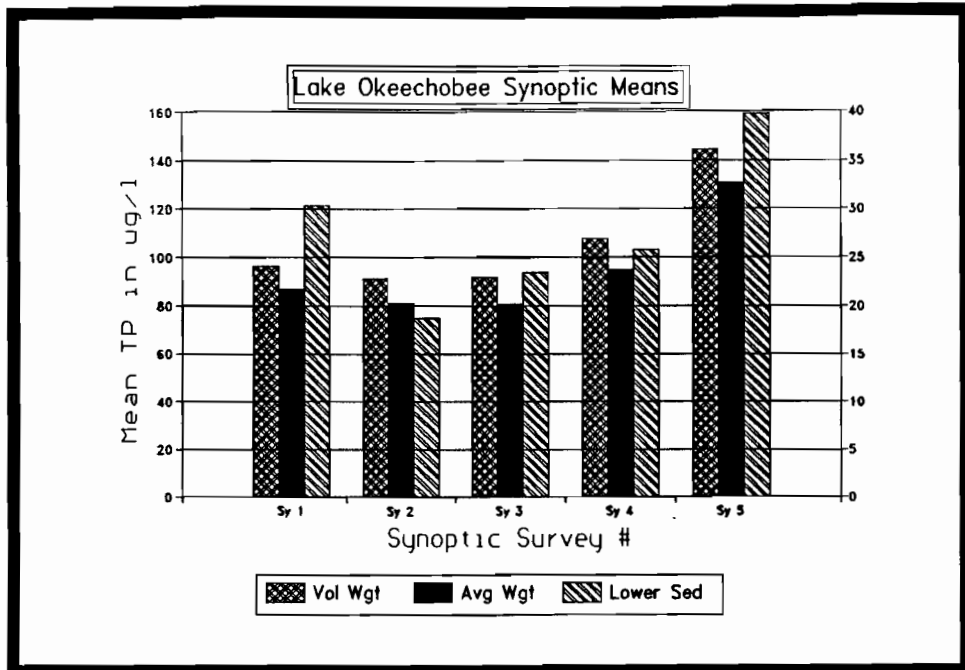


Figure 14-3 Mean synoptic total phosphorus and suspended sediment concentrations in 1989.

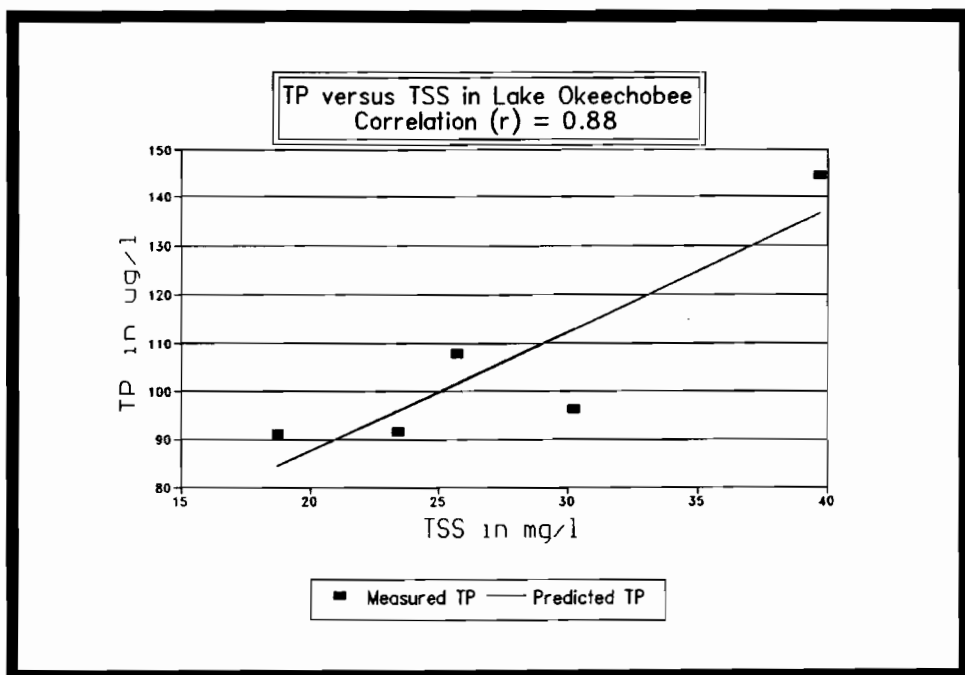


Figure 14-4 Straight line relationship obtained by linear regression between the mean synoptic TP and TSS for the five synoptic surveys during the spring of 1989.

the intensive synoptic data also relate to the discussion in Chapter 5 concerning the long term correlation between TP and both TSS and turbidity.

Initial conditions for each run are established from 25 locations around the lake sampled at the beginning of the six day period. Measurements of TP, SRP and total dissolved phosphorus (TDP) were made at one or two depths. Following the lead of the UF COE group, the 25 values at two depths are interpolated (and extrapolated) into every grid cell, first by reciprocal square weighting in the x and y directions, and then vertically by linear interpolation and extrapolation. The final measured phosphorus concentrations at each grid cell (at the end of a synoptic survey, for comparison purposes) are determined similarly, from the 25 measured values.

The synoptic survey data sets contain 22 to 25 stations with two vertical measurements of SRP, total dissolved phosphorus (TDP), TP and suspended sediments. The data are first interpolated vertically to the five σ levels and then are interpolated in the x and y directions using the nearest three synoptic stations. The north lake, South Bay, and littoral area of Lake Okeechobee have few synoptic data stations, as a consequence the phosphorus concentrations are actually extrapolated based on the nearest mud or sand zone synoptic data stations.

The weighting function is the sum of the inverse squared distance of the three nearest data stations, except for cells corresponding to a synoptic station. Measured synoptic SRP is the starting SRP in the simulation. Measured suspended sediment concentrations are used to initialize the PIP and organic sediment phosphorus (ORG) concentration fields using the partition coefficients described in Chapter 13. Measured DRP minus SRP is the initial concentration field of DOP. The remaining residual total phosphorus is apportioned among green algae, blue-green algae, and zooplankton. An initial estimate is 1/2 the residual TP which is defined as:

$$\text{Residual} = \text{TP} - \text{DRP} - \text{PIP} - \text{ORG} \quad (14.2-2)$$

The residual is detrital organic (colloidal and particulate) phosphorus. This is added to the initial DOP concentration to account for detrital particulate phosphorus not associated with the suspended sediment. The remaining residual TP is assumed to be 60 percent blue-green algae, 38 percent green algae and 2 percent zooplankton.

Lake sub-areas and volumes are compared in Figure 14-5. Peak concentrations are in the mud zone bordering the sand and macrophyte zones of Lake Okeechobee. The concentrations in the north lake, west littoral zone, and South Bay are extrapolated based on the three nearest synoptic stations in the sand and mud zones since there are few synoptic stations in these lake boxes. The model fitness should not be based on a comparison of the north lake, South Bay, and macrophyte zone concentrations.

The creation of the shaded plots of concentrations, reactions, and advective-diffusive movements presented in this chapter is discussed in Chapter 11. The shaded contour map (SCMAP) integrates the vertically differentiated model. That is, shading represents the depth-averaged concentrations.

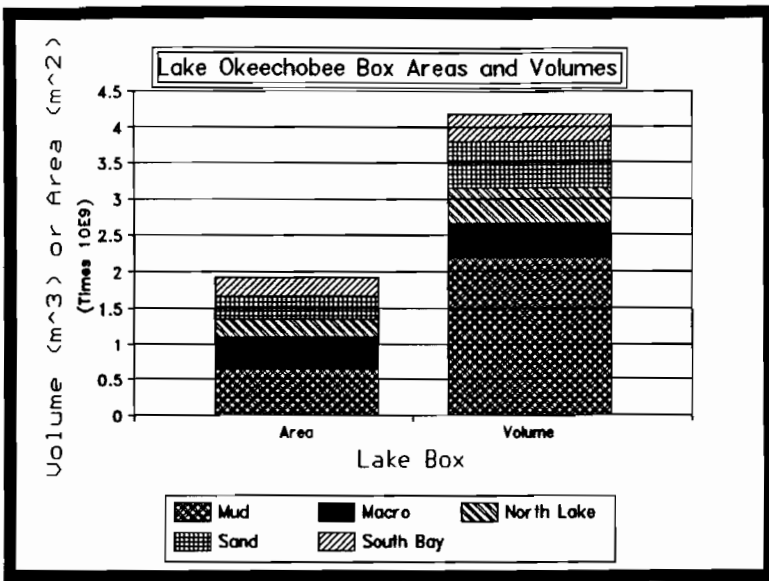


Figure 14-5 Box depths, areas, and volumes for the measured synoptic surveys during the spring of 1989.

Hydrologic and phosphorus concentration data have been assembled for Lake Okeechobee and its tributaries for all available years, but generally commencing in 1973 with the most complete data since 1980 (Carey and Huber, 1990). Flows, stages and total phosphorus (TP) and soluble reactive phosphorus (SRP) concentrations are stored on diskettes in a data base format. The primary data deficiency is wind speeds for which no routine weather service monitoring is performed. Wind speeds can only be obtained for this project by direct monitoring during the project, as is being done by the SFWMD and UF COE group at the locations shown in Figure 14-1.

14.3 Results

14.3.1 Interfacing and Time Steps

Model LOP3D cannot "stand alone." All runs of LOP3D were made in cooperation with parallel hydrodynamic and sediment model (EHSM3D) runs of the UF COE group (Sheng et al., 1991a). LOP3D relies on the UF COE hydrodynamic and sediment models for time-step input (usually every 3 hours) of velocities, diffusivities, elevations, and sediment concentrations at every one of the 496 x 5 cells of the finite difference grid. LOP3D time steps are usually 3 hours (although completely variable) because there is no apparent advantage to using shorter values, on the basis of considerable model testing. Finite difference grids are 2 km on a side, and the five depth layers are adjusted during the simulation according to the σ -layer schematization discussed in Chapter 10. During the course of a 7 day simulation, this adjustment is only on the order of millimeters (see Section 14.3.4).

The one-week simulation described in this chapter was done without including inflows to the lake. This is justifiable, because the influence of these loadings is very small over such a short time period. However, the model can (and has, in a 3-month simulation) include these fluxes into and out of the lake. This is done on the basis of boundary velocities at inflow cells (e.g., mouth of the Kissimmee River) calculated by the EHSM3D model, and concentrations of SRP and dissolved organic phosphorus (DOP, assumed equal to TP-SAP). The concentrations are interpolated from semi-monthly or monthly monitoring data. The combination of the hydrodynamic advective velocity into (or out of) the lake at such boundary cells and the interpolated concentrations permits the proper advective flux of phosphorus to enter (or leave) the lake during the simulation.

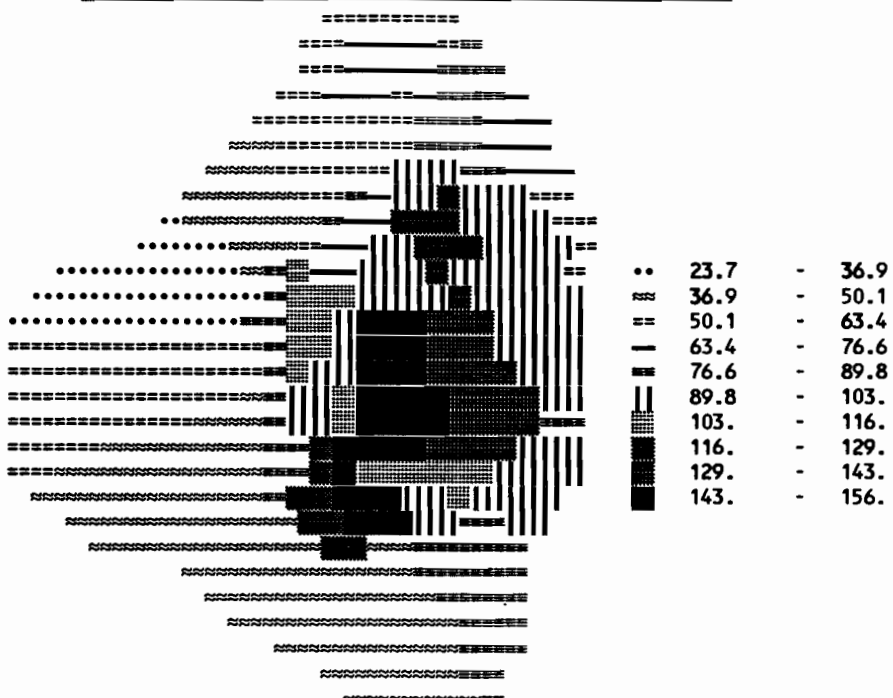
14.3.2 TP and SRP Comparisons

Initial TP and SRP concentrations in the lake are shown in Figures 14-6 and 14-7 for the synoptic period beginning 12 noon on Julian day 89147 (May 27, 1989). This is the second synoptic data period in the spring 1989 synoptic survey. Measured and predicted concentrations of at the end of seven days (Julian day 89154, June 3, 1989) are shown in Figures 14-8 and 14-9 for TP and in Figures 14-10 and 14-11 for SRP. Comparisons (Figures 14-8 and 14-9) are quite reasonable for total phosphorus (the sum of the eight components modeled). The total TP varies little over the period and thus does not test the model predictivity very much. Deviation of predicted and measured SRP concentration contours is somewhat greater, as can be seen in Figures 14-10 and 14-11 although the magnitudes are definitely correct. The model tends to predict a somewhat larger areal spread of SRP than observed, but concentrations on the fringes are similar to those observed.

Measured versus predicted differences can be compared on a cell by cell basis in Figures 14-12 and 14-13. Although at first glance these do not look so flattering, the mean difference between measured and predicted TP concentrations is only 6.2 ug/l and 0.03 ug/l for SRP. Thus, in spite of locally high differences, the LOP3D model does a good job on the average.

Synoptic concentrations of SRP are high in the South Bay and lower mud zone of Lake Okeechobee. Evaluating measured and predicted SRP on Julian day 89154 (Figures 14-10 and 14-11), at the end of the seven day simulation the high concentration of SRP has moved to the central mud zone and decreased in the South Bay of Lake Okeechobee. The concentrations of SRP in the model lake are vertically averaged on the figures to correspond to synoptic data on 89154. Based on the "mean box" concentrations printed beneath the figures, measured and predicted box-averaged SRP values show remarkably good agreement, in spite of not accounting for all possible phosphorus pathways, e.g., the algal mat at the bottom of the South Bay. Predicted SRP in the macrophyte zone is less than that of the measured synoptic data, possibly indicating the need for a macrophyte submodel in the 3-D model, although concentrations are very low (measured = 2.9 ug/l, predicted = 1.6 ug/l).

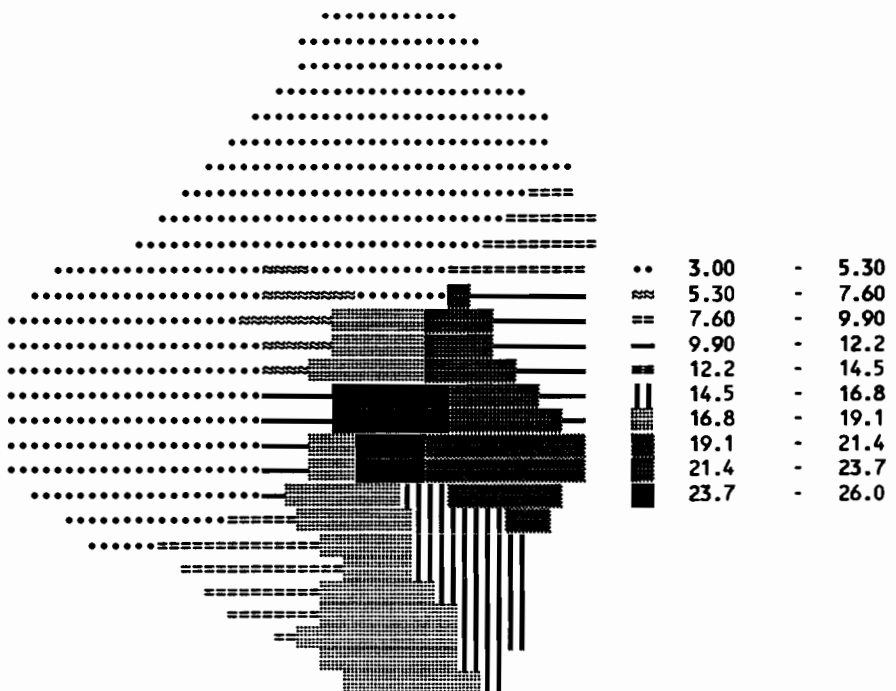
Mean	76.01	Max	156.0	Min	23.68
------	-------	-----	-------	-----	-------



	Mud zone	Macrophyte North	Lake Sand zone	South Bay	Whole Lake
Mean Box	113.	46.4	72.5	57.5	64.9
Layer 5 Total P	110.134	43.151	68.886	54.229	64.559
Layer 4 Total P	111.488	44.784	70.690	55.869	64.727
Layer 3 Total P	112.843	46.418	72.494	57.509	64.895
Layer 2 Total P	114.197	48.051	74.298	59.149	65.063
Layer 1 Total P	115.552	49.685	76.103	60.790	65.231
Layer 5 ZOO	0.520	0.328	0.557	0.396	0.408
Layer 4 ZOO	0.511	0.345	0.554	0.410	0.399
Layer 3 ZOO	0.502	0.363	0.550	0.425	0.389
Layer 2 ZOO	0.493	0.380	0.547	0.440	0.380
Layer 1 ZOO	0.484	0.397	0.543	0.454	0.371
Layer 5 PIP	0.296	0.000	0.103	0.042	0.000
Layer 4 PIP	0.310	0.000	0.108	0.046	0.000
Layer 3 PIP	0.325	0.000	0.112	0.050	0.001
Layer 2 PIP	0.339	0.000	0.117	0.054	0.001
Layer 1 PIP	0.354	0.000	0.122	0.058	0.001
Layer 5 OrgP-Sed	37.062	0.000	6.702	2.092	0.003
Layer 4 OrgP-Sed	38.711	0.000	7.048	2.286	0.018
Layer 3 OrgP-Sed	40.361	0.000	7.394	2.480	0.032
Layer 2 OrgP-Sed	42.010	0.000	7.740	2.675	0.047
Layer 1 OrgP-Sed	43.660	0.000	8.085	2.869	0.062
Layer 5 Sediment	21.758	0.000	10.426	10.253	0.015
Layer 4 Sediment	22.658	0.000	10.639	11.206	0.087
Layer 3 Sediment	23.559	0.000	10.852	12.158	0.159
Layer 2 Sediment	24.460	0.000	11.066	13.111	0.231
Layer 1 Sediment	25.360	0.000	11.279	14.063	0.303

Figure 14-6 Starting TP synoptic concentrations in ug/l on 89147.

Mean	9.144	Max	26.00	Min	3.000
------	-------	-----	-------	-----	-------



	Mud zone	Macrophyte	North Lake	Sand zone	South Bay	Whole Lake
Mean Box	14.3	3.60	3.41	5.62	16.2	8.61
Layer 5 SRP	13.839	3.655	3.131	5.354	14.818	
Layer 4 SRP	14.050	3.628	3.270	5.487	15.496	
Layer 3 SRP	14.261	3.601	3.410	5.620	16.174	
Layer 2 SRP	14.472	3.574	3.549	5.753	16.852	
Layer 1 SRP	14.683	3.546	3.689	5.886	17.530	
Layer 5 DOP	32.935	23.096	31.090	26.946	29.354	
Layer 4 DOP	32.859	23.890	32.579	27.525	29.286	
Layer 3 DOP	32.783	24.684	34.068	28.103	29.219	
Layer 2 DOP	32.708	25.477	35.557	28.682	29.152	
Layer 1 DOP	32.632	26.271	37.046	29.261	29.084	
Layer 5 Greens	9.881	6.232	10.587	7.522	7.746	
Layer 4 Greens	9.712	6.561	10.521	7.799	7.572	
Layer 3 Greens	9.543	6.891	10.454	8.077	7.398	
Layer 2 Greens	9.374	7.220	10.388	8.355	7.224	
Layer 1 Greens	9.205	7.550	10.321	8.632	7.050	
Layer 5 Blues	15.602	9.839	16.716	11.877	12.230	
Layer 4 Blues	15.335	10.360	16.611	12.315	11.956	
Layer 3 Blues	15.068	10.880	16.506	12.753	11.681	
Layer 2 Blues	14.800	11.400	16.401	13.192	11.407	
Layer 1 Blues	14.533	11.921	16.296	13.630	11.132	

Figure 14-7 SRP Synoptic concentrations in ug/l on 89147.

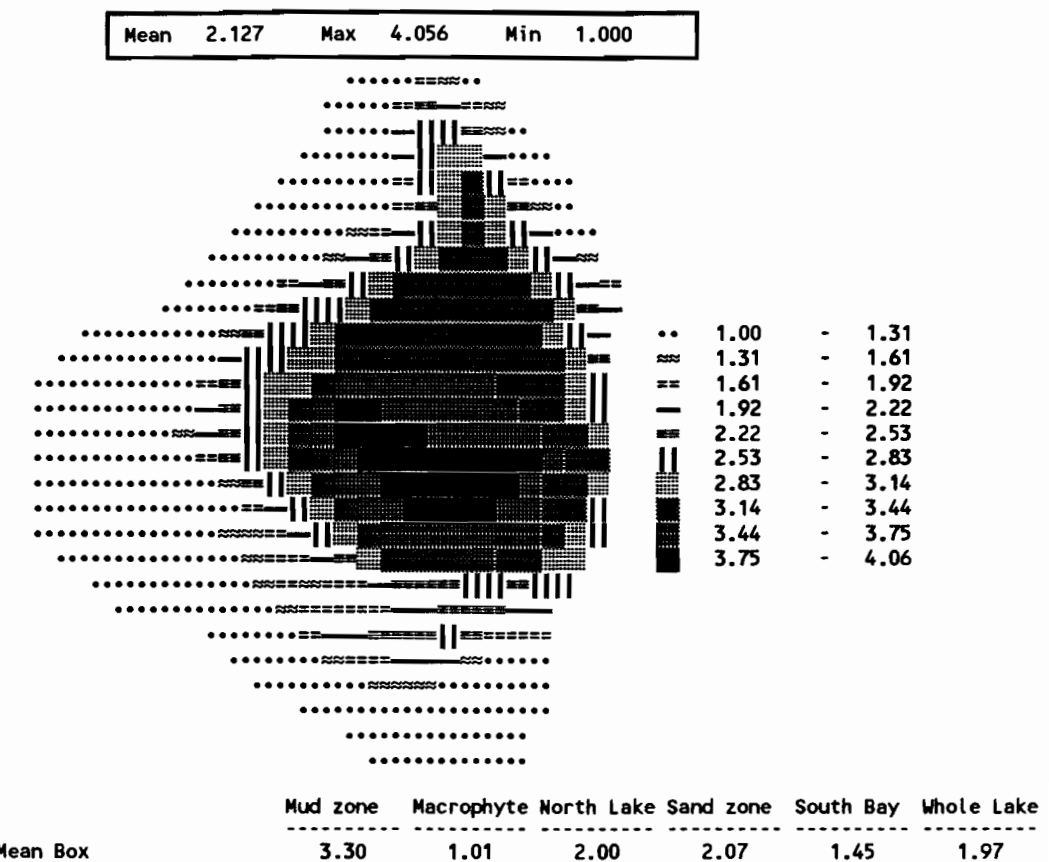


Figure 14-8 Center cell depth on Julian day 89147.

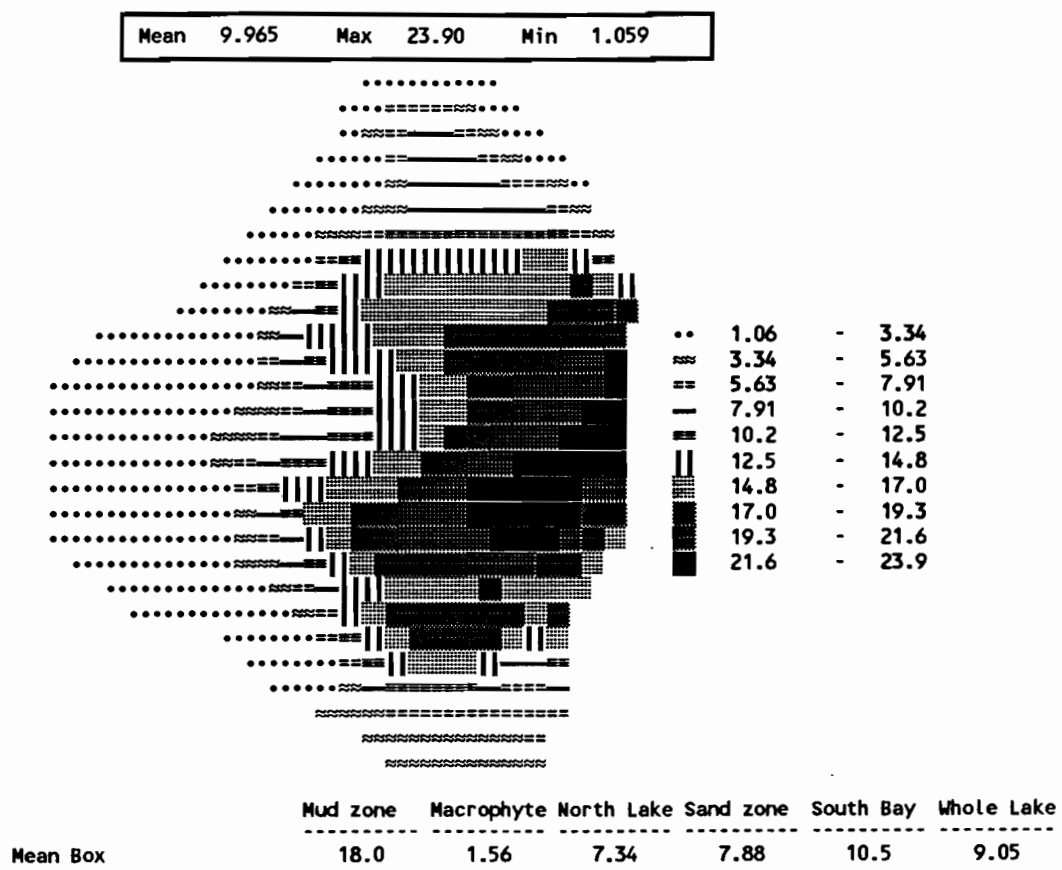


Figure 14-9 Predicted SRP concentration in ug/l on day 89154.

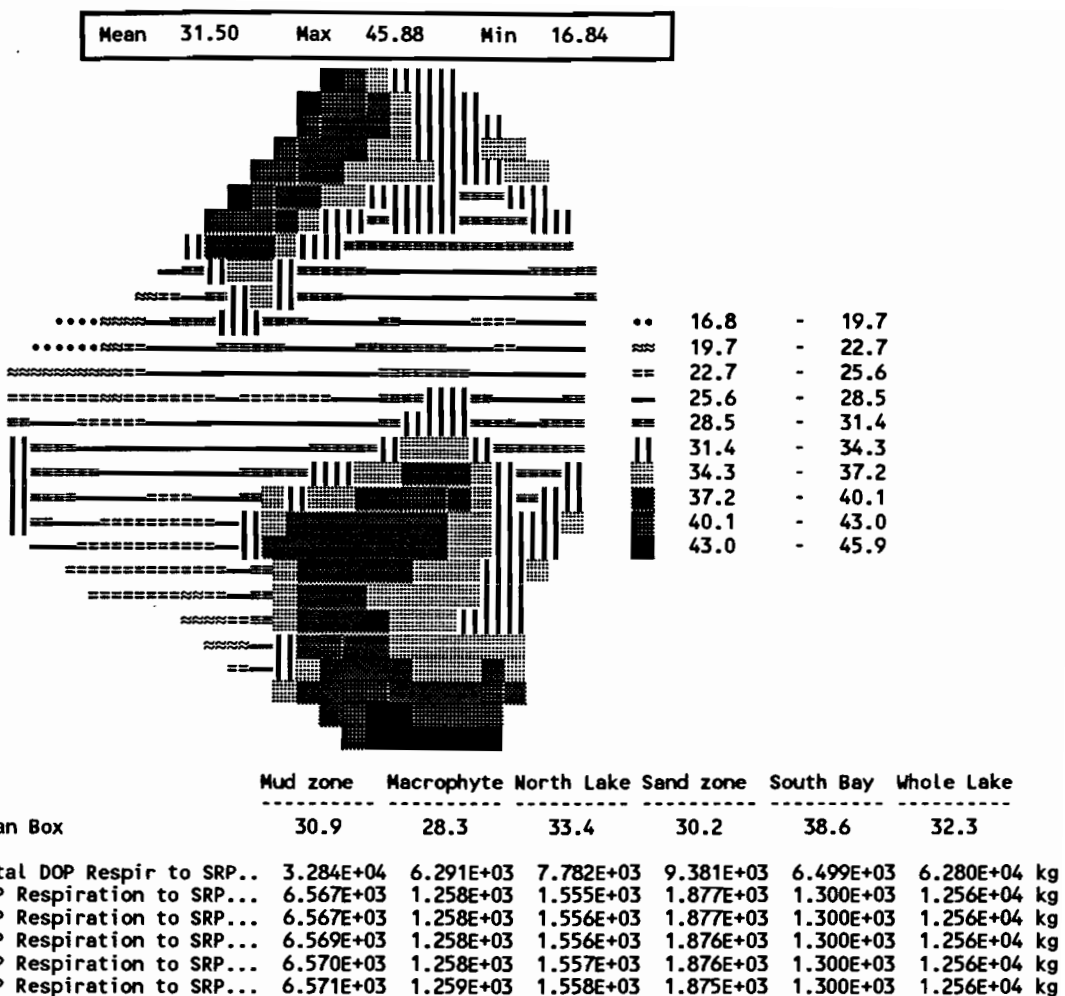
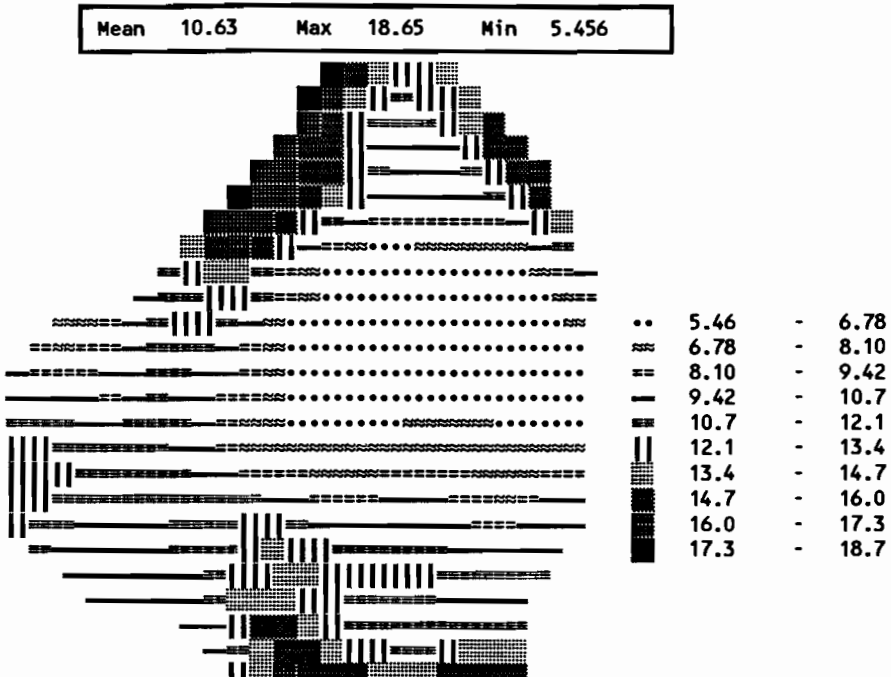


Figure 14-10 Predicted concentration for constituent DOP, ug/l.



	Mud zone	Macrophyte	North Lake	Sand zone	South Bay	Whole Lake
Mean Box	7.57	11.9	11.7	10.8	14.6	11.3
Total Green uptake of SRP	2.937E+04	1.112E+04	9.472E+03	1.066E+04	1.057E+04	7.119E+04
Green uptake of SRP.....	2.581E+04	2.928E+03	5.027E+03	6.661E+03	6.030E+03	4.645E+04
Green uptake of SRP.....	3.141E+03	2.853E+03	2.598E+03	2.484E+03	3.402E+03	1.448E+04
Green uptake of SRP.....	364.	2.491E+03	1.108E+03	936.	930.	5.827E+03
Green uptake of SRP.....	46.8	1.804E+03	517.	389.	178.	2.934E+03
Green uptake of SRP.....	7.19	1.049E+03	222.	188.	33.0	1.500E+03
Total Green decay to SRP.	1.761E+04	5.319E+03	5.108E+03	6.072E+03	5.055E+03	3.917E+04
Green decay to SRP.....	7.498E+03	1.204E+03	1.652E+03	2.124E+03	1.803E+03	1.428E+04
Green decay to SRP.....	2.986E+03	1.190E+03	1.165E+03	1.291E+03	1.272E+03	7.904E+03
Green decay to SRP.....	2.424E+03	1.117E+03	864.	974.	771.	6.150E+03
Green decay to SRP.....	2.357E+03	980.	744.	862.	619.	5.562E+03
Green decay to SRP.....	2.347E+03	828.	684.	821.	591.	5.270E+03
Total Green decay to DOP.	1.189E+04	3.128E+03	3.240E+03	3.968E+03	2.973E+03	2.520E+04
Green decay to DOP.....	2.475E+03	629.	663.	816.	614.	5.197E+03
Green decay to DOP.....	2.366E+03	629.	652.	796.	601.	5.044E+03
Green decay to DOP.....	2.351E+03	627.	644.	788.	589.	5.000E+03
Green decay to DOP.....	2.348E+03	624.	641.	785.	585.	4.983E+03
Green decay to DOP.....	2.346E+03	620.	639.	784.	584.	4.973E+03

Figure 14-11 Predicted concentration for constituent greens, ug/l.

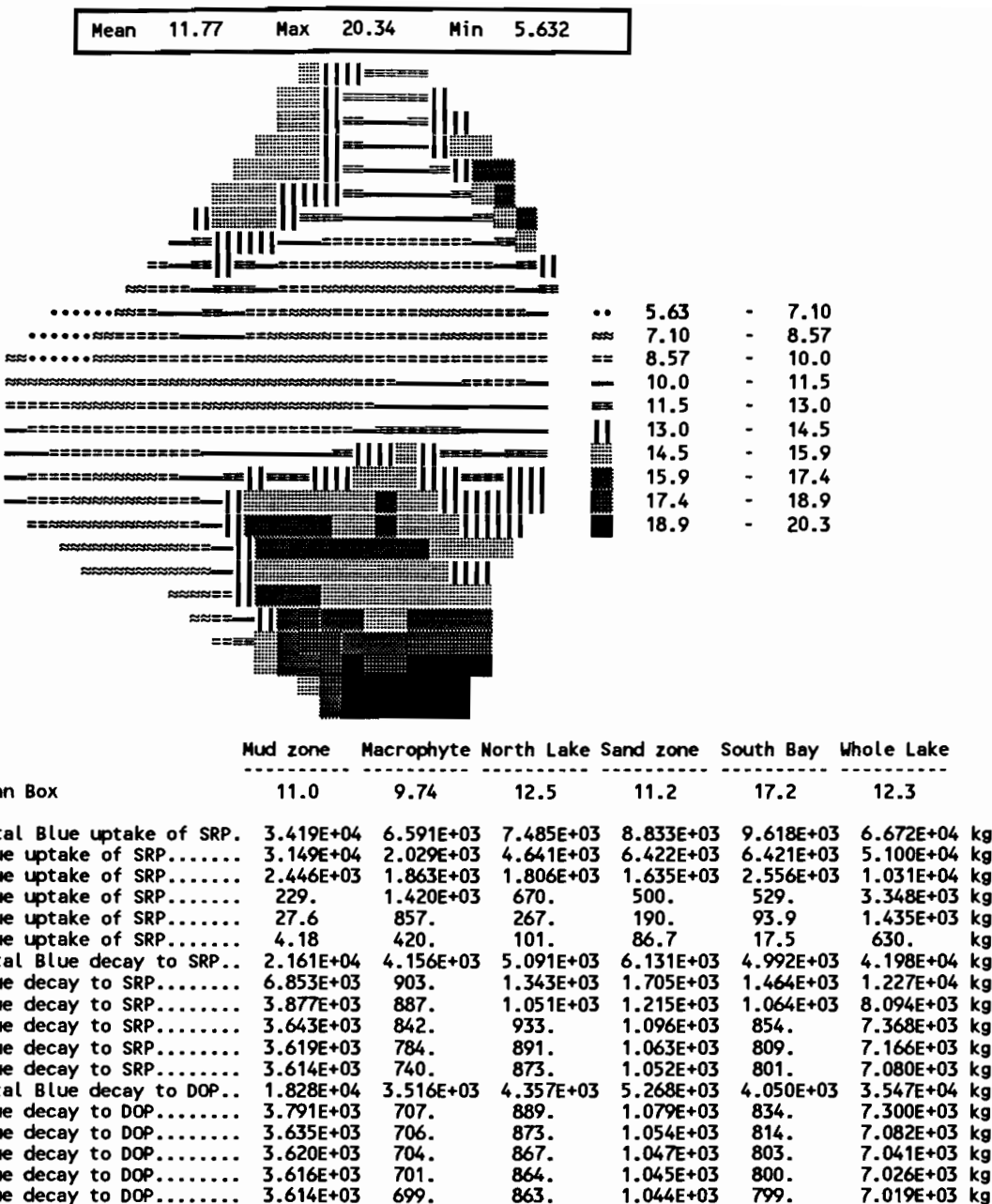
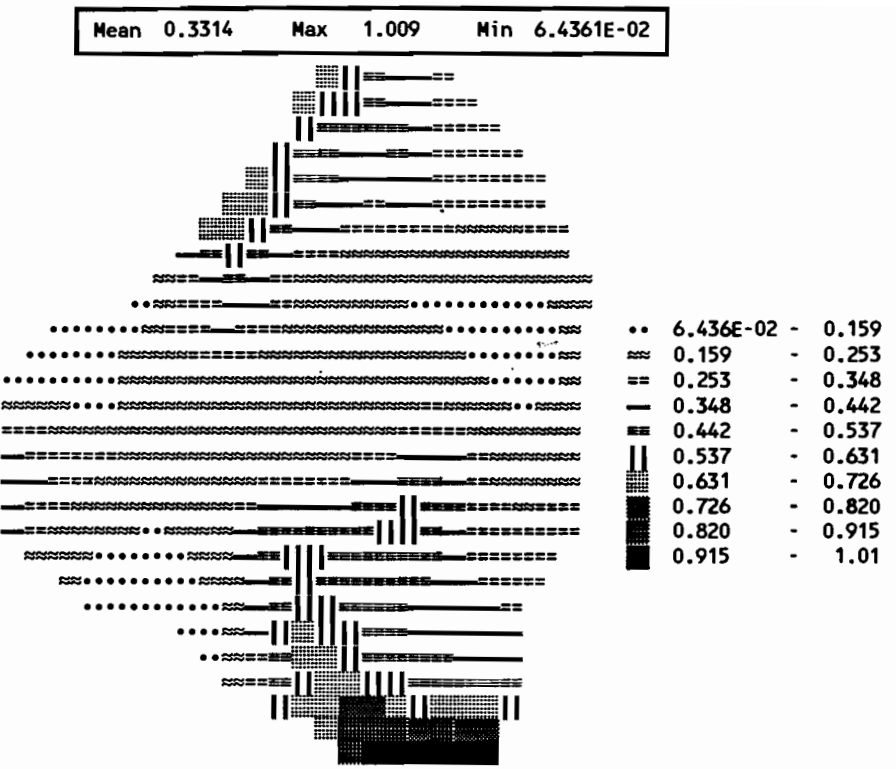


Figure 14-12 Predicted concentration for constituent blue-greens, ug/l.



	Mud zone	Macrophyte	North Lake	Sand zone	South Bay	Whole Lake
Mean Box	0.263	0.280	0.348	0.299	0.613	0.361
Total Zoo uptake of GRN...	2.615E+03	499.	720.	763.	710.	5.308E+03 kg
Zoo uptake of Greens.....	534.	100.	146.	155.	144.	1.079E+03 kg
Zoo uptake of Greens.....	522.	100.	144.	153.	143.	1.062E+03 kg
Zoo uptake of Greens.....	520.	99.9	144.	152.	141.	1.057E+03 kg
Zoo uptake of Greens.....	520.	99.7	143.	152.	141.	1.055E+03 kg
Zoo uptake of Greens.....	519.	99.4	143.	152.	141.	1.054E+03 kg
Total Zoo uptake of Blues	321.	53.7	83.2	88.6	80.7	628. kg
Zoo uptake of Blues.....	65.3	10.8	16.8	17.9	16.3	127. kg
Zoo uptake of Blues.....	64.1	10.8	16.7	17.7	16.2	125. kg
Zoo uptake of Blues.....	64.0	10.7	16.6	17.7	16.1	125. kg
Zoo uptake of Blues.....	64.0	10.7	16.6	17.6	16.1	125. kg
Zoo uptake of Blues.....	64.0	10.7	16.6	17.6	16.1	125. kg
Total Zoo decay to SRP...	1.693E+03	305.	439.	480.	390.	3.307E+03 kg
Zoo decay to SRP.....	339.	60.9	87.8	96.1	78.0	662. kg
Zoo decay to SRP.....	339.	60.9	87.8	96.0	78.0	661. kg
Zoo decay to SRP.....	339.	60.9	87.8	96.0	78.0	661. kg
Zoo decay to SRP.....	339.	60.9	87.8	96.0	77.9	661. kg
Zoo decay to SRP.....	339.	60.9	87.8	96.0	77.9	661. kg
Total Zoo decay to DOP...	1.693E+03	305.	439.	480.	390.	3.307E+03 kg
Zoo decay to DOP.....	339.	60.9	87.8	96.1	78.0	662. kg
Zoo decay to DOP.....	339.	60.9	87.8	96.0	78.0	661. kg
Zoo decay to DOP.....	339.	60.9	87.8	96.0	78.0	661. kg
Zoo decay to DOP.....	339.	60.9	87.8	96.0	77.9	661. kg
Zoo decay to DOP.....	339.	60.9	87.8	96.0	77.9	661. kg

Figure 14-13 Predicted concentration for constituent ZOO, ug/l.

Soluble reactive phosphorus is the most dynamic and reactive of the phosphorus species because it is involved in most reaction pathways, and has a residence time of only 1 - 2 days in the lake. SRP has turned over 1 to 4 times in a one week simulation of Lake Okeechobee.

From the "mean box" values printed beneath the diagrams, the South Bay and macrophyte areas of Lake Okeechobee do not show a good measured-predicted match between TP concentrations, but the other three areas of the lake have a close match between the predicted concentration field and the synoptic concentration field. The macrophyte and South Bay predicted TPs (51.8 and 81.5 ug/l, respectively) are greater than the measured interpolated TP concentrations (31.9 and 69.2 ug/l, respectively), perhaps indicative of sources/sinks or mechanisms not modeled.

14.3.3 Other Phosphorus Parameters

This section will deal with the multitude of other information that can be extracted from the LOP3D model, most of which has no measured counterpart. This output is presented in the remainder of the figures in this chapter.

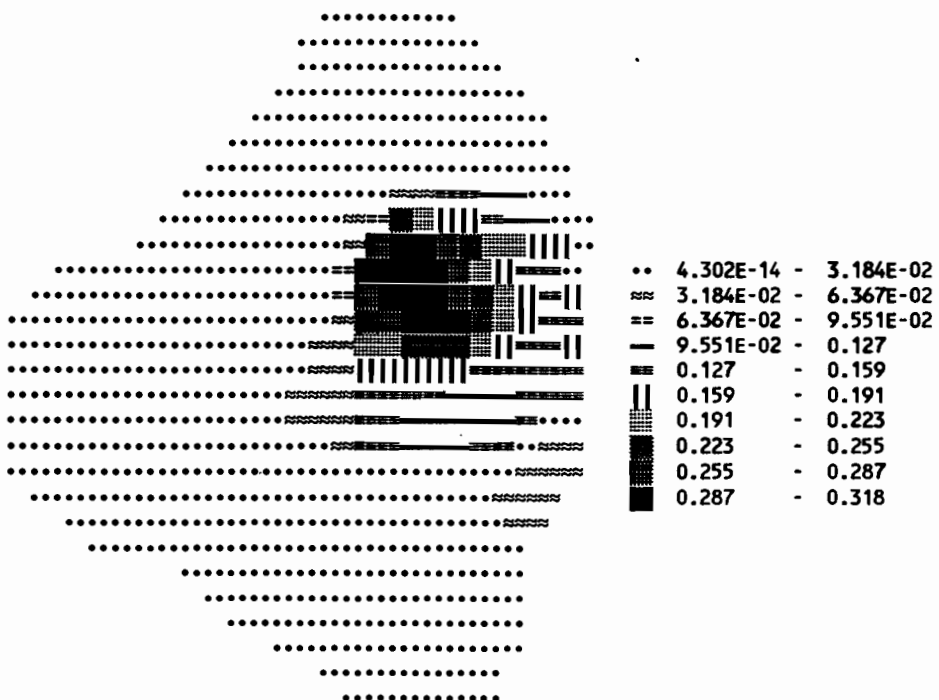
Predicted DOP (Figure 14-14) is somewhat higher than the measured synoptic DOP (not shown) indicating that the rate constant for the transformation of DOP to SRP should be increased in the model. Green algae (Figure 14-15) are likewise over-predicted (measured not shown) in Lake Okeechobee. The mud zone measured and predicted green algae concentrations are close but the other four areas of the lake have over-predicted green algal concentrations. This can be adjusted by changing the green algae uptake, respiration and excretion parameters to decrease the predicted concentrations. The blue-green algae (Figure 14-16, measured not shown) are slightly under-predicted in Lake Okeechobee.

Zooplankton (Figure 14-17) have a small concentration of particulate phosphorus but nonetheless important because they increase the rate of internal phosphorus cycling in the lake. The zooplankton are a consumer of algae and a source of SRP to the pelagic phytoplankton in Lake Okeechobee. The change in phosphorus directly attributable (by the model) to zooplankton is comparable to the magnitude of the green and blue-green algal pathways. The largest PIP (Figure 14-18) concentration naturally occurs in the mud zone of Lake Okeechobee. Overall this is a small pathway but significant because a single cell may be both a source or sink of pelagic SRP.

The concentration (Figure 14-19) of organic sediment phosphorus (ORG) is connected to the suspended sediment (Figure 14-20) and thus tied to the reliability of the 3-D suspended sediment simulation. ORG is approximately 40 percent of the total phosphorus in the mud zone.

Algal uptake (Figures 14-21 and 14-22) is 4 times higher in the upper σ -level than in the lowest σ -level of the whole lake and 10-12 times higher in the upper σ level than the lowest σ level because of the shading of the suspended sediments. The algal respiration and excretion losses (Figures 14-23 and 14-24) are more evenly distributed in the pelagic region of Lake Okeechobee.

Mean 4.0672E-02 Max 0.3184 Min 4.3025E-14



	Mud zone	Macrophyte	North Lake	Sand zone	South Bay	Whole Lake
Mean Box	0.119	3.951E-05	5.161E-03	3.739E-03	8.205E-05	2.559E-02
Total desorption onto SED	-1.760E+03	-1.10	-100.	-82.8	-2.36	-1.947E+03
Desorption onto sediment.	-341.	-0.221	-18.7	-15.3	-0.387	-376.
Desorption onto sediment.	-347.	-0.221	-19.4	-15.9	-0.424	-382.
Desorption onto sediment.	-350.	-0.220	-20.1	-16.5	-0.471	-388.
Desorption onto sediment.	-355.	-0.220	-20.8	-17.2	-0.517	-393.
Desorption onto sediment.	-367.	-0.218	-21.5	-17.9	-0.559	-408.
Total adsorption onto SED	1.268E+03	1.04	32.8	41.7	1.89	1.346E+03
Adsorption onto sediment.	256.	0.210	6.61	8.51	0.383	272.
Adsorption onto sediment.	254.	0.210	6.60	8.41	0.380	270.
Adsorption onto sediment.	251.	0.209	6.57	8.34	0.379	266.
Adsorption onto sediment.	249.	0.209	6.53	8.27	0.376	265.
Adsorption onto sediment.	258.	0.207	6.47	8.20	0.371	273.

Figure 14-14 Predicted concentration for constituent PIP, ug/l.

Mean	14.75	Max	108.7	Min	7.7648E-11
------	-------	-----	-------	-----	------------

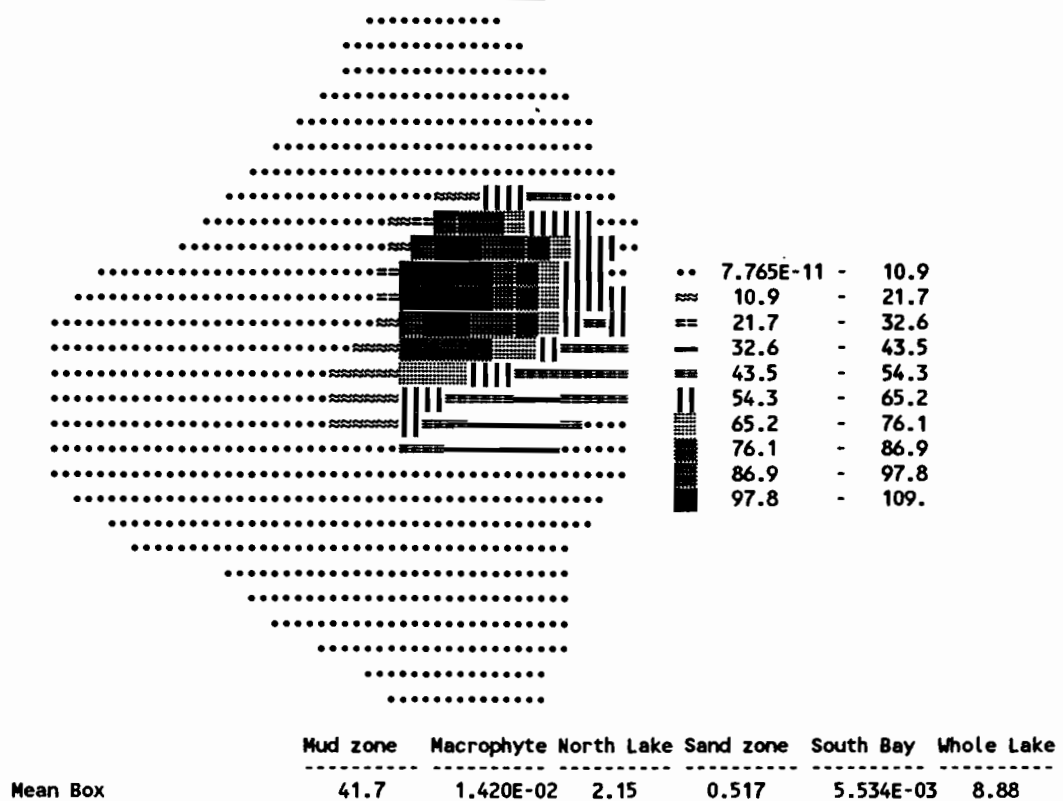


Figure 14-15 Predicted concentration for constituent OrgP-Sed, ug/l.

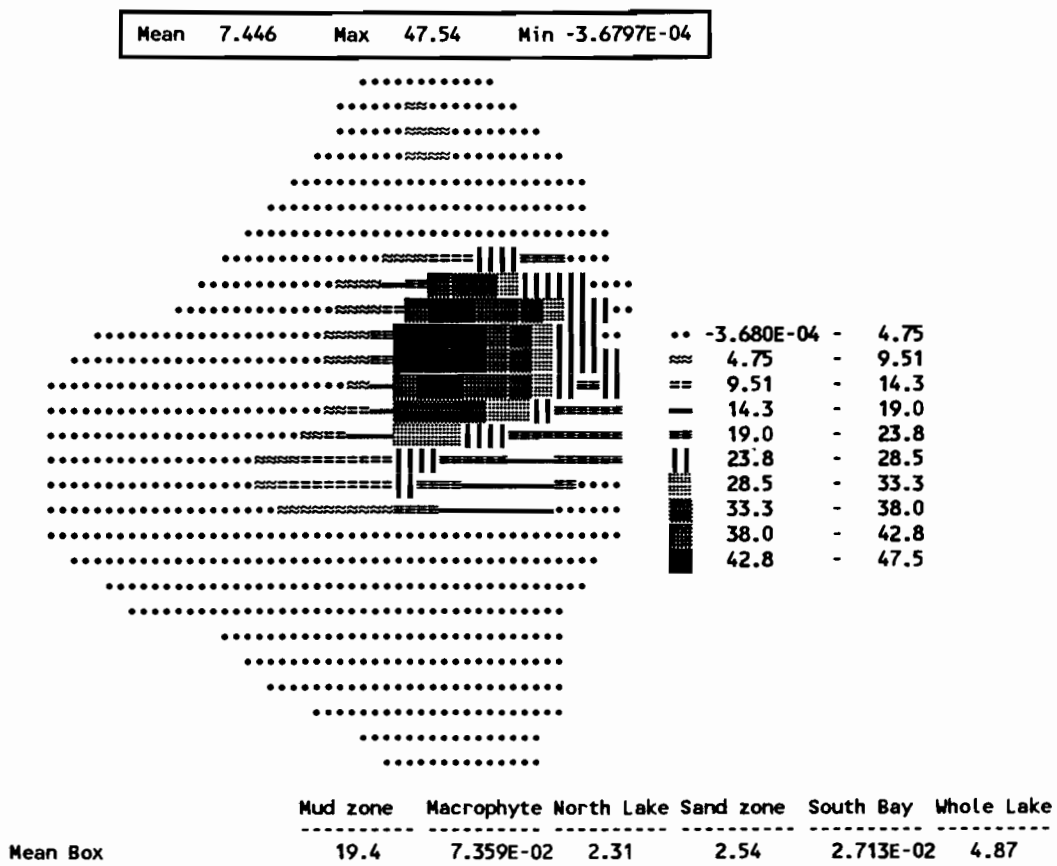
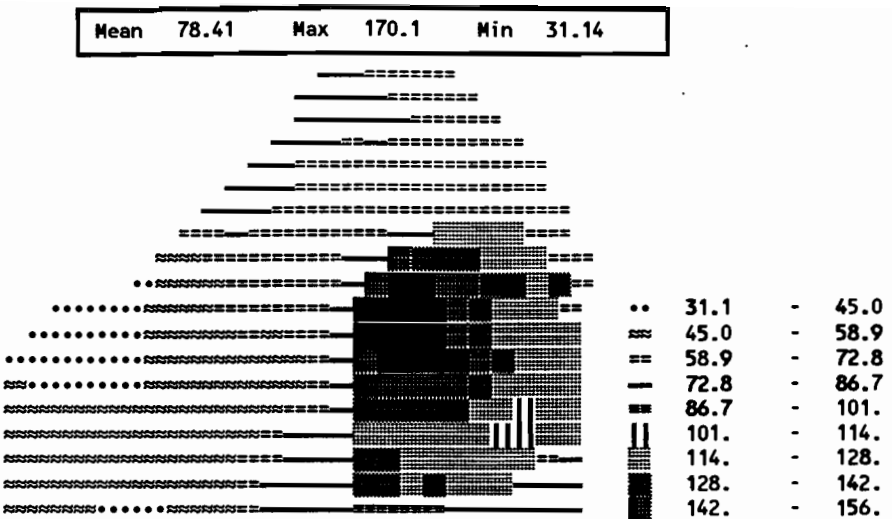


Figure 14-16 Predicted concentration for constituent sediment, mg/l.



	Mud zone	Macrophyte	North Lake	Sand zone	South Bay	Whole Lake
Mean Box	110.	51.8	67.5	60.9	81.5	74.3
Mean Total P for layer 5	108.	51.8	67.6	60.9	81.4	ug/l
Mean Total P for layer 4	109.	51.8	67.6	60.9	81.4	ug/l
Mean Total P for layer 3	109.	51.8	67.6	60.9	81.5	ug/l
Mean Total P for layer 2	110.	51.8	67.5	60.9	81.5	ug/l
Mean Total P for layer 1	111.	51.8	67.4	60.8	81.5	ug/l
Erosion flux of Org-P....	1.335E-05	4.072E-16	3.510E-18	0.000	0.000	1.335E-05 kg
Deposition flux of Org-P..	8.171E-04	2.445E-06	7.303E-05	6.246E-05	1.081E-06	9.561E-04 kg
Erosion flux of Org-P....	8.844E-08	2.727E-18	2.294E-20	0.000	0.000	8.844E-08 kg
Deposition flux of Org-P..	-4.523E-09	-4.488E-11	-8.231E-10	-5.569E-10	-1.211E-11	-5.960E-09 kg
Erosion flux of PIP.....	0.000	0.000	0.000	0.000	0.000	0.000 kg
Deposition flux of PIP...	7.828E-11	4.833E-15	1.290E-12	1.999E-12	3.337E-15	8.158E-11 kg
Change in TP.....	-448.	-55.9	-74.1	-108.	10.9	-675. kg
Change in SRP.....	8.995E+03	-1.949E+03	1.091E+03	2.136E+03	-3.644E+03	6.629E+03 kg
Change in DOP.....	-2.682E+03	354.	-186.	-145.	524.	-2.134E+03 kg
Change in Green algae....	-132.	2.677E+03	1.124E+03	616.	2.545E+03	6.830E+03 kg
Change in Blue-Greens....	-5.689E+03	-1.082E+03	-1.962E+03	-2.566E+03	576.	-1.072E+04 kg
Change in PIP.....	-492.	-5.559E-02	-67.6	-41.1	-0.470	-601. kg
Change in Zooplankton....	-450.	-56.1	-74.5	-108.	10.7	-678. kg
Change in Sediment Org P..	-8.038E-04	-2.445E-06	-7.303E-05	-6.246E-05	-1.081E-06	-9.428E-04 kg
Diagenetic flux of SRP...	1.94	0.229	0.427	0.247	0.207	3.05 kg
Calc change in Sed Org P.	1.405E+03	6.85	-3.074E+03	-1.381E+03	-15.6	-3.060E+03 kg
Calc change in Sediment ..	-8.806E+06	3.549E+04	-4.161E+06	-6.772E+06	-7.647E+04	-1.978E+07 kg

Figure 14-17 Predicted TP concentration in ug/l on day 89154.

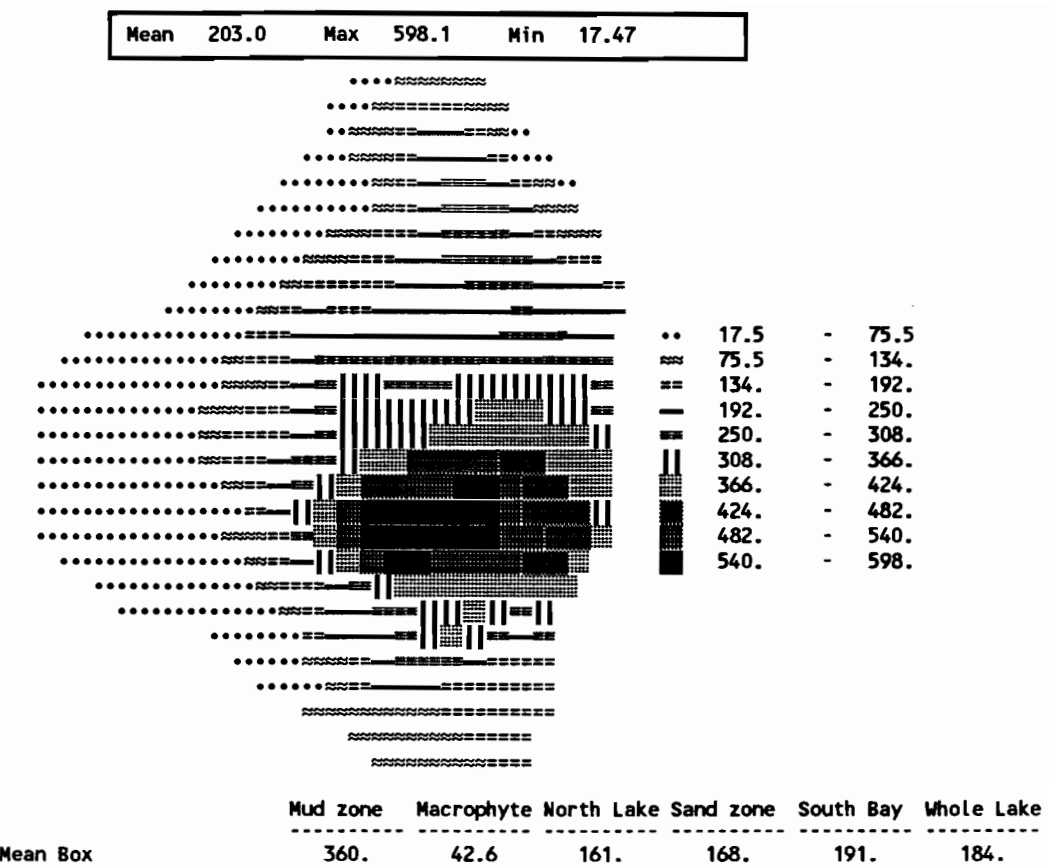


Figure 14-18 Upper layer uptake for all algae species in kilograms.

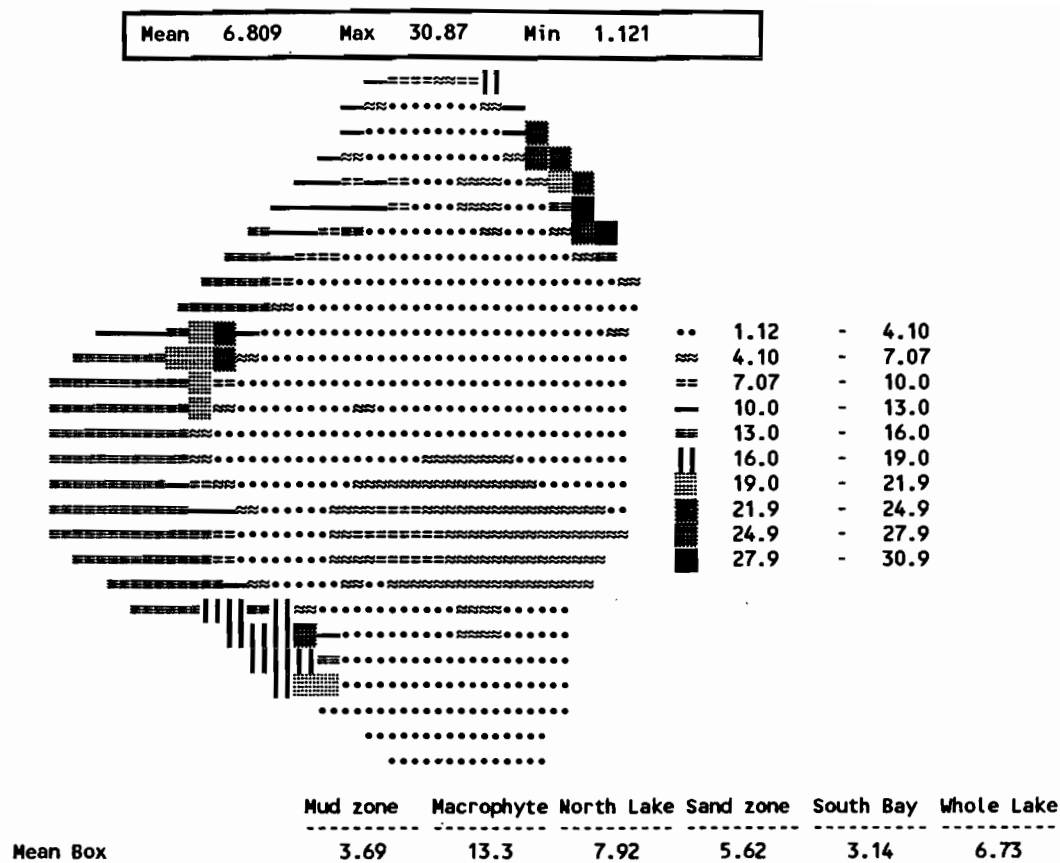


Figure 14-19 Lower layer uptake for all algae species in kilograms.

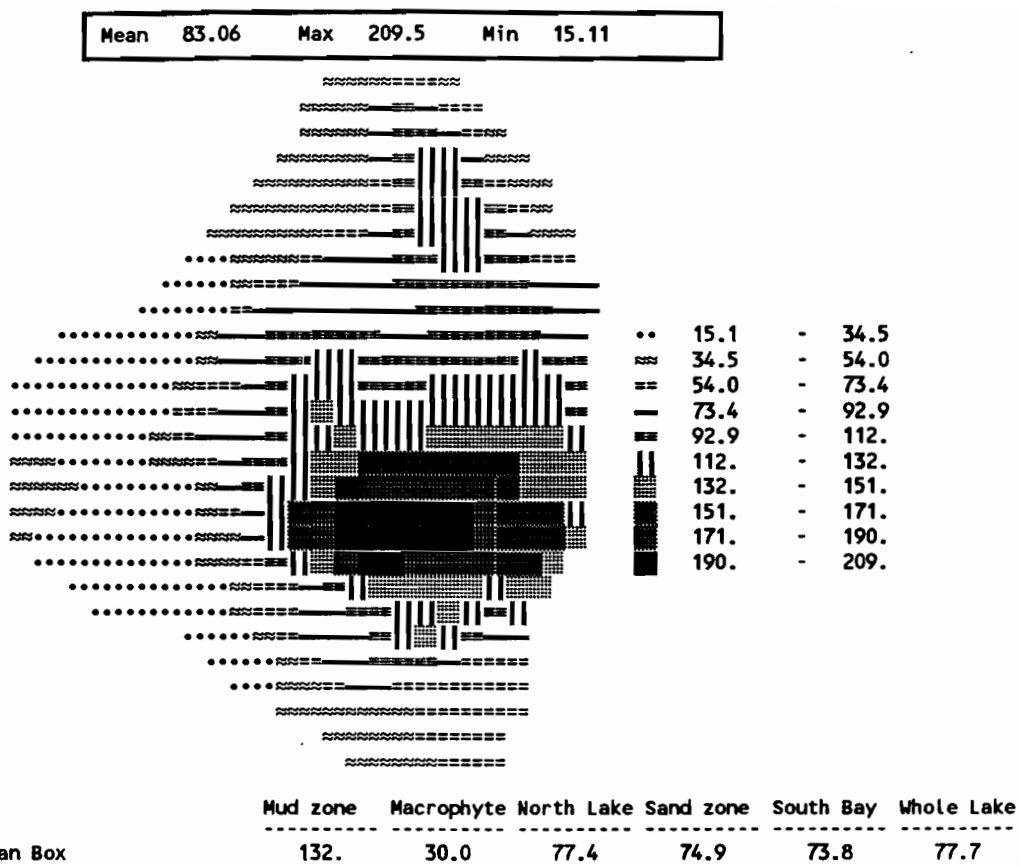


Figure 14-20 Upper layer losses for all algae species in kilograms.

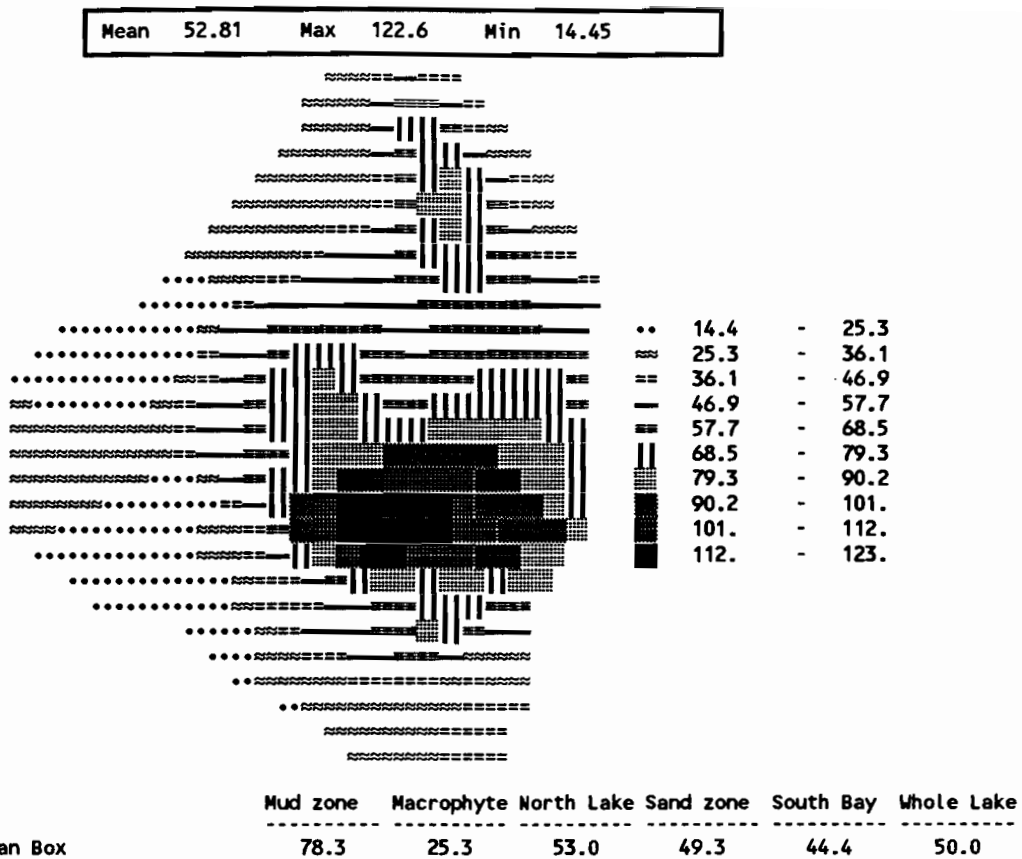


Figure 14-21 Lower layer losses for all algae species in kilograms.

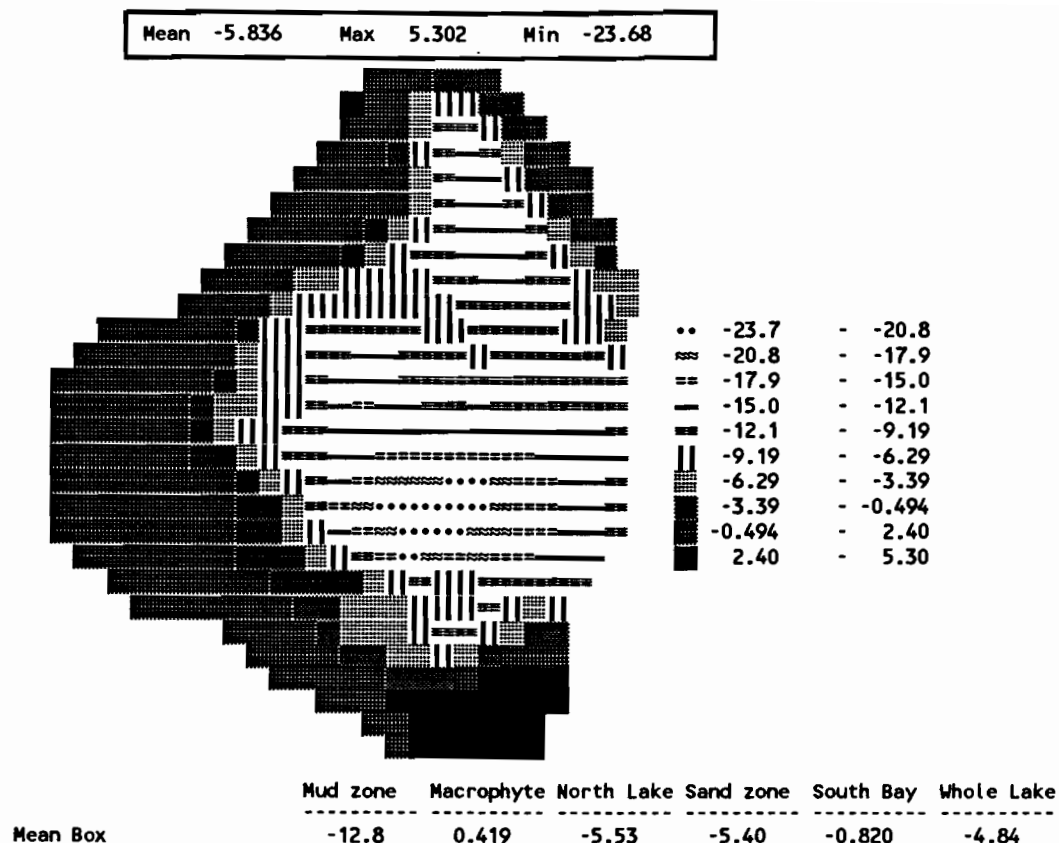


Figure 14-22 Total reaction change of zooplankton in kilograms.

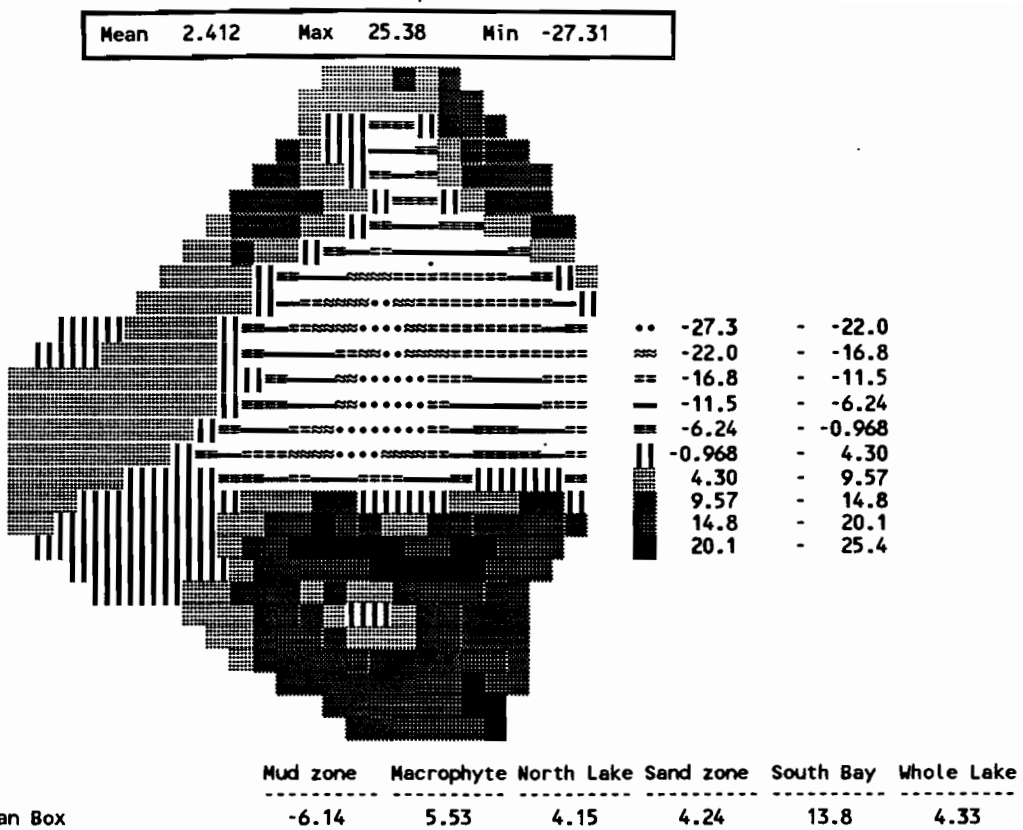


Figure 14-23 Total cell change of DOP in kilograms.

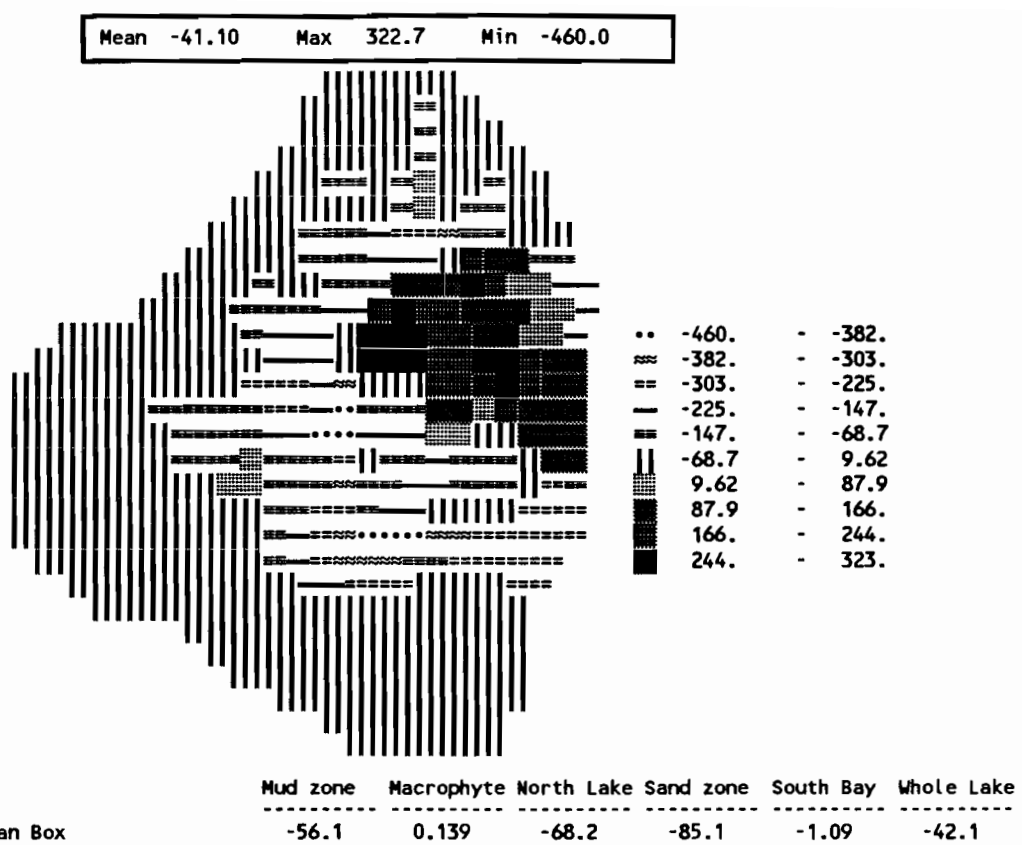


Figure 14-24 Total cell change of SED in kilograms.

Chlorophyll a concentrations (Figure 14-25) follow algal concentrations (Figures 14-15 and 14-16) closely as would be expected. Predicted Secchi depths (Figure 14-26) are highest in the quiescent macrophyte zone and lowest in the turbid mud zone.

There appears to be a "hot spot" of change above the rocky reef in the center of Lake Okeechobee. DOP is increasing at the edge of the lake and decreasing in the center of Lake Okeechobee (Figure 14-27). SRP and DOP move from the center of the lake to the perimeter following the mass flux of water (Figures 14-28 and 14-29). The greatest SRP reactions occur near the border of the mud zone and sand zone (Figure 14-30), while zooplankton reactions (Figure 14-31) follow the green and blue-green algae (Figures 14-15 and 14-16).

The diagenetic flux of PIP is primarily in the mud zone of Lake Okeechobee (Figures 14-32, 14-33 and 14-34). Similarly, the strongest adsorption occurs in the mud zone as well (Figures 14-35 and 14-36). Sediment (Figure 14-37) is deposited in the center of the mud zone and eroded in the perimeter of the mud zone (negative accumulation in Figure 14-37).

The flux of total phosphorus is greatest in "corners" subject to movement of lake currents (Figure 14-38), but otherwise does not exhibit strong spatial groupings. The flux of algae and zooplankton (Figures 14-39 and 14-40) occurs in the area of strongest gradient between the South Bay and central mud zone.

14.3.4 Water Depths

Water depths at the beginning of the simulation are shown in Figure 14-41. These are fairly typical of spring depths in Lake Okeechobee. An indication of the vertical "motion" of the lake can be obtained by comparing the thickness of the center cell (of five vertical layers) at the beginning (Figure 14-42) and end (Figure 14-43) of the simulation. There is almost no change in these values, the most noticeable being the decrease in the average thickness of the center (vertically) cells in the north lake from 19.0 cm to 18.9 cm. This 1 mm decrease corresponds to movement of water from the north lake into the remainder of Lake Okeechobee. In other words, this simulation period did not correspond to significant changes in lake volumes and depths. Hence, changes in simulated parameters are due primarily to reactions, as would be expected anyway in finite-difference grids 2 km on a side.

14.4 Three-Month Simulation

A joint effort between the UF Coastal and Oceanographic Engineering Department (UF COE) and UF Environmental Engineering Sciences Department (UF ENV) produced a three-month simulation using the combined EHMS3D and LOP3D models (Sheng et al., 1991b). The simulation time period began in April 1989 during the synoptic surveys and lasted until July 24, 1989 using monitored in situ winds and loads. Synoptic survey data were thus available for comparison with approximately the first five weeks of the simulation. Wind data from one or more of the five UF COE lake stations (Figure 14-1) were used to

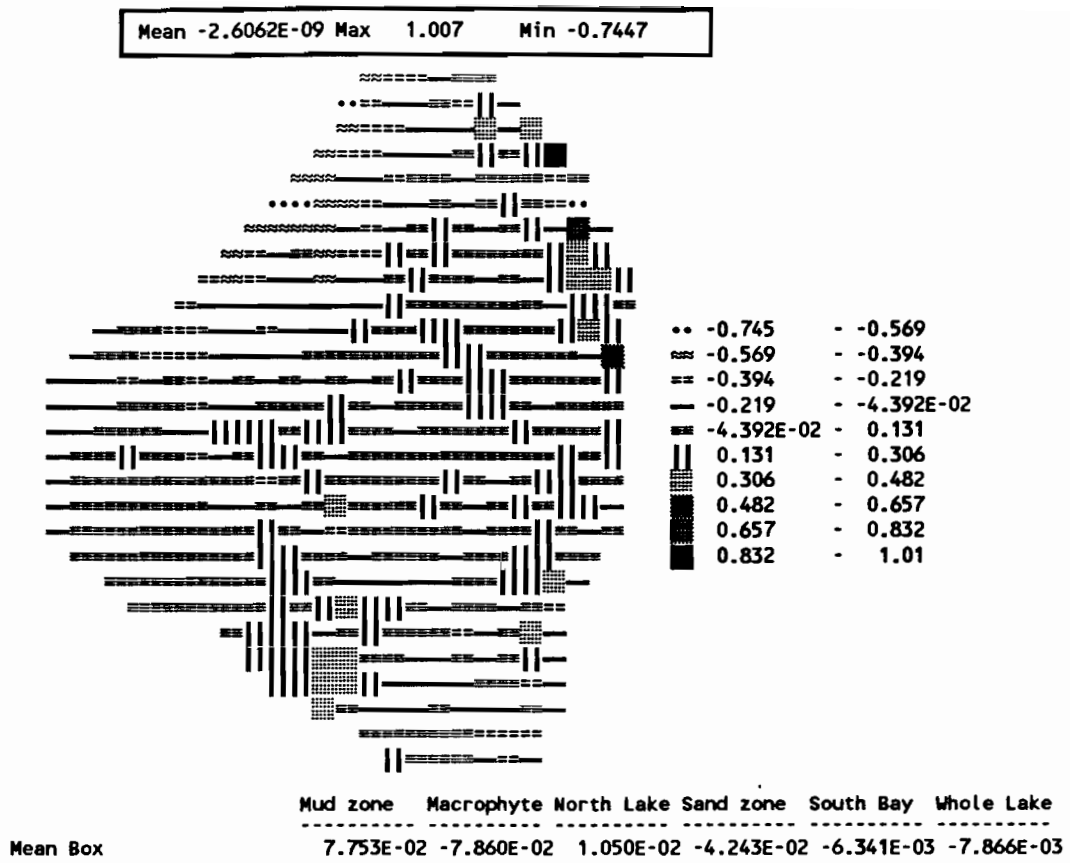


Figure 14-25 Total mass flux of TP in an I,J center cell.

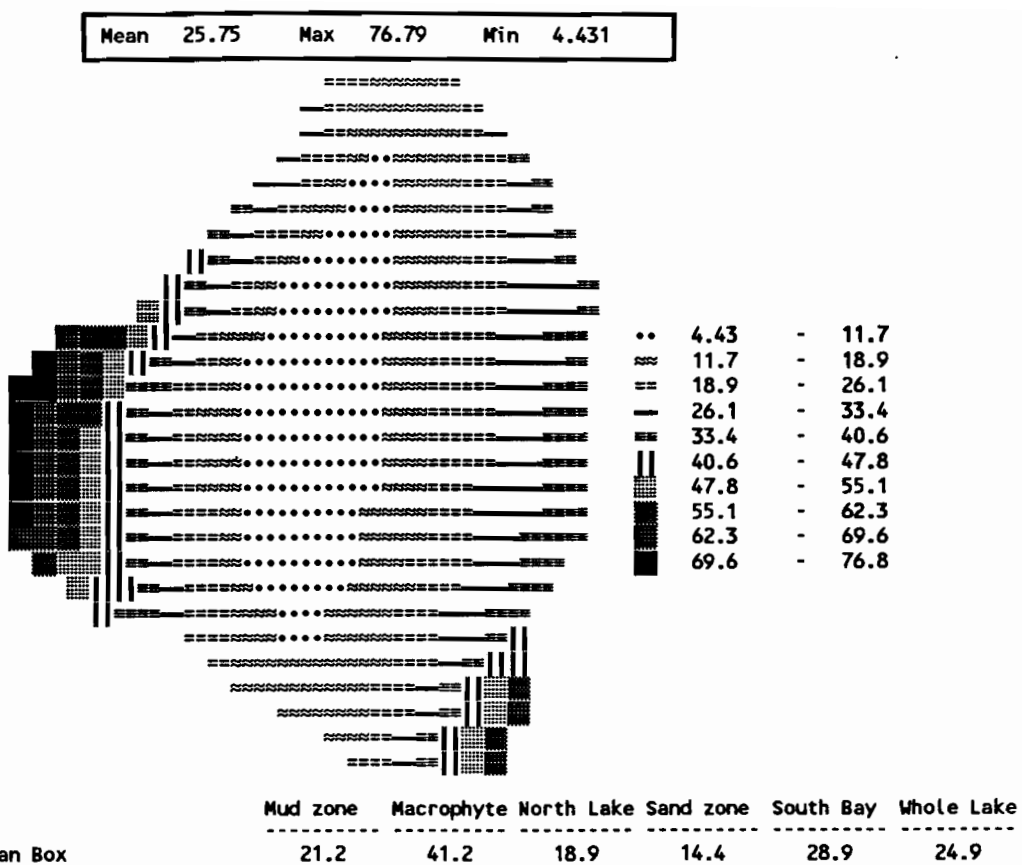


Figure 14-26 Total adjusted thickness (cm) of cell at end of simulation.

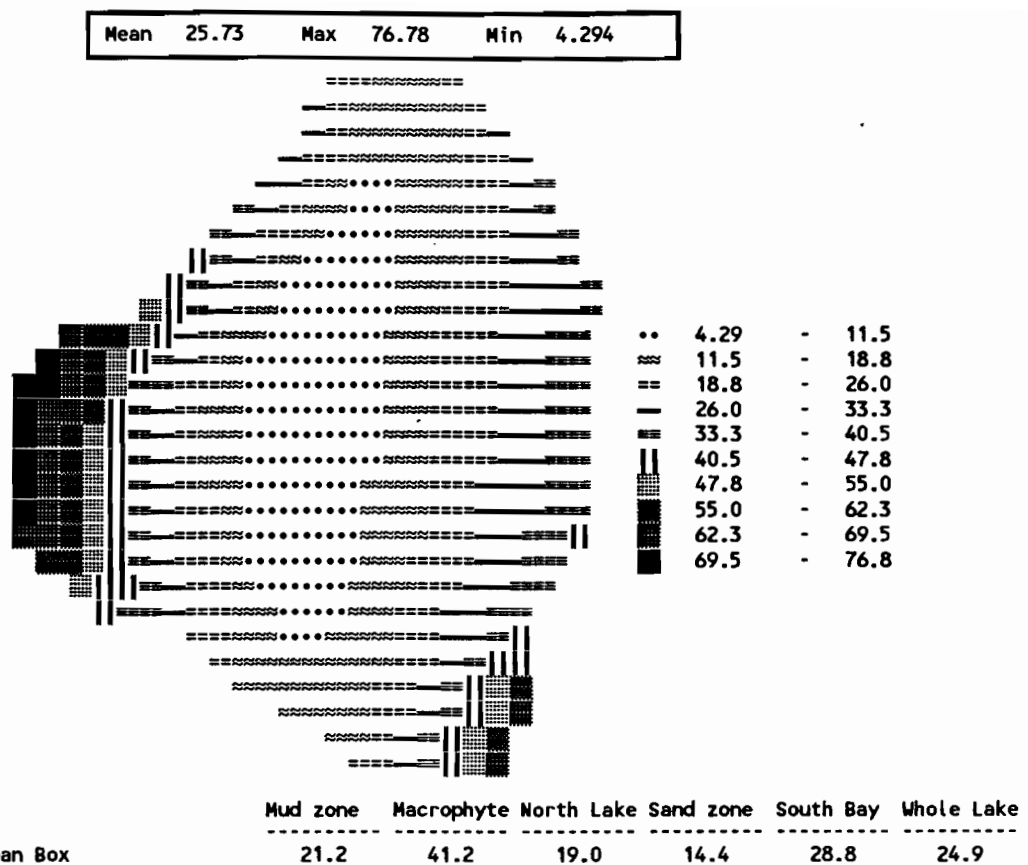


Figure 14-27 Total original thickness (cm) of center cell.

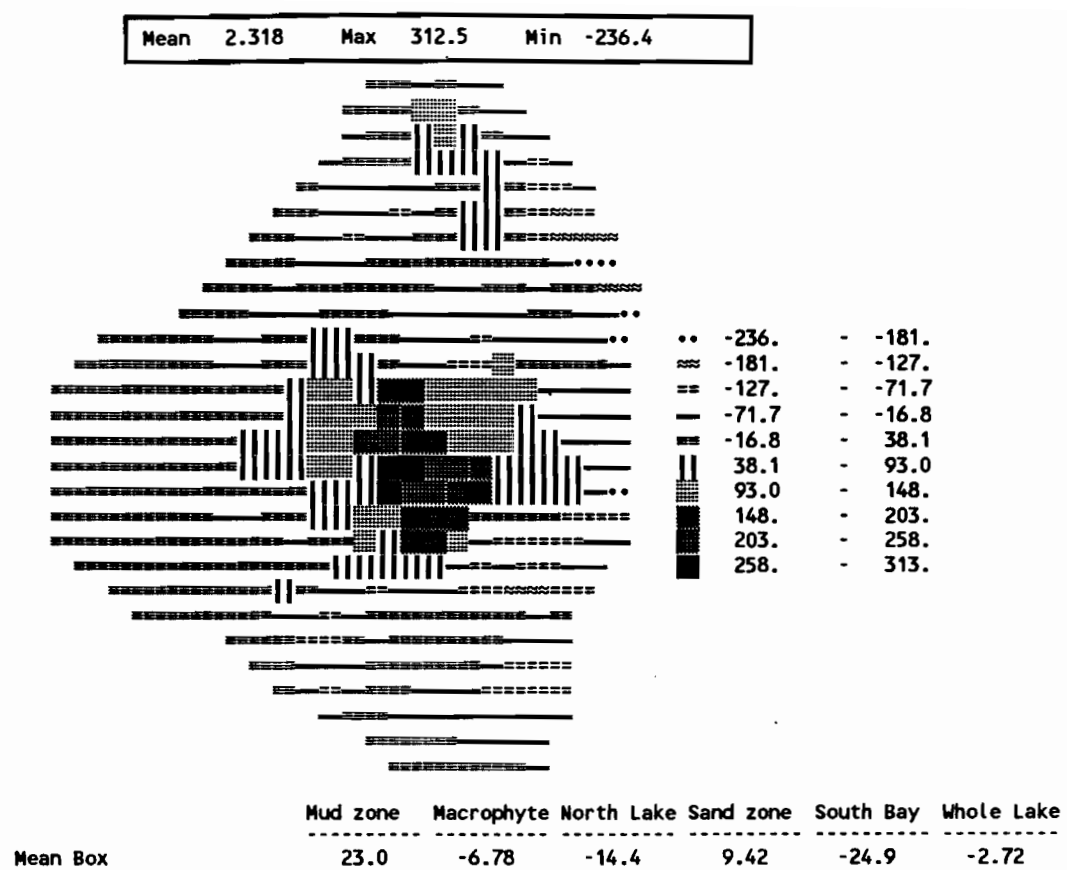


Figure 14-28 Total advection-diffusion SRP change in kilograms.

Mean 0.2653 Max 319.9 Min -216.4

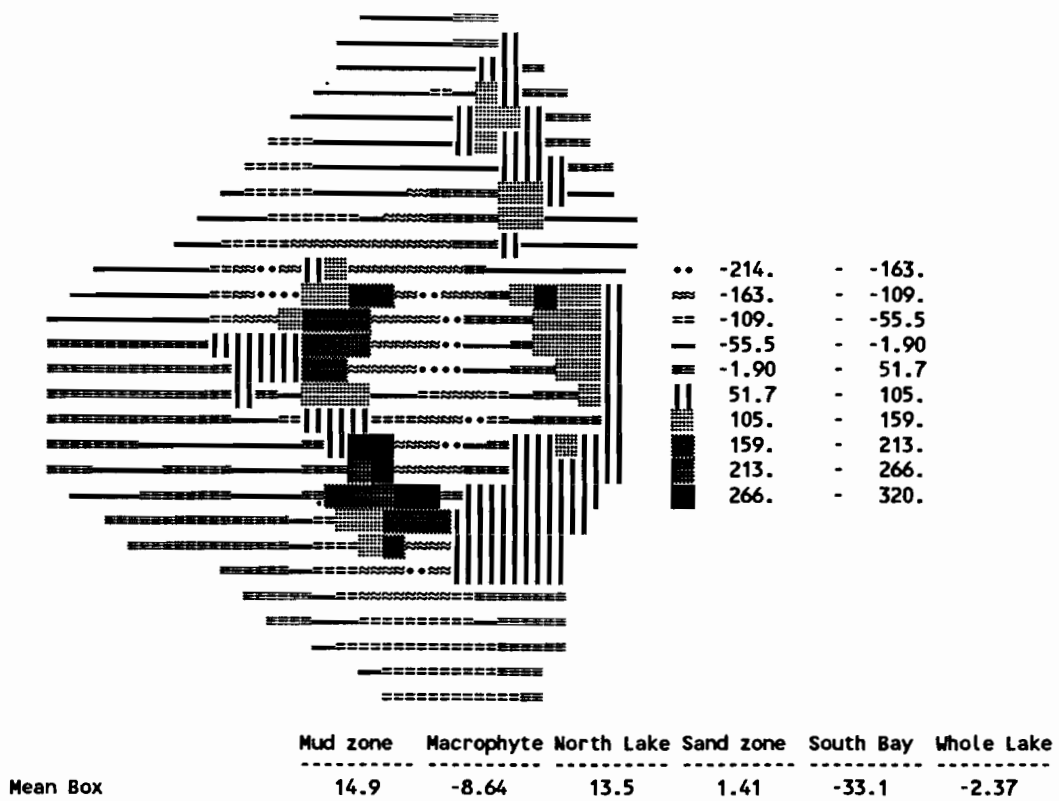


Figure 14-29 Total advection-diffusion DOP change in kilograms.

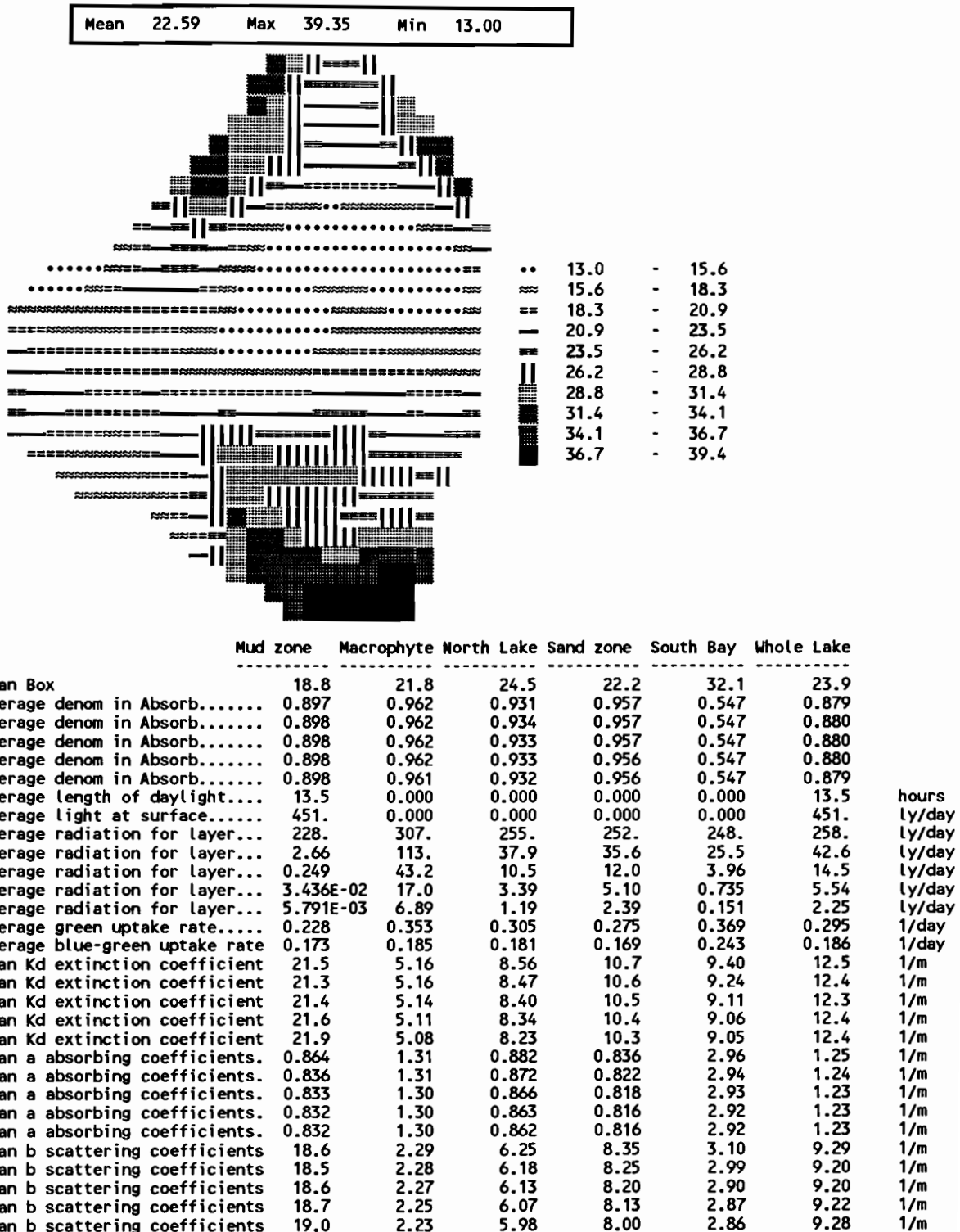


Figure 14-30 Predicted chlorophyll a in ug/l.

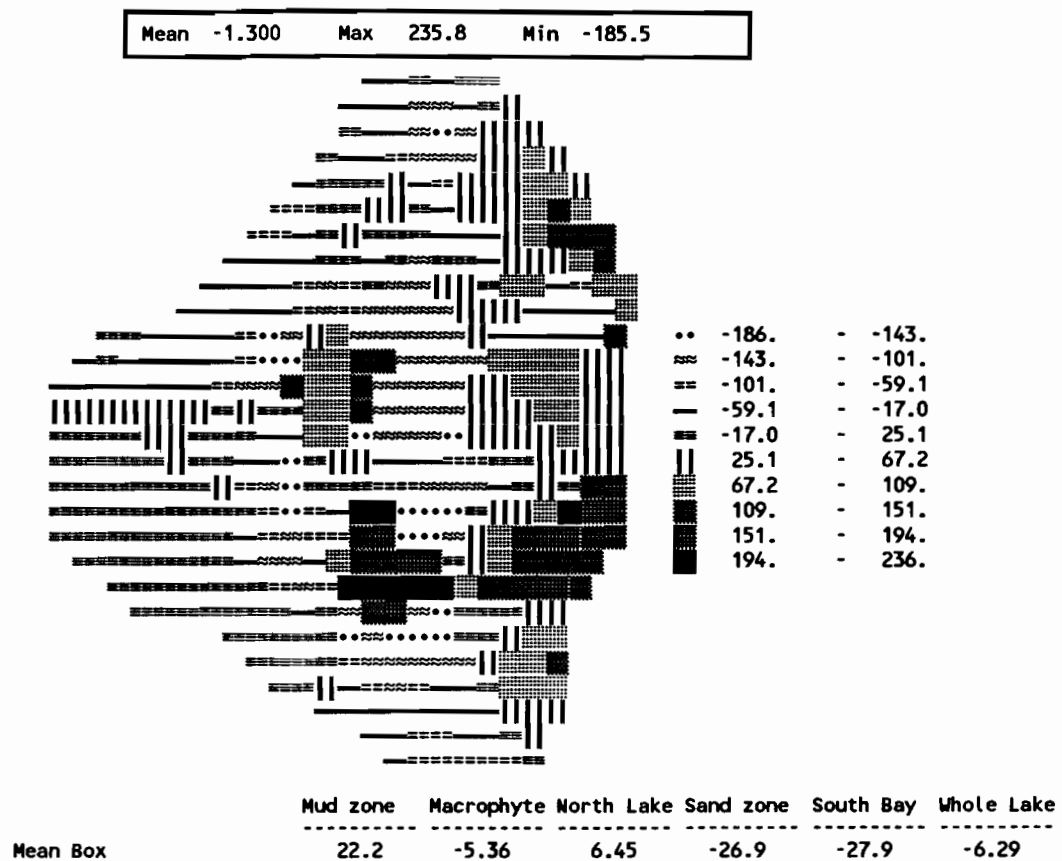


Figure 14-31 Total advection-diffusion algae change in kilograms.

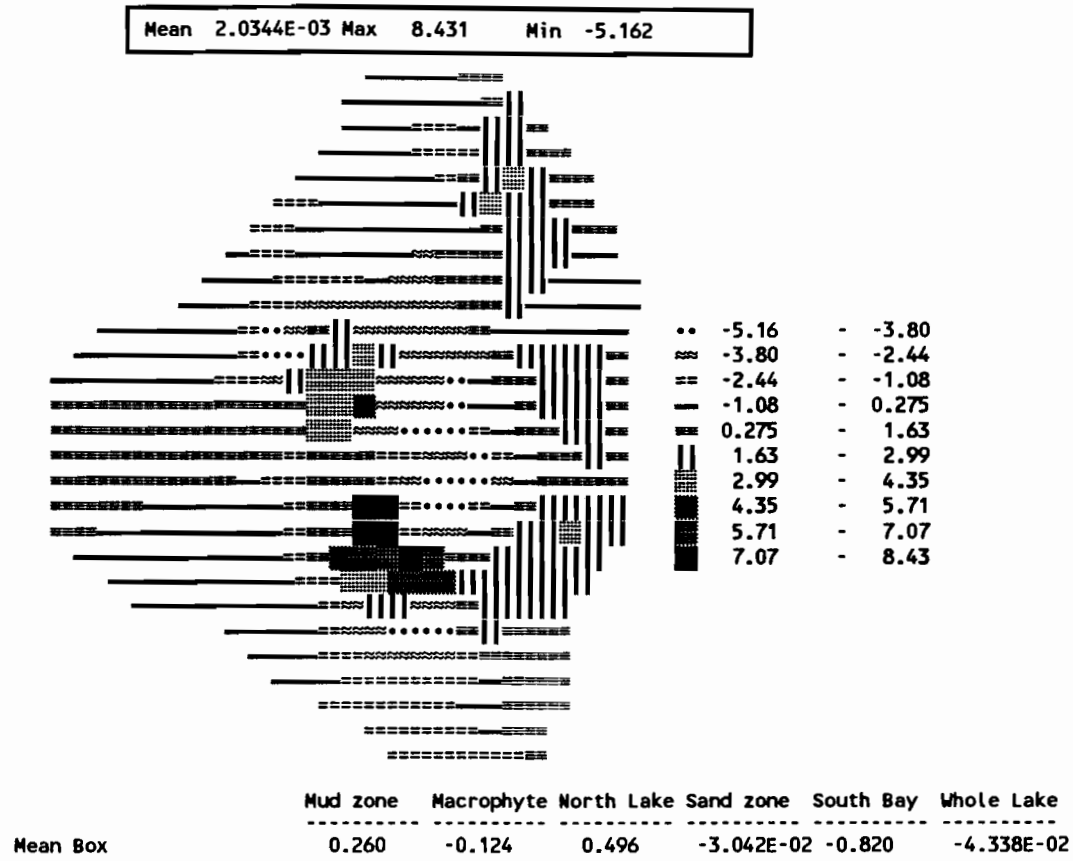


Figure 14-32 Total advection-diffusion ZOO change in kilograms.

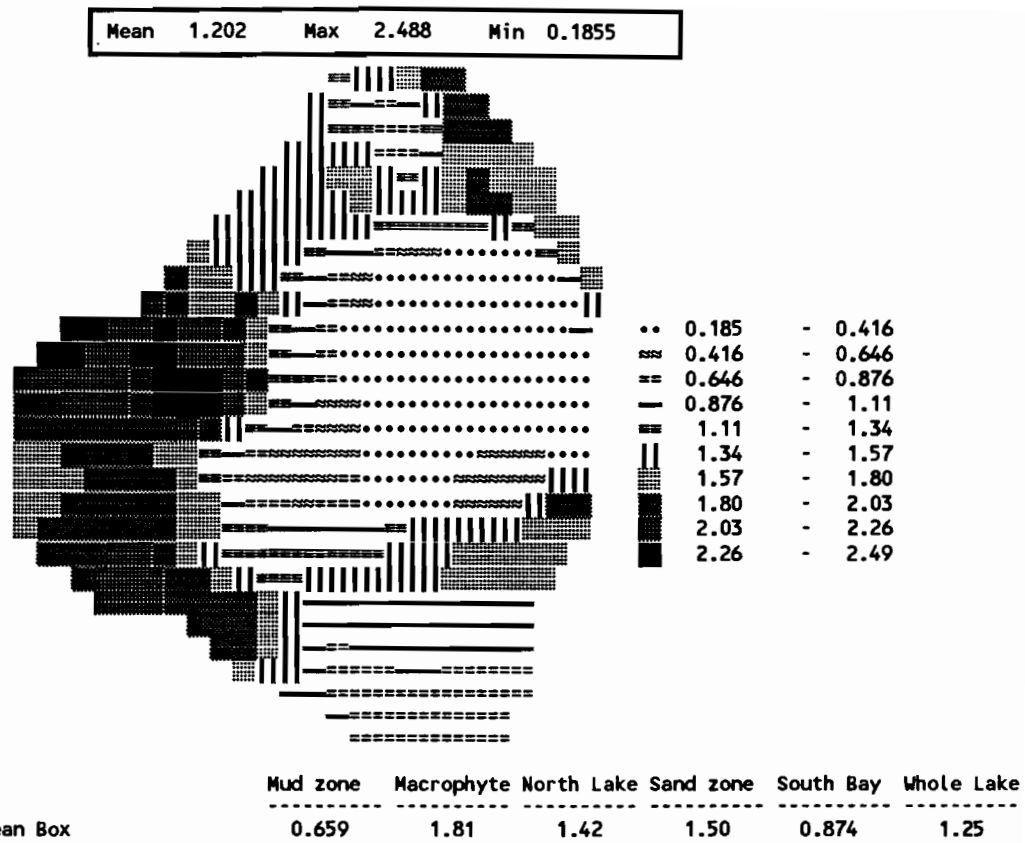


Figure 14-33 Predicted Secchi depth, meters.

Mean	20.53	Max	171.8	Min	-176.0
------	-------	-----	-------	-----	--------

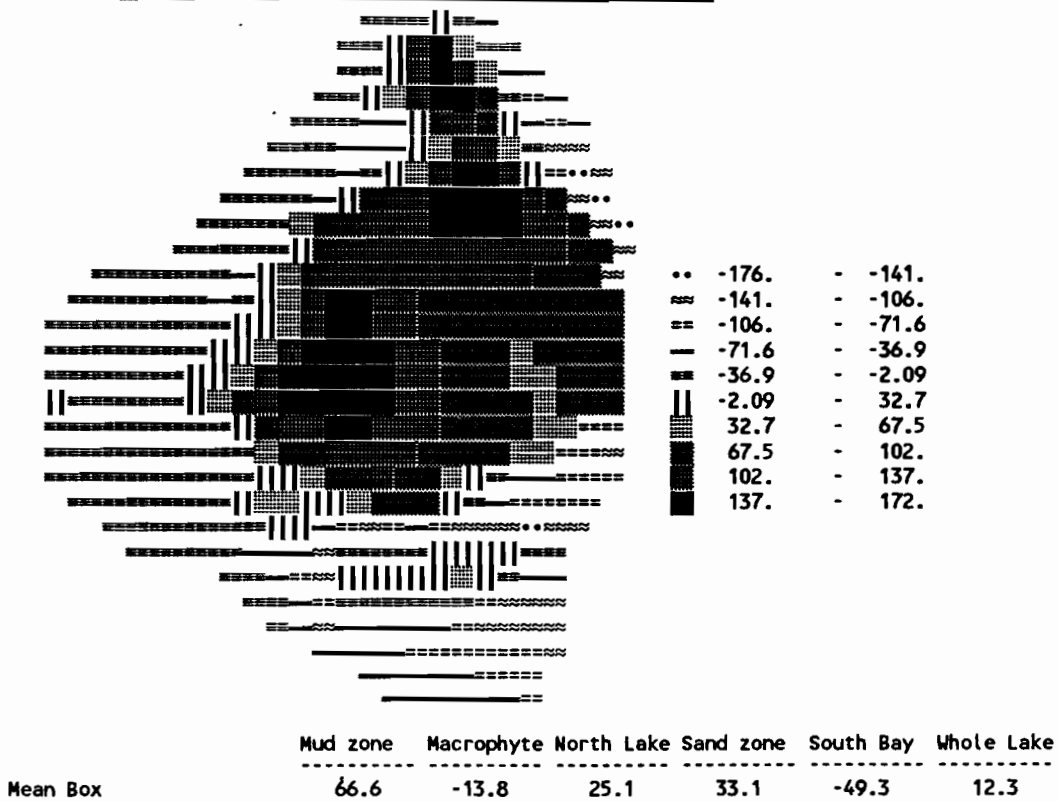


Figure 14-34 Total reaction SRP change in kilograms.

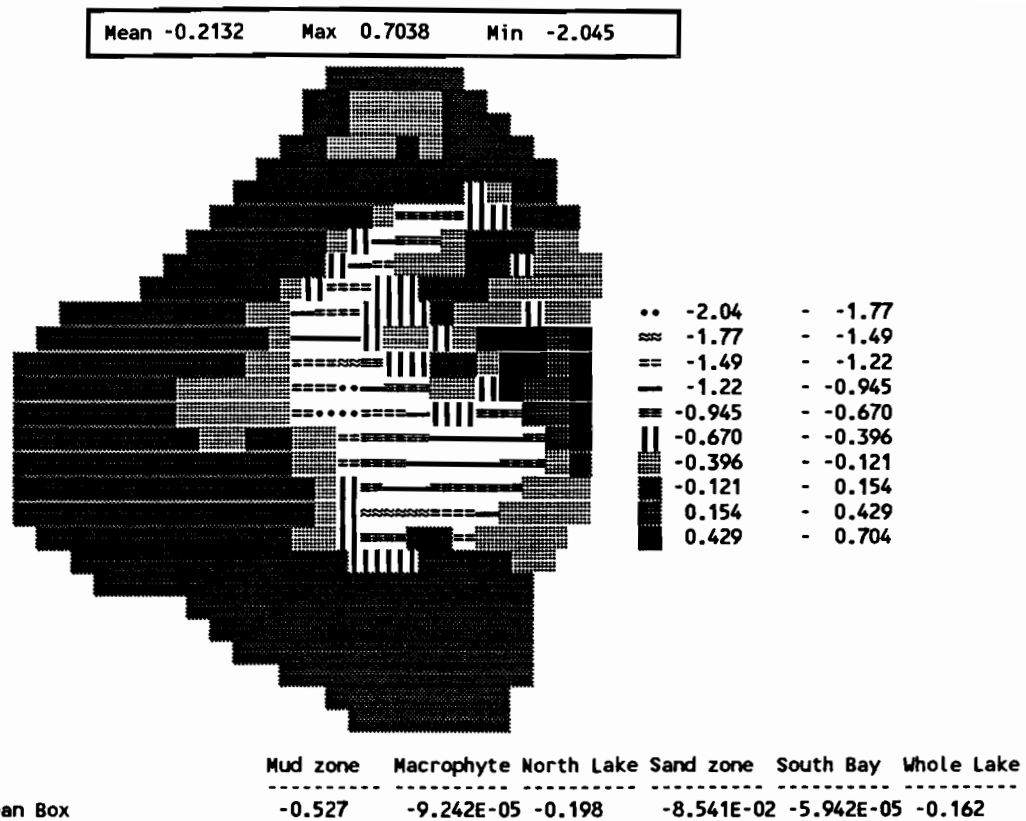


Figure 14-35 Upper layer adsorption in kilograms.

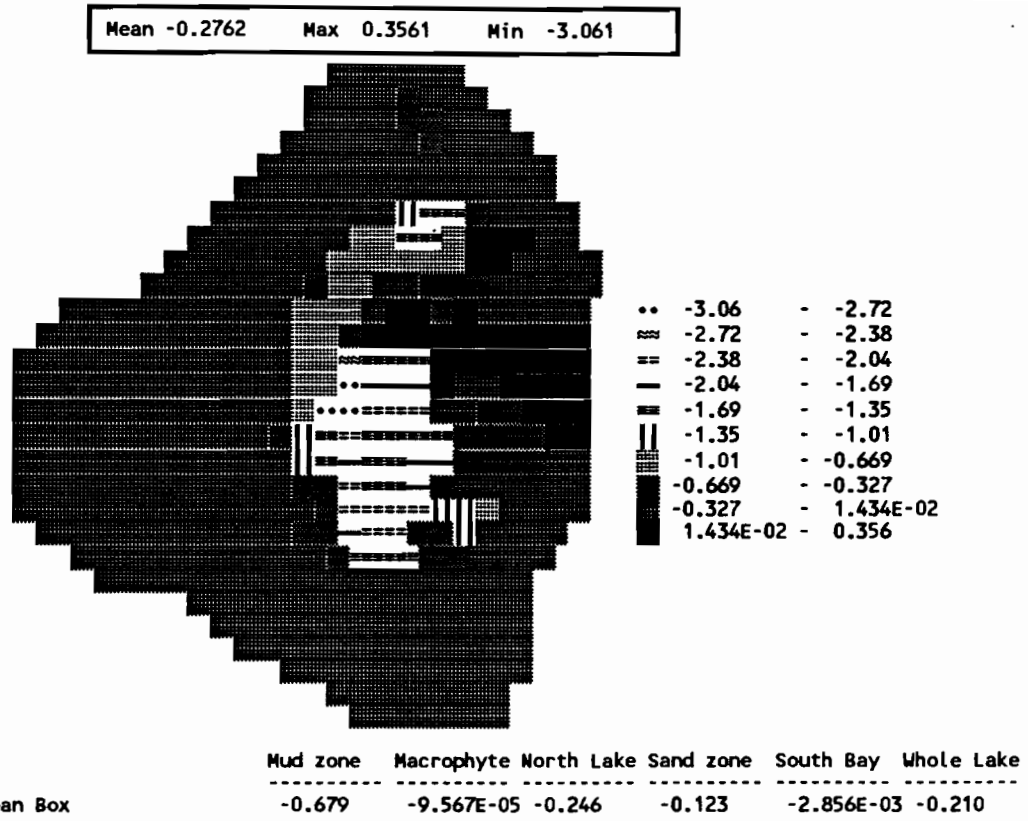


Figure 14-36 Lower layer adsorption in kilograms.

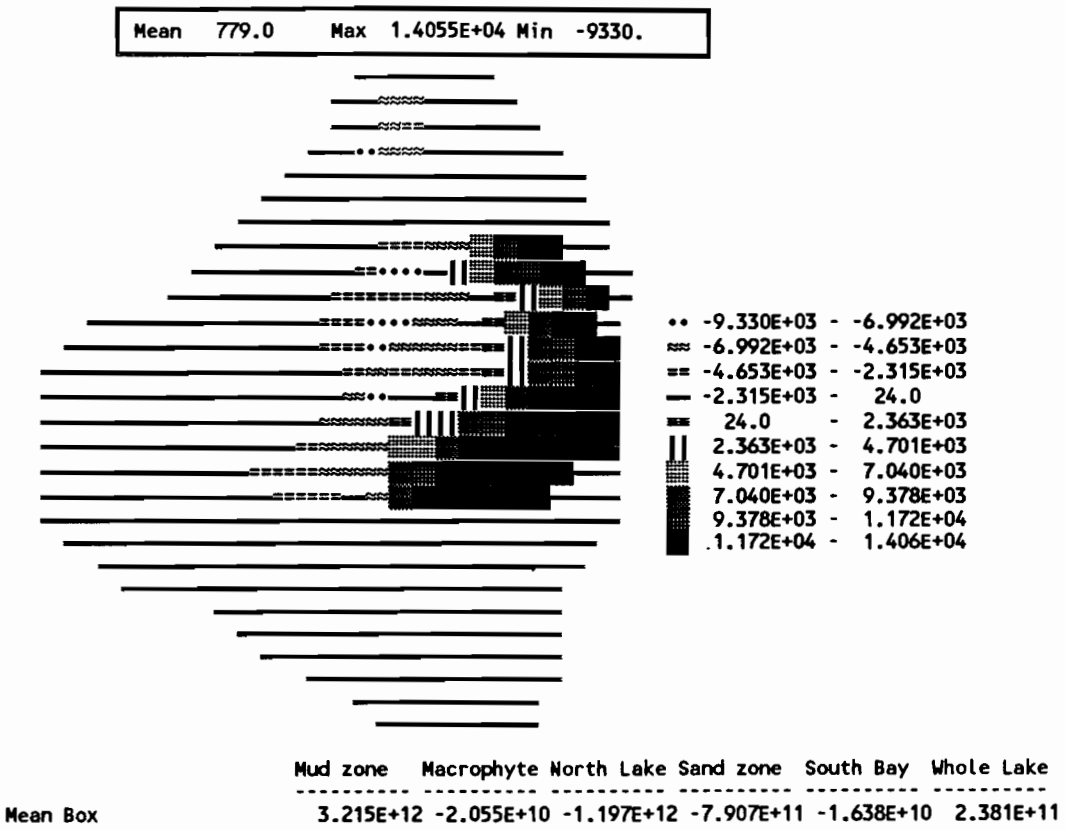


Figure 14-37 Total sediment organic flux in kilograms.

Mean 0.3938 Max 0.8839 Min 1.8913E-11

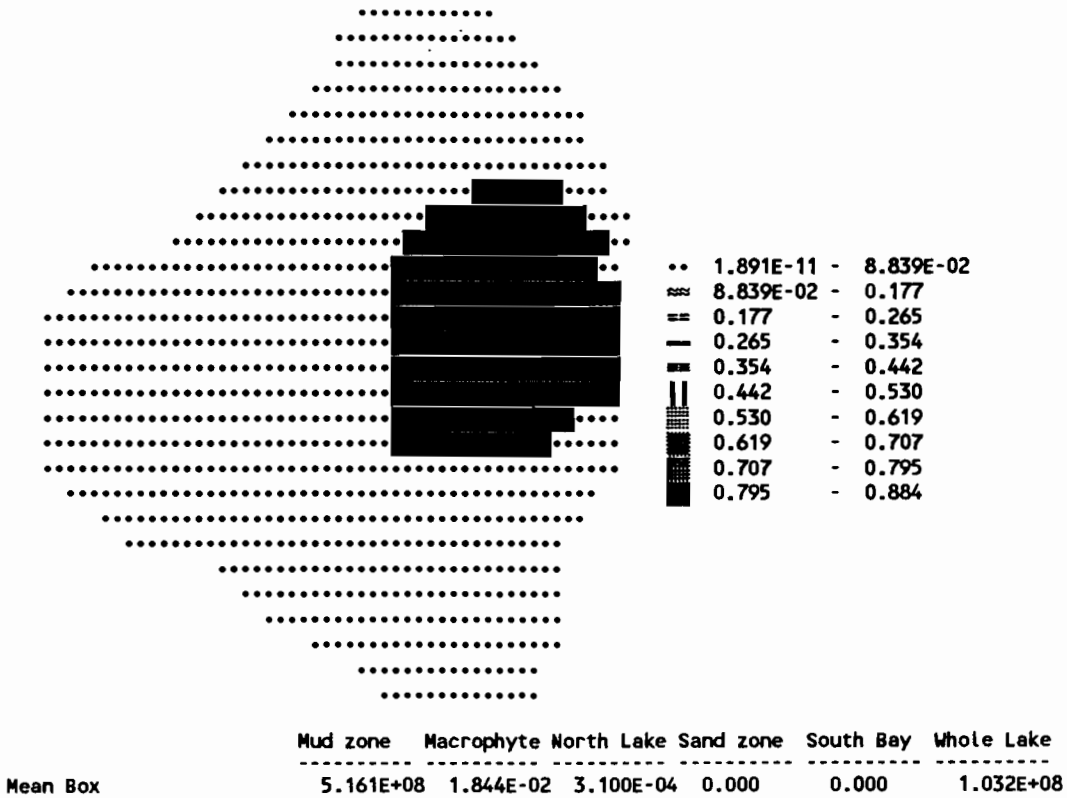


Figure 14-38 Total PIP flux from sediment to pelagic in kilograms.

Mean 1.6785E-04 Max 2.9300E-03 Min 2.7693E-24

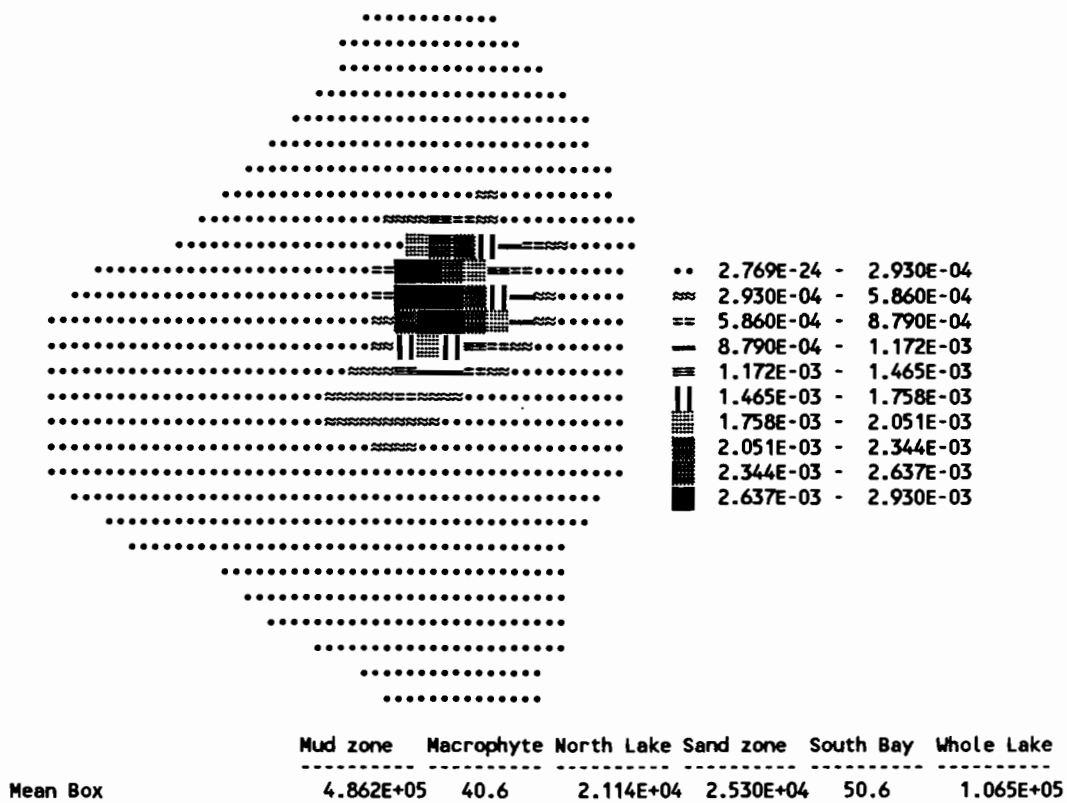
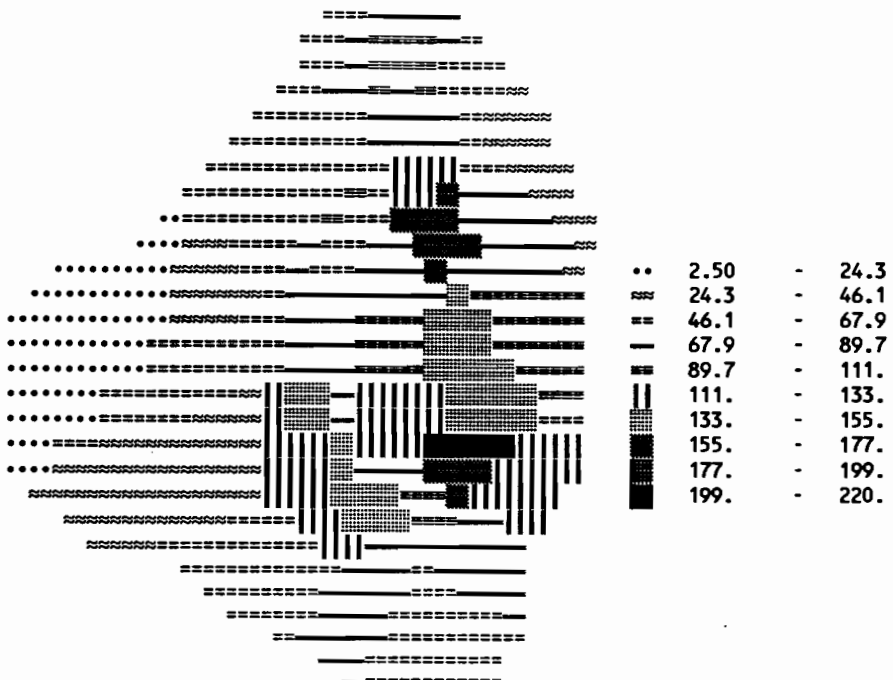


Figure 14-39 Total PIP flux from pelagic to sediment in kilograms.

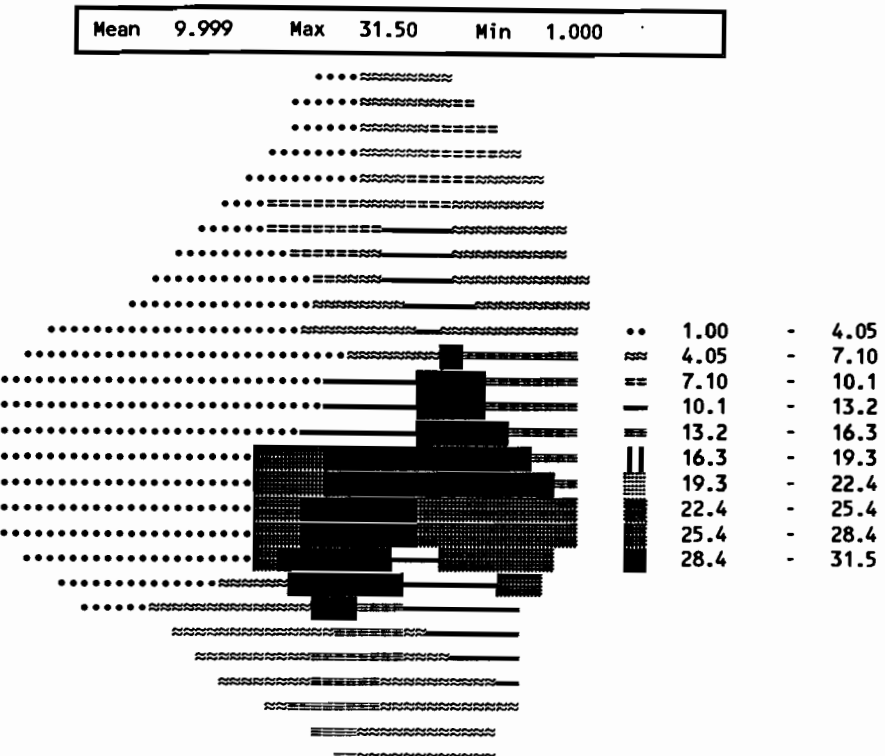
Mean	72.37	Max	220.5	Min	2.500
------	-------	-----	-------	-----	-------



	Mud zone	Macrophyte	North Lake	Sand zone	South Bay	Whole Lake
--	----------	------------	------------	-----------	-----------	------------

	Mud zone	Macrophyte	North Lake	Sand zone	South Bay	Whole Lake
Mean Box	111.	31.9	70.7	59.2	69.2	68.3
Layer 5 Total P	104.633	30.134	68.008	57.015	66.606	
Layer 4 Total P	107.663	31.014	69.360	58.094	67.896	
Layer 3 Total P	110.692	31.894	70.711	59.174	69.186	
Layer 2 Total P	113.722	32.774	72.062	60.253	70.477	
Layer 1 Total P	116.752	33.654	73.413	61.332	71.767	
Layer 5 ZOO	0.385	0.242	0.435	0.406	0.503	
Layer 4 ZOO	0.380	0.244	0.438	0.414	0.516	
Layer 3 ZOO	0.375	0.245	0.441	0.421	0.529	
Layer 2 ZOO	0.371	0.247	0.444	0.428	0.542	
Layer 1 ZOO	0.366	0.249	0.447	0.435	0.555	
Layer 5 PIP	0.348	0.000	0.207	0.052	0.002	
Layer 4 PIP	0.370	0.000	0.202	0.058	0.002	
Layer 3 PIP	0.393	0.000	0.197	0.065	0.002	
Layer 2 PIP	0.415	0.000	0.192	0.072	0.002	
Layer 1 PIP	0.438	0.000	0.187	0.079	0.003	
Layer 5 OrgP-Sed	44.011	0.000	13.553	2.575	0.105	
Layer 4 OrgP-Sed	46.424	0.000	13.237	2.910	0.111	
Layer 3 OrgP-Sed	48.838	0.000	12.922	3.246	0.116	
Layer 2 OrgP-Sed	51.251	0.000	12.606	3.582	0.121	
Layer 1 OrgP-Sed	53.665	0.000	12.290	3.917	0.127	
Layer 5 Sediment	25.447	0.000	20.672	12.620	0.515	
Layer 4 Sediment	27.557	0.000	19.980	14.266	0.542	
Layer 3 Sediment	29.668	0.000	19.287	15.911	0.568	
Layer 2 Sediment	31.778	0.000	18.594	17.557	0.595	
Layer 1 Sediment	33.888	0.000	17.902	19.203	0.621	

Figure 14-40 Measured TP synoptic concentrations in ug/l on day 89154.



		Mud zone	Macrophyte	North Lake	Sand zone	South Bay	Whole Lake
Mean Box		17.6	2.86	6.36	7.75	10.4	8.99
Layer 5	SRP	15.466	1.950	3.492	7.190	11.106	
Layer 4	SRP	16.530	2.405	4.926	7.468	10.754	
Layer 3	SRP	17.593	2.861	6.361	7.747	10.402	
Layer 2	SRP	18.657	3.317	7.795	8.025	10.049	
Layer 1	SRP	19.720	3.773	9.230	8.304	9.697	
Layer 5	DOP	25.572	16.092	28.985	26.884	30.249	
Layer 4	DOP	25.338	16.428	29.077	26.982	31.238	
Layer 3	DOP	25.105	16.764	29.169	27.080	32.227	
Layer 2	DOP	24.872	17.100	29.261	27.178	33.216	
Layer 1	DOP	24.638	17.436	29.353	27.276	34.205	
Layer 5	Greens	7.310	4.595	8.273	7.720	9.554	
Layer 4	Greens	7.220	4.629	8.329	7.857	9.801	
Layer 3	Greens	7.130	4.662	8.384	7.994	10.047	
Layer 2	Greens	7.040	4.696	8.439	8.131	10.293	
Layer 1	Greens	6.950	4.729	8.494	8.268	10.539	
Layer 5	Blues	11.542	7.255	13.063	12.189	15.086	
Layer 4	Blues	11.400	7.308	13.150	12.405	15.475	
Layer 3	Blues	11.258	7.361	13.238	12.621	15.864	
Layer 2	Blues	11.116	7.414	13.325	12.838	16.252	
Layer 1	Blues	10.974	7.467	13.412	13.054	16.641	

Figure 14-41 Measured SRP synoptic concentrations in ug/l on day 89154.

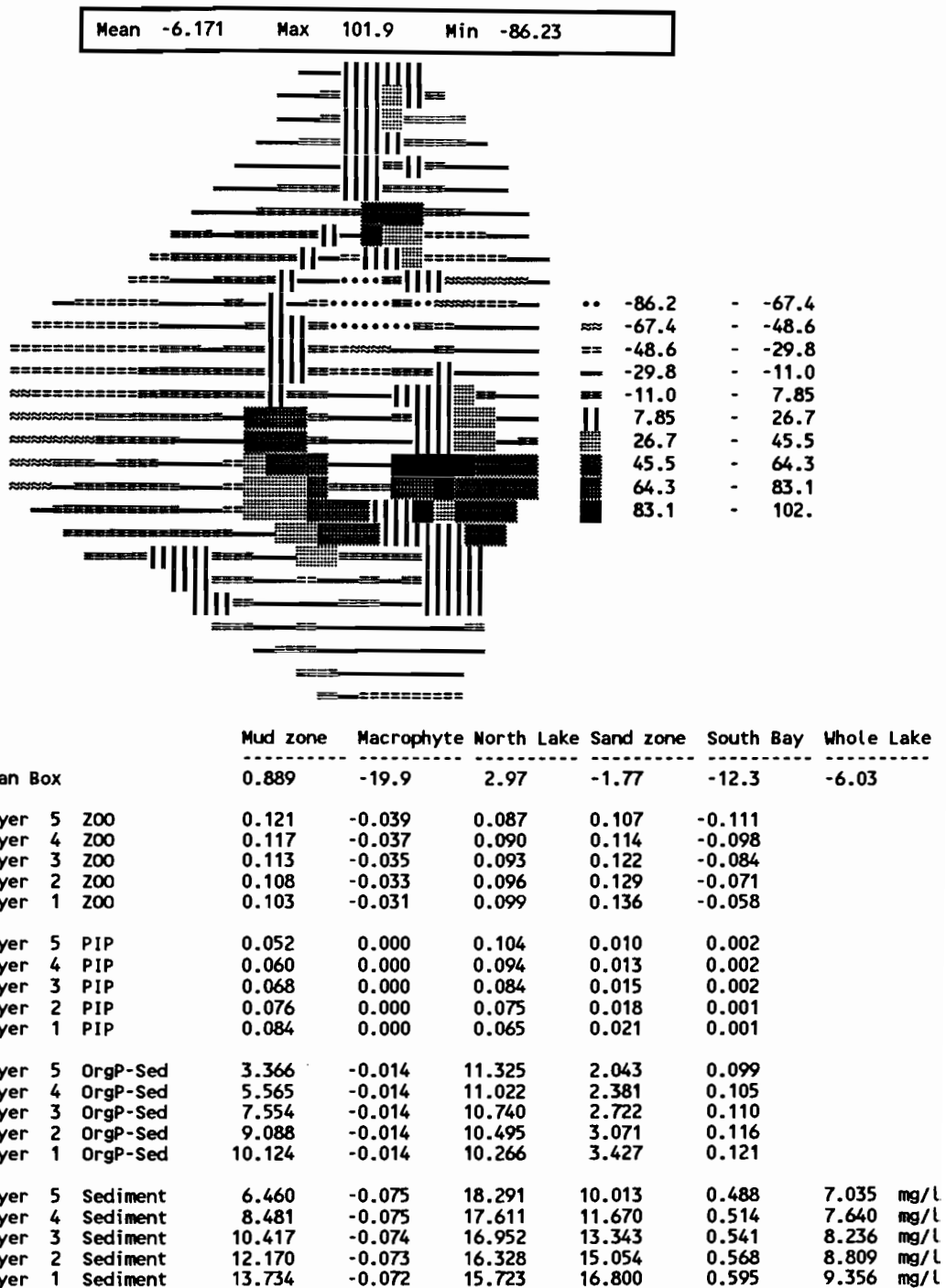
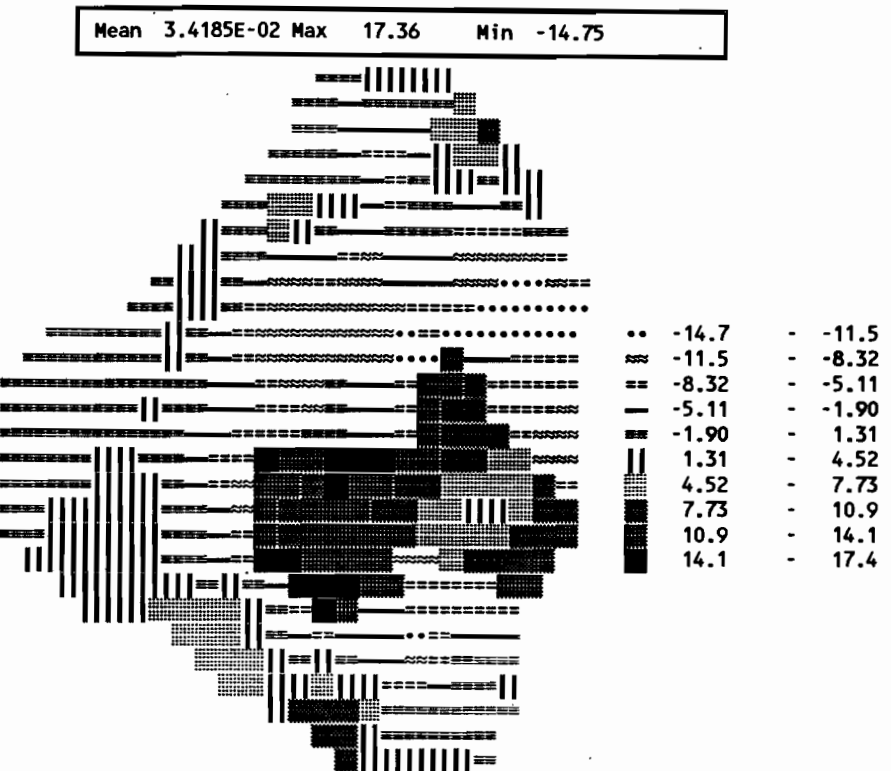


Figure 14-42 Ending TP concentration differences in ug/l.



	Mud zone	Macrophyte	North Lake	Sand zone	South Bay	Whole Lake
Mean Box	-0.397	1.30	-0.977	-0.130	-5.879E-02	-5.322E-02
Layer 5 SRP	0.181	0.600	-2.296	0.927	3.367	
Layer 4 SRP	-1.656	1.048	-1.803	0.212	1.501	
Layer 3 SRP	-1.135	1.430	-1.250	-0.539	-0.900	
Layer 2 SRP	-0.193	1.635	-0.335	-0.683	-1.900	
Layer 1 SRP	0.816	1.769	0.799	-0.568	-2.362	
Layer 5 DOP	-5.297	-12.217	-4.467	-3.302	-8.395	
Layer 4 DOP	-5.515	-11.879	-4.364	-3.195	-7.400	
Layer 3 DOP	-5.750	-11.540	-4.257	-3.087	-6.400	
Layer 2 DOP	-5.988	-11.200	-4.155	-2.984	-5.408	
Layer 1 DOP	-6.224	-10.860	-4.057	-2.884	-4.420	
Layer 5 Greens	-1.381	-7.447	-4.224	-3.859	-6.278	
Layer 4 Greens	-0.307	-7.411	-3.763	-3.312	-5.490	
Layer 3 Greens	-0.123	-7.354	-3.234	-2.619	-4.167	
Layer 2 Greens	-0.157	-7.192	-2.884	-2.214	-3.498	
Layer 1 Greens	-0.225	-6.950	-2.633	-1.970	-3.183	
Layer 5 Blues	-1.038	-2.596	-0.266	0.142	-3.519	
Layer 4 Blues	0.531	-2.536	0.357	0.937	-2.171	
Layer 3 Blues	0.645	-2.432	0.853	1.622	-0.831	
Layer 2 Blues	0.559	-2.256	1.168	1.994	-0.227	
Layer 1 Blues	0.443	-2.092	1.362	2.266	0.198	

Figure 14-43 Ending SRP concentration differences in ug/l.

drive the resuspension algorithms. Inflow concentrations were interpolated from daily flows and semi-monthly phosphorus measurements. Chlorophyll *a* was predicted assuming a 1:1 ratio with algae. Finally, a loading/no-loading scenario was run to evaluate the relative impact of inflows to the lake.

This combination of the UF COE and ENV models is essentially the product delivered to the SFWMD as a result of this project. The results are presented in detail by Sheng et al. (1991c). Briefly, paraphrasing these authors, the sediment flux of organic phosphorus from the sediments was substantial and overwhelms the contribution from any other source on a daily basis. But over a 3-month period the net flux of deposited and eroded organic phosphorus on the suspended sediment rivals the algal uptake, algal decay, and dissolved organic phosphorus transformation pathways in total mass flux. The SRP concentration in the northern end of the lake is much higher in the loading scenario than in the no-load scenario, consistent with chlorophyll *a* evidence of Jones and Federico (1984).

Thus, the detailed 3-D transient models can realistically be used to for predictive purposes. A useful manner in which to operate would be to perform broad scale evaluations using the long-term LOP0D model, followed by EHMS3D/LOP3D simulations for detailed evaluation and possible design criteria.

14.5 Sensitivity

The most sensitive parameters of the 3-D model are the uptake parameters of the green and blue-green algae. The respiration and excretion parameters of SRP, DOP, and the algal components are slightly less sensitive based on the total mass change of the phosphorus components. The least sensitive parameters are the zooplankton and sorption-desorption parameters.

Associated physical parameters that affect uptake are important in the five layer model. Light shading by sediment and self shading by algae are very important since the different light conditions in the five layers shift algal uptake to the top two or three layers.

14.6 Summary

The three-dimensional, transient LOP3D model includes advection, diffusion and reaction of seven phosphorus species that total to TP. It relies for its transport calculations for hydrodynamic and sediment input from the UF COE EHSM3D model. The mathematical and finite difference formulation and testing is described in Chapters 10 and 11. Reactions are discussed in Chapter 12 and additionally in Chapter 13. Reactions tend to dominate the predictive calculations for simulations on the order of one week, as for the results described in this chapter.

When compared on a grid cell by grid cell basis, measured and predicted TP and SRP concentrations show a broad spatial agreement, with local differences. When compared on a lake sub-area basis (e.g., mud zone, South Bay, etc.), agreement between measured and

predicted SRP concentrations is remarkably good. Agreement for TP is similarly good with the exception of the South Bay and macrophyte areas, for which TP is over-predicted. It is clearly difficult to include all possible phosphorus mechanisms and pathways into any model. Moreover, the input data for a model of this detail are necessarily sparse (i.e., concentration data are interpolated into 496 cells from about 25 locations, and meteorological data are interpolated from only 5 or 6 in-lake locations (Figure 14-1). Thus, given the complexities of this level of modeling, the agreement between predicted and measured TP and SRP concentrations is good. Nonetheless, there will be ample opportunity for model improvement in the hands of the South Florida Water Management District.

REFERENCES

Note: This reference list is incomplete. Missing references (indicated by "TBA") will be obtained as soon as possible and an updated reference list supplied to report recipients. WCH 7/16/92

- Achen, C.H., 1982. *Interpreting and Using Regression*, Sage Publications, Series/Number 07-029, Beverly Hills, CA.
- Adelaja, C.M. and E.E. Adams, 1990. *Comparison of Cooling Lake Mathematical Models for Mount Storm Lake*, MIT Ralph M. Parsons Laboratory Technical Report Technical Report No. 328, Cambridge, MA.
- Agusti, S., 1991. "Light Environment Within Dense Algal Populations: Cell Size Influences on Self-Shading," *Journal of Plankton Research*, 13(4):863-871.
- Ahl, T., 1988. "Background Yield of Phosphorus from Drainage Area and Atmosphere: An Empirical Approach," *Hydrobiologia*, 170:34-44.
- Ahlgren, G., 1988. "Phosphorus as Growth-Regulating Factor Relative to Other Environmental Factors in Cultured Algae," *Hydrobiologia*, 170:191-210.
- Ahlgren I, T. Frisk and L. Kamp-Nielson, 1988. "Empirical and Theoretical Models of Phosphorus Loading, Retention and Concentration vs. Lake Trophic State," *Hydrobiologia*, 170:285-303.
- Ambrose, R.B., S. A. Vandergrift and T.A. Wool, 1986. *WASP3, A Hydrodynamic and Water Quality Model -- Model Theory, User's Manual, and Programmers Guide*. EPA-600/3-86-034, Athens, GA, September.
- Anderson, E.R., 1954. "Energy Budget Studies," in *Water Loss Investigations - Lake Hefner Studies*, USGS Prof. Paper 269, Washington, DC.
- Anderson, G., W. Graneli and J. Stenson, 1988. "The Influence of Animals on Phosphorus Cycling in Lake Ecosystems," *Hydrobiologia*, 170:267-284.
- Babajiimopoulos and Papadopoulos, 1968. ***TBA
- Baker, L.A., P.L. Brezonik and C.R. Kratzer, 1981. *Nutrient Loading-Trophic State Relationships in Florida Lakes*, Publication No. 56, Water Resources Research Center, University of Florida, Gainesville.
- Balling, R.C. and R. S. Cerveny, 1983. "Spatial and Temporal Variations in Long-Term Normal Percent Possible Solar Radiation Levels in the United States," *Journal of Climate and Applied Meteorology*, 22:1726-1732.

- Bannister, T.T., 1990. "Empirical Equations Relating Scalar Irradiance to a, b/a, and Solar Zenith Angle," *Limnol. Oceanogr.*, 35(1):173-177.
- Banse, K. 1975. "Rates of Growth, Respiration and Photosynthesis of Unicellular Algae as Related to Cell Size," *J. Phycol.*, 12:135-140.
- Barholic J.F., Bill R.G. and L.H. Allen Jr., 1978. *Measurement of Evaporation From Lake and Ponds in Florida*, Publication No. 43, Water Resources Research Center, University of Florida, Gainesville, September.
- Barica, J. and R.J. Allan, 1988. "Utility of Soluble Reactive Phosphorus Measurements in Great Lakes Surveillance Programs: A Summary," *J. Great Lakes Research*, 14(3):377-379.
- Barnstan et al., 1983. ***TBA
- Beaver, J.R., T. L. Crisman and J. S. Bays, 1981. "Thermal Regimes of Florida Lakes," *Hydrobiologia*, 83:267-273.
- Beck, M.B., 1985. *Water Quality Management: A Review of the Development and Application of Mathematical Models*, Springer-Verlag, New York.
- Berner, 1980. ***TBA
- Berseneva, 1984. ***TBA
- Bierman, V.J., D.M. Dolan, E.F. Stoermer, J.E. Gannon and V.E. Smith, 1980. *The Development and Calibration of a Spatially Simplified Multi-Class Phytoplankton Model for Saginaw Bay, Lake Huron*, Great Lakes Environmental Planning Study, Contribution No. 33.
- Blosser, M.C., 1986. "Phosphorus Models for Lake Okeechobee, Florida," M.E. Thesis, Department of Environmental Engineering Sciences, University of Florida, Gainesville.
- Blumberg, A.F., 1986. *Turbulent Mixing Processes in Lake, Reservoirs, and Impoundments*, Chapter 4, in (W. Gray, editor) *Physics-Based Modeling of Lakes, Reservoirs and Impoundments*, American Society of Civil Engineers, New York.
- Boers, P., L. Van Ballegooijen, and J. Uunk, 1991. "Changes in Phosphorus Cycling in a Shallow Lake Due to Food Web Manipulations," *Freshwater Biology*, 25:9-20.
- Bowie, G.L., Mills, W.B., Porcella, D.B., Campbell, C.L., Pagenkopf, J.R., Rupp, G.L., Johnson, K.M, Chan, P.W.H., Gherini, S.A. and C.E. Chamberlin, 1985. *Rates, Constants and Kinetics Formulations in Surface Water Quality Modeling*

(Second Edition), EPA/600/3-85/040, Environmental Protection Agency, Athens, GA, June.

Bostrom, B., Persson, G. and B. Broberg, 1988. "Bioavailability of Different Phosphorus Forms in Freshwater Systems," *Hydrobiologia*, 170:133-155.

Brezonik, P.L. and E.E. Shannon, 1981. *Trophic State of Lakes in North Central Florida*, Publication No. 13, Florida Water Resources Research Center, Gainesville.

Brezonik, P.L., E.C. Blancher, V.B. Myers, C.L. Hilty, M.K. Leslie, C.R. Kratzer, C.D. Marbury, B.R. Snyder, T.L. Crisman and J.J. Messer, 1979. *Factors Affecting Primary Production in Lake Okeechobee, Florida*, Report No. 07-79-01 to the Florida Sugar Cane League, Department of Environmental Engineering Sciences, University of Florida, Gainesville.

Brezonik, P.L., D.R. Engstrom and T. Huang, 1989. *Phosphorus Accumulation Rates in Lake Okeechobee, Florida*, Annual progress report submitted to the South Florida Water Management District, April 1989.

Brezonik, P.L., W.C. Huber, C. Pollman, M. Blosser, S. Zoltewicz, C. Miles and L. Lane, 1983. *Evaluation and Modeling of Internal Nutrient Cycling Processes in Lake Okeechobee, Florida*, Completion Report, Dept. of Environmental Engineering Sciences, University of Florida, to South Florida Water Management District, West Palm Beach, March 1983.

Brooks, H.K., 1974. "Lake Okeechobee," in P.J. Gleason (ed.), *Environments of South Florida: Past and Present. Memoir 2*, Miami Geological Society, Miami, FL.

Bricaud, A., A-L. Bedhomme and A. Morel, 1988. "Optical Properties of Diverse Phytoplankton Species: Experimental Results and Theoretical Interpretation," *Journal of Plankton Research*, 10(5):851-873.

Broberg, B. and G. Persson, 1988. "Particulate and Dissolved Phosphorus Forms in Freshwater: Composition and Analysis," *Hydrobiologia*, 170:61-90.

Brutsaert, W.H., 1980. *Evaporation into the Atmosphere*, D. Reidel Publishing Co., Boston.

Butaka, R.P., J.H. Jerome and J.E. Bruton, 1989. "Determination of Irradiation and Primary Production Using a Time-Dependent Attenuation Coefficient," *J. Great Lakes Res.*, 15(2):327-338.

Canale, R.P. and S.W. Effler, 1989. "Stochastic Phosphorus Model for Onondaga Lake," *Water Research*, 23(8):1009-1016.

Canale and Vogel, 1974. ***TBA

Canfield, D.E., 1983. "Prediction of Chlorophyll Concentrations in Florida Lakes: The Importance of Phosphorus and Nitrogen," *Water Resources Bulletin*, 19(2):255-262.

Canfield, D.E., S.B. Linda and L.M. Hodgson, 1984. "Relations Between Color and Some Limnological Characteristics of Florida Lakes," *Water Resources Bulletin*, 20(3):323-330.

Canfield, D.E., S.B. Linda and L.M. Hodgson, 1985. "Chlorophyll-Biomass-Nutrient Relationships for Natural Assemblages of Florida Phytoplankton," *Water Resource Bulletin*, 21(3):381-391.

Canfield, D.E. and M.V. Hoyer, 1989. "The Eutrophication of Lake Okeechobee," *Lake and Reservoir Management*, 4:91-99.

Carey, J.S. and W.C. Huber, 1990. *Assembly and Time Series Analysis of Historical Flow and Phosphorous Data for Lake Okeechobee*, Volume VIII, Final Report, Department of Environmental Engineering Sciences, University of Florida, to South Florida Water Management District, West Palm Beach, FL, July.

Carlson, R.E., 1977. "A Trophic State Index for Lakes," *Limnol. Oceanogr.*, 22:361-369.

Chapra, S.C. and K.H. Reckhow, 1983. *Engineering Approaches for Lake Management, Volume 2: Mechanistic Modeling*, Butterworth Publishers, Woburn, MA.

Chen, C.W. and D.J. Smith, 1985. "Preliminary Insights Into a Three-dimensional Ecological-Hydrodynamic Model," Chapter 10, in (D. Scavia and A. Robertson, eds.) *Perspectives on Lake Ecosystem Modeling*, Ann Arbor Science, Ann Arbor, MI.

Chmyr, V.D. and G.P. Berseneva, 1983. "Content of Carbon and Chlorophyll in Planktonic Algae," *Ekologiya*, 5:18-25.

Cole, J.J., 1982. "Interactions Between Bacteria and Algae in Aquatic Ecosystems," *Ann. Rev. Ecol. Syst.*, 13:291-314.

Crisman, T.L. and J.R. Beaver, 1988. ***TBA

Crisman, T.L., P. Scheurman, R.W. Bienert, J.R. Beaver and J.S. Bays, 1984. "A Preliminary Characterization of Bacterioplankton Seasonality in Subtropical Florida Lakes," *Verh. Internat. Verein. Limnol.*, 22:620-626.

Crisman, T.L. and H. M. Kennedy, 1982. *The Role of Grizzled Shad (Dorosoma cepedianum) in Eutrophic Florida Lakes*, Publication No. 64, Water Resources Research Center, University of Florida, Gainesville, October.

- Currie, D.J. and J. Kalff, 1984. "The Relative Importance of Bacterioplankton and Phytoplankton in Phosphorus Uptake in Freshwater," *Limnol. Oceanogr.*, 29(2):311-321.
- Dake, J.M.K. and D.R.F. Harleman, 1969. "Thermal Stratification in Lakes: Analytical and Laboratory Studies," *Water Resources Research*, 5(2):484-495.
- Davies-Colley, R.J., W.N. Vant and R.J. Wilcock, 1988. "Lake Water Color: Comparison of Direct Observations with Underwater Spectral Irradiance," *Water Resources Bulletin*, 24(1):11-18.
- Davies-Colley, R.J. and W.N. Vant, 1988. "Estimation of Optical Properties of Water from Secchi Disk Depths," *Water Resources Bulletin*, 24(6):1329-1335.
- Davis, B.L. and A. C. Frederico, 1984. *Phytoplankton, Chlorophyll a, and Primary Production in Lake Okeechobee*, South Florida Water Management District, Tech. Pub. No. 84-4, West Palm Beach, FL, 33 pp.
- Davis, S.M., 1984. *Cattail Leaf Production, Mortality, and Nutrient Flux in Water Conservation Area 2A*, South Florida Water Management District, Tech. Pub. No. 84-8, West Palm Beach, FL, 40 pp.
- DeBusk, T.A. and F. E. Dierberg, 1989. "Effects of Nutrient Availability on Water Hyacinth Standing Crop and Detritus Deposition," *Hydrobiologia*, 174:151-159.
- De Groot, W.T., 1983. "Modelling the Multiple Nutrient Limitation of Algal Growth," *Ecological Modelling*, 18:99-119.
- De Pinto et al., 1986. ***TBA
- Devol, A.H., 1979. "Zooplankton Respiration and its Relation to Plankton Dynamics in Two Lakes of Contrasting Trophic State," *Limnol. Oceanogr.*, 24(5):893-905.
- Dickinson et al., 1986. ***TBA
- Dillon, P.J. and F.H. Rigler, 1974. "The Phosphorus-Chlorophyll Relationship in Lakes," *Limnol. Oceanogr.*, 19(5):767-773.
- DiToro, D.M., 1980. "Applicability of Cellular Equilibrium and Monod Theory to Phytoplankton Growth Kinetics," *Ecological Modelling*, 8:201-218.
- Draper, N.R. and H. Smith, 1981. *Applied Regression Analysis*, John Wiley & Sons, New York.
- Droop, 1968. ***TBA

- Duarte, C.M., 1990. "Time Lags to Algal Growth: Generality, Causes and Consequences," *Journal of Plankton Research*, 12(4):873-883.
- Echternacht, K.L., 1975. *A Study of the Precipitation Regimes of the Kissimmee River-Lake Okeechobee Watershed*, State of Florida Department of Environmental Regulation Technical Series Vol. 1, No. 3, Tallahassee, FL.
- Edson, J.E. and R. C. Jones, 1988. "Spatial, Temporal, and Storm Runoff-Related Variations in Phytoplankton Community Structure in a Small, Suburban Reservoir," *Hydrobiologia*, 169:353-362.
- Effler, S.W., S.D. Field, J.V. DePinto, E.M. Owens, J.S. Dobi and M.A. Preda, 1982. "Predicting Phosphorus Levels in a Future Reservoir," *Journal of the Environmental Engineering Division, ASCE*, 108(EE4):689-704, August.
- Effler, S.W. and D.L. Johnson, 1987. "Calcium Carbonate Precipitation and Turbidity Measurements in Otisco Lake, New York," *Water Resources Bulletin*, 23(1):73-79.
- Effler, S.W., M.G. Perkins, H. Greer and D.L. Johnson, 1987a. "Effect of "Whiting" on Optical Properties and Turbidity in Owasco Lake, New York," *Water Resources Bulletin*, 23(2):189-196.
- Effler, S.W., C.M. Brooks, M.G. Perkins, M. Meyer and S.D. Field, 1987b. "Aspects of the Underwater Light Field of Eight Central New York Lakes," *Water Resources Bulletin*, 23(6):1193-1201.
- Effler, S.W. and M.T. Auer, 1987. "Optical Heterogeneity in Green Bay," *Water Resources Bulletin*, 23(6):937-941.
- Effler, S.W., R. Roop and M.G. Perkins, 1988. "A Simple Technique of Estimating Absorption and Scattering Coefficients," *Water Resources Bulletin*, 24(2):397-404.
- Effler, S.W., 1988. "Secchi Disc Transparency and Turbidity," *Journal of Environmental Engineering*, 114(6):1436-1447.
- Eidsvik, K.L. and T. Utne, 1991. "Changes in Phosphorus Cycling in a Shallow Lake Due to Food Web Manipulations," *Coastal Engineering*, 15:247-256.
- Eisenreich, S.J., P.J. Emmling and A.M. Beeton, 1977. "Atmospheric Loading of Phosphorus and Other Chemicals to Lake Michigan," *J. Great Lakes Research, Inter. Assoc. Great Lakes Research*, 3(3-4):291-304.
- Ewel, K.C. and T.D. Fontaine, 1983. "Structure and Function of a Warm Monomictic Lake," *Ecological Modelling*, 19:139-161.

- Falkowski, P.G., 1981. "Light Shade Adaptation and Assimilation Numbers," *Journal of Plankton Research*, 3(2):203-216.
- Falkowski, P.G., Z. Dubinsky and K. Wyman, 1985. "Growth-Irradiance Relationships in Phytoplankton," *Limnol. Oceanogr.*, 30(2):311-321.
- Federico, A.C., Dickson, K.G., Kratzer, C.R. and Davis, F.E., 1981. *Lake Okeechobee Water Quality Studies and Eutrophication Assessment*. South Florida Water Management District, Tech. Pub. No. 81-2, West Palm Beach, FL, 270 pp.
- Ferrara, R.A. and D.R.F. Harleman, 1978. *A Dynamic Nutrient Cycle Model for Waste Stabilization Ponds*, MIT Ralph M. Parsons Laboratory Technical Report 237, Dept. of Civil Engineering, MIT, Cambridge, MA.
- Ferrara, R.A., 1986a. "Introduction to the Modeling of Lakes, Reservoirs and Impoundments," Chapter 1, in (W. Gray, editor) *Physics-Based Modeling of Lakes, Reservoirs and Impoundments*. American Society of Civil Engineers, New York.
- Ferrara, R.A., 1986b. "Modeling Pollutant Transformation Processes," Chapter 5, in (W. Gray, editor) *Physics-Based Modeling of Lakes, Reservoirs and Impoundments*. American Society of Civil Engineers, New York.
- Field, S.D. and S.W. Effler, 1982. "Light-Productivity Model for Onondaga Lake, N.Y.," *Journal of Environmental Engineering*, 109(4):830-843.
- Field, S.D. and S.W. Effler, 1988. "Temperature and the Productivity-Light Relationship," *Water Resources Bulletin*, 24(2):325-328.
- Florida Dept. of Administration, 1976. *Final Report on the Special Project to Prevent Eutrophication of Lake Okeechobee*. Tallahassee, FL.
- Forsberg, C. and S. Ryding, 1980. "Eutrophication Parameters and Trophic State Indices in 30 Swedish Waste-Receiving Lakes," *Arch. Hydrobiol.*, 89:189-207.
- Furumai, H. and S. Ohgaki, 1989. "Adsorption-Desorption of Phosphorus by Lake Sediments Under Anaerobic Conditions," *Water Research*, 3(6):677-683.
- Furumai, H., T. Kondo and S. Ohgaki, 1989. "Phosphorus Exchange Kinetics and Exchangeable Phosphorus Forms in Sediments," *Water Research*, 23(6):685-691.
- Gayle, T.L., 1975. "Systems Models for Understanding Eutrophication in Lake Okeechobee, Florida," M.S. Thesis, Department of Environmental Engineering Sciences, University of Florida, Gainesville, 119 pp.

Goda, T. and Y. Matsuoka, 1986. "Synthesis and Analysis of a Comprehensive Lake Model - with the Evaluation of Diversity of Ecosystems," *Ecological Modelling*, 31:11-32.

Goldman, J.C., 1979. "Outdoor Algal Mass Cultures- II. Photosynthetic Yield Limitations," *Water Research*, 13:119-136.

Goldman, J.C., D.B. Porcella, E.J. Middlebrooks and D.F. Toerien, 1972. "The Effect of Carbon on Algal Growth - Its Relationship to Eutrophication," *Water Research*, 6:637-679.

Granberg, K. and H. Harjula, 1982. "On the Relation of Chlorophyll a to Phytoplankton Biomass in Some Finnish Freshwater Lakes," *Arch. Hydrobiol. Beih. Ergeb. Limnol.*, 16:63-75.

Graneli, W. and D. Solander, 1988. "Influence of Aquatic Macrophytes on Phosphorus Cycling in Lakes," *Hydrobiologia*, 170:245-266.

Griffin, H. and R.A. Ferrara, 1984. "A Multicomponent Model of Phosphorus Dynamics in Reservoirs," *Water Resources Bulletin*, 20(5):777-788.

Grobbelaar, J.U., 1985. "Carbon Flow in the Pelagic Zone of a Shallow Turbid Impoundment," Wuras Dam, *Arch. Hydrobiol.*, 103(1):1-24.

Grover, J.P., 1989. "Phosphorus-dependent Growth Kinetics of 11 Species of Freshwater Algae," *Limnol. Oceanogr.*, 34(2):341-348.

Haire, W.J., C. Price, R.E. Curtisand C. Lietz, 1987. *Water Resources Data Florida. Water Year 1985. Volume 2A. South Florida Surface Water*, USGS Water-Data Report FL-85-2A, Miami, FL.

Haire, W.J. and C. Price, 1990. *Water Resources Data Florida. Water Year 1989. Volume 2A. South Florida Surface Water*, USGS Water-Data Report FL-89-2A, Miami, FL.

Hakanson, L., 1984. "On the Relationship Between Lake Trophic Level and Lake Sediments," *Water Research*, 18(3):303-314.

Haltermann, S.G. and D.W. Toetz, 1984. "Kinetics of Nitrate Uptake by Freshwater Algae," *Hydrobiologia*, 114:209-214.

Harleman, D.R.F., 1988. "Transport Processes in Environmental Engineering," Unpublished lecture notes, Dept. of Civil Engineering, MIT, Cambridge, MA.

Heggen, R.J., 1983. "Thermal Dependent Physical Properties of Water," *J. Hydraulic Engineering, ASCE*, 109(2):298-302.

Hellstrom, 1991. ***TBA

Henderson-Sellers, B., 1986. "Calculating the Surface Energy Balance for Lake and Reservoir Modeling: A Review," *Reviews of Geophysics*, 24(3):625-649.

Holtan H., I. Kamp-Nielsonand A. O. Stuanes, 1988. "Phosphorus in Soil, Water and Sediment: An Overview," *Hydrobiologia*, 170:19-34.

Holstag, A.A.M. and A.P. Van Ulden, 1983. "A Simple Scheme for Daytime Estimates of the Surface Fluxes from Routine Weather Data," *Journal of Climate and Applied Meteorology*, 22(4):517-529.

Huber, W.C. and A. I. Perez, 1970. *Prediction of Solar and Atmospheric Radiation for Energy Budget Studies of Lakes and Streams*, Publication No. 10, Water Resources Research Center, University of Florida, Gainesville, October.

Huber, W.C., P.L. Brezonik, J.P. Heaney, R.E. Dickinson, S.D. Preston, D.S. Dwornikand M.A. DeMaio, 1982. *A Classification of Florida Lakes*, Publication No. 72, Florida Water Resources Research Center, University of Florida, Gainesville.

Hunters, B.L. and E.A. Laws, 1981. "ATP and Chlorophyll a as Estimators of Phytoplankton Carbon Biomass," *Limnol. Oceanogr.*, 26(5):944-956.

Hutchinson, G.E., 1957. *A Treatise on Limnology, Volume I, Part 1 - Geography and Physics of Lakes*, John Wiley and Sons, New York.

Hutchinson, G.E., 1961. "The Paradox of the Plankton," *The American Naturalist*, XCV(882):137-145, May-June.

Hwang, K.N., 1989. "Erodibility of Fine Sediment in Wave-Dominated Environment," MS Thesis, University of Florida, Gainesville.

Hwang, K.N. and A.J. Mehta, 1989. *Fine Sediment Erodibility in Lake Okeechobee, Florida*, Report UFL/COEL-89/019, Dept. of Coastal and Oceanographic Engineering, Univeristy of Florida, to South Florida Water Management District, West Palm Beach, FL, November.

Ibelings, B.W., L.R. Mur and A.E. Walsby, 1991. "Diurnal Changes in Buoyancy and Vertical Distribution of Microcystis in Two Shallow Lakes," *Journal of Plankton Research*, 13(2):419-433.

Idso, S.B., 1981. "A Set of Equations for Full Spectrum and 8- to 14- μm and 10.5- to 12.5- μm Thermal Radiation from Cloudless Skies," *Water Resources Research*, 17(2):295-304.

- Idso, S.B. and R.D. Jackson, 1969. "Thermal Radiation from the Atmosphere," *J. Geophysical Research*, 74:5397-5403.
- Istvanovics, V., 1988. "Seasonal Variation of Phosphorus Release from the Sediments of Shallow Lake Balaton(Hungary)," *Water Research*, 22(12):1473-1481.
- Istvanovics, V., S. Herdodekand F. Szilagy, 1989. "Phosphate Adsorption by Different Sediment Fractions in Lake Balaton and its Protecting Reservoirs," *Water Research*, 23(11):1357-1366.
- Jaffe, P.R., 1988. "Tropical Eutrophic Lake Modeling and Parameter Discrimination," *Water Resources Bulletin*, 24(3):585-592.
- Jansson, M., 1988. "Phosphate Uptake and Utilization by Bacteria and Algae," *Hydrobiologia*, 170:177-189.
- Jirka, G.H., D.N. Brocard, K.A.H. Octavio, M. Watanabe and D.R.F. Harleman, 1977. *Analysis of Cooling Effectiveness and Transient Long-Term Simulations of a Colling Lake*, R.M. Parsons Laboratory for Water Resources and Hydrodynamics, Report No. 232, MIT, Cambridge, MA.
- Jointe, I., 1991. "The Allometric Determination of Pelagic Production Rates," *Journal of Plankton Research*, Supplement, 13:69-81.
- Jones, B. and A. Federico, 1984. *Phytoplankton and Chlorophyll in Lake Okeechobee*, Technical Report No. 84-2, South Florida Water Management District, West Palm Beach.
- Jones, J.R. and R.W. Bachmann, 1976. "Prediction of Phosphorus and Chlorophyll Levels in Lakes," *J. Water Pollution Control Federation*, 48:2176-2182.
- Jorgensen, S.E., 1981. "Model for Lake Glumsø, Denmark," in (A.E. Biswas, ed.) *Models for Water Quality Management*, McGraw-Hill, New York.
- Jorgensen, S.E., 1983. "Modeling the Ecological Processes," Chapter 5 in (G.T. Orlob, ed.) *Mathematical Modeling of Water Quality: Streams, Lakes and Reservoirs*, John Wiley and Sons, New York.
- Joyner, B.F., 1974. *Chemical and Biological Conditions of Lake Okeechobee, Florida (1969-1972)*, USGS Report Investigation No. 71, Tallahassee, FL.
- Kalff, J. and R. Knoechel, 1978. "Phytoplankton and Their Dynamics in Oligotrophic and Eutrophic Lakes," *Ann. Rev. Ecol. Syst.*, 9:475-495.

Kasten, F., 1964. *A New Table and Approximation Formula for the Relative Optical Air Mass*, U.S. Army Material Command, Cold Regions Research and Engineering Laboratory, Technical Report No. 136, Hannover, NH.

Keenan, J.D. and M.T. Auer, 1974. "The Influence of Phosphorus Luxury Uptake on Algal Bioassays," *Journal WPCF*, 46(3):532-542.

Keesman, K. and G. Van Straten, 1990. "Set Membership Approach to Identification and Prediction of Lake Eutrophication," *Water Resources Research*, 26(11):2643-2652.

Kempf, J., L. Duckstein and J. Cash, 1984. "Relaxation Oscillations and Other Non-Michaelian Behavior in a Slow-Fast Phytoplankton Growth Model," *Ecological Modelling*, 23:67-90.

Kilham, P. and S.S. Kilham, 19910 "Endless Summer: Internal Processes Dominate Nutrient Cycling in Tropical Lakes," *Freshwater Biology*, 22(4):379-389.

Kirby R.R., C.H. Hobbs and A.J. Mehta, 1989. *Fine Sediment Regime in Lake Okeechobee, Florida*, Report UFL/COEL-89/009, Coastal and Oceanographic Engineering Department of the University of Florida, Gainesville.

Kirk, J.T.O., 1981. "Monte-Carlo Study of the Nature of the Underwater Light Field in, and the Relationships Between Optical Properties of Turbid Yellow Waters," *Australian J. Marine and Freshwater Research*, 32(3):517-532.

Klemer and Borko, 19???. ***TBA

Knowton, M.F., M.V. Hoyer and J.R. Jones, 1984. "Sources of Variability in Phosphorus and Chlorophyll and Their Effects on Use of Lake Survey Data," *Water Resources Bulletin*, 20(3):397-407.

Kozerski, H.P., H. Behrendt and G. Schellenberger, 1988. "Investigations of the Lake Ecosystem Model EMSY by Means of the Simulation System SONCHES," *Ecological Modelling*, 41:193-200.

Kratzer, C.R., 1979. "Application of Input-Output Models to Florida Lakes," M.S. Thesis, Department of Environmental Engineering Sciences, University of Florida, Gainesville.

Kratzer, C.R. and P.L. Brezonik, 1981. "A Carlson-Type Trophic State Index for Nitrogen in Florida lakes," *Water Resources Bulletin*, 17(4):713-715.

Kromkamp, J. and A.E. Walsby, 1990. "A Computer Model of Buoyancy and Vertical Migration in Cyanobacteria," *Journal of Plankton Research*, 12(1):161-183.

Kunikane, S.M., M. Kaneko and R. Maehara, 1981. "Steady State Analysis of Algal Cultures Grown Under Simultaneous Limitation of Nitrogen and Phosphorus," *Verh. Internat. Verein. Limnol.*, 21:1454-1457.

Kunikane, S. and M. Kaneko, 1984. "Growth and Nutrient Uptake of Green Alga, Scenedesmus Dimorphous, Under a Wide Range of Nitrogen/Phosphorus Ratio-II," *Water Research*, 18(10):1313-1326.

Lam, D.C.L., 1986. *Basic Equations for Pollutant and Heat Transports in Lakes*, Chapter 3, in (W. Gray, editor) *Physics-Based Modeling of Lakes, Reservoirs and Impoundments*. American Society of Civil Engineers, New York, N.Y.

Lamonds, A.G, 1975. *Chemical Characteristics of the Lower Kissimmee River, Florida--with Emphasis on Nitrogen and Phosphorus*, Water-Resources Investigation 45-75, U.S. Geological Survey, Tallahassee, FL.

Lang, G.A., Lang, J.A. Morton and T.D. Fontaine," 1988. "Total Phosphorus Budget for Lake St. Clair: 1975-80," *J. Great Lakes Research*, 14(3):257-266.

Langdon, C., 1988. "On the Causes of Interspecific Differences in the Growth-Irradiance Relationship for Phytoplankton. II. A General Review," *Journal of Plankton Research*, 10(6):1291-1312.

Lastein, E. and E. Gargas, 1978. "Relationship Between Phytoplankton Photosynthesis and Light, Temperature and Nutrients in Shallow Lakes," *Verh. Internat. Verein. Limnol.*, 20:678-689.

Lazzaro, X., 1987. "A Review of Planktivorous Fishes: Their Evolution, Feeding Behaviors, Selectivities, and Impacts," *Hydrobiologia*, 146:97-167.

Lean, D.R.S., 1973. "Movements of Phosphorus Between its Biologically Important Forms in Lake Water," *Journal Fisheries Research Board of Canada*, 30(10):1525-1536.

Lehman, J.T., D.B. Botkin and G.E. Likens, 1975. "The Assumptions and Rationales of a Computer Model of Phytoplankton Population Dynamics," *Limnology and Oceanography*, 3:343-364.

Lennox, L.J., 1984. "Sediment-Water Exchange in Lough Ennell with Particular Reference to Phosphorus," *Water Research*, 18(12):1483-1485.

Leslie, M.K., 1979. "Measurement of Phosphorus Limitation in the Phytoplankton of Lake Okeechobee by Limiting Nutrient Bioassays," M.S. Thesis, Department of Environmental Engineering Sciences, University of Florida, Gainesville.

List, R.J., ed., 1966. *Smithsonian Meteorological Tables*, Smithsonian Institution, Washington, DC.

Lynch, D.R., 1986. "Basic Hydrodynamic Equation for Lakes," Chapter 2, In (W. Gray, editor) *Physics-Based Modeling of Lakes, Reservoirs and Impoundments*. American Society of Civil Engineers, New York, N.Y.

McQueen, D.J. and J.R. Post, 1988. "Cascading Trophic Interactions: Uncoupling at the Zooplankton-Phytoplankton Link," *Hydrobiologia*, 159:277-296.

Malone, T.C., 1982. "Phytoplankton Photosynthesis and Carbon-Specific Growth: Light-Saturated Rates in a Nutrient-Rich Environment," *Limnol. Oceanogr.*, 27(2):226-235.

Marshall, M.L., 1977. *Phytoplankton and Primary Productivity Studies in Lake Okeechobee During 1974*, South Florida Water Management District, Technical Publication No. 77-2.

MacIntyre, D.F., 1986. "A Quantitative Review of the Hydrology of Lake Jackson, Florida, 1971-81," ME Thesis, Department of Environmental Engineering Sciences, University of Florida, Gainesville.

MacVicar, T.F., 1983. *Rainfall Averages and Selected Extremes for Central and South Florida*, South Florida Water Management District, Tech. Pub. No. 83-2, West Palm Beach, FL, 31 pp.

MacVicar, T.F., 1984. *South Florida Water Model Documentation Report*, South Florida Water Management District, Tech. Pub. No. 84-3, West Palm Beach, FL, 130 pp.

Melack, J.M., 1985. "Interactions of Detrital Particulates and Plankton," *Hydrobiologia*, 125:209-220.

Messer J.J., P.L. Brezonik and B.R. Snyder, 1979. *Denitrification in Lake Okeechobee, Florida*, Report No. 07-79-03 to the South Florida Water Management District. Department of Environmental Engineering Sciences, University of Florida, Gainesville.

Maurersberger, P., 1982. "Logistic Growth Laws for Phyto-and-Zooplankton," *Ecological Modelling*, 17:57-63.

Milleson, J., 1987. *Vegetation Changes in the Lake Okeechobee Littoral Zone 1092-1982*. South Florida Water Management District, Technical Publication No. 87-3, West Palm Beach, FL.

- Nalewajko, C., K. Leeand H. Shear, 1981. "Phosphorus Kinetics in Lake Superior: Light Intensity and Phosphate Uptake in Algae," *Can. J. Fish. Aquat. Sci.*, 38:224-232.
- Niebauer, H.J. and W.O. Smith, 1989. "A Numerical Model of Mesoscale Physical-Biological Interactions in the Fram Strait Marginal Ice Zone," *Journal of Geophysical Research*, 94:1615-1675.
- Odum, H.T., 1983. *Systems Ecology: An Introduction*, John Wiley and Sons, New York.
- OECD, 1982. ***TBA
- Orlob, G.T., ed., 1983. *Mathematical Modeling of Water Quality: Streams, Lakes and Reservoirs*, John Wiley and Sons, New York.
- Owens, E.M., S.W. Effler and F. Trama, 1986. "Variability in Thermal Stratification in a Reservoir," *Water Resources Bulletin*, 22(2):219-227.
- Pace, M.L., 1984. "Zooplankton Community Structure, But Not Biomass, Influences the Phosphorus-Chlorophyll a Relationship," *Can. J. Fish. Aquat. Sci.*, 41:1089-1096.
- Padisak, J., L.G. Toth and M. Rajczy, 1988. "The Role of Storms in the Summer Succession of the Phytoplankton Community in a Shallow Lake (Lake Balaton, Hungary)," *Journal of Plankton Research*, 10(2):249-265.
- Parker, R.A., 1991. "Eddy Diffusion of Phytoplankton and Nutrients: Estimating Coefficients from Simulated and Observed Vertical Distributions," *Journal of Plankton Research*, 13(4):815-830.
- Pedlosky, J., 1982. *Geophysical Fluid Dynamics*. Springer-Verlag, New York, N.Y.
- Peng, T.H. and W.S. Broecker, 1987. "C/P Ratios in Marine Detritus," *Global Biogeochemical Cycles*, 1(2):155-161.
- Persson, G., 1984. "Characterization of Particulate and Colloidal Phosphorus Forms in Water by Continuous Flow Density Gradient Centrifugation," *Verh. Internat. Verein. Limnol.*, 22:149-154.
- Pesnell and Brown, 1977. (?? SFWMD) ***TBA
- Peters, R.H., 1981. "Phosphorus Availability in Lake Memphremagog and its Tributaries," *Limnol. Oceanogr.*, 26(6):1150-1161.

- Peterson, W.A. and I. Dirmhirn, 1981. "The Ratio of Diffuse to Direct Solar Irradiance (Perpendicular to the Sun's Rays) with Clear Skies - A Conserved Quantity," *Journal of Applied Meteorology*, 20:826-828.
- Peyret, R. and T.D. Taylor, 1983. *Computational Methods for Fluid Flow*, Springer-Verlag, New York.
- Pielke, R.A., 1974. "A Three-Dimensional Numerical Model of the Sea Breeze Over South Florida," *Monthly Weather Review*, 102:115-139.
- Platzman, G.W., 1963. "The Dynamical Prediction of Wind Tides on Lake Erie," *Meteorological Monographs*, 4(26), American Meteorological Society, Boston, September.
- Pollman, C.D., 1983. "Internal Loading in Shallow Lakes," Ph.D. Dissertation, Department of Environmental Engineering Sciences, University of Florida, Gainesville.
- Pollman, C.D., 1991. *Development of a Phosphorus Diagenetic Model for Lake Okeechobee Sediments*, KBN Engineering and Applied Sciences, Gainesville, FL, Final Report to South Florida Water Management District, West Palm Beach, FL, September.
- Prepas, E.E. and J. Vickery, 1984. "Seasonal Changes in Total Phosphorus and the Role of Internal Loading in Western Canadian Lakes," *Verh. Internat. Verein. Limnol.*, 22:303-308.
- Randazzo, A.F., 1983. *Mineralogical Model of the Floridan Aquifer in the Southwest Florida Water Management District*, Publication No. 68, Florida Water Resources Research Center, University of Florida, Gainesville.
- Reckhow, K.H. and S.C. Chapra, 1983. *Engineering Approaches for Lake Management, Volume 1: Data Analysis and Empirical Modeling*, Butterworth Publishers, Woburn, MA.
- Reddy, R., 1990. *Lake Okeechobee Progress Report*, Soil Science Dept., University of Florida, Gainesville.
- Reddy, K.R. et al., 1991. *Lake Okeechobee Phosphorus Dynamics Study: Biogeochemical Processes in the Sediments, Volume III*. Final Report, Soil Science Dept., University of Florida, to South Florida Water Management District, West Palm Beach, FL, May.
- Reddy, R. and D.B. Ivanoff, 1990. "Mineralization of Organic Phosphorus in Sediments," Chapter 6 in *Lake Okeechobee Progress Report*, Soil Science Dept., University of Florida, Gainesville.

Redfield, A.C., Ketchum, B.H. and F.A. Richards, 1966. Chapter 2 in *The Sea, Vol. II*, M.N. Hill, Ed., Wiley-Interscience, New York.

Reeder, P.B. and S. M. Davis, 1983. *Decomposition, Nutrient Uptake and Microbial Colonization of Sawgrass and Cattail Leaves in Water Conservation Area 2A*, South Florida Water Management District, Tech. Pub. No. 83-4, West Palm Beach, FL, 24 pp.

Rhee, G-Y. and I.J. Gotham. 1981a. "The Effect of Environmental Factors on Phytoplankton Growth: Temperature and the Interactions of Temperature with Nitrate Limitation," *Limnol. Oceanogr.*, 26(4):635-648.

Rhee, G-Y. and I.J. Gotham. 1981b. "The Effect of Environmental Factors on Phytoplankton Growth: Light and the Interactions of Light with Nitrate Limitation," *Limnol. Oceanogr.*, 26(4):649-659.

Riemann, B., P. Simonsenand L. Stensgaard, 1989. "The Carbon and Chlorophyll Content of Phytoplankton from Various Nutrient Regimes," *Journal of Plankton Research*, 11(5):1037-1045.

Rigler, F.H., 1975. "Nutrient Kinetics and the New Typology," *Verh. Internat. Verein. Limnol.*, 19:197-210.

Rigler, F.H., 1973. *A Dynamic View of the Phosphorus Cycle in Lakes*, in Griffith, E.J., Beeton, A., Spencer, J.M. and D.T. Mitchell, *Environmental Phosphorus Handbook*, New York, John Wiley & Sons, pp. 539-572.

Riley, M.J. and H.G. Stefan, 1988. "MINLAKE: A Dynamic Lake Water Quality Simulation Model," *Ecological Modelling*, 43:155-182.

Roache, P.J., 1972. *Computational Fluid Dynamics*, Hermosa Publishers, Albuquerque, N.M.

Rose, K.A., G.G. Swartzman, A.C. Kindigand F.B. Taub, 1988. "Stepwise Iterative Calibration of a Multi-Species Phytoplankton-Zooplankton Simulation Model Using Laboratory Data," *Ecological Modelling*, 42:1-32.

Ryan, P.J. and D.R.F. Harleman, 1971. *Prediction of the Annual Cycle of Temperature changes in a Stratified Lake or Reservoir: Mathematical Model and User's Manual*, MIT Ralph M. Parsons Laboratory Technical Report 137, Dept. of Civil Engineering, MIT, Cambridge, MA.

Sakamoto, M., 1966. "Primary Production by Phytoplankton Community in Some Japanese Lakes and its Dependence on Lake Depth," *Arch. Hydrobiol.*, 62:1-28.

Salas, H.S. and R.V. Thomann, 1975. *The Chesapeake Bay Waste Load Allocation Study*, Hydroscience, Inc. for the Maryland Dept. of Natural Resources Administration, Annapolis, MD.

Salhotra, A.M., E.E. Adams and D.R.F. Harleman, 1986. *A Coupled Heat, Salt and Water Balance Model of Evaporation and Stratification in Saline Terminal Lakes: An Application to the Dead Sea*, R.M. Parsons Laboratory, Report No. 311, M.I.T., Cambridge, MA.

Scavia, D., 1980. "An Ecological Model for Lake Ontario," *Ecol. Model.*, 8:49-78.

Scavia, D., 1981. "Conceptual Model of Phosphorus Cycling," in (D. Scavia and R. Moll, eds.) *Nutrient Cycling in the Great Lakes: A Summarization of Factors Regulating the Cycling of Phosphorus*, Great Lakes Research Division Special Report No. 83, University of Michigan, Ann Arbor, MI.

Scavia, D., W.F. Powers, R.P. Canale and J.L. Moody, 1981a. "Comparison of First-Order Error Analysis and Monte Carlo Simulation in Time-Dependent Lake Eutrophication Models," *Water Resources Research*, 17(4):1051-1059.

Scavia, D., R.P. Canale, W.F. Powers and J.L. Moody, 1981b. "Variance Estimates for a Dynamic Eutrophication Model of Saginaw Bay, Lake Huron," *Water Resources Research*, 17(4):1115-1124.

Scavia et al., 1984. ***TBA

Schelske, C.L., 1989. "Assessment of Nutrient Effects and Nutrient Limitation in Lake Okeechobee," *Water Resources Bulletin*, 25(6):1119-1130.

Schindler, D.W., 1978. "Factors Regulating Phytoplankton Production and Standing Crop in the World's Freshwaters," *Limnol. Oceanogr.*, 23(3):478-486.

Schnoor, J.L. and D.J. O'Connor, 1980. "A Steady State Eutrophication Model for Lakes," *Water Research*, 14:1651-1665.

Schwab, D.J. and J.A. Morton, 1984. "A Computer Model of Buoyancy and Vertical Migration in Cyanobacteria," *J. Great Lakes Research*, 10(1):68-72.

Seki, H. and Takahashi, E., 1983. "Spring Bloom in a Hypereutrophic Lake, Lake Kasumigaura, Japan-I. Succession of Phytoplankters with Different Accessory Pigments," *Water Research*, 17:441-445.

SethuRaman and Raynor, 1981. ***TBA

SFWMD, 1990. *Comprehensive Annual Financial Report for the Fiscal Year Ended September 30, 1990*, Prepared by the Department of Finance and Administration, West Palm Beach, FL.

Shanahan, P. and D.R.F. Harleman, 1981. *Linked Hydrodynamic and Biogeochemical Models of Shallow Lake Water Quality*, MIT Ralph M. Parsons Laboratory Technical Report 268, Dept. of Civil Engineering, MIT, Cambridge, MA.

Sheng, Y.P., 1983. *Mathematical Modeling of Three-Dimensional Coastal Currents and Sediment Dispersion: Model Development and Application*, Technical Report CERC-83-2, Coastal Engineering Research Center, U.S. Army Corps of Engineers, Waterways Experiment Station, Vicksburg, MS.

Sheng, Y.P., 1986. "Finite-Difference Models for Hydrodynamics of Lakes and Shallow Seas," Chapter 6, in (W. Gray, editor) *Physics-Based Modeling of Lakes, Reservoirs and Impoundments*. American Society of Civil Engineers, New York.

Sheng, Y.P., D.E. Eliason, J.-K. Choi, X.-J. Chen and H.-K. Lee, 1991a. *Numerical Simulation of Three-Dimensional Wind-Driven Circulation and Sediment Transport in Lake Okeechobee During Spring 1989*. Coastal and Oceanographic Engineering Department, University of Florida, Report to South Florida Water Management District, West Palm Beach, February.

Sheng, Y.P., D.E. Eliason, R.E. Dickinson and J.-K. Choi, 1991b. *A Three-Month Simulation of Wind-Driven Circulation, Sediment Transport, and Phosphorus Transport in Lake Okeechobee*. Coastal and Oceanographic Engineering Department, University of Florida, Report to South Florida Water Management District, West Palm Beach, July.

Sheng, Y.P. and W. Lick, 1980. *A Two-Mode Free-Surface Numerical Model for the Three-Dimensional Tide-Dependent Currents in Large Lakes*, EPA-600/3-80-047, May.

Sheng, Y.P., Y. Luo and V. Cook, 1991c. *Effect of Sediment Resuspension on Internal Loading of Phosphorus in Lake Okeechobee*. Coastal and Oceanographic Engineering Department, University of Florida, Report to South Florida Water Management District, West Palm Beach.

Shih, S.F. 1980. "Water Budget Computation for a Shallow Lake - Lake Okeechobee, Florida," *Water Resources Bulletin*, 16(4):724-728.

Smith, R.A., 1980. "The Theoretical Basis for Estimating Phytoplankton Production and Specific Growth Rate from Chlorophyll, Light and Temperature Data," *Ecological Modelling*, 10:243- 264.

Smith, V.H., 1982. "The Nitrogen and Phosphorus Dependence of Algal Biomass in Lakes: An Empirical and Theoretical Analysis," *Limnol. Oceanogr.*, 27(6): 1101-1112.

Smith V.H., E. Willenand and B. Karlsson, 1987. "Predicting the Summer Peak Biomass of Four Species of Blue-Green Algae (Cyanophyta/Cyanobacteria) in Swedish Lakes," *Water Resources Bulletin*, 23(3):397-402.

Spencer, C.N. and D.L. King, 1989. "Role of Light, Carbon Dioxide and Nitrogen in Regulation of Buoyancy, Growth and Bloom Formation of *Anabaena Flos-aquae*," *Journal of Plankton Research*, 11(2):283-296.

Staley and Jurica, 1972. ***TBA

Stauffer, R.E., 1991. "Environmental Factors Influencing Chlorophyll v. Nutrient Relationships in Lakes," *Freshwater Biology*, 25:279-295.

Stefan, H.G., S. Dhamotharan and F.R. Schiebe, 1982. "Temperature/Sediment Model for a Shallow Lake," *J. Environmental Engineering Division, ASCE*, 108(EE4):750-765 August.

Steinle, P. and R. Morrow, 1989. "An Implicit Flux-Corrected Transport Algorithm," *J. Computational Physics*, 80:61- 71.

Strickland, 1960. ***TBA

Stumm, 1977. ***TBA

Stumm, W. and J.J. Morgan, 1981. *Aquatic Chemistry*, John Wiley and Sons, New York.

Summers, J.K., 1985. "A Simulation Model of Carbon and Oxygen Dynamics in a Reservoir," *Ecological Modelling*, 28:279-309.

Swinbank, W.C., 1963. "Long-wave Radiation from Clear Skies," *Quart. J. Royal Met. Soc.*, 89:339-348.

Takamura, N and M. Yasuno, 1988. "Sedimentation of Phytoplankton Populations Dominated by *Microcystis* in a Shallow Lake," *Journal of Plankton Research*, 10(2):283-299.

Thackston, 1974. ***TBA

Topper et al., 1981. ***TBA

- Trimble, P., 1986. *South Florida Regional Routing Model*. South Florida Water Management District, Tech. Pub. No. 86-3, West Palm Beach, FL, 147 pp.
- Trimble, P.J. and J.A. Marban, 1988. *Preliminary Evaluation of the Lake Okeechobee Regulation Schedule*, South Florida Water Management District, Tech. Pub. No. 88-5, West Palm Beach, FL, 130 pp.
- Trimble, P.J. and J.A. Marban, 1989. "A Proposed Modification to Regulation of Lake Okeechobee," *Water Resources Bulletin*, 25(6):1249-1257.
- Tyler, J.E., 1968. "The Secchi Disc," *Limnology and Oceanography*, 13(1):1-6.
- U.S. Army Coastal Engineering Research Center (CERC), 1977. *Shore Protection Manual*, Dept. of the Army, Corps of Engineers, Ft. Belvoir, VA, Vol. 1.
- Van Benschoten, J.E. and W.W. Walker, 1984. "Calibration and Application of Qual-II to the Lower Winooski River," *Water Resources Bulletin*, 20(1): 109-117.
- Van Duin, E.H.S. and L. Lijklema, 1988. "Modelling Photosynthesis and Oxygen in a Shallow Hypereutrophic Lake," *Ecological Modelling*, 45:243-260.
- Vincent, W.F., et al., 1984. "Seasonal Dynamics of Nutrient Limitation in a Tropical High-Altitude Lake (Lake Titicaca, Peru- Bolivia): Application of Physiological Bioassays," *Limnol. Oceanogr.*, 29(3):540-552.
- Virtanen, M., J. Koponen, K. Dahlbo and J. Sarkkula, 1986. "Three-Dimensional Water-Quality-Transport Model Compared with Field Observations," *Ecological Modelling*, 31:185-199.
- Voinov, A.A. and Y.M. Svirezhev, 1984. "A Minimax Model of Eutrophication in Freshwater Ecosystems," *Ecological Modelling*, 23:277-292.
- Voinov, A.A. and A.A. Akhremenkov, 1990. "Simulation Modeling System for Aquatic Bodies," *Ecological Modelling*, 51:181-205.
- Vollenweider, R.A., 1969. "Possibilities and Limits of Elementary Models Concerning the Budget of Substances in Lakes," *Arch. Hydrobiol.*, 66(1):1-36.
- Vollenweider, R.A., 1985. "Elemental and Biochemical Composition of Plankton Biomass; Some Comments and Explorations," *Arch. Hydrobiol.*, 103(1):11-29.
- Wang, M. and D.R.F. Harleman, 1982. *Hydrothermal-Biological Coupling of Lake Eutrophication Modeling*, MIT Ralph M. Parsons Laboratory Technical Report No. 270, Department of Civil Engineering, MIT, Cambridge, MA.

- Weller, M.W., 1981. *Freshwater Marshes*, University of Minnesota Press, Minneapolis, MN.
- Wetzel, R.G., 1983. *Limnology*, Saunders College Publishing, New York.
- Wofsy, S.C., 1983. "A Simple Model to Predict Extinction Coefficients and Phytoplankton Biomass in Eutrophic Waters," *Limnol. Oceanogr.*, 28(6):1144-1152.
- Wroblewski, J.S., J.L. Sarmiento and G.R. Flierl, 1988. "An Ocean Basin Scale Model of Plankton Dynamics in the North Atlantic 1. Solutions for the Climatological Oceanographic Conditions in May," *Global Biogeochemical Cycles*, 2(3):199-218.
- Yentsch, C.M. and J.W. Campbell, 1991. "Phytoplankton Growth: Perspective Gained by Flow Cyclometry," *Journal of Plankton Research*, 13, Supplemental, pp. s83-s108.
- Zaffke, A.C., 1984. *Wading Bird Utilization of Lake Okeechobee Marshes 1977-1981*. South Florida Water Management District, Tech. Pub. No. 84-9, West Palm Beach, FL, 38 pp.
- Zalesak, S.T., 1979. "Fully Multidimensional Flux-Corrected Transport Algorithms for Fluids," *J. Computational Physics*, 31:335-362.

Appendix A: Dictionary of FORTRAN Variables

This appendix is a compilation of the FORTRAN variables used in the Lake Okeechobee phosphorus models LOP0D and LOP3D.

Variable	Description
ADEEP	Two dimensional character array for hexa plots.
ADKON	Partition coefficients for PIP (liter/kg).
ADEV	Advection in sigma direction. One dimensional array.
ADVEC	Advection in X and Y directions. Two dimensional array.
AHR	Constant value for diffusion in X direction (cm**2/sec)
AK	Adsorption coefficient (liter/kg) in diagenetic model.
AKON	Diagonal coefficient for tridiagonal solution.
AMAX	Light saturation constant in units of cal/cm**2-min.
AMASS	Added inflow phosphorus mass.
ANGLAT	Latitude of lake.
AR	Computational cells in the model lake.
ARDN	Index for type of down cell boundary condition. One dimensional array.
ARLF	Index for type of left cell boundary condition. One dimensional array.
ARRI	Index for type of right cell boundary condition. One dimensional array.
ARUP	Index for type of up cell boundary condition. One dimensional array.
ARLOW	Area parameter.
ASED	Analytical SRP concentration in diagenetic model.
ATTITLE	General simulation title.
ATRAN	Difference in inter-box CTRAN values.
AVR	Reference value for diffusion in sigma direction (cm**2/sec).
BAR	Box model outlines for Lake Okeechobee. 0 - Not part of lake. 1 - Mud zone. 2 - Macrophyte zone. 3 - North lake. 4 - Sandy fringe. 5 - South Bay zone.
BFMASS	Added diagenetic phosphorus mass.
BLUN	Blue-Green algae phosphorus concentration at old time step. Three dimensional array.
BLU	Blue-Green algae phosphorus concentration at new time step. Three dimensional array.

Variable	Description
BMASS	Beginning phosphorus mass.
BTFLUX	Added atmospheric phosphorus mass.
BQMAS2	Beginning quadratic phosphorus mass.
BNAME	Name of the lake sector.
BTOTAL	Two dimensional array summing advective, diffusive and reaction pathways during the simulation in the diagenetic model.
BTRAN	Difference in inter-box CTRAN values.
BVOL	Beginning volume of the lake.
CALBOX	= 'N' No reactions simulated in sector I. = 'Y' Reactions simulated in sector I.
CBIG	Maximum concentration of phosphorus species calculated during the simulation. Three dimensional array.
CDOWN	Phosphorus concentration in cell one down.
CDP	Daily diffusive flux of SRP from the sediments.
CENTER	Phosphorus concentration in cell.
CEQQ	Equilibrium concentration for lowest layer of diagenetic model.
CLAYER	Current phosphorus species concentration in the layers of the cell.
CLEFT	Phosphorus concentration in cell to left.
CLOWER	Lowest allowable phosphorus species concentration.
CMEAN	Ending collector mean phosphorus concentration.
CMASS	Ending collector phosphorus mass.
CNAME	Name of the phosphorus species.
COLD	Old time step center cell depth.
CORB	Corbicula mass in a computational cell.
	Two dimensional array.
CQMAS2	Ending collector quadratic phosphorus mass.
CRIGHT	Phosphorus concentration in cell to right.
CSED	Calculated SRP concentration in diagenetic model.
CSURFN	Variable used to sum SRP and TP for SURFER plotting.
CSUSP	Erosion parameter.
CTIME	Time history of phosphorus concentrations in each sector printed at the end of simulation. Three dimensional array.
CTOP	SRP concentration at sediment-water interface.
CTOTAL	Two dimensional array summing advective, diffusive and reaction pathways during the simulation.
CTRAN	Phosphorus concentration in box model.
CUP	Phosphorus concentration in a cell one up.
CUPPER	Highest allowable phosphorus species concentration.

Variable	Description
D	Down cell in Y direction.
DAY	Day of the week.
DAYSEC	Number of seconds in one day.
DIFF	Diffusion in X and Y directions. Two dimensional array.
DIFV	Diffusion in sigma direction. One dimensional array.
DD	Diffusion (cm**2/yr) in pore water in diagenetic model.
DD1	Real variable used for weighting time steps less than the hydrodynamic time step.
DD2	Real variable used for weighting time steps less than the hydrodynamic time step.
DLAMB	Diffusion (cm**2/yr) for solid phase in diagenetic model.
DEPN	Deposition in a cell at old time step. Two dimensional array.
DEP	Deposition in a cell at new time step. Two dimensional array.
DEPLOW	Minimum depth allowed in simulation (m).
DIAG	Diagonal elements for tridiagonal solution.
DIFCON	Inter-box diffusive-transport coefficient.
DOPN	Dissolved organic phosphorus concentration at old time step. Three dimensional array.
DOP	Dissolved organic phosphorus concentration at new time step. Three dimensional array.
DRHO	Sediment density for diagenetic model.
DTIME	Simulation time from coastal interface file.
DX	Open water cell X length (cm).
DX1	Aerobic layer space increment.
DX2	Anaerobic layer space increment.
DY	Open water cell Y length (cm).
DTLONG	Time in minutes for hour correction.
EE3	Reciprocal of NSIG squared.
EH1	Old time step time-weighting parameter for X, Y diffusion.
EH2	New time step time-weighting parameter for X, Y diffusion.
EM	Total change in cell phosphorus mass during the simulation. Two dimensional array.
EMASS	Ending phosphorus mass.
ENAME	Name of uptake pathways.
EQMAS2	Ending quadratic phosphorus mass.
ERON	Erosion in a cell at old time step. Two dimensional array.
ERO	Erosion in a cell at new time step. Two dimensional array.
EZDIF	Diffusion in vertical direction at new and old time steps. Two dimensional array.

Variable	Description
FLOW	Tributary inflows. One dimensional array.
FWIND	Wind parameter.
GOI	Integer array used to read coastal interface file.
GBN	Vertical diffusion at old time step. 3-D array.
GB	Vertical diffusion at new time step. 3-D array.
GRNN	Green algal phosphorus concentration at old time step. Three dimensional array.
GRN	Green algal phosphorus concentration at new time step. Three dimensional array.
HKON	Constant lake depth for all cells.
HNEW	New time step center cell depth.
HOLD	Old time step center cell depth.
HOWINT	= '1' EHSM interpolation. = '2' Average interpolation.
HUN	U cell face velocity at the new time step. Two dimensional array.
HU	U cell face velocity at the new time step. Two dimensional array.
HULF	Left U face cell depth at old and new time steps. One dimensional array.
HURI	Left U face cell depth at old and new time steps. One dimensional array.
HV	V cell face velocity at the new time step. Two dimensional array.
HVBT	Bottom V face cell depth at old and new time steps. One dimensional array.
HVN	V cell face velocity at the new time step. Two dimensional array.
HVTB	Top V face cell depth at old and new time steps. One dimensional array.
HYTIME	Hydrodynamic time step in seconds.
IADPHI	Key for adding surface elevation to center cell and cell face depths.

Variable	Description
IBOX	One dimensional array for index of I points of collector.
ICOL	One dimensional array for index of I points of source.
ICOMP	Index for computational cell. Two dimensional array.
IJTOT	1-D array for total number of cells in a lake sector.
IM	Array dimensions in X direction.
IMAX	= 0 use minimum value of 0.0 in concentration plots. = 1 use actual minimum value in concentration plots.
INAME	Name of the solution used in advection-diffusion scheme.
ISD	Bottom sediment flag. Two dimensional array. 0 - sandy area 1 - mud zone 2 - macrophyte area 3 - peat area
ISOL	Solution technique for advection. = 1 Upwind method. = 2 Donor cell method. = 3 Sheng combined upwind - central difference. = 4 Central difference. = 5 ZIP difference.
IT1	Beginning iteration number.
IT2	Ending iteration number.
ITNUM	Iteration number from coastal interface file.
ITS	Iteration time step.
ITSTOP	Stop reading data at this iteration.
JBOX	One dimensional array for index of J points of collector.
JCHAN	Print total change in cell phosphorus mass.
JCOL	One dimensional array for index of J points of source.
JCONC	= 0 Constant initial concentration. = 1 Synoptic survey initial concentration. = 2 Beginning and ending Synoptic survey concentrations.
JHR	Hour of the day.
JLIN	Print ending concentrations every JLIN layers.
JM	Array dimensions in Y direction.
JPATH	= '1' Advection-Diffusion only. = '2' Advection-Diffusion-Reaction. = '3' Reactions only.
JPDSM	Print divergence in cell.
IDIV	= 0 Spart fraction used to calculate PIP. > 0 Partition coefficient used to calculate PIP.
IDO	Counter for number of time interface file from coastal engineering is called for new data.

Variable	Description
JPLOT(1)	= 'N' do not create a SURFER grid file. = 'Y' Create a SURFER grid file on NSCRAT(1) of initial concentration values.
JPLOT(2)	= 'N' do not create a movie output file. = 'Y' Create a movie file on NSCRAT(2).
JPLOT(3)	= 'N' do not create a SURFER grid file. = 'Y' Create a SURFER grid file on NSCRAT(1) of final concentration values.
JPRINT	= 'N' do not print initial lake data. = 'Y' Print all initial lake data.
JSEC	Second.
JULDAY	Julian date.
JVEL	= 0 Use coastal engineering data set for cells. = 1 Use a constant velocity field.
JLAYER	= 'N' Do not print all final layer information. = 'Y' Do print all final layer information.
KSROW	Starting computational row in model.
KEROW	Ending computational row in model.
KSCOL	Starting computational column in model.
KSCOL	Ending computational column in model.
LDIAG	Lower diagonal elements for tridiagonal solution.
LAYERS	Number of layers in diagenetic model.
LOWLAY	Lowest aerobic layer in diagenetic model.
LF	Left cell in X direction.
LIGHT	Average solar radiation at each layer for a time step.
LOW	Lower (anaerobic) layer of diagenetic model.
LXXX	I subscript array for inflow - outflow nodes.
LYYY	J subscript array for inflow - outflow nodes.
KL	K - 1 sigma layer.
KC	K sigma layer.
KH	K + 1 sigma layer.
KM	Array dimensions in sigma direction.
KMIN	Michaelis-Menton constant for uptake (ug/l).
KO	Sum of K-1, K, and K+1 layers at old time step.
KORG	Precipitation rate in diagenetic model (1/yr).
KPPT	Precipitation rate in diagenetic model (1/yr).
KPRINT	Print input information KPRINT layers in diagenetic model.

Variable	Description
MATYPE	= 'P' PC computer. = 'V' VAX computer. = 'S' Silicon graphics computer.
MASOL	= 'P' PC computer code. = 'E' EHSM modified code.
MDAY	Integer used to calculate the day of the year.
MDP	Maximum dimension for tridiagonal solution.
MEAT	A phosphorus species eaten by another species.
MINUTE	Minute of hour.
MAKUNF	= 'N' Do not make an unformatted input file. = 'Y' Make an unformatted input file.
MONTH	Integer number for month of year.
MTIME	The number of iterations simulated starting at one.
NBOX	Number of sectors in model.
NBOX1	Number of sectors in model + entire lake.
NCOL	The number of columns simulated.
NDAY	Day of the month.
NISS	Number of stations with initial concentration data.
NREAC	Number of reacting phosphorus species.
NROW	The number of rows simulated.
NSED	Number of sediment types in diagenetic model.
NSIG	The number of layers in sigma direction.
NSOUR	Number of inflow and outflow sources.
NQ	Array dimension for moving quality parameters.
NQ1	Array dimension for total quality parameters + sediment.
NQ2	Array dimension for total quality parameters + suspended sediment and total phosphorus.
NQMOV	Number of advective phosphorus species.
NQUAL	Number of total phosphorus species.
OMEGA	Omega at new time step. One dimensional array.
OMEGAN	Omega at old time step. One dimensional array.
OPFRAC	Organic P in sediment (mg/kg).
OPMEAN	Uptake for current time step for an uptake pathway.
ORG	Sediment organic phosphorus concentration. 3-D array.
PIP	Particulate inorganic phosphorus concentration. 3-D array.
PNAME	Name of excretion or decay pathways.
POR	Porosity (fraction) in sediment.

Variable	Description
PORG	Two dimensional array for organic phosphorus in each layer of the diagenetic model.
PSTAR	Dimensionless density in aerobic and anaerobic layers of the diagenetic model.
PTOP	Organic concentration in top layer of diagenetic model.
QMOV	Integer value corresponding to WQ constituents in model. 1 ==> SRP 2 ==> DOP 3 ==> GRN 4 ==> BLU 5 ==> ZOO 6 ==> PIP 7 ==> OPSED 8 ==> Sediment
RAD	Average solar radiation at noon for Lakeland, Fla. 2-D array.
RB1	Old time step time-weighting parameter for X and Y direction advection.
RB2	New time step time-weighting parameter for X and Y direction advection.
RCTERM	Control reaction terms. One dimensional array.
RDFORM	= '1' Input data from COE is unformatted. = '2' Input data from COE is unformatted and adjusted. = '3' Input data from COE is from SG.
REDLOW	Ratio of tributary loadings to be used in simulation to values in input data file.
RESPIR	Respir coefficients for NQUAL constituents (1/day).
RHS	Right hand side vector for tridiagonal solution.
RI	Right cell in X direction.
SDIST	The reciprocal of NSIG.
SEDIM	Two dimensional array for reading suspended sediment synoptic concentrations.
SETTL	Maximum settling rate (1/day).
SOLP	Two dimensional array for reading soluble phosphorus synoptic concentrations.
SMEAN	Beginning source mean phosphorus concentration.
SMASS	Beginning source phosphorus mass.
SPART	PIP in sediment (fraction).
SPEED	Interbox advection parameter (m/day).
SQMAS2	Beginning source quadratic phosphorus mass.
SRPP	Two dimensional array for reading SRP synoptic concentrations.
SRHO	Suspended sediment density (gm/cm**3).
SSC	Self-shading coefficients. One dimensional array.
SVOL	The volume in one cell layer of open water.
SRAD	Average radiation over lake during time step.
SRPN	SRP concentration at old time step. 3-D array.
SRP	SRP concentration at new time step. 3-D array.

Variable	Description
SYLINE	Diagenetic simulation title.
T1FLUX	Top flux of SRP (mg/m**2-yr).
T2FLUX	Top flux of DOP (mg/m**2-yr).
TBMAX	Maximum shear stress (dyne/cm**2).
TCONC	Maximum TP concentration allowed in Nubbin Slough/Taylor Creek tributary inflow.
TEMP	Average monthly lake temperature in degrees C.
TEMPER	Modeled water temperature of lake in degrees C.
THETA	Theta values for temperature adjustment.
TIMDAY	Time of day in seconds.
TMASS	Input concentrations for inflow nodes. Two dimensional array.
TOTP	Two dimensional array for reading total phosphorus synoptic concentrations.
UDIAG	Upper diagonal elements for tridiagonal solution.
UKON	Constant U velocity for unreal simulations.
UL	Left U face cell velocity at old and new time steps.
UMAX	One dimensional array.
UP	Maximum U velocity or Uref.
UPMAX	Up cell in Y direction.
UPMIN	Maximum uptake rate (1/day).
UPMXX	Minimum allowable maximum uptake rate (1/day).
UR	Maximum allowable maximum uptake rate (1/day).
UPP	Right U face cell velocity at old and new time steps.
UREF	One dimensional array.
USED	Upper (aerobic) layer of diagenetic model.
VAR	Reference value for velocity in X and Y directions (cm/sec).
VAVG	Multiplier to get maximum daily wind speed from average.
VEL	Unknown solution vector for tridiagonal solution.
VV	Average layer volume.
VDN	Mass balance in cell during a time step.
VKON	Two dimensional array.
VMAX	Burial velocity (cm/yr) in diagenetic model.
VU	Bottom V face cell velocity at old and new time steps.
	One dimensional array.
	Constant V velocity for unreal simulations.
	Maximum V velocity or Uref.
	Top V face cell velocity at old and new time steps.
	One dimensional array.

Variable	Description
W1	Old time step time-weighting parameter for sigma advection.
W2	Old time step time-weighting parameter for sigma advection.
WD1	Old time step time-weighting parameter for sigma diffusion.
WD2	Old time step time-weighting parameter for sigma diffusion.
WKON	Constant W velocity for unreal simulations.
WMAX	Maximum W velocity or Wref.
WREF	Reference value for velocity in sigma direction.
XTRANS	Distance between model boxes (km).
YTRANS	Inter-box boundary length (km).
ZREF	Reference value for depth (cm).
SREF	Reference value for water surface elevation (cm).
ZOON	Zooplankton concentration at old time step.
ZOO	Three dimensional array. Zooplankton concentration at new time step. Three dimensional array.

Appendix B: List of Symbols

a	Light absorption coefficient for water particles.
a_t	Atmospheric transmission coefficient.
A_k	Cross sectional area of a lake box.
A_v	Vertical diffusion coefficient (cm^2/s).
A_s	Shortwave albedo or reflection coefficient.
A_l	Longwave albedo or reflection coefficient.
b	Light scattering coefficient for particles in water.
B_r	Bowen ratio.
c_p	Heat capacity of water (cal/g).
C_{aq}	Concentration of SRP in sediment pore (interstitial) water.
C_l	Fraction of sky covered by clouds.
C_{srp}	Porewater SRP in the sediment (ug/l).
C_{susp}	Coefficient of suspension (s/cm).
D_L	Length of day (hours).
D_{eff}	Effective aerobic diffusion coefficient in the sediment (cm^2/s).
D_Γ	Effective aerobic diffusion coefficient due to bioturbation in the sediment (cm^2/s).
DIFCON	Coefficient for diffusive-type transport in LOP0D (m/s).
e_a	Vapor pressure of atmosphere (mbar).
e_s	Saturation vapor pressure (mbar) at the surface water temperature.
E	Evaporation rate (m/sec).
E_ϕ	Latitude of a location on earth.
$f_1(T)$	Temperature function modifying reaction rates.
$f_2(I)$	Light function modifying algal uptake.
F	Formation factor.
F_d	Rate of deposition (gm/cm^2).
F_e	Rate of resuspension or erosion (gm/cm^2).
f_w	Dimensionless wave friction factor.
F_w	Diffuse fraction of the total subsurface radiation.
g	Gravitational acceleration (m/s^2)
HR_α	Hour angle.
HR_{sr}	Hour of sunrise.
HR_{ss}	Hour of sunset.
I_{noon}	Standard year, clear sky, solar noon irradiance.
I_o	Surface irradiance.
I_z	Irradiance at a depth z .
I_{od}	Light half saturation coefficient for DIA.
I_{oG}	Light half saturation coefficient for GRN.
I_{oB}	Light half saturation coefficient for BLU.
k_{rG}	New growth respiration coefficient of GRN.
k_{rB}	New growth respiration coefficient of BLU.
k_{rd}	New growth respiration coefficient of DIA.
k_{rz}	New growth respiration coefficient of ZOO.
K_{SP}	Partition coefficient between pelagic PIP and SRP.

K_{Chl}	Phosphorus to chlorophyll ratio.
K_G	Michaelis-Menten half saturation constant for GRN uptake of SRP (ug/l)
K_B	Michaelis-Menten half saturation constant for BLU uptake of SRP (ug/l).
K_d	Michaelis-Menten half saturation constant for DIA uptake of SRP (ug/l).
K_{ZG}	Michaelis-Menten half saturation constant for ZOO uptake of GRN (ug/l).
K_{ZB}	Michaelis-Menten half saturation constant for ZOO uptake of BLU (ug/l).
K_{Zd}	Michaelis-Menten half saturation constant for ZOO uptake of DIA (ug/l).
K_D	Bacterial mineralization of DOP to SRP (1/day).
K_L	Saturation light intensity at which algal growth is a maximum.
K_{Gd}	Mortality of GRN (1/day).
K_{Bd}	Mortality of BLU (1/day).
K_{dd}	Mortality of DIA (1/day).
K_{Zd}	Mortality of ZOO (1/day).
K_{sp}	Partition coefficient between pelagic PIP and SRP (liter/mg).
K_{org}	Organic phosphorus partition coefficient in pelagic sediment (ug/l / mg/l = ug/mg).
K_{spip}	Settling velocity of PIP (m/day).
K_{sorg}	Settling velocity of ORG (m/day).
K_{sht}	Surface heat transfer coefficient (ly/day/°C).
K_d	Vertical irradiance attenuation coefficient.
K_{vsun}	Vertical irradiance attenuation coefficient for the direct component of $E(0, \Theta_r)$.
K_{vsky}	Vertical irradiance attenuation coefficient for the diffuse component of $E(0, \Theta_r)$.
K^*	Modified linear adsorption coefficient.
L	Deep water wavelength (m).
L_w	Latent heat of vaporization (kcal/kg).
L_ϕ	Western longitude in radians.
M	Optical air mass.
M_{day}	Day of the year from 1 to 365 (ignoring leap years)
ΔM	Concentration change due to diffusion.
ΔMM	Concentration change due to advection.
R_h	Relative humidity expressed as a fraction.
r_{rad}	Normalized earth-sun radius.
r_{oG}	Maintenance respiration rate of GRN (1/day).
r_{oB}	Maintenance respiration rate of BLU (1/day).
r_{od}	Maintenance respiration rate of DIA (1/day).
r_{oZ}	Maintenance respiration rate of ZOO (1/day).
S	Velocity coefficient for LOP0D advection (m/s).
SD	Secchi depth (m).
S_L	Solar longitude.

t	Universal time (hours).
T_a	Air temperature 2 meters above the ground ($^{\circ}\text{C}$).
T_e	Equilibrium temperature ($^{\circ}\text{C}$).
T_s	Water temperature ($^{\circ}\text{C}$).
T_c	Critical temperature for algal growth ($^{\circ}\text{C}$).
T_{opt}	Optimum temperature at which growth rate is maximum ($^{\circ}\text{C}$).
T_{\min}	Temperature at which growth rate is zero ($^{\circ}\text{C}$).
T_{\max}	Upper temperature tolerance limit at which the growth rate is zero ($^{\circ}\text{C}$).
T_n	Turbidity (JTU or NTU).
T_s	Surface water temperature ($^{\circ}\text{C}$).
ν_{aq}	Burial rate of interstitial water in the sediment (cm/yr).
ν_s	Burial rate of sediment particles in the sediment (cm/yr).
v_{sG}	Settling rate of GRN (m/day).
v_{sB}	Settling rate of BLU (m/day).
v_{sd}	Settling rate of DIA (m/day).
V_k	Volume of a lake box (m^3).
x_i	Inter-box distance (km). = DIFCON $\cdot Y_i/x_i$.
X_i	Depth of lake box (m).
y_k	Inter-box boundary distance (km).
Y_i	Depth dimension in diagenetic model (m).
z_s	Zenith angle.
Z	Solar altitude.
α	A constant ranging from 0.8 to 1.27 $\text{NTU} \cdot \text{m}$
α_n	The long wave fraction of the incoming radiation at the water surface or the fraction of solar radiation adsorbed in the surface layer.
β	Concentration of sediment phosphorus.
Γ	Earth's declination.
δ_{decl}	Extinction coefficient for solar radiation in water.
ϵ	Atmospheric emissivity.
ϵ_a	Extinction coefficient of water.
ϵ_w	Extinction coefficient of water due to color.
ϵ_{col}	Linear self shading extinction coefficient for green algae (GRN).
ϵ_G	Linear self shading extinction coefficient for blue green algae (BLU).
ϵ_B	Linear self shading extinction coefficient for diatom algae (DIA).
ϵ_d	Linear self shading coefficient for suspended sediment (SED).
ϵ_s	Dynamic viscosity of water ($\text{g}/\text{cm}\cdot\text{s}$).
η	Blue-green algae density (g/cm^3).
ρ_B	Green algae density (g/cm^3).
ρ_G	Diatom algae density (g/cm^3).
ρ_d	Sediment density (g/cm^3).
ρ_s	Water density (gm/cm^3).
ρ_w	Coefficient for temperature dependence.
Θ	Carbon to Chlorophyll ratio.
Θ_c	In-water refracted angle.
Θ_r	Sediment porosity.
ϕ	

ϕ_a	Incoming long wave radiation from the atmosphere (ly/day).
ϕ_{an}	Net incoming longwave radiation from the atmosphere (ly/day).
ϕ_{ar}	Reflected long wave radiation = $A_l \cdot \phi_a$ (ly/day).
ϕ_{br}	Back radiation emitted by the water (ly/day).
ϕ_c	Energy advected from or to the water surface (ly/day).
ϕ_e	Energy utilized by evaporation (ly/day).
ϕ_n	Net surface heat flux (ly/day).
ϕ_s	Shortwave radiation incident to water surface (ly/day).
ϕ_{sc}	Solar constant (ly/day).
ϕ_{sn}	Net shortwave radiation incident to the water surface (ly/day).
ϕ_{sr}	Reflected shortwave radiation = $A_s \cdot \phi_s$ (ly/day).
ϕ_z	Shortwave solar radiation at depth z in water column (ly/day).
σ_{sb}	Stefan-Boltzmann constant = 8.26×10^{-11} , cal/cm ² /min/°K ⁴ .
τ_o	Threshold shear stress below which suspension does not occur in the lake (dynes/cm ²).
τ_b	Stress (dynes/cm ²).
μ_d	Maximum uptake of SRP by DIA (1/day).
μ_G	Maximum uptake of SRP by GRN (1/day).
μ_B	Maximum uptake of SRP by BLU (1/day).
μ_{ZC}	Maximum uptake of DIA by ZOO (1/day).
μ_{ZG}	Maximum uptake of GRN by ZOO (1/day).
μ_{ZB}	Maximum uptake of BLU by ZOO (1/day).
ΣR_{aq}	Sum of all chemical reactions affecting C _{aq} .
ΣR_Γ	Sum of all chemical reactions affecting Γ .

Appendix C: Lake Okeechobee SRP and TP-SRP Trends

The trend of 1979-1988 in-lake concentrations of the nutrients SRP and TP-SRP (TP minus SRP) was investigated using linear regression with the nutrients as the dependent variable and a cubic function of time as the independent variable. For example, for SRP:

$$\text{SRP} = \text{Intercept} + A \cdot \text{date} + B \cdot \text{date}^2 + C \cdot \text{date}^3 \quad (\text{C-1})$$

A similar equation applies for TP-SRP.

The eight long term stations discussed in Chapter 5 plus a combination of the central mud zone stations and non-mud zone stations are examined in this section. The non-mud stations are: L001, L003, and L007. The mud stations are: L002, L003, L004, L006, and L008. The correlation coefficients, r , of twenty regressions are presented in Table C-1. (Their statistical significance has not been assessed because of autocorrelation between adjacent data points.) Plots of the cubic functions are shown for the eight individual stations in Figures C-1 - C-8 for SRP and C-9 - 16 for TP-SRP. Similar plots for SRP and TP-SRP are shown for mud and non-mud stations in Figures C-17 - C-20.

There is generally a decreasing trend in SRP data after 1984 and no trend in the TP-SRP difference after 1984. In particular, although the plot of SRP versus time shown in Figure 1-4 seems to indicate an increasing trend in TP and SRP concentrations, Figures C-1 - C-8 clearly indicate that at all stations SRP concentrations "level off" after the early 1980s, with two stations (L003 and L004) indicating a sharp decline. Both mud (Figure C-17) and non-mud (Figure C-19) stations indicate a similar rise in concentration until the early 1980s, followed by a gradual decline.

The TP-SRP fits are more ambiguous with some stations indicating an increase in the latter 1980s, and others not. The mud stations (Figure C-18) tend to show more of an increase than do the non-mud stations (Figure C-20). This is possibly due to the higher erosional capability of the mud zone.

Table C-1 Correlation coefficient (r) between dependent variables SRP and TP-SRP and the independent variables consisting of a cubic function of time for nutrient data between the years 1972 and 1989.

Station	SRP	TP-SRP
L001	0.33	0.31
L002	0.28	0.35
L003	0.45	0.35
L004	0.52	0.37
L005	0.12	0.37
L006	0.44	0.39
L007	0.33	0.35
L008	0.29	0.35
Mud	0.46	0.42
Non-Mud	0.46	0.41

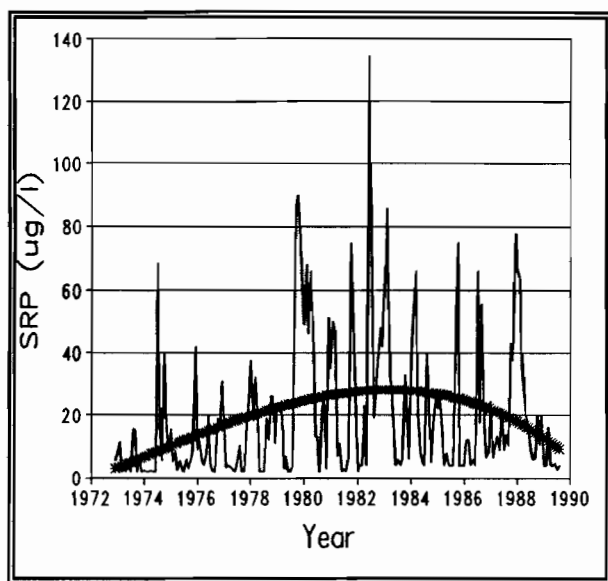


Figure C-1 Station L001 SRP.

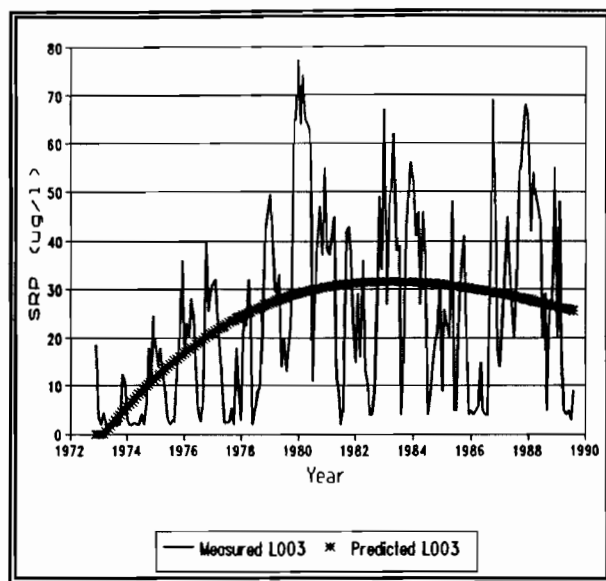


Figure C-3 Station L003 SRP.

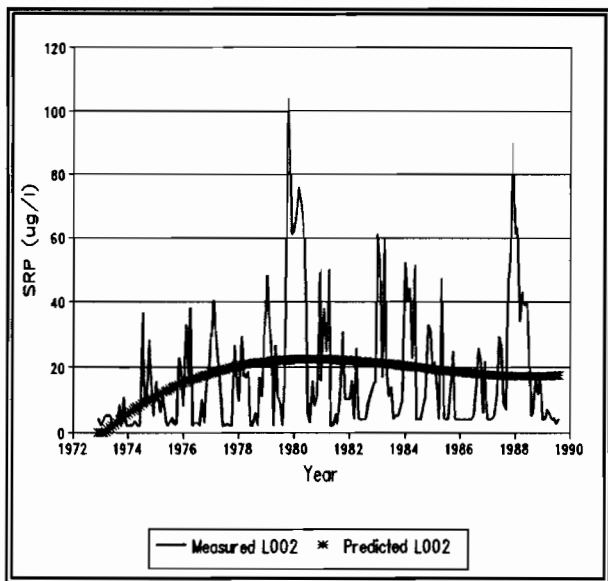


Figure C-2 Station L002 SRP.

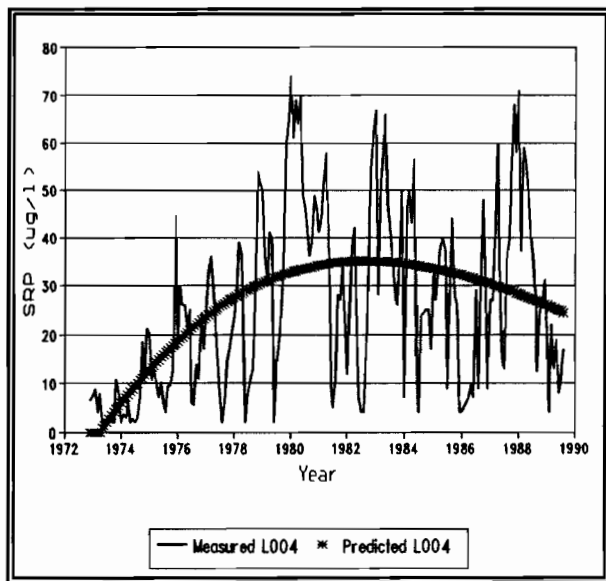


Figure C-4 Station L004 SRP.

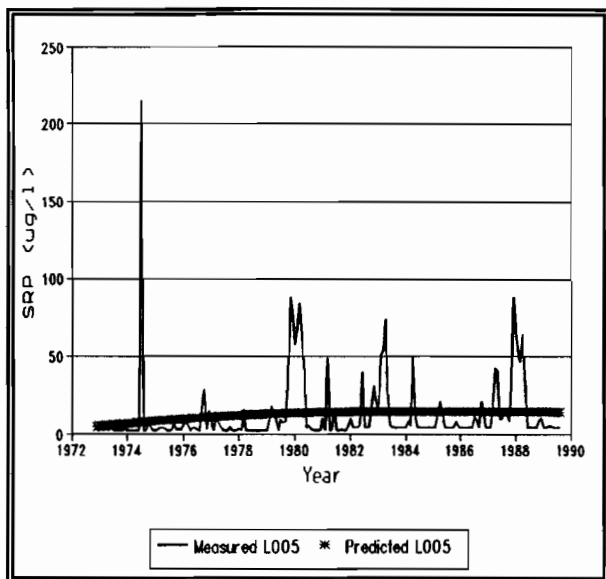


Figure C-5 Station L005 SRP.

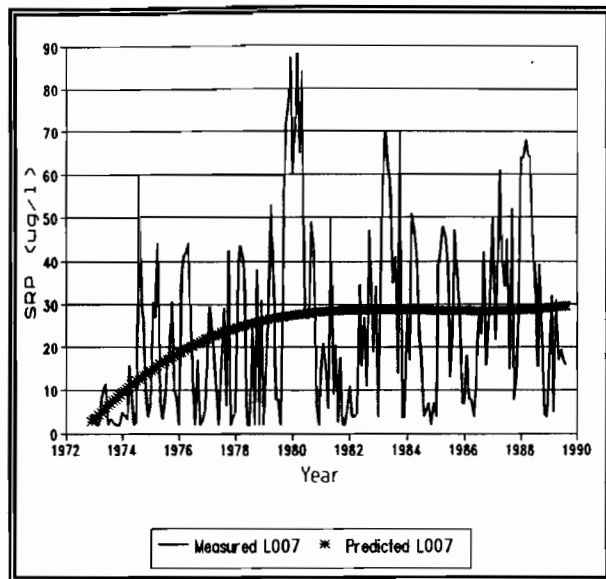


Figure C-7 Station L007 SRP.

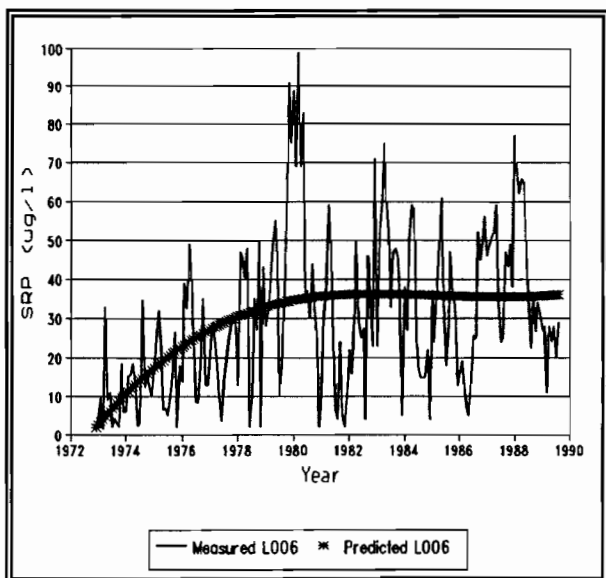


Figure C-6 Station L006 SRP.

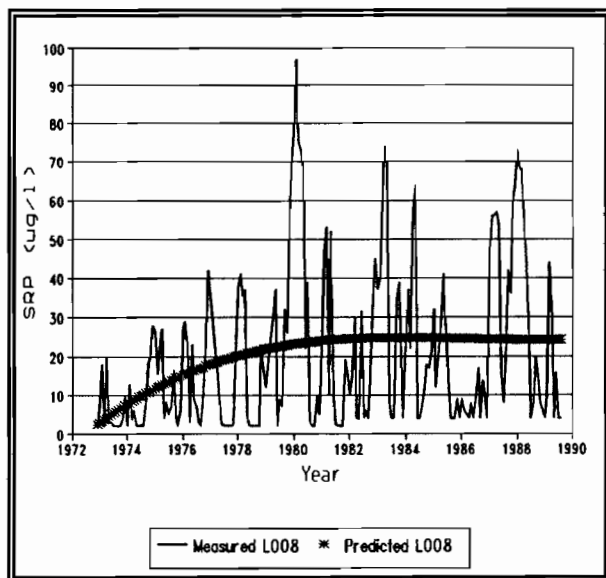


Figure C-8 Station L008 SRP.

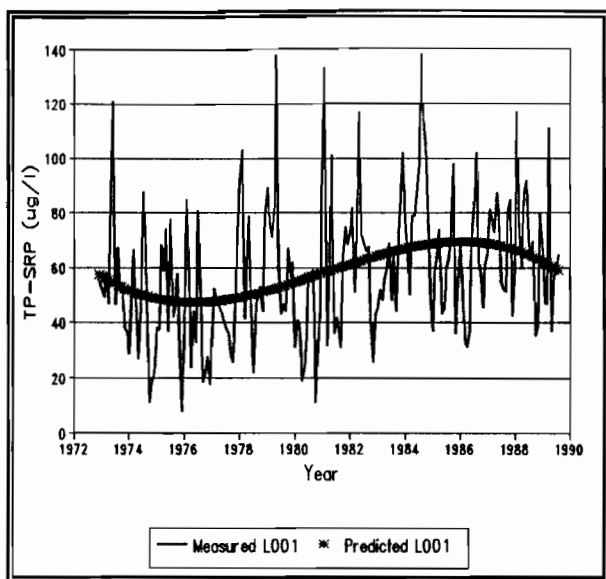


Figure C-9 Station L001 TP-SRP.

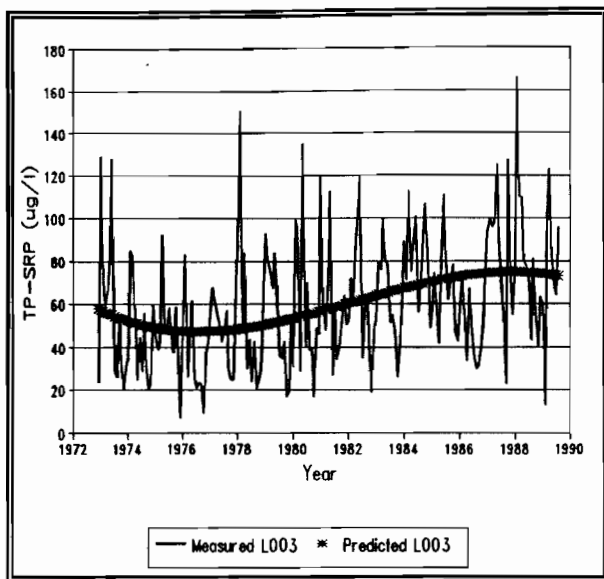


Figure C-11 Station L003 TP-SRP.

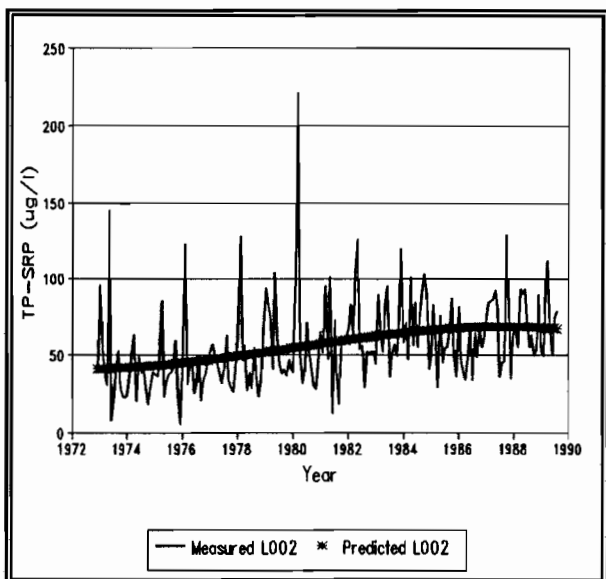


Figure C-10 Station L002 TP-SRP.

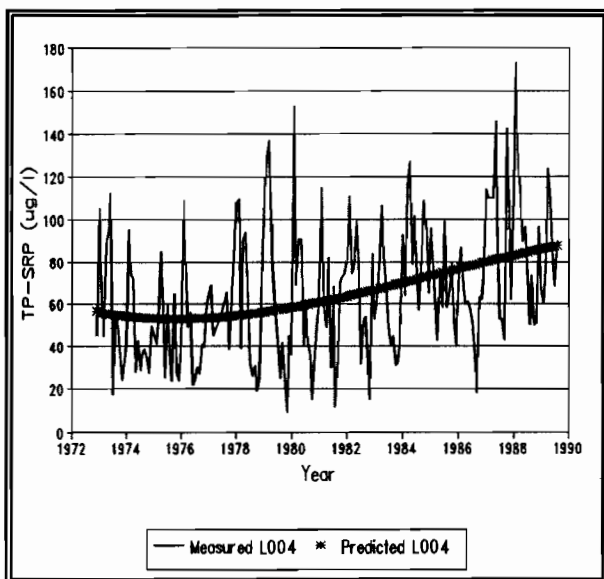


Figure C-12 Station L004 TP-SRP.

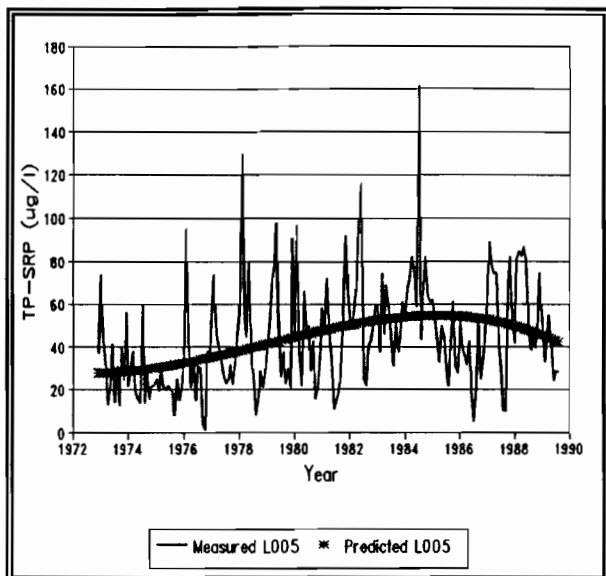


Figure C-13 Station L005 TP-SRP.

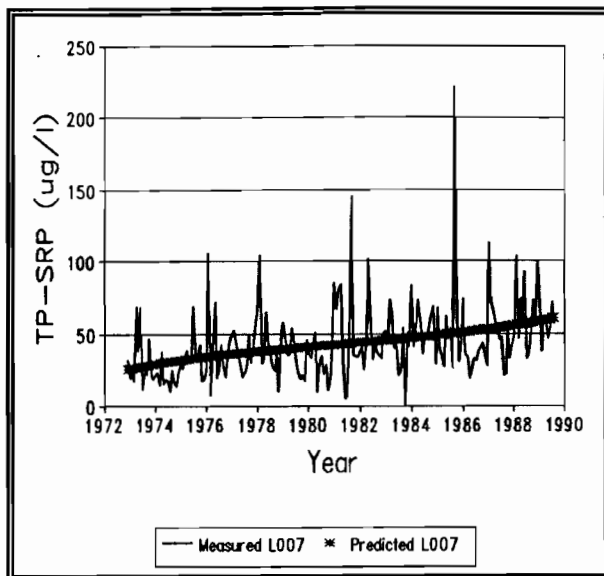


Figure C-15 Station L007 TP-SRP.

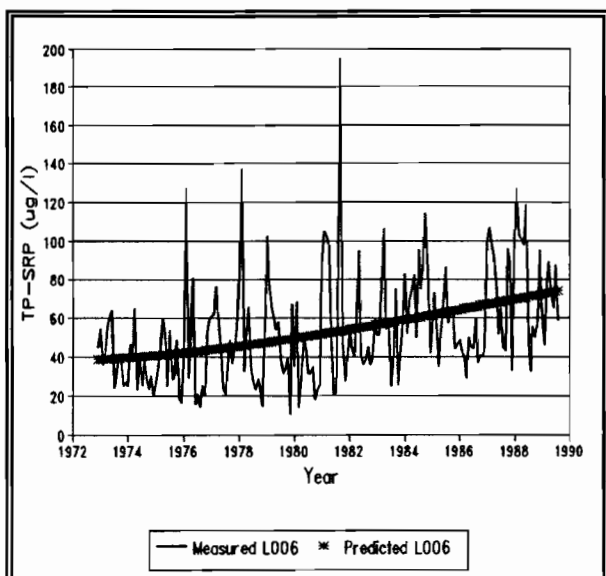


Figure C-14 Station L006 TP-SRP.

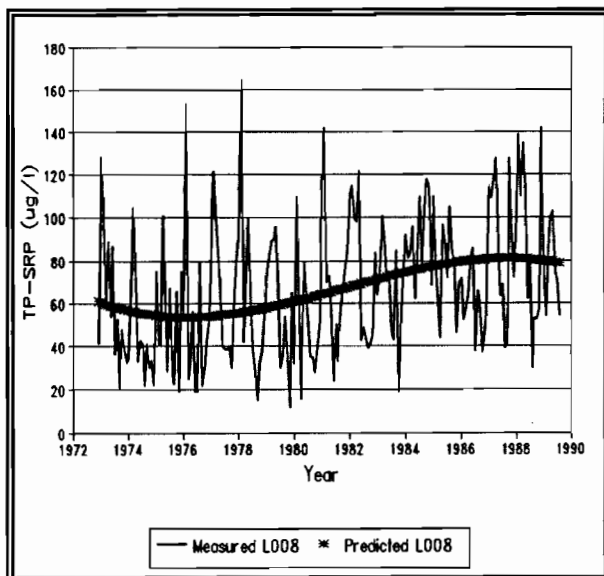


Figure C-16 Station L008 TP-SRP.

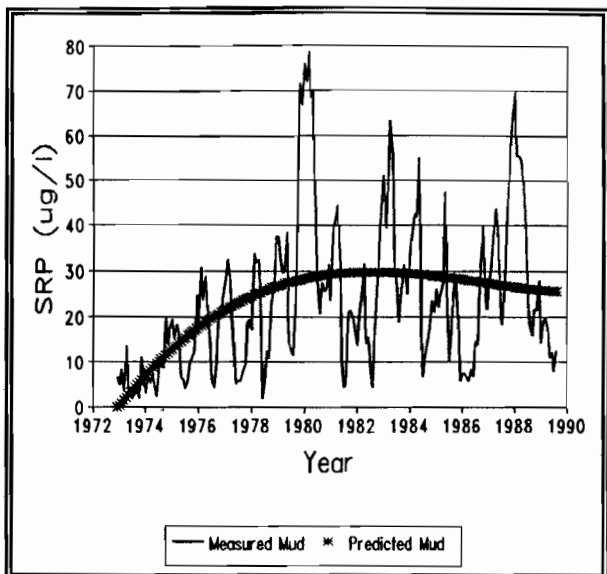


Figure C-17 MUD station SRP.

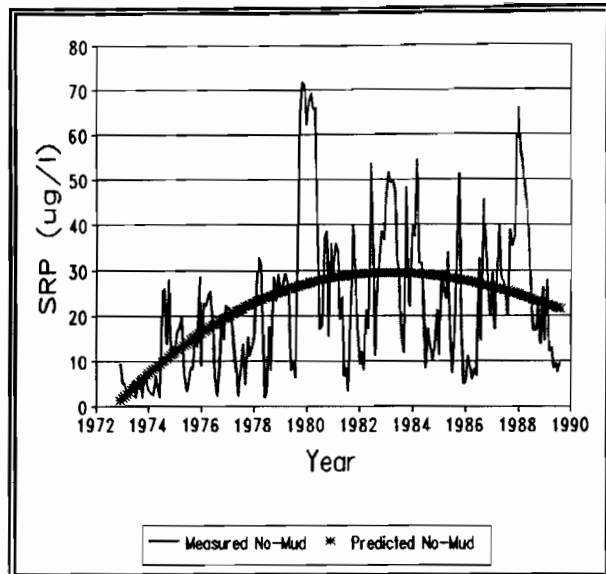


Figure C-19 Non-MUD station SRP.

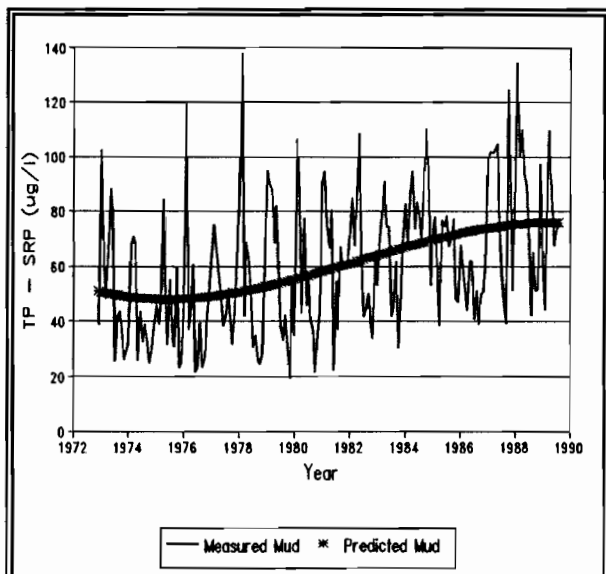


Figure C-18 MUD station TP-SRP.

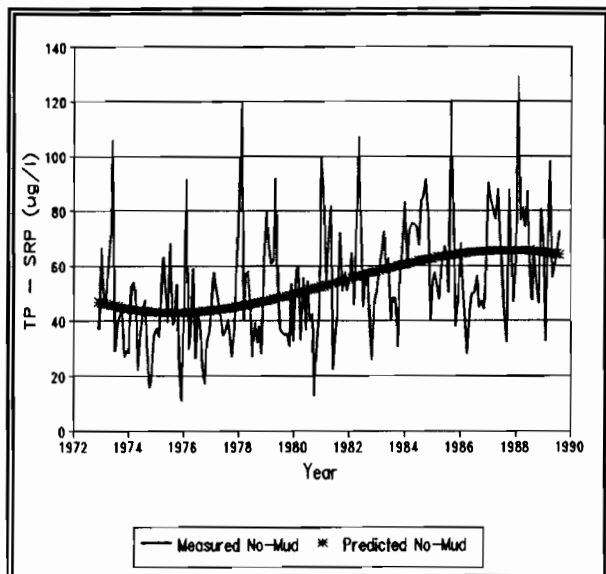


Figure C-20 Non-MUD TP-SRP.

Appendix D: Output from Baseline Run of LOP0D

See Table 13-11 for index to figures.

Figure D-01 Inflow

NLake		
10.4		
Littoral	Sand	Mud
1.04	0.000	0.000
Sbay	Lake Okee	
1.07	12.6	meters

Figure D-02 Outflow

NLake		
0.000		
Littoral	Sand	Mud
-3.08	0.000	-0.453
Sbay	Lake Okee	
-2.54	-6.07	meters

Figure D-03 Evaporation

NLake		
-16.5		
Littoral	Sand	Mud
-17.9	-16.5	-16.5
Sbay	Lake Okee	
-16.5	-16.7	meters

Figure D-04 Precipitation

NLake		
8.64		
Littoral	Sand	Mud
8.62	8.64	8.64
Sbay	Lake Okee	
8.64	8.63	meters

Figure D-05 Mean box stage

NLake		
4.44		
Littoral	Sand	Mud
4.44	4.44	4.44
Sbay	Lake Okee	
4.44	4.44	meters

Figure D-06 Mean box depth

NLake	2.68
Littoral	2.68
Sand	2.68
Mud	2.68
Sbay	2.68
Lake Okee	2.68
meters	

Figure D-07 SRP mean box concentration

NLake	35.6
Littoral	16.2
Sand	19.0
Mud	30.4
Sbay	28.4
Lake Okee	25.4
mg/m ³	

Figure D-08 DOP mean box concentration

NLake	28.4
Littoral	36.4
Sand	36.6
Mud	23.9
Sbay	30.2
Lake Okee	30.4
mg/m ³	

Figure D-09 GRN mean box concentration

NLake	3.30
Littoral	9.22
Sand	9.25
Mud	3.02
Sbay	4.27
Lake Okee	5.75
mg/m ³	

Figure D-10 BLU mean box concentration

NLake	8.33
Littoral	7.31
Sand	8.02
Mud	7.59
Sbay	10.4
Lake Okee	8.05
mg/m ³	

Figure D-12 ZOO mean box concentration

NLake	1.62
Littoral	2.45
Sand	2.45
Mud	1.53
Sbay	1.80
Lake Okee	1.95
mg/m ³	

Figure D-13 PIP mean box concentration

NLake	0.686
Littoral	1.517E-06
Sand	1.782E-02
Mud	0.701
Sbay	0.157
Lake Okee	0.345 mg/m ³

Figure D-14 ORG mean box concentration

NLake	26.7
Littoral	6.845E-05
Sand	3.96
Mud	34.8
Sbay	13.4
Lake Okee	17.5 mg/m ³

Figure D-15 SED mean box concentration

NLake	61.0
Littoral	1.321E-05
Sand	0.809
Mud	62.4
Sbay	15.4
Lake Okee	30.8 mg/m ³

Figure D-16 TP mean box concentration

NLake	105.
Littoral	71.6
Sand	79.3
Mud	102.
Sbay	88.7
Lake Okee	89.4 mg/m ³

Figure D-17 SRP time integrated burden

NLake	1.238E+06
Littoral	5.536E+05
Sand	6.576E+05
Mud	1.063E+06
Sbay	9.891E+05
Lake Okee	8.831E+05 mg/m ²

Figure D-18 DOP time integrated burden

NLake	9.973E+05
Littoral	1.269E+06
Sand	1.294E+06
Mud	8.413E+05
Sbay	1.071E+06
Lake Okee	1.068E+06 mg/m ²

Figure D-19 GRN time integrated burden

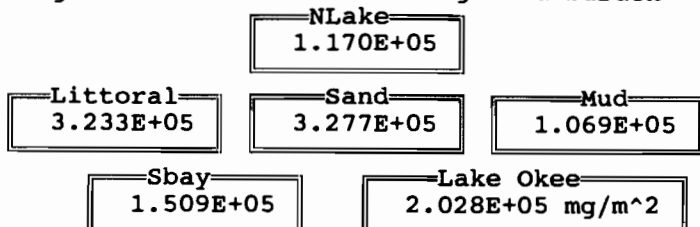


Figure D-20 BLU time integrated burden

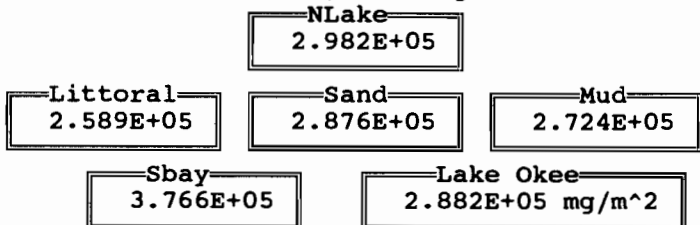


Figure D-22 ZOO time integrated burden

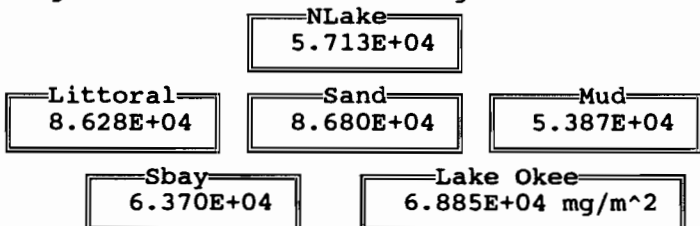


Figure D-23 PIP time integrated burden

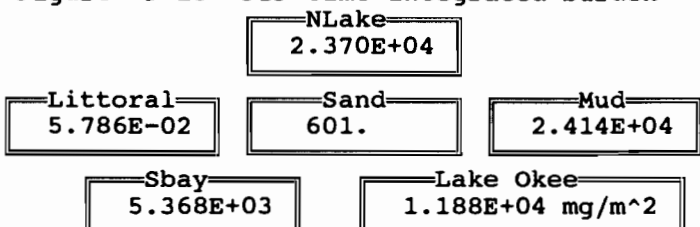


Figure D-24 ORG time integrated burden

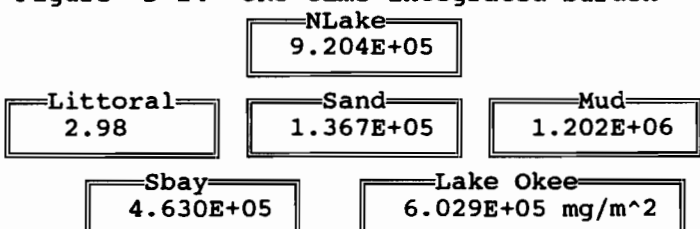


Figure D-25 SED time integrated burden

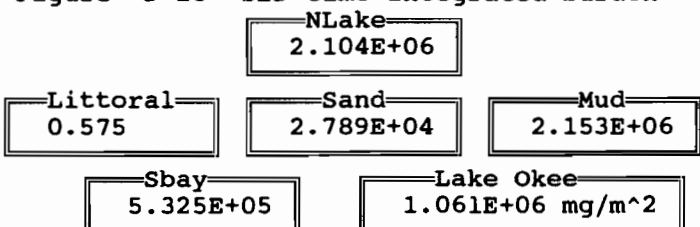


Figure D-26 SRP remineralization from DOP

NLake	1.130E+04
Littoral	3.893E+04
Sand	5.212E+04
Mud	5.782E+04
Sbay	3.448E+04
Lake Okee	3.303E+04 mg/m^2

Figure D-27 GRN uptake of SRP

NLake	5.872E+03
Littoral	6.164E+04
Sand	8.427E+04
Mud	2.860E+04
Sbay	2.628E+04
Lake Okee	3.308E+04 mg/m^2

Figure D-28 GRN respiration to SRP

NLake	2.011E+03
Littoral	2.119E+04
Sand	2.854E+04
Mud	1.131E+04
Sbay	7.986E+03
Lake Okee	1.142E+04 mg/m^2

Figure D-29 GRN death to DOP

NLake	1.642E+03
Littoral	1.913E+04
Sand	2.624E+04
Mud	3.169E+03
Sbay	7.564E+03
Lake Okee	9.136E+03 mg/m^2

Figure D-30 BLU uptake of SRP

NLake	1.111E+04
Littoral	1.963E+04
Sand	3.029E+04
Mud	5.497E+04
Sbay	3.977E+04
Lake Okee	2.686E+04 mg/m^2

Figure D-31 BLU respiration to SRP

NLake		
3.106E+03		
Littoral	Sand	Mud
5.238E+03	8.195E+03	1.590E+04
Sbay	Lake Okee	
1.127E+04	7.542E+03 mg/m^2	

Figure D-32 BLU death to DOP

NLake		
6.154E+03		
Littoral	Sand	Mud
9.590E+03	1.538E+04	3.210E+04
Sbay	Lake Okee	
2.147E+04	1.467E+04 mg/m^2	

Figure D-36 ZOO uptake of GRN

NLake		
2.572E+03		
Littoral	Sand	Mud
1.773E+04	2.358E+04	1.442E+04
Sbay	Lake Okee	
9.649E+03	1.113E+04 mg/m^2	

Figure D-37 ZOO uptake of BLU

NLake		
1.352E+03		
Littoral	Sand	Mud
4.687E+03	6.559E+03	7.519E+03
Sbay	Lake Okee	
4.486E+03	4.155E+03 mg/m^2	

Figure D-38 ZOO respiration to SRP

NLake		
1.962E+03		
Littoral	Sand	Mud
1.121E+04	1.507E+04	1.097E+04
Sbay	Lake Okee	
7.067E+03	7.643E+03 mg/m^2	

Figure D-39 ZOO death to DOP

NLake		
2.029E+03		
Littoral	Sand	Mud
1.096E+04	1.464E+04	1.135E+04
Sbay	Lake Okee	
7.000E+03	7.625E+03 mg/m^2	

Figure D-40 Desorption. PIP to SRP.

NLake			
-41.3			
Littoral	Sand	Mud	
-5.033E-02	-755.	-680.	
Sbay	Lake Okee		
-1.175E+03	-399.	mg/m^2	

Figure D-41 Adsorption. SRP to PIP.

NLake			
2.929E+03			
Littoral	Sand	Mud	
1.215E-02	8.015E-04	9.420E+03	
Sbay	Lake Okee		
745.	2.832E+03	mg/m^2	

Figure D-42 Mean GRN uptake rate

NLake			
0.709			
Littoral	Sand	Mud	
1.23	1.22	0.678	
Sbay	Lake Okee		
0.910	0.937	1/day	

Figure D-43 Mean GRN respiration rate

NLake			
0.932			
Littoral	Sand	Mud	
0.932	0.932	0.932	
Sbay	Lake Okee		
0.932	0.932	1/day	

Figure D-44 Mean GRN death rate

NLake			
0.312			
Littoral	Sand	Mud	
0.312	0.315	0.123	
Sbay	Lake Okee		
0.313	0.248	1/day	

Figure D-45 Mean BLU uptake rate

NLake			
0.750			
Littoral	Sand	Mud	
0.702	0.728	0.713	
Sbay	Lake Okee		
0.789	0.727	1/day	

Figure D-46 Mean BLU respiration rate

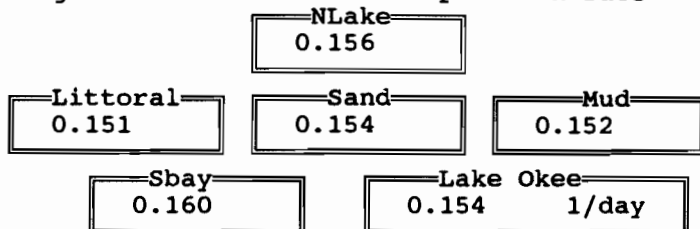


Figure D-47 Mean BLU death rate

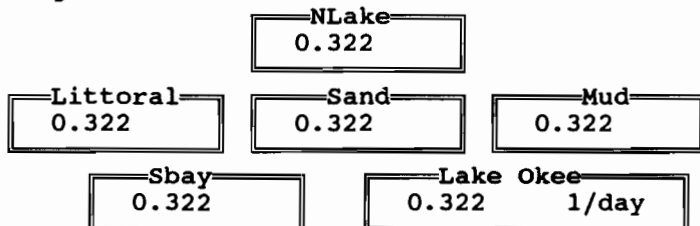


Figure D-51 Mean ZOO uptake of GRN

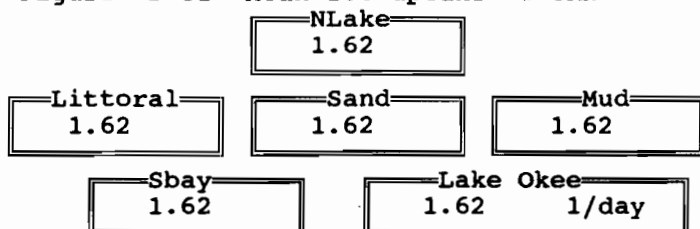


Figure D-53 Mean ZOO uptake of BLU

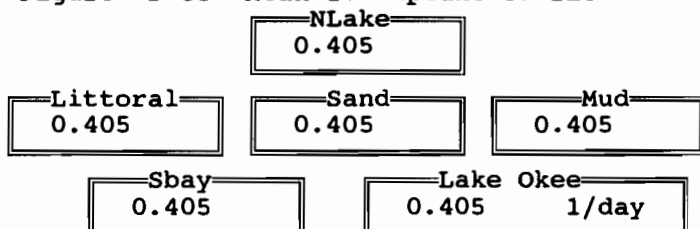


Figure D-54 Mean ZOO respiration rate

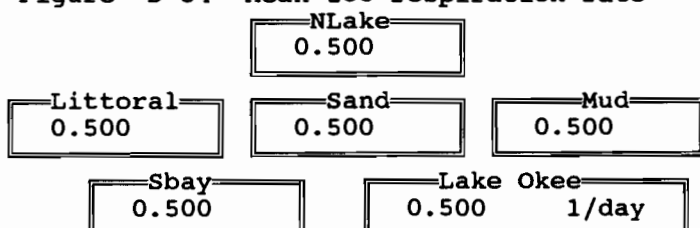


Figure D-55 Mean ZOO death rate

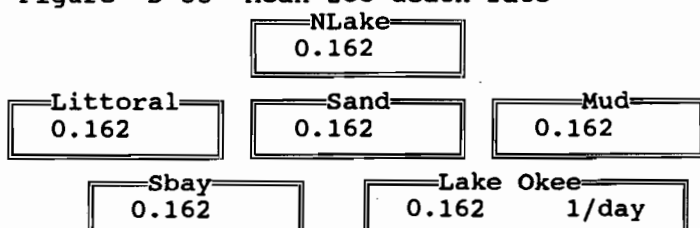


Figure D-56 Green algal settling loss

NLake	916.
Littoral	2.162E+03
Sand	2.210E+03
Mud	856.
Sbay	1.143E+03
Lake Okee	1.377E+03 mg/m^2

Figure D-57 Blue-green settling loss

NLake	505.
Littoral	417.
Sand	457.
Mud	455.
Sbay	600.
Lake Okee	476. mg/m^2

Figure D-59 Total algal settling loss

NLake	1.422E+03
Littoral	2.579E+03
Sand	2.667E+03
Mud	1.311E+03
Sbay	1.743E+03
Lake Okee	1.853E+03 mg/m^2

Figure D-60 Added SRP loading from rainfall

NLake	302.
Littoral	302.
Sand	302.
Mud	302.
Sbay	302.
Lake Okee	302. mg/m^2

Figure D-61 Added DOP loading from rainfall

NLake	130.
Littoral	129.
Sand	130.
Mud	130.
Sbay	130.
Lake Okee	130. mg/m^2

Figure D-62 Net diagenetic SRP diffusion

NLake	383.
Littoral	376.
Sand	830.
Mud	682.
Sbay	84.6
Lake Okee	528. mg/m^2

Figure D-63 Up diagenetic SRP diffusion

NLake 383.		
Littoral 376.	Sand 830.	Mud 682.
Sbay 88.4	Lake Okee 528.	mg/m ²

Figure D-64 Down diagenetic SRP diffusion

NLake -2.531E-02		
Littoral -7.903E-02	Sand 0.000	Mud 0.000
Sbay -3.81	Lake Okee -0.560	mg/m ²

Figure D-65 Equilibrium PC (EPC)

NLake 35.4		
Littoral 16.2	Sand 19.0	Mud 30.3
Sbay 28.4	Lake Okee 25.3	mg/m ³

Figure D-66 Days SRP > EPC

NLake 2.135E+03		
Littoral 1.513E+03	Sand 1.554E+03	Mud 2.022E+03
Sbay 1.671E+03	Lake Okee 8.894E+03	

Figure D-67 Days SRP < EPC

NLake 1.153E+03		
Littoral 1.775E+03	Sand 1.734E+03	Mud 1.266E+03
Sbay 1.617E+03	Lake Okee 7.546E+03	

Figure D-68 Diagenetic boundary flux

NLake 0.116		
Littoral 0.113	Sand 0.252	Mud 0.207
Sbay 2.564E-02	Lake Okee 0.156	mg/m ²

Figure D-69 Top SRP concentration

NLake		
35.6		
Littoral	Sand	Mud
16.2	19.0	30.4
Sbay	Lake Okee	mg/m ³
28.4	25.4	

Figure D-70 Top diagenetic layer

NLake		
36.7		
Littoral	Sand	Mud
17.4	19.9	32.3
Sbay	Lake Okee	mg/m ³
28.6	26.7	

Figure D-71 Top diagenetic organic P (mg/kg)

NLake		
2.236E+03		
Littoral	Sand	Mud
191.	202.	1.752E+03
Sbay	Lake Okee	mg/m ³
1.125E+03	1.093E+03	

Figure D-72 Mean GRN settling rate (m/day)

NLake		
7.314E-02		
Littoral	Sand	Mud
7.314E-02	7.314E-02	7.314E-02
Sbay	Lake Okee	
7.314E-02	7.314E-02	

Figure D-73 Mean BLU settling rate (m/day)

NLake		
1.829E-02		
Littoral	Sand	Mud
1.829E-02	1.829E-02	1.829E-02
Sbay	Lake Okee	
1.829E-02	1.829E-02	

Figure D-74 Organic phosphorus erosion

NLake		
4.351E+05		
Littoral	Sand	Mud
1.207E-04	3.883E+04	3.411E+05
Sbay	Lake Okee	mg/m ²
2.189E+05	2.214E+05	

Figure D-75 Organic phosphorus deposition

NLake		
	4.353E+05	
Littoral	0.991	Sand
	3.882E+04	Mud
Sbay	2.190E+05	Lake Okee
		2.215E+05 mg/m^2

Figure D-76 Diagenetic SRP sediment advec

NLake		
	6.73	
Littoral	9.346E-09	Sand
	1.79	Mud
Sbay	5.32	Lake Okee
		4.16 mg/m^2

Figure D-77 Inorganic phosphorus erosion

NLake		
	2.959E+03	
Littoral	6.502E-07	Sand
	765.	Mud
Sbay	2.998E+03	Lake Okee
		1.980E+03 mg/m^2

Figure D-78 Inorganic phosphorus deposition

NLake		
	1.120E+04	
Littoral	1.421E-02	Sand
	198.	Mud
Sbay	2.569E+03	Lake Okee
		4.413E+03 mg/m^2

Figure D-79 Total SRP interbox mass transfer

NLake		
	-1.206E+04	
Littoral	3.507E+03	Sand
	6.078E+03	Mud
Sbay	3.553E+03	Lake Okee
		-1.905E-03 mg/m^2

Figure D-80 Total DOP interbox mass transfer

NLake		
	-5.081E+03	
Littoral	-1.298E+03	Sand
	-4.020E+03	Mud
Sbay	-3.522E+03	Lake Okee
		7.388E-04 mg/m^2

Figure D-81 Total GRN interbox mass transfer

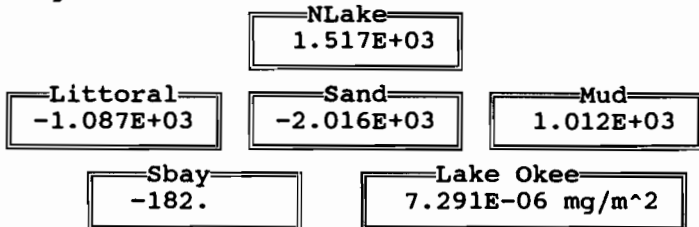


Figure D-82 Total BLU interbox mass transfer

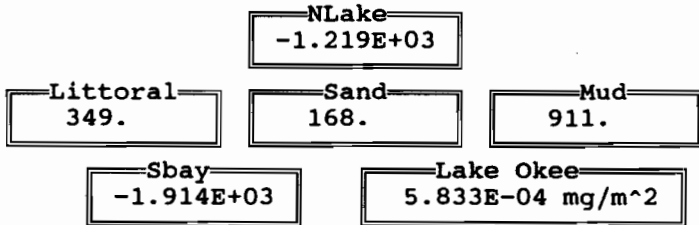


Figure D-83 Total DIA interbox mass transfer

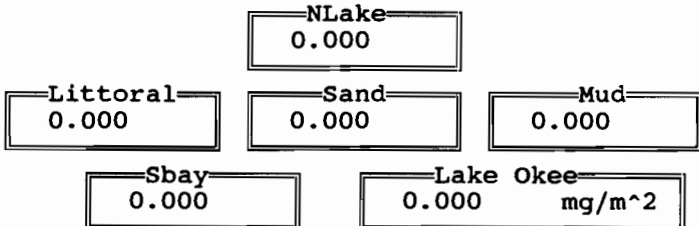


Figure D-84 Total ZOO interbox mass transfer

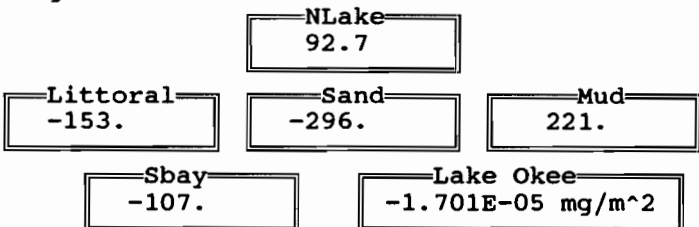


Figure D-85 Total PIP interbox mass transfer

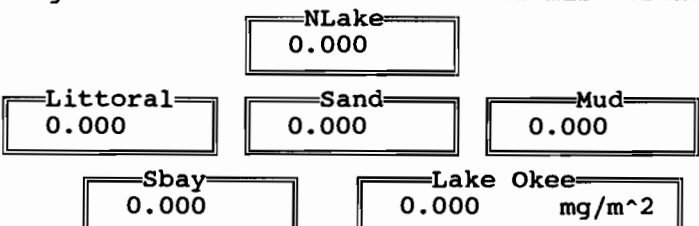


Figure D-86 Total ORG interbox mass transfer

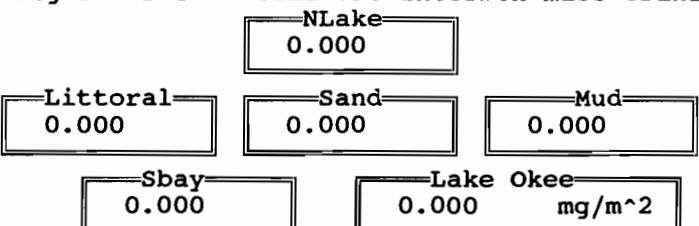


Figure D-87 Advection SRP mass transfer

NLake 445.		
Littoral 310.	Sand 909.	Mud -967.
Sbay 612.	Lake Okee $-1.750E-04 \text{ mg/m}^2$	

Figure D-88 Advection DOP mass transfer

NLake 1.348E+03		
Littoral -479.	Sand -192.	Mud -542.
Sbay 1.025E+03	Lake Okee $4.569E-04 \text{ mg/m}^2$	

Figure D-89 Advection GRN mass transfer

NLake 391.		
Littoral -213.	Sand -245.	Mud -32.3
Sbay 297.	Lake Okee $1.264E-04 \text{ mg/m}^2$	

Figure D-90 Advection BLU mass transfer

NLake 292.		
Littoral -7.75	Sand 108.	Mud -198.
Sbay 127.	Lake Okee $-1.920E-04 \text{ mg/m}^2$	

Figure D-92 Advection ZOO mass transfer

NLake 102.		
Littoral -39.8	Sand -21.3	Mud -35.8
Sbay 77.2	Lake Okee $1.580E-05 \text{ mg/m}^2$	

Figure D-93 Advection PIP mass transfer

NLake 0.000		
Littoral 0.000	Sand 0.000	Mud 0.000
Sbay 0.000	Lake Okee 0.000 mg/m^2	

Figure D-94 Advection ORG mass transfer

NLake		
0.000		
Littoral	Sand	Mud
0.000	0.000	0.000
Sbay	Lake Okee	
0.000	0.000	mg/m ²

Figure D-95 Secchi disc depth

NLake		
0.186		
Littoral	Sand	Mud
1.12	0.930	0.178
Sbay	Lake Okee	
0.372	0.557	meters

Figure D-96 KDD - light attenuation coeff

NLake		
25.3		
Littoral	Sand	Mud
2.04	2.45	27.0
Sbay	Lake Okee	
8.21	14.2	

Figure D-97 KAA - sum of absorbing agents

NLake		
0.596		
Littoral	Sand	Mud
0.616	0.623	0.588
Sbay	Lake Okee	
0.621	0.606	

Figure D-98 KBB - sum of scattering agents

NLake		
22.8		
Littoral	Sand	Mud
0.718	1.08	24.5
Sbay	Lake Okee	
6.43	12.3	

Figure D-99 Erosion of sediment

NLake		
13.9		
Littoral	Sand	Mud
2.537E-08	7.74	13.9
Sbay	Lake Okee	
15.3	9.63	

Figure D-100 Deposition to sediment

NLake		
13.9		
Littoral	Sand	Mud
1.509E-04	7.74	13.9
Sbay	Lake Okee	
15.3	9.63	

Figure D-101 Macrophyte sink of SRP

NLake		
0.000		
Littoral	Sand	Mud
827.	817.	0.000
Sbay	Lake Okee	
817.	409.	mg/m ²

Figure D-102 Macrophyte loading of DOP

NLake		
0.000		
Littoral	Sand	Mud
817.	827.	0.000
Sbay	Lake Okee	
827.	410.	mg/m ²

Table D-1 Further summary output from LOPOD -- baseline simulation.

Parameter	North Lake	Littoral	Sand Zone	Mud Zone	South Bay	Whole Lake
TP import NB/Slough	594.	0.000	0.000	0.000	0.000	594. mg/m^2
TP import Kissimmee	582.	0.000	0.000	0.000	0.000	582. mg/m^2
Other SRP import	1.063E+03	132.	0.000	0.000	167.	1.362E+03 mg/m^2
Other DOP import	424.	63.8	0.000	0.000	54.4	542. mg/m^2
SRP export	0.000	-34.5	0.000	-9.80	-43.8	-88.1 mg/m^2
DOP export	0.000	-110.	0.000	-9.38	-66.4	-186. mg/m^2
GRN export	0.000	-30.0	0.000	-1.36	-10.6	-42.0 mg/m^2
BLU export	0.000	-19.4	0.000	-3.44	-23.2	-46.1 mg/m^2
PIP export	0.000	-2.938E-06	0.000	-3.935E-07	-2.230E-06	-5.561E-06 mg/m^2
ZOO export	0.000	-7.58	0.000	-0.641	-4.24	-12.5 mg/m^2
ZOO export	0.000	-2.956E-06	0.000	-0.215	-0.282	-0.497 mg/m^2
ZOO export	0.000	-5.496E-06	0.000	-12.8	-30.0	-42.8 mg/m^2
Total TP export	0.000	-201.	0.000	-37.6	-179.	-417. mg/m^2
Total TP import	2.663E+03	196.	0.000	0.000	222.	3.081E+03 mg/m^2
Total TP loading error	-481.	mg/m^2				
Beginning lake burden	450.	mg/m^2				
Ending lake burden	266.	mg/m^2				